

Light and Temperature Triggered Triazolinedione Reactivity for On Demand Bonding and Debonding of Polymer Systems

Zur Erlangung des akademischen Grades eines

DOKTORS DER NATURWISSENSCHAFTEN

(Dr. rer. nat.)

von der KIT-Fakultät für Chemie und Biowissenschaften
des Karlsruher Instituts für Technologie (KIT)

genehmigte

DISSERTATION

von

M. Sc. Hannes Houck

geboren in Vilvoorde, Belgien

KIT Dekan: Prof. Dr. Reinhard Fischer

Referent: Prof. Dr. Christopher Barner-Kowollik and Prof. Dr. Filip E. Du Prez

Korreferent: Prof. Dr. Patrick Théato

Tag der mündlichen Prüfung: 13.12.2018

Die vorliegende Arbeit wurde von Januar 2015 bis Oktober 2018 im Rahmen einer Cotutelle Vereinbarung zwischen KIT und der Universität Gent, Belgien unter Anleitung von Prof. Dr. Christopher Barner-Kowollik am Karlsruher Institut für Technologie (KIT) - Universitätsbereich und unter Anleitung von Prof. Dr. Filip E. Du Prez an der Universität Gent, Belgien angefertigt.

Erklärung

Hiermit erkläre ich, dass die vorliegende Arbeit im Rahmen der Betreuung durch Prof. Dr. Christopher Barner-Kowollik (KIT) und Prof. Dr. Filip E. Du Prez (Universität Gent, Belgien) selbstständig von mir verfasst wurde und keine anderen als die angegebenen Quellen und Hilfsmittel verwendet wurden. Die wörtlich oder inhaltlich übernommenen Stellen wurden als solche kenntlich gemacht. Die Regeln zur Sicherung guter wissenschaftlicher Praxis des Karlsruher Instituts für Technologie (KIT) wurden beachtet und die Abgabe und Archivierung der Primärdaten gemäß Abs. A (6) der Regeln zur Sicherung guter wissenschaftlicher Praxis des KIT beim Institut ist gesichert. Die elektronische Version der Arbeit stimmt mit der schriftlichen überein. Die Arbeit wurde im Rahmen der bestehenden Cotutelle-Vereinbarung zwischen dem KIT und der Universität Gent gemeinschaftlich durchgeführt und ist ebenfalls an der ausländischen Universität als Bestandteil einer Prüfungs- oder Qualifikationsleistung zur Erlangung des dortigen Doktorgrades (Doctor of Science in Chemistry) vorgelegt. Des Weiteren erkläre ich, dass ich keine vorausgegangenen Promotionsversuche unternommen habe und mich derzeit nur in dem oben genannten laufenden Cotutelle-Promotionsverfahren befinde.

Hannes Houck

Karlsruhe, 30.10.2018



Research funded by the Research Foundation – Flanders

Onderzoek gefinancierd door het Fonds Wetenschappelijk Onderzoek - Vlaanderen.

“Science may set limits to knowledge,

but should not set limits to imagination”

Bertrand Russel

British author

mathematician

philosopher

Nobel prize laureate

Acknowledgements

Although this is the part of the dissertation I looked forward to write the most, it turned out to be the hardest one to put down on paper. Not because I do not know who to thank, but because there is no way I can acknowledge everyone who has been involved during the course of this joint PhD project in just a few pages. Nonetheless, as the journey is coming to an end, I could not find a more symbolic place to write my acknowledgements than on the train from Ghent to Karlsruhe.

Departure from Ghent. The starting point of my journey today in Ghent, reminds me of the one exactly 4 years ago when I walked into the office of Prof. Filip Du Prez and not just told him that I wanted to do a PhD, but also that I wanted to do it abroad. A phone call to Prof. Christopher Barner-Kowollik later marked the start of this incredible journey. I would like to express my deepest gratitude to the both of you, Filip and Christopher, for the opportunity you have provided me. I truly appreciate the unique environment you created for me and the scientific freedom I was offered by both of you to approach this challenging PhD project from a more fundamental and conceptual approach, yet keeping the application ever in mind (let's say a perfectly merged view of both). Especially the out-of-the-box ideas that were created during our many jointly meetings and the high risk they came with, were taken as a real motivation to persue them. Thanks to all the support and chances you gave me, I was able to challenge and develop myself as a researcher on a daily basis, which will definitely help me in my future career.

Stopping in Brussels. This is the point I spontaneously think of the many stopovers I held in the office of Prof. Johan Winne from the organic synthesis lab in Ghent, especially during the first two years of my PhD. Your door was always open for me to bother you with yet another synthesis problem and no matter how busy you were, you always took the time to listen. I cannot recall a single moment I left your office without an answer ... or at least an additional question to be answered.

Crossing the border. The train continues from Belgium into Germany, equally effortless as I travelled between the two research groups as a result of the unique working atmosphere, discussions and many fun outside-of-the-lab activities, at both sides of the border. I would therefore like to thank all the remarkable people I was fortunate to work with in both research groups, in particular some that I have worked with most closest. First of all, there is not a font size small enough that allows me to express my gratitude to Josh on just one page. From the day we met on teambuilding having a dreadful green cocktail that only tastes delicious after a spoon of vegemite, to the many years later sharing an apartment and seeing you as a brother, your support has truly been unconditional. Especially during the frustrating and stressful moments in the few weeks preceding this thesis (I guess I am back on cleaning and cooking duties

again now...). I also need to thank Kevin, for all the things you have done for me, from the guidance during my undergrad to the fun moments in lab 4, yet most importantly for staying a close friend afterwards. Matze, thanks for the fun times sharing coffees, beers, frustrations and a fume hood together. Also for taking care of my black synthesis residue that I keep promising to column one day (you can actually read what it is in Chapter III). Eva and Patrick for the extremely nice collaboration and sharing exciting ideas when others might not so much. Hatice M. for bringing me food when working late at night, blinded by sleep and laser goggles, and simply every other individual from both the PCR and MacroArc group for the nice memories and fun moments I will treasure (teambuildings, Christmas parties, skiing trips, Cheese and Wine evenings, ...).

Approaching Cologne. The announcement that the train cannot continue due to a technical issue readily reminds me of an SEC system or rheometer out of service. The train company can only wish for the brilliant technical support that I received during my research. Thank you Bernhard for not only being fascinated about trains, but also for keeping the lab in Ghent on the rails every day. Many thanks to Bastiaan for the brilliant atmosphere and support in lab 4. That co-authored contribution is far from enough to reflect your impact the past 4 years. Further, I would like to thank Katharina, Vincent and Frau Schneider for providing me the best conditions in the Karlsruhe group, as well as Tim, Dieter and Jan for the excellent NMR and LC-MS service.

Changing in Cologne. The midway point between Ghent and Karlsruhe. This is where I always get lost in the flock of people searching their way to the platforms. It reminds me of the amount of paper work that has been involved at both universities to set up and carry out this joint PhD program. I would have been lost without the administrative help from Evelyn, Veerle, Paul, Queenie, Christel and Carine.

Passing Frankfurt international airport. The second part of my journey makes me realise how privileged I was to spend 7 months in Brisbane, Australia at the Queensland University of Technology. An experience that will stay with me for the rest of my life. Not only a scientific eye-opener, but definitely also a personal one. I only hold the best memories of my time there, especially the Monday morning coffees on the bridge with Matthias, the many weekend trips with wonderful people (Hendrik, Matze, David, Andrea, Waldemar, ...) and the road trip with two of the warmest colleagues/friends (delete where applicable, Hendrik and Federica).

Arriving in Karlsruhe. I arrive in the city of rising construction sites rather than buildings, which I call my second home. I had great times here not only developing myself as a scientist but also on a person level. Regardless from where I was at which time, I need to thank all my friends in Belgium and Germany for taking part in this incredible journey.

Texting my parents I arrived well. This finally leaves me to thank my parents and sister for always being so supportive and caring about me, for as long as I can remember. I couldn't have achieved all this without you and I can only hope you are as proud of me as I am of you.

Table of Contents

Acknowledgements	xi
Table of Contents	xiii
Chapter I. General introduction, aim and outline	1
I.1 Introduction and aim	1
I.2 Outline	3
Chapter II. Theoretical background	7
II.1 Triggered bonding and debonding of polymer systems	8
II.1.1 General introduction.....	8
II.1.2 Thermally triggered bonding and debonding.....	9
II.1.3 Photochemically triggered bonding and debonding	15
II.1.4 Conclusions	30
II.2 Introduction to triazolinedione chemistry	31
II.2.1 General introduction.....	31
II.2.2 Synthesis of 4-substituted triazolinediones	33
II.2.3 Triazolinedione reactivity	41
II.2.4 Applications of TAD-based reactions in polymer synthesis.....	54
II.2.5 Conclusions.....	60
Chapter III. Tunable thermoreversible blocking agents for triazolinediones	61
III.1 Introduction	62
III.2 Potential candidates for suitable TAD-blocking agents.....	63
III.3 In-depth investigation of the reversible TAD-indole reaction platform.....	65
III.3.1 Exploration of novel TAD-reactive indole substrates	67
III.3.2 Kinetic thermoreversibility studies	70
III.3.3 Theoretical rationalisation	75
III.4 Substituted indoles enabling tunable deblocking temperatures.....	78
III.4.1 Synthesis of a 2,3-disubstituted indole library	78
III.4.2 Kinetic thermoreversibility studies	79
III.4.3 Additional influences on the temperature of reversibility.....	82

III.5	Blocked triazolinediones for temperature controlled bonding of polymer systems...	84
III.5.1	Case study 1: temperature triggered polymer modification.....	84
III.5.2	Case study 2: on demand polymer crosslinking.....	88
III.6	Orthogonal indole-to-indole exchange reaction.....	93
III.7	Conclusions and perspectives of the blocked triazolinedione concept	96
III.8	Notes on the collaboration.....	98
Chapter IV. Photodeactivation of triazolinediones enabling light-switchable reactivity		99
IV.1	Introduction.....	100
IV.2	Photopolymerisation as the key to photodeactivation.....	101
IV.2.1	Photopolymerisation	102
IV.2.2	Photodeactivation	105
IV.3	Orthogonality with different colours of light	108
IV.3.1	Introducing TAD to UV-induced conjugation.....	109
IV.3.2	Combination of UV- and visible light-induced reaction channels.....	110
IV.4	Light play: switchable TAD reactivity	112
IV.5	Valorisation in sub-diffraction laser lithography	114
IV.6	Conclusions and perspectives of light-switchable TAD reactivity	116
IV.7	Notes on the collaboration.....	117
Chapter V. Light-stabilised dynamic materials through triazolinedione-based cycloaddition.....		119
V.1	Introduction.....	119
V.2	Investigations on low molecular weight compounds	122
V.2.1	Visible light-induced polymerisation versus cycloaddition	122
V.2.2	Covalent debonding in the dark.....	125
V.2.3	Light-stabilised dynamic covalent bonds.....	128
V.3	Introducing light-stabilised dynamic bonds into polymers	129
V.3.1	Monomer design	129
V.3.2	Polymer design and crosslinking test	135
V.4	Light-stabilised dynamic materials	138
V.4.1	Rheological behaviour	138

V.4.2	Macroscopic demonstrations	144
V.5	Conclusions and perspectives of light-stabilised materials	146
Chapter VI.	Photoaddition of triazolinediones to polyethers	149
VI.1	Introduction	150
VI.2	Model studies of the photoaddition reaction	151
VI.2.1	Investigations on low molecular weight compounds	151
VI.2.2	Backbone modification of poly(ethylene glycol).....	154
VI.2.3	Hydrolytic stability.....	158
VI.2.4	Concluding remarks on the model studies	159
VI.3	Writing and cleaving of poly(ethylene glycol)-based materials	160
VI.3.1	Macroscopic investigation	160
VI.3.2	Direct laser written microstructures	162
VI.4	Conclusions and perspectives	167
VI.5	Notes on the collaboration	168
Chapter VII.	General conclusions and perspectives	169
VII.1	Conclusions.....	169
VII.2	Future perspectives	171
Chapter VIII.	Abstract	175
Chapter IX.	Samenvatting	177
Chapter X.	Zusammenfassung.....	179
Appendix A.	Materials and instrumentation.....	181
A.1	Materials	181
A.2	Instrumentation	182
Appendix B.	Experimental section Chapter III.....	187
B.1	Additional figures.....	187
B.2	Experimental procedures.....	193
B.2.1	Kinetic thermal reversibility studies of TAD-indole systems.....	193
B.2.2	Calculation of the observed activation energies.....	194
B.2.3	Time-controlled modification of polyisoprene with indole-blocked TAD-dyes	196
B.2.4	Temperature triggered transfer of indole-blocked TAD-dyes from solution onto an insoluble resin.....	197

B.2.5	On demand polymer crosslinking of a diene-containing polyurethane.....	197
B.2.6	Orthogonal indole-to-indole TAD-exchange reaction	198
B.3	Computational methods and theoretical data	201
B.4	Synthetic procedures	202
B.4.1	Synthesis of indole model compounds	202
B.4.2	Synthesis of triazolinedione model reagents	216
B.4.3	Synthesis of model TAD-indole adducts	217
B.4.4	Synthesis of 4-(4-azobenzene)-1,2,4-triazoline-3,5-dione (31).....	222
B.4.5	Synthesis of indole-blocked TAD-dye adducts 32 and 33	224
B.4.6	Synthesis of TAD-reactive network.....	226
B.4.7	Synthesis of diene-containing polyurethane (HDEO-PU, 35)	227
B.4.8	Synthesis of triazolinedione crosslinking agents	229
B.4.9	Synthesis of indole-blocked triazolinedione crosslinking agents 38-43	231
B.4.10	Synthesis of poly(ethylene glycol)-supported blocked TAD-dye 45	234
Appendix C. Experimental section Chapter IV		237
C.1	Additional figures and table	237
C.2	Experimental procedures	245
C.2.1	Photopolymerisation of BuTAD (1) upon visible light irradiation	245
C.2.2	Photostability assessment of BuTAD (1) as a function of the applied wavelength	246
C.2.3	Trapping experiment to demonstrate the photodeactivation of BuTAD (1) .	248
C.2.4	Kinetic study of the photopolymerisation of BuTAD (1)	248
C.2.5	Regeneration kinetics of BuTAD (1) after photopolymerisation.....	249
C.2.6	Photostability assessment of <i>o</i> -methylbenzophenone (5) and <i>trans</i> -5-decene (10)	250
C.2.7	Photostability assessment of BuTAD (1) under UV-light	251
C.2.8	Light-induced photoenol reaction of 1 with 5	251
C.2.9	Reduction of the photoenol product mixture 8a+8b into cyclic 9	252
C.2.10	Alder-ene addition of 1 to 10 in the dark	253
C.2.11	Light-switchable reaction manifold	253
C.2.12	STED-inspired sub-diffraction lithography experiments	255

C.3	Synthetic procedures	256
C.3.1	Synthesis of 4- <i>n</i> -butyl-triazoline-3,5-dione (BuTAD, 1)	256
C.3.2	Synthesis of triethoxysilane-containing photoenol precursor 12	256
C.3.3	Synthesis of bromine-containing triazolinedione 13	256
Appendix D. Experimental section Chapter V		259
D.1	Additional figures	259
D.2	Experimental procedures	263
D.2.1	Visible light-induced formation of cycloadduct 3	263
D.2.2	Visible light-induced cycloaddition or polymerisation	264
D.2.3	Kinetic measurements of the cycloreversion process	265
D.2.4	Reduction of cycloadduct 3 into 4	267
D.2.5	Thermal cycloreversion test of reduced cycloadduct 4	268
D.2.6	Light-stabilised formation of cycloadduct 3	268
D.2.7	Photo-induced crosslinking of triazolinedione-naphthalene networks	269
D.3	Synthetic procedures	270
D.3.1	Synthesis of 4- <i>n</i> -butyl-triazoline-3,5-dione (BuTAD, 1)	270
D.3.2	Synthesis of potassium azodicarboxylate	270
D.3.3	Synthesis of naphthalene model compounds	271
D.3.4	Synthesis of naphthalene-containing methacrylate monomers	275
D.3.5	Synthesis of naphthalene-containing polymers	277
D.3.6	Synthesis of bisfunctional triazolinedione crosslinker 16	279
Appendix E. Experimental section Chapter VI		281
E.1	Additional figures	281
E.2	Experimental procedures	285
E.2.1	Photoaddition to low molecular weight compounds	285
E.2.2	Photoaddition to <i>tert</i> -butyl endcapped poly(ethylene glycol)	287
E.2.3	Removal of urazole byproducts via dialysis	287
E.2.4	Hydrolysis of BuTAD-poly(ethylene glycol) conjugates	288
E.2.5	Light-induced macroscopic network formation and cleavage	288
E.2.6	Direct laser writing and cleavage of microscopic structures	289

E.3	Synthetic procedures	289
E.3.1	Synthesis of 4- <i>n</i> -butyl-triazoline-3,5-dione (BuTAD, 1).....	289
E.3.2	Synthesis of <i>tert</i> -butyl end capped poly(ethylene glycol)s (<i>t</i> BuPEG)	290
E.3.3	Synthesis of bisfunctional triazolinedione crosslinker 6	290
Appendix F. List of abbreviations.....		291
Appendix G. List of publications arising from this dissertation.....		295
Appendix H. Bibliography		297

Chapter I.

General introduction, aim and outline

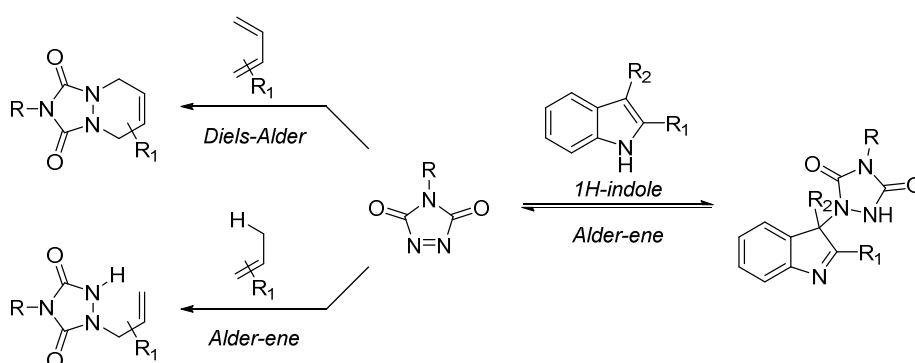
I.1 Introduction and aim

The field of polymer chemistry is often regarded as a separate discipline by many chemists, yet the synthesis, properties and application of macromolecules are inherently interdisciplinary. Indeed, the study of how small building blocks can be combined into complex macromolecules or materials whereby the final macroscopic properties can be manipulated on a molecular level, relies on fundamental concepts in various research domains, most importantly organic, physical and analytical chemistry. Especially organic chemistry provides the polymer scientist with a plethora of efficient bond forming and bond breaking reactions that can serve as tools to affect perturbations on a molecular level in order to introduce a desired macroscopic response. In this context, the click chemistry concept¹ – which emerged at the beginning of the 21st century – introduced a new reaction paradigm, leading to a vast array of robust, fast and high-yielding reactions. Polymer science has vastly benefited from these spring loaded ‘click’ approaches, particularly in the design of unprecedented and highly complex macromolecular architectures.² Moreover, additional criteria such as equimolarity and large scale purification have been implemented to specifically address polymer-polymer conjugation reactions.³

Despite the many modular reactions, some with ‘click’ characteristics, that have been exploited throughout the years,⁴ the development of more advanced ligation protocols with tailored responsive behaviour is highly desired in contemporary polymer synthesis. Indeed, the incorporation of covalent linkages into polymer materials that can be modulated by an external stimulus enables highly attractive materials that can adapt their structure and properties on demand, simply by a change in their surrounding environment.⁵ A key attribute to introduce adaptive properties such as dynamic rearrangement, self-repair and reprocessing is found in reversible covalent chemistries that can undergo bonding and/or debonding in response to an external trigger such as temperature or light.⁶

The chemistry of triazolinediones (TADs) represents an ideal combination of both irreversible and reversible click-type reactivity, which has recently been identified in our own research group at Ghent University.⁷ Whereas TAD reagents have been well-studied in highly efficient ligation methods,⁸⁻⁹ gaining the reputation of most reactive dienophiles that are to be isolated,¹⁰ these highly reactive compounds recently regained considerable interest in polymer synthesis.¹¹ In particular, the irreversible Diels-Alder and Alder-ene-type addition to conjugated and isolated alkenes (refer to

Scheme I.1, left) have been exploited by us for the ultrafast formation of defined block copolymers^{7, 12} and also crosslinked materials from plant oil feedstock.¹³ Notably, TAD-based reactions swiftly proceed at ambient temperature, and even far below (e.g. at -78 °C), without the need of a catalyst and typically reach quantitative conversions in only seconds to minutes, even with macromolecular substrates. Furthermore, when indole moieties are applied as TAD reaction partner instead of plain alkenes, the corresponding Alder-ene adduct comprises a reversible linkage (Scheme I.1, right). The dynamic nature of the TAD-indole reaction thus allows for a triggered debonding at elevated temperatures, thereby enabling thermoreversible polymer conjugations and healable crosslinked materials.^{7, 14}



Scheme I.1. Irreversible (left) and reversible (right) TAD-based click-like addition reactions.

Although TAD chemistry has found many applications in organic chemistry, bioconjugation and polymer science,¹⁵ the general perception that is associated with TAD reagents, together with some remaining fundamental issues, still hampers its widespread use. For example, no general synthetic strategy is available to afford tailored TAD compounds, as the synthesis of such functional derivatives typically suffers from chemoselectivity issues. Moreover, whereas TADs are praised for their ultrafast reaction kinetics, their use is often refrained from applications that require a controlled reactivity. In the coating industry, for example, a certain time delay is required to allow for a coating formulation to be applied onto a substrate, before the actual curing can be initiated. Hence, chemistries that have too fast curing kinetics are considerably less attractive. The high reactivity is also reflected in the ultrafast crosslinking of polydienes upon addition of bivalent TAD reagents, which typically results in inhomogeneous materials. In addition, the inherent reactivity of TADs also translates into a rather limited stability and moisture sensitivity, imposing continuous or even *in situ* synthesis efforts.

The general aim of the current doctoral work is two-fold: Initially, the development of externally triggered TAD-based reactions as a promising on-and-off switch over their unique reactivity was explored (Figure I.1). Temperature and light were identified as interesting stimuli to provide a selective start and stop switch, which would ideally resolve the above noted shortcomings of TAD

reagents in terms of synthesis, stability and controlled reactivity. Secondly, the introduction of triggered TAD-based reactions for the controlled design of polymer materials was intended so as to make TAD chemistry also feasible in temporally and spatially resolved applications. Thus, the ultimate goal is to develop triggered TAD reactivity from a polymer materials perspective and establish conceptual, unprecedented TAD-based materials that can adapt in a controllable and/or repeatable manner via temperature or light-induced bonding and/or debonding reactions.

To increase the success rate of achieving the postulated aims, the current doctoral study was subject to an intense and international collaborative project between the Macromolecular Architectures (Christopher Barner-Kowollik) research group at the Karlsruhe Institute of Technology (KIT), Germany and the polymer chemistry research group (Filip Du Prez) at Ghent University, Belgium. These joint PhD efforts have endowed the combination of two renowned areas of expertise that have been developed at both research groups, i.e. on the one hand, the highly efficient TAD ligation chemistry (Du Prez group),^{7, 15} and on the other hand, the development of light-induced modular (polymer) conjugation strategies (Barner-Kowollik group).

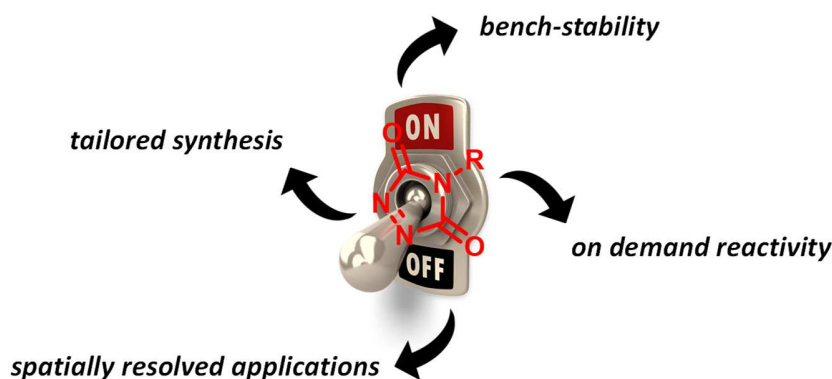


Figure I.1. Aim of the presented doctoral work to develop externally triggered triazolinedione-reactivity, paving the way for an improved synthesis and increased bench-stability, as well as enabling on demand applications that require temporal and/or spatial control.

I.2 Outline

Chapter II, at the beginning of the current dissertation, serves as a theoretical background consisting of two parts that outlines some of the fundamental principles on externally triggered concepts and chemical ligation platforms that have been used throughout the doctoral work. The **first part** offers a concise review of thermally and photochemically triggered reactions that have been described in (recent) literature for the on demand bonding and debonding of polymer systems. In particular, special attention is devoted to the use of molecular photoresponsive switches that allow

for a light-modulated control of reactivity and hence external accessibility to different material properties. In addition, two spatially resolved applications are highlighted that were used in the course of the joint PhD project. Given the extraordinary reputation that TAD reagents possess, the **second part** of Chapter II begins with offering the reader insights into the synthesis of these unique reagents. Furthermore, an overview of the different modes of both thermal and photochemical reactivity wherein TAD reagents can participate is provided, followed by some representative TAD-based polymer modification and crosslinking applications.

Since the current doctoral work aims to establish triggered TAD-based reactions featuring an on-and-off switch over their reactivity, **Chapter III** discusses the exploration of suitable blocking agents that can release TAD compounds on demand upon heating. Apart from introducing indole compounds as highly promising blocking agents, a full insight in TAD-indole reactivity is provided from which structural alterations on both the indole and TAD compounds are identified to greatly influence the blocking and deblocking properties. The resulting indole-blocked TAD systems with distinct deblocking temperatures are next used to demonstrate the practicality of the obtained on demand TAD reactivity in the context of polymer science through time delayed modification and crosslinking.

Light is also an efficient and more defined stimulus to selectively switch chemical reactivity on or off. Hence, **Chapter IV** demonstrates the possibility to activate or deactivate TAD compounds through visible light irradiation. This switchable reactivity is achieved via the homopolymerisation of TADs when subjected to green light, followed by their subsequent depolymerisation when standing in the dark. An additional level to the light-controllable TAD on-and-off switch is next provided via the combination of a UV-induced as well as thermal TAD-based conjugation to establish a tunable product selectivity. In addition to the temporally controlled application of TAD chemistry, developed in Chapter III, the obtained spatio-resolved feature over the TAD reaction outcome is finally explored to open potential in sub-diffraction surface lithography.

Light not only serves as a highly interesting gate to control the reaction outcome of a chemical transformation, it also plays a pivotal role in the design of adaptable and responsive materials. Motivated to devise a TAD-based material that can be transformed by a light stimulus, **Chapter V** introduces *light-stabilised dynamic materials* that allow to be reversibly switched from a covalently crosslinked network upon irradiation, to a viscous liquid when kept in the dark. Moreover, as long as the applied colour of visible light is kept switched on, the material's integrity is maintained. To generate such a unique material, the visible light-induced cycloaddition of TADs to naphthalene substrates is fully reinvestigated and next translated to the material level by the incorporation of the naphthalene scaffolds into a polymer. The resulting light-controlled bonding and debonding of

the TAD-naphthalene crosslinks is addressed by rheological measurements and further demonstrated by macroscopic experiments.

In addition to the reversible photoinduced reaction with naphthalenes, TADs also undergo addition reactions with ether substrates when irradiated. While this photochemical mode of reactivity was originally classified as a side reaction, **Chapter VI** demonstrates its use for the straightforward backbone functionalisation of polyethers. Apart from the visible light triggered modification of poly(ethylene glycol)s (PEGs), an advanced TAD-based PEG-photoresist is designed that can be crosslinked through multiphoton absorption lithographic techniques. This is evidenced by the fabrication of three dimensional microscopic objects through direct laser writing, whereby the resulting structures can be cleaved under extremely mild aqueous conditions as a result of the hydrolytic instability of the formed TAD-ether crosslinks. This potentially serves as a highly enabling platform to provide support structures in subtractive photoresist development or even cell scaffolds that can be removed without the need for an additional (chemical) trigger.

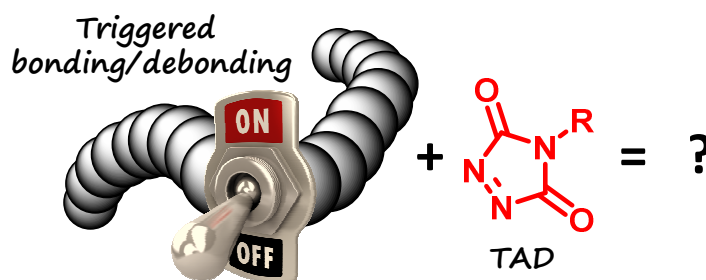
A general conclusion of the current doctoral work is provided in **Chapter VII**, wherein some future perspectives are also addressed.

Finally, an English, Dutch and German abstract of the manuscript is presented in **Chapters VIII, IX and X**, respectively.

Chapter II.

Theoretical background

Brief motivation and content



Following the introduction of the click chemistry philosophy, a plethora of efficient modular reactions have been introduced that allow for the design of complex macromolecules, in particular addressing polymer-polymer conjugations. A highly desired feature in contemporary polymer synthesis is to implement tailored responsive behaviour such as dynamic rearrangement, self-repair and reprocessing that can be remotely triggered, simply by a change in their surrounding environment. A key aspect to incorporate such adaptive properties into polymer materials is found in reversible covalent chemistries that undergo bonding and/or debonding in response to an external trigger, particularly temperature and light.

The chemistry of triazolinediones (TADs) is of particular interest for polymer chemistry because of the ultrafast, ambient temperature and additive-free formation of irreversible conjugates with simple olefins, whereas with indole substrates a dynamic covalent bond forming process can be achieved. However, no external control over the inherently reactive TADs is currently available, which considerably hinders its widespread use, especially in more demanding applications that require temporal and spatial control. The development of triggered TAD reactivity is thus a highly desired feature for the future development of these highly enabling reagents.

In the first part of this chapter, a concise overview of commonly adopted thermally and photochemically triggered reactions in polymer science are described that can serve as inspiration to develop triggered TAD-based reactions. Following the insights concerning on demand bonding and debonding covalent chemistries, a detailed discussion on the synthesis of TAD compounds is next provided. Moreover, the unique modes of both thermal and photochemical TAD reactivity are discussed, followed by their most important applications in the field of polymer science.

Partially adapted from

K. De Bruycker, S. Billiet, H. A. Houck, S. Chattopadhyay, J. M. Winne, F. E. Du Prez, *Chemical Reviews* **2016**, *116*, 3919-3974.

With permission from the American Chemical Society. Copyright 2016 American Chemical Society.

II.1 Triggered bonding and debonding of polymer systems

II.1.1 General introduction

The development of modular, spring-loaded and chemoselective orthogonal reactions made a profound impact on numerous research fields, ranging from drug discovery and bioconjugation¹⁶⁻¹⁷ to soft matter material sciences.^{4, 18} Some of these approaches, meeting the stringent click chemistry criteria,^{1, 3} proved particularly useful from a polymer synthesis point of view as they readily enabled polymer modification reactions¹⁹ as well as the design of unprecedented and complex macromolecular architectures in an equimolar manner without the need for complex purification.^{2, 20-21}

Shortly after their widespread application in the polymer community, a defined control over these efficient reactions emerged as a highly desired feature. Indeed, the ability to modulate chemical reactivity with an external stimulus was found critical for the construction of programmable, adaptive and stimuli-responsive materials.²²⁻²³ Moreover, the potential of on demand triggered reactivity can eliminate some inherent issues associated with even the most efficient click reactions, such as toxicity and bench stability of the starting components or even too pronounced reaction kinetics. Many external triggers have thus been implemented throughout the years, leading to a vast availability of chemical transformations that can be accessed on demand. The applied stimulus can either be physical (e.g. temperature, light, mechanical), chemical (e.g. pH, reagent) or biological (e.g. enzymatic).²⁴ Specifically temperature and light-induced protocols have been intensively studied for the on demand construction of (complex) macromolecules via newly coined concepts such as transclick^{7, 25} and photoclick reactions.²⁶⁻²⁷

A key aspect to provide triggered behaviour in polymer systems is the incorporation of dynamic or reversible linkages which can bond and/or debond when exposed to the external stimulus. The pioneering work of Cram, Lehn and Pederson in the field of supramolecular chemistry has inspired the development of dynamic covalent chemistry, which encompasses a library of chemical reactions that result in reversible covalent bond formation under thermodynamic equilibrium.²⁸ Polymer chemists eagerly exploited the highly attractive concept of dynamic covalent chemistries since a change on a molecular level is rapidly translated into a macroscopic response.⁶ Hence, material properties can be regulated on demand, introducing self-healing and reprocessing or recycling, controlled degradation and other types of smart and adaptive behaviour.²⁹ A recent example of the latter is the introduction of so-called macromolecular metamorphosis, whereby dynamic covalent chemistry prompted the reversible debonding and bonding of polymers to undergo dramatic topological transformations.³⁰

The current chapter provides an overview on two of the most widely adopted stimuli to introduce on demand bonding and/or debonding reactivity in polymer systems, which have also been applied in the current doctoral work. The first section is devoted to **temperature**

triggered reactivity (II.1.2) and covers some illustrative examples of thermoreversible covalent chemistries (II.1.2.1). In a following section, one particular thermoreversible system is highlighted to showcase the importance of thermally induced polymer crosslinking, more specific in an industrial context (II.1.2.2). Another example of thermally triggered bonding and debonding applications is presented in II.1.2.3 by the design of crosslinked polymer materials that exhibit adaptable properties such as self-healing, stress-relieving and reprocessing upon heating.

Next to temperature, a second section aims to provide insights in **photochemically induced protocols (II.1.3)**. More specifically, after getting acquainted with some basic fundamental concepts of photochemistry (II.1.3.1), selected light-triggered conjugation and cleavage reactions as well as photoreversible chemistries are discussed (II.1.3.2). In addition, the strongly emerging feature of light to afford a switchable modulation of material properties is highlighted in II.1.3.3 in a brief discussion on molecular photoswitches. Finally, the principles of two spatially resolved applications that have been employed in the current doctoral work, i.e. direct laser writing and sub-diffraction lithography, are presented in II.1.3.4.

II.1.2 Thermally triggered bonding and debonding

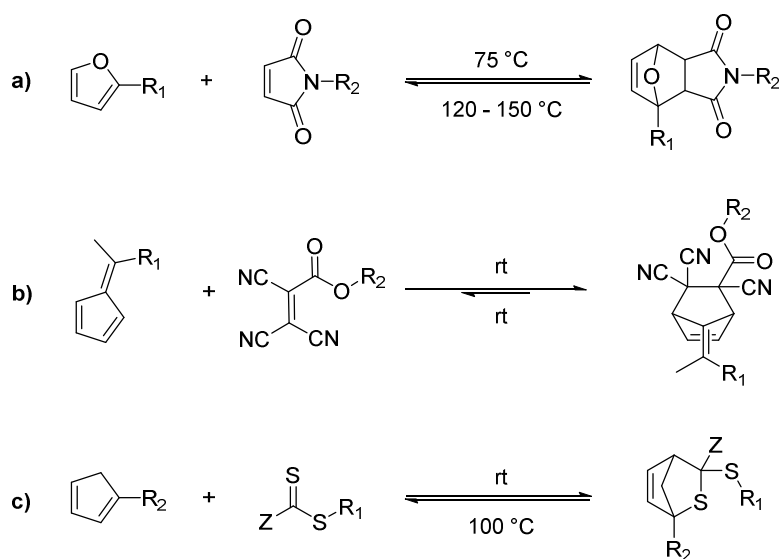
Temperature is perhaps one of the most commonly exploited triggers to selectively form or break a covalent bonding interaction with an on demand control. Essentially all bimolecular addition reactions are thermoreversible, which to some extent is highlighted by the temperature dependence of the associated equilibrium constants.³¹ In most cases, however, the required temperature range wherein the reversible reaction starts to dominate greatly exceeds the practical temperature regime and often suffers from preliminary induced side reactions or even thermal decomposition processes.

In the following, a few commonly applied thermoreversible covalent chemistries will be discussed that allow for a time-controlled bonding and/or debonding in relatively low temperature regimes, i.e. < 200 °C (II.1.2.1). Next, a key example will be outlined in II.1.2.2 to demonstrate how a dynamic system can be modulated on a molecular level in order to adjust user's application demands. Moreover, the potential of the listed thermally triggered covalent chemistries to serve as a design strategy for thermally adaptable materials will be highlighted in II.1.2.3.

II.1.2.1 Thermoreversible covalent chemistries

Many covalent chemistries have been explored throughout the years whereby the retro-reaction can be triggered at reasonably mild temperatures (i.e. < 200 °C).³² Rather than providing a complete overview on thermally induced dynamic covalent chemistries,³³⁻³⁴ the current section will merely cover some examples that have found widespread use in the design of thermoresponsive polymer materials and are considered relevant to the current doctoral work.

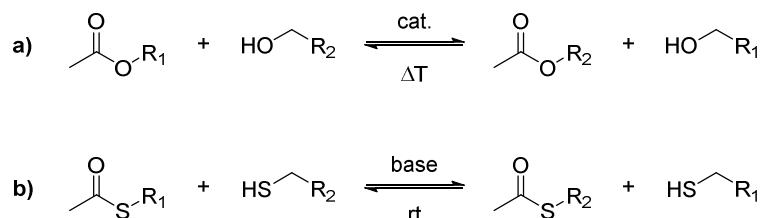
The Diels-Alder cycloaddition reaction is arguably one of the most frequently adopted thermoreversible covalent linkage that has been incorporated into a variety of polymer matrices. In particular, the furan-maleimide system found numerous applications since its introduction by Chen *et al.* to generate a remendable and self-healing, yet highly-crosslinked polymer material (Scheme II.1a).³⁵ Whereas crosslinking was initiated at 75 °C, the retro-Diels-Alder reaction was found to dominate upon treatment of the resulting material at temperatures above 120 °C. Hence, debonding of the initially formed crosslinks was triggered, introducing reshaping and healing behaviour into the material. Furthermore, by making use of bifunctional furan and maleimide moieties, a thermoreversible linear rather than crosslinked polymer was obtained that started to depolymerise above 100 °C, with a quantitative monomer regeneration above 140 °C.³⁶



Scheme II.1. Selection of thermoreversible Diels-Alder systems. a) Widely adopted furan-maleimide combination. b) Room-temperature dynamic fulvene-tricyanoethylene ester pair. c) Heteroatom-based cyclopentadiene-dithioester reaction partners (e.g. Z = -CN).

A highly interesting feature of the Diels-Alder/retro-Diels-Alder systems is the control over thermal reversibility that is readily achieved by the careful selection of the starting reagents.³² Hence, many alternative combinations have been explored that allow for the tunable dynamic behaviour to be triggered at considerably higher or lower temperatures.³⁷ In fact, based on the cycloaddition reaction of fulvenes with cyanoolefins (Scheme II.1b), Lehn and coworkers even developed so-called Diels-Alder dynamers, materials that can be healed already at room temperature when damage is inflicted.³⁸ A common strategy to allow for relatively low-temperature reversibility (approx. < 120 °C) can also be found in the use of heteroatom-containing building blocks. An elegant example forms the hetero-Diels-Alder reaction between cyclopentadiene and dithioester moieties (Scheme II.1c).³⁹⁻⁴⁰ The latter reagents can be readily incorporated into polymers via their corresponding commodity chain transfer agents used in controlled radical polymerisations. As a result, the cyclopentadiene/dithioester systems emerged as efficient tools in the design of adaptable complex macromolecular architectures,⁴¹⁻⁴³ self-healing materials,⁴³⁻⁴⁴ and on demand bonding/debonding adhesives.⁴⁵

Transesterification reactions (Scheme II.2a) are another type of covalent reversible chemistries that have been extensively studied in polymer science,⁴⁶ for example in the synthesis of linear polymers from cyclic ester building blocks.⁴⁷ These prototypical exchange reaction are readily incorporated into polymer materials through traditional crosslinking procedures such as epoxide curing to introduce reversible properties at elevated temperatures. A substantial drawback of transesterification-based thermoreversible reactions, however, is the need for a catalyst to achieve efficient dynamic covalent bonding/debonding within a reasonable time frame.⁴⁶ Nonetheless, Leibler and coworkers gave the required catalyst added value in the welding process of epoxy-acid and epoxy-anhydride thermosets.⁴⁸ Indeed, by simply changing the concentration of a metal catalyst, a defined control over welding kinetics and strength was established. An alternative approach that allows for dynamic covalent reactions to proceed at room temperature, is based on the thiol-thioester exchange (Scheme II.2b).⁴⁹ In particular the compatibility of this thiolate-mediated exchange with aqueous reaction media, has driven its application in the field of biochemistry,⁵⁰ including protein synthesis through native peptide ligation.⁵¹

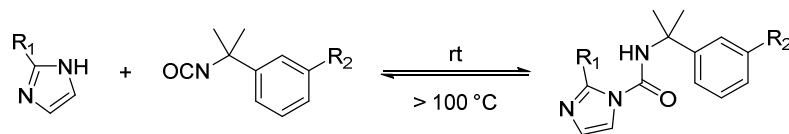


Scheme II.2. Examples of thermoreversible exchange reactions. a) Transesterification at elevated temperatures in the presence of a catalyst. b) Thiol-thioester exchange reaction through thiolate anions at room temperature.

Nucleophilic addition reactions can also provide well-suited thermoreversible systems, although a good leaving group is required to allow for the retro-reaction to occur within a practical temperature regime. The additions of alcohols and amines to aliphatic isocyanates, for instance, do possess a dynamic nature but dissociation often only occurs above 250 °C,⁵² which is rather inadequate in many polymer applications. Therefore, isocyanate-based addition reactions are typically used for irreversible polymer formation and crosslinking. For example, the combination of bifunctional isocyanates and alcohols swiftly results in the formation of linear polyurethanes that exhibit high mechanical strength, elasticity and abrasion resistance.⁵³ Their crosslinked analogues starting from multifunctional isocyanates are also found in a wide array of industrial bulk applications, including packaging and insulation as well as adhesive and coating technologies.⁵³

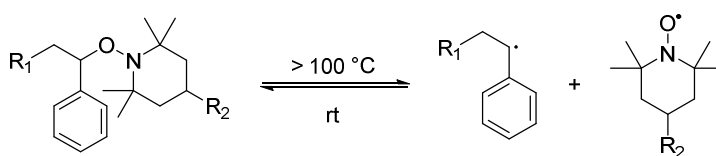
Regardless of the irreversible nature of isocyanate adducts at user-friendly temperatures, perturbations on the small molecule level can greatly influence the temperature window at which dissociation takes place. Indeed, the thermoreversible addition of imidazoles to isocyanates was successfully incorporated in vinyl polymers whereby the formed urea crosslinks can undergo dissociation when heated above 100 °C (Scheme II.3), thereby resulting in the transition of a gel

into a liquid-like state.⁵⁴ In the following section, this molecular engineering of the dynamic behaviour will be discussed into more detail in the context of blocked isocyanates.



Scheme II.3. Isocyanate addition of imidazoles readily gives the corresponding urea at room temperature, which is prone to dissociation upon heating.

A final example of thermoreversible covalent systems relates to the homolytic cleavage of alkoxyamines, which has been exploited in controlled nitroxide-mediated reversible-deactivation radical polymerisation.⁵⁵ Homolytic bond cleavage of the C-O bond in alkoxyamines occurs above 100 °C and results in the concomitant formation of both a stable, non-propagating, radical and a more reactive one (Scheme II.4). The latter radical, however, typically suffers from irreversible termination reactions and thereby prevents the initial covalent bond to be quantitatively reformed. Despite being considerably less applicable in materials that require multiple cycles of reversibility,^{31, 56} alkoxyamines do provide a temperature controlled on demand debonding of polymer systems.⁵⁷



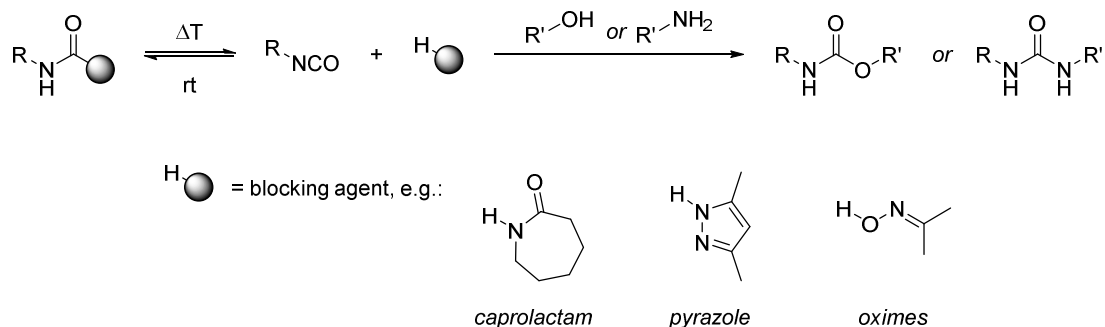
Scheme II.4. Homolytic cleavage of the covalent N-O bond in alkoxyamines upon heating with the generation of two radical species.

II.1.2.2 Temperature controlled curing through blocked isocyanates

An important aspect of thermally reversible covalent bonds is their molecular engineering that allows for the dynamic behaviour to be finetuned. A prototypical example of how modulated thermoreversible systems can be used to an advantage is presented in isocyanate based chemistry. The high reactivity of isocyanate reagents typically comes at the cost of a limited shelf life and difficult handling, originating from its facile hydrolysis and toxicity. Nonetheless, isocyanate-based addition reactions form one of the most basic and industrially relevant covalent ligation platforms, particularly in the tailor-made synthesis of polymers and crosslinked materials.⁵⁸

In response to the issues associated with isocyanates, Wicks expressed the need to provide an on demand and temporal control over their reactivity.⁵⁹ Hence, the strategy of ‘blocked’ or ‘masked’ isocyanates was developed whereby the reactive and moisture sensitive isocyanate functionality can readily be protected upon reaction with a suitable blocking agent. Most prevalent blocking agents are oximes,⁶⁰⁻⁶¹ caprolactams⁶¹⁻⁶² and pyrazoles,⁶³ which give bench stable adducts at room temperature (see Scheme II.5). Heating of the blocked chemical in the presence of a coreactant, such as an alcohol or amine, results in the thermal deprotection or deblocking.⁶⁴ The thus *in situ* activated isocyanate subsequently reacts with the coreactant,

allowing for a temporally triggered addition reaction to occur. This temporal control over the fast isocyanate reaction kinetics has found widespread interest in an industrial context. Indeed, besides a greatly prolonged shelf life and safer handling, blocked isocyanates resulted in the use of bench-stable and waterborne one-pot crosslinking formulations wherein curing is only initiated on demand upon heating.⁶⁵



Scheme II.5. Blocked isocyanate strategy, whereby suitable blocking agents readily react with isocyanates to give bench stable adducts. Heating of the blocked compound results in the *in situ* release of the isocyanate moiety, making it available to react with alcohols or amines in a temporally controlled manner.

Interestingly, the temperatures needed to induce the isocyanate deblocking reaction can be readily tuned via alterations on the molecular level, which most often relies on the structure of the blocking agent. Additionally, the nature of the isocyanate itself also has a pronounced effect on the dynamic behaviour of the blocked adduct, with aromatic derivatives being susceptible to lower temperatures of deblocking than their aliphatic counterparts.⁶⁶ Given the broad chemical diversity in blocking agents and isocyanates, a range of tunable temperatures of deblocking are accessible and can hence be judiciously selected in view of the envisioned application.

II.1.2.3 Covalent adaptable networks and vitrimers

Another attractive application of thermoreversible covalent bonds embedded into a polymer matrix is the design of covalent adaptable networks (CANs).³¹ The dynamic crosslinks that are distributed throughout CANs give rise to materials that exhibit a unique combination of both plastic and thermosetting properties.⁶⁷ Although the network is fixed at service conditions, efficient and reliable covalent bond exchange reactions can be triggered by an external stimulus, such as temperature, to provide macroscopic flow to the material without introducing structural damage or a permanent loss in final properties.⁶⁸ The unique transition of CANs from a viscoelastic solid into a viscoelastic liquid has been vastly implemented in a variety of stimuli responsive applications, including self-healing,⁶⁹ reduced shrinkage stress⁷⁰⁻⁷¹ and nanoimprinting.⁷²

Whereas in theory any thermoreversible reaction can be introduced into the strategic design of CANs, favourable reaction kinetics are required so that bond rearrangement occurs on appropriate time scales to allow for the network to adapt to the applied stimulus.³¹ Moreover, the formation of side products at elevated temperatures should be avoided. Nonetheless, many

of the reported thermoreversible covalent chemistries were shown to proceed at practical rates in a chemoselective manner without the need for a catalyst and have thus been introduced into CANs.³¹

Similar to the blocked isocyanate concept (*cf.* II.1.2.2), the applied covalent dynamic bond exchange can proceed via two different mechanisms.⁷³ A first mechanism is based on a dissociative process whereby chemical linkages are first broken before they are reformed, commonly referred to as reversible addition (Figure II.1a). A second pathway to introduce the net replacement of covalent bonds proceeds via an associative exchange mechanism, in which the original crosslinks are only broken once another connection is made first (Figure II.1b).

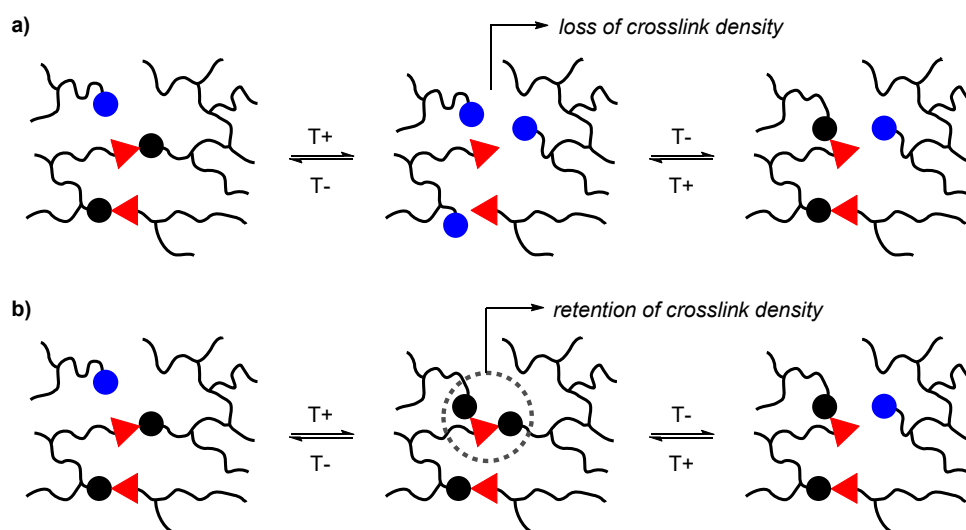


Figure II.1. Two types of covalent adaptable networks (CANs). a) Dissociative CANs based on a fragmentation-addition bond shuffling, leading to a loss of the crosslinking density and hence network integrity. b) Associative CANs through an addition-fragmentation covalent bond exchange, with retention of the crosslinking density. Reproduced from Ref.⁷³ with permission from the Royal Society of Chemistry.

Although the overall outcome of reshuffled covalent bonds is the same, the network will behave very differently when the exchange reactions are triggered. Indeed, if a dissociative CAN is subjected to an appropriate trigger, e.g. heat, the chemical equilibrium of the covalent bonds will be shifted to the open form (*i.e.* to the side of the reagents), resulting in the net dissociation of crosslinking points (Figure II.1a). Hence, the thermoset is transformed into a thermoplast with liquid-like behaviour that allows for reprocessing, reshaping and recycling of the polymer material.³⁵ Once heating or irradiation is discontinued, the initial crosslinks are reformed and the thermoset material properties, including stiffness and solvent resistance, are reinstated. Commonly adopted chemistries for the construction of dissociative CANs are found in reversible Diels-Alder cycloadditions, archetypical of furan with maleimides.

In contrast to dissociative CANs, the crosslink density in their associative counterparts remains constant and therefore the integrity of the material is maintained at all times when the dynamic bond reshuffling is triggered (Figure II.1b). In other words, the material exists as a permanent

network, yet enables interesting flow and stress-relaxation properties under certain conditions. Chemistries that are applicable to this type of CANs are found in reversible addition-fragmentation reactions such as transesterifications.⁷⁴

In 2011, Leibler and coworkers reported on a superior class of associative CANs based on transesterification reactions upon addition of an appropriate catalyst to a polyester-based network with an excess of pending hydroxyl groups.⁷⁴ By heating the resulting composition above 200 °C, the transesterification exchange reaction with alcohols could thus be triggered, which resulted in a gradually decreasing viscosity while the network remained permanently connected instead of a sudden drop as observed in thermoplasts. As the observed viscosity profile showed distinct similarities to that of vitreous silica (i.e. glass), the term vitrimers was coined for materials that exhibit this exceptional behaviour. Following the pioneering system of Leibler, vitrimers emerged as a new class of polymer networks and numerous types of associative thermally exchangeable chemistries are under continuous investigation.⁷³ Amongst others, our own research group (Ghent University) also actively investigates vitrimer materials with an emphasis on the introduction of new types of covalent exchange reactions (e.g. based on vinylogous urethanes⁷⁵⁻⁷⁶ and trialkylsulfonium salts⁷⁷) and the future development thereof.⁷⁸⁻⁷⁹

II.1.3 Photochemically triggered bonding and debonding

Next to the above alluded thermally triggered reactions, the use of light as an external stimulus also provides a powerful paradigm in polymer science.⁸⁰ Indeed, the ability to control a material's formation, structure and mechanical properties simply by switching a modular light source on-and-off remains one of the most fascinating tools a chemist holds, both in fundamental research as well as in a vast array of industrial applications.

Light in general is regarded as a much more defined trigger compared to temperature as it allows for chemical transformations to be initiated much faster and at ambient temperature. Furthermore, photochemically induced processes can be performed with the additional feature of spatial control, thereby enabling more demanding applications, including site-selective surface lithography and three dimensional structure fabrication.

The following sections will address the use of light-induced reactivity from a polymer synthesis perspective. First, some of the basic fundamentals of photochemistry are presented in II.1.3.1, followed by a comprehensive overview of some photochemical bonding, debonding as well as photoreversible reactions that have been successfully introduced into material sciences (II.1.3.2). While light as a trigger is typically recognised for its spatio-temporal control, their potential to serve as a gate to enhance or reduce chemical reactivity is rather unexplored. The next section (II.1.3.3) is therefore devoted to molecular photoswitches that introduce a switchable reactivity between distinct pathways. Finally, two specific spatially resolved applications that have been used in the current doctoral work, i.e. direct laser writing and sub-diffraction lithography, are discussed in II.1.3.4.

II.1.3.1 Basic concepts of photochemistry

The typical photochemical processes that take place during the interaction of molecules with light can be summarised by a Jablonski diagram. Such a diagram represents the relative energies of the ground state as well as singlet and triplet excited states of a molecule in a simplified manner, whereby a photochemical process can be schematically illustrated by connecting the relevant transitions that are involved. In the current section, some photophysical processes are discussed based on the Jablonski diagram depicted in Figure II.2.

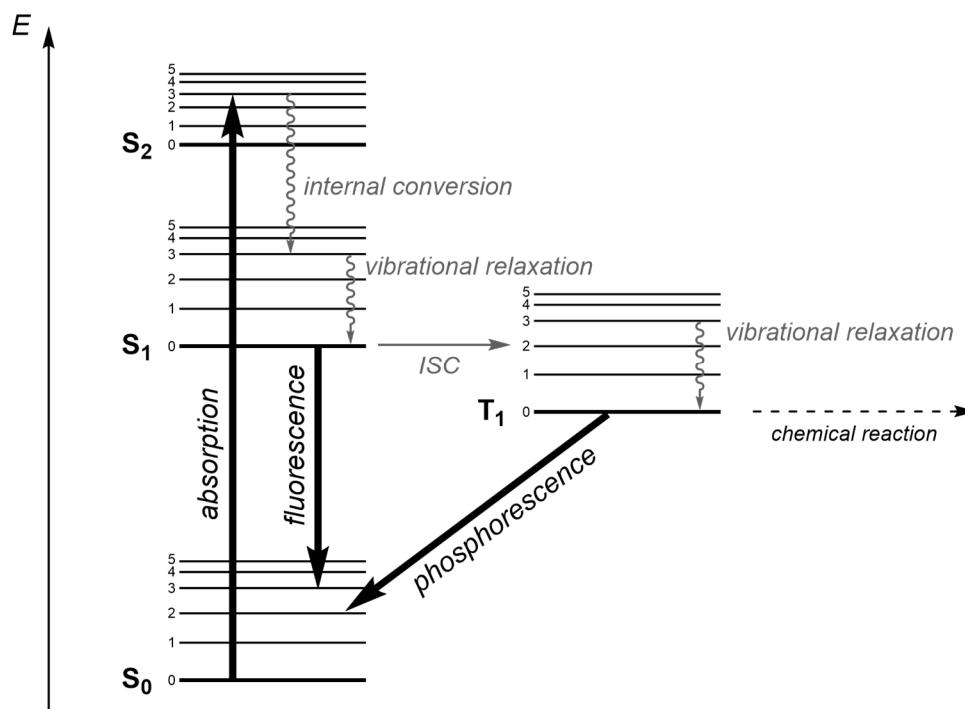


Figure II.2. Jablonski diagram. Simplified representation of the relative energies of ground electronic singlet state S₀, singlet excited states S₁ and S₂ as well as first triplet excited state T₁ along with their vibrational states. The possible photochemical processes are schematically represented with straight arrows (black) for radiative transitions and wavy arrows (grey) for non-radiative energy dissipation, with the exception of intersystem crossing (ISC) displayed by a horizontal arrow (grey) which is a non-radiative process without energy dissipation.

Absorption

Every photochemical process starts with the absorption of photons which promotes a molecule from its singlet ground state S₀ into an excited singlet state S_{1,2,3,...}, a process that typically occurs on a time scale of 10⁻¹⁵ seconds. Excitation beyond the first excited state S₁ is possible, yet highly unlikely and higher excited states are therefore considerably less populated and can often be neglected. The energy difference between two electronic states that needs to be overcome during the excitation typically corresponds to the energy of visible light and UV photons (with E_{photon} = $h c \lambda^{-1}$, with the Planck constant h and speed of light c).

As the distribution of the electrons around the nuclei changes upon light absorption, excited molecules generally show a different chemical reactivity compared to their counterparts that reside in their electronic ground state. Beer-Lambert's law quantitatively describes the absorption

of photons by molecules at a given wavelength, referred to as the molar extinction coefficient ϵ , as a function of its concentration and the path length of the incident light (Equation II.1).

$$A = -\log \frac{I}{I_0} = \epsilon lc$$

Equation II.1. Beer-Lambert law describing the absorption A as the transmitted light intensity I with respect to the incident light intensity I_0 , which is proportional to the molar extinction coefficient ϵ , concentration c and the path length l of the absorbed light.

Each electronic state consists out of different vibrational levels, which can be presented by means of a potential energy diagram (Figure II.3). Importantly, the intensity of vibrational transitions allow to explain the molecular absorption spectrum based on the Frank-Condon principle. This principle states that the nuclear configuration of the initial excited state, formed immediately after absorption, is the same as the ground state. In other words, nuclear motion can be neglected as a result of the sufficiently fast arising excitation between two electronic levels. Thus, electronic transitions are considered to take place at fixed nuclear coordinates, i.e. in a vertical manner as shown in Figure II.3, thereby resulting in a higher vibrational level being occupied.

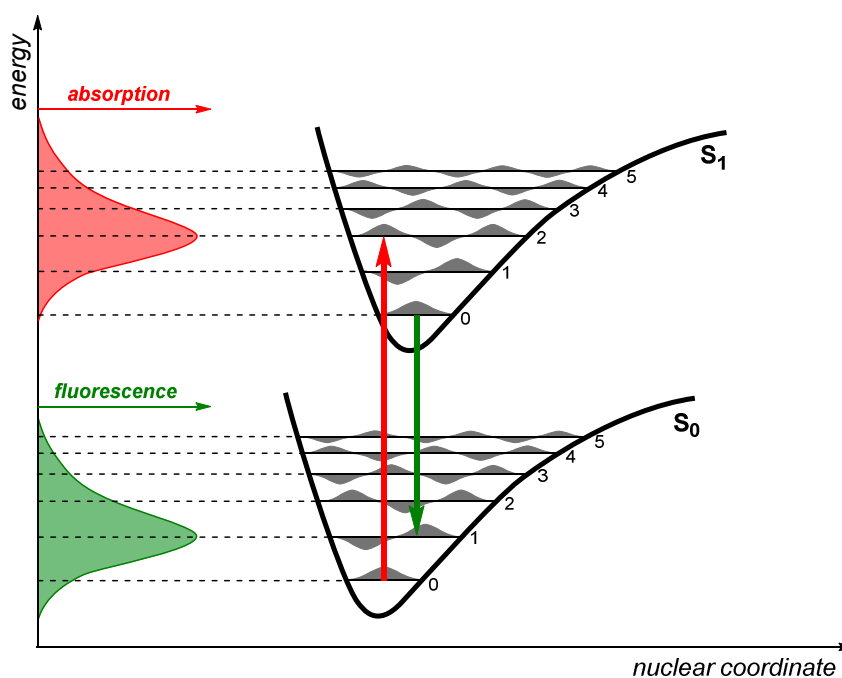


Figure II.3. Energy diagram demonstrating the Frank-Condon principle. The vertical transition from the singlet ground state S_0 to the first excited state S_1 is governed by the overlap integral of the vibrational wave functions (red arrow). The maximal overlap integral is associated with the highest probability to occupy a certain vibrational level and hence results in the highest absorption intensity (red, left). In a similar manner, the intensity of fluorescence can be rationalised (depicted in green). Figure adapted from Ref.⁸¹ with permission from IOP, published under the Creative Commons License (CC-BY-3.0).

The intensities that are associated with each transition are defined by the overlap integral of the corresponding wave functions and can be correlated to the experimentally observed absorption spectrum. The maximal overlap integral of the vibrational wave functions translates

to the highest observed absorption intensity (Figure II.3, red). Although excitation initially comes with a retention of the nuclear coordinates, promoting an electron into an antibonding orbital in a higher excited state eventually leads to an elongation of the equilibrium bond and thus in a displacement of the nuclear configuration of the excited state. In a similar manner, the Frank-Condon principle also enables to understand fluorescence spectra by taking into account the shifted potential energy diagram of S_1 compared to S_0 (Figure II.3, green).

Vibrational relaxation

Vibrational relaxation is the very fast (i.e. 10^{-14} to 10^{-11} s)⁸² dissipation of the gained photon energy by relaxing from a higher vibrational level to a lower one within the same electronic state, usually the vibrational ground state. Given the fast time scale, the relaxation process is likely to occur immediately after the absorption event.

Internal conversion

Internal conversion is a similar process to vibrational relaxation but occurs between two vibrational levels of a different electronic state. This non-radiative transition thus takes place from an excited electronic state to a lower one and offers a fast pathway for deactivation (i.e. 10^{-14} to 10^{-11} s).⁸²

Fluorescence

An alternative manner to respond to the given energy upon photon absorption is by emitting a photon so to reach an energetically lower electronic state. This process, termed fluorescence, is rather slow (with a half life of 10^{-8} - 10^{-9} s)⁸² and can only compete with non-radiative energy dissipation when it occurs from the first electronically excited state S_1 to the ground state S_0 . At higher electronic states, energy is predominantly lost through internal conversion and vibrational relaxation, which are significantly much faster processes. The resulting fluorescent photons are always less energetic than the incident absorbed photons because of energy loss that arises during non-radiative processes. Hence, fluorescence is observed at longer wavelengths compared the molecular absorption.

Intersystem crossing (ISC)

Intersystem crossing is marked by a change of spin multiplicity, whereby a molecule in an excited singlet state is transferred into an excited triplet state to give two unpaired electrons of the same spin. It is a relatively slow process (i.e. up to 10^{-8} s) as it entails a spin forbidden transition and is therefore unlikely to occur. The probability of the transition increases, however, when the vibrational levels of the involved excited electronic states overlap.

Phosphorescence

Once intersystem crossing into a triplet excited state is achieved, a direct transition back to S_0 is offered by phosphorescence. This is again a slow spin forbidden transition with a corresponding lifetime of 10^{-3} seconds up to 1 second and longer.⁸² As a result of this slow photon emission, competitive chemical reactions from the triplet state become feasible.

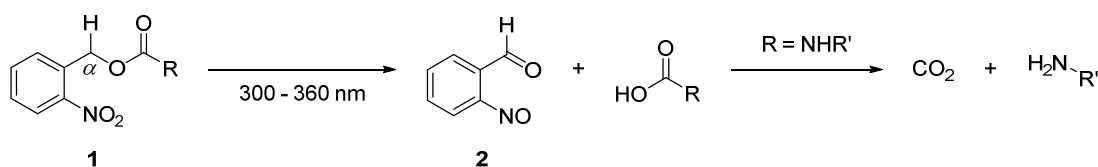
II.1.3.2 Photo-induced cleavage and conjugation reactions

A plethora of photochemically triggered covalent bonding and debonding reactions have been established over the years. Although a detailed discussion exceeds the scope of the current doctoral work, some widely adopted photo-induced reactions are listed in the current section to make the reader acquainted with some prominent examples of how light serves as a highly enabling tool to cleave and/or form bonds on demand.⁸³

Photocleavage

Many light-triggered degradation reactions have been developed in recent decades that enable the site selective cleavage of covalent bonds upon irradiation. Initially driven by their use as protecting groups in (bio)organic synthesis,⁸⁴ photocleavage reactions – mainly based on *o*-nitrobenzyl,⁸⁵⁻⁸⁷ 3',5'-dimethoxybenzoin⁸⁵⁻⁸⁶ and/or coumarin derivatives⁸⁶⁻⁸⁷ – rapidly received a growing interest in polymer science as they allow for the external and on demand manipulation of material properties.⁸⁸⁻⁸⁹ The polymer community thus highly benefited from the plethora of photocleavable units that were introduced in, for instance, the uncaging of bioactive molecules⁹⁰⁻⁹¹ or the controlled release of therapeutics.⁹²

One of the most extensively investigated photocleavable scaffolds comprises *o*-nitrobenzyl derivatives (**1**, Scheme II.6).⁹³ Barltrop *et al.* first reported on this photosensitive group in 1966 for the UV-triggered release of carboxylic acids and amines.⁹⁴ A few years later, *o*-nitrobenzyls were introduced as a protecting group in amino acids that can be quantitatively removed by means of a UV-induced tautomerisation to the corresponding nitrosobenzaldehyde (**2**, Scheme II.6).⁹⁵ However, the formation of the nitrosobenzaldehyde as a byproduct of the cleavage reaction has been of particular concern as it readily competes with the substrate for the incident light. Hence, low yields as well as secondary photoproducts were obtained. A dramatic improvement was found in the use of α -substituted derivatives, which give less reactive aromatic ketone byproducts after photoremoval of the protecting group. An interesting evolution of *o*-nitrobenzyl moieties is their exploitation as photoacid⁹⁶ and photobase⁹⁷ generators, which found widespread use in photodirected synthesis and material sciences.⁹⁸ For example, Bowman and coworkers reported on a responsive material that can be changed from a solid to a fluid state at room temperature upon exposure to light to generate an acid or base catalyst.⁹⁹ Among other applications, photocleavable *o*-nitrobenzyl bonds have predominantly been employed in photolithography,¹⁰⁰ UV-degradable networks¹⁰¹ and photocleavable linkers in bioconjugates¹⁰² and solid supports.¹⁰³

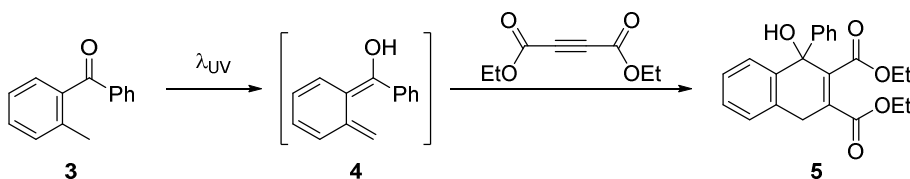


Scheme II.6. Photocleavage of *o*-nitrobenzyl derivatives **1** into nitrosobenzaldehyde **2** upon UV-irradiation, which serves as a photoprotecting group strategy for carboxylic acids and amines.

A highly attractive feature of light as a trigger is the potential to remove different protecting groups in a highly selective and orthogonal manner, simply by using light of a different wavelength. In 2001, Bochet introduced this revolutionary concept of wavelength-orthogonal – also referred to as λ -orthogonal – uncaging after the observed chemoselective cleavage of two differently protected carboxylic acids.^{85, 104} Following this seminal work, many alternative wavelength-orthogonal photoprotecting groups have been developed that allow for the externally controlled sequential activation of molecules,^{87, 105-106} for example on surfaces.^{86, 107} Moreover, several guidelines for their design of orthogonal photochemically cleavable systems have been postulated.⁹³ A notable development is the rational substitution of the chromophores to shift the corresponding absorption spectra away from that of its pristine derivative, so to allow orthogonality within the same molecular family. Especially the design of photoprotecting groups that can be cleaved on demand with light in the visible range the spectrum is a highly emerging field,¹⁰⁸⁻¹¹⁰ particularly in biologically oriented applications as a result of increased penetration depths.¹¹¹

Photoconjugation

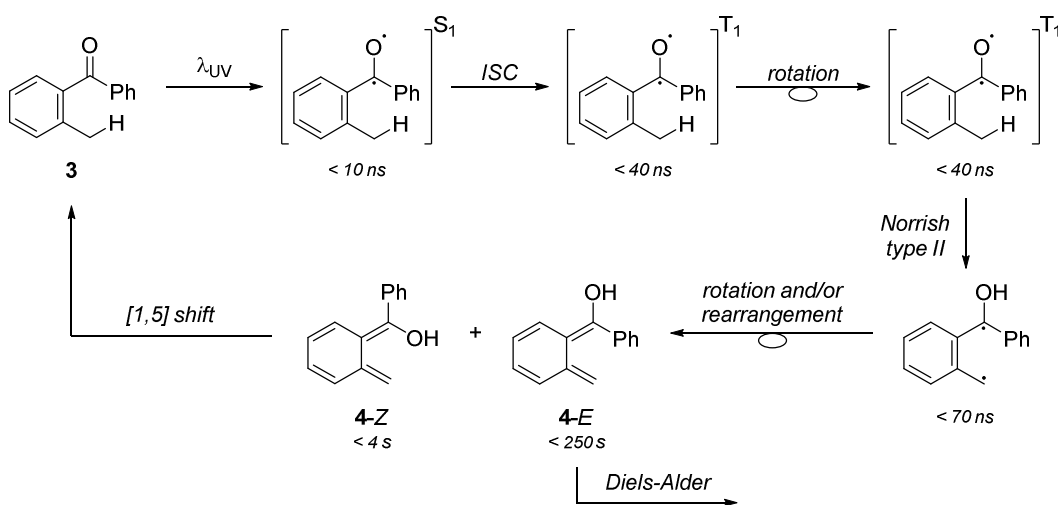
Next to covalent bond cleavage reactions, light also serves as a powerful tool in modular conjugation reactions. To date, the tool box of photo-induced transformations that are applicable to both small molecule synthesis as well as spatially resolved biochemistry and adaptive polymer design continues to expand,¹¹² in part due to efforts in our own research group (Karlsruhe Institute of Technology).¹¹³ One of the workhorses in our own laboratories is the UV-induced formation of *o*-quinodimethanes (**4**, Scheme II.7) which are highly susceptible substrates in Diels-Alder cycloaddition reactions. Yang and Rivas were the first to describe the generation of *o*-quinodimethane transients **4** from *o*-methylbenzophenone **3** in the 1960s, which was confirmed by trapping the photocaged diene with dimethyl acetylenedicarboxylate into the high-yielding cycloadduct **5** (Scheme II.7).¹¹⁴ Repeating studies later verified the true Diels-Alder nature of the formed adduct through the stereospecific addition of maleic and fumaric acid to **4**.¹¹⁵



Scheme II.7. Seminal report by Yang and Rivas¹¹⁴ on the formation of *o*-quinodimethane **4** upon UV-irradiation of *o*-methylbenzophenone **3**. The formation of the transient diene was confirmed by the formation of a Diels-Alder cycloadduct **5**.

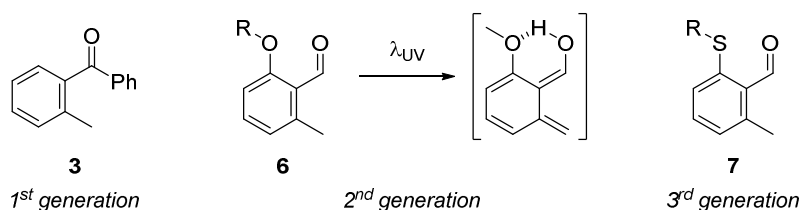
The underlying mechanism of the *o*-quinodimethane species, often referred to as photoenols, was only elucidated several years later when flash photolysis experiments allowed for the detection of the transient intermediates and their lifetimes (refer to Scheme II.8).¹¹⁶⁻¹¹⁷ The first step in the photoenolisation process was identified as the excitation of the carbonyl group to the excited singlet state via an $n \rightarrow \pi^*$ transition and its subsequent intersystem crossing to the triplet

state. Following rotation around the aryl-carbon radical in the triplet state, a hydrogen abstraction occurs from the benzylic position via a Norrish type II pathway with the formation of a biradical intermediate (Scheme II.8). Rearrangement of the formed intermediate eventually results in two isomeric enol moieties, i.e. 4-*E* and 4-*Z*, that have a considerably different lifetime. Whereas the *Z* isomer has a very short lifetime and readily converts back to the initial starting reagent **3** via a [1,5] sigmatropic rearrangement, the lifetime of the *E* isomer is sufficiently long to undergo a thermal Diels-Alder follow-up reaction. An extremely elegant exploitation of the different reactivity of the formed *E/Z*-photoenol isomers was found in sub-diffraction laser lithography (*vide infra*).¹¹⁸



Scheme II.8. Mechanism of *o*-quinodimethane **4** formation upon UV-irradiation of *o*-methylbenzophenone **3**, postulated based on flash photolysis experiment. Lifetimes, obtained in cyclohexane, are displayed under the corresponding transient intermediates.¹¹⁶⁻¹¹⁷

Inspired by the photoenolisation and the click-like characteristics of the sequential Diels-Alder cycloaddition,¹¹⁹ the *o*-methylbenzophenones/maleimide system was successfully employed in the efficient and equimolar coupling of macromolecules.¹²⁰ Moreover, a second generation photoenol precursor was introduced based on 2-methoxy-6-benzaldehydes (**6**, Scheme II.9). As a result of an internal hydrogen-bond stabilisation, both the amount and the lifetime of the enol *E*-isomer was enhanced, thereby increasing its Diels-Alder reactivity. Indeed, this second generation of photoenols also swiftly reacted with modular acrylates, thereby greatly expanding the product scope of the photo-click reaction and introducing orthogonal multiblock copolymer formation¹²¹⁻¹²² as well as efficient surface functionalisation.¹²³⁻¹²⁴ Very recently, our team replaced the ether by a thioether aryl substituent, leading to an advanced generation of photoenol precursors (**7**, Scheme II.9), whereby the activation wavelength for the diene intermediate could be shifted into the visible range of the spectrum (i.e. up to 430 nm).¹²⁵



Scheme II.9. Generations of photoenol precursors, applicable in the UV-triggered or visible light-induced Diels-Alder cycloaddition reaction.

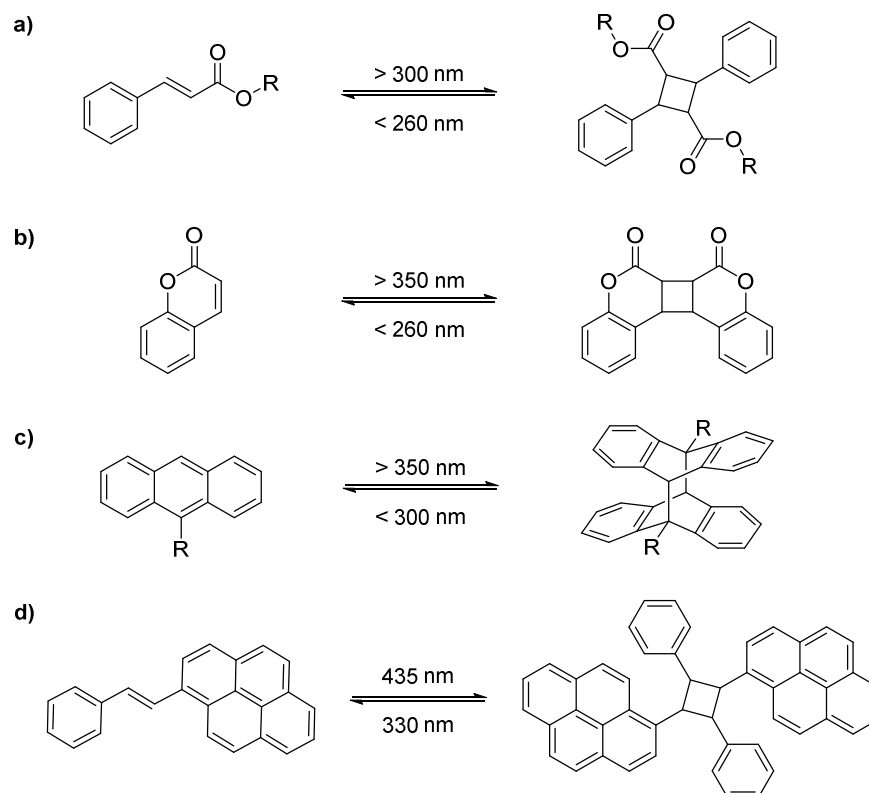
Since the non-reactive 4-*Z* isomer formed during the photoenolisation reverts back to the initial starting reagent, the overall process can in principle be reinitiated (*cf.* Scheme II.8). This is, however, only if a suitably activated dienophile is continuously provided to conduct the final Diels-Alder step.¹²⁶ Indeed, irradiation of the second photoenol precursor **6** in the absence of such a suitable reaction partner leads to a mixture of dimers being formed. By deliberately accessing this dimerisation pathway, photocuring of an *o*-methylbenzaldehyde containing polymer was made possible without the need for additional crosslinking agents.¹²⁷ It should be noted that this photoenol dimerisation is expected to be considerably less pronounced during the UV-induced reactions with *o*-methylbenzophenone **3**, as they are reported to be much more stable towards photodegradation.¹¹⁶⁻¹¹⁷

To date, a vast majority of the established photo-triggered conjugation reactions are conducted under UV-light. Contemporary synthetic photochemistry is therefore challenged by the quest for equally efficient covalent bond forming reactions, yet under much more benign conditions of irradiation.¹²⁸ Visible light-induced conjugation reactions therefore remain under continuous investigation.¹²⁹⁻¹³² A well-embedded strategy to pursue visible light transformations can be found in altering the electronic environment of existing chromophores with electron donating substituents to shift the absorption to longer wavelengths. A prototypical example of substituents that cause such a bathochromic effect are found in pyrenes, which can readily increase the absorption wavelength by over 100 nm.^{129-130, 133} Since these visible light triggered covalent bonding processes have not been employed in the current doctoral work, the interested reader is directed to state-of-the-art review literature that covers this emerging field in photochemistry.¹³⁴

Photoreversible transformations

The majority of light-induced processes trigger irreversible photoproduct formation. The ability to combine photocleavage and -conjugation reactions proved highly interesting as it would introduce a dynamic switch between reactants and reagent, yet truly photoreversible chemistries are rather unique. Ideally, the overall process should be wavelength-selective whereby different colours of light can be employed to trigger the forward, or the backward photoreaction.¹³⁵ Two types of transformations have been actively researched in order to develop ideal photoreversible systems. In the current section, photoreversible cycloaddition reactions will be discussed as they allow for the covalent bonding and debonding between two different molecular entities. The second type, based on photoswitches, typically comprises intramolecular isomerisation reactions

whereby the bimolecular follow-up reaction, i.e. the covalent bond forming step, is a thermal process and can intrinsically not be activated by light.¹³⁶ Nonetheless, these photo-switches have enormous potential to introduce a gated reaction selectivity between light-induced and thermal reaction pathways and will be discussed in section II.1.3.3.

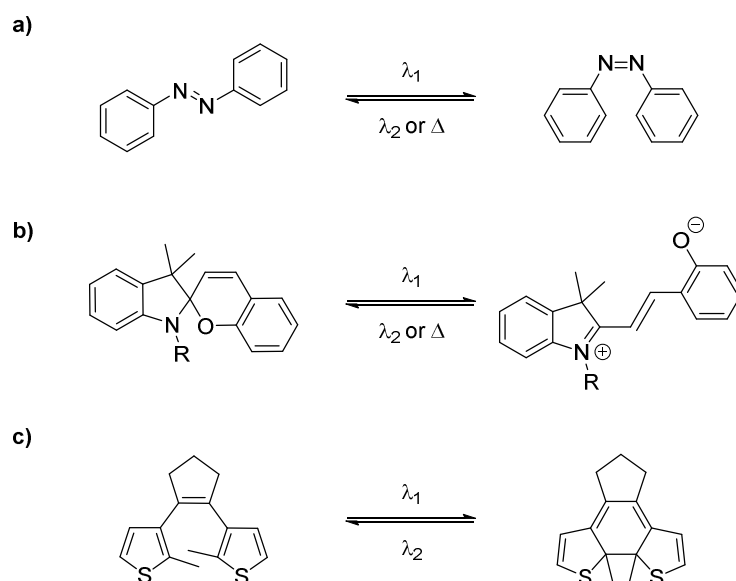


Scheme II.10. Selected photoreversible cycloaddition reactions. a) [2+2] cycloaddition of cinnamates, b) coumarin dimerisation, c) [4+4] dimerisation of anthracenes, and d) [2+2]-cycloaddition of styrylpyrene moieties. Only one potential isomer is depicted for each listed reaction.

Photo-cycloaddition reactions, are by far the most interesting type of transformations to introduce wavelength-orthogonal bonding and debonding of a single reaction system.¹³⁷⁻¹³⁹ Amongst the most widely adopted reversible photosystems, particularly in polymer chemistry, are the [2+2] dimerisation of cinnamates and coumarins as well as the [4+4] cycloaddition of anthracenes (Scheme II.10a-c).¹⁴⁰⁻¹⁴¹ Given these systems are extensively studied throughout the years, many applications have exploited photodimerisation reactions, for example in reversible surface patterning,¹⁴² photoresists¹⁴³ and self-healing materials.^{140, 144-145} The defining challenge, however, is to replace the necessity of harsh UV-light to affect both the forward and backward cycloaddition reaction, by more benign visible light-induced strategies. Recently, the [2+2] cycloaddition of styrylpyrene (Scheme II.10d) regained attention in this context since the forward reaction can be triggered with visible light irradiation ($\lambda = 435$ nm) whilst the cycloreversion can be affected in the UV-range (330 nm).¹⁴⁶ Nonetheless, visible light is usually too low energetic to enable covalent bond breaking reactions⁸⁰ and the challenge to enable cycloreversions at wavelengths above 400 nm by rational molecular design remains to be tackled.¹⁴⁷

II.1.3.3 Photo-switchable reactivity

Photoswitches hold great potential to serve as a gate to switch between photochemical and thermal reaction channels as a result of a reversible change in the geometry, polarity or charge distribution of the chromophore when subjected to light.¹⁴⁸ Most common photoswitches, depicted in Scheme II.11, are based on azobenzene, spiropyran or diarylethene moieties and operate through a photo-induced *cis-trans* isomerisation or intramolecular ring-closure. Many of these photoswitches are accessible in the visible range of the spectrum, either via direct or indirect excitation, and made a considerable impact to tune the behaviour and properties of materials.¹⁴⁹ Especially the exploitation of photoswitches in molecular devices that are fuelled by light is highly recognised, not in the least by the 2016 Nobel prize in chemistry.¹⁵⁰⁻¹⁵¹



Scheme II.11. Selected examples of molecular photoswitches. a) light-induced *cis-trans* isomerisation of azobenzene, b) ring-opening of spiropyran moieties upon irradiation with the formation of a dipole, and c) light triggered electrocycloisomerisation of diarylethenes.

The working principle of a photoswitch relies on the photodynamic equilibration of the two generated isomers upon photoexcitation, which is next exemplified for the *cis-trans* isomerisation of azobenzenes (*cf.* Scheme II.11a).¹⁵⁰ If the chemical system is not irradiated, only the ground state of the thermodynamic more stable *trans* configuration is occupied (Figure II.4a). At a given temperature, such as room temperature, the activation barrier to populate the *cis*-configuration of the azobenzene is too high to be overcome. Upon irradiation, however, the *trans*-azobenzene molecules can be transferred into an excited state, thereby passing a higher energy surface potential, and can subsequently relax into the metastable *cis*-analogues (Figure II.4b-c). Eventually, the *cis*-isomers return to the more thermodynamically favoured *trans*-azobenzene, either thermally or via a second photoexcitation process (typically with a longer wavelength as a higher energy state is reached, Figure II.4d). Generally, a wavelength-selective excitation of only one isomer is not perfectly feasible and hence the photochemical system is continuously subjected to both forward (*trans* \rightarrow *cis*) and backward events (*cis* \rightarrow *trans*) in a dynamic

equilibration. Eventually, a photostationary state is obtained that reflects the equilibrium ratio of the formed isomers in the given photoswitch upon irradiation. Importantly, when the formed metastable isomer has a non-negligible thermal lifetime, the photochemical system can potentially be near-quantitatively pushed out-of-equilibrium as long as photons are continuously supplied to system.

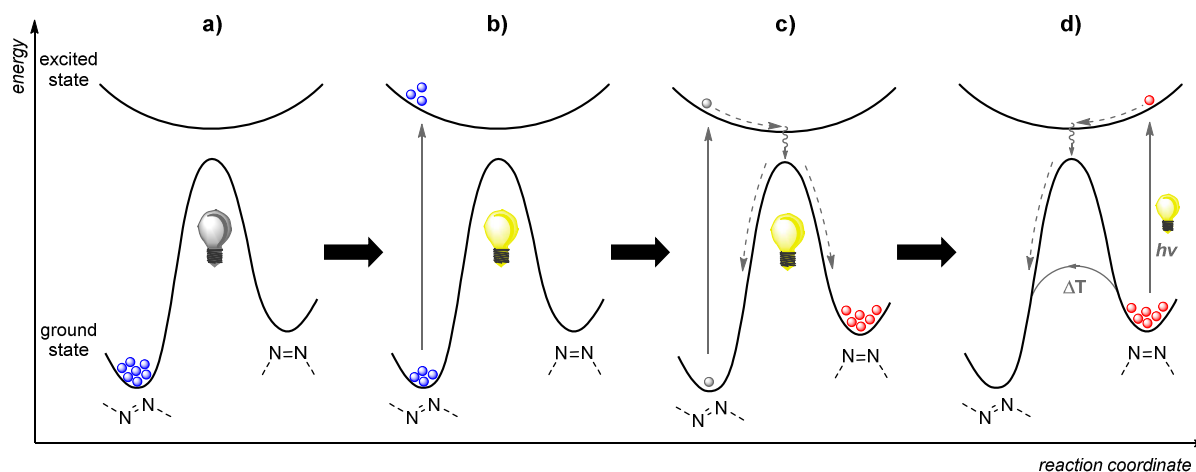
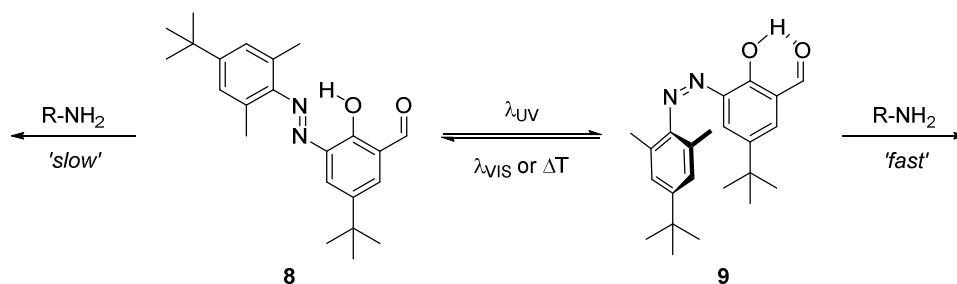


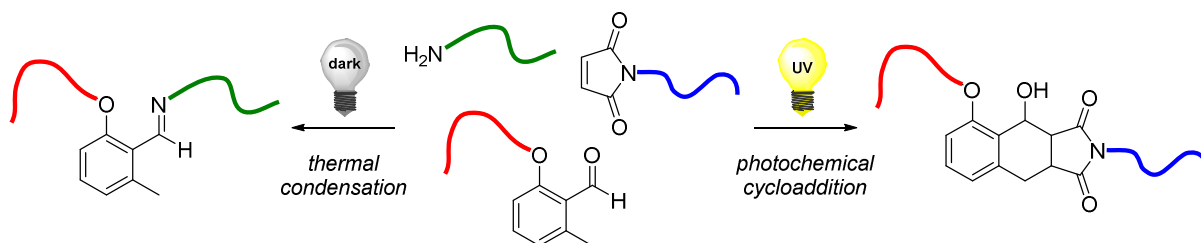
Figure II.4. Working principle of molecular photoswitches, illustrated for the *cis/trans* photoisomerisation of azobenzenes. a) Under ambient temperature conditions, only the thermodynamically most stable *trans*-state is populated and the activation barrier is too high to be overcome. b) Irradiation, however, readily transforms the *trans*-isomers into an excited state. c) The excited *trans*-azobenzenes subsequently relax back to their initial configuration or transform into the *cis*-analogue, thereby resulting in an enriched population of the meta-stable *cis*-state. d) Eventually, the *cis*-isomer state is depopulated, either thermally or via a second photoexcitation process. Adapted from Ref.¹⁵⁰ with permission from the Royal Society of Chemistry.

An interesting application of photoswitches is their use as a gate to switch between light-induced and thermal reaction pathways so to manipulate the output of a one-pot reaction system.¹⁵²⁻¹⁵⁵ Hecht and coworkers designed several of these switchable reactivity systems and incorporated them into dynamic covalently crosslinked networks so to provide an on/off switch over thermal healing abilities.^{153, 156-157} A fascinating example of a light-switchable system was provided based on the condensation reaction of aldehydes with amines, which under thermal ambient conditions results in a rather slow imine formation.¹⁵³ By cleverly incorporating the aldehyde onto photoswitches, however, a difference in the aldehyde reactivity was established which enabled to significantly influence the thermal condensation reaction kinetics. For example, by connecting an aldehyde functionality to the azobenzene photoswitch **8**, a rather slow imine condensation product is formed (Scheme II.12). Subsequent UV-light irradiation flips the *trans*-isomer **9** into its *cis*-derivative **10**, thereby enhancing the reactivity of the aldehyde through an intramolecular hydrogen bond and leading to an accelerated imine formation (i.e. 2.4 times faster). Thus, by tuning the electrophilicity of the aldehyde, the outcome of a dynamic covalent bonding reaction could be modulated.



Scheme II.12. Illustrative example of the photoswitchable kinetics of an imine condensation reaction developed by Hecht and coworkers. Whilst the reaction of amines with aldehyde **8** is a rather slow thermal process, UV-irradiation transforms **8** into its *cis*-isomer **9**, which enhances the nucleophilicity of the aldehyde through an intramolecular hydrogen bonding, thereby significantly accelerating the imine condensation process.¹⁵³

Another example of light-switchable reactivity was recently introduced by our own research group (Karlsruhe Institute of Technology). Here, the photoisomerisation of *o*-methylbenzaldehydes into reactive diene transients (*cf.* II.1.3.2) was exploited in combination with the thermal imine condensation reaction to enable selective block copolymer synthesis.¹⁵⁵ The resulting one-pot reaction manifold, consisting of the benzaldehyde, an amine and a maleimide, was demonstrated to either undergo a thermal imine condensation (benzaldehyde + amine) when kept in the dark, or a Diels-Alder cycloadduct formation (benzaldehyde + maleimide) upon UV-irradiation (see Scheme II.13). Regardless of the aforementioned systems being highly elegant examples of how an external trigger such as light can modulate a reaction outcome, their thermal reaction pathways cannot be completely halted, which identifies a key next challenge in photochemical reactivity, which will be addressed in Chapter IV.



Scheme II.13. Selective block copolymer formation based on a light-switchable one-pot reaction manifold comprising an *o*-methylbenzaldehyde, amine and maleimide. A different block copolymer composition can be obtained depending on whether the UV-light is switched on (right) or off (left).¹⁵⁵

II.1.3.4 Direct laser writing and sub-diffraction lithography

The above alluded types of light-induced processes are highly attractive in the design of complex micro- and nanoscale patterns, both in two dimensional lithography as well as in three dimensional (3D) material design. In particular direct laser writing (DLW) has emerged as a versatile technique to generate 3D structures with sub-100 nm resolution without restraints onto the shape of the eventually created objects.¹⁵⁸ As a result of the superior resolution, DLW has found applications in highly demanding fields, including the design of 3D cell scaffolds.¹⁵⁹⁻¹⁶⁰ In the current section, some elementary principles of the DLW technique will be presented to provide a basic understanding of its use in high resolution phototriggered material design. A

detailed physical background of DLW falls outside the scope of the present doctoral work but can be found in specialised literature.^{158, 161}

Microstructure fabrication via DLW is based on the non-linear absorption of multiple photons in a suitable photoresist, which is caused by a femtosecond tightly focussed laser beam inside a small volume or voxel. Most commonly, the DLW photoresist undergoes a two-photon absorption process (2PA) whereby two photons are simultaneously absorbed in a single quantum moment. 2PA processes are rare events and require the use of high intensity light sources to increase their probability of occurring. In contrast to the conventional direct one-photon absorption from the singlet ground state into the corresponding excited state, the two photons that are involved in the 2PA process are only half as energetic and excitation proceeds via a virtual intermediate state (see Figure II.5).¹⁶² Hypothetically, this implies that classical photochemical transformations that require 350 nm UV-light can be accessed by means of a 2PA with two 700 nm photons. Thus, harsh UV-light can effectively be replaced by considerably milder infrared wavelengths making the technique more viable for biological applications.

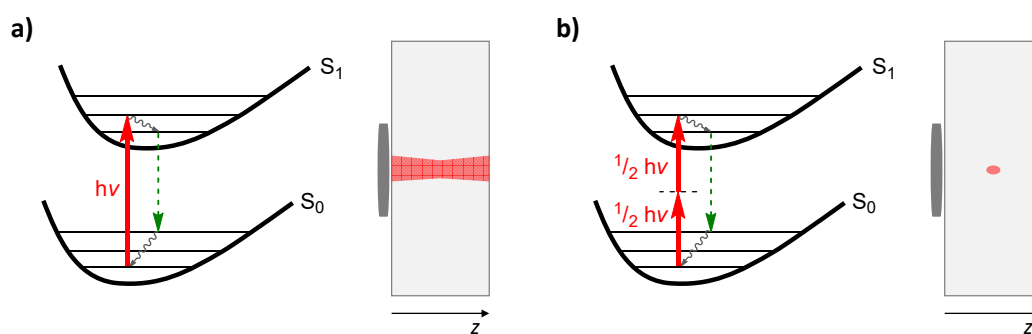


Figure II.5. Comparison of one and two photon absorption processes and the resulting laser beam focus. a) one photon absorption proceeds via direct excitation from the singlet ground state S_0 to the excited state S_1 , characterised by a constant energy profile in the z -direction. b) In a two photon absorption process, excitation to S_1 occurs via a virtual state upon the simultaneous absorption of two photons that are only half as energetic as in the one photon excitation. The energy profile of the resulting laser beam is proportional to z^2 , resulting in a very confined laser focus. Full arrows (red): excitation. Dashed arrows (green): fluorescence. Wavy arrows (grey): vibrational relaxation.

The 2PA process is crucial in DLW as it allows for lateral resolution in three dimensions instead of two. This 3D aspect originates from the non-linearity of the two-photon absorption, which is a second-order process and therefore proportional to the squared light intensity. Next to the x,y -directionality observed in 1PA processes, this ultimately leads to a restricted absorption along the vertical z -axis as well. Hence, the absorption – and thus photochemical reactivity – can be confined in a small 3D volume. The difference in the excitation pattern of a 2PA versus 1PA process is depicted in Figure II.5 and was visually demonstrated via the fluorescence of an appropriate dye.¹⁶³ Because of the high photon density that is generated in such confined volume, relatively low laser powers that operate at a wavelength of 700 – 900 nm can be applied in DLW.¹⁶⁴

With the obtained control in the z-direction, complex 3D patterns can be written by moving the substrate relative to the laser focus according to a computer assisted design. The voxel is thereby freely moved into the resist and photocuring only takes place within the focal point (see Figure II.6, with a negative-tone photoresist). When the writing is finalised, development of the resist washes away non-reactive material and leaves the 3D patterned material with sub-100 nm dimensions behind. Amongst the many applications of such microscale structures is the fabrication of microchips¹⁶⁵ and cell scaffolds.¹⁶⁶

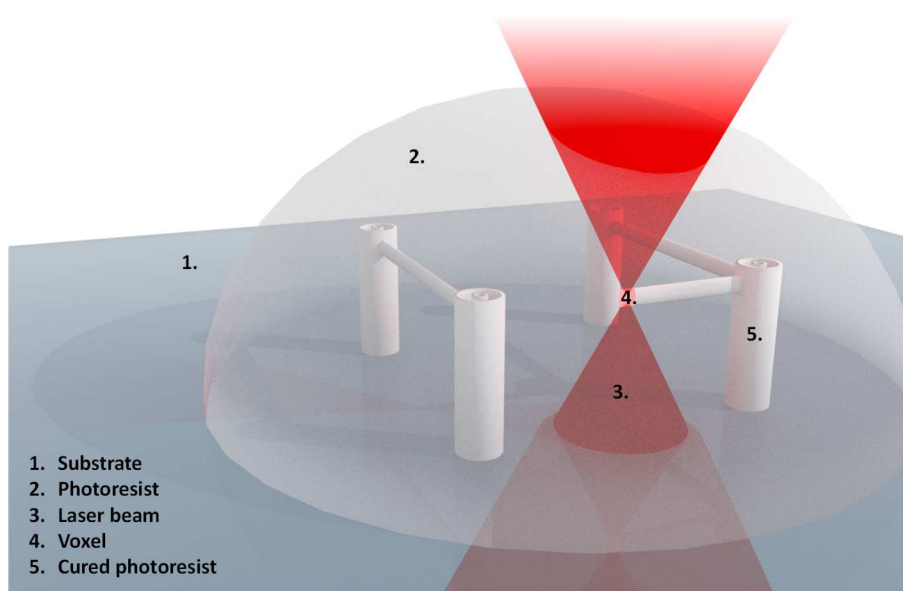


Figure II.6. Graphical representation of the direct laser writing process with a negative-tone resist. A drop of the photoresist (1) is placed onto the substrate holder (2) and moved relative to the laser beam (3). The photochemical reaction is only induced into the voxel (4) of the laser beam, which in the case of a negative-tone photoresist, leads to a crosslinked three dimensional material (5). Figure courtesy of Markus Zieger (Karlsruhe Institute of Technology).

Commercially available resists for DLW are based on acrylate- or epoxide-curing chemistries, yet tailored photoresists are readily applicable to the experimental setup.¹⁶⁷⁻¹⁶⁹ This latter aspect of custom photoresist design is of critical importance to answer today's challenges in DLW.¹⁷⁰ Indeed, using different colours of light for the wavelength-selective writing in the same resist would allow for tailored structures with multiple properties that can be externally accessed,¹⁷¹ for instance in the site selective cleavage of 3D scaffolds to control the growth of cell cultures.^{166, 172} Furthermore, incorporating photocleavable entities in confined 3D materials that can be cleaved upon an extremely mild stimuli (e.g. near-infrared light) would pave the way for many more biological applications.

Next to the fabrication of 3D structures, DLW can also be used for precisely controlled surface patterning, simply by moving the substrate only in the x,y-direction and applying the laser focus near the interface of the substrate and the photoresist (i.e. the z-direction). Whereas in general resolutions below 100 nm are routinely achieved, DLW is limited by the diffraction barrier postulated by Abbe, which is not much smaller than half the size of the applied wavelength. To overcome this diffraction boundary, the ingenious concept of stimulated emission depletion

(STED), introduced by Stefan Hell in optical fluorescence microscopy¹⁷³ to access spectacular resolutions down to 10 nm,¹⁷⁴ was applied to DLW in order to eliminate the wavelength dependence of the resolution.^{161, 170}

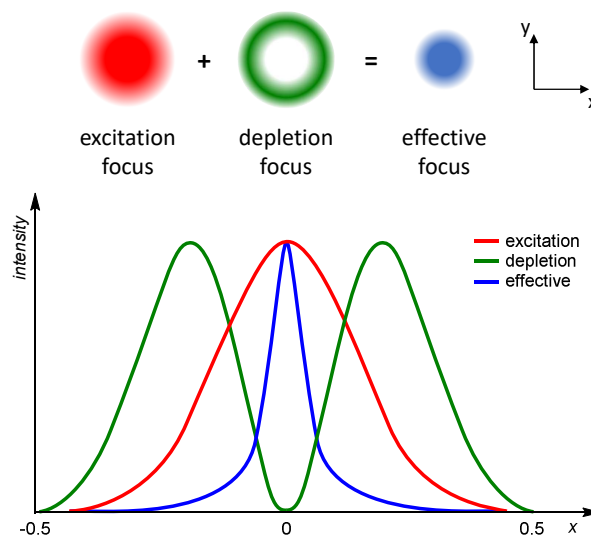
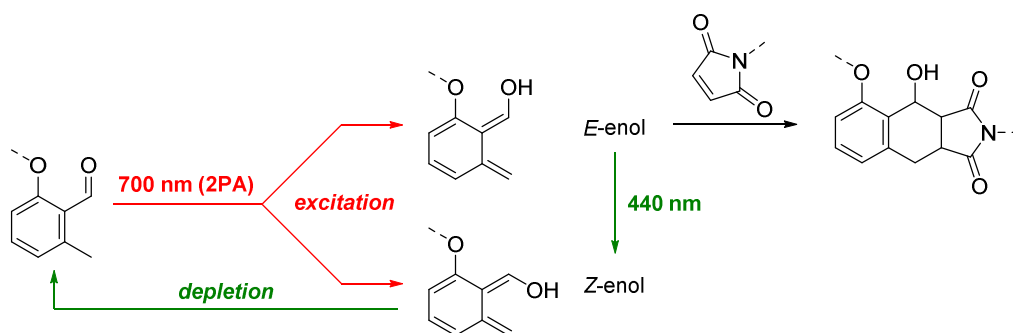


Figure II.7. Principle of stimulated emission depletion (STED) inspired laser lithography. Superimposition of an excitation laser focus (red) with a depletion focus (green) generates a significantly reduced effective focus wherein a photochemical reaction can be triggered. The intensity profiles depict the zero intensity donut shape depletion focus which cancels out the initial excitation intensity. Adapted from Ref.¹⁷⁰ with permission from WILEY-VCH Verlag.

In essence, the two dimensional STED technique rests on the introduction of a second laser with a donut shaped focus – called depletion laser – that is emerged with the initial excitation laser (see Figure II.7). Both lasers employed have a Gaussian focus that is precisely overlaid. Hence, those areas wherein the initial excitation focus overlaps with the depletion laser are effectively deactivated by reducing the intensity near zero, thereby leading to a much smaller volume that is truly subjected to excitation. In STED-based lithographic applications, for example, the enabling feature of combining a depletion with excitation effect has been illustrated to considerably reduce the line width (i.e. down to 65 nm)¹⁷⁵ during surface patterning by ‘erasing’ the edges of the writing laser.¹⁷⁶ Moreover, the concept was also translated to three dimensional optical lithography, allowing for the fabrication of sub-diffraction structures through STED-inspired DLW. Yet, a crucial aspect to successfully implement STED into DLW is found in the tailored design of suitable photoresists.¹⁷⁶

The main requirement for a photoresist to be applicable to STED-lithography comprises a triggered chemical switching behaviour between an activated and deactivated state. In other words, it should be possible to switch the reactivity of a molecule on-and-off by the action of the excitation and depletion laser, respectively. An attractive way to provide such an on/off switchability is through reversible photodeactivation pathways whereby the chemical reactivity of a certain chromophore can be inhibited.¹⁷⁰ The above discussed photoenol chemistry was found to be a suitable candidate for such a photoswitchable reactivity (Scheme II.14).¹¹⁸ The key step

in this example is the formation of two photoisomers, whereby only the *E*-enol is susceptible to undergo a Diels-Alder cycloaddition (*cf.* II.1.3.2). Irradiation at 400 nm, however, readily converts the *E*-enol into its unreactive *Z*-counterpart which results in the effective depopulation of the Diels-Alder reaction substrate. Whilst the photoenol depletion system has elegantly been exploited in surface lithography to achieve 60 nm line width patterns, the development of photoresists to enable sub-diffraction lithography in three dimensions constitutes a crucial next step to fully explore the potential sub-10 nm resolution fabrication of 3D structures.¹⁷⁶



Scheme II.14. Molecular switch enabling STED-inspired lithography, based on the *cis/trans*-isomerisation of photogenerated enols. Upon a two-photon absorption (2PA), two isomeric forms of the resulting photoenol are obtained of which only the *E*-configuration has a sufficient lifetime to react in a Diels-Alder cycloaddition with maleimides. Irradiation with 440 nm light, however, transforms the reactive *E*-enol into its unreactive *Z*-analogue, thereby providing the depletion pathway required for the STED process.¹¹⁸

II.1.4 Conclusions

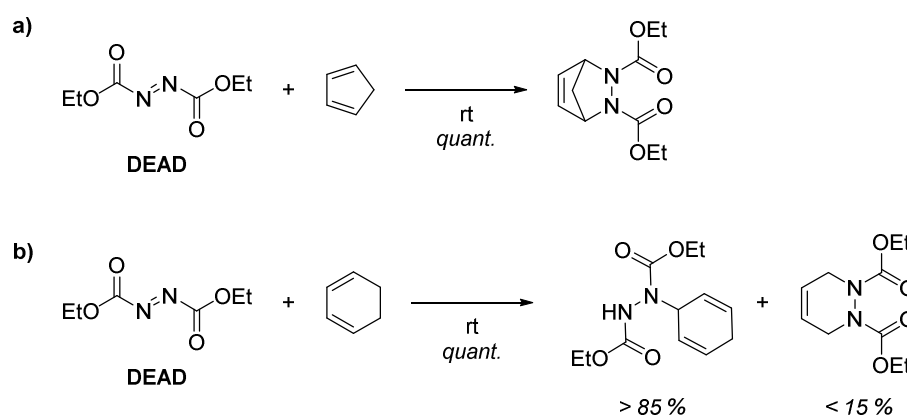
Many external triggers have been investigated throughout the years that allow for the precise control over complex and multicomponent reaction systems. Temperature and light-induced processes are by far most studied and have been promptly incorporated into a vast array of polymer materials that contain adaptive properties. Numerous dynamic covalent chemistries have been introduced throughout the years to allow for tailored material features such as self-healing, stress-relieving, reprocessing or even triggered degradation for on demand release. Yet, new chemistries are still being explored as the meticulous design on a molecular level readily provides a tunable macromolecular response.

In this context, the presented doctoral work aimed to gain an external control over triazolinedione (TAD) compounds, powerful coupling reagents in biomedical and polymer research,¹⁵ in order to selectively switch their reactivity on and off. Ideally, this would enable the rational design of functional and responsive TAD-based polymer materials, as well as dynamic molecular systems with tunable properties, that can be accessed ‘on demand’ by temperature or light.

II.2 Introduction to triazolinedione chemistry

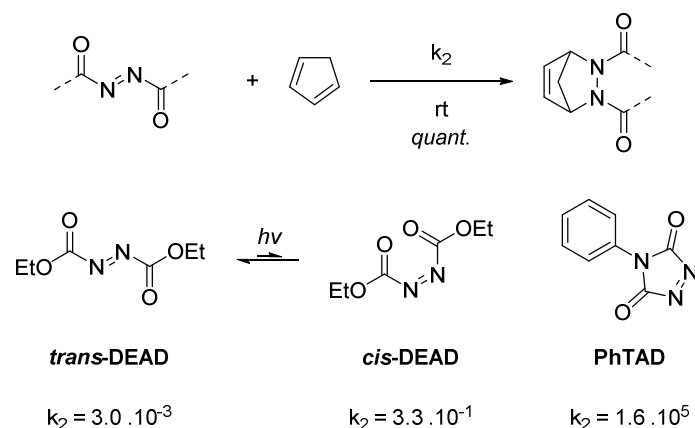
II.2.1 General introduction

The 1925 seminal finding by Otto Diels, Jacob H. Blom and Werner Koll of the swift and quantitative bond-forming reactivity of azodicarbonyl compounds with simple hydrocarbons that contain conjugated double bonds, serves as one of the most powerful transformations in contemporary organic chemistry.¹⁷⁷ In what was later coined a Diels-Alder reaction,¹⁷⁸ diethyl azodicarboxylate (DEAD) was found to spontaneously and quantitatively form a 1:1 heterocyclic addition product with cyclopentadiene at – and even below – room temperature (Scheme II.15a). Despite the pronounced dienophilic properties of DEAD, the aza-dienophile was outperformed by more accessible alternatives, such as maleic anhydride and *N*-substituted maleimides, as it failed to selectively yield Diels-Alder cycloadducts with 1,3-cyclohexadiene.¹⁷⁹⁻¹⁸⁰ Instead, an allylic addition product was predominantly formed via a competing Alder-ene reaction, attributed to the *trans* conformation of the azobond (Scheme II.15b).¹⁸¹⁻¹⁸²



Scheme II.15. a) Seminal Diels-Alder reaction of diethyl azodicarboxylate (DEAD) with cyclopentadiene.¹⁷⁷
b) Addition of DEAD to 1,3-cyclohexadiene predominantly forms an allylic substitution product with only traces of the expected Diels-Alder adduct to be detected.¹⁷⁹⁻¹⁸⁰

In an attempt to enhance Diels-Alder product selectivity, *trans*-DEAD was irradiated with UV-light to give a photostationary equilibrium containing up to 30% of the *cis*-DEAD isomer, the latter exhibiting a 100 times faster Diels-Alder reactivity compared to its *trans*-analogue (Scheme II.16).¹⁸³⁻¹⁸⁴ At the same time, Cookson and co-workers investigated the dienophilic reactivity of the cyclic azodicarbonyl derivative 4-phenyl-1,2,4-triazoline-3,5-dione (PhTAD, Scheme II.16), which was found to be of extraordinary nature, attributed to the locked *cis*-azo configuration.¹⁸⁵⁻¹⁸⁶ Today, 4-substituted 1,2,4-triazoline-3,5-diones (triazolinediones or TADs) are notorious for their instantaneous reaction with cyclopentadiene, even at $-78\text{ }^{\circ}\text{C}$,¹⁸⁵ and are considered as the most reactive yet bench-stable dienophiles and enophiles.¹⁰



Scheme II.16. Rate coefficients k_2 ($\text{L mol}^{-1} \text{s}^{-1}$) of *trans*- and *cis*-diethyl azodicarboxylate (DEAD) and 4-phenyl-1,2,4-triazoline-3,5-dione (PhTAD) aza-dienophiles in their Diels-Alder cycloaddition reaction with cyclopentadiene (at 25°C in toluene).^{183, 187}

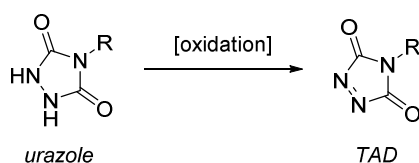
Although initially hampered by their problematic synthesis and ‘exotic’ reputation, Cookson’s procedure (*vide infra*) allowed for simple 4-alkyl and 4-aryl substituted TAD reagents to be isolated as carmine red crystals which could be stored for months in a dark and cold environment.⁹ In fact, PhTAD has been commercially available since 1981,¹⁸⁸ making it a prominent reagent in a multitude of organic transformations, in particular for the construction of condensed heterocycles.¹⁸⁹⁻¹⁹¹ Over the past decades, other simple TAD derivatives (e.g. 4-methyl, 4-*n*-butyl) also evolved as versatile and reliable synthetic tools in other research disciplines, including polymer^{11, 192} and bioconjugation sciences,¹⁹³⁻¹⁹⁴ and by efforts in our research groups (Ghent University) emerged to be a highly interesting click chemistry platform.^{7, 12, 25}

Whereas simple TAD reagents are readily obtained on multigram scale via the oxidation of a bench-stable precursor, the synthesis of more complex and functional TAD reagents is often tedious and serves as a major bottleneck to fully harness the potential of TAD chemistry, especially in more demanding and advanced applications.¹⁵ The first section of the current chapter (II.2.2) therefore provides a brief overview on the most frequently adopted synthetic routes to obtain both simple as well as tailored TAD reagents from easily accessible building blocks. The following section (II.2.3) aims to provide a comprehensive understanding of triazolinedione reactivity. Given the interest of this PhD work in triggered TAD-based reactions, a subdivision is made between their thermal (II.2.3.1) and photochemical (II.2.3.2) reactivity. As can be expected from such highly activated species, TADs can participate in a wide range of reactions and thus has great potential in a multitude of applications, of which macromolecular (bio)conjugation is highlighted in section II.2.4. Finally, some important considerations (II.2.5) regarding the practical use of TAD reagents throughout this PhD thesis are outlined.

II.2.2 Synthesis of 4-substituted triazolinediones

Since the present PhD thesis focuses on the development of triggered TAD-based reactions in polymer systems rather than the synthesis of new and more sophisticated TAD compounds, a rather informative overview with regard to the synthesis of triazolinediones related to the current work is provided in the following section. A more elaborate overview of the available synthetic routes, in particular for tailored TAD reagents bearing additional functionalities, is discussed in our review article.¹⁵

Triazolinediones were first reported in the 1894 pioneering work of Thiele and Stange, who designed a synthetic protocol towards 4-substituted 1,2,4-triazolidine-3,5-diones or so-called urazole moieties (the dihydro-TAD-derivative, see Scheme II.17).¹⁹⁵ At that time, reduction and oxidation reactions were commonly applied analytical techniques for structure elucidation and to support the successful formation of a synthesis target. Hence, the first routes towards 4-substituted urazoles typically encompassed a final oxidation experiment that yielded a brightly red coloured solution, which was attributed to the formation of the corresponding azodicarboxamide derivative, or TAD (see Scheme II.17).¹⁹⁵⁻¹⁹⁷



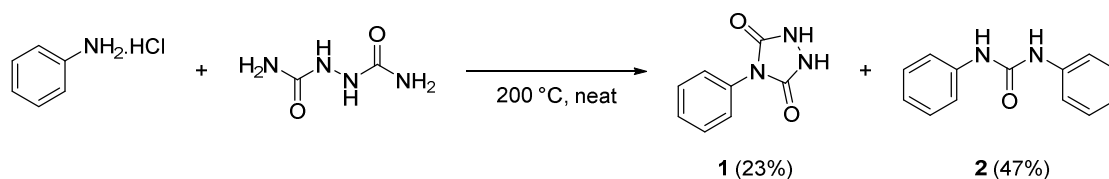
Scheme II.17. Oxidation of a 4-substituted urazole into its corresponding triazolinedione (TAD).

Although triazolinediones were described as early as 1894, their synthesis remained elusive due to a problematic isolation as well as stability issues related to their extreme reactivity.^{185, 198} Nevertheless, the initial strategy of generating TAD reagents by means of a straightforward oxidation of their bench-stable urazole precursor (cfr. Scheme II.17), remains the exclusively applied synthesis strategy to date.

In the following, the synthesis of the parent urazole compounds from readily available starting materials is discussed in more detail. Emphasis will lie on the preparation of 1-alkoxycarbonyl semicarbazides, well-established key intermediates, that can be assembled in a number of efficient protocols and are readily converted into their urazole counterparts upon cyclisation under basic conditions (II.2.2.1.). While a large structural variety in urazoles can be obtained in this manner, a vast range of chemical functionalities is not compatible with the aforementioned reaction conditions. The next section (II.2.2.2.) is therefore devoted to the transformation of simple 4-substituted urazoles into more elaborate ones, either *via* post-modification of a latent functionality or *via* removal of a protecting group. Following some brief conclusions on urazole syntheses (II.2.2.3.), some commonly applied oxidation procedures to ultimately obtain triazolinedione reagents are listed in section II.2.2.4.

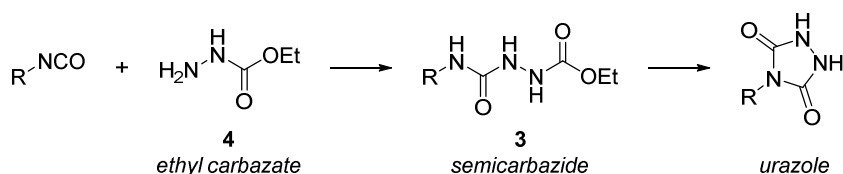
II.2.2.1 Urazole synthesis

The earliest report on 4-substituted urazoles describes the formation of 4-phenylurazole (**1**, Scheme II.18) upon heating a neat mixture of biurea and aniline hydrochloride to 200 °C.¹⁹⁵ However, significant amounts of a diphenylurea side product (**2**) were observed, which proved hard to separate from the desired urazole target. Multiple variations of this low-yielding original procedure were reported in order to improve the overall efficiency, but all suffered from tedious optimisation of the reaction conditions.^{197, 199-203} Furthermore, the overall substrate scope proved to be limited as a result of the harsh reaction conditions, making this synthetic strategy far superseded.



Scheme II.18. Original synthesis of 4-phenylurazole, obtained upon heating biurea and aniline hydrochloride.¹⁹⁵

In 1961, Zinner and Deucker proposed a significant improvement upon Thiele's original procedure.²⁰⁴ Rather than using biurea substrates, 4-phenyl- and 4-*n*-butylurazole were obtained under much milder conditions through cyclisation of their corresponding 4-substituted 1-(ethoxycarbonyl)semicarbazides (**3**, Scheme II.19). These later key intermediates, in this work simply referred to as 'semicarbazides', are easily derived from isocyanates and ethylcarbazate **4**, which in turn is a readily available and rather cheap condensation product of hydrazine and diethyl carbonate. Although the reported two-step approach resulted in significantly higher overall yield (i.e. 93% for R = Ph and 83% for R = *n*Bu, Scheme II.19), the optimised urazole synthesis procedure did not gain much attention. This changed, however, when Cookson and co-workers presented the first efficient isolation of 4-phenyl-1,2,4-triazoline-3,5-dione (PhTAD) as carmine-red crystals, through the reaction of phenyl isocyanate and ethyl carbazate followed by ring closure to 4-phenylurazole (i.e. according to Zinner and Deucker) and its subsequent oxidation.²⁰⁵ As this overall reaction sequence became of paramount importance in modern TAD synthesis, it is commonly referred to as the Cookson method²⁰⁶ with PhTAD regularly coined as Cookson's reagent.²⁰⁷⁻²⁰⁸

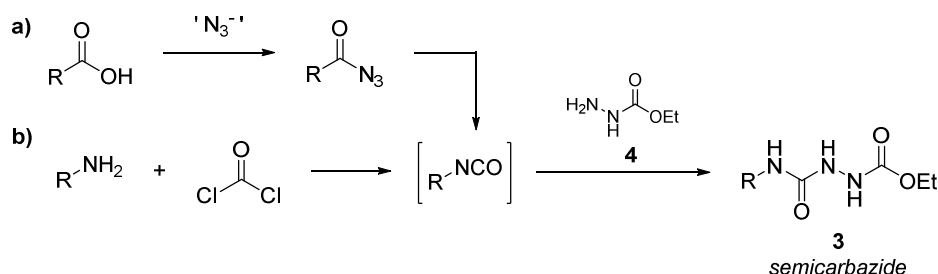


Scheme II.19. Modern and highly efficient synthetic pathway to 4-substituted urazoles via the cyclisation of semicarbazides, obtained from the addition of ethylcarbazate to isocyanates (R = Ph, *n*Bu).²⁰⁴

Throughout the years, the Cookson method has found many application for the synthesis of 4-substituted urazoles whereby the main alterations are found in the synthesis of the semicarbazide intermediate **3**. The most straightforward and still widely adopted synthetic

strategy to generate semicarbazides exploits the high reactivity of isocyanate reagents towards ethyl carbazate (**4**, cf. Scheme II.19). Typically, the addition reaction is carried out in hydrophobic solvents from which the resulting semicarbazide can be collected in near-quantitative yields by simple filtration. Importantly, the substrate scope was quickly expanded to other commercially available isocyanates, thus simply altering the structural identity of the urazole targets.^{15, 209-212} In particular diisocyanates, such as 4,4'-methylene diphenyl (MDI)^{210, 213} and 1,6-hexamethylene diisocyanates (HDI)²¹⁴⁻²¹⁵ (bulk chemicals used in polyurethane industries), received much attention in the field of polymer chemistry as they ultimately yield bivalent TAD crosslinking reagents (bisTADs, cf. II.2.4.).

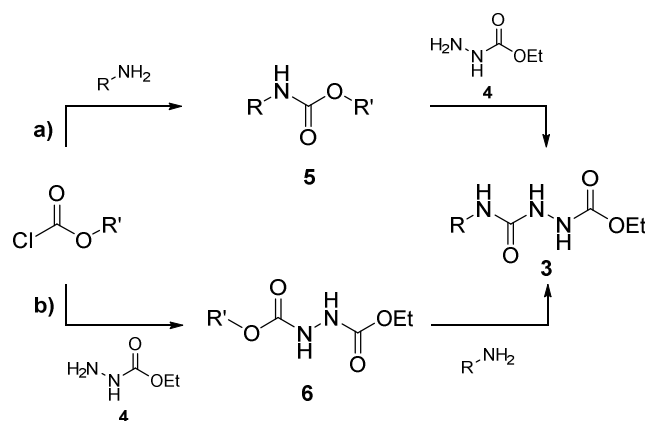
Despite its ease and reliability, the Cookson method is limited by the structural variety that is found in commercially available isocyanates. As a result, the substrate scope was expanded to carboxylic acids that are readily converted into acyl azides.²¹⁶ The resulting crude product can then be subjected to a Curtius rearrangement²¹⁷⁻²¹⁹ upon heating to give the corresponding isocyanate, which is subsequently reacted *in situ* with ethyl carbazate **4** to form the semicarbazide **3** (route a, Scheme II.20).²²⁰ This extension of the Cookson method was successfully applied to a range of fluorescent and chromophore carboxylic acids of which the resulting TADs were used for the detection of vitamin D analogues.²²⁰⁻²²³ In a similar manner, isocyanates can also be obtained *in situ* from amines in combination with phosgene (route b, Scheme II.20), as was demonstrated in the synthesis of chiral semicarbazides starting from optically pure amines.²²⁴⁻²²⁵



Scheme II.20. Extended Cookson procedures for the synthesis of semicarbazides whereby isocyanates are generated *in situ*. a) Starting from carboxylic acids followed by azidation and subsequent Curtius rearrangement. b) From amines in combination with phosgene.

More modern research efforts have been devoted to the development of isocyanate-free methods for the production of semicarbazides from amines, as the latter are more readily available.^{206, 226-227} Two strategies have been established that avoid the use and even intermediate formation of hazardous isocyanate reagents. A first strategy, introduced by Mallakpour and co-workers, utilises activated carbamate intermediates **5**, obtained upon reaction of an amine with chloroformate (route a, Scheme II.21).²²⁶ The reactivity of the resulting carbamate in the follow-up reaction with ethyl carbazate to yield the desired semicarbazide **3** greatly depends on the chloroformate reagent used, with 4-nitrophenyl chloroformate (R' = 4-NO₂Ph, Scheme II.21a) identified as the most reactive one.²²⁸ Later, a one-pot procedure was developed using an excess of chloroformate and ethyl carbazate thereby circumventing the isolation of the carbamate

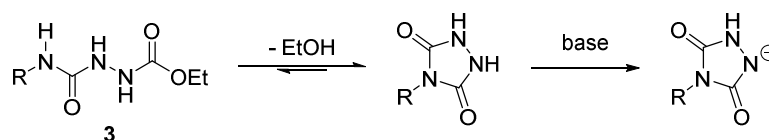
intermediate.^{193-194, 229} In an alternative strategy, designed by Breton and co-workers, ethyl carbazate **4** is firstly activated to the hydrazine dicarboxylate **6**, followed by addition of the amine (reaction pathway b, Scheme II.21).^{206, 230-231} The transformation of aliphatic amines with (4-nitro)phenyl chloroformate ($R' = \text{Ph}$ or $4\text{-NO}_2\text{Ph}$ in Scheme II.21b) proved to be very successful, yet aniline failed to acquire the phenyl-substituted urazole precursor **3** ($R = \text{Ph}$) in all cases. Inspired by the above discussed strategies of Mallakpour and Breton, our research group recently reported on the use of diphenyl carbonates as a more environmentally friendly alternative to chloroformates.²²⁷ Whereas no significant improvements in urazole yield or substrate scope were observed, considerably shorter reaction times were obtained as a result of the solvent-free conditions. Despite isocyanate-based routes tend to be higher yielding, their non-isocyanate alternatives offer an important addition to the TAD synthesis toolbox. Indeed, even though methyl isocyanate, traditionally used in the synthesis of the benchmark MeTAD reagent, is no longer commercially available, methyl-substituted semicarbazide (**3** with $R = \text{Me}$), still remains accessible on multigram scale via Breton's isocyanate-free procedure.²⁰⁶



Scheme II.21. Isocyanate-free synthetic strategies for the preparation of semicarbazides from amines with chloroformates ($R' = \text{Et}, \text{Ph}, 4\text{-NO}_2\text{Ph}$).

The above discussed semicarbazides can be readily cyclised to their corresponding urazoles and hence, only a limited amount of procedures are documented throughout literature reports. In general, the ring closure of the urazole precursor is effected under mildly basic conditions in a protic solvent.^{204, 209, 232}

In the original procedures, e.g. Cookson's method, cyclisation is effected by the simple treatment of the semicarbazide in a boiling aqueous potassium hydroxide solution. It is important to note that although the ring closing reaction is an intrinsic reversible process, it is driven by an irreversible deprotonation step as a result of the relatively low pK_a value (i.e. ≈ 5)²³³⁻²³⁴ of the formed urazole (Scheme II.22). The solvated urazolyl anion is finally isolated in nearly quantitative yields upon acidification (to $\text{pH} = 1\text{-}2$), since the neutral compound typically precipitates from the aqueous reaction mixture. This cyclisation procedure is thus the method of choice for 4-aryl substituted urazoles that easily crystallise from the acidic solution.²³⁵

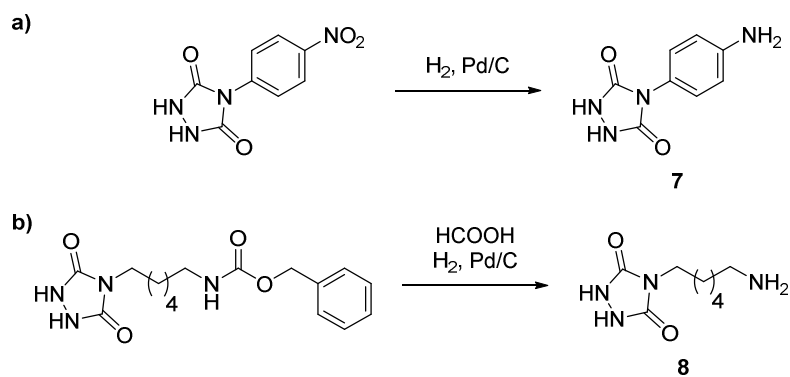


Scheme II.22. Cyclisation of semicarbazides (**3**) to their urazole derivatives under basic conditions. The process is driven by the irreversible formation of the urazolyl anion through deprotonation of the heterocyclic product.

An alternative method to the aqueous potassium hydroxide-mediated cyclisation is presented by sodium ethoxide in ethanol at reflux temperatures, which also allows for the isolation of urazoles in high yields, albeit after longer reaction times (i.e. up to 24 hours). Since this procedure is compatible with a non-aqueous work-up, it is often the method of choice if the 4-substituent on the urazole prevents it from precipitating out of an aqueous solution as is commonly observed for aliphatic derivatives.^{216, 235} Similarly, potassium carbonate can be used as a much milder base in both alcoholic and aqueous media,²²² leading to improved results with more problematic substrates such as 4-(pentafluorophenyl) semicarbazides, where the para-fluorine atom is readily displaced during hydroxide-mediated ring closure.²³²

II.2.2.2 Urazole modification

Whereas a large structural variety in 4-substituted urazoles is already accommodated for by the aforementioned synthetic procedures, quite a few chemical functionalities are not compatible with the commonly applied reaction conditions. Hence, more elaborate urazole functionalities are most often introduced during a post-modification reaction of a latent urazole functionality, i.e. after the base-mediated cyclisation of the semicarbazide has been affected (*cf.* II.2.2.1.). An elegant example is presented in the formation of 4-(4-aminophenyl)-substituted urazole **7** upon hydrogenation of the nitro-group, the latter not interfering in the urazole synthesis (Scheme II.23a).^{7, 236} Another approach is to strategically incorporate protecting groups at or before the semicarbazide level that are preserved during the urazole formation and can be readily removed afterwards. Typically, urazoles substituted with an aliphatic amine, e.g. **8**, are accessible in this manner upon removal of a carboxybenzyl protecting group (Scheme II.23b).²³⁷



Scheme II.23. Examples of urazole post-modification strategies. a) Transformation of a latent functionality such as a nitro-group. b) Using protection/deprotection chemistries.

Overall, reactive chemical functionalities that are initially incompatible with the conventional urazole syntheses (e.g. amines, but also alcohols and carboxylic acids) can be introduced via the outlined post-modification strategies. Importantly, these reactive groups can serve as functional handles for further derivatisation. Amino-functional urazoles, for instance, are prone to amidation reactions and have evolved as valuable intermediates, particularly in the synthesis of urazole-containing polymerisation initiators^{7, 238} and chain transfer agents.^{12, 239} However, the amide bond formation is typically assisted by relatively strong bases ($pK_a > 5$) that readily deprotonate the neutral urazole N-H. Thus, the formed urazolyl anion (*cf.* Scheme II.22) acts as a competitive nucleophile during the amidation reaction which often results in undesired acylation byproducts.²³⁷ This competing side reaction is even more pronounced during modification of urazoles via hydroxyl functionalities, which are therefore considerably less explored.²²² The use of carboxylic acid moieties as functional handles for further derivatisation is also very limited explored. This is likely because the urazole itself is expected to greatly interfere with carboxylic acid reactions considering their similar acidity.²³⁶ Conventional coupling reactions, such as the widely adopted carbodiimide assisted esterifications, are therefore extremely challenging.

II.2.2.3 Concluding remarks on urazole synthesis

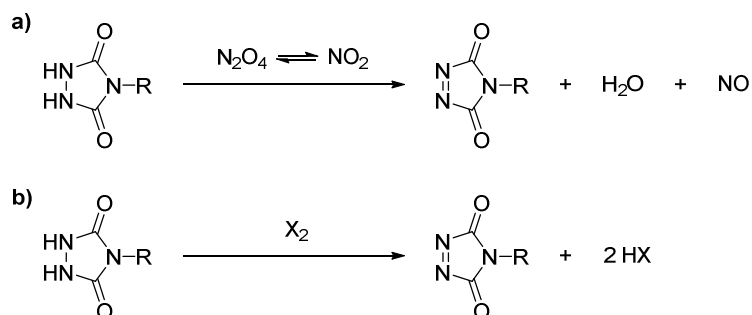
Common 4-substituted urazole substrates (e.g. 4-phenyl- and 4-*n*-butylurazole) and numerous bisfunctional derivatives are readily synthesised on a large scale and in high yields from cheap and bulk starting materials such as isocyanates. However, very few urazoles bearing an additional functionality are easily accessible or commercially available and often require elaborate multistep synthesis procedures as well as expert knowledge. This limited versatility in urazole products, and as a result in final TAD compounds, remains one of the main limitations of TAD chemistry today. Ongoing research efforts within our groups are therefore devoted to the development of short, scalable and versatile synthetic protocols to tailored urazole reagents.

II.2.2.4 Oxidation of urazoles to their corresponding triazolinediones

Until today, all practical procedures to synthesise triazolinediones proceed via a final oxidation step of the corresponding urazole precursor. It is important to keep in mind that while the oxidation of urazoles is a very straightforward reaction that can be affected by numerous oxidants, it is often a true bottleneck in TAD synthesis. The oxidation of urazoles can indeed become challenging because of two interrelated issues, namely the chemoselectivity of the oxidant and the reactivity of the thus formed TAD compound.¹⁵ Moreover, isolation of the desired TADs can sometimes be tedious. Ideal oxidation protocols should therefore be highly chemoselective, afford only one single triazolinedione product, and generate no or readily removable oxidation by-products. For some applications, the *in situ* generation of TADs is preferred. Although this circumvents difficulties that might arise during TAD isolation, the chemoselectivity problem is usually aggravated. Importantly, both the initial oxidant as well as its reduced form should not react with the TAD moieties that are targeted.

Unfortunately, no general guidelines are available to carry out urazole oxidations and the development of a myriad of successful protocols was therefore often based on trial and error. While a complete overview is presented in our extensive TAD chemistry review,¹⁵ only the most important oxidation methods that are used in the crucial final stage of TAD synthesis are described below.

The first oxidation procedures to transform urazoles into their brightly colored TADs simply comprised the addition of concentrated nitric acid.^{195, 240} Although nitric acid solutions are cheap and easy to handle, an aqueous work-up procedure was typically required to remove the oxidation by-products (e.g. acids, water). Consequently, the obtained TAD yields were rather moderate as a result of their limited stability towards hydrolysis (see below, II.2.3.3.). As a result, Stickler and Pirkle developed a straightforward acid-free oxidation protocol by making use of gaseous dinitrogen tetroxide (N_2O_4),²⁰⁹ which exists in equilibrium with nitrogen dioxide²⁴¹ and is regarded as a milder and dehydrated form of nitric acid (Scheme II.24a).²⁴² The gaseous oxidant readily converts urazoles into their corresponding TADs in an almost traceless and quantitative manner and can easily be used in excess without affecting the isolation of pure TADs. The reaction is typically carried out in the presence of an appropriate desiccant to avoid the interference of generated water and can also be performed in more polar solvents (e.g. ethyl acetate), which broadens the substrate scope considerably compared to the classical nitric acid procedure that is limited to the synthesis of chloroform or dichloromethane soluble TAD reagents.^{198, 209, 243}



Scheme II.24. a) General scheme for the dinitrogen tetroxide-mediated oxidation of urazoles into their triazolinedione counterparts. b) Halogen-mediated oxidation protocol.

To date, the N_2O_4 -mediated oxidation is still the most widely applicable method to many urazole substrates, even though electron rich 4-aryl-substituted derivatives tend to give competitive aromatic nitration reactions, as was evidenced for 4-(4-hydroxyphenyl)urazole.²⁴⁴ Yet, the highly effective N_2O_4 reagent has several unfavourable aspects, including high toxicity, high cost and unreliable quality. Hence, Mallakpour developed a lab-scale set-up for the controlled generation of neat N_2O_4 gas via the combustion of dried lead nitrate.²⁴⁵ More recently, heterogenous oxidation protocols have been developed that are based on the adsorption and/or complexation of gaseous N_2O_4 onto an insoluble solid support, including poly(ethylene glycol).²⁴⁶⁻

Besides nitrogen-mediated reagents, a second major class of urazole oxidants comprises halogens and their derivatives (Scheme II.24b). Both elemental chlorine²³⁷ and bromine¹⁰ were reported to readily oxidise 4-substituted urazoles into TADs, albeit in low yields and with only limited chemoselectivity. Cookson achieved a more controlled oxidation by using *tert*-butyl hypochlorite in dry acetone at low temperatures (i.e. below $-50\text{ }^{\circ}\text{C}$).¹⁸⁵ Quantitative yields at room temperature were later obtained feasible by changing the solvent to dioxane or ethyl acetate.^{186, 205} The Cookson oxidation method remains a well-established procedure and can be performed on a large scale and in the presence of a broad range of 4-urazole substituents, including electron-rich aromatic groups.²⁴⁴

In order to avoid the use and handling of hazardous elemental chlorine, bromine and other active halogen-based oxidants, a multitude of alternative reagents have been developed that rely on the slow and *in situ* release of active halogen species. A well-known replacement for bromine that is capable of oxidising a variety of monofunctional, bivalent and polymeric urazoles is *N*-bromosuccinimide (NBS, Figure II.8).²⁴⁹⁻²⁵⁰ However, an extensive aqueous workup is needed to remove the resulting succinimide oxidation by-product, which is considerably less suitable for water-sensitive TADs. It is therefore advisable to omit this workup by using the crude TAD reaction mixture as such.

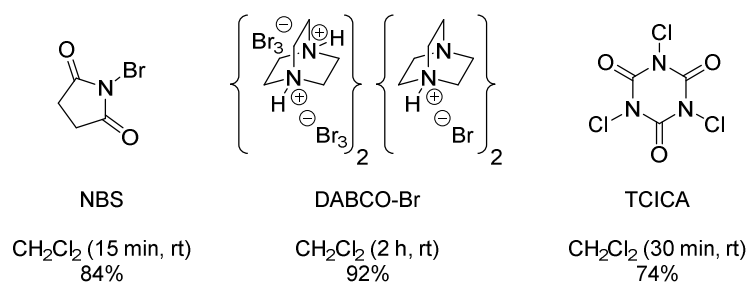


Figure II.8. Commonly applied urazole oxidants for the *in situ* generation of active halogen species along with their reaction conditions and yields for the conversion of 4-phenylurazole. NBS: *N*-bromosuccinimide.²⁵¹ DABCO-Br: tetrameric 1,4-diazabicyclo[2.2.2]octane-bromine complex.¹³ TCICA: trichloroisocyanuric acid.²⁵²

Alternatively, heterogeneous reagents were introduced to enable a more efficient removal of the oxidation waste products via a simple filtration of the formed salts. A particularly useful heterogeneous reagent in this respect is the tetrameric complex of 1,4-diazabicyclo[2.2.2]octane with bromine (DABCO-Br, Figure II.8) that generates active bromine species *in situ*.²⁵³ Besides the conversion of a variety of low molecular weight urazoles, this bromine complex was also found suitable for the quantitative oxidation of urazole polymer end groups into their TAD counterparts.^{7, 12, 239}

Although DABCO-Br oxidants – which require the in-house synthesis from elemental bromine – are well-embedded into our own research groups, trichloroisocyanuric acid (TCICA, Figure II.8) can be considered as a more elegant reagent owing to its commercial availability.²⁵² Indeed, TCICA is a convenient and cheap source for the active chlorine species capable of oxidising

urazoles to TADs in excellent yields in various solvents as well as under solvent-free conditions. Moreover, faster reaction times are observed since the oxidant itself typically dissolves in the reaction medium whereas the subsequently formed oxidation by-products precipitate during the course of the oxidation and can be removed by simple filtration.²⁵⁴ It is an exceptionally mild method that can be used for notoriously sensitive urazole substrates, such as the hydrochloride salt of 4-aniline-urazole, and is currently the method of choice in our laboratories to conduct the crucial final TAD synthesis step.

II.2.3 Triazolinedione reactivity

TAD reagents are generally regarded as being the structural analogue of the more widely known maleimides – a well-established class of synthetic tools in a range of applications, including bio-conjugation and polymer chemistry²⁵⁵⁻²⁵⁶ – in which the C=C double bond has been replaced by a N=N double bond. Nevertheless, TADs are five to six orders of magnitude more reactive in Diels-Alder reactions with cyclopentadiene compared to their maleimide mimics.^{187, 257} Although both their modes of reactivity show certain similarities, TAD reagents have a higher intrinsic thermodynamic driving force and participate in a much wider variety of pericyclic reactions, even with simple and isolated olefinic substrates.^{15, 258-259} In contrast, TADs showcase a lack of (controlled) reactivity towards common nucleophiles such as alcohols and amines.²⁶⁰

Despite the structural resemblance with maleimide, from a reactivity point of view, TADs are best compared with singlet oxygen.⁹ Indeed, similarly to singlet oxygen, TADs possess a multiform high reactivity in Diels-Alder reactions,¹⁸⁶ (Alder-)ene reactions²⁶¹ and [2+2] cycloadditions²⁶² with electron-rich or non-polarised olefins. This corresponding reactivity pattern can be explained by the arrangement and very similar energies of the filled and empty π^* -type frontier molecular orbitals, as depicted in Figure II.9.²⁶³ TADs possess both a high-energy HOMO and a low-energy LUMO and have an essential preference for orbital-controlled reactions.²⁶⁴ Their remarkable reactivity lies in the dual character of the geometrically orthogonal p-type antibonding orbitals, only one of which is occupied. The low-energy LUMO acts as the main source for the electrophilic character of TAD molecules.

TADs are useful reagents to investigate mechanistic aspects of singlet oxygen additions because of their similar reactivity, yet improved practicality.⁹ Indeed, many TAD model compounds have a superior lifetime and can be isolated and stored, in contrast to singlet oxygen, which is typically generated *in situ* and only has a lifetime up to seconds (depending on the organic solvent used).²⁶⁵ Additionally, triazolinediones offer the potential to introduce additional functionalities during chemical transformations (expressed in their R-group), instead of solely effecting oxygenations.

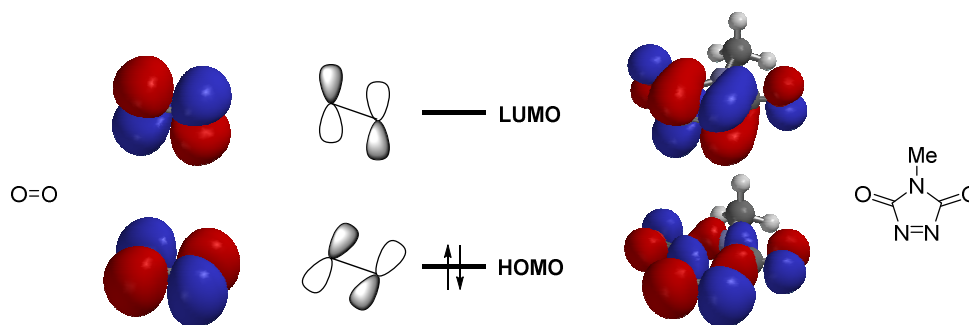
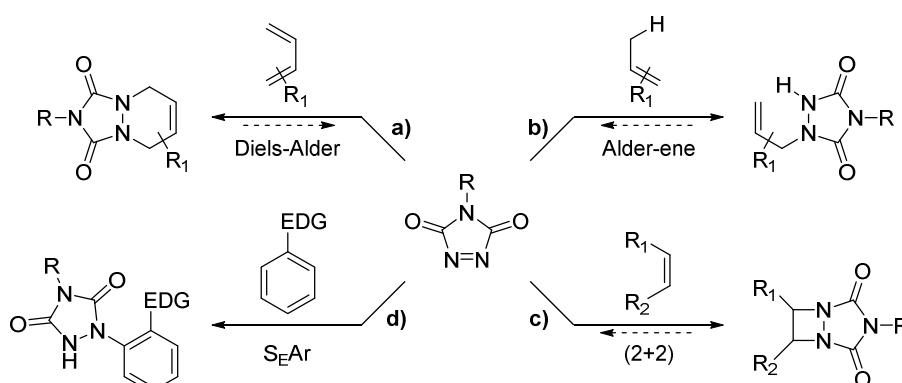


Figure II.9. The similar reactivity pattern of singlet oxygen (left) with 4-methyltriazolinedione (MeTAD) (right) can be related to the similar geometry of their frontier molecular orbitals. In both cases, the π^* -type antibonding highest occupied and lowest unoccupied molecular orbital, HOMO and LUMO respectively, are of similar energies.

In what follows, the TAD-based reactions that are most relevant to this doctoral research will be discussed. The first two sections are dedicated to the thermal (II.2.3.1.) and photochemical TAD-based reactivity (II.2.3.2.), which are typically very fast with a predictable kinetic selectivity. The final section (II.2.3.3.) will briefly highlight some secondary modes of reactivity, which proceed much slower and often lack a clear selectivity. While the latter reactions are often negligible compared to those of interest for this work, they can often escalate to undesirable side reaction and are thus important to take into consideration during the design of TAD experiments. More in depth insights into the realm of TAD-based reactions, specifically with regard to the underlying mechanisms, are discussed in various review articles and book chapters.^{9, 15, 190-191}

II.2.3.1 Thermal reactivity

A general overview of the key TAD-based reactions that spontaneously occur at ambient temperatures (and often far below) are depicted in Scheme II.25. Given the interest of this work in the development of triggered triazolinedione-based reactions, particular attention will be given to those substrates that readily react with TADs, but of which the resulting adducts show dynamic behaviour upon heating.

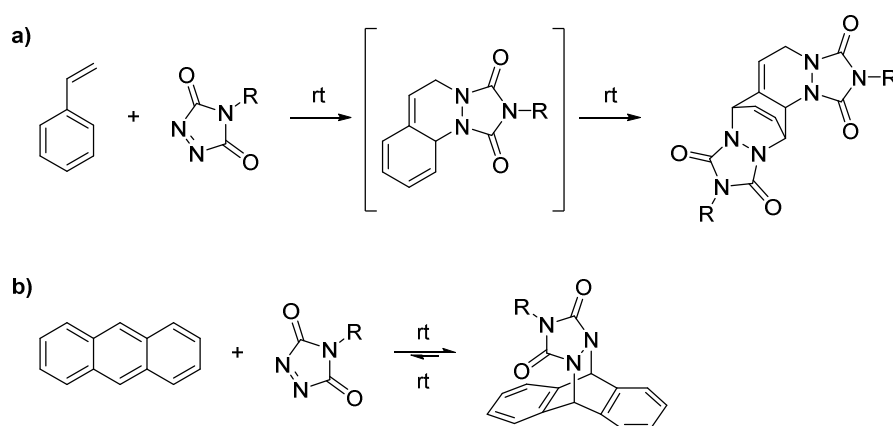


Scheme II.25. Overview of thermal TAD-based conjugation reactions. a) Diels-Alder reaction, b) Alder-ene reaction, c) [2+2] cycloaddition, and d) electrophilic aromatic substitution (S_{EAr}).

Diels-Alder reaction (Scheme II.25a)

The Diels-Alder reaction has emerged as one of the most efficient and widely adopted bond-forming reactions that allows for the simultaneous formation of two C-C sigma bonds and the introduction of up to four stereocenters.²⁶⁶ Regardless of the complexity of the resulting reaction products, the [4+2] cycloaddition proceeds with high levels of predictable regio- and stereoselectivity and is extremely tolerant to a variety of functional groups. Diels-Alder reactions usually proceed at elevated temperatures, but can be carried out at lower temperatures in the presence of a catalyst, e.g. Lewis acids.²⁶⁷

The Diels-Alder reaction is well-known for its immense substrate scope and was initially investigated with azodicarbonyl compounds (*cf.* II.2.1.), yet TADs were rather late entries as dienophiles (*cf.* Scheme II.25a).¹⁸⁵ This ultrafast, yet quantitative low-temperature reactivity towards a range of conjugated dienes has been extensively illustrated since, giving TADs the reputation as fastest dienophiles that can be isolated.²⁶³ In fact, the reactivity is so pronounced that calculations suggest the cycloaddition is concerted, but highly asynchronous whereby one C-N bond is formed far ahead of the other.²⁶⁴ Also with less reactive dienes, Diels-Alder reactions with TAD still proceed smoothly at ambient temperature. Indeed, the reaction with styrene even results in the quantitative formation of a 1:2 Diels-Alder adduct, although an equimolar substrate ratio is used (Scheme II.26a).¹⁸⁶



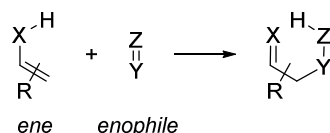
Scheme II.26. a) Diels-Alder cycloaddition reaction of TAD with styrene gives a 1:2 adduct via the formation of a highly reactive diene intermediate. b) The reaction of TAD with anthracene results in a self-contained dynamic Diels-Alder equilibrium at room temperature.

In theory, the bond-forming process in the Diels-Alder reaction can be reversed to release the original reaction partners.²⁶⁸⁻²⁶⁹ Examples of this reverse or retro-Diels-Alder reaction are well-known in organic synthesis to temporarily protect dienes,²⁷⁰ scavenge dienes from complex mixtures²⁷¹ or capture and subsequently release transient intermediates.²⁷² Reversible Diels-Alder systems have also gained much attention in polymer synthesis for the design of dynamic polymer architectures and covalent adaptable networks, leading to numerous bonding/de-bonding applications (*cf.* II.1.2)^{67, 273} Anthracenes are well documented substrates that enable retro-Diels-Alder reactions upon heating, which is driven by their regained aromaticity. With TAD as a

dienophile, the Diels-Alder reaction with anthracene already shows reversibility at room temperature, resulting in a self-contained dynamic equilibrium mixture that is very quickly established upon mixing both substrates (see Scheme II.26b).^{10, 259}

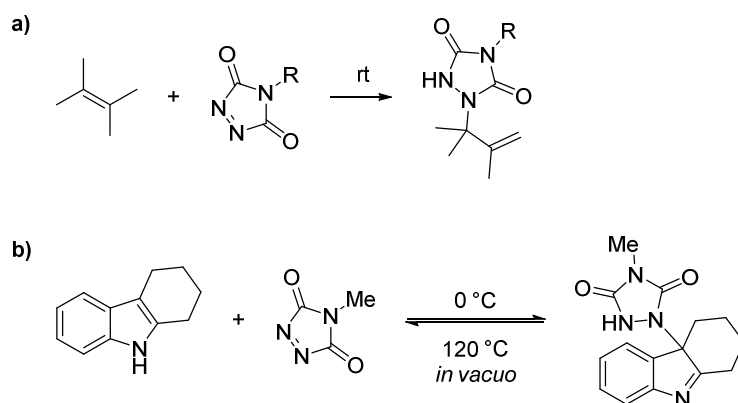
Alder-ene reaction (Scheme II.25b)

The Alder-ene reaction (often shortened to ene reaction) was first described by Kurt Alder in 1943 and comprises the bond forming process between an alkene that contains an allylic hydrogen and a double (or triple) bond, called the ene and enophile, respectively (Scheme II.27).²⁷⁴ The reaction was classified as an indirect substitution addition or ene synthesis during his 1950 Nobel lecture.²⁷⁵ It is a pericyclic reaction characterized by migration of the π -bond, formation of a new σ -bond and simultaneous shift of the allylic hydrogen, as depicted in Scheme II.27.²⁷⁶



Scheme II.27. General representation of an Alder-ene reaction (with X = C, N, O and Y=Z = C=O, C=N, C=S, C=C, etc.).

The Alder-ene reaction received considerably less attention than its Diels-Alder counterpart, presumably because of the unfavourable activation barrier that can be related to the highly ordered transition state with relatively poor orbital overlap.²⁷⁷ Alder-ene type addition reactions therefore often require quite harsh conditions (i.e. high pressure and temperatures above 200 °C) and are more commonly observed in intramolecular transformations, i.e. ene cyclisations.²⁷⁸ The inauguration of extremely reactive enophiles, however, has paved the way to more reliable and intermolecular ene reactions. The use of TADs as potent enophiles was established in its ambient temperature reactivity with plain mono-olefin substrates, e.g. 2,3-dimethyl-2-butene, to give the corresponding ene adducts in quantitative yields (Scheme II.28a).²⁷⁹ Furthermore, the reaction rate of TAD-addition was found to be highly dependent on the degree of the double bond substitution, i.e. the amount of inductively electron-donating groups, with terminal alkene substrates performing slowest (i.e. > 1 hour).²⁸⁰ As a result, the TAD-ene reaction kinetics (and selectivity) can be tailored, which was elegantly displayed in the modification and cross-linking of unsaturated fatty acids with varying degrees of double bond substitution (*vide infra*).¹³



Scheme II.28. a) The addition of TAD to a tetrasubstituted alkene swiftly forms the corresponding Alder-ene adduct at room temperature. b) The reversible Alder-ene reaction of TAD with indoles can be used as a protection group strategy since the volatile MeTAD can be removed upon heating *in vacuo* thereby releasing the initial indole substrate.

In contrast to the retro-Diels-Alder reaction, the reverse Alder-ene addition is only very rarely observed, owing to the high activation barriers that need to be overcome.²⁷⁵ Since most of the desired retro-Alder-ene reactions require near-pyrolysis conditions, the synthetic value of this backward transformation remained underappreciated.²⁷⁸ With the much more reactive TAD compounds as enophiles, however, the retro-ene reaction might be expected to be susceptible to much more reasonable temperature intervals. Indeed, Baran and co-workers reported on the – thus far only – thermoreversible TAD-ene reaction when they sought to protect an indole functionality,²⁸¹ a highly interesting scaffold in natural and synthetic biologically active compounds.²⁸² They found that the Alder-ene adducts of MeTAD with indoles were readily formed, even at 0 °C, and disassemble upon heating of the resulting TAD-indole adduct (see Scheme II.28b). Upon removal of the volatile MeTAD *in vacuo*, the initial indole substrate could thus be quantitatively recovered.

[2+2] cycloaddition (Scheme II.25c)

[2+2] cycloaddition reactions can generally be regarded as thermally forbidden processes because of geometrical constraints on the frontier molecular orbitals of the involved π -bonds to approach one another to achieve the required orbital overlap (Figure II.10a). Consequently, the concerted [2+2] cycloaddition of olefins is only observed under photochemical conditions (Figure II.10b) and today constitutes one of the most important and frequently adopted photoinduced transformations.¹³⁸ Nonetheless, in the case of less sterically constrained alkenes such as ketenes, the thermal [2+2] reaction is not orbital symmetry forbidden and does result in the concerted formation of cycloadducts via a perpendicular approach of the HOMO and LUMO (Figure II.10c). These ketene-alkene [2 π_s +2 π_a] cycloadditions lead to the formation of cyclobutanone products, which found a vast utility in total synthesis.²⁸³⁻²⁸⁴

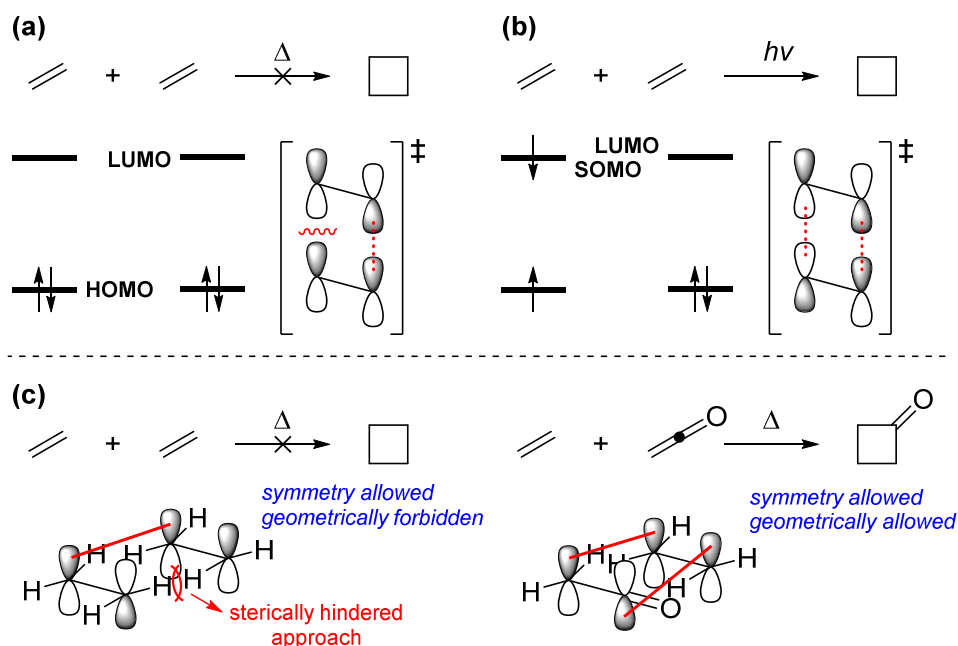
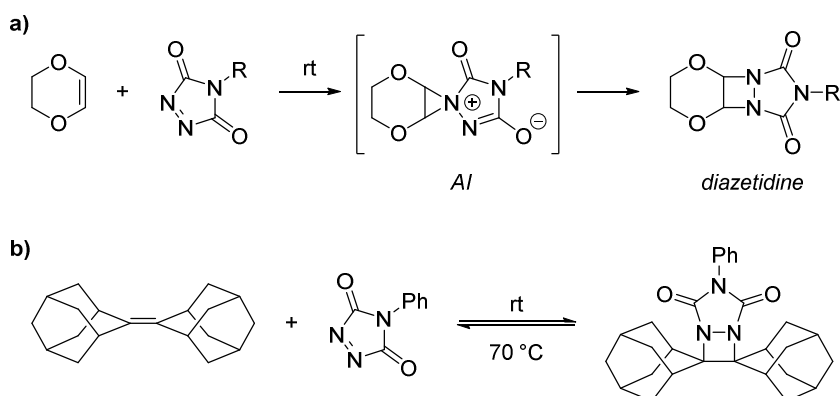


Figure II.10. a) Geometrically forbidden [2+2] cycloaddition under thermal conditions as a result of an unfavourable orbital overlap. b) Under photochemical conditions, however, the required HOMO-LUMO interaction is feasible and a [2+2] cycloadduct is formed. c) Although the thermal [2+2] cycloaddition is geometrically forbidden, it is not symmetry forbidden and can still proceed when a combination of a suprafacial and antarafacial orbital approach is feasible (simplified representation). Whereas this is not the case for the dimerisation of ethene because of steric hindrance (left), the reaction of an alkene with a ketene, for instance, can thereby still proceed thermally.

As a result of their frontier orbital arrangement (*cf.* Figure II.9), TADs are also capable to undergo antarafacial [2+2] cycloadditions with electron rich olefins, such as 1,4-dioxene, to give the corresponding diazetidines (Scheme II.29a).^{262, 285-287} Actually, the TAD-based [2+2] cycloaddition reaction proceeds via a stepwise, rather than a concerted, mechanism with the formation of an aziridinium imide intermediate (AI) that subsequently rearranges to the neutral four-membered ring.²⁸⁸⁻²⁸⁹ The existence of a biradical intermediate was ruled out since no acceleration of the [2+2] addition was observed upon visible light irradiation.²⁸⁶



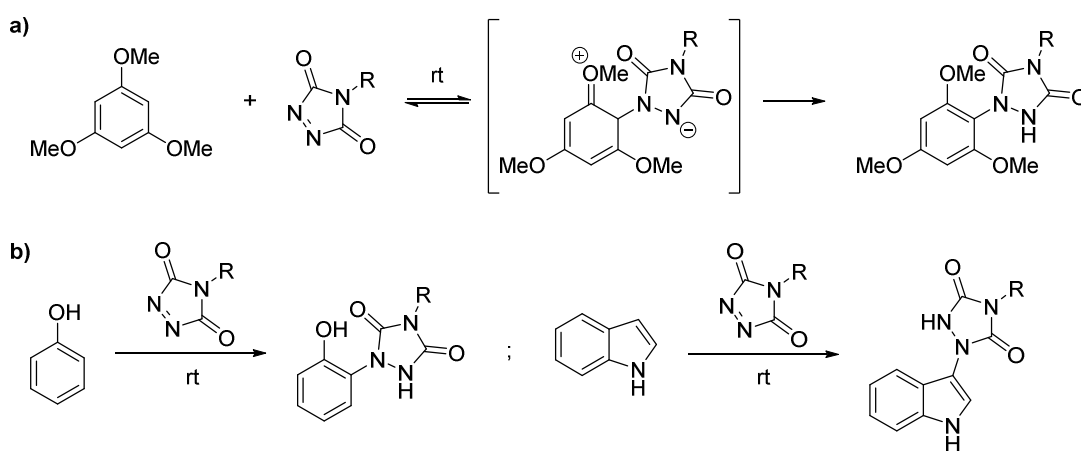
Scheme II.29. a) The reaction of TAD with 1,4-dioxene gives a thermal [2+2] diazetidine cycloadduct in a stepwise process via the formation of an aziridinium intermediate (AI). b) Even with the sterically demanding adamantylidene adamantane [2+2] cycloaddition proceeds quickly and the resulting adduct was shown to revert back to the original reagents upon heating.

An important consideration of TAD-based [2+2] cycloaddition reactions is that the olefin substrate should not contain (transferable) allylic hydrogens, otherwise an Alder-ene reaction will take place with the formation of the more thermodynamically preferred ene adducts. Nonetheless, the remarkable [2+2] reactivity of TADs was demonstrated by the quantitative addition to the bulky adamantylidene adamantane (Scheme II.29b).^{280, 288, 290} Interestingly, the resulting [2+2] adduct was found to be labile and reverted back to the reactants upon heating.

Electrophilic aromatic substitution (Scheme II.25d)

TADs also readily participate in electrophilic aromatic substitution reactions ($S_{E}Ar$) with (highly) activated aromatic substrates to give 1-aryl substituted urazoles. Although TADs are pronounced electrophiles, only a few studies on its $S_{E}Ar$ reaction have been reported. 1,3,5-trimethoxybenzene was found to be a relatively efficient substrate towards TAD, yielding the corresponding 1-substituted urazole in 74% yield in less than an hour (Scheme II.30a).²⁹¹ Hall and co-workers observed that the reaction times could be reduced when the reaction mixture was exposed to ambient laboratory light and although the formation of a charge transfer complex was postulated, its mechanistic role in the substitution reaction remained unclear.²⁹¹⁻²⁹² Recently, Breton and co-workers significantly expanded the substrate scope for TAD-based $S_{E}Ar$ to plain (poly)aromatic systems (e.g. substituted benzenes) by using trifluoroacetic acid as a catalyst.²⁹³⁻

294



Scheme II.30. a) TAD-based electrophilic aromatic substitution reaction with 1,3,5-trimethoxybenzene. b) phenol- and indole-type substrates also undergo electrophilic TAD-substitution reactions, although the process can also be regarded as an Alder-ene-type addition.

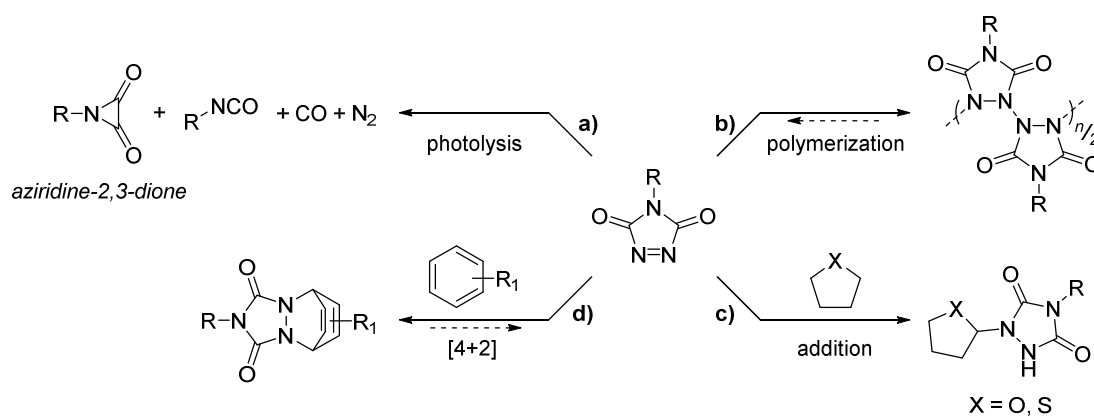
A highly interesting substrate that is susceptible towards TAD-reactions are phenols which, despite being less activated compared to trialkoxybenzenes, react much faster (i.e. within 5 minutes) and can be applied in aqueous media (see Scheme II.30b).^{193, 295} Consequently, TADs have been used in the site-selective and click-like bioconjugation with the phenolic side chain of native tyrosine residues.²²⁹ In a similar manner, the pending indole groups of tryptophan were modified with a variety of TAD reagents (Scheme II.30b).²⁹⁶ Although the reaction of TAD with phenols is listed here as an electrophilic aromatic substitution reaction, it can also be regarded as an Alder-ene reaction whereby the resulting ketone tautomerises to the enol with a

concomitant restoration of the aromaticity.¹⁵ Nonetheless, the underlying mechanism is still a matter of debate,²⁹⁷ the phenolic proton does seem to have an influence on the reaction course, as alkoxy-type substrates are outperformed by their phenol analogues.

II.2.3.2 Photochemical reactivity

In addition to the above discussed thermal TAD-based reactions, the truly exceptional reactivity of TADs is also expressed in their photochemical modes of reactivity. TADs exhibit rather unique photophysical properties which can be attributed to the presence of two very strong chromophoric groups, i.e. an azo and carbonyl moiety, that besides being in close proximity are also connected through conjugation.²⁹⁸ The absorption spectra of 4-substituted TADs reveal two principal electronic excitations in the UV- and visible region that are assigned to a $\pi \rightarrow \pi^*$ and $n \rightarrow \pi^*$ type transition, respectively.²⁹⁸ The latter transition is responsible for the typically observed red-purple colour of TAD reagents and is of low-energy, which allows for their visible light-induced excitation. As a result, TADs show fascinating reactivity when they are subjected to both UV- as well as visible light.²⁹⁹

In contrast to their thermal reaction pathways, TAD-based photoreactions are considerably less explored owing to a lack of information on their excited state behaviour.³⁰⁰ Following our interests to introduce light-triggered TAD-reactions in the field of polymer synthesis, this section is devoted to provide an overview of the few reported photochemical modes of TAD reactivity, which are depicted in Scheme II.31.



Scheme II.31. Overview of TAD-based photochemical reactivity. a) Photolysis, b) photopolymerisation, c) α -photoaddition to (thio)ethers, and d) light-induced [4+2] cycloaddition reaction.

Photolysis (Scheme II.31a)

TAD solutions in non-reactive solvents (e.g. CCl_4 , CH_2Cl_2 , MeCN, EtOAc) have been reported to readily decompose upon irradiation. Wamhoff and Wald carried out a detailed investigation on the photolytic behaviour of plain solutions of PhTAD in acetonitrile and dichloromethane.²⁵¹ They found that upon irradiation with UV-light ($\lambda > 313$ nm) the TAD compound decomposed into the corresponding isocyanate with the loss of nitrogen and carbon monoxide gas ($\text{R} = \text{Ph}$, Scheme II.31a). The kinetics of the photolytic degradation were monitored spectroscopically by

the disappearance of the $n \rightarrow \pi^*$ transition at $\lambda_{\max}(\text{MeCN}) = 532 \text{ nm}$ and up to 73 % of the phenyl isocyanate degradation product was detected after 8 hours of irradiation. Similar decomposition products were identified upon photolysis of MeTAD and PhTAD isolated in argon matrices at 10 K, although transients of 1-substituted aziridine-2,3-diones were also detected (Scheme II.31a, R = Me, Ph).³⁰¹ Critically, irradiation of the triazolinediones with visible light ($\lambda > 514 \text{ nm}$) resulted in much slower photodecomposition rates.

Unfortunately, the photolytic instability of TADs severely hampers the development of photo-induced TAD-based reactions. Indeed, TADs are advised to be stored in a dark environment and special caution should be taken when carrying out TAD-based reactions, even in the presence of ambient light. However, the common opinion that TADs cannot be used under any conditions of irradiation is a misconception. Instead, a careful assessment of the photolysis of TADs should be made keeping in mind the kinetic chemoselectivity aspect. In other words, the question that should be asked is whether TAD could react faster rather than it would decompose under those specific irradiation conditions.

Photopolymerisation (Scheme II.31b)

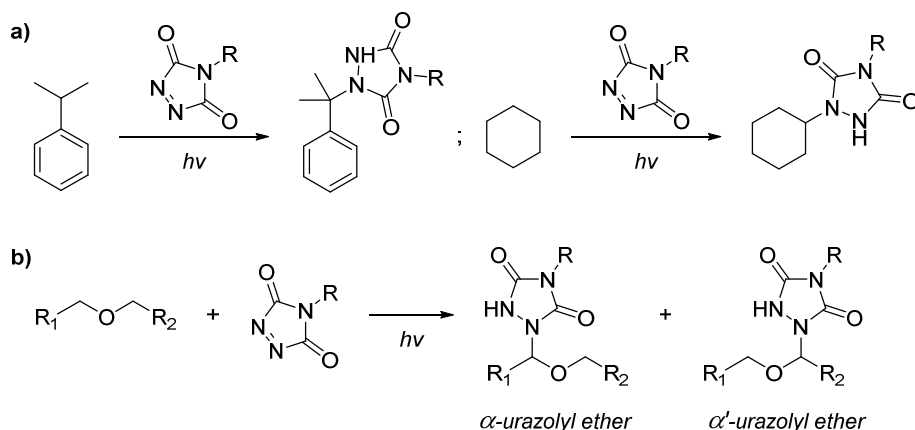
In 1970, Pirkle and Stickler reported the formation of an exotic polymer when they irradiated a carbon tetrachloride solution of 4-*n*-butyl-TAD (BuTAD) with visible light (R = *n*Bu in Scheme II.31b).³⁰² Vapour pressure osmometry of the resulting colourless solution pointed to the generated BuTAD homopolymer with an average molecular weight of 4200 Da. The repeating unit was identified based on infrared spectral data and an all-nitrogen-containing backbone polymer was postulated.

As can be expected from all-nitrogen backboned polymers,³⁰³ the TAD photopolymer was found to be thermally unstable and the initial red coloured monomer was slowly regenerated over time with up to 80% of the depolymerisation detected after several days.³⁰² Remarkably, the photopolymerisation was observed to be strongly solvent-dependent. Only those solvents in which the TAD compounds fluoresce (e.g. CCl_4 , CH_2Cl_2 , EtOAc) resulted in the successful formation of the TAD polymer. Aromatic solvents that quench TAD fluorescence were assumed to reduce the lifetime of the excited TAD, thereby inhibiting the photopolymerisation. In contrast to the 4-alkyl substituted TADs, aromatic analogues such as PhTAD failed to photopolymerise because of a self-quenching effect that is reflected by lack of fluorescence.²⁹⁹

Photoaddition (Scheme II.31c)

Besides the photopolymerisation, Stickler also found that excited TADs exhibit good hydrogen abstraction reactivity.^{302, 304} Indeed, hydrogen donor substrates such as cyclohexane and cumene undergo photoreaction with 4-substituted TADs to give the corresponding urazole adducts (see Scheme II.32a). Similar to the photopolymerisation, a difference in reactivity was observed between alkyl- and aryl-substituted TAD reagents, with PhTAD being significantly less reactive in the hydrogen abstraction process compared to MeTAD. Again, this was attributed to the fact

that PhTAD does not fluoresce, which indicates a rapid non-radiative depopulation of the excited state from which the photoaddition reaction is assumed to take place.²⁹⁹



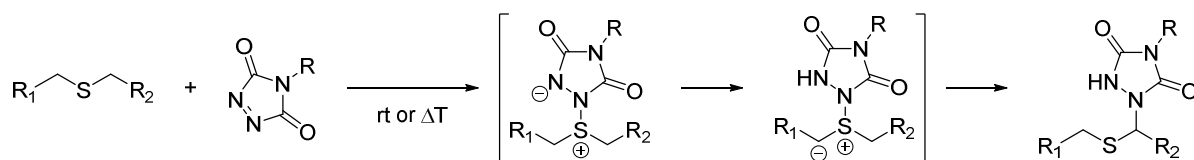
Scheme II.32. Examples of photochemical addition reactions of TAD. a) Hydrogen abstraction with cumene and cyclohexene. b) Photoaddition to aliphatic ethers.

A more common hydrogen-donor substrate can be found in ethers ($X = O$, Scheme II.31c). In fact, the photoreaction of diethyl azodicarboxylate (DEAD) with ethers was already studied by Cookson and co-workers in 1965.³⁰⁵ Wamhoff and Wald described a similar photoaddition reaction of TADs when conducting their photolysis experiments (*vide supra*) in ether solvents.²⁵¹ Rather than photodegradation, they observed the formation of α -C-H insertion side products, which is likely established via the initial hydrogen abstraction at the α -carbon next to the oxygen (Scheme II.32b).

Whereas cyclic ethers (e.g. tetrahydrofuran, 1,4-dioxane and crown ethers) yield the corresponding α -urazolyl ether adducts both under irradiation as well as upon heating, their acyclic analogues (e.g. diethyl ether) exclusively react with TAD under photochemical conditions.^{251, 306} Moreover, no difference in the mono-substituted product selectivity is noted when UV-light ($\lambda \geq 313$ nm) or green laser light ($\lambda = 515$ nm) is applied, although for unsymmetrical acyclic ethers two regioisomers are typically formed (i.e. α - and α' -urazolyl ether, Scheme II.32b).³⁰⁶ Alongside the expected reaction product, minor traces of the parent urazole (< 10 %) are also formed. This indicates that the photoaddition can in fact be regarded as a photoreduction process in which H-abstraction of the ether leads to a reactive urazolyl radical intermediate. The latter eventually recombines with the ether radical to give the overall α -addition product.³⁰⁷ It should be noted that with aromatic ether substrates (e.g. anisole and 1,3,5-trimethoxybenzene), no α -C-H insertion products but solely electrophilic aromatic substitution products are obtained.¹²⁰ Although this reaction is known to proceed thermally (*cf.* Scheme II.30a), it was witnessed to be significantly accelerated when subjected to light.²⁹²

Thioethers were shown to be superior hydrogen-donor substrates for TAD-based addition reactions compared to their ether analogues ($X = S$, Scheme II.31c). Indeed, Ando and co-workers displayed the formation of urazole insertion products upon simply mixing PhTAD with some

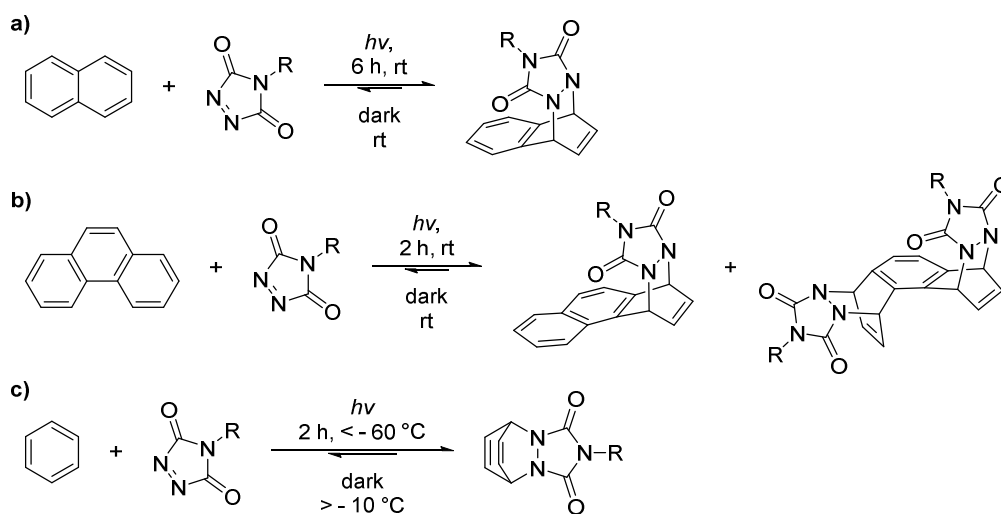
α -hydrogen-containing disubstituted sulfides at room temperature (Scheme II.33).³⁰⁸ No irradiation was required to affect the reaction, although only low yields of the addition products were detected after reaction times up to 48 hours. Heating of the reaction mixture was later shown to enhance the α -C-H insertion product formation.³⁰⁹ Even though the addition of TAD to the α -carbon of thioethers proceeds under thermal conditions, it is likely to be expected that the reaction also swiftly proceeds upon irradiation. A similar dual reactivity is well-studied for the thioether addition of DEAD, which is a well-representative acyclic TAD-mimic.³¹⁰⁻³¹³



Scheme II.33. Addition reaction of TAD with α -hydrogen containing thioethers.

Photo-induced [4+2] cycloaddition (Scheme II.31d)

Photochemical Diels-Alder reactions are allegedly forbidden by orbital symmetry according to the Woodward-Hoffmann rules,³¹⁴ yet mechanisms have been proposed that by-pass these rules in the case of very polar cycloadditions that have a substantial amount of charge-transfer character.³¹⁵⁻³¹⁶

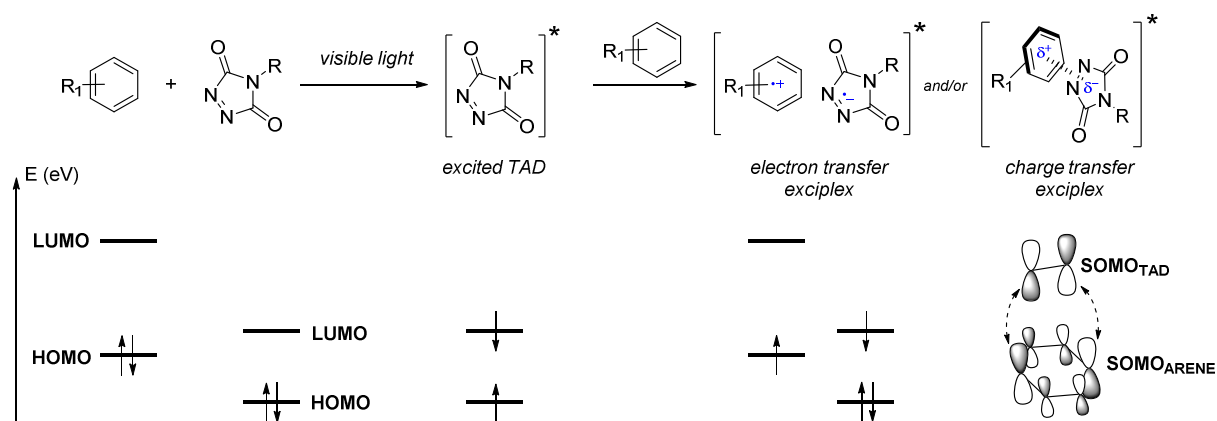


Scheme II.34. Visible light-induced TAD-based [4+2] cycloaddition reactions. a) Cycloaddition to naphthalene, b) phenanthrene, and c) benzene.

Kjell and Sheridan found that while MeTAD and naphthalene do not readily react upon mixing, visible light irradiation resulted in the formation of a new 1:1 addition product, which was assigned as the [4+2] cycloadduct (Scheme II.34a).^{300, 317} The formed product was thermally labile and quickly regenerated the starting materials upon slight heating. Several years later, Breton and Newton further investigated the photochemical TAD-naphthalene Diels-Alder reaction into more detail and assessed the effect of naphthalene substitution and solvent dependence on both the photochemical adduct formation as well as the thermal cycloreversion process.³¹⁸ Besides naphthalene, also phenanthrene was reported to undergo [4+2] cycloaddition of MeTAD upon

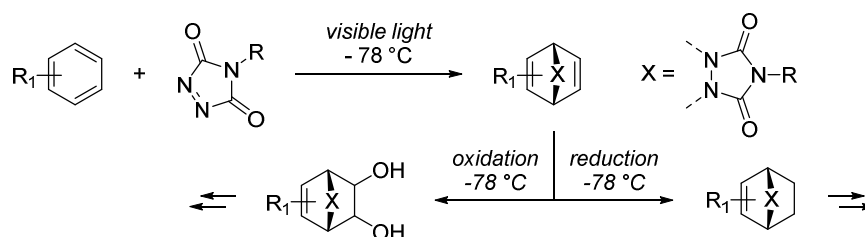
visible light irradiation, yielding a mixture of mono and double cycloadducts (Scheme II.34b).³¹⁹ Monocyclic aromatic substrates such as plain benzene were also successfully transformed into their corresponding TAD-cycloadducts but extremely low temperatures are needed (i.e. < -60 °C) in order to prevent rapid cycloreversion (Scheme II.34c).³²⁰

Although the reaction outcome of the photochemical TAD-based cycloadditions appears simple, the underlying mechanism is surprisingly complex with quantum yield data indicating the involvement of both excited singlet as well as triplet TAD in a concerted pathway.³⁰⁰ In any case, the electron deficient TAD reagent rather than the aromatic compound was found to be electronically excited upon irradiation with visible light.³²⁰ Based on the initial observations of Sheridan and co-workers, excited TADs likely react with arenes through exciplex formation of the electron transfer and/or charge transfer type (refer to Scheme II.35).³²¹⁻³²² The resulting exciplexes subsequently collapse into the resulting [4+2] cycloadducts, providing sufficient overlap of the single occupied molecular orbitals (SOMO). Importantly, electron transfer can only occur if both the HOMO and LUMO energies of TAD are within range of the aromatic substrate, which is indeed the case for the benzene-MeTAD reaction system.



Scheme II.35. Mechanistic representation for the visible-light-induced TAD-based [4+2] cycloaddition reaction with aromatic compounds. The excited state of TAD allows for the formation of an electron and/or charge transfer exciplex upon combination with the ground state arene, which eventually collapses to give the cycloadduct.³²¹⁻³²²

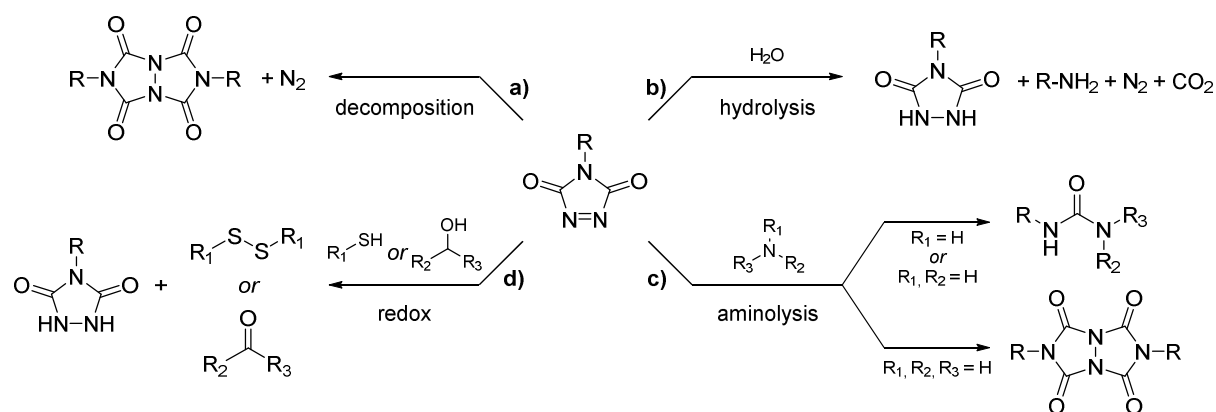
Despite the unique visible light-induced adduct formation of TADs with simple aromatic hydrocarbons, the synthetic utility of this transformation remained extremely little explored. In fact, the only application of TAD-based photochemical cycloadditions was found in the functionalisation of [60]fullerene and derivatives upon irradiation at 420 nm, albeit in very low yields.³²³ During the course of this doctoral work, however, the organic synthesis group of David Sarlah at the University of Illinois developed an extremely elegant procedure to transform simple and readily available aromatic building blocks into highly functionalized cyclohexenes and -dienes.³²² The key step in their procedure is the visible light-induced cycloaddition of TADs to arenes at -78 °C, followed by their *in situ* oxidation^{322, 324} or reduction³²⁵⁻³²⁶ (Scheme II.36).



Scheme II.36. Dearomative procedure developed by the David Sarlah group to transform simple aromatic building blocks into highly substituted cyclohexenes and cyclohexadienes. The key step is the visible light-induced TAD-based [4+2] cycloaddition.³²¹

II.2.3.3 Secondary modes of reactivity

As the two previous sections demonstrated, TAD moieties are highly reactive towards a range of electron rich substrates, both under thermal as well as photochemical conditions. Whereas the above discussed modes of reactivity are almost exclusively adopted in various research fields (e.g. organic synthesis, bioconjugation, polymer chemistry), TADs are susceptible to undergo many more reactions in the absence of a suitable reaction partner. These reactions are outlined in Scheme II.37 and are often observed as undesired decomposition or side reactions. Fortunately, the reaction kinetics related to these secondary reactions are much slower than the reaction types described in sections II.2.3.1. and II.2.3.2. Consequently, the primary TAD-based reactions still proceed surprisingly chemoselective, even in the presence of competing reaction partners. Nonetheless, it is crucial to take these secondary modes of reactivity in consideration during the design and application of TAD-based reactions.



Scheme II.37. Overview of secondary TAD-based reactions that are often observed as side reactions. a) Decomposition into a dimeric species upon heating, b) hydrolysis, c) aminolysis, and d) oxidation of thiols and alcohols.

As previously stated, the inherent reactivity of TADs directly translates to a limited stability which makes their isolation sometimes cumbersome. Whereas some TAD reagents cannot be isolated at all, most can be obtained in a crystalline form and are reported to decompose before melting.³²⁷ Yet, PhTAD was found to be relatively stable up to 160 °C, which is considerably higher than many other azocarbonyl compounds.²⁵¹ Diethyl azodicarboxylate (DEAD), for instance, explodes violently when heated to 100 °C.³²⁸ PhTAD has never been observed to be explosive but instead dimerises into a self-condensation product with the loss of nitrogen gas

when heated above 160 °C (Scheme II.37a).²⁵¹ TAD-based reactions thus have an upper temperature limit which is imposed by their thermolysis.

Next to the thermal stability, another important consideration when working with TADs is their moisture sensitivity.¹⁹⁷ Although some TAD reactions are successfully conducted in buffered aqueous media, TAD compounds are prone to slow hydrolysis with the formation of the corresponding urazole along with amine decomposition products (Scheme II.37b). In many occasions, hydrolysis can be avoided upon storage and usage of TADs under dry conditions. Primary alcohols also result in the decomposition of TADs, although more complex products are formed.^{190, 329-330}

Unlike water and primary alcohols, basic amines lead to a much more pronounced degradation of triazolinediones. Primary and secondary amines give rise to urea products whereas decomposition by tertiary amines proceeds via a less straightforward pathway with the ultimate formation of a dimeric aza-product (Scheme II.37c).^{260, 330} These degradation processes are rapidly observed and conducting TAD reactions in the presence of amines can therefore be quite troublesome. Careful design of the reaction conditions is thus required to suppress TAD aminolysis. Common strategies include the prior protonation of the amines by adjusting the pH of the reaction medium, or using substrates that are kinetically preferred over the present amines (e.g. Diels-Alder type substrates). In contrast, aniline is much more tolerant to TADs although it is known to undergo electrophilic aromatic substitution (*cf.* Scheme II.25d).³³¹

TAD compounds are easily generated via the oxidation of their urazole precursors (*cf.* II.2.2.4) and therefore also act as mild oxidants in redox reactions. Mainly thiols³³² and secondary alcohols³³³ are readily converted into the corresponding disulfide and carbonyl derivatives with the sacrificial formation of the parent 4-substituted urazole (Scheme II.37d). Moreover, the formed urazole by-product can easily be removed via filtration and retransformed into its TAD analogue by means of the conventional oxidation procedures.³³² As a result, clean and efficient TAD-mediated oxidation reactions are actually synthetically useful as they are typically carried out under neutral conditions.³³³

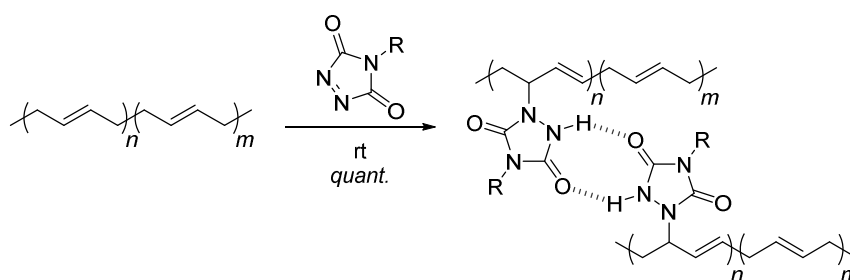
II.2.4 Applications of TAD-based reactions in polymer synthesis

Following the profound impact that TAD reagents made in organic synthesis in the 1960s, their remarkable room temperature reactivity towards unsaturated compounds quickly received interest from the polymer community as well. Primarily the Diels-Alder and Alder-ene type TAD-addition reactions emerged since the 1970s as elegant approaches for the modification of a variety of polydienes. Despite the ongoing interests to influence material properties via straightforward polymer modification reactions,¹⁹ TAD reagents somehow remained in the background. Recently, the assessment of their *click* behaviour^{1, 3} in our laboratories (Ghent University) revived the use of TAD-based reactions in polymer synthesis.⁷

In the remainder of this chapter that covers the chemistry of triazolinediones, a brief overview with regard to their application scope in polymer chemistry is provided. First, the use of TAD reagents as polydiene modifiers and crosslinkers is discussed into more detail and a distinct example is provided on how the exceptional reactivity of TAD allowed for the synthesis of new materials from low molecular weight unsaturated feedstocks (II.2.4.1.). Next, irreversible and reversible TAD-based polymer (bio)conjugation reactions are highlighted (II.2.4.2.), which enabled the synthesis of recyclable and healable polymer materials (II.2.4.3.).

II.2.4.1 Modification and crosslinking of polydienes and plant oils

The major application of TADs in polymer science, thus far, comprises the low-temperature modification and crosslinking of polydienes, which is particularly relevant in an industrial context.³³⁴⁻³³⁸ Saville was the first to introduce the atom efficient, site-selective and fast TAD-alkene reaction for the instantaneous crosslinking of natural rubbers in the early 1970s.²¹³ Later, Butler expanded the scope of TAD-based modification to other polydiene substrates, including polybutadiene, polyisoprene and copolymers thereof (e.g. random styrene-butadiene copolymers) (Scheme II.38).^{11, 192, 210} Although multiple TAD reagents can theoretically add to one repeating unit because the double bond is not consumed but shifted along the polymer backbone, subsequent reactions are usually kinetically disfavoured. Polymer modification degrees of 5 up to 100 % can be obtained upon TAD addition, resulting in either an elastic material at low conversions, or a rigid and amorphous one at higher conversions. The modified polymers were demonstrated to have higher glass transition temperatures (T_g) and improved solubility in polar media compared to their non-functionalized counterparts. Furthermore, inter- and intramolecular secondary interactions via hydrogen bonding of the highly polar pendant urazole moieties were observed at high degrees of modification (Scheme II.38), leading to changes in thermal and tensile strength behaviour.³³⁹⁻³⁴⁶

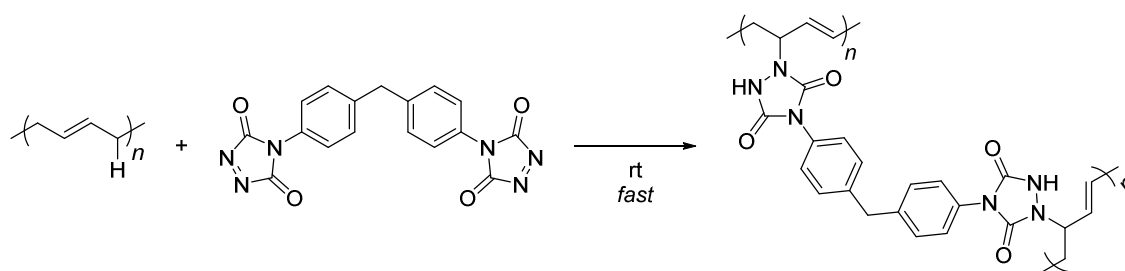


Scheme II.38. Room temperature modification of polybutadiene with TAD can result in the formation of secondary hydrogen-bonding crosslinking interactions.

In continuation of the urazole-based hydrogen bonding networks, polydiene modification with a range of additionally functionalized TAD moieties was explored to further influence the observed supramolecular behaviour.³⁴⁷ These additional functional groups are easily introduced onto the polymer backbone via the R-group of the TAD reagent. Hence, hydroxyl- and carboxylgroups were easily introduced. It was demonstrated that the addition of hydroxyl groups

via 4-(4-hydroxyphenyl)-triazolinedione resulted in the formation of extended hydrogen bonding zones rather than point-like linkages.³⁴⁶ Polydiene modification with 4-(4-carboxyphenyl)-TAD resulted in stronger hydrogen-bonding interactions with the resulting material shown to be equivalent to a covalently crosslinked material up to 80 °C.³⁴⁸⁻³⁵⁰ Moreover, the mechanical properties were found to be superior than the plain PhTAD hydrogen-bonded supramolecular networks.²⁴³

Besides monofunctional triazolinediones, also bivalent TAD reagents were widely adopted in reactions with polydienes, which resulted in the swift formation of highly covalently crosslinked polymer networks at room temperature in a few seconds.^{210, 351} As a result of these ultrafast crosslinking kinetics, however, achieving homogeneous material properties can often be troublesome, particularly when working under solvent-free conditions.²¹³ Nonetheless, the crosslinking of polybutadiene with 4,4'-(4,4'-methylenediphenyl)-bis-(1,2,4-triazoline-3,5-dione) (MDI-bisTAD, derived from the readily available corresponding diisocyanate, *cf.* II.2.2.) in solution was well-studied by Stadler and coworkers (Scheme II.39).³⁵² The reaction served as a model system to monitor cross-linking kinetics as a function of the gelation process and the initial molecular weight of the polymer matrix.³⁵³⁻³⁵⁴ In later studies, other polymer matrices³³⁷⁻³³⁸ and TAD crosslinking agents containing different spacer units, e.g. azo-dyes³⁵⁵ and poly(ethylene glycol),³⁵⁶⁻³⁵⁷ were also applied and different network properties were obtained.



Scheme II.39. Crosslinking of polybutadiene with bivalent TAD reagents readily occurs at room temperature in only a few seconds.

In contrast to solution modification of polydienes, also TAD-based surface modification reactions were studied and their influence on the surface properties was investigated. Surface treatment of vulcanized unsaturated elastomers, for instance, was found to enhance adhesion behaviour and improved resistance to peeling whilst the surface tack was reduced.³⁵⁸ TAD-modification was preferred over the state-of-the-art techniques (e.g. chlorination) because of the relative non-corrosiveness and non-toxicity of the TAD reagents used. A similar strategy of covalent surface modification was reported on electrospun styrene-butadiene-styrene (SBS) fibres to give tunable mechanical properties depending on the degree of PhTAD and MDI-bisTAD used.³⁵⁹⁻³⁶⁰ More recently, De Bruycker *et al.* reported on the synthesis of fluorinated TAD reagents which were covalently attached to commercial polybutadiene-containing polymers, including acrylonitrile butadiene styrene terpolymers (ABS), thereby drastically changing the surface wetting properties.³⁶¹

Following the assessment of the click behaviour of TAD-based reactions by the Polymer Chemistry Research group at Ghent University,⁷ the use of TADs as highly enabling tools in polymer science quickly expanded.¹⁵ In particular TAD-based post-polymerisation reactions are continuously introduced for a wide variety of olefin-containing polymers. For instance, both mono- and bifunctional TADs were efficiently employed to functionalise macromolecules obtained via both ring opening³⁶² and acyclic diene³⁶³⁻³⁶⁵ metathesis polymerisation (ROMP and ADMET, respectively) via the residual carbon-carbon double bonds.

A highly attractive example that truly demonstrates the powerful reactivity and versatility of triazolinediones was found in the modification and crosslinking of crude and readily available natural plant oils.^{13, 366} Even though plant oils as a feedstock contain a large number of unsaturations, only a limited number of chemical transformations, which often require harsh conditions and/or catalysts, can be affected. TADs, however, readily react with a wide range of plant oils already at room temperature. Because of the high conversions that are reached, bivalent TADs were shown to successfully transform the natural plant oil monomers into crosslinked materials (Figure II.11). Variable gelation kinetics and material properties were obtained depending on the plant oil composition, with higher fractions of polyunsaturated fatty acids leading to shorter gelation times and higher T_g materials. Next to low molecular weight fatty acids, also plant oil-based triblock copolymers were readily modified with TAD reagents, leading to improved mechanical properties such as tensile strength and elastic recovery.³⁶⁷

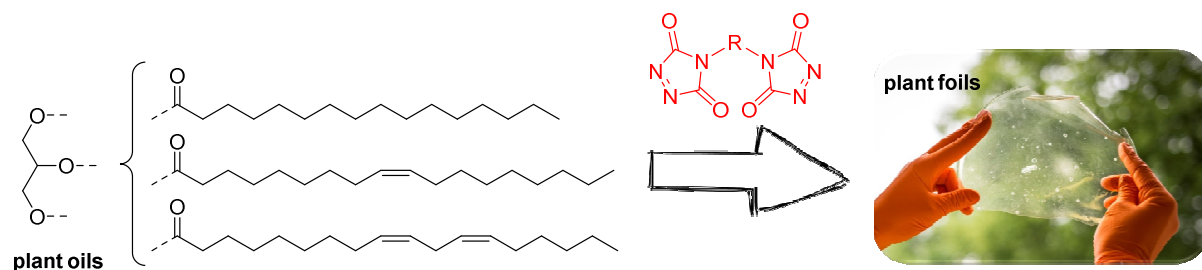


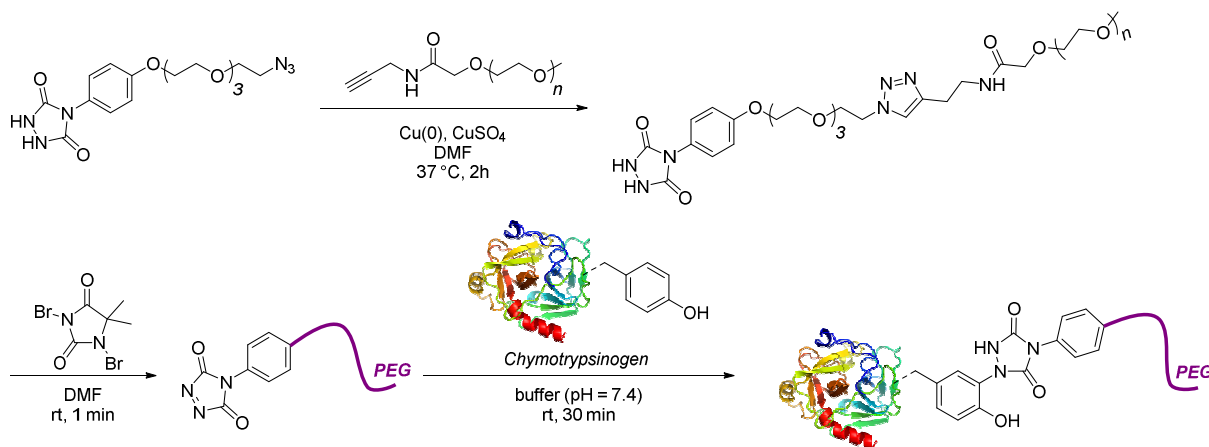
Figure II.11. TAD-based crosslinking of triglycerides into crosslinked plant foils via the Alder-ene reactions with mono- and polyunsaturated fatty acid residues.

II.2.4.2 Polymer- and bioconjugation of TAD-containing macromolecules

Besides the post-modification and crosslinking of polydienes, the click-like reactivity of TADs towards unsaturated substrates gained a lot of interest in more challenging polymer-bioconjugation and polymer-polymer ligation reactions. Although (functional) TADs have explicitly been used in bioconjugation strategies with tyrosine¹⁹³⁻¹⁹⁴ and (unnatural) furylalanine³⁶⁸ residues in peptides and proteins (refer to II.2.3.1), TAD-containing polymer ligations are only rarely explored.

Barbas and co-workers were the first to report a successful polymer-protein conjugation through TAD-based adduct formation in 2013.²²⁹ For this, a 5 kDa poly(ethylene glycol) (PEG) chain bearing a urazole end group was prepared via the copper-induced cycloaddition of an azide-

functional urazole precursor with an alkyne-containing PEG polymer (see Scheme II.40). Upon oxidation of the resulting urazole, the reactive TAD end group was thus instated, which was immediately clicked onto a chymotrypsinogen, a tyrosine-containing enzyme. The PEGylation reaction was carried out in a buffer solution at pH 7.4 and yielded predominantly the mono-addition product, which pointed to a site-selective modification.

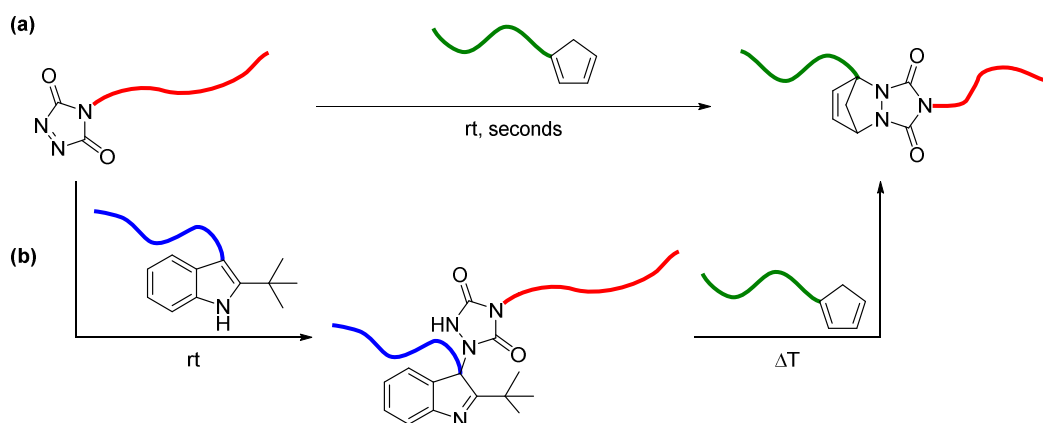


Scheme II.40. Synthesis of a urazole end functional poly(ethylene glycol) (PEG), its oxidation into a reactive polymeric TAD end group and subsequent PEGylation of Chymotrypsinogen via the TAD-tyrosine electrophilic aromatic substitution reaction.

Inspired by Barbas' seminal work, the Börner research group in collaboration with ours very recently developed an easy and efficient protocol to transform N-terminal amino groups of peptides into a reactive TAD-moiety.³⁶⁹ The resulting TAD-containing peptides were subsequently clicked onto a diene-end capped polycaprolactone to give peptide-polymer conjugates in a chemoselective manner. Almost simultaneously, the performance of the TAD-tyrosine bioconjugation between a poly(*N,N*-dimethylacrylamide) TAD-containing polymer and the bovine serum albumin protein was explored in detail.³⁷⁰ Not much later, Heise and co-workers investigated the crosslinking reaction of tyrosine³⁷¹ and tryptophan³⁷¹⁻³⁷² residues of some synthetically prepared polypeptides with bisTADs.

Until recently, the implementation of TAD chemistry for the modular synthesis of polymer conjugates, both with biologically relevant substrates as well as other polymeric structures, proved to be extremely challenging as a result of the rather inefficient and non-scalable synthesis of functional TAD compounds. Applications such as polymer-polymer conjugations therefore remained unexplored. A major breakthrough in this regard was the introduction of a versatile synthesis method to incorporate clickable TAD groups in a multitude of polymer segments that are prepared via reversible-deactivation radical polymerisations. Hence, TAD end functional polymers based on acrylate, acrylamide and styrene monomers became available that could be transformed into well-defined block copolymers in only a few seconds upon reaction with a conjugated diene-end capped macromolecular reaction partner (Scheme II.41a).^{7, 12} Importantly, when the conjugated diene on the polymeric substrate is replaced by an indole moiety, the resulting block copolymer can be debonded at elevated temperatures via the thermoreversible

TAD-indole linkage (Scheme II.41b). The liberated TAD-polymer can subsequently be trapped with a diene-polymer to give a newly formed irreversible polymer-polymer conjugate. Alternatively, the end standing diene reaction partner could also be incorporated into the polymer side chains on which the TAD polymers can be grafted onto, resulting in more complex macromolecular architectures such as bottlebrush copolymers.²³⁹ Future development of complex TAD-based polymeric architectures in combination with reversible linkages offers great potential in stimuli-induced topological macromolecular transformations.³⁰



Scheme II.41. a) Irreversible polymer-polymer conjugation occurs within seconds via a Diels-Alder reaction between a TAD and diene polymer end group. b) When an indole is installed at the polymer end instead of a diene, a reversible block copolymer formation becomes possible. Heating of the latter in the presence of a diene end capped polymer can eventually lead to a newly formed macromolecular conjugate.

II.2.4.3 Healable and recyclable polyurethane networks

Inspired by Baran's TAD-based click-and-unclick reaction with indoles, our research group at Ghent University described the combination of a highly thermodynamically driven forward addition reaction with a rarely observed kinetically feasible backward reaction.⁷ Normally, such a dynamic process is associated with either low addition yields, or uncontrollable free radical cleavage chemistry. The uniquely controlled dynamic nature of the TAD-indole reaction thus opened unprecedented applications in the field of polymer chemistry.

To demonstrate the unique properties that TAD-indole materials can possess, a linear polyurethane with pending indole side chains was synthesised.⁷ The latter was then crosslinked upon addition of a bivalent TAD reagent and the resulting polyurethane network, containing thermoreversible TAD-indole crosslinks, could be healed, recycled and reprocessed at elevated temperatures without the loss of its material properties. As a striking example, the initially crosslinked material could be broken into small pieces and placed in a mould, from which a pristine sample was retrieved after applying pressure for 30 minutes at 120 °C. In a follow-up study, polycaprolactone was included in the polyurethane matrix to enable shape-memory assisted intrinsic healing of TAD-indole-based materials.¹⁴ The networks were shown to recover from a 1 mm deep cut whereby the shape-recovery and the healing process are triggered in one single heating step.

II.2.5 Conclusions

Triazolinediones are highly reactive compounds that can swiftly participate in a wide range of reactions with simple (non-activated) electron rich olefin substrates. Rightfully so, they gained the reputation of being the most reactive dienophiles and enophiles that are to be isolated. In contrast, TADs are also given a reputation as ‘exotic’ reagents that are unstable, which often forms an obstacle in their general use. Nonetheless, simple non-functional TADs can be readily isolated whereas functional and more sensitive TAD analogues require to be generated and used *in situ*. Until today, the only practical route to synthesise TAD reagents is via the oxidation of their bench-stable urazole precursors, which can be quite cumbersome and marks a real challenge in tailored TAD synthesis (II.2.2).

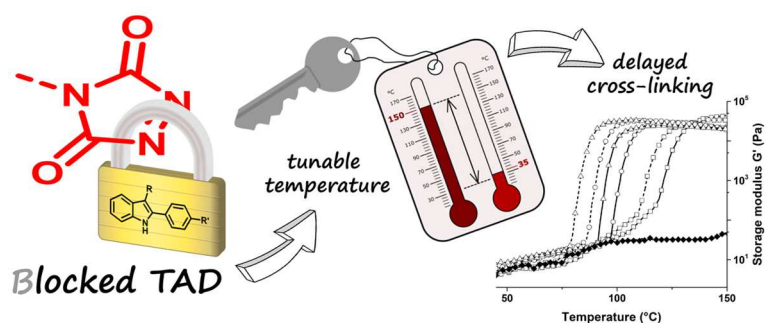
Fortunately, common TADs, including 4-alkyl-, 4-aryl- and a range of bisTADs are available on a large scale from simple bulk reagents. Many TAD reactions are therefore well-studied and were found to proceed with high levels of kinetic selectivity. Predominantly the low-temperature yet ultrafast Diels-Alder and Alder-ene transformations, even with less activated reaction partners, are well illustrated throughout the years (II.2.3.1). Moreover, these addition reactions meet the so-called click chemistry requirements and are therefore highly enabling tools in organic synthesis, (bio)conjugation and polymer chemistry (II.2.4). The interest of using TADs in these kind of applications has clearly shown a revival during the past decade, undoubtedly related to the ongoing search for modular click chemistry platforms. Apart from their renowned thermal modes of reactivity, the photochemistry of TADs is considerably less explored (II.2.3.2). Although it truly demonstrates their exceptional reactivity, light-induced TAD-reactions remain rarely applied, particularly in the field of polymer chemistry.

Despite the progress made over recent years, some fundamental TAD issues such as tailored synthesis, inherent instability and gaining control over their extremely high reactivity remain untackled. As this would considerably hamper the future widespread use of TAD chemistry, this gave a good benchmark for this doctoral work to develop triggered TAD-based reactivity to introduce both temporal and spatial control into the realm of TAD chemistry.

Chapter III.

Tunable thermoreversible blocking agents for triazolinediones

Brief motivation and content



The remarkable reactivity of triazolinediones (TADs) towards simple olefinic substrates highlights them as highly attractive click-like reagents in modular conjugation methods, in particular for polymer modification and crosslinking. Critically, the ultrafast reaction rates associated with TAD-additions result in handling issues and rather limited shelf life, whereas a particular concern for TAD-based polymer material applications is homogeneous network formation. In this chapter, an in-depth study is provided aimed at investigating indole compounds as promising blocking agents for TADs. Specifically, the thermoreversible TAD-indole reaction gives bench stable reagents at ambient temperatures, from which the initial TADs can be released *in situ* upon heating. A set of easy-accessible and rationally designed indole blocking agents are hence introduced and evaluated in terms of their TAD-blocking capabilities. Guided by mechanistic considerations, supported by theoretical calculations, various substitution patterns were incorporated onto the indole scaffold, thereby leading to a precise control over the temperature of deblocking, ranging from 35 °C up to over 100 °C. The established TAD-indole blocking platform enables the synthesis of a tailored TAD-dye demonstrator, which is used in the time-controlled modification of polydienes. Furthermore, delayed crosslinking of a one-pot diene-containing polyurethane system is illustrated via rheological measurement, even at low temperatures. Finally, an unprecedented orthogonal TAD-dye exchange from one indole to another is evidenced, without sacrificing the dynamic properties of the resulting adducts.

Adapted from

H. A. Houck, K. De Bruycker, S. Billiet, B. Dhanis, H. Goossens, S. Catak, V. Van Speybroeck, J. M. Winne, F. E. Du Prez, *Chemical Science* **2017**, *8*, 3098-3108.

H. A. Houck, K. De Bruycker, C. Barner-Kowollik, J. M. Winne, F. E. Du Prez, *Macromolecules* **2018**, *51*, 3156-3164.

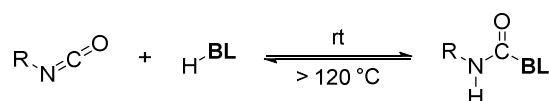
With permission from the Royal Society of Chemistry, and with permission from the American Chemical Society. Copyright 2018 American Chemical Society.

III.1 Introduction

This doctoral work aimed to develop triggered triazolinedione-based reactions that provide the feature to selectively switch TAD conjugation reactions on and/or off. It was anticipated that such controlled TAD reactivity would enable the rational design of functional and responsive polymer materials, as well as dynamic macromolecular systems, with tunable properties that can be accessed ‘on demand’ by the action of external triggers.

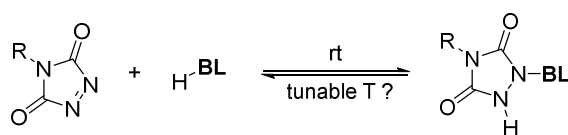
As discussed in Chapter II, triazolinedione compounds (TADs) possess an extremely high reactivity to electron rich substrates and TAD-based conjugation reactions often proceed very rapidly and are highly exergonic, even far below room temperature (*cf.* -78 °C for the instantaneous Diels-Alder reaction with cyclopentadiene).¹⁸⁵ The inherent reactivity of TADs also results in (ultra)fast crosslinking kinetics of polyunsaturated substrates (e.g. polydienes and plant oils), already at room temperature. Achieving homogeneous material properties can therefore be troublesome, especially when working under solvent-free conditions.²¹³ This chapter was hence devoted to gain a temporal control over TAD-based reactions through the development of latent TAD precursor moieties or ‘blocked TADs’ that can be activated *in situ* upon heating. Introducing such a concept in the realm of TAD chemistry is expected to not only resolve TAD-handling issues (i.e. limited stability and shelf-life), but yet also enable ‘on demand’ TAD-based polymer modification and curing applications.

Blocked isocyanate strategy...



H-BL = oximes, caprolactams, pyrazoles, ...

... as inspiration for blocked TAD reagents



H-BL = indoles

Scheme III.1. General representation of the blocked isocyanate strategy (left), which was taken as inspiration for the development of blocked triazolinediones (right).

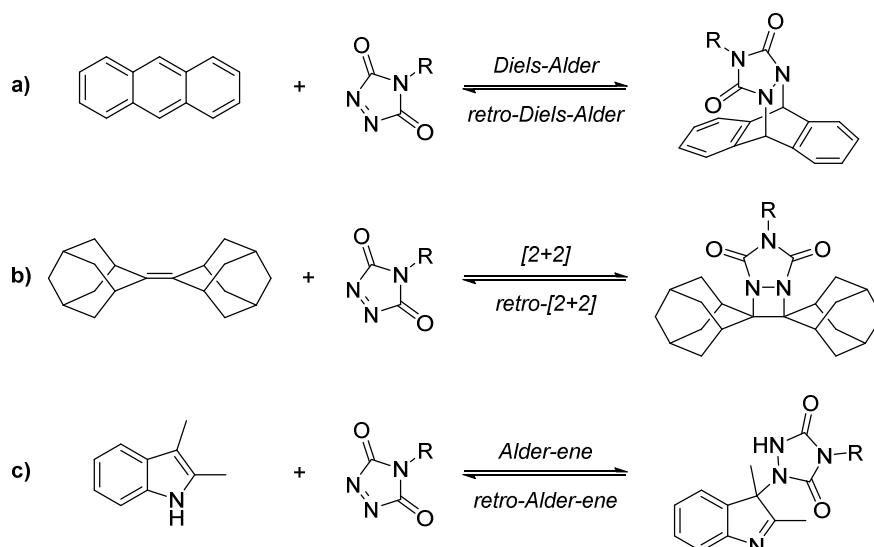
For the development of blocked TAD reagents, inspiration was taken from the well-established concept of blocked isocyanates, which was introduced to protect the reactive and moisture sensitive isocyanate functionality (see Scheme III.1).^{59, 64-65} The concept of blocked isocyanates and their application in triggered polymer synthesis has already been discussed earlier (*cf.* II.1.2.2), but in short the isocyanate moiety is reacted with suitable hydrogen compounds (e.g. oximes,⁶⁰⁻⁶¹ caprolactams,⁶¹⁻⁶² pyrazoles⁶³) to form bench-stable, inactive, adducts at room temperature. Heating of the blocked chemical (typically exceeding 120 °C) in the presence of a co-reactant, such as an alcohol or amine, then results in the *in situ* deprotection or ‘deblocking’ of the isocyanate functionality, making it available to react.

This chapter will provide an overview on the introduction, as well as the development of, blocked triazolinedione reagents. First, the few reported thermoreversible TAD-based reactions will be screened in terms of their potential blocking capabilities towards TAD reagents (III.2). After having identified substituted indole compounds as most promising blocking agents, novel indole substrates will be explored and a full account of their reversible reactivity with TADs will be given, including some theoretical rationalisations (III.3). Once a full understanding of the TAD-indole reaction is provided, additional structural alterations onto the indole core will be made in order to precisely tune the deblocking capabilities over a considerably broad temperature range (III.4). The practicality and importance of the established versatile blocked TAD platform will then be highlighted by two case studies in polymer sciences (III.5). Finally, two particular TAD-indole blocking systems will be selected that allows for a directed indole-to-indole transfer of TAD moieties, including a water soluble blocked TAD-dye demonstrator (III.6).

III.2 Potential candidates for suitable TAD-blocking agents

In order to develop a robust blocked TAD platform, potential candidates that can act as suitable blocking agents were first screened and evaluated. For this, in similarity to the blocked isocyanate concept, some important considerations need to be fulfilled in the context of TAD reactivity. At first, the blocking agent candidate needs to have a tendency to swiftly and quantitatively yield bench-stable TAD-adducts at room temperature. Furthermore, the resulting adducts need to be thermally labile to ensure the triggered *in situ* release of TAD reagents upon heating. Critically, the temperature of deblocking should not exceed 150 °C in order to avoid thermal degradation of the liberated TAD compounds (*cf.* II.2.3.3).

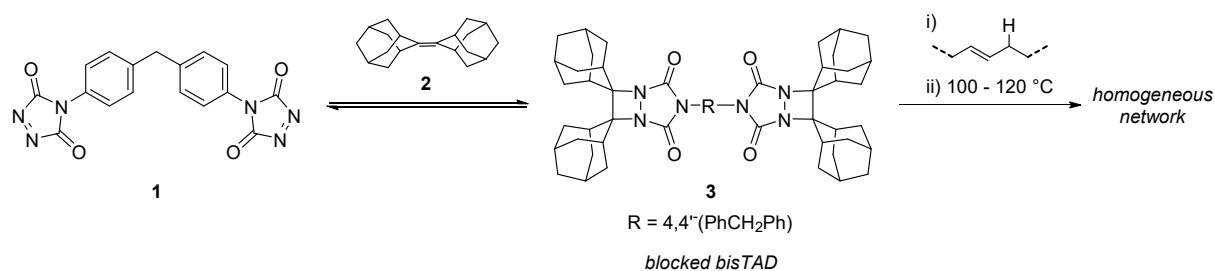
Only a few particular cases of TAD-based additions are known to enable the retro-reaction to dominate in a useful temperature regime (i.e. < 150 °C). The key to establish such thermoreversible TAD-systems lies in the careful selection of a complementary reaction partner with a moderate reaction enthalpy. Thus far, only anthracenes,³⁷³ adamantylidene adamantane²⁸⁸ and indoles²⁸¹ have been reported to give thermally labile TAD adducts (see Scheme III.2a-c, resp.). A certain driving force for the backward reaction, such as the release of steric constraints or regained aromaticity is thereby typically present. For a detailed discussion of the reversible TAD-systems, the reader is referred to the dedicated section in Chapter II that discusses the thermal reactivity of TADs.



Scheme III.2. Potential TAD-blocking reactions with (a) anthracenes, (b) adamantylidene adamantane and (c) indoles that result in the formation of thermally labile TAD-adducts.

All three TAD reactions depicted in Scheme III.2 give rise to TAD adducts that can be easily reverted to the corresponding starting reagents and thus form potential candidates to serve as TAD blocking reactions. Closer evaluation of the three systems was therefore made based on the efficiency of the initial, forward, TAD blocking reaction. In this regard, anthracenes were found to be disfavoured blocking agents since the formed TAD-anthracene Diels-Alder adducts are reported to already be reversible at room temperature (Scheme III.2a).³⁷³ Since the TAD deblocking reaction is already initiated at ambient temperatures, no temporal control over TAD reactivity would thus be provided. However, quantitative yields of the TAD-anthracene addition were made possible via substitution of the anthracene core with electron donating alkoxy groups.³⁷³⁻³⁷⁴ Nevertheless, such electron rich anthracene compounds suffer from chemoselectivity issues upon TAD addition since electrophilic aromatic substitution reactions also readily take place and render the adduct formation irreversible.³⁷³ Anthracenes in general are therefore not considered as suitable TAD blocking agents.

In contrast to anthracenes, adamantylidene adamantane and indole substrates both give clean and quantitative addition products with TADs at room temperature, whilst the corresponding retro-reaction is only induced at elevated temperature. In fact, a sole example of a blocked TAD crosslinking reagent has already been reported over 30 years ago by Jacobi and Stadler to allow for the controlled crosslinking of polybutadiene under solvent-free condition.³⁷⁵ For this, they made use of the thermoreversible (2+2) cycloaddition reaction of 4,4'-(4,4'-methylenediphenyl)-bis-(1,2,4-triazoline-3,5-dione) (MDI-bisTAD, **1**) with adamantylidene adamantane (**2**) to first protect the TAD-based crosslinker (see Scheme III.3). Upon heating a mixture of the polydiene and the blocked bivalent TAD compound **3** at 100 - 120 °C *in vacuo*, a homogenous network was formed, thereby illustrating for the first time the potential of thermally triggered TAD-based reactions in polymer science.



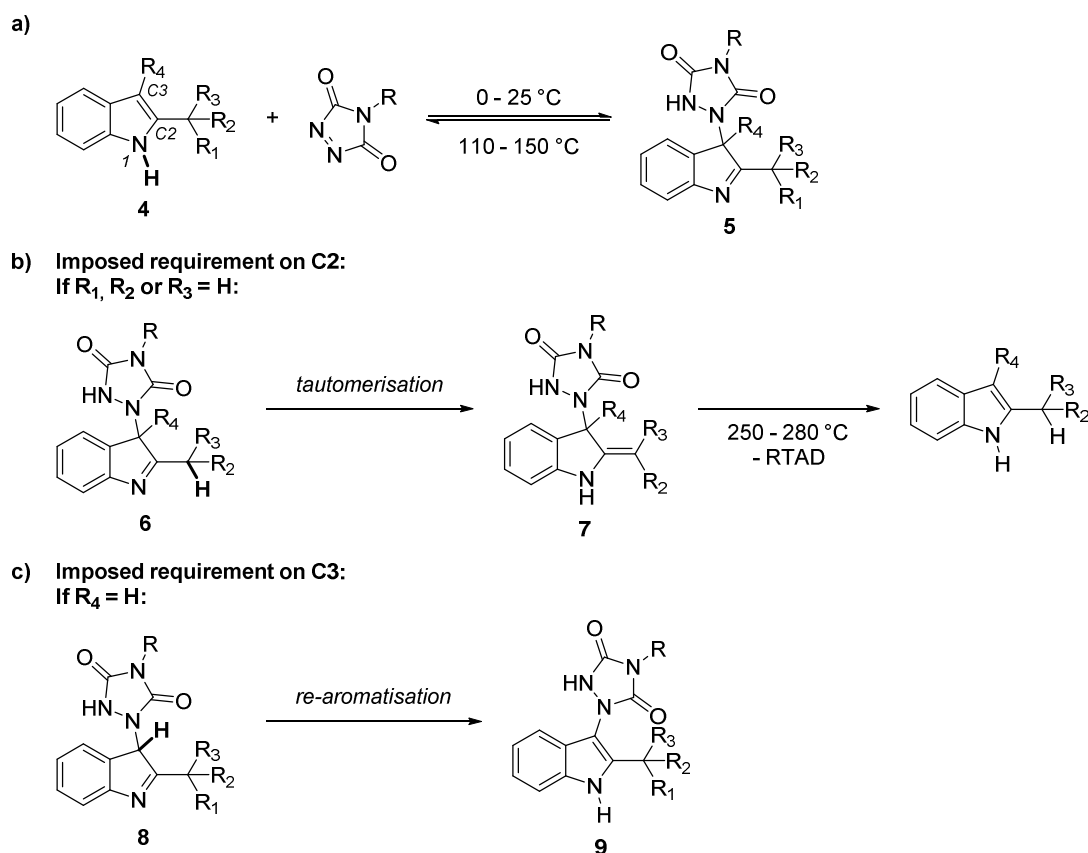
Scheme III.3. First and only reported blocking reaction of a TAD crosslinking agent with adamantylidene adamantane, enabling a homogeneous network formation upon heating.

Indoles represent an alternative class of promising blocking agents since they exhibit a similar dynamic behaviour at elevated temperatures when reacted with TADs yet are more readily available than adamantylidene adamantane. Indeed, indoles are straightforward heterocyclic scaffolds that are easily prepared from widely accessible starting reagents via a range of synthetic protocols, e.g. the Fischer indole reaction (*vide infra*).³⁷⁶ Furthermore, indoles have found a widespread use as fine chemicals in pharmaceuticals³⁷⁷ and fragrances,³⁷⁸ and are common additives in bulk polymer materials.³⁷⁹ Critically, the indole core structure provides an extensive freedom towards substitution, which opens the highly attractive possibility to precisely finetune the retro-TAD-indole reaction, as was already demonstrated with substituted anthracenes (*vide supra*). Since no such structural alterations that would influence the TAD reactivity are possible for the adamantylidene adamantane-blocking agent, indoles were regarded as the most promising class of TAD-blocking agents and are thus investigated in the current chapter.

III.3 In-depth investigation of the reversible TAD-indole reaction platform

With the identification of indole compounds to potentially serve as highly attractive blocking agents, the TAD-indole reaction was subjected to an in-depth investigation. The seminal work of Baran in 2003 provided a sound basis of some important structural indole characteristics in order to ensure a reversible nature of the TAD-indole system and allow for the backward reaction to proceed at appropriate temperatures.²⁸¹ Indeed, whilst the TAD-indole adducts are still swiftly formed at – and even below – room temperature (i.e. 0 – 25 °C), the required temperature to affect the retro-TAD-indole reaction strongly depends on the substitution pattern of the indole substrate (**4**, Scheme III.4a). Particularly the indole C2-position is of crucial importance. Initially, the Alder-ene reaction between TAD and indole **4** results in the formation of the imine product **5**, with a characteristic retro-reaction temperature in the range of 100 – 150 °C (refer to Scheme III.4a). If however, allylic protons are present in the indole C2-position, the formed imine **6** readily tautomerises into the corresponding enamine **7**, which is considerably more stable, i.e. up to 250 – 280 °C (see Scheme III.4b). To prevent undesired side reactions such as TAD decomposition, the subsequent formation of the enamine tautomer should thus be avoided. Additionally, reversibility of the TAD-indole reaction can only be ensured by the presence of a

substituent on the indole C3-position in order to exclude re-aromatisation of adduct **8** into **9** (Scheme III.4c). In conclusion, reliable TAD-reactive indole compounds should have an appropriate 2,3-substitution pattern in order to qualify as suitable blocking agents.

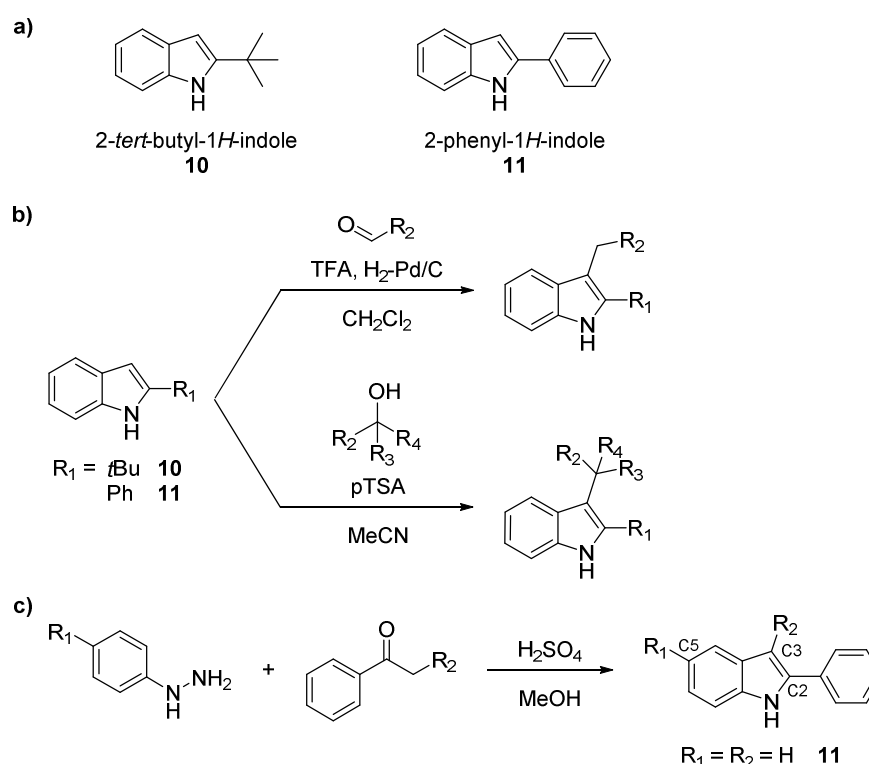


Scheme III.4. Overview of the imposed requirements on the indole substrate to ensure thermal reversibility of the resulting TAD-adducts at appropriate temperatures. a) Reaction of 2,3-disubstituted 1*H*-indoles **4** with TAD readily gives the imine adduct **5**, which reverts back to the starting reagents at temperatures above 110 °C. b) When allylic hydrogens are present on the indole C2-substituent, the formed TAD-indole imine **6** tautomerises to the enamine **7**, which is considerably more stable with retro-reaction temperatures above 250 °C. c) When the indole C3-position is not substituted, the TAD-indole adduct **8** will undergo re-aromatisation to an irreversible adduct **9**.

For the original exploration of the TAD-indole click reaction, 3-alkylsubstituted 2-*tert*-butylindoles (**10**, $R_1 = R_2 = R_3 = \text{Me}$ in Scheme III.4a) were used as model substrates whereby the quaternary indole 2-substituent preserves reliable TAD reactivity.⁷ The 2-*tert*-butyl-1*H*-indole building block from which these structures were derived is commercially available and can be prepared on a relatively large lab scale (> 50 g), but requires a multistep synthesis route and harsh basic conditions, which greatly affects the substrate scope.³⁸⁰ As a result, more easily accessible and cheaper indole building blocks were explored and rationally designed with regard to their TAD reactivity (III.3.1). Besides the forward TAD-indole reaction, also the retro-reaction with these novel indole substrates will be fully characterised and some important parameters will be introduced to evaluate the thermoreversibility and hence the efficiency of the TAD-deblocking reaction (III.3.2). Finally, theoretical rationalisation supported by Density Functional Theory (DFT) calculations will be provided, leading to a full understanding of the TAD-indole reaction.

III.3.1 Exploration of novel TAD-reactive indole substrates

Taking into account the imposed requirement for the indole C2-position not to contain allylic hydrogens to ensure selective imine adduct formation with TADs (*cf.* Scheme III.4b), 2-phenyl-1*H*-indoles **11** were identified as a more easily accessible, cheaper and versatile building block than the formerly applied 2-*tert*-butyl-1*H*-indole core **10** (Scheme III.5a). Interestingly, plain 2-phenyl-1*H*-indole **11** is a common stabiliser – often used to more than 1 wt %³⁷⁹ – in bulk poly(vinyl chloride) materials, including food packaging plastics. Moreover, the necessary 3-substituent on the indole (to retain thermoreversibility, *vide supra*) is easily introduced by exploiting the nucleophilicity of the C3-position, for example via a reductive alkylation with aldehydes or via an acid-catalysed alkylation with alcohols (Scheme III.5b).³⁸¹⁻³⁸²



Scheme III.5. a) Formerly applied and newly introduced TAD-reactive 2-*tert*-butyl- (**10**) and 2-phenyl-1*H*-indole (**11**) scaffolds, respectively. b) Substitution on the indole C3-position is readily performed by exploiting its nucleophilicity in a reductive alkylation with aldehydes or acid-catalysed alkylation with alcohols. c) Fischer indole synthesis allows for the one-step preparation of the 2-phenylindole scaffold and simultaneous introduction of versatile substituents.

Although commercially available on a large scale, an additional advantage of the 2-phenyl-1*H*-indole as newly projected TAD-reactive scaffold, is its alternative preparation from readily available aromatic hydrazine and ketone starting reagents via the well-known Fischer indole synthesis (see Scheme III.5c). In this way, a wide range of 2-phenylindoles were readily prepared via a one-step procedure, making it possible to introduce different substituents and additional functionalities at once, both on the indole C2/C3- and C5-positions, by simply changing the phenylketone or phenylhydrazine reaction partner, respectively. Along with the non-functional 2-*tert*-butyl-3-isopentyl-1*H*-indole **12**, the model substrate used in the original TAD-indole study,

its 2-phenyl analogue **13** and a range of differently 3-substituted 2-phenylindole derivatives **14-20** were synthesised on a multigram scale according to the above described methods (Figure III.1).

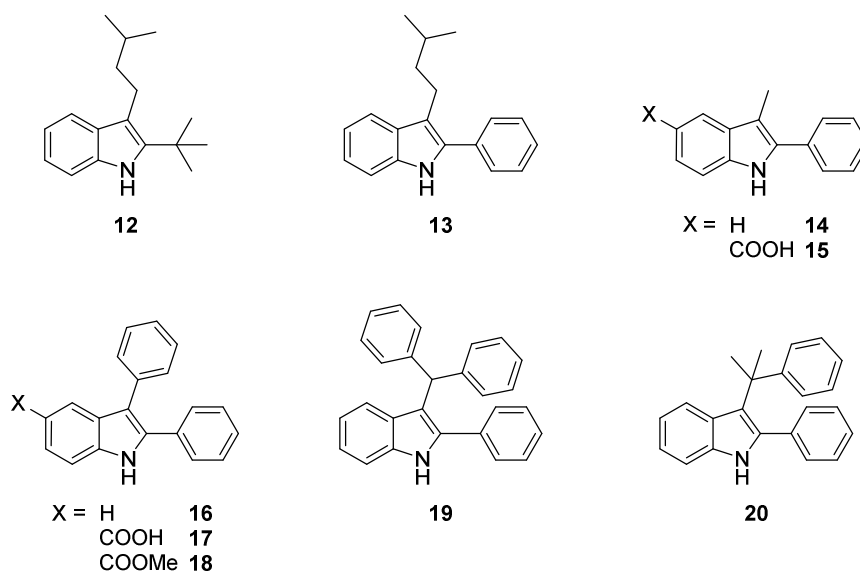


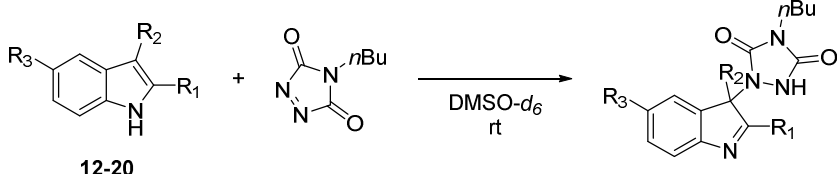
Figure III.1. Overview of the investigated 2,3-disubstituted indole substrates.

Following their synthesis, the reactivity of the new indole compounds towards TADs was next investigated. Prior to exploring the effect of the different substitution patterns on the reversibility of the TAD-indole reaction, the corresponding forward reaction was briefly investigated in terms of efficiency and chemoselectivity. For this assessment, 4-*n*-butyl-1,2,4-triazolinedione (BuTAD) was used as the model reagent of choice and qualitative information was readily obtained by the self-reporting nature of TADs, as their characteristic reddish colour disappears upon reaction.

At first, the effect of replacing the indole 2-*tert*-butyl group by a phenyl group was investigated into more detail. Thus, 2-phenyl-3-isopentylindole **13** (Figure III.1) was reacted with equimolar aliquots of BuTAD in deuterated DMSO- d_6 (0.04 M) and the reaction outcome was verified by proton nuclear magnetic resonance spectroscopy ($^1\text{H-NMR}$). The reaction was observed to go to completion in only a few seconds, as judged by the disappearance of the characteristic reddish TAD-colour, and resulted in a single 1:1 addition product (Table III.1). A slight acceleration of the TAD-addition was observed compared to the 2-*tert*-butyl-3-isopentylindole **12** counterpart, which went to completion in less than a minute. This minor difference in reaction kinetics is most likely attributed to the conjugation of the 2-phenyl group with the reactive indole 2,3- π -bond, making the indole substrate more electron rich. Similar results were obtained when the 3-isopentyl substituent was replaced by a much shorter methyl group, *cf.* 3-methyl-2-phenyl-1*H*-indole **14**. This latter result is quite important since indole **14** can be easily obtained via a Fischer indolisation in one high yielding step (*i.e.* > 93 %), thereby eliminating the need of an additional post-modification reaction (*cf.* Scheme III.5b for the synthesis of 2-Ph-3-isopentylindole **13**). Subsequently, 5-carboxy-3-methyl-2-phenyl-1*H*-indole **15** was explored to

assess the effect of an additional functionality on the indole C5-position, which was used in a later stage as a functional handle to incorporate the model 3-Me-2-Ph-indole compound (**14**) into polymeric systems. Again, no significant difference in reaction rate and efficiency with BuTAD was observed, despite the presence of an electron withdrawing substituent, which in theory might lead to a reduced nucleophilicity of the indole core. Thus, 2-phenylindoles were concluded to react in the orders of seconds with BuTAD, independent of the aliphatic chain length on the indole C3- or the presence of an electron withdrawing functional handle in the C5-position.

Table III.1. Indicative forward BuTAD-addition reaction times for investigated indoles **12-20** (0.04 M in DMSO- d_6 at room temperature).

				
	R ₁	R ₂	R ₃	Reaction time
12	<i>t</i> Bu	isopentyl	H	< 1 min
13	Ph	isopentyl	H	< 10 s
14	Ph	Me	H	< 10 s
15	Ph	Me	COOH	< 10 s
16	Ph	Ph	H	< 3 h
17	Ph	Ph	COOH	< 3 h
18	Ph	Ph	COOMe	< 3 h
19	Ph	CHPh ₂	H	no full conversion
20	Ph	CMe ₂ Ph	H	no reaction

In addition to the aliphatic 3-substituted substrates, aromatic groups were also easily incorporated onto the indole scaffold. Similar BuTAD addition tests were therefore also performed with 2-phenylindoles **16-20** (Figure III.1). As the steric bulk around the reactive indole C3-site is significantly increased compared to the previously investigated aliphatic substituents, a more pronounced effect on the reactivity with TADs could be expected. At first, the reaction of BuTAD with the sterically more demanding 2,3-diphenylindoles **16-18** was investigated. It became apparent that TAD-addition to the plain 2,3-diphenyl-1*H*-indole **15** in DMSO- d_6 required significantly extended reaction times to quantitatively form the TAD-indole adduct (i.e. up to 3 hours compared to a few seconds, Table III.1). Again, introducing a carboxylic acid or ester functional handle on the indole core did not influence the reactivity towards TAD reagents, as was qualitatively judged by a comparable efficiency (single reaction product) and forward reaction rate of BuTAD addition to indole **17** and **18**. Thus, although the reaction takes considerably longer, the introduction of a sterically constrained 3-phenyl group does not affect the TAD-indole reaction outcome.

When the steric bulk at the C3-position was increased even further, as for 3-benzhydryl-2-phenylindole **19**, the reaction with BuTAD did not go to full conversion as evidenced by the persisting red colour, even after prolonged reaction times (i.e. 48 hours). Instead, a dynamic equilibrium at room temperature was obtained (**19**:**[BuTAD-19]** = 74:26 in DMSO-*d*₆). Indeed, when the reaction mixture was subjected to column chromatography, isolated fractions of the resulting colourless **BuTAD-19** adduct quickly reinstated a reddish TAD-colour upon standing. By introducing tertiary substituents on the indole C3-position, here illustrated by 2-phenyl-3-(2-phenylpropan-2-yl)-1*H*-indole **20**, not even a trace of the expected BuTAD adduct was detected at room temperature, nor at lower or elevated temperatures.

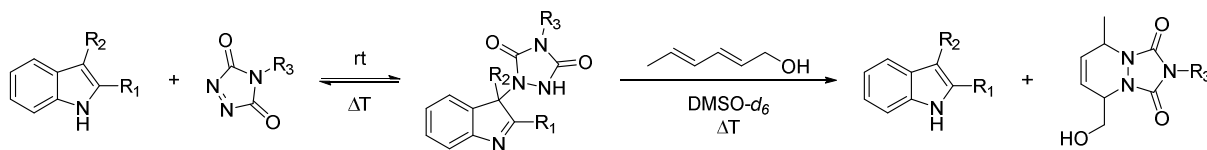
III.3.2 Kinetic thermoreversibility studies

Encouraged by the observed differences in the forward TAD-addition reaction rates, yet the retention of their ‘click’ efficiency, also for the sterically hindered indole substrates (i.e. quantitative yields and single reaction product under equimolar conditions), the thermoreversibility of the newly introduced BuTAD-indole adducts was next investigated.

Although ¹H-NMR spectroscopy was identified as the perfect way to study the forward BuTAD-indole reaction, the analysis technique failed to deliver information on the retro-addition process as no traces of the BuTAD or indole starting compounds could be detected after heating the adduct. A similar problem arose during high temperature online NMR measurements. Most likely, the TAD-indole system is far too favoured over the starting reagents and/or equilibration is far too rapidly. This is indeed confirmed by the absence of a red colour when a solution of the BuTAD-adduct with 3-methyl-2-phenylindole **14** is heated. In contrast, such a red colouration was observed with the more sterically hindered and significantly slower 2,3-diphenylindole **16** (*cf.* Figure III.1). Nonetheless, a general strategy was required to enable a comparative study of the dynamic behaviour of the different TAD-indole systems.

To resolve the issue of fast TAD-indole (re)equilibration, a straightforward analytical protocol was designed to kinetically examine the backward TAD-indole reaction. The key to success for the kinetic thermoreversibility studies was the subsequent addition of a slight excess of the conjugated diene *trans,trans*-2,4-hexadien-1-ol (HDEO) to a solution of the BuTAD-indole adduct under investigation (see Scheme III.6). In this manner, a kinetic and thermodynamic trap for triazolinediones is instated which irreversibly quenches any TAD that is liberated from the initial TAD-indole adduct via a Diels-Alder reaction. Thus, when the TAD-indole adduct is heated and opens up, the released TAD has two options, i.e. either to recombine with the original indole or to be trapped in the irreversible TAD-HDEO adduct. Critically, the Diels-Alder reaction kinetics exceed the forward TAD-indole addition rate by several orders of magnitude (i.e. $k_{\text{TAD-HDEO}} > 10^3 k_{\text{TAD-indole}}$), thus neglecting the TAD-indole recombination reaction at elevated temperatures. Hence, the amount of TAD-HDEO adduct that is formed within a certain time period upon heating can be directly related to the total amount of TAD molecules that haven

been released from the TAD-indole adduct. As a result, valuable information concerning the retro-reaction barriers can be obtained.



Scheme III.6. General reaction scheme of the kinetic thermal reversibility study used to investigate the TAD-indole retro-reaction.

By means of illustration, the kinetic thermal reversibility study for 3-methyl-2-phenyl-1*H*-indole **14** is here discussed in more detail. At first, equimolar solutions of the indole and BuTAD reagents were prepared in dichloromethane (0.2 M) and mixed together at room temperature to quantitatively form the corresponding TAD-indole adduct **BuTAD-14** (Figure III.2a). An important advantage of using dichloromethane, especially with the more sterically hindered indole substrates (*vide supra*), is the faster TAD-addition times compared to the adduct formation in DMSO-*d*₆ (*cf.* Table III.2) Moreover, the volatile solvent is easily removed *in vacuo* to give the TAD-indole adducts as solid residues. The isolated **BuTAD-14** adduct was then dissolved in DMSO-*d*₆ (0.04 M) and mixed with a slight excess of HDEO in order to quantify the amount of released BuTAD during the thermal treatment (Figure III.2b). The resulting [TAD-indole]-HDEO solutions are eventually heated for 15 minutes at well-defined temperatures in the range of 40 - 160 °C, with 10 °C intervals, and monitored via offline ¹H-NMR spectroscopy.

A selection of the NMR spectra obtained during the reversibility study of **BuTAD-14** is depicted in Figure III.2c. Several well-resolved NMR signals could be followed during the course of the retro-TAD-indole-reaction and allowed to monitor the equilibrium mixture as a function of temperature. For instance, the urazole N-H signal (*a*) of the **BuTAD-14** adduct decreased at the expense of the N-H signal (*m*) with a typical down-field resonance shift that is associated with the released indole **14**. Simultaneously, the increase in intensity of signal (*s*) indicated the formation of the **BuTAD-HDEO** Diels-Alder adduct, which can be directly correlated to the amount of *in situ* released TAD at the relevant temperature. Despite the clear shift in the *NH* resonances, the urazole proton of **BuTAD-14** is quite acidic (p*K*_a ≈ 5) and is thus prone to exchange reactions which not only results in characteristic peak broadening, but also affects the integration values. Therefore, the resolved aromatic signals (*c*) and (*o*) of the TAD-indole adduct and the released indole, respectively, were preferred to set the integration values that correspond to the amount of **BuTAD-14** and **14** in the reaction mixture. In the particular cases that signal (*o*) overlaps with other signals in the aromatic region, the resolved resonance peaks denoted with (*) could be used instead to determine the indole concentration. Importantly, all signals in the final spectrum of the reversibility study perfectly correspond to a reference spectrum (Figure III.2c, bottom), obtained by mixing indole **14** with a preformed **BuTAD-HDEO** adduct at room temperature. Thus, the occurrence of any side reactions at the applied temperatures can be excluded.

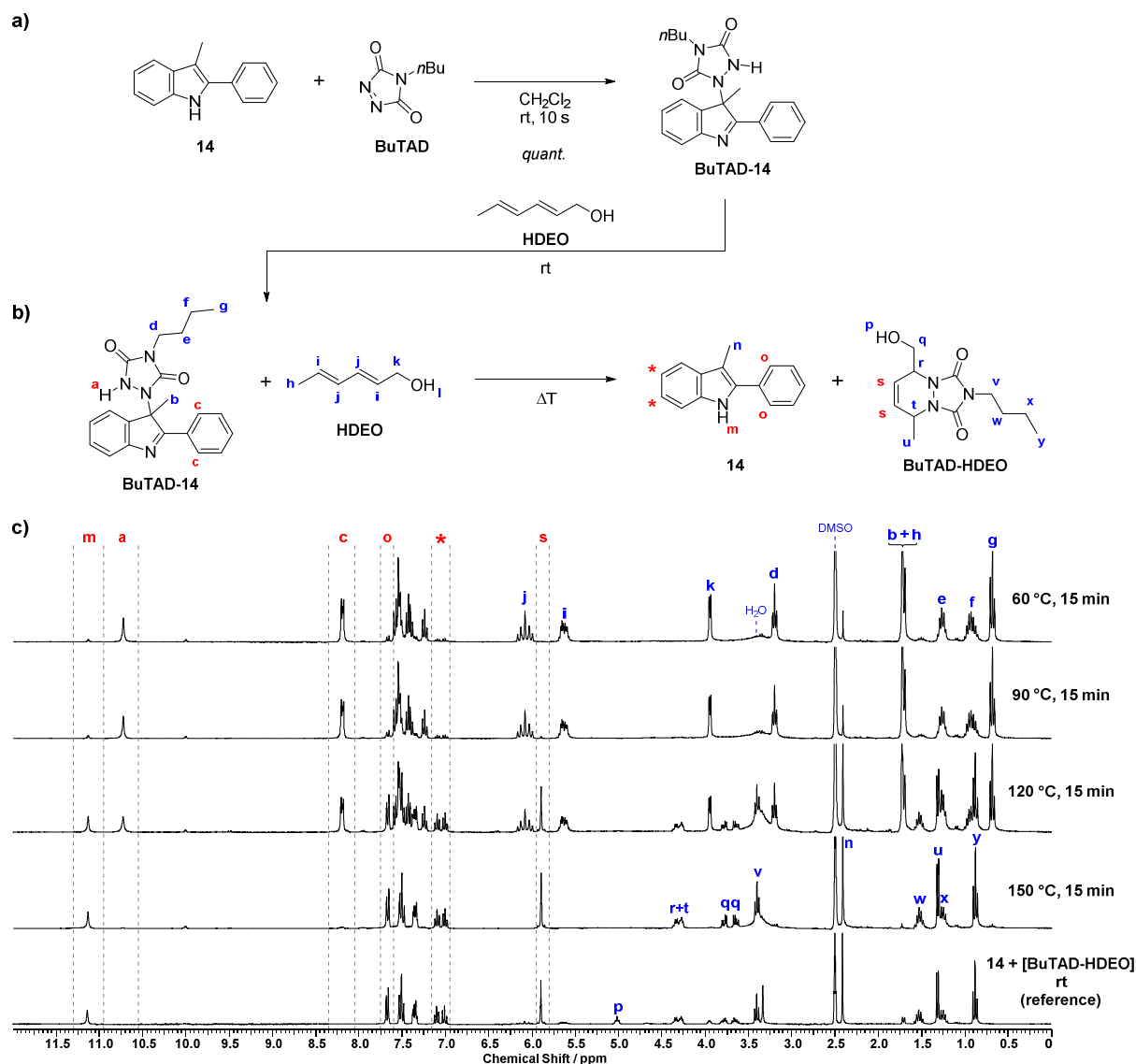


Figure III.2. a) Reaction of 3-methyl-2-phenyl-1*H*-indole **14** with BuTAD to quantitatively form the corresponding TAD-indole adduct. b) Addition of a slight excess of HDEO allows for the quantitative analysis of the TAD-indole retro-reaction by trapping the liberated TAD upon heating in the irreversible **BuTAD-HDEO** Diels-Alder adduct. c) Integration of well-resolved signals in the resulting offline ^1H -NMR spectra after 15-minute heating periods allows for the determination of the equilibrium concentrations, from which a kinetic thermal reversibility profile can be deduced.

By taking the integration ratios of the well-resolved NMR signals for each TAD-indole blocking system under investigation (i.e. indoles **13-18**), including the pioneering 2-(*tert*-butyl)-3-isopentyl-1*H*-indole **12**, the respective TAD-indole equilibrium mixtures were fully quantified as a function of temperature and their so-called thermal reversibility profiles could be deduced (*cf.* Figure III.3). These profiles represent the total amount of TAD that has been released or ‘deblocked’ from its corresponding indole adduct in a 15-minute period at a given temperature. It should be stressed that this is indeed a kinetic measurement whereby the fraction of deblocking corresponds to the amount of TAD-indole adducts that have at least opened up once. Since the opening of the TAD-indole adduct is a first order fragmentation, and the reverse TAD-indole reaction can be neglected compared to the TAD-trapping reaction (as discussed earlier), the

thermal reversibility profiles readily display the temperature at which the TAD-indole combinations have a half-life time of 15 minutes (i.e. $t_{1/2} = 15$ min, the intersection of the sigmoid curve with the 50 % deblocking line). To enable a better comparison between the different TAD-indole systems, a ‘TAD deblocking temperature’ is introduced as a useful indicator and defined as the initial temperature at which 5 % of the indole has been released over a 15-minute period (i.e. $t_{1/20} = 15$ min). In fact, this deblocking temperature can be regarded as a macroscopic reversibility temperature whereby the TAD-indole reaction becomes dynamic enough to show stress relaxation or self-healing properties in specific polymer material applications.⁴⁰ Additionally, the obtained data points allow for the determination of the experimentally observed first-order deblocking reaction rate coefficient k_{obs} and activation energies (by fitting $\ln k_{\text{obs}}$ vs T^{-1}) that are associated with the TAD-deblocking reaction.

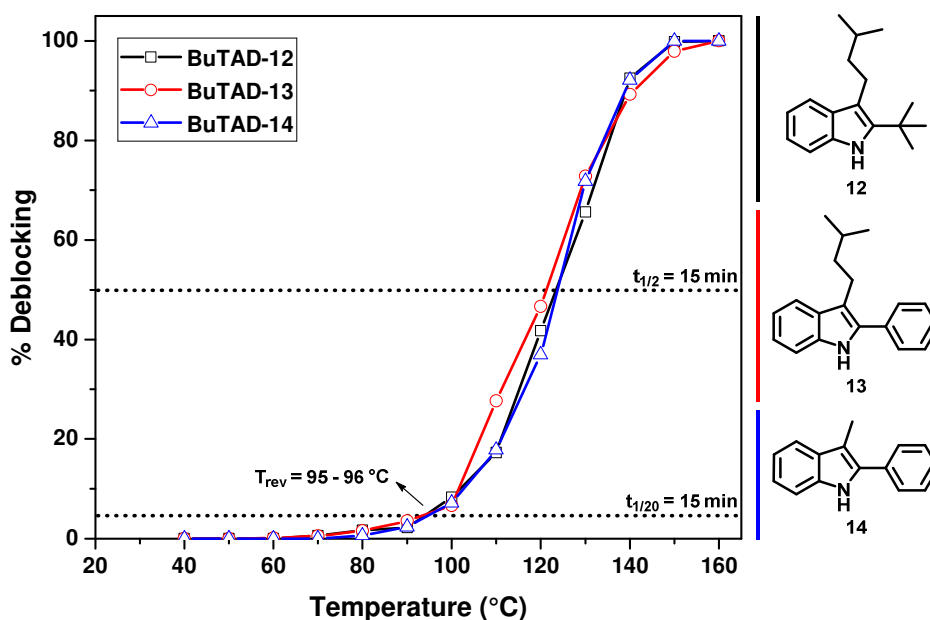


Figure III.3. Thermal reversibility profiles of the BuTAD adducts with 2-(*tert*-butyl)-3-isopentyl-1*H*-indole **12** and its 2-phenyl-1*H*-indole derivatives **13** and **14**, reflecting the amount of deblocking at distinct temperatures after a 15-minute heating period in the presence of *trans,trans*-2,4-hexadien-1-ol ($[\text{BuTAD-indole}]_0 = 0.04$ M, $\text{DMSO-}d_6$).

For the 2-*tert*-butyl-3-isopentylindole **12** used in the original TAD-indole studies, then BuTAD-deblocking reaction has a half-life of 15 minutes at 121 °C and a corresponding activation barrier of 116.5 ± 6.0 kJ mol⁻¹ (refer to Figure III.3 and Table III.2). Despite the minor differences in their forward BuTAD-adduct formation, the reversibility profiles of 2-phenyl-3-isopentylindole **13** and 3-methyl-2-phenylindole **14** were found to be superimposable with the one of reference indole **12**, and showed deblocking temperatures of 95 °C (for indole **13**) and 96 °C (for indole **14**), which were in perfect agreement with the observed 95 °C for reference indole **12** (Figure III.3). Kinetic fitting of the first order deblocking reaction gave statistically indistinguishable activation energies (Table III.2). It can thus be seen that replacement of the indole C2-substituent

from a *tert*-butyl to a phenyl group (**12** -> **13**) does not affect the dynamic behaviour of the TAD-indole system. Furthermore, alteration of the size of the 3-alkyl group (isopentyl vs. methyl, i.e. **13** -> **14**) also does not significantly influence the deblocking reaction barriers. Nonetheless, the findings so far allowed for the identification of 2-phenylindoles as preferred TAD-reactive indole substrates because of their more straightforward synthetic design and broader availability.

Table III.2. Overview of the investigated indole-blocked BuTAD-systems with their indicative forward TAD-addition reaction time (0.2 M, CH₂Cl₂, room temperature) as well as their deblocking temperature (5 % release), half-life temperature and experimentally observed activation energies ($E_{a, \text{obs}}$) for a 15-minute heating period ($[\text{BuTAD-indole}]_0 = 0.04 \text{ M}$, DMSO-*d*₆).

R ₁	R ₂	R ₃	Reaction time	Deblocking T (°C)	Half-life T (°C)	$E_{a, \text{obs}}$ (kJ mol ⁻¹)
12	<i>t</i> Bu	isopentyl	< 2 min	95	123	116.5 ± 6.0
13	Ph	isopentyl	< 1 min	95	121	114.8 ± 7.1
14	Ph	Me	< 1 min	96	123	114.5 ± 4.7
16	Ph	Ph	< 15 min	70	98	103.8 ± 1.4
18	Ph	Ph	COOMe	< 15 min	70	106.4 ± 4.0

The deblocking reactions of the 2,3-diphenyl-substituted indole substrates **16-18** that contained a more pronounced steric bulk at the indole C3-reaction site were next investigated. As it was previously found that the steric crowding has a significant effect on the forward reaction rates, it was expected that the backward TAD-indole reaction might be accelerated. As evidenced from the thermal reversibility profiles, a remarkably different dynamic nature of **BuTAD-16** was indeed noticed with deblocking temperatures that are lowered by 20 – 25 °C compared to their 3-methyl-substituted analogues (Figure III.4). A 15-minute reaction half-life was now observed at 98 °C (vs. 123 °C for indole **14**), whereas the deblocking temperature dropped to 70 °C (vs. 96 °C for **14**). The corresponding experimental activation energy for the BuTAD deblocking dropped from 114.5 ± 4.7 kJ mol⁻¹ for **14** to 103.8 ± 1.4 kJ mol⁻¹ for 2,3-diphenyl-1*H*-indole **16** (Table III.2). In line with the forward reaction, no significant effect – evidenced by an almost superimposable thermal reversibility profile – is seen on the retro-reaction when the ester-functionalised indole **18** is used instead of the unsubstituted parent indole **16** (Figure III.4).

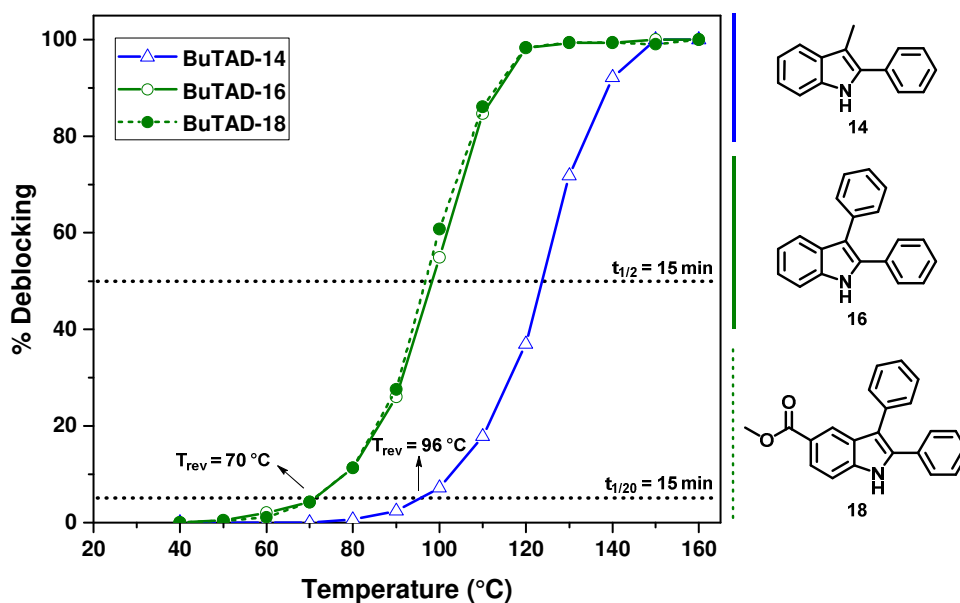


Figure III.4. Thermal reversibility profiles of the BuTAD adducts with 3-methyl-2-phenyl-1*H*-indole **14** (blue) and its more bulky C3-substituted 2,3-diphenyl-1*H*-indole derivatives **16** and **18** (green), reflecting the amount of deblocking at distinct temperatures after a 15-minute heating period in the presence of *trans,trans*-2,4-hexadien-1-ol ([BuTAD-indole]₀ = 0.04 M, DMSO-*d*₆).

III.3.3 Theoretical rationalisation

In order to unroll a versatile and robust indole-blocked TAD platform, it is crucial to obtain an in-depth understanding on *how* the TAD-indole chemistry exactly works. The next phase of this project was thus devoted to rationalising the observed differences in both the forward as well as the thermally triggered backward TAD-indole reaction when slight alterations to the indole core are made.

Before this doctoral work started, an *in silico* mechanistic study of the reversible TAD-indole reaction of BuTAD with 2-*tert*-butyl-3-alkylindole (*cf.* **12**, Figure III.1) was reported by our research group in collaboration with the group of prof. Veronique Van Speybroeck at the *Centre for Molecular Modeling* (Ghent University). Based on density functional theory (DFT) calculations, a stepwise mechanism was proposed that proceeds via an open iminium-urazolide zwitterionic intermediate that is readily converted into the TAD-indole adduct by means of a simple proton transfer.⁷ Under the assumption that the retro-TAD-indole-reaction follows the same trajectory, an activation energy of 140 kJ mol⁻¹ for the transfer of the TAD compound from its initial indole-adduct to a second reaction partner, such as HDEO, was calculated. An alternative mechanism that would proceed via homolytic cleavage of the TAD-indole adduct, thereby leading to an indolyl and urazolyl radical, could be experimentally discarded.³⁸³

With the new experimental data concerning the TAD-indole reaction that was obtained by introducing structural variations onto the indole scaffold, the collaboration with the molecular modelling group was reinitialized in order to rationalise the remarkable effects of the indole substitution patterns. Consequently, the theoretical model could be revised by including the

experimental observations and a correction was made for the high polarity of DMSO, the solvent that was used for the thermal reversibility studies.

The calculated Gibbs free activation energies – carried out by Hannelore Goossens (Ghent University) – for the forward and backward TAD-indole reaction with **12-18** are shown in Table III.3 and clearly reproduce the experimentally observed trends of lower forward reaction rates for the 2,3-diphenylindoles **16** and **17** compared to the 3-alkyl substituted indole derivatives **12-15**. However, the calculations point towards a somewhat slower TAD-reaction for the 5-carboxylic acid containing indoles **15** and **17** with regard to their unsubstituted analogues, although no qualitative difference in forward addition rates were experimentally found. This discrepancy might be attributed to the generally observed acid-enhanced TAD reactivity,³²⁷ which might not have been included into the applied theoretical model.

Table III.3. Calculated Gibbs free activation energies for the forward (CH_2Cl_2) and backward (DMSO) reaction of the investigated indoles **12-18** with MeTAD, and comparison to their indicative forward reaction time (0.2 M, CH_2Cl_2) and experimentally observed activation energy ($E_{a, \text{obs}}$, DMSO- d_6) with BuTAD. Polarizable continuum model with $\epsilon = 8.93$ (CH_2Cl_2 , forward reaction) or 46.7 (DMSO, retro-reaction), M06-2X/6-31++G(d,p). n.d.: not determined.

R ₁	R ₂	R ₃	$\Delta G_{\text{forward}}^{\ddagger}$ (kJ mol ⁻¹)	Reaction time	$\Delta G_{\text{backward}}^{\ddagger}$ (kJ mol ⁻¹)	$E_{a, \text{obs}}$ (kJ mol ⁻¹)
12	<i>t</i> Bu	isopentyl	77.5	< 2 min	135.2	116.5 ± 6.0
13	Ph	isopentyl	78.9	< 1 min	140.6	114.8 ± 7.1
14	Ph	Me	80.9	< 1 min	140.4	114.5 ± 4.7
15	Ph	Me	89.5	< 1 min	141.8	n.d.
16	Ph	Ph	95.5	< 15 min	132.8	103.8 ± 1.4
17	Ph	Ph	102.2	< 15 min	132.9	n.d.
18	Ph	COOMe	n.d.	< 15 min	n.d.	106.4 ± 4.0

Next to the forward reaction, differences with regard to the reversible TAD-indole conjugation can also be rationalised. Since this backward reaction has been examined under kinetic conditions, a more useful comparison can be made by screening the trends between the observed activation barriers and calculated backward free energy barriers. For the two different groups of indoles, with either an alkyl chain or a sterically demanding phenyl group installed on the indole C3-position, a clear difference in calculated backward free energy barriers was found (Table III.3), which perfectly correlates with the experimentally observed separation in activation barriers by 10 kJ mol⁻¹. From the Gibbs free energy profiles (refer to Figure III.5), the lower backward reaction barrier for 2,3-diphenylindole **16** can be attributed to a significant reduction in

exergonicity of the forward TAD-indole addition (i.e. approx. 20 kJ mol⁻¹ less exergonic than 3-methyl-2-phenylindole **14**). However, the 3-phenyl group only destabilises the transition state by 13 kJ mol⁻¹.

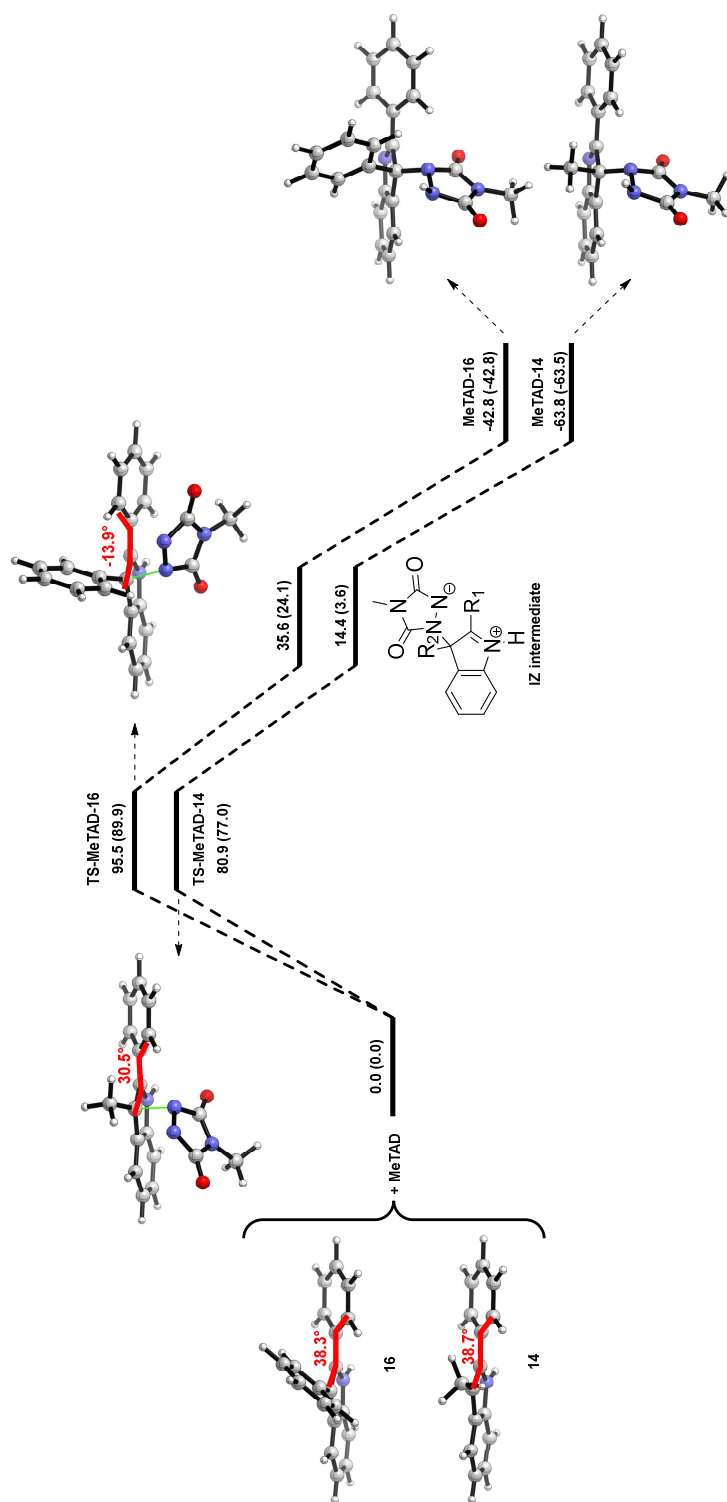


Figure III.5. Gibbs free energy profiles (in kJ mol⁻¹) for the reaction trajectory of TAD-addition to 3-methyl-2-phenylindole **14** and 2,3-diphenylindole **16**, calculated at 298 K and 1 atm. Polarisable continuum model with $\epsilon = 8.93$ (CH₂Cl₂, forward reaction) or 46.7 (DMSO, retro-reaction, in parenthesis). M06-2X/6-31++G(d,p). IZ: iminium-urazolide zwitterionic intermediate. Dihedral angles are displayed in red.

An interesting insight is that the theoretical rationalisations also point towards an additional electronic effect of the phenyl C3-substituent during the reaction course. This is hinted by the remarkable difference in conformation of the optimised geometries of the 3-Me- and 3-Ph-indole transition states (see Figure III.5). In calculations with 3-methyl-2-phenylindole **14**, the TAD molecule approaches the reactive indole C3-position with its electron poor unsaturated ring system oriented in close proximity to the electron rich indole ring system. The presence of a more sterically demanding phenyl group at C3 as in **16**, however, was found to alter the trajectory of TAD-addition which now approaches from the other side, i.e. from the 2-phenyl substituent (Figure III.5). Furthermore, the C2-phenyl moiety becomes significantly more coplanar with the heterocyclic scaffold in the transition state (dihedral angle of -14° for **TS-MeTAD-16**) which is considerably less the case for the transition state of the 3-methylindole derivative ($+31^\circ$), or even the isolated indole **16** as such ($+38^\circ$).

The calculations thus lead to conclude that the 2-phenyl ring is expected to have a pronounced electronic effect during the TAD-indole reaction trajectory, even though there is little electronic conjugation in the ground states of the starting indole and formed TAD-indole adduct. In fact, this insight may be of particular interest in the further rational design of indole substrates that show altered thermal reversibility profiles.

III.4 Substituted indoles enabling tunable deblocking temperatures

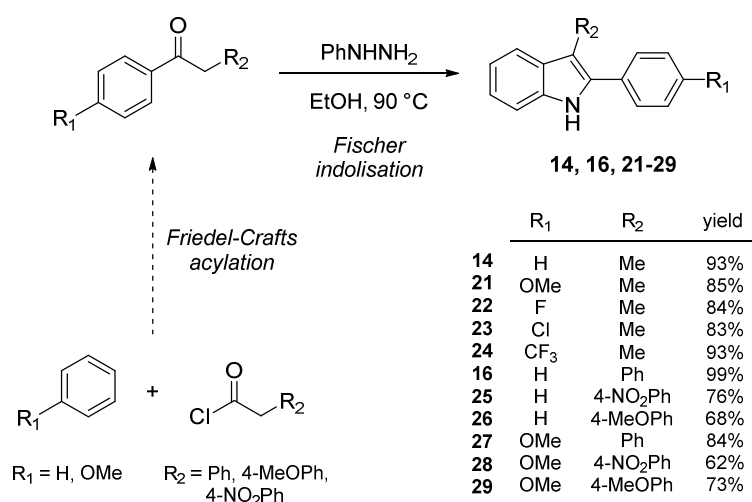
Guided by the mechanistic rationalisation, clear insights were gained into how subtle structural alterations, such as sterical hindrance, can greatly modulate the dynamic properties of the TAD-indole systems. Furthermore, the theoretical calculations hinted towards an additional electronic effect that could influence the deblocking reaction barriers (*cf.* Figure III.5).

Having gained an in-depth understanding of both the forward as well as backward TAD-indole reaction, the objective to precisely tune the deblocking temperature of TAD-indole adducts was projected. In an ideal scenario, the development of such a tunable blocked TAD platform would result in a variety of different TAD-indole combinations from which the reversible behaviour can be triggered in a specific user-defined temperature window in view of the targeted application.

III.4.1 Synthesis of a 2,3-disubstituted indole library

As a first step towards the development of tunable indole blocking agents, steric and/or electronic effects were introduced on the previously identified TAD-reactive 2-phenylindole scaffolds. Hence, a library of 3-Me- and 3-Ph-substituted 2-phenyl-1*H*-indoles, containing electron donating and/or withdrawing groups, was synthesized in good to excellent yields (i.e. 62 - 99 %) via the classical Fischer indolisation reaction of the corresponding acetophenones (see Scheme III.7). The used acetophenone starting substrates were either commercially available or could be

readily synthesized from very cheap bulk starting materials via a Friedel-Crafts acylation. Importantly, the latter in-house acetophenone synthesis ensured the desired diversity in substituent combinations that are feasible. Briefly, the resulting library contains a range of potential indole-blocking agents which can be subdivided based on the sterical hindrance near the indole reaction site. On the one hand, the indole library comprises a series of 3-methyl-2-phenylindole analogues **14**, **21-24** with varying electron density on the 2-aryl group (R = OMe, F, Cl, CF₃), while on the other hand a series of 2,3-diphenyl- and 2-(4-methoxyphenyl)-3-phenylindoles (**16**, **25-26** and **27-29**, respectively), with their nitro and methoxy-substituted derivatives was obtained.



Scheme III.7. Library of 2,3-disubstituted indoles **14**, **16**, **21-29** synthesised via a Fischer indolisation of their corresponding acetophenones. The starting ketone is either commercially available or can be generated by a Friedel-Crafts acylation.

In line with our previous investigations (*cf.* III.3.1), the newly synthesised indole compounds were next screened towards their TAD-based addition reaction. Again, BuTAD was selected as the model TAD reagent which swiftly converted all indole substrates into their corresponding TAD-indole adducts. As expected, all reactions promptly proceeded at room temperature and exclusively gave the indole-blocked BuTAD compounds (verified by ¹H-NMR and LC-MS) in quantitative yields with reaction times ranging from a few seconds up to 30 minutes. Theoretical calculations of the forward Gibbs free energy barriers accurately reproduced the observed trends in TAD reactivity (Table III.4). Thus, also with the novel electronically altered indole scaffolds, the click-type characteristics of the TAD-indole addition reaction were retained.

III.4.2 Kinetic thermoreversibility studies

Subsequently, the deblocking behaviour of each TAD-indole system was assessed by subjecting the blocked compounds to kinetic thermal reversibility studies. Similar as before (*cf.* III.3.2), the TAD-indole deblocking reaction was monitored via offline ¹H-NMR analysis, from which the fraction of initial blocking agent could be determined, that is released from the BuTAD-indole adducts during a 15-minute heating period in the presence of a conjugated diene (*i.e.* HDEO,

which acts as a kinetic trap for the *in situ* liberated TAD). The resulting thermal reversibility profiles, depicted in Figure III.6, now show a broad but finely interspaced array of temperature ranges wherein the specific BuTAD-indole systems exhibit a dynamic behaviour. From these reversibility plots, the deblocking temperatures (i.e. the temperature at which 5 % of indole blocking agent, and thus TAD, is released from the adduct over a 15-minute period) and half-life temperatures ($t_{1/2} = 15$ min) were next derived for each BuTAD-indole combination (see Table III.4).

With the full kinetic profiling of the indole-blocked BuTAD systems, the influence of the indole substitution pattern in terms of their TAD-blocking capability could again be rationalised. From the thermal reversibility profiles, three major classes of blocking indoles could be distinguished.

1) A first class contains the least dynamic 3-methyl-substituted indole adduct, which shows half-life temperatures in the range of 117 - 131 °C (Figure III.6). Electronic substitution of the 2-phenyl ring was thus found to have a small yet significant influence on the deblocking reaction, as was predicted from the theoretical calculations (*cf.* III.3.3). The electron donating effect of a methoxy substituent in **21** was observed to lower the deblocking reaction barrier (i.e. 6 °C drop vs. plain 3-Me-2-Ph-indole **14**), while electron withdrawing groups (e.g. -F, -Cl, -CF₃ in **22-24**) were shown to have the opposite effect and shift the thermal reversibility profiles to higher temperatures with half-life values up to 131 °C (i.e. an 8 °C increase compared to **14**). The observed trends in deblocking correlate with shifts in activation energies of up to 10 kJ mol⁻¹ (Table III.4).

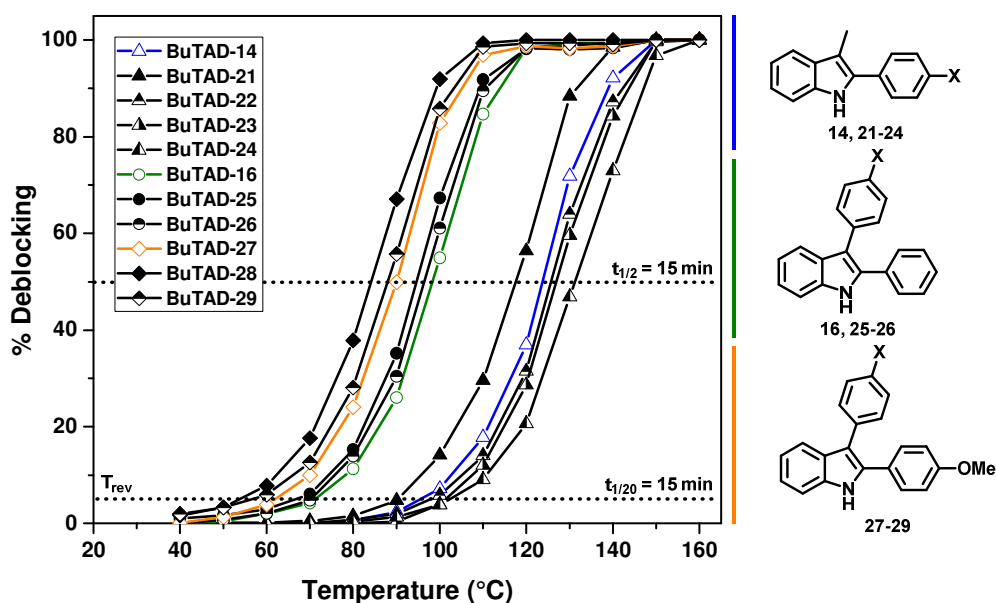


Figure III.6. Thermal reversibility profiles of the BuTAD adducts with the synthesised library of 2-phenylindoles **14**, **16** and **21-29**, reflecting the amount of deblocking at distinct temperatures after a 15-minute heating period in the presence of *trans,trans*-2,4-hexadien-1-ol ($[\text{BuTAD-indole}]_0 = 0.04$ M, DMSO-*d*₆).

2) A second class of blocking agents is made up by the bulky 3-substituted 2-phenylindoles (Figure III.6). Initially, the drop in activation barriers to affect the deblocking reaction with 2,3-diphenylindole **16** (103.8 kJ mol⁻¹ vs 114.5 kJ mol⁻¹ for its 3-methyl analogue) was believed to originate from the steric destabilisation of the TAD-indole adduct. However, a minor but notable shift of the corresponding reversibility profiles was found when the 3-phenyl group was additionally substituted with a nitro- (**25**) and methoxy- (**26**) moiety. Nonetheless, the calculated deblocking activation barriers fall within the measurement error margin (Table III.4) and the observed differences are therefore considered as non-significant.

Table III.4. Overview of the investigated indole-blocked BuTAD-systems with their indicative forward reaction time (0.2 M, CH₂Cl₂, room temperature), temperature of deblocking (5 % release), half-life temperature and experimentally observed activation energy ($E_{a, \text{obs}}$) for a 15-minute heating period ($[\text{BuTAD-indole}]_0 = 0.04 \text{ M}$, DMSO-*d*₆). A comparison is provided by respective forward (CH₂Cl₂) and backward (DMSO) Gibbs free energy barriers, obtained from theoretical calculations of the addition reaction with MeTAD. Polarisable continuum model with $\epsilon = 8.93$ (CH₂Cl₂, forward reaction) or 46.7 (DMSO, retro-reaction), M06-2X/6-31++G(d,p). n.d.: not determined.

14, 16, 21-29 + MeTAD $\xrightarrow[\text{DMSO-}d_6, \Delta T]{\text{CH}_2\text{Cl}_2, \text{rt}}$ **BuTAD-(14, 16, 21-29)**

R ₁	R ₂	Reaction time	$\Delta G_{\text{forward}}^\ddagger$ (kJ mol ⁻¹)	Deblocking T (°C)	Half-life T (°C)	$E_{a, \text{obs}}$ (kJ mol ⁻¹)	$\Delta G_{\text{backward}}^\ddagger$ (kJ mol ⁻¹)	
14	H	Me	< 1 min	80.9	95	123	114.5 ± 4.7	140.4
21	OMe	Me	< 1 min	74.8	90	117	110.0 ± 4.2	127.7
22	F	Me	< 1 min	81.5	98	126	116.3 ± 4.4	132.5
23	Cl	Me	< 1 min	83.8	101	127	118.5 ± 4.3	133.2
24	CF ₃	Me	< 3 min	n.d.	102	131	122.0 ± 5.1	n.d.
16	H	Ph	< 15 min	95.5	71	98	103.8 ± 1.4	132.8
25	H	4-NO ₂ Ph	< 30 min	101.6	67	94	102.3 ± 1.5	135.1
26	H	4-MeOPh	< 10 min	93.6	70	96	102.3 ± 2.0	127.8
27	OMe	Ph	< 10 min	87.3	62	90	96.2 ± 3.4	120.5
28	OMe	4-NO ₂ Ph	< 15 min	93.2	54	83	90.9 ± 0.3	117.0
29	OMe	4-MeOPh	< 4 min	84.6	56	87	95.1 ± 1.3	119.8

3) In a third and final class of indole substrates, the most activating 2-methoxyphenyl group identified from class 1 was installed on the different 3-phenyl modified indoles from class 2. This resulted in an apparent synergistic effect, leading to even further enhanced dynamic behaviour of the (2-(4-methoxyphenyl)-3-arylindole **27-29** BuTAD-adducts (Figure III.6), which was confirmed by additional theoretical calculations (Table III.4). The derived half-life temperatures were all significantly lower compared to the plain diphenylindole **16** and were even more reduced when a nitro- (**28**) or methoxy- (**29**) group is introduced on the 3-phenyl ring. Generally, the

methoxy-group on the 2-phenyl substituent lowers the half-life temperatures of the BuTAD-adducts by 10 °C and the deblocking barrier by approximately 5 - 10 kJ mol⁻¹ (Table III.4). As a result, deblocking temperatures as low as 54 °C were established (with indole **29**).

In conclusion, the rational design of structurally different substituted 2-phenylindoles allows for a meticulous regulation of the TAD-indole deblocking reaction. This makes it possible to conduct temporally controlled TAD-based reactions in a tunable temperature regime whereby TAD-deblocking takes place from 102 °C down to 54 °C in a 15-minute interval.

III.4.3 Additional influences on the temperature of reversibility

Thus far, the thermal reversibility profiles of a range of indole compounds were determined by making use of their corresponding ‘non-functional’ 4-*n*-butyl-TAD adducts. The choice for this aliphatic TAD model reagent is mainly attributed to the distinct ¹H-NMR chemical shift values of the *n*-butyl protons, which allows for a straightforward identification of TAD-addition products and improves the detection of possible side product formation. In contrast, the aromatic PhTAD reagent was considered far less relevant to probe the forward and backward TAD-indole reactions because of overlapping proton resonances of the 4-phenyl TAD-substituent with the aromatic signals of the 2-phenylindole substrates. Nonetheless, PhTAD is commercially available and is by far more generally recognised as a benchmark to monitor TAD reactions compared to its BuTAD derivative. Moreover, aromatic TAD compounds have been reported in literature to be more reactive than their aliphatic counterparts.³²⁷ Therefore, next to the effect of structural indole variations, the influence of the TAD-substituent on the TAD-indole deblocking process was also investigated.

Three representative indole blocking agents, one from each of the identified classes in III.4.2, were selected, i.e. **14**, **16** and **27** (*cf.* Scheme III.7), and reacted with the 4-phenyl TAD reagent to give the respective blocked aromatic TAD adducts. As expected, the forward blocking reaction proceeds considerably faster with PhTAD compared to the aliphatic BuTAD reagent (Table III.5).

After subjecting the aromatic PhTAD-indole systems (i.e. **PhTAD-14**, **PhTAD-16** and **PhTAD-27**) to kinetic reversibility studies, a consistent downward shift of the reversibility curves by 20 °C with regard to their aliphatic counterparts was identified (see dotted vs. full line in Figure III.7 and Table III.5). The most dynamic indole-blocked PhTAD system with 2-(4-methoxyphenyl)-3-phenyl-1*H*-indole **27** now shows a deblocking temperature as low as 33 °C (instead of 54 °C for **BuTAD-27**), and in fact shows a non-negligible TAD-release already at room temperature. This room temperature release was also evidenced from the fact that a freshly prepared NMR-solution of the corresponding blocked PhTAD reagent gradually started to turn pink, indicating free TAD formation. Furthermore, traces of an electrophilic aromatic substitution on the methoxy-activated phenyl groups were detected upon standing for several

days. Thus, this indole-blocked PhTAD system had to be stored in the fridge at 4 °C as the extremely low temperature of deblocking has a severe impact on its shelf-life stability. Thus, further decreasing the temperature at which deblocking takes place by the design of next generation indoles – which is theoretically possible – would not result in any additional benefits for temperature triggered TAD-based reactivity.

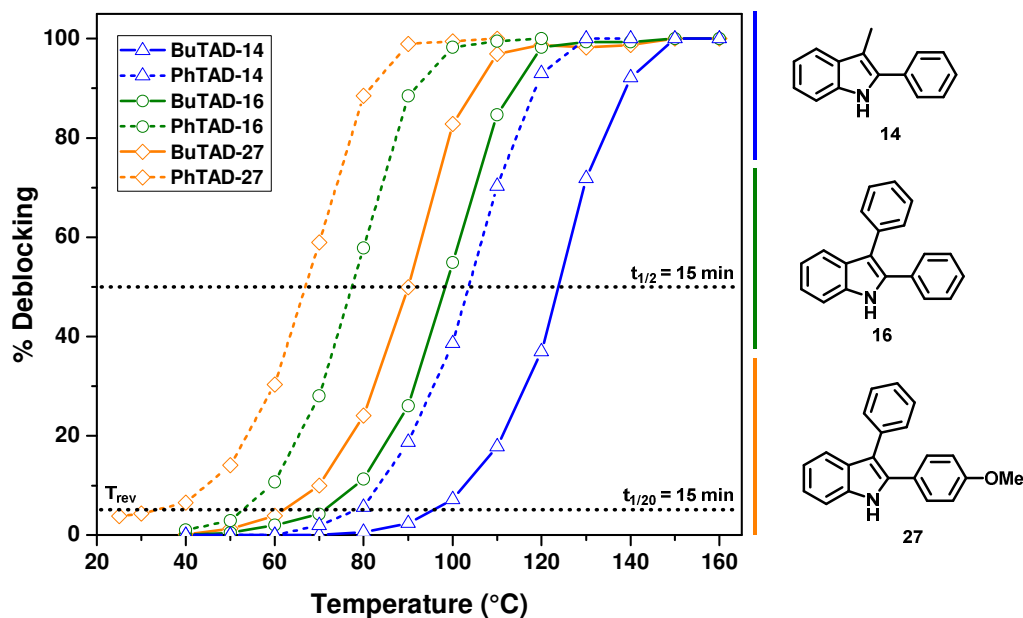


Figure III.7. Thermal reversibility profiles of the BuTAD and PhTAD adducts with 3-methyl-2-phenyl-1*H*-indole **14**, the more bulky C3-substituted 2,3-diphenyl-1*H*-indole **16** and its 2-(4-methoxyphenyl)-3-phenyl-1*H*-indole derivatives **27**, reflecting the amount of deblocking at distinct temperatures after a 15-minute heating period in the presence of *trans,trans*-2,4-hexadien-1-ol ($[\text{RTAD-indole}]_0 = 0.04 \text{ M}$, DMSO- d_6).

In summary, a remarkable shift in reversibility profiles is observed by switching the nature of the TAD-substituent from a butyl chain to a phenyl ring. Overall, by simple structural changes in both the indole and TAD reaction partners, the deblocking temperatures of the resulting blocked TAD chemicals can be finetuned, almost at will, over a broad temperature range (i.e. over 50 °C).

Table III.5. Indicative forward reaction time (0.2 M, CH₂Cl₂, room temperature), temperature of deblocking (5 % release), half-life temperature and experimentally observed activation energies ($E_{a, \text{obs}}$) for a 15-minute heating period ($[\text{BuTAD-indole}]_0 = 0.04 \text{ M}$, DMSO-*d*₆) derived for the blocking and deblocking of BuTAD and PhTAD with indoles **14**, **16** and **27**.

$\text{R}_3 = n\text{Bu}$ **BuTAD-(14, 16, 17)**
 $\text{R}_3 = \text{Ph}$ **PhTAD-(14, 16, 17)**

	R ₁	R ₂	R ₃	Reaction time	Deblocking T (°C)	Half-life T (°C)	$E_{a, \text{obs}}$ (kJ mol ⁻¹)
BuTAD-14	H	Me	<i>n</i> Bu	< 1 min	95	123	114.5 ± 4.7
PhTAD-14	H	Ph	<i>n</i> Bu	< 10 s	78	104	108.9 ± 4.0
BuTAD-16	H	Ph	<i>n</i> Bu	< 15 min	71	98	103.8 ± 1.4
PhTAD-16	H	Me	Ph	< 5 min	53	77	98.7 ± 0.7
BuTAD-27	OMe	Ph	Ph	< 10 min	62	90	96.2 ± 3.4
PhTAD-27	OMe	Ph	Ph	< 1 min	33	67	84.2 ± 1.9

III.5 Blocked triazolinediones for temperature controlled bonding of polymer systems

After having investigated the blocking and deblocking behaviour of the molecular engineered indoles with low molecular weight TAD compounds, the practicality of the established blocked TAD platform was demonstrated in a ‘more realistic’, macromolecular context.

The following two case studies will showcase the gained time-resolved control over TAD reactivity in two of their most widely adopted polymer applications. The first case study will illustrate how the indole-blocking concept enables the synthesis of highly reactive, yet bench-stable functional TAD reagents that can be activated in a controlled fashion to induce temperature triggered *modification* of unsaturated polymers (III.5.1). In a second study, the indole blocking agents will be applied to bivalent TAD reagents to allow for on demand TAD-based *crosslinking* reactions whereby the curing temperature can be finetuned by simply changing the bisTAD-indole blocking system (III.5.2).

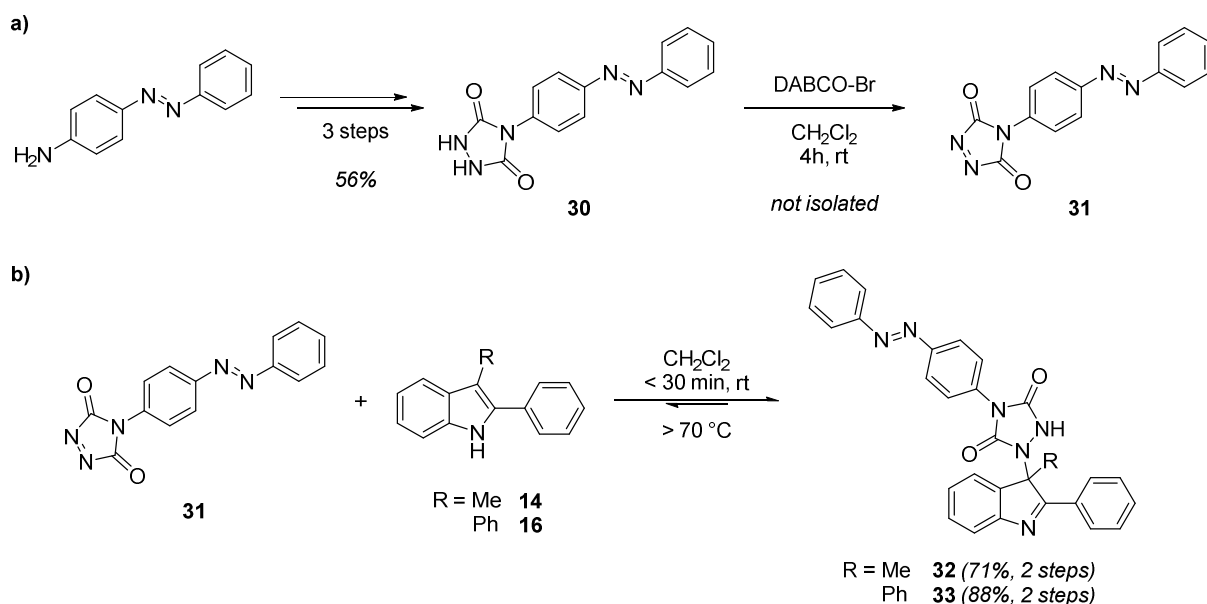
III.5.1 Case study 1: temperature triggered polymer modification

The highly efficient low-temperature modification of polydienes is one of the most striking examples of how TAD reagents have emerged as highly enabling ‘click’ tools in polymer chemistry. An attractive application of click chemistries in general involves the covalent introduction of dyes onto a variety of substrates, including macromolecules. In this regard, research efforts within

our groups have been focussed on the synthesis of dye-containing TAD reagents as they can be used as unsophisticated probes to visually detect unsaturations without the need for advanced analytical techniques.³⁸³

The synthesis of dye-containing TAD reagents, however, can be extremely challenging. Indeed, functional TADs are very reactive and readily self-react over prolonged periods of time, which necessitates their generation from their corresponding urazole precursors *in situ* or only shortly before use. In fact, such an issue was identified during the synthesis of a TAD-dye compound bearing an azobenzene-type chromophoric unit (see Scheme III.8a). Although the brightly orange urazole precursor **30** could be readily obtained from 4-aminoazobenzene via an extended Cookson procedure (*cf.* II.2.2.1), the resulting TAD-dye compound **31** was shown too reactive to be isolated after the final oxidation step. As a result, the azobenzene TAD-dye had to be generated *in situ* and reacted subsequently without isolation, and hence without knowing the exact TAD concentration in the reaction mixture (since monitoring the conversion of the final urazole oxidation can be tedious). These issues were elegantly resolved, however, by using the developed 2-phenylindoles as attractive blocking agents, as they give bench-stable TAD-dye adducts that can be isolated.

In this first case study, two blocked TAD dyes (i.e. **32** and **33**, Scheme III.8b) were introduced based on 3-methyl-2-phenyl- and 2,3-diphenylindole blocking agents, respectively, and their use in temperature-controlled covalent staining of unsaturated macromolecular substrates was validated.



Scheme III.8. a) Synthesis of the azobenzene-containing TAD-dye **31**, which was too reactive to be isolated. b) Using the indole blocking concept, however, the TAD-dye can be readily transformed into its bench-stable indole-blocked derivatives **32** and **33**.

At first, however, the influence of the inherently more reactive 4-azobenzene TAD-dye (**31**) on the indole deblocking reaction was investigated. Hence, a thermal reversibility profile was obtained for the newly introduced 2,3-diphenylindole-TAD-dye combination **33** (Figure III.8). Interestingly, the dynamic behaviour of the blocked TAD-dye was again shifted to a lower temperature range compared to that of the plain phenyl-substituted TAD reagent, *with* a characteristic deblocking temperature already observed at 40 °C (vs. 53 °C for **PhTAD-16**) and an associated drop in the activation barrier for the deblocking reaction with approximately 10 kJ mol⁻¹ (see Table III.6). In fact, the low-temperature deblocking of a tailored TAD reagent around 40 °C offers highly interesting potential in bioconjugation reactions with a controllable TAD reactivity.

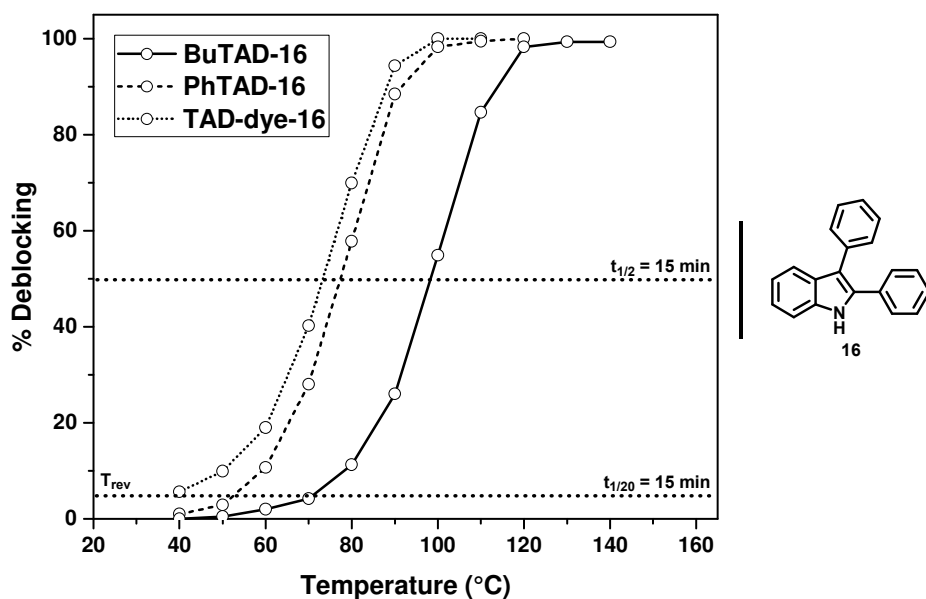
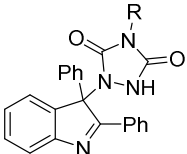


Figure III.8. Thermal reversibility profile of the azobenzene-containing TAD-dye **31** with 2,3-diphenyl-1*H*-indole **16** relative to its BuTAD and PhTAD analogues, reflecting the amount of deblocking at distinct temperatures after a 15-minute heating period in the presence of *trans,trans*-2,4-hexadien-1-ol ([RTAD-**16**]₀ = 0.04 M, DMSO-*d*₆).

Table III.6. Comparative temperatures of deblocking (5 % release), half-life temperatures and experimentally observed activation energies ($E_{a,obs}$) for a 15-minute heating period ([BuTAD-indole]₀ = 0.04 M, DMSO-*d*₆) derived for the blocking and deblocking of BuTAD, PhTAD and the azobenzene-containing TAD-dye **31** with 2,3-diphenylindole **16**.

	R	Deblocking	Half-life	$E_{a,obs}$	
		T (°C)	T (°C)	(kJ mol ⁻¹)	
	BuTAD- 16	<i>n</i> Bu	71	98	103.8 ± 1.4
	PhTAD- 16	Ph	53	77	98.7 ± 0.7
	TAD-dye- 16 (= 33)	4-azobenzene	40	73	87.3 ± 1.3

After the deblocking reaction was probed, the triggered TAD-dye conjugation reaction with polyisoprene **34** ($M_n = 35$ kDa), a common polydiene that contains suitable TAD-reactive sites along the polymer backbone, was next demonstrated (Figure III.9a). Since the polymer is insoluble in DMSO, the triggered TAD-dye conjugation reaction was performed in deuterated chloroform-*d* and monitored via $^1\text{H-NMR}$ analysis (refer to Appendix B). Thus, the indole-blocked dyes **32** and **33** were dissolved with polyisoprene in a pressure tube and heated in an oil bath set at 120°C . With the more sterically hindered 2,3-diphenylindole-blocked TAD-dye **33**, a complete transfer of the dye onto the polymer backbone was observed within 40 min, whilst longer reaction times were needed for its 3-methyl-2-phenylindole-blocked analogue **32** to reach full conversion of the polymer-dye conjugate (i.e. 105 min, see Figure III.9b). Moreover, the most dynamic TAD-dye adduct **33** could also be completely transferred to polyisoprene at lower temperatures, i.e. $60 - 65^\circ\text{C}$, within 24 hours (Figure III.9c). In the latter case, the covalent attachment of the azobenzene dye onto the polymer was confirmed by precipitation of the resulting reaction mixture in methanol (Figure III.9c, inset), which gave a dark orange polymeric residue together with a clear supernatant that exclusively contained the released indole blocking agent **16** and traces of dissolved parent polymer **34** (refer to Appendix B for $^1\text{H-NMR}$ spectra).

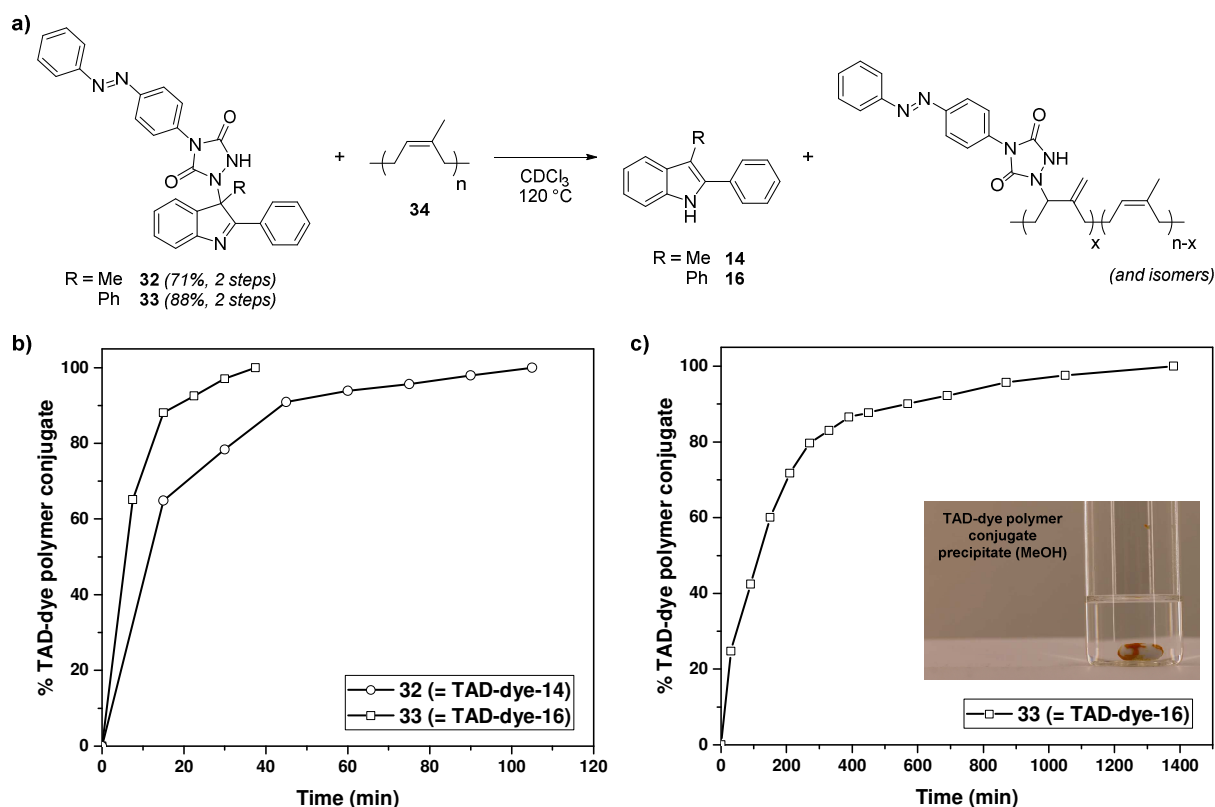


Figure III.9. a) Use of indole-blocked TAD-dyes **32** and **33** for the temperature triggered covalent staining of polyisoprene **34**. b) Reaction kinetics for the transfer of azobenzene-containing TAD-dye from indoles **14** and **16** onto the polymer backbone at 120°C (CDCl_3 , external temperature). c) The most dynamic blocked TAD-dye **33** also enables the complete transfer of the TAD-dye under milder reflux conditions (i.e. $60 - 65^\circ\text{C}$, CDCl_3) within 24 hours. The resulting polymer-dye conjugate could be isolated from the reaction mixture by precipitation (inset).

In a more challenging triggered polydiene modification experiment, the TAD-dye was also transferred from a solution onto an insoluble but swollen TAD-reactive polymeric resin. To provide such a resin, a network was first synthesised by crosslinking an alkene-trimer (derived from a multifunctional isocyanate) with a sub-equimolar amount of a bivalent TAD, so that an excess of residual TAD-reactive unsaturations was guaranteed (see Figure III.10). Upon heating this network in a solution of the blocked TAD-dye **32** or **33**, an orange stained material was recovered (Figure III.10). Again, the covalent attachment of the TAD-dye was verified, this time by the persisting orange colour of the material after subjecting it to a Soxhlet extraction.

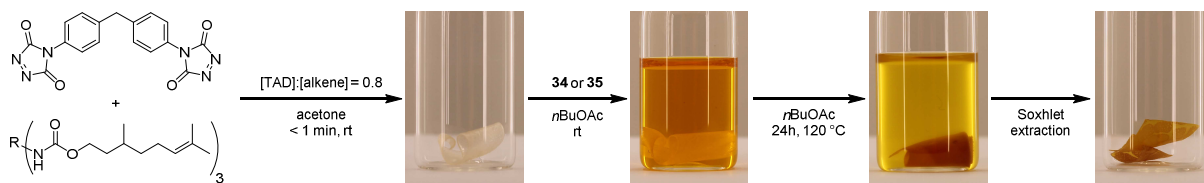
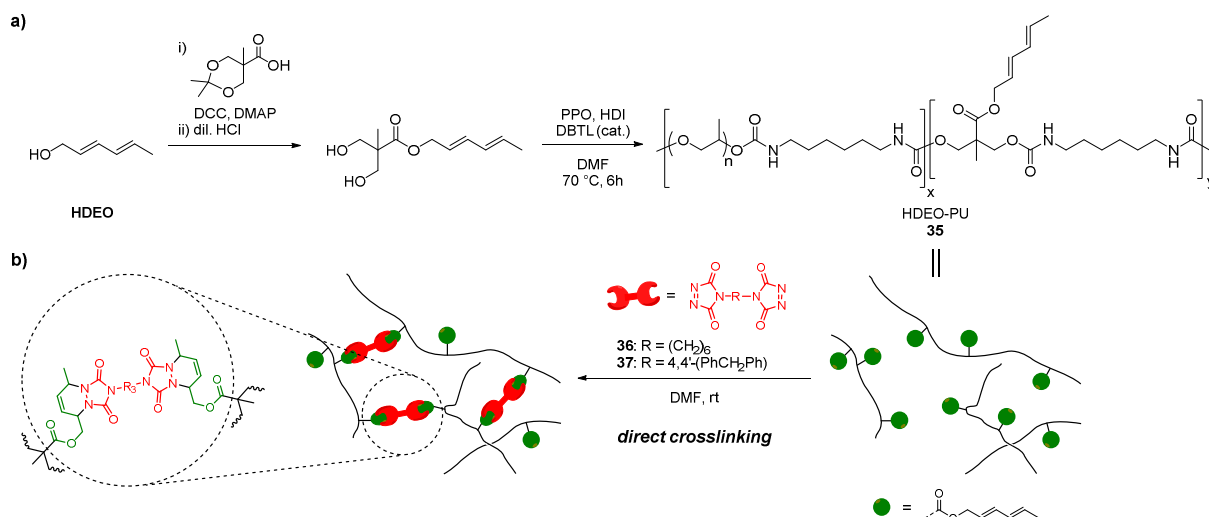


Figure III.10. Temperature triggered transfer of a blocked TAD-dye from a solution onto an insoluble network, containing residual TAD-reactive sites. Besides the visual feedback, the covalent attachment of the orange azobenzene-dye was confirmed by the persisting orange colour after subjecting the insoluble polymer resin to a Soxhlet extraction.

III.5.2 Case study 2: on demand polymer crosslinking

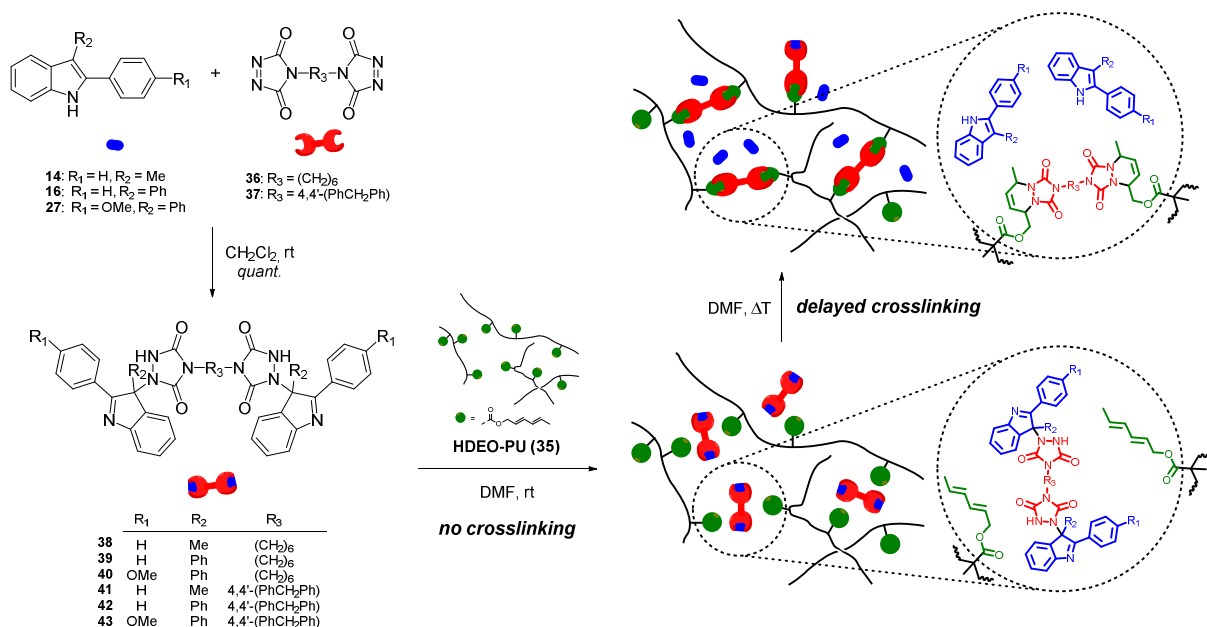
The low-temperature crosslinking of polydienes can still be considered as one of the most industrially relevant applications of TAD chemistry. Also throughout the course of the current doctoral work, TAD reactions have gained a continued attention from industry leading to several conceptual screening meetings and the valorisation of collaborative projects, including a recently approved Horizon 2020 project. Typically, TAD-based crosslinking reactions are praised for reaching high conversions with ultrafast associated kinetics. However, very fast crosslinking times can also be highly undesirable. In coating applications, for instance, a certain time delay over the curing reaction is often required, not only to ensure thorough mixing of the components but also to allow ample time for the formulation to be applied onto a substrate.

Inspired by the need for time-controlled crosslinking reactions, a second case study aimed to validate the tunable indole-blocking concept by exploiting the on demand controlled release of TAD-based crosslinkers. For this, the conjugated HDEO diene – used earlier in the TAD-indole thermoreversibility studies (*cf.* III.3.2, Scheme III.6) – was transformed into a diol monomer and subsequently incorporated into a linear polyurethane (see Scheme III.9a). The HDEO-derived diol was therefore used as a comonomer (15 wt%) with poly(propylene oxide) (PPO, $M_n = 2.0$ kDa) and hexamethylene diisocyanate (HDI) to generate the linear polyurethane **35** (HDEO-PU, $M_n = 12.5$ kDa, Scheme III.9a) that contains TAD-reactive diene side chains.



Scheme III.9. a) Modification of *trans,trans*-2,4-hexadien-1-ol (HDEO) into a diol, which is subsequently used as a comonomer with poly(propylene oxide) (PPO, $M_n = 2.0$ kDa) and hexamethylene diisocyanate (HDI) to give a diene-containing TAD-reactive linear polyurethane (**35**, HDEO-PU, $M_n = 12.5$ kDa). b) Addition of an aliphatic or aromatic bivalent TAD reagent (**36** or **37**, respectively) to the resulting polyurethane leads to a directly crosslinked material.

When an aliphatic or aromatic TAD-based crosslinking agent (i.e. **36** or **37**, Scheme III.9b) is added to a solution of the diene-containing HDEO-PU at room temperature, a swift and ultrafast gelation is detected within 5 seconds and the complete curing of the resulting network – visualised by the disappearance of the red TAD colour – was observed in less than 1 minute. As a result of these fast curing times, the crosslinking reaction was found to lack any form of control, leading to rather inhomogeneous networks.



Scheme III.10. Schematic representation of the delayed TAD-based crosslinking experiments of the linear HDEO-PU **35**. (left) Treatment of the TAD-based crosslinker **36** or **37** with two equivalents of a suitable indole blocking agent (**14**, **16** or **27**) retains the reactivity of the crosslinking agent. (bottom) When the blocked TAD crosslinkers (**38-43**) are now added to the HDEO-PU, no room-temperature gelation is induced. (right) Only upon heating the bench-stable formulation, the TAD crosslinker is released to initiate the on demand crosslinking.

To better control the polyurethane curing reaction, three representative indole blocking agents (i.e. **14**, **16** and **27**, *cf.* Figure III.7) were used to create the blocked aliphatic and aromatic bisTAD crosslinking agents **38-43** (Scheme III.10, left). Addition of these blocked bisTADs to the HDEO-PU (**35**) solution now resulted in a bench-stable non-crosslinked formulation (Scheme III.10, bottom left). Only upon heating of this mixture were the TAD crosslinking agents released from their indole blocking moieties and the controlled TAD-diene crosslinking reaction was triggered (see Scheme III.10, right).

To illustrate the on demand temperature triggered curing of the polyurethane formulations, rheological experiments under oscillatory shear mode were performed with the blocked TAD-based crosslinkers **38-43**. The delayed crosslinking process was monitored by following the viscoelastic response upon heating from 25 °C to 150 °C at a constant rate of 2.25 °C min⁻¹ (see Figure III.11a). The storage and loss moduli G' and G'', respectively, were determined from the torque which was measured throughout the heating process. Strain sweeps of the cured materials were carried out to ensure that the experiments were conducted within the linear viscoelastic regime.

The curing profiles obtained for the blocked bisTAD/polyurethane formulations (0.1 M blocked bisTAD **38-43** in a 0.4 g mL⁻¹ solution of polymer **35** in DMF), depicted in Figure III.11a, indicated very low initial G' values (close to the limit of detection) which slightly increase upon mild heating. A reference sample of the bare linear polymer was characterised with a similar upward increase from which a reference baseline was established (Figure III.11a). Further heating of the curing formulations resulted in an abrupt increase of G' for all samples that contained the latent bisTAD crosslinkers **36** or **37**, indicating a liquid to solid-like transition. These sol-gel transition, which was obviously not observed for the HDEO-PU reference sample, can be attributed to the (extended) deblocking reaction whereby the bisTAD crosslinker is activated within the formulation, making it available to react with the diene side chains of the polymer to form a crosslinked gel. At higher temperatures, the storage modulus eventually reached a plateau which indicated the complete curing of the resulting material.

Although similar storage moduli were obtained at 150 °C, each specific indole-blocked bisTAD was characterised by different on-set temperatures at which the sol-gel transitions occurs. Moreover, the observed trends in the curing profiles are consistent with those that were derived from the thermal reversibility model studies (*cf.* Figure III.6). Indeed, the delayed crosslinking formulations with the aromatic blocked bisTADs **41-43** gave markedly earlier sol-gel transitions compared to their aliphatic counterparts (**38-40**). Additionally, the indole blocking agents **27** were cleaved off at considerably lower temperatures than **16** and **14** for the same TAD crosslinker (see Table III.7).

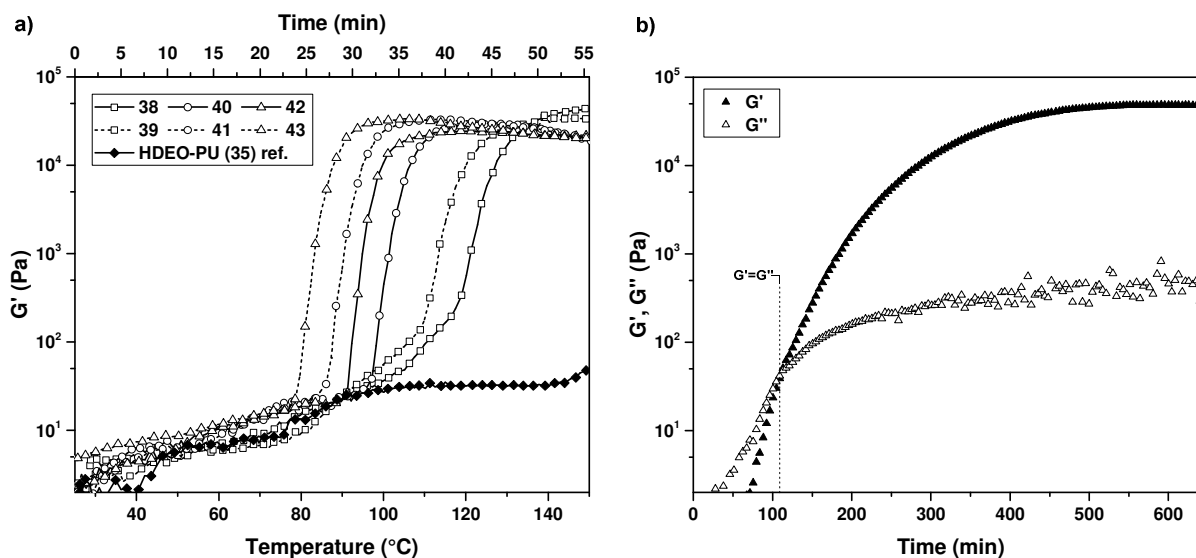


Figure III.11. a) Rheological assessment of the tunable delayed crosslinking upon heating of a solution of HDEO-PU **35** and indole-blocked bisTADs **38-43** from 25 °C to 150 °C at 2.25 °C min⁻¹. b) The most dynamic bisTAD-indole system enabled low-temperature curing of HDEO-PU at 50 °C with a sol-gel transition reached after 110 minutes, here defined as the intersect of the storage and loss moduli G' and G'' , respectively.

In a follow-up rheology experiment, the delayed polyurethane curing with the most dynamic blocked bisTAD crosslinker, i.e. **43**, was repeated under isothermal conditions instead of continuous heating. At 50 °C, a sol-gel transition was reached after 110 minutes, which was observed from the rheological behaviour as the intersect of the storage and loss modulus (Figure III.11b). The low-temperature curing was fully completed after 7 hours as the storage modulus reached a plateau at 50 kPa, which perfectly correlates to the networks obtained upon continuous heating.

The indole-blocking platform was thus demonstrated to enable delayed TAD-based crosslinking at user-defined temperatures without affecting the final viscoelastic properties of the cured materials. It is important to note, however, that the released indole blocking agents will remain present in the polymer networks and are thus expected to influence the thermal properties of the final materials to a certain extent. Therefore, the cured and dried materials were subjected to differential scanning calorimetry (DSC) and thermal gravimetric analysis (TGA) to determine some characteristic properties such as the glass transition temperature T_g and the onset temperature of degradation $T_{d,5\%}$ – here defined at 5 % weight loss. Whereas no distinct changes were recorded in thermal stability of the delayed compared to the directly crosslinked polyurethane materials (i.e. without the presence of indoles), a notable effect on the T_g was observed. Although the influence on T_g of small molecules in a polymer matrix is well known, the cured networks containing the 2-phenylindole blocking agents surprisingly showed an increase in T_g (> - 57 °C) rather than the expected decrease, with a more pronounced effect found for the 3-aryl substituted indole blocking agents (e.g. **39-40** and **42-43** in Table III.7). In a repeating set of experiments, this unusual effect on the T_g was found to be reproducible. When the

remaining indole blocking agent was successfully removed from the isothermally cured HDEO-PU network by means of a Soxhlet extraction (verified by $^1\text{H-NMR}$, refer to Appendix B), a decrease in T_g to the original value of the directly crosslinked network was detected (Table III.7). Thus, the exceptional increase in T_g of the on demand crosslinked materials can be attributed to the interactions of the indole blocking agent with the polymer matrix. A similar anti-plasticising effect was observed with non-crystallising additives in poly(vinyl alcohol) and poly(*N*-vinylpyrrolidone) matrices.³⁸⁴⁻³⁸⁵

Table III.7. Overview of the crosslinker systems used for the direct and delayed HDEO-PU curing experiments with their sol-gel transition temperature range observed during continuous heating from 25 °C to 150 °C at 2.25 °C min⁻¹. Glass transition temperatures (T_g) and onset temperatures of degradation T_d (defined at 5 % weight loss) of the dried networks were determined via DSC and TGA, respectively.

Crosslinker	Blocking agent	R ₁	R ₂	R ₃	Sol-gel transition temperature (°C)	T _g (°C)	T _{d, 5%} (°C)
36	-	-	-	(CH ₂) ₆	rt	-57	253
37	-	-	-	4,4'-(PhCH ₂ Ph)	rt	-57	278
38	14	H	Me	(CH ₂) ₆	120 – 150	-52	225
39	14	H	Me	4,4'-(PhCH ₂ Ph)	110 – 140	-53	232
40	16	H	Ph	(CH ₂) ₆	95 – 115	-36	253
41	16	H	Ph	4,4'-(PhCH ₂ Ph)	85 – 105	-37	242
42	27	OMe	Ph	(CH ₂) ₆	90 – 110	-34	260
43	27	OMe	Ph	4,4'-(PhCH ₂ Ph)	80 – 100	-39	253

III.6 Orthogonal indole-to-indole exchange reaction

After the identification and the extensive study of the different 2-phenylindoles with their own characteristic forward and backward TAD reactivity, an additional research question was postulated whether it would be possible to selectively exchange a certain TAD compound between two different indole substrates. In other words, *would the difference in reactivity of the various 2-phenylindoles offer the possibility to create a directed transfer of TADs from one indole derivative to another, thereby opening unprecedented dynamic macromolecular systems?*

For the selective transfer of a TAD reagent to be successful, the two selected indole moieties should possess clearly distinct properties on two levels. A first level is related to a preferred *thermal reversibility* of the TAD-adducts formed with the ‘donor’ indole over the ‘acceptor’ indole. Thus, at a certain temperature, the release of TAD compounds from the initial donor indole should be highly dominating over the second indole that acts as the TAD acceptor. A second level takes into account the *kinetic selectivity*, which should drive the equilibrium of the TAD exchange into the direction of the acceptor indole. Thus, once the TAD compound is released from the donor indole, the follow-up reaction with the acceptor donor should be significantly faster than the reformation of the donor TAD-indole adduct. From the previously conducted model studies, an indole combination that exactly fulfils the desired behaviour was found in the combination of 3-methyl-2-phenyl-1*H*-indole **14** and 2,3-diphenyl-1*H*-indole **16**, as the acceptor and donor indole, respectively (*cf.* Figure III.4).

The intriguing idea of an orthogonal indole-to-indole exchange reaction was first investigated with low molecular weight model compounds. A similar protocol as the one used to investigate the thermal reversibility profiles of the TAD-indole blocking systems was therefore applied, albeit by using the second indole instead of a diene to act as a TAD trapping agent. Thus, aliquots of 3-methyl-2-phenylindole **14** as the acceptor were added to a DMSO-*d*₆ solution of the BuTAD-adduct with the sterically hindered donor 2,3-diphenylindole **16** (see Figure III.12a). As can be seen from the ¹H-NMR spectrum, the resulting two-component mixture is stable at room temperature with all BuTAD bound to the donor indole (*cf.* signals *a* and *b* in spectrum *I*, Figure III.12c). Upon heating of the reaction mixture, the TAD compound is released from the donor indole **16** and made available to undergo reaction with either of the indole substrates. Since the acceptor indole **14** is demonstrated to react faster with TADs whilst being more sluggish in the retro-reaction, a kinetically controlled net transfer of BuTAD from the donor to the acceptor indole took place, which was indicated by the disappearance of signals *a*, *b* and *c* and appearance of *e*, *f* and *g* in the ¹H-NMR spectrum (*II*, Figure III.12c). This kinetic selectivity for the acceptor indole is also observed by the exclusive formation of the corresponding **BuTAD-14** adduct upon addition of the TAD reagent to an equimolar mixture of **14** and **16** at room temperature (refer to appendix B for NMR analysis of this competition experiment). The indole-to-indole transfer reaction was shown to be completed (> 99 %, Figure III.12d) already after 15 minutes at 120 °C.

At higher temperatures, no decrease in TAD-addition to the acceptor indole was observed, which indicated a strong thermodynamic preference for the newly formed **BuTAD-14** adduct.

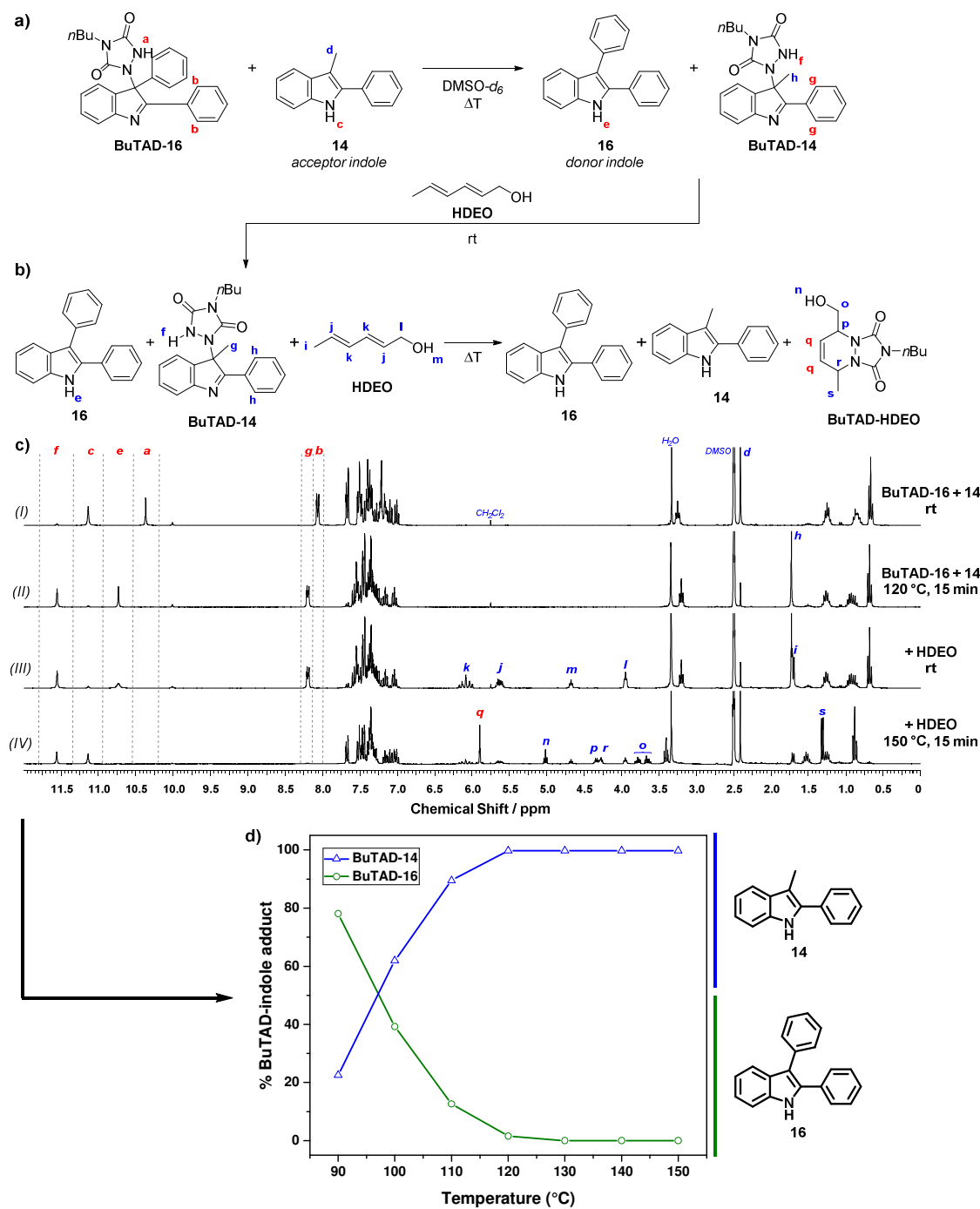
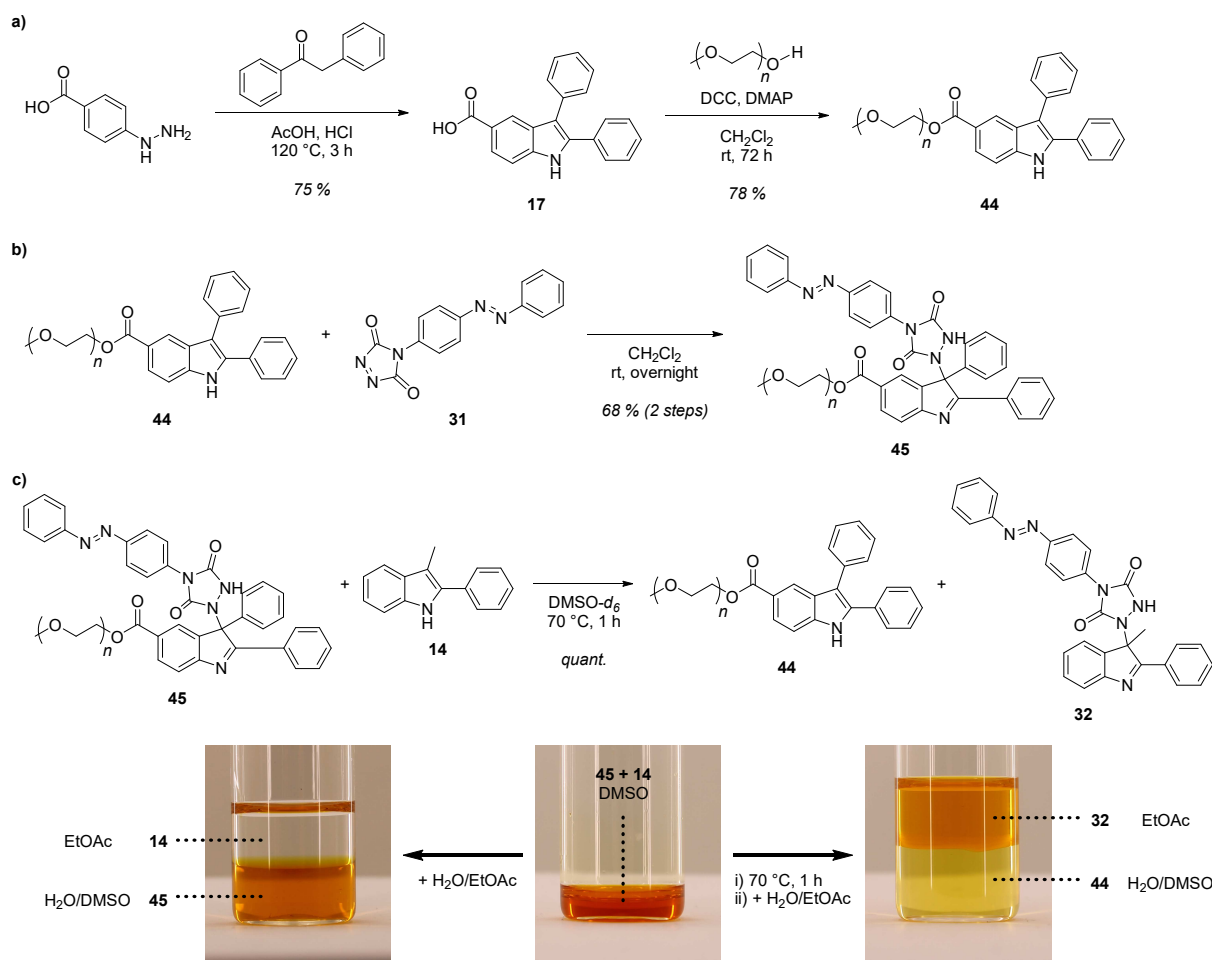


Figure III.12. a) Selective transfer of BuTAD from the donor indole **16** to acceptor indole **14** upon heating. b) Addition of HDEO to the reaction mixture and subsequent heating at 150 °C eventually converts all BuTAD into the irreversible Diels-Alder adduct with the release of both original indole substrates. c) $^1\text{H-NMR}$ spectra of the orthogonal indole-to-indole exchange reaction before and after heating for 15 minutes (spectra *I* and *II*) and the consecutive irreversible TAD-transfer to the conjugated diene HDEO upon a second 15-minute heating period at 150 °C (*III* and *IV* before and after heating, resp.). d) Graphical representation of the indole-to-indole TAD-transfer reaction as a function of temperature indicates the complete and orthogonal transformation of **BuTAD-16** into **BuTAD-14** within 15 minutes at 120 °C.

In a subsequent low molecular weight experiment, the reaction mixture after complete indole-to-indole BuTAD transfer was treated with one equivalent of the conjugated HDEO diene and heated a second time at 150 °C for 15 minutes (Figure III.12b). Analysis of the $^1\text{H-NMR}$ spectrum before and after heating (Figure III.12c, *III* and *IV*, resp.) clearly showed all BuTAD trapped in the HDEO Diels-Alder adduct (signal *s*) with the concomitant release of the acceptor indole **14**. Thus, a TAD reagent could be successfully transferred from one indole substrate to another, thereby retaining its reversible nature and making it possible to be transferred irreversibly in a third consecutive one-pot reaction.



Scheme III.11. a) Synthesis of 2,3-diphenyl-1*H*-indole-5-carboxylic acid **17** and its use in the post-modification of poly(ethylene glycol) to give the indole end-functionalised indole **44**. b) Reaction of the PEGylated indole with azobenzene TAD-dye **31** yields the water soluble blocked TAD-dye **45**. c) The selective indole-to-indole reaction was visually demonstrated by the transfer of the orange TAD-dye from the aqueous phase before, to the organic phase after heating the blocked TAD-dye **45** in the presence of the acceptor indole **14**.

The practicality of this orthogonal indole-to-indole reaction was once more demonstrated in a macromolecular context by means of a visual TAD-dye phase transfer experiment. To this end, the carboxylic acid functionalised 2,3-diphenylindole **17**, with the lowest temperature of reversibility, was modified with poly(ethylene glycol) monomethyl ether (*m*PEG, $M_n = 2.0$ kDa) to provide the donor indole end-capped polymer **44** (Scheme III.11a). The PEGylated indole was

then used as a blocking agent for the earlier introduced azobenzene TAD-dye **31** to yield a water soluble blocked TAD-dye **45** (Scheme III.11b). The resulting *m*PEG-TAD-dye conjugate **45** was subsequently incubated together with an equimolar amount of acceptor indole **14** in deuterated DMSO-*d*₆ and heated for 1 hour at 70 °C (Scheme III.11c). After a clear transfer of the TAD-dye from PEGylated donor indole **44** to non-functional acceptor indole **14** was evidenced by ¹H-NMR (refer to Appendix B), the reaction mixture was added to water, followed by the addition of ethyl acetate to induce a phase separation (Scheme III.11c). The newly formed indole-dye conjugate **32** was found to reside preferentially in the organic phase (refer to Appendix B for ¹H-NMR spectra), thereby visually demonstrating the phase transfer of the orange TAD-dye out of the aqueous phase.

III.7 Conclusions and perspectives of the blocked triazolinedione concept

In the current chapter, a series of easy-to-synthesise indole moieties were introduced and evaluated to act as suitable blocking agents for highly reactive TAD compounds. The possibility to engineer the TAD-indole systems in order to modulate both the forward blocking and backward deblocking reactivity was identified, leading to a tunable behaviour of the temperature at which the deblocking process can be triggered.

At first, the synthetic protocol to generate the TAD-reactive indoles was optimised to a more upscalable and highly versatile route thereby swiftly enabling the introduction of a variety of different substituents onto the indole scaffold, including functional handles for their straightforward incorporation into polymers. Whereas the introduction of a phenyl group at the indole C2-position was shown to slightly enhance the forward reaction kinetics, the additional incorporation of a phenyl group near the TAD-reaction site at the C3-position lead to a significant reduction of the deblocking reaction barriers by more than 20 °C.

The remarkable control over the dynamic nature of the TAD-indole systems was then rationalised by theoretical calculations which provided insights into the underlying reaction mechanism. Moreover, the information gained from the theoretical model identified the prospect to further finetune the indole blocking agent reactivity. This resulted in the synthesis of a 2-phenylindole library with the additional introduction of varying sterically demanding substituents as well as electron withdrawing and/or donating groups. The blocking capabilities of all indoles under investigation were assessed via kinetic thermal reversibility profiles, which were obtained by monitoring the deblocking kinetics at elevated temperatures. The resulting temperatures of deblocking, half-life temperatures and experimentally observed activation energies were determined and found to span an extraordinary wide temperature range to promote the TAD-indole deblocking reaction from above 100 °C down to 54 °C. Additionally, the nature

of the TAD substituent was shown to have a significant effect, systematically lowering the deblocking behaviour by approximately 20 °C. Overall, the various indole-TAD systems allowed for the careful modulation of the deblocking temperatures over a 50 °C interval, thereby paving the way for temperature controlled TAD reactivity as low as 35 °C. Interestingly, the careful selection of two blocked TAD-indole systems with an orthogonal reactivity was shown to create an unprecedented indole-to-indole exchange reaction that allows for the selective transfer of a TAD moiety without sacrificing its dynamic characteristics.

The applicability of the indole-blocked TAD reagents was demonstrated by means of two representative case studies of TAD chemistry in a polymer context. A first example of the added value that blocked TAD reagents have to offer was found in the formation of a bench-stable TAD-dye that was used in time-controlled polymer modification. A second case study validated the tunability of the blocking concept with bivalent TAD-based crosslinkers to provide on demand curing of a diene-containing polyurethane at distinct temperatures. As the blocking agents remain in the material after the temperature triggered gelation, the effect of the indoles on the thermal properties was investigated.

The developed blocked triazolinedione concept undoubtedly opens a whole new range of applications for TAD chemistry that require an external and temporal control. Next to on demand polymer modification and crosslinking reactions, the newly identified and tunable dynamic TAD-indole systems can also be easily incorporated into dynamic materials via functional handles on the indole core, which would enable triggered debonding applications. Ongoing research efforts are also devoted to the design of dynamic macromolecular architectures with tunable properties that can be triggered at distinct temperatures. Furthermore, the use of indole blocking agents that release tailored TAD reagents *in situ* at ambient temperatures, e.g. 40 °C, show highly interesting opportunities in the field of bioconjugation. Whereas TADs readily hydrolyse when exposed to water, the use of hydrophilic TAD-indole combinations, such as the PEGylated blocked TAD-dye introduced in this chapter, might serve as a valuable and general approach to deliver TAD compounds to a suitable reaction partner in a controlled manner, even in aqueous media.

One of the main limitations of TAD chemistry has been the access to functional TAD reagents. In particular, the chemoselectivity issue that is observed during the post-modification of 4-functionalised urazoles as a result of their acidity and nucleophilicity prevents the access to conventional ligation methods, such as amide bond formation. Therefore, next to the time-controlled activation of TAD reactivity, the developed indole blocking agents are currently also applied within our laboratories as a protecting group strategy in tailored TAD synthesis. By incorporating the indole groups onto the TAD moiety, the undesired reactivity of the formed urazole NH is shielded by the steric bulk of the indole, thereby greatly facilitating post-modification of the TAD precursor. This has already marked a real breakthrough with regard to

the availability and scalability of highly tailored TAD reagents, which was considered a true bottleneck of TAD chemistry thus far.

Finally, the selective exchange of the orange TAD-dye via an orthogonal indole-to-indole reaction is also envisioned to be applicable for the transfer of a functional TAD moiety between two resins that are not in physical contact with one another. In such a system, the most dynamic TAD-indole system would be bound to a bead and selectively transferred to a solid-supported diene. By submerging both of the resins in a solution of a suitable acceptor indole, which acts as the messenger, the TAD compound will be selectively transferred from one bead onto another upon heating. Ideally, the TAD reagent that is used in this ‘molecular courier system’ would carry a fluorescent tag or a biologically active molecule of interest.

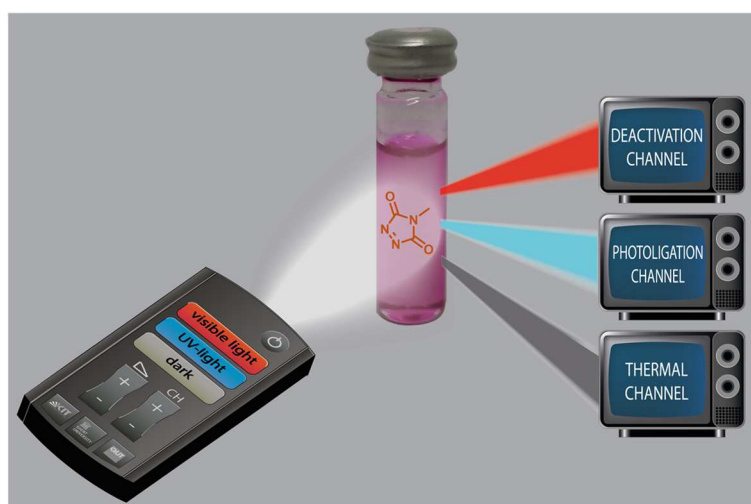
III.8 Notes on the collaboration

A collaboration with the research group of Prof. Veronique Van Speybroeck at the *Centre for Molecular Modeling* (Ghent University) was initiated to gain mechanistic insights into the TAD-indole reaction. The DFT calculations that are presented in III.3.3 were carried out by Hannelore Goossens (Ghent University), in close collaboration with Prof. Johan Winne from the Organic Synthesis group at Ghent University. All collaboration partners involved discussed and commented on the obtained results at all stages.

Chapter IV.

Photodeactivation of triazolinediones enabling light-switchable reactivity

Brief motivation and content



The ability to selectively switch a one-pot reaction system between a thermally and photochemically activated reaction channel by an external and defined stimulus constitutes a key frontier within the realm of chemical reaction control. In this chapter, the reactivity of triazolinediones (TADs) is demonstrated to be effectively modulated by an external photonic field. Specifically, the visible light-induced polymerisation of TADs leads to their quantitative photodeactivation, while the thus formed labile homopolymer slowly releases the initial monomers upon standing in the dark. Hence, a well-defined on-and-off switch is provided over the thermal reactivity of these unique TAD coupling agents. Based on the identified photodeactivation, a reaction manifold is pioneered whereby light serves as a gate to switch between a UV-induced Diels-Alder conjugation with photocaged dienes and a thermal TAD-addition reaction with simple alkenes. Importantly, the obtained modulation of the reactivity by light is reversible and the individual reaction pathways can be repeatedly accessed. The addressed photochemically controlled reactivity not only enables a step change in small molecule ligations, yet is also explored in controlled site-selective surface design, potentially opening sub-diffraction laser lithography.

Adapted from

H. A. Houck, F. E. Du Prez, C. Barner-Kowollik, *Nature Communications* **2017**, *8*, 1869.

With permission from Nature Publishing Group, published under the Creative Commons License (CC-BY-4.0).

IV.1 Introduction

The introduction of external stimuli to gain a defined control over spring-loaded and chemoselective reactions – some of which meeting the stringent click chemistry requirements^{1, 3} – forms a critical milestone in the design of adaptive, self-reporting and programmable materials.²² Specifically temperature and light are well developed triggers that allow for the on demand generation of complex macromolecules via newly coined concepts such as *transclick*^{7, 25} and *photoclick*²⁶⁻²⁷ approaches.

In the previous chapter (III), controlled triazolinedione-based polymer modification and crosslinking reactions have been established via the development of suitable blocking agents that can activate TADs on demand upon heating. Whereas thermally triggered TAD reactivity enables a selective on-switch over their chemical transformation, light-induced protocols are considered much more defined as they also offer spatial resolution next to temporal control. This spatio-temporal feature of light-induced processes has vastly been exploited in precision applications that require site-selective reactivity, most prominently in surface functionalisation,^{121, 386} three dimensional laser lithography^{167, 172, 387} and *in vitro* protein imaging.^{27, 388} Consequently, the possibility to switch TAD reactivity on-and-off by light was projected in order to open TAD chemistry to the realm of spatio-resolved applications.

In addition, light-triggered reactions also offer the potential to conduct sequential photochemical reactions in a highly orthogonal manner by carefully activating different chromophores each at a distinct wavelength.^{135, 389} Elegant examples of such wavelength-orthogonal processes are found in the many photocleavage reactions⁸⁵⁻⁸⁶ that were developed for the selective uncaging of bioactive molecules.^{87, 89, 390} More recently, λ -orthogonal light-induced conjugation reactions have also been introduced (*cf.* II.1.3.2), thereby enabling the site-selective design of defined macromolecular architectures.^{135, 391} Besides investigating the potential of light to serve as an on/off trigger for TAD reactivity (IV.2), their combination with existing photochemical protocols will also be targeted in the current chapter (IV.3).

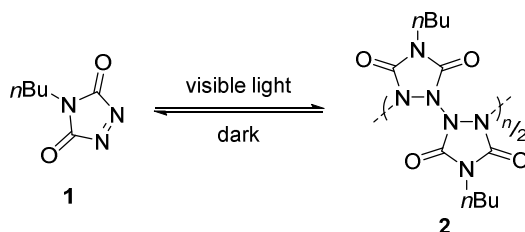
A final highly interesting, yet almost non-explored feature of light, is its exploitation as a gate in order to switch between a thermally activated and photochemically induced reaction channel.¹⁵⁵ To date, the few examples that are capable of regulating the outcome of a chemical one-pot process via an outer photonic field are based on the isomerisation reaction of photoswitches (*cf.* II.1.3.3).¹⁵²⁻¹⁵³ Whereas this allows for the modulation of the chromophore's reactivity, their thermal reactivity, however, can never be fundamentally halted. In other words, once the one-pot manifold is generated, the system will be active and always be forced into one reaction avenue or the other. With the development of a light-controllable off-switch over TAD reactivity, an unprecedented one-pot reaction manifold will be pioneered whereby the outcome can not only be selectively switched from thermal to photochemical reaction products, but can also be completely halted (IV.4). The applicability of such an ultimately controllable system will

eventually be explored in selective on demand bonding onto surfaces by means of laser lithography (IV.5).

IV.2 Photopolymerisation as the key to photodeactivation

While the idea to photochemically deactivate TAD compounds is theoretically simple, the ability to control these highly reactive moieties is quite challenging, since TAD-based ligations often proceed extremely rapidly, even far below ambient temperature. Visible light irradiation even enhances the reactivity of TADs, which makes them eligible to undergo cycloaddition reactions even with simple aromatic substrates such as benzene and derivatives thereof (*cf.* II.2.3.2).

The starting point for the photodeactivation strategy was the peculiar series of events that was rather serendipitously observed in the laboratory with a left-over NMR solution of 4-*n*-butyl-1,2,4-triazoline-3,5-dione (BuTAD) in deuterated chloroform. The purple BuTAD solution was found to slowly turn colourless over time when it was exposed to sunlight. Remarkably, the loss of colour could not be attributed to photolytic TAD degradation as the initial purple colour was regained overnight. After an extensive literature screening, a similar observation was found in the report by Pirkle and Stickler in the 1970s, who attributed the colour change to the exclusive photopolymerisation of BuTAD (**1**, Scheme IV.1) under visible light irradiation to provide the homopolymer **2**.³⁰² Not surprisingly, the all-nitrogen containing backbone polymer was found to be unstable and slowly regenerated the purple TAD monomer over time, with up to 80 % release after several days.



Scheme IV.1. Transformation of 4-*n*-butyl-1,2,4-triazoline-3,5-dione **1** into its homopolymer **2** under visible light irradiation.

While one avenue to photodeactivate molecules can be provided by changing its electronic properties, thereby preventing a thermal chemical reaction to proceed, a viable alternative can be offered by means of a reversible light-induced transformation (e.g. photoisomerisation) of the target substrate into a non-reactive moiety. In the latter context, the photopolymerisation of TADs was first re-investigated (IV.2.1) and subsequently examined as an avenue to photochemically deactivate thermal TAD reactivity (IV.2.2).

IV.2.1 Photopolymerisation

Initial experiments were aimed to reproduce the formation of polymeric **2** under visible light irradiation as was observed by Pirkle and Stickler. In their original report, a 150 W quartz-iodine tungsten lamp was applied as the visible light source to affect the photopolymerisation of **1**, yet no details concerning the emission source were provided.³⁰² Therefore, the wavelength at which the TAD polymerisation can be executed was first established by means of a wavelength-tunable laser system. Green laser light irradiation (4 mW cm^{-2} , 100 Hz) of a 0.3 M deaerated carbon tetrachloride solution of sublimed **1** at the wavelength of maximum absorption $\lambda_{\text{max}} = 544 \text{ nm}$, resulted in a colourless solution after 10 minutes (Figure IV.1). A similar experiment was conducted with the aromatic PhTAD reagent, but did not result in photobleaching, in contrast to its aliphatic counterpart. Stickler reported a similar observation, which was attributed to the self-quenching of the 4-aryl TAD-substituent (*cf.* II.2.3.2).^{302, 304}

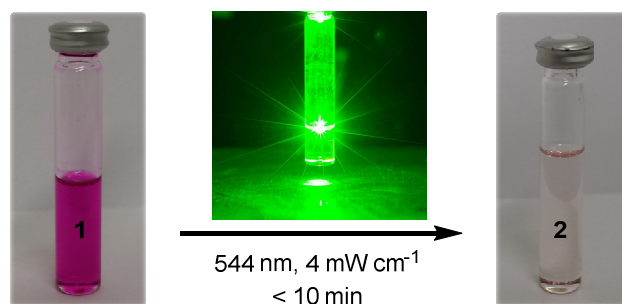


Figure IV.1. Decolouration of a BuTAD solution (**1**, 0.3 M in CCl_4) observed after 10 minutes of green laser light irradiation (544 nm , 4 mW cm^{-1} , 10 min).

Upon standing in the dark, the characteristic purple colour of **1** was slowly regenerated, as indicated by visual and UV/vis analysis (see Figure IV.2). Consecutive irradiation experiments resulted in the repeatable photobleaching without affecting the subsequent regeneration of the purple colour in the dark. Thus, the photochemical system entails a reversibly switchable behaviour. Irradiation at lower wavelengths – down to 440 nm, whilst keeping the amount of incident photons constant (*cf.* Appendix C.2.2) – gave similar results, albeit after prolonged irradiation times (i.e. up to 30 minutes).

Having reproduced the reversible colour switch of the BuTAD solutions, the formation of the photopolymer **2** was next evidenced. $^1\text{H-NMR}$ analysis immediately after irradiation of **1** in deuterated chloroform (0.3 M, 544 nm , 4 mW cm^{-2}) supported the formation of polymeric **2** by the characteristic peak broadening of the *n*-butyl proton signals (Figure IV.3), which was confirmed via high-resolution electrospray ionisation mass spectrometry (ESI-MS, refer to Figure IV.4a and Appendix C). Furthermore, the rapid decay of the polymeric distribution in the mass spectrum showcased the thermal instability of **2** upon standing in the dark (Figure IV.4b and c).

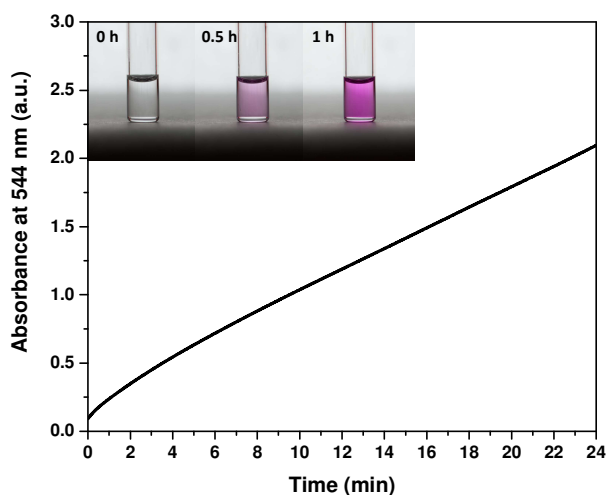


Figure IV.2. UV/vis measurement (5 minute time delay) of a 0.3 M solution of **1** in CCl_4 after a 10-minute irradiation period with visible light (544 nm, 4 mW cm^{-1}), indicating the regeneration of the purple colour over time (inset).

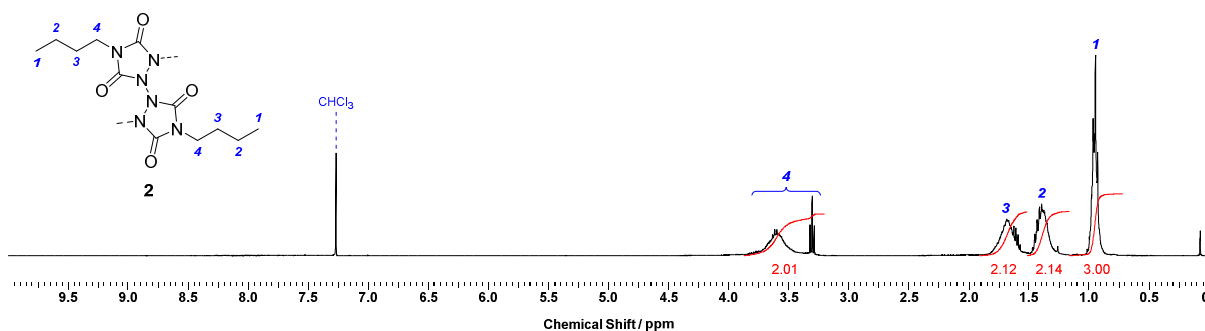


Figure IV.3. $^1\text{H-NMR}$ spectrum of photopolymer **2**, recorded 7 minutes after a 10-minute irradiation period of BuTAD **1** (0.3 M, CDCl_3) with green laser light (544 nm, 4 mW cm^{-1}), indicating peak broadening of the *n*-butyl proton signals.

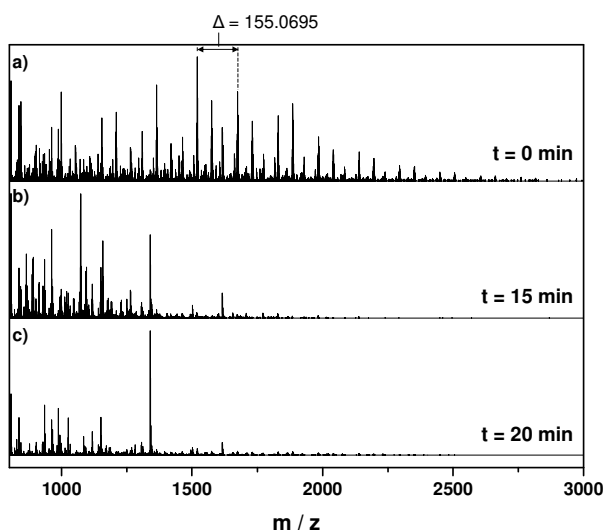


Figure IV.4. a) ESI-MS spectrum recorded immediately after a 10-minute irradiation period of BuTAD **1** (0.3 M, CDCl_3) with green laser light (544 nm, 4 mW cm^{-1}), indicating the presence of polymeric compound **2**. b) The fast decrease of the polymeric signals after standing in the dark for 15 minutes demonstrated the thermal instability of the thus formed polymer. c) Within 20 minutes of standing in the dark, barely any polymeric species were detected.

Interestingly, the photopolymerisation of **1** was observed to be a strongly solvent-dependent process. In acetonitrile, for instance, no polymer formation was detected even after prolonged irradiation times (i.e. 1 hour at 544 nm, 4 mW cm⁻²), which was judged by the superimposable absorption spectra obtained shortly after irradiation and upon standing in the dark for 16.5 h (see Figure IV.5a). It should be noted that the slight decrease in absorption intensity compared to a non-irradiated reference sample could be attributed to photodegradation (*cf.* II.2.3.2). In fact, acetonitrile solutions of **1** could be used to obtain qualitative insights with regard to the photostability of BuTAD, without interference of the photopolymerisation process. Thus, BuTAD solutions in acetonitrile were subjected to light in both the UV- and visible wavelength regime. More specifically, irradiation was performed by a wavelength-tunable laser from 320 to 560 nm in 10 nm intervals, thereby keeping the amount of incident photons constant^{131, 392} (refer to Appendix C.2.2). The fraction of photostability was readily determined by comparing the UV/vis absorption spectra recorded before and after irradiation with a distinct colour of light. From the results, depicted in Figure IV.5b, isolated BuTAD solutions were shown to be surprisingly stable under the applied conditions of irradiation, particularly in the visible light range of the spectrum (i.e. above 400 nm). This is not only an important finding in the context of the ongoing research efforts to develop modular light-induced transformations that can be triggered by more benign visible light, but also with regard to the future endeavours related to the current doctoral work (i.e. Chapter V and VI).

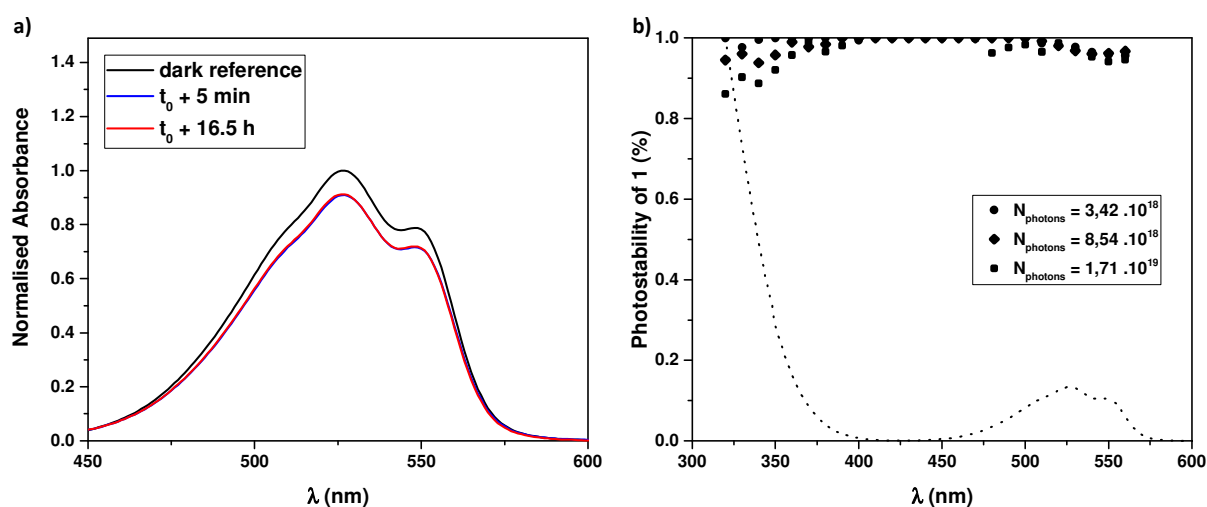


Figure IV.5. a) UV/vis spectra (MeCN) obtained after a 1-hour irradiation period of BuTAD **1** in acetonitrile (0.3 M, 544 nm, 4 mW cm⁻¹), showing only a minor decrease in absorption intensity (attributed to photodegradation). No complete disappearance of **1**, nor its regeneration after standing in the dark for 16.5 h is detected. b) Acetonitrile solutions of **1** hence enable a photostability assay (MeCN, 5 mg mL⁻¹) between 320 and 560 nm with 10 nm intervals at a constant number of incident photons, indicating the pronounced stability of TADs in the visible range of the spectrum. The dashed line represents the absorption spectrum of **1** in acetonitrile.

IV.2.2 Photodeactivation

Following the establishment of the most efficient conditions to affect the polymerisation in combination with the photostability assay of **1**, the ability of the photochemical TAD switch to act as a deactivation channel for their unique thermal reactivity was probed in a critical next step. Specifically, a trapping experiment was devised that is able to detect any presence of active TAD moieties during irradiation. Importantly, the thermal reaction partner of choice should result in the instantaneous formation of an irreversible TAD-adduct, which can be readily identified via offline analytical tools.

Here, cyclopentadiene (**C_p**) was selected as the preferred complementary reaction partner as it is notorious for its ultrafast Diels-Alder reaction with TAD (*cf.* $k_2^{25\text{ }^\circ\text{C}} = 1.6 \cdot 10^5 \text{ L mol}^{-1} \text{ s}^{-1}$ for the reaction of PhTAD with **C_p** in toluene). Thus, **C_p** acts as a reliable probe to identify active TAD molecules. Indeed, addition of a slight excess of **C_p** (1.2 eq.) to a 0.3 M reference solution of **1** in CDCl₃ kept in the dark, immediately resulted in the discolouration of the purple solution with the formation of the corresponding Diels-Alder product **3** (Figure IV.6a). The remaining non-reacted **C_p** was ultimately compensated for by the sequential addition of *N*-ethylmaleimide (1.4 eq.) to give a second Diels-Alder adduct **4**. Analysis of the ¹H-NMR spectrum confirmed the formation of both Diels-Alder adducts and indicated the complete consumption of **1** and **C_p** (Figure IV.6c, spectrum *I*). Moreover, the absence of any remaining TAD was supported by the lacking regeneration of a purple colour in the final reaction mixture.

In a sister experiment, the TAD solution was first subjected to visible light irradiation (544 nm, 4 mW cm⁻¹) for 10 minutes to completely transform **1** into its photopolymer **2**, after which the cyclopentadiene trap (1.2 eq.) was injected into the solution under continued irradiation (see Figure IV.6b). The resulting mixture was subsequently kept irradiated for an additional minute to ensure the complete detection of any active TAD species into the corresponding **C_p**-adduct **3**. Eventually, the residual amount of cyclopentadiene was again quenched with *N*-ethylmaleimide (1.4 eq.) before the visible light was switched off and the resulting non-reactive mixture was analysed via offline ¹H-NMR spectroscopy. In contrast to the reference experiment performed in the absence of visible light, the initial colourless reaction mixture quickly regained a faint purple colour, which served as a first indication for the regeneration of **1**. Critically, no trace of the TAD-Diels-Alder adduct **3** could be observed in the ¹H-NMR spectrum (*II*, Figure IV.6c, indicated by the dashed red line). This unambiguously demonstrated the complete absence of any active TAD molecules during the course of the visible light irradiation. In other words, converting **1** into its photopolymer **2** resulted in the quantitative light-induced deactivation of its thermal reactivity.

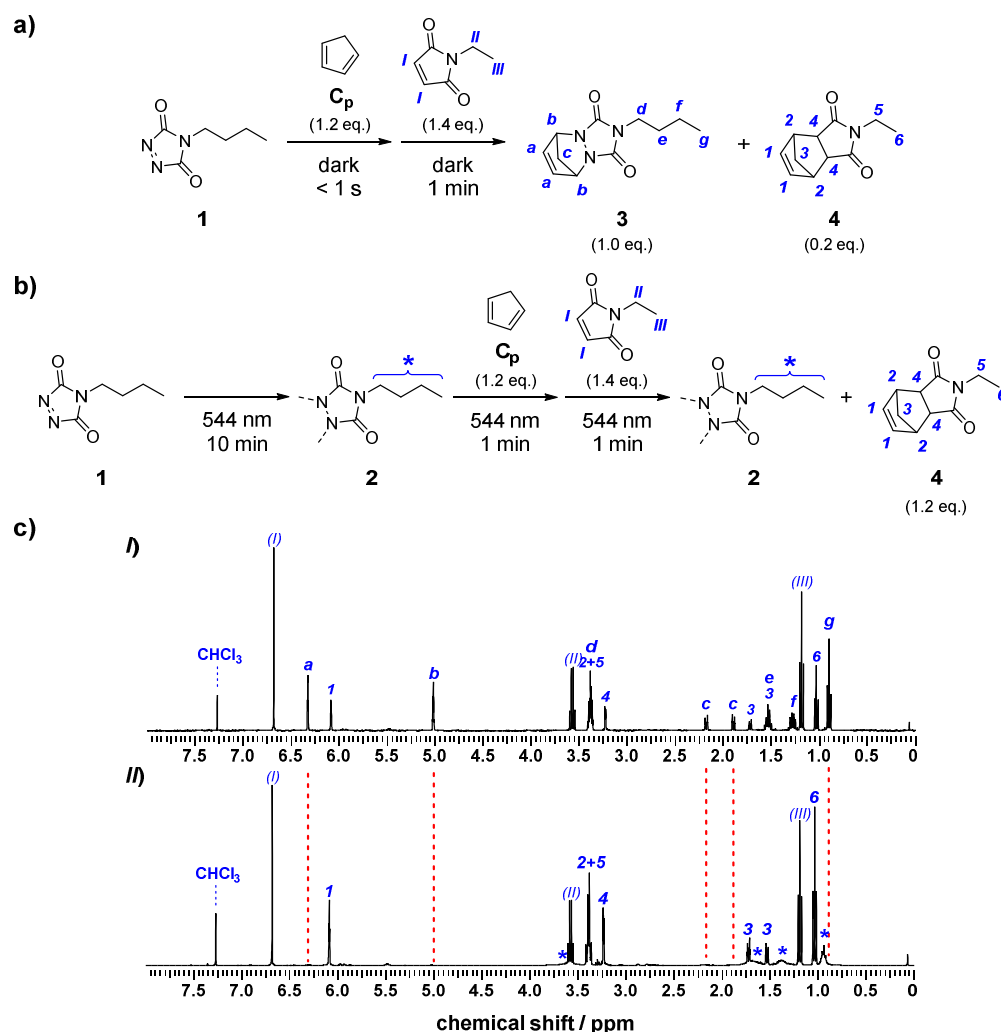


Figure IV.6. Trapping experiment as a proof of deactivation. a) Reference experiment carried out in the dark of the sequential addition of cyclopentadiene (1.2 eq.) and *N*-ethylmaleimide (1.4 eq.) to a solution of **1** (0.3 M in CDCl₃, 1.0 eq.). b) Experiment under continued green light irradiation (544 nm, 4 mW cm⁻²) whereby the mixture of trapping agents is added after the photopolymerisation of **1** into **2**. c) Whereas the dark reaction shows the complete trapping of **1** by cyclopentadiene (spectrum I), no such adduct formation is detected when the visible light is switched on (spectrum II, dashed red line), thus indicating the ability to photodeactivate **1** and switch off its thermal reactivity.

Since the amount of reactive versus deactivated triazolinediones can be swiftly determined via the cleverly designed cyclopentadiene/maleimide trapping experiment, a more quantitative analysis of the BuTAD photopolymerisation kinetics could be made. Indeed, by repeating the above experiment after distinct irradiation times, the monomer conversion was determined as a function of time (Figure IV.7a), indicating the complete polymerisation of **1** – and thus photodeactivation – to occur within 5 minutes (0.3 M in CDCl₃, 544 nm, 4 mW cm⁻¹).

Whereas the photodeactivation of **1** was shown to be a rather fast process with a half-life time of 1.7 min (CDCl₃, 18 °C, Figure IV.7b), the monomer release in the dark proceeded considerably slower with up to 4 % of regenerated **1** after 2 h (Figure IV.7c). Even in the presence of cyclopentadiene as a trap, the depolymerisation was only slightly accelerated (i.e. 5 % release within 2 h). Remarkably, the depolymerisation of **2** was also verified to occur under UV-

irradiation ($\lambda_{\max} = 320$ nm, Arimed B6, 3 x 36 W), although a more pronounced acceleration of monomer release was observed (approx. 7 %). This rather unexpected result was attributed to the higher temperature inside the photoreactor (25 °C) during the UV-irradiation compared to the regeneration monitored in the dark (i.e. at 18 °C). Indeed, a significant effect of increasing temperature on the regeneration rate was observed via isothermal UV/vis measurements (Figure IV.7d), which agrees with the thermal instability of the formed TAD polymer that was noted earlier (*cf.* IV.2.1).

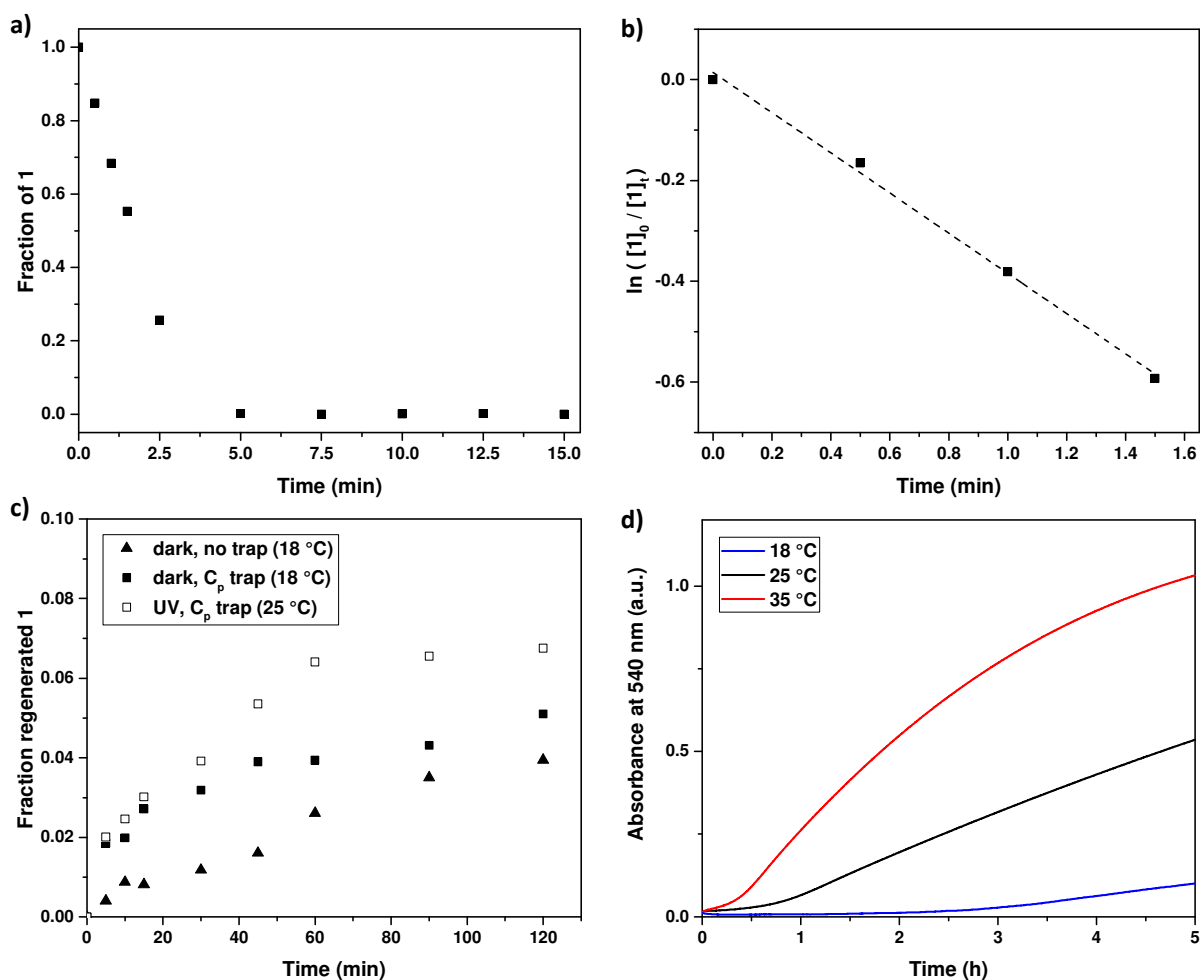


Figure IV.7. a) Photopolymerisation kinetics of **1** (0.3 M, $CDCl_3$) when irradiated at 544 nm (4 mW cm^{-2}) whereby the monomer conversion over time is determined via offline $^1\text{H-NMR}$ analysis by means of a dual cyclopentadiene/*N*-ethylmaleimide trapping experiment. b) First-order reaction kinetics are observed from which $t_{1/2} = 1.7$ min and $k_{\text{obs}} = 0.4 \text{ min}^{-1}$ are calculated. c) Regeneration kinetics of **1** from the photopolymer **2** at 18 °C in the dark with or without cyclopentadiene as an *in situ* trap. An accelerated release of **1** is observed under the UV-irradiation conditions applied to induce the phenol reaction ($\lambda_{\max} = 320$ nm, Arimed B6, 3 x 36W), which was attributed to the higher temperature in the photoreactor (25 °C). d) Effect of temperature on the depolymerisation of **2** assessed via UV/vis kinetic measurements ($CHCl_3$) at 18 °C (blue), 25 °C (black) and 35 °C (red), recorded after a 5-minute irradiation period of **1** (0.3 M, $CHCl_3$) with green laser light (544 nm, 4 mW cm^{-2}).

IV.3 Orthogonality with different colours of light

After having established a photochemical way to deactivate TADs in the visible light regime, the combination with a second light-induced conjugation reaction was next examined in order to design a truly wavelength-orthogonal reaction system. Since our research group at the Karlsruhe Institute of Technology (Germany) is renowned for their expertise with regard to photo-triggered ligation reactions, the current project highly benefitted from the vast amount of efficient bond-forming reactions that have been developed throughout the years and are accessible by both UV- and visible light.^{113, 123, 129, 132, 134, 146, 393}

With the photopolymerisation of TADs triggered by visible light whilst being unaffected in the UV-range of the spectrum, a UV-triggered conjugation reaction was sought after as to provide the best changes for the λ -orthogonal manifold to succeed. Here, one of the workhorses of our previously established photochemistries, i.e. the photoenol reaction, was selected based on its attractive complementary absorption spectrum (Figure IV.8). In the following, the compatibility of TAD with the existing photoenol reaction will be accounted for (IV.3.2) and the combination with the photodeactivation will be explored (IV.3.1).

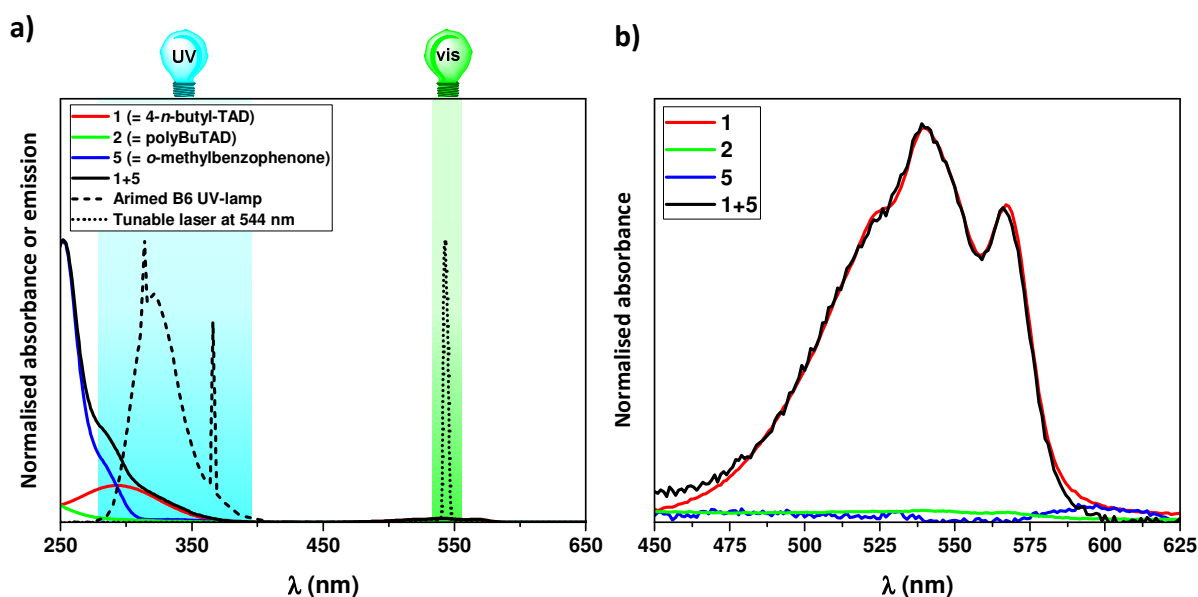
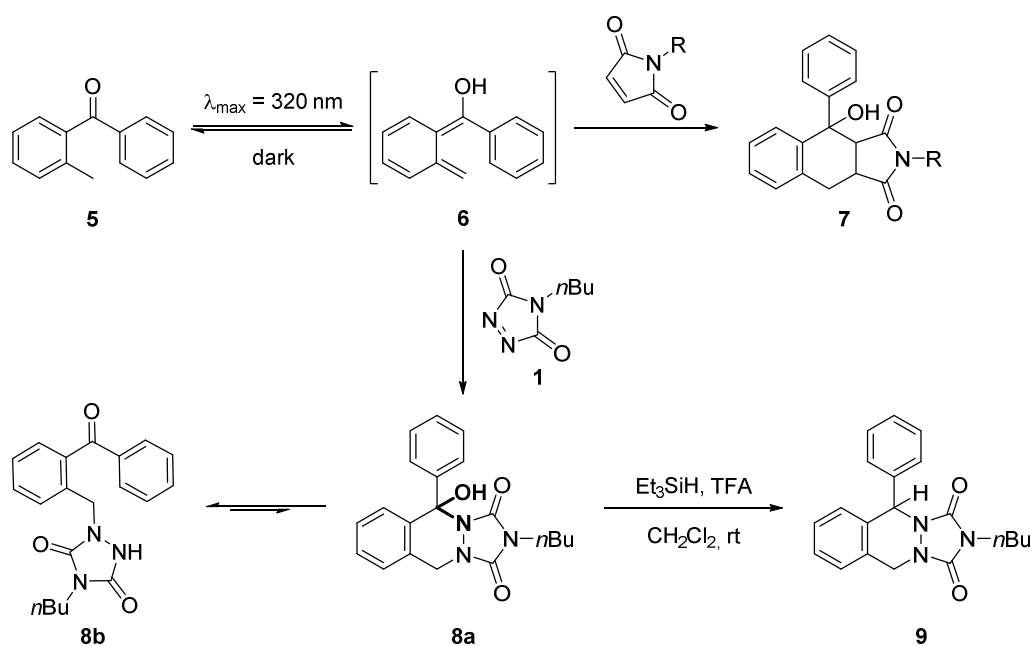


Figure IV.8. a) Absorption (in CHCl₃, 25 °C) and emission spectra illustrating the required wavelength-dependent excitation of the reagents **1** (red), **2** (green) and **5** (blue) together with the light sources (UV-emitting fluorescent lamp (dashed) and green laser light (dotted)) applied to create a λ -orthogonal reaction system **1** + **3** (black). b) Zoom of the visible light absorbance of the reagents and reaction mixture involved.

IV.3.1 Introducing TAD to UV-induced conjugation

In order to develop an orthogonal reaction manifold that is steered by two different wavelengths, the UV-induced isomerisation of *o*-methylbenzophenones **5** to their *o*-quinodimethane derivatives **6** was exploited as the photochemical reaction pathway (Scheme IV.2). The formation of photoenol **6** upon irradiation is a well-established and highly attractive substrate that swiftly participates in light-induced [4+2] reactions with electron-deficient olefins, including *N*-substituted maleimides, to give the resulting cycloadducts (e.g. **7**, Scheme IV.2).^{114, 126} Although TADs are structurally similar to maleimides yet intrinsically more reactive, they remained unexplored dienophiles in the photoenol ligation reaction. The light-induced [4+2] cycloaddition reaction of TADs with *o*-methylbenzophenone was therefore first investigated.



Scheme IV.2. UV-induced photoisomerisation of *o*-methylbenzophenone **5** into the diene-containing photoenol **6**, which readily reacts with *N*-substituted maleimides to give the [4+2] cycloadduct **7**. With BuTAD **1** as the dienophile, the photoenol reaction leads to a mixture of two photoproducts **8a** and **8b**, which are in equilibrium with one another, most likely via the labile hemiaminal-type bond (in bold), as was evidenced by the reduction of the reaction mixture into the exclusive formation of cyclic **9**.

Surprisingly, the straightforward irradiation of **5** in the presence of BuTAD (**1**) with compact fluorescent lamps emitting around $\lambda_{\max} = 320$ nm – typically employed to induce the formation of the photocaged diene **6**¹²⁰ – only gave minor traces of the expected Diels-Alder adduct **8a** (Scheme IV.2). Instead, the Alder-ene type adduct **8b** was assigned as the major photoproduct in a combined (i.e. for **8a** + **8b**) isolated yield of 74 % (verified by 2D-NMR in combination with LC-MS, refer to Appendix C for structure elucidation). Peculiarly, a solvent-dependent product ratio was observed which altered from **8a**:**8b** = 1:14 in CDCl_3 to 1:3 in $\text{DMSO}-d_6$. Together with the unsuccessful separation of the two adducts by means of column chromatography (verified by their co-existence in the LC trace), this pointed towards an equilibrium between the formed photoproducts, which is most likely established via the labile

hemiaminal-type moiety in **8a** (highlighted in bold in Scheme IV.2). The dynamic equilibrium between the closed and open adduct was further evidenced by subjecting the crude reaction mixture to a triethylsilane reduction. This resulted in the complete conversion of both **8a** as well as **8b** into the exclusively observed cyclic product **9** (verified via NMR and LC-MS, refer to Appendix C for structure elucidation). As upon reduction the predominantly formed open adduct **8b** cannot directly be transformed into **9**, the complete conversion of the photoproduct **8b** can only be explained by means of an equilibration to **8a** before the hydroxyl-substitution with the mild hydride donor takes place. Critically, the observed dynamic interrelationship of the two formed photoaddition products does not undermine the envisaged wavelength-orthogonal reaction manifold since they are both generated via the same photo-induced reaction pathway.

IV.3.2 Combination of UV- and visible light-induced reaction channels

After having assessed the photostability of BuTAD (**1**) under UV-irradiation ($\lambda_{\max} = 320$ nm for 4 h) and *o*-methylbenzophenone (**5**) upon UV- and visible light impact (4 h at $\lambda_{\max} = 320$ nm and 1 h at $\lambda = 544$ nm, respectively) (refer to Appendix C for $^1\text{H-NMR}$ spectra before and after irradiation), the above established UV-induced photoenol reaction with BuTAD was combined with its visible light-induced deactivation. Moreover, the ability to conduct both photochemical processes orthogonally to one another was investigated.

In a first irradiation experiment, an equimolar solution (0.15 M, CDCl_3) of **1** and **5** was exposed to 544 nm green laser light to deactivate **1** via the formation of the photopolymer **2** in the presence of the benzophenone derivative **5**. Subsequently, the resulting colourless solution containing **2** + **5** was transferred into a photoreactor and irradiated with UV-light ($\lambda_{\max} = 320\text{nm}$) to provide the photodiene **6** in the presence of the photopolymer. Following the slow depolymerisation in the absence of green light, the *in situ* released **1** was immediately trapped to give the photoenol products **8a** + **8b** with 6.8 % conversion over 2 hours, which is in perfect agreement with the regeneration kinetics observed under the exact same conditions (*cf.* Figure IV.7c). It should be noted that in addition to the expected photoadducts, also minor traces of a 1:2 double TAD addition product were detected (refer to Appendix C for NMR and LC-MS data). When the UV-light was eventually switched off, the generation of the reactive photodiene species was discontinued, which resulted in the reaction mixture to unfold a purple colour through the continued release of **2**.

Close to identical results were observed in a second irradiation experiment upon reversing the order of the used colours of light (i.e. 320 nm followed by 544 nm). Slightly higher conversions to **8a** + **8b** (i.e. 8.2 % after 2 h) were achieved when the UV-induced [4+2] reaction was carried out before the TAD-deactivation, since the light-induced cycloaddition reaction was now the rate determining step instead of the *in situ* regeneration of **1** (see Figure IV.9 for comparative kinetics with or without subsequent green light irradiation). Thus, the UV- and visible light-induced reaction pathways were shown to be accessible independent of the applied light sequence and thus to have a λ -orthogonal nature.

Whereas the selective and sequential photochemical transformation of **1** in the presence of **5**, and vice versa, of **5** in the presence of **1** was demonstrated, the formation of a deeply purple coloured charge transfer complex [**1+5**] was found to have an undesired effect on the irradiation times that were needed to fully convert **1** into its photopolymer (i.e. 45 min instead of 5 min at 544 nm). Therefore, it was greatly favoured to conduct the photodeactivation of TAD with green laser light prior to the addition of the photoenol precursor **5**.

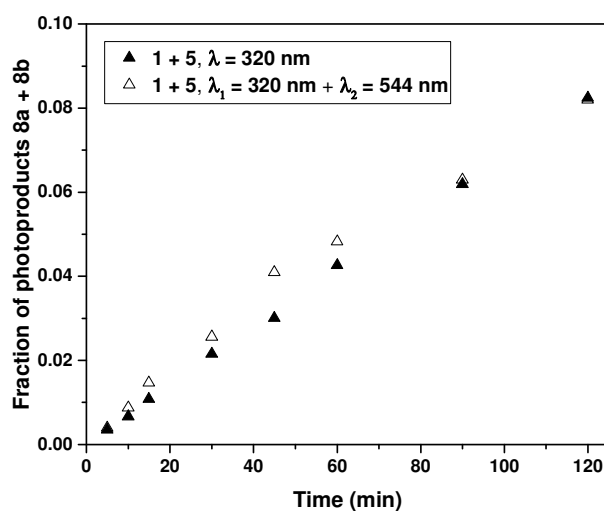
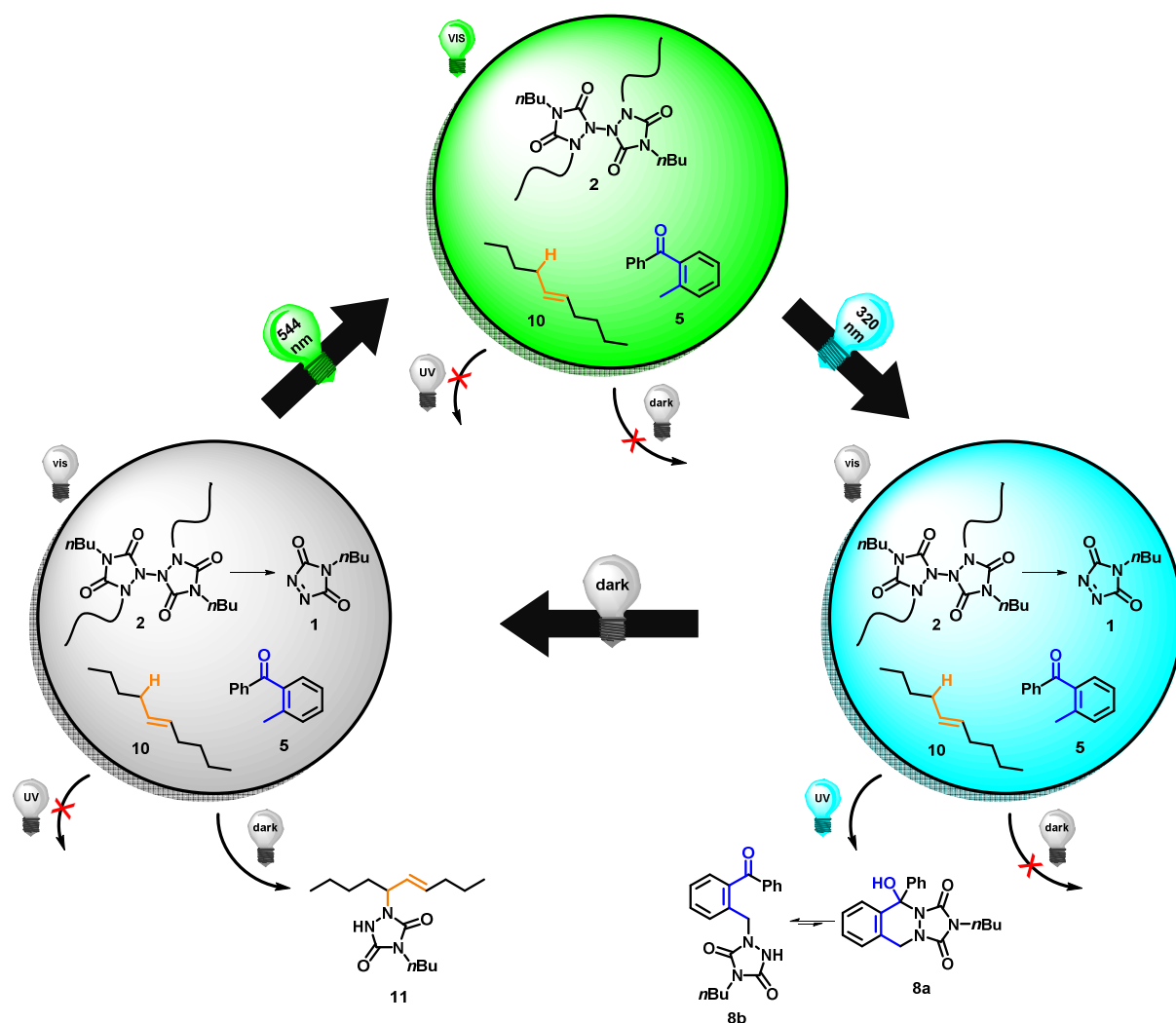


Figure IV.9. Fraction of photoproducts **8a** + **8b**, formed upon UV-irradiation ($\lambda_{\max} = 320$ nm, Arimed B6, 3 x 36W) of an equimolar solution of **1** and **5**. Similar conversions are obtained with (open) and without (closed) subsequent green light irradiation (544 nm, 4 mW cm⁻²).

IV.4 Light play: switchable TAD reactivity

The λ -orthogonal reaction system was finally extended by the introduction of a thermal TAD-based conjugation reaction in order to pioneer a one-pot reaction manifold that exhibits a light-switchable output. Here, *trans*-5-decene (**10**, Scheme IV.3) was selected as an ideal thermal TAD-substrate as it was shown to be stable under the projected conditions of irradiation (i.e. both UV- and visible light) and results in the quantitative formation of a well-defined 1:1 Alder-ene TAD-addition product **11** (refer to Appendix C for $^1\text{H-NMR}$ spectra). Importantly, the associated reaction kinetics of the adduct formation are not too fast to compete with the photoenol reaction, and nor too slow to ensure the complete trapping of any released TAD from its polymer.



Scheme IV.3. Representation of the designed light-switchable TAD reaction manifold, obtained after the visible light-induced photodeactivation of **1** into **2** followed by the addition of aliquots of the photochemical *o*-methylbenzophenone reaction partner **5**, and *trans*-5-decene **10** as the thermal TAD-substrate. The resulting mixture of **2** + **5** + **10** (0.15 M, CDCl_3) showed no reactivity as long as the green light is kept switched on (top). When the green light is switched off, however, UV-light act as a gate to selectively alter the reaction outcome between the photoproducts **8a** + **8b** and thermal TAD-addition product **11** (bottom).

The envisioned manifold system was eventually established by green laser light irradiation of **1** (0.3 M in CDCl₃) at 544 nm for 5 minutes, after which an equimolar mixture of the photochemical *o*-methylbenzophenone **5** and the thermal *trans*-5-decene **10** reaction partners were added (Scheme IV.3, top). Hence, a one-pot reaction mixture was thereby obtained that was non-reactive as long as the green light source remained switched on. Subsequently, the mixture was subjected to UV-light ($\lambda_{\text{max}} = 320$ nm) for 2 hours and kept in the dark for an additional 8 hours. The conversion to the respective reaction products at the end of each phase was determined by integrating the well-resolved product peaks in the ¹H-NMR spectrum and reproduced in threefold (refer to Appendix C). The reaction outcome over time is displayed in Figure IV.10 and show the exclusive formation of the photoproducts **8a** and **8b** upon irradiation with UV-light, whilst the thermal mode of reactivity was completely suppressed (Scheme IV.3, right). Only when the reaction mixture was placed in the dark and the photochemical pathway was blocked, the thermal addition product **11** was formed (Scheme IV.3, left). Moreover, both reaction pathways could be completely halted upon green light irradiation during which no TAD-conjugation took place (Scheme IV.3, top and Figure IV.10). To illustrate that the different reaction channels could be repeatably accessed, a second on/off cycle of UV-light and dark time was carried out to re-initiate the conversion to the photo- and thermal products, respectively (Figure IV.10).

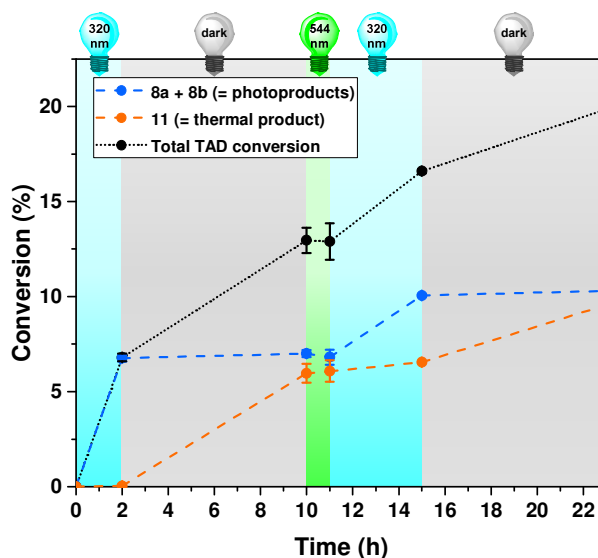


Figure IV.10. The switchable and selective reaction outcome of the manifold was evidenced from the product conversion (determined from ¹H-NMR with error bars indicating the standard deviation of three measurements) throughout the light cycles. Upon irradiation with UV-light (2 hours), followed by standing in the dark (8 hours) only photoenol products **8a** + **8b** and thermal addition products **11** are formed, respectively. A second on-and-off cycle demonstrates the possibility to re-access both reaction channels.

IV.5 Valorisation in sub-diffraction laser lithography

The designed reaction manifold was demonstrated to provide a switch over TAD-based reactivity whereby a photochemical and thermal reaction channel can be selectively accessed. In other words, the outcome of the TAD conjugation reaction could be readily modulated by the presence or absence of light. Next to the small molecule ligations shown above, this photonic field controlled reactivity was anticipated to also stimulate an array of opportunities in lithographic applications, where the reactivity of surface areas can be selectively switched-off or rendered reactive by using light of different wavelengths. Hence, a collaborative project was initiated with the physics group of Martin Wegener (Karlsruhe Institute of Technology, Germany) to exploit the established molecular TAD switch in sub-diffraction laser lithography.

The translation of the stimulated-emission depletion (STED) concept from microscopy to maskless lithographic techniques, such as 3D direct laser writing (3D-DLW), constituted a step change in the fabrication of super-resolution, sub-diffraction nano-scaled structures (*cf.* II.1.3.4).³⁸⁷ In the ongoing quest to reduce the linewidth that can be achieved with STED-lithography, challenges on both the physical and chemical involved aspects need to be addressed.^{170, 174, 176}

From a chemical point of view, the prerequisite is to provide efficient photochemical systems that exhibit a molecular switch between an activated and deactivated state, which can be selectively triggered by two different colours of light (refer to II.1.3.4 for a discussion of STED-lithography). Exactly such a switch was identified in the currently investigated TAD-photoenol system. Indeed, UV-light can be applied to induce the formation of the TAD-reactive photodiene which provides the activation channel, whereas under green light irradiation the TAD reagent will be transformed into its photopolymer and thereby deactivated. The applicability of the UV/visible light-switchable TAD-photoenol reaction was thus explored in STED-inspired laser lithography.

To provide a suitable experimental set-up, a glass substrate was functionalised with a triethoxysilane-containing *o*-methylbenzaldehyde moiety (**12**, Figure IV.11a) – a second generation photoenol precursor applied in previous STED experiments (*cf.* II.1.3.4).¹¹⁸ Subsequently, a TAD solution in chloroform was added as a drop onto the UV-active surface, which was held in place in a custom-built sample holder that was specifically designed to prevent solvent evaporation. Photolithography was next conducted with an in-house laser setup by Patrick Müller from the Wegener group at KIT. The sample was subjected to femtosecond pulsed laser irradiation centred around 700 nm for the two-photon excitation and continuous-wave green laser light at 532 nm to affect the depletion. Only in those areas of the surface that are solely exposed to the excitation light, the TAD-photoaddition reaction to the photoenol moiety is expected to be observed (Figure IV.11b). In those regions that are simultaneously irradiated with the depletion light as well, the TAD reagents will be deactivated via their photopolymerisation

and thus no TAD reaction with the photodiene will occur. To achieve a reduction in the linewidth, the depletion beam could be modulated with a phase mask, resulting in a distinct focus so that depletion is only effective at the edges of the written line profiles (Figure IV.11c). Ideally, such a depletion would result in a considerable reduction of the linewidth during the surface patterning.

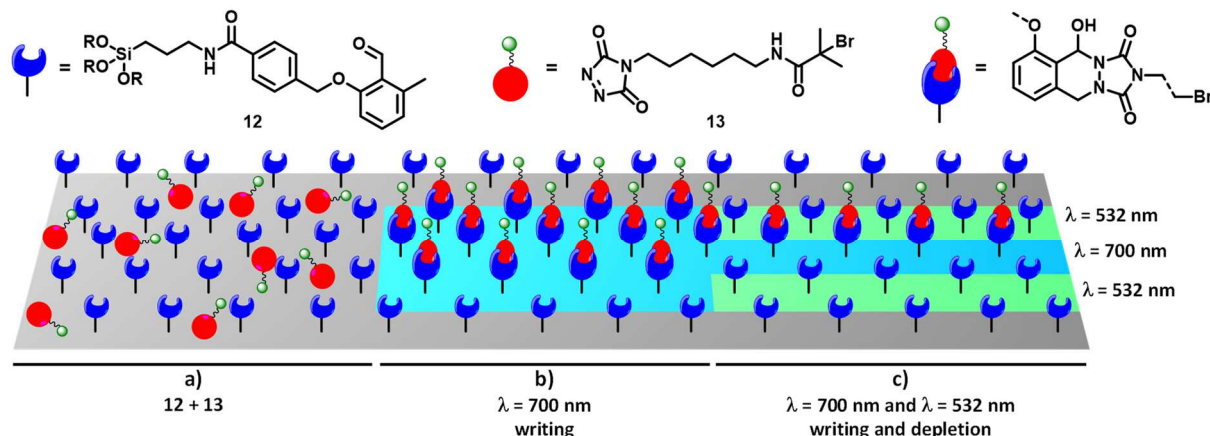


Figure IV.11. a) STED-inspired laser lithography through the combination of surface bound photoenol precursor moieties **12** and bromine-containing TAD compounds **13** in solution. b) After addition of a drop of the TAD reagent to the photo-activatable surface, laser light at 700 nm can be used to trigger a site-selective surface functionalisation through two-photon excitation. c) When a 532 nm depletion source is simultaneously applied at the edges of the writing profile, the TAD reactants are photopolymerised and hence deactivated, resulting in a reduction of the linewidth.

The projected site-selective surface functionalisation was first put to the test by studying the depletion effect when the sample was exposed to a writing pattern as depicted in Figure IV.12a. Whereas the excitation laser was permanently kept on, the depletion laser was only switched on in the region shortly before and after the initial beam path would be crossed (i.e. the hatched area in Figure IV.12a). In order to visually express the patterns written onto the surface, the tailored TAD reagent **13** (*cf.* Figure IV.11) bearing a bromine-containing initiator was synthesised, thereby taking into account the requirement on the TAD-substituent to be aliphatic to allow for its photodeactivation (*cf.* IV.2.1). Following the patterning experiment, the covalently attached TAD-initiators were applied in a surface-initiated atom-transfer radical polymerisation (SI-ATRP) of poly(ethylene glycol) methyl ether methacrylate (300 Da) and the grown polymer brushes were characterised via atomic-force microscopy (AFM).³⁹⁴ Hence, the lithographic patterns were revealed by the AFM height profile and the depletion of the TAD reagents could be assessed since the obtained brush height directly relates to the surface functionalisation density.³⁹⁵ Unfortunately, the AFM profiles of the surface patterning experiments conducted at low depletion powers only indicated a vaguely suppressed surface functionalisation (see Figure IV.12b and c). Although a considerably more pronounced depletion was observed at higher laser power (i.e. 3 mW), the surface was again not completely deactivated (Figure IV.12d). Further increasing the power eventually lead to irreversible effects. Yet, the experimental data indicated that the two necessary prerequisites for STED-inspired laser lithography are fulfilled. Firstly, the previously written line patterns were not affected by the

depletion beam. Secondly, the local depletion effect was observed to be reversible, which was demonstrated by the continued writing process when passing through a previously depleted region.

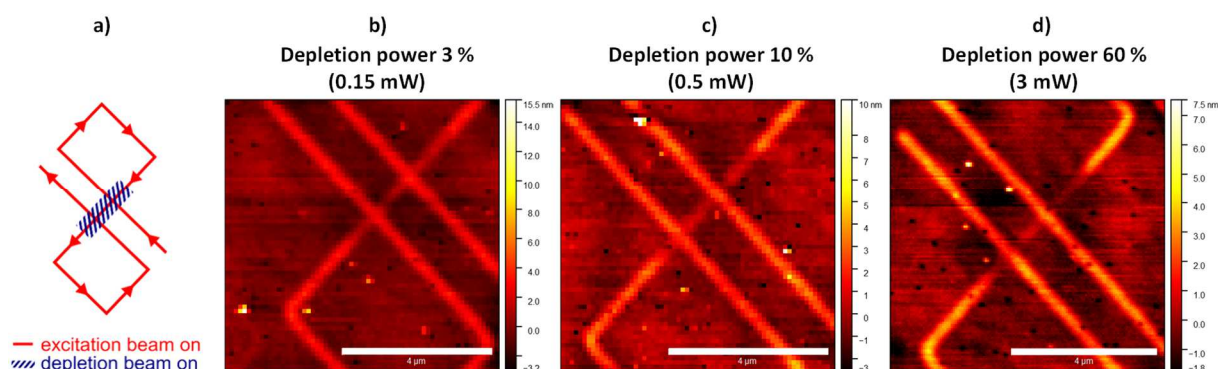


Figure IV.12. a) Writing pattern used to investigate the depletion effect. Just before and after the initially written line would have passed, the depletion laser (5 mW) is switched on (hatched region). b-d) The experimental pattern obtained at different depletion powers (i.e. 3, 10 and 60 %) was visualised via AFM measurements after SI-ATRP with the initiator-containing TAD **13**. The excitation laser power was fixed at 2 mW. Scale bars correspond to 4 μm.

Despite efforts of the collaboration partner at the end of the current PhD project to optimise the parameters of the depletion source, the TAD deactivation was just not found efficient enough. Thus, sub-diffraction laser lithography was not feasible. This can most likely be attributed to a much slower TAD polymerisation reaction caused by a charge transfer complexation of TAD in the presence of the benzaldehyde motives attached onto the surface. Indeed, such a retardation of the photodeactivation was also observed previously during the wavelength-orthogonal investigation of the TAD-polymerisation in combination with the photoenol reaction (*cf.* IV.3.2). In fact, the increased electron density caused by the alkoxy-substituent on benzaldehyde **12** compared to **5**, is expected to give an even more pronounced charge transfer complexation.

Future research efforts should therefore aim to optimise the TAD depletion effect with an *o*-methylbenzophenone (**5**) functionalised surface, although the design of a suitable surface reactive derivative thereof is considerably less straightforward.³⁹⁶

IV.6 Conclusions and perspectives of light-switchable TAD reactivity

In the present chapter, the sole report on the visible light-induced photopolymerisation of triazolinediones was reinvestigated and exploited as a highly defined switch to completely halt the unique thermal reactivity of TADs. Importantly, the photostability of TAD reagents under both UV- and visible light irradiation was assessed. This was a critical finding which indicated that the general opinion of TAD reactivity being incompatible with light should be revisited. Instead, the photostability of TAD reagents should be carefully evaluated as a function of the specific irradiation conditions applied.

The approach to photochemically deactivate the highly reactive TAD moiety was successfully combined with the well-established UV-induced photoenol conjugation reaction and both were shown to be selectively and orthogonally triggered in the presence of one another. Critically, this resulted in a photonic field modulated reaction manifold in which the outcome can be switched between a photochemically and thermally induced TAD-based conjugation reaction. Moreover both reaction channels can be repeatedly accessed, simply by using different colours of light.

The pioneered light-switchable TAD reactivity provides an array of synthetic opportunities not only in small molecule design, yet also in site-selective surface design whereby the reactivity in distinct regions can be switched on-and-off. The on/off behaviour of TADs effectively represents a depletion system that was briefly explored in sub-diffraction STED-inspired laser lithography. Although the thus far obtained results indeed showcased the desired features for the devised TAD switchable reactivity to be compatible with the STED-principle, future endeavours are needed to improve the deactivation efficiency. Given the deactivation process can indeed be optimised, this would potentially enable sub-diffraction surface lithography and eventually also the design of advanced TAD-based photoresists for laser writing in three dimensions. Regardless of the required optimisation of the depletion process, however, surface patterning experiments did point out the efficient UV-induced TAD-conjugation reaction and thus opening TAD chemistry to the realm of spatially controlled applications.

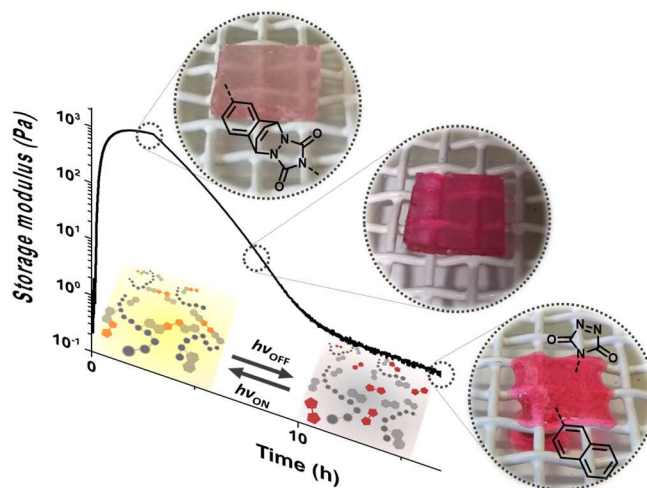
IV.7 Notes on the collaboration

A collaboration with the research group of Prof. Martin Wegener at the Karlsruhe Institute of Technology, Germany was initiated to investigate the applicability of the established TAD-photodeactivation pathway in sub-diffraction lithography. Patrick Müller and Dr. Eva Blasco (Karlsruhe Institute of Technology) designed and conceived the STED-inspired experiments described in section IV.5. Hannes Houck synthesised the urazole precursor containing an ATRP-initiator via an aliphatic spacer, which can be converted into its TAD counterpart upon oxidation. All collaboration partners involved discussed and commented on the obtained results at all stages.

Chapter V.

Light-stabilised dynamic materials through triazolinedione-based cycloaddition

Brief motivation and content



The ability of photoswitches to efficiently and reversibly undergo a photochemical response continues to highly impact the field of materials science, most notably in the design of molecular machines that can undergo translational or rotary motion that is fuelled by light. Yet, existing photoswitches are exclusively based on photo-induced intramolecular transformations such as isomerisation and cyclisation processes. In other words, no constitutional dynamic behaviour in the sense of bimolecular covalent bonding or debonding can be directly established by the applied trigger. Motivated to devise a material that can undergo a repeatable change in topology from a covalently crosslinked material to a liquid polymer formulation, simply by switching one colour of light on-and-off without the need for any additional triggers, an unprecedented concept in the field of light-switchable materials is introduced. Specifically, the visible light-driven cycloaddition reaction of triazolinediones (TADs) with naphthalenes is exploited as a suitable dynamic covalent crosslinking system because the photostationary state is almost quantitatively populated by the cycloadduct, whereas the resulting photoproducts readily dissociate upon standing in the dark. Following model investigations of this unique feature, the TAD-naphthalene-based polymer materials are developed and the light-switchable states of matter are characterised through rheology. Critically, the mechanical integrity of the polymer materials is retained as long as the green light is kept switched on, which is also evidenced by macroscopic demonstrations. The observed extraordinary behaviour of the TAD-naphthalene-based networks lead us to pioneer the concept of light-stabilised dynamic materials.

Adapted from

H. A. Houck, E. Blasco, F. E. Du Prez, C. Barner-Kowollik, *Journal of the American Chemical Society* **2019**, *141*, 31, 12329-23337.

With permission from the American Chemical Society. Copyright 2019 American Chemical Society.

V.1 Introduction

Molecular photoswitches are not just capable of serving as a light-controllable gate to tune the outcome of a chemical transformation as was demonstrated in Chapter IV. They also play a pivotal role in the design of adaptable and responsive materials, in particular in a biologically oriented context,³⁹⁷⁻³⁹⁸ for example in peptide folding and unfolding.³⁹⁹⁻⁴⁰⁰ Driven by these tremendous opportunities, ongoing research efforts are devoted to design specific photochromic systems that result in a tailored mechanical, electrical or optical response that is externally controlled or even fuelled by light.^{150, 154} A truly fascinating application of photoswitchable dynamic behaviour can be found in the design of molecular machines that are continuously driven out-of-equilibrium by light, thereby achieving translational and rotary motion on the nanoscale.⁴⁰¹

In the context of bulk materials, photoswitches have been successfully incorporated to enable adaptable behaviour such as reversible colouration for sensing applications,⁴⁰²⁻⁴⁰³ switchable repair¹⁵⁶ or contraction/expansion⁴⁰³⁻⁴⁰⁴ in a non-invasive manner.¹³⁶ However, existing photoswitches are exclusively based on photo-induced isomerisation or intramolecular cyclisation reactions (*cf.* II.1.3.3). Thus, no constitutional dynamic behaviour in the sense of bimolecular covalent bonding and/or debonding is directly established by the applied stimulus. Photoswitches are therefore typically incorporated into materials either via irreversible linkages into the polymer backbone or as pendant side chains through a postpolymerisation modification. This allows for the photoswitchable behaviour to be embedded in a tailored material to induce a change in size or mechanical properties,⁴⁰⁵ yet does not enable to reversibly switch its topology from a crosslinked state into a decrosslinked one.

Recently, Hecht and coworkers reported an elegant implementation of a photoswitch into a thermoreversible furan-maleimide system that allowed for the healing capabilities of the resulting material to be switched on or off by two colours of light.¹⁵⁶ Nonetheless, heating of the system was still required to induce the thermoreversible covalent bond shuffling process. In fact, the necessity of temperature as an additional trigger to provide the triggered bonding/debonding in a material somehow defeats the controllable aspect that is provided by light. In other words, rather than relying on a combination of different triggers, including two complementary colours of light, the ability to induce bonding/debonding behaviour in a material should ideally be provided by one single, preferentially much milder and non-invasive trigger.

Motivated to devise a material that can be transformed from a crosslinked to a decrosslinked state by only one single wavelength and without the need for a change in temperature, the current chapter aims to introduce a two-fold conceptual approach to design advanced light-switchable materials:

At first, the intramolecular reactivity and subsequent thermal follow-up reaction that is provided by the conventional photoswitches should be replaced by a bimolecular light-induced

process. This would ensure that the crosslinking reaction can be directly triggered by light and would guarantee the facile incorporation of the desired photoreversible system into polymer materials. Critically, the covalent bonding interaction should retain its dynamic nature that can be repeatedly accessed by light, preferentially in the visible range of the spectrum.

A second level of the conceptual approach relies on the use of light-stabilised covalent bonds, whereby the crosslinking density is determined by the obtained photostationary state and is near-quantitatively populated by the bonded covalent interaction upon irradiation to retain the materials integrity. Lehn and coworkers very recently introduced the term photodynamic covalent bonds to describe covalent interactions that are stable under ambient temperature, yet readily dissociate upon photoexcitation.⁴⁰⁶ Here, an opposite approach is preferred whereby the covalent crosslinks are kept stable under continuous irradiation, but efficiently dissociate upon standing in the dark at ambient temperature. Hence, the targeted decrosslinking of the material would be made feasible on demand by exploiting the mildest trigger of all, i.e. simply switching the light off.

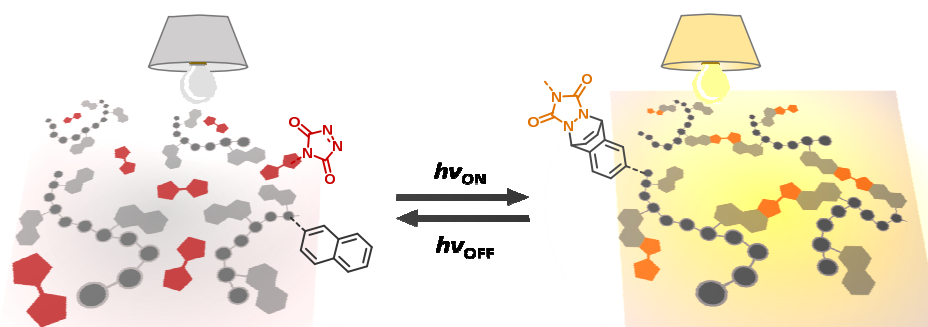


Figure V.1. Representation of the light-stabilised dynamic material introduced in the current chapter, based on the light-induced cycloaddition crosslinking reaction and thermal cycloreversion dissociation of triazolinediones with naphthalenes.

In continuation of our quest to develop triggered triazolinedione-based reactivity, the visible light-induced cycloaddition of TAD with naphthalene was identified as a highly promising platform to address the introduced conceptual approach into a material context. Indeed, many functional naphthalene building blocks are commercially available, which allows for their incorporation into a range of polymer matrices. Moreover, several bivalent TAD reagents are accessible on a large scale and can serve as low molecular weight crosslinking agents. Thus, it should be perfectly feasible to translate the TAD/naphthalene system to the macromolecular level. Hence, a material formulation would be provided that can be cured upon irradiation through the light-driven TAD/naphthalene cycloaddition reaction, whilst the resulting labile adducts can dissociate at room temperature, simply by switching the light off (Figure V.1). As long as the system is irradiated, however, a crosslinked integrity would be retained, thus providing an unprecedented *light-stabilised dynamic material*.

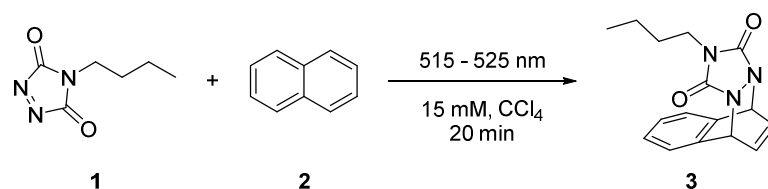
To generate light-stabilised dynamic materials (LSD materials), the initially reported visible light-induced TAD-naphthalene cycloaddition reaction will first be fully reinvestigated (V.2). This forms a critical aspect in line with the results obtained in Chapter IV, where the photopolymerisation of TADs was observed to be triggered upon visible light irradiation as well. Next, functionalities will be introduced onto the naphthalene substrate to enable the light-stabilised bonding/debonding system to be incorporated into a polymer matrix, thereby taking into account the effect of such molecular modulations on both the cycloaddition as well as cycloreversion process (V.3). Following the TAD/naphthalene system to be successfully integrated into polymers, the rheological behaviour of the targeted light-stabilised materials will be evaluated and some macroscopic applications will be demonstrated (V.4).

V.2 Investigations on low molecular weight compounds

While the photochemical [4+2] cycloaddition reaction of TADs to naphthalene has already been explored to enable the synthesis of some theoretically interesting low molecular weight structures,^{322, 325} no mention what so ever is included in these reports with regard to TAD's ability to undergo photopolymerisation. With the knowledge that was derived from Chapter IV, the TAD-naphthalene model reaction will therefore be first reinvestigated and the possible competition between visible light-induced polymerisation and cycloaddition will be addressed (V.2.1). After the identification of suitable reaction conditions to affect the cycloaddition reaction under visible light irradiation, insights in the transient nature of the corresponding cycloadduct will be obtained (V.2.2). Finally, the possibility to continuously push the characteristic dynamic nature to covalent bond formation whilst keeping the system irradiated will be examined (V.2.3).

V.2.1 Visible light-induced polymerisation versus cycloaddition

Initially, the visible light-induced TAD-based [4+2] cycloaddition reaction with naphthalene was reinvestigated. Thus, a 15 mM solution of BuTAD **1** and plain naphthalene (**2**, Scheme V.1) in CCl₄ was subjected to green laser light at 544 nm (4 mW cm⁻²) to give a colourless solution within 5 minutes. UV/vis spectra before and after irradiation clearly indicated the complete consumption of **1** (Figure V.2). A purple colour was rapidly regenerated upon standing in the dark, which indicated the release of BuTAD into the reaction mixture. Interestingly, similar results were obtained when 3 x 3 W green LEDs ($\lambda = 515 - 525$ nm) were applied as irradiation source. Although the use of LEDs resulted in slightly prolonged times needed to reach full cycloadduct conversion, i.e. 20 minutes, they are a much more convenient and accessible light source and are thus used in the remainder of the current chapter.



Scheme V.1. Visible light irradiation of BuTAD with plain naphthalene **2** results in the quantitative formation of cycloadduct **3**.

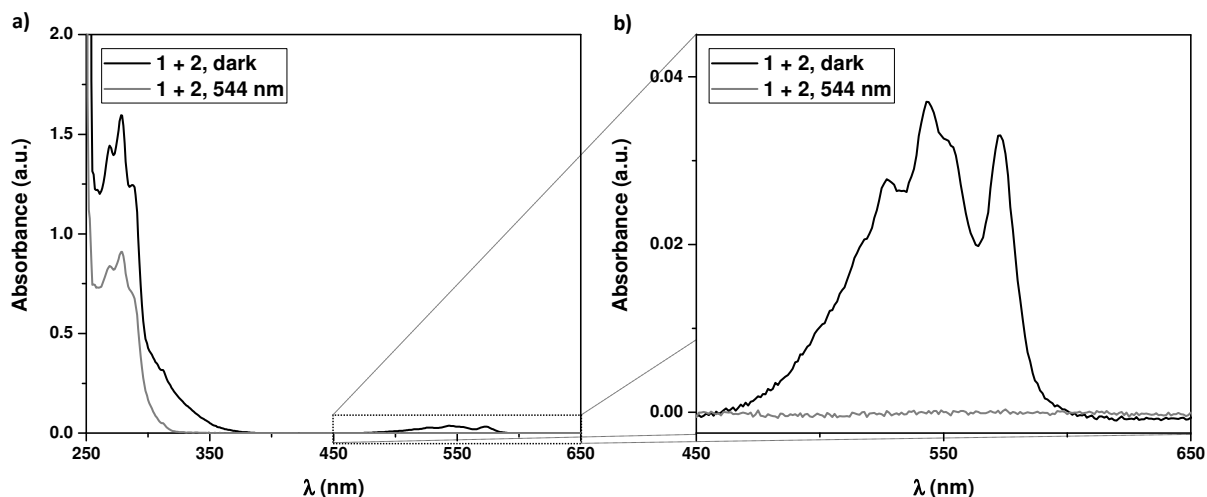


Figure V.2. a) UV/vis absorption spectra (CCl_4) before (black) and after (grey) irradiation of a BuTAD-naphthalene solution (15 mM, CCl_4) with green laser light ($\lambda = 544\text{ nm}$, 4 mW cm^{-2}). b) Zoom in the visible region of the spectrum indicated the complete disappearance of BuTAD upon visible light irradiation.

Whilst the above experimental observations are in perfect agreement with the reported TAD-naphthalene cycloadduct formation, they might as well be explained by the photopolymerisation that was previously studied in Chapter IV. To elucidate whether the cycloaddition of TAD with naphthalene suffers from competitive photopolymerisation, the reaction mixtures obtained after irradiation were subjected to $^1\text{H-NMR}$ analysis. At first, a blank solution of BuTAD **1** in deuterated chloroform (15 mM) was irradiated for 20 minutes with green LEDs ($\lambda = 515 - 525\text{ nm}$, $3 \times 3\text{ W}$). As expected, the obtained $^1\text{H-NMR}$ spectrum of the colourless solution exclusively contained the photopolymer (Figure V.3a). In the presence of naphthalene **2** (1.2 eq., CDCl_3), however, the [4+2] cycloadduct **3** was near-quantitatively formed under similar conditions, with only a very minor trace (i.e. $< 2\%$) of the TAD-polymer detected (Figure V.3b). Moreover, less than 1% of cycloadduct **3** was observed in the spectrum of a reference solution of **1 + 2** kept in the dark for 20 minutes (Figure V.3c), thus indicating the truly photo-induced nature of the cycloaddition reaction. This was also indicated by the observed equilibrium concentration upon standing in the dark for 24 hours (i.e. 2%), which did not increase over the course of 48 hours (refer to Appendix D for $^1\text{H-NMR}$ spectra). Importantly, not a single trace of the TAD-polymer was observed in the presence of **2** when increasing the reagent concentration to 0.3 M (CDCl_3 , refer to Appendix D). Presumably, this was attributed to the formation of a deep red [1+2] charge transfer complex that somehow inhibits the photopolymerisation reaction or benefits the cycloaddition process.

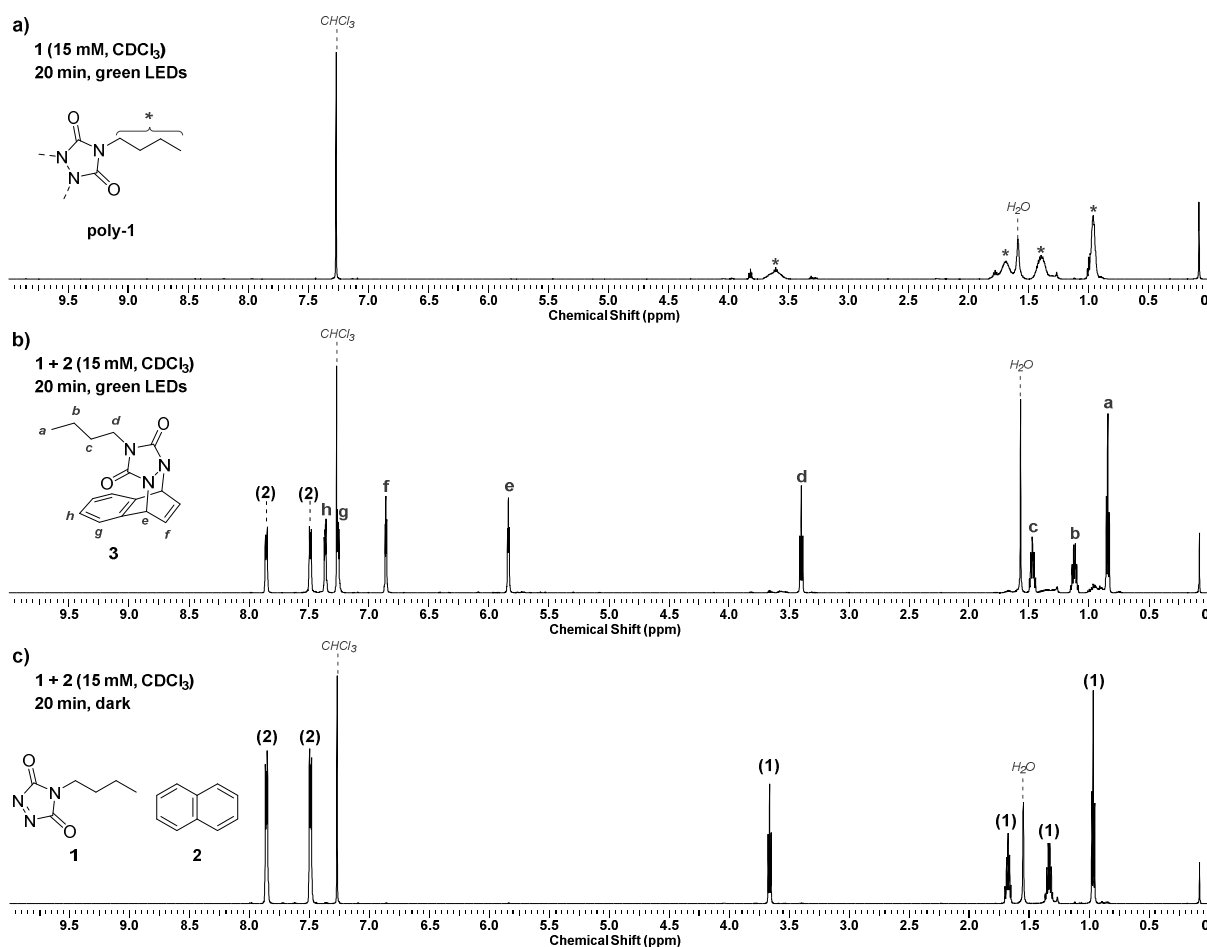


Figure V.3. Assessment of competitive TAD-based photopolymerisation and cycloaddition upon visible light impact (**1**, 15 mM, CDCl₃). a) ¹H-NMR spectrum of photopolymer **2**, obtained after green light irradiation ($\lambda = 515 - 525$ nm, 3 x 3 W LEDs, 20 min) of a blank BuTAD solution (**1**, 15 mM, CDCl₃). b) In the presence of naphthalene **2** (1.2 eq.), the cycloadduct **3** is almost quantitatively formed, with only minor traces (i.e. < 2 %) of photopolymer **2** being detected. c) Less than 1 % of adduct **3** is observed in a reference experiment whereby **1** and **2** are kept in the dark, indicating the light-induced nature of the TAD-naphthalene cycloaddition.

The photopolymerisation of TAD is a strongly solvent-dependent process whereas the light-induced cycloaddition reaction has been reported to proceed in a range of organic media. Thus, by simply changing the solvent to acetonitrile, competitive TAD-photopolymerisation was also proven to be completely excluded without influencing the formation of the [4+2] cycloadducts. Yet, longer irradiation times (i.e. up to 1 hour instead of 20 min) were required to reach full conversion of **1** into **3**. Moreover, the aromatic PhTAD analogue as a reagent with **2** also successfully provided the naphthalene cycloadduct, whilst it was previously demonstrated in this doctoral work not to undergo self-reaction to its homopolymer (*cf.* IV.2.1).

Although the model TAD reagents that were used to investigate the cycloaddition reaction with naphthalene were soluble in chloroform at the applied concentrations, bivalent TAD-based crosslinkers suffer from very poor solubility in halogenated solvents. Since the aim of the current chapter is to develop TAD/naphthalene-based crosslinked materials, assuring good solubility of the TAD-crosslinking agent is of critical importance. Moreover, a good solvent for the envisioned

polymer matrix is also required. Since the current chapter focusses on the conceptual design of light-stabilised materials, poly(methyl methacrylate) (PMMA) was selected as a bench-mark polymer system. Given the poor solubility of PMMA in acetonitrile, a compatible solvent for both bisTAD crosslinkers and the polymeric substrate was found in acetone. Hence, the photo-induced cycloaddition of **1** (15 mM, 1.0 eq.) and **2** (1.2 eq.) was also tested in deuterated acetone- d_6 . Upon standing in the dark, no trace of the expected cycloadduct **3** was observed in the $^1\text{H-NMR}$ spectrum of the deep purple reaction mixture (Figure V.4a). In contrast, a 45-minute irradiation period with green LEDs ($\lambda = 515 - 525 \text{ nm}$, $3 \times 3 \text{ W}$) resulted in a clear colourless solution of **3**, together with a slight excess of unreacted naphthalene **2** (Figure V.4b). Interestingly, the purple colour that is assumed to originate from the released TAD upon cycloreversion, was shown to unfold much faster compared to the adduct formation in chloroform.

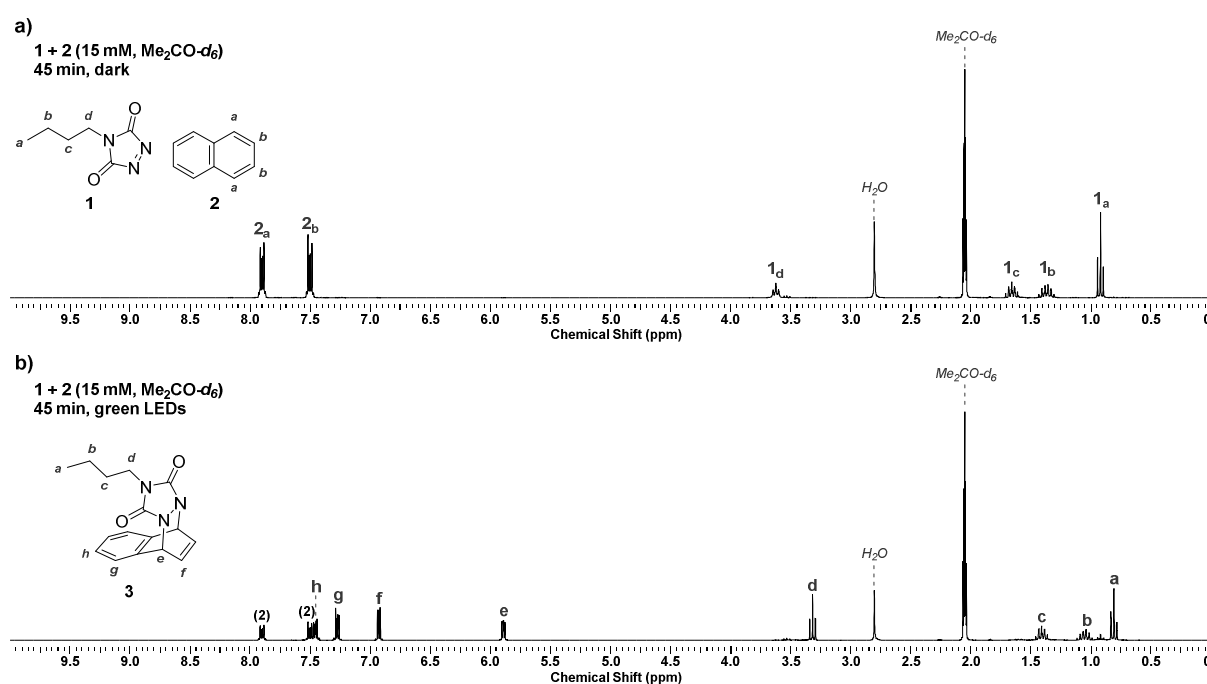


Figure V.4. $^1\text{H-NMR}$ analysis of the TAD-naphthalene cycloaddition reaction in deuterated acetone (**1** + **2**, 15 mM, $\text{Me}_2\text{CO-}d_6$). a) No cycloadduct formation was observed when the mixture was kept in the dark. b) Only upon visible light irradiation for 45 minutes ($\lambda = 515 - 525 \text{ nm}$, $3 \times 3 \text{ W}$ green LEDs), a colourless solution containing cycloadduct **3** was obtained.

V.2.2 Covalent debonding in the dark

After the forward TAD-naphthalene reaction was investigated, the thermal cycloreversion process was studied. In 2000, Breton and Newton already investigated the thermal retro-TAD-naphthalene reaction rate of the isolated cycloadduct **3** via offline NMR analysis.³¹⁸ However, in order to measure the rate of cycloreversion more conveniently, their studies comprised the use of 2,3-dimethyl-2-butene as an irreversible Alder-ene trap for the released TAD. Indeed, by quenching the TAD reagent, the reformation of the cycloaddition process could be discarded. In the context of the current investigations, however, the TAD/naphthalene system was aimed to be used as an autonomous dynamic covalent bond that is embedded into polymer materials.

Hence, in contrast to the thermal reversibility studies of **3** reported earlier, and to those that have been conducted previously in Chapter III to screen the deblocking reaction of TADs with indoles, no irreversible trap for the released TAD was added in the cycloreversion study discussed below.

The backward reaction of the cycloadduct **3** was monitored independently by means of online $^1\text{H-NMR}$ kinetic measurements. Specifically, a solution of **1** (15 mM, 1.0 eq.) and **2** (1.2 eq.) in deuterated acetone- d_6 was first irradiated with green LEDs for 45 minutes until complete photobleaching was observed. The quantitative conversion of **1** was confirmed by $^1\text{H-NMR}$ after which the resulting colourless solution was shielded from light and kept at 25 °C. A faint purple colour was quickly reinstated upon standing in the dark and a $^1\text{H-NMR}$ spectrum was recorded every hour from which the amount of cycloadduct **3** could be determined. The thermal cycloreversion monitored over time is depicted in Figure V.5 and shows a first order decrease in **3** with an observed rate coefficient $k_{\text{obs}} = 2.03 \cdot 10^{-5} \text{ s}^{-1}$, corresponding to a half-life time of 9.5 hours. This qualitatively relates well to the $3.94 \cdot 10^{-5} \text{ s}^{-1}$ found by Breton and Newton for the retro-reaction of **3** in $\text{Me}_2\text{CO-}d_6$ at 29 °C,³¹⁸ taking into account the higher temperature as well as the presence of an irreversible trap for TAD which drives the equilibrium more towards free naphthalene **2**. The dynamic BuTAD/naphthalene system eventually reached an equilibrium value of 2 % cycloadduct **3** after 60 hours, which perfectly agreed to the amount of cycloadduct that was detected in a reference sample of **1** + **2** kept in the dark.

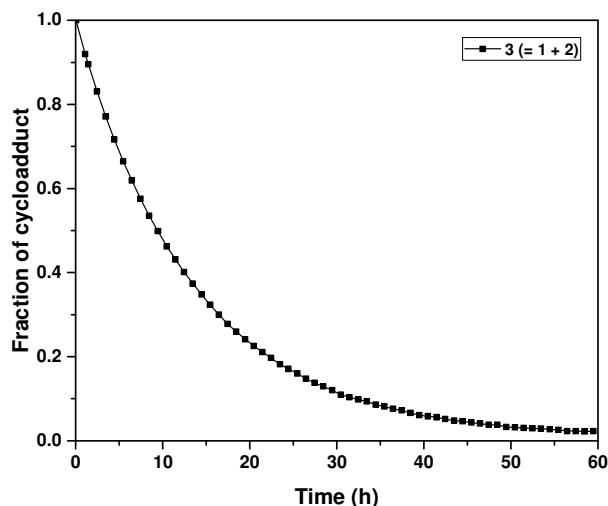
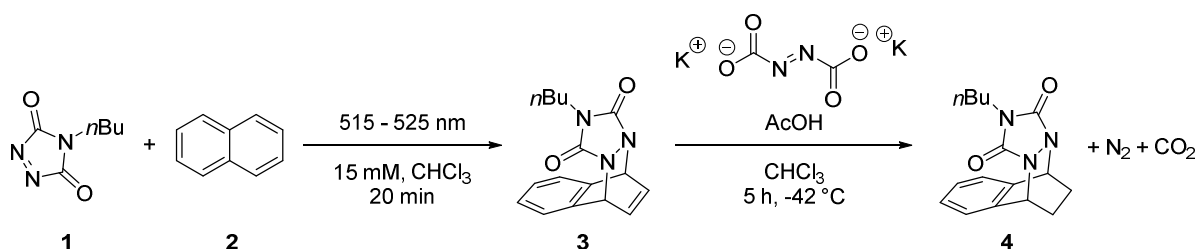


Figure V.5. Thermal reversion of cycloadduct **3** at 25 °C, obtained after visible light irradiation (45 min, green LEDs, $\lambda = 515 - 525 \text{ nm}$, 3 x 3 W) of a 15 mM solution of BuTAD **1** and naphthalene **2** in deuterated acetone- d_6 .

The interesting dynamic behaviour of cycloadduct **3** to return to the original reagents was believed to be caused by the regained aromaticity. To assess this driving force of the cycloreversion, the adduct **3** formed upon green light irradiation was subjected to a diimide-mediated reduction in an attempt to remove the isolated double bond (see Scheme V.2). Purification of the reaction mixture resulted into the successful isolation of **4** and the complete

disappearance of the isolated double bond was confirmed by ^1H - and ^{13}C -NMR (refer to Appendix D for structure elucidation). As expected, no purple colour was reinstated upon dissolving the reduced cycloadduct **4**, visually indicating the absence of a thermally reversible nature at room temperature. Moreover, when **4** was heated in the presence of *trans,trans*-2,4-hexadien-1-ol (HDEO) for 30 minutes at 150 °C, no change in the ^1H -NMR spectrum was evidenced (see Figure V.6). Furthermore, no newly formed TAD-HDEO Diels-Alder adduct was detected in the reaction mixture, indicating the complete absence of liberated TAD compounds at elevated temperatures. Thus, the driving force of the cycloreversion could be clearly attributed to the existing isolated endocyclic double bond, which upon removal prevents the re-aromatisation to the naphthalene substrate to occur.



Scheme V.2. Visible light-induced formation of cycloadduct **3** and subsequent diimide-mediated reduction of the isolated double bond to give adduct **4**.

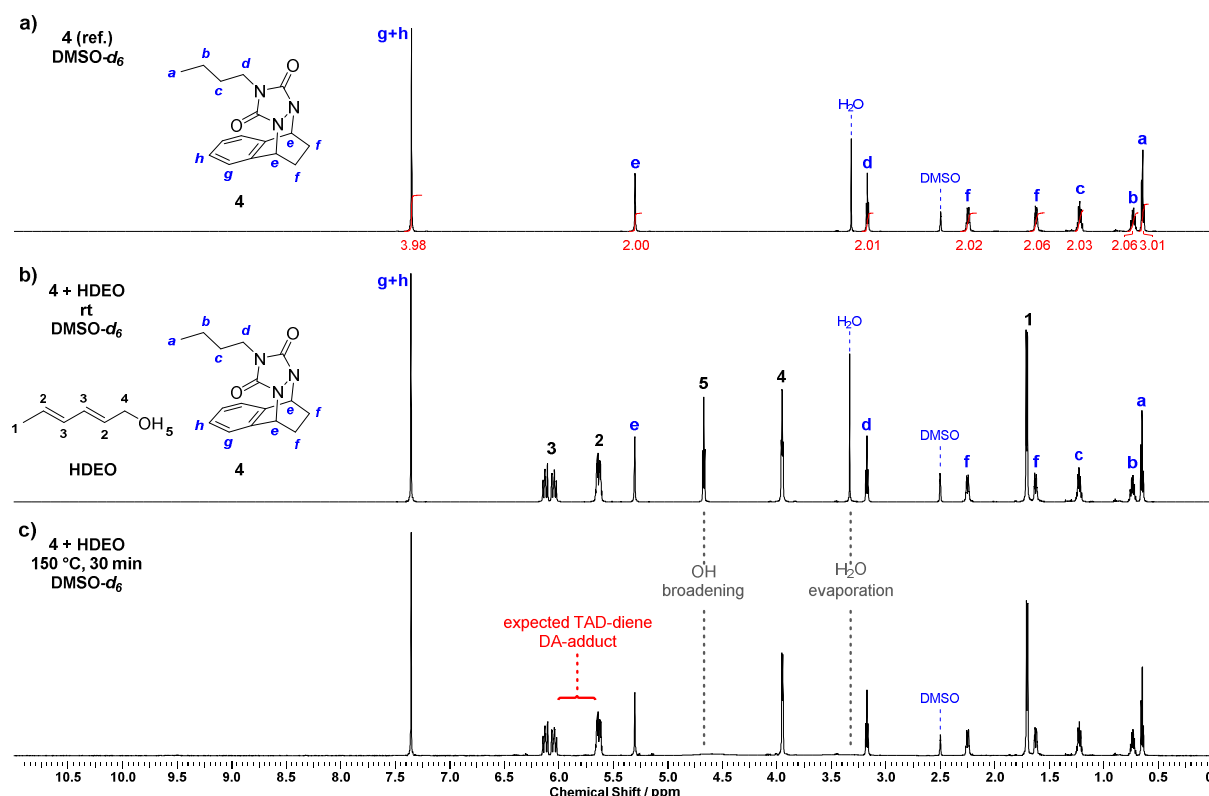


Figure V.6. Thermal reversibility test of cycloadduct **4**, obtained upon reduction of TAD-naphthalene adduct **3**. a) ^1H -NMR spectrum of **4** in $\text{DMSO-}d_6$ indicates the room temperature stability. b) No change of TAD-adduct is observed upon addition of the conjugated diene HDEO, which acts as a trap for any free BuTAD. c) Heating of **4** in the presence of HDEO at 150 °C for 30 minutes confirms the irreversible nature of the TAD-naphthalene adduct when the isolated double bond is removed.

V.2.3 Light-stabilised dynamic covalent bonds

A final question that remained unanswered was whether the covalent nature of the dynamic bond can be kept intact upon continuous green light irradiation. This is an important aspect as the crosslinking density of the targeted TAD/naphthalene-based material could be directly influenced during the irradiation process. An elegant trapping experiment based on the sequential addition of cyclopentadiene and *N*-ethylmaleimide was previously designed to enable the detection of free TAD moieties during green light irradiation (*cf.* IV.2.2, used to provide proof of the photodeactivation). The same trapping experiment was applied here to determine the amount of covalent TAD/naphthalene bonds that are opened under prolonged irradiation times.

Initially, green light ($\lambda = 515 - 525 \text{ nm}$, 3 x 3 W LEDs) was applied to completely transform a solution of BuTAD **1** (15 mM in CDCl_3 , 1.0 eq.) in the presence of a slight excess naphthalene **2** (1.1 eq.) into the corresponding [4+2] cycloadduct **3** (see Figure V.7a). While the green light was kept switched on, cyclopentadiene (1.2 eq.) was next added to the resulting mixture and irradiation was continued for an additional 2 hours to allow for any free TAD to be irreversibly trapped by the diene. Eventually, the residual non-reacted cyclopentadiene was quenched upon addition of *N*-ethylmaleimide (1.4 eq.) and the light was subsequently switched off.

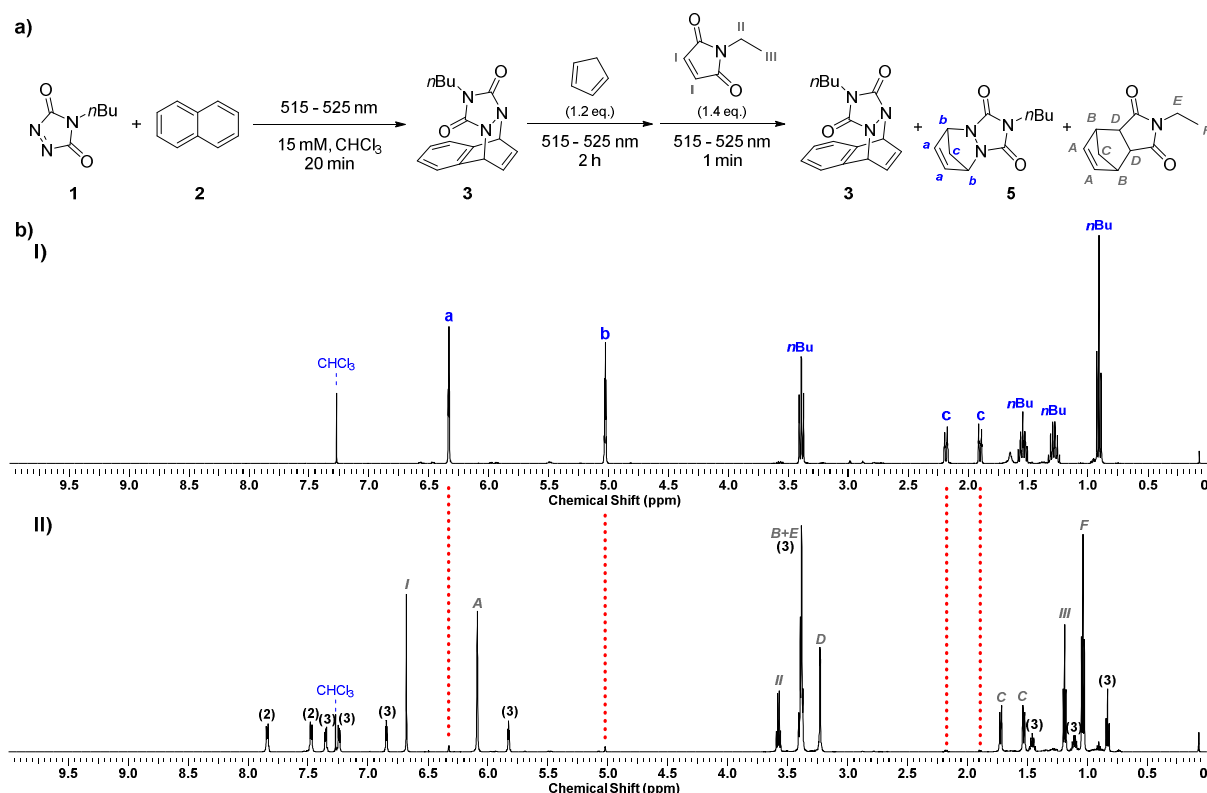


Figure V.7. a) Trapping experiment consisting of the sequential addition of cyclopentadiene and *N*-ethyl maleimide designed to detect the amount of TAD that is released from cycloadduct **3** under continuous green light irradiation (2 h, $\lambda = 515 - 525 \text{ nm}$, 3 x 3 W LEDs). b) $^1\text{H-NMR}$ analysis before (I) and after (II) irradiation indicates the dynamic behaviour of **3** upon irradiation in the presence of cyclopentadiene, although the closed covalently bonded cycloadduct remains near-quantitatively formed (*i.e.* > 95 %).

Inspection of the obtained $^1\text{H-NMR}$ spectrum of the resulting mixture indicated a minor fraction of trapped **1** (i.e. less than 5 %) into the cyclopentadiene Diels-Alder adduct **5** (depicted by the red dotted lines, Figure V.7b). Although the TAD/naphthalene system is thus still dynamic under the applied conditions of irradiation, the equilibrium concentration remains predominantly shifted to the closed cycloadduct (i.e. > 95 %). Moreover, the trace fraction of cycloreversion was determined in the presence of an irreversible TAD trap, which considerably overestimates the amount of retro-cycloaddition that would occur in the envisioned autonomous TAD/naphthalene system. The term *light-stabilised dynamic covalent bonds* was introduced here to describe the formation of a dynamic system whereby the photostationary state of two reactants remains near-quantitatively populated by the covalently bound reaction products under continuous irradiation. In other words, no macroscopic reversibility can be detected since the covalent bond remains predominantly formed as long as the light is kept switched on.

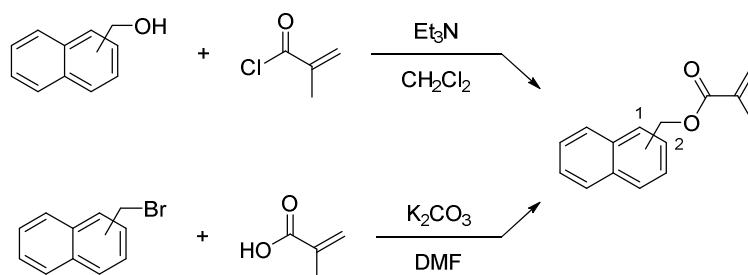
V.3 Introducing light-stabilised dynamic bonds into polymers

The unique characteristics derived from the BuTAD/naphthalene model study, i.e. fast bonding upon visible light impact in combination with a relatively slow debonding when kept in the dark, were next validated into a macromolecular context. Thus, at least one of the two reagents involved needed to be embedded into a polymer system to enable an on demand triggered bonding/debonding switch. In contrast to the rather challenging synthesis of functional TAD compounds that allow for their incorporation into polymers (*cf.* II.2), low molecular weight bisfunctional TAD reagents are much more accessible and were hence selected to act as small molecule crosslinking agents. Consequently, functional derivatives of the plain naphthalene scaffold had to be screened and transformed into a suitable monomer (V.3.1) before being incorporated into a linear polymer to provide the targeted light-stabilised materials (V.3.2).

V.3.1 Monomer design

In contrast to anthracenes, naphthalene compounds are considerably less frequently applied monomers. Nonetheless, many functional naphthalene derivatives are commercially available and can be readily transformed into a polymerisable moiety. Given the aim of the current chapter to validate the proposed conceptual design, the synthesis of naphthalene-containing methacrylates – commonly employed bench-mark monomers – was targeted.

The most widely adopted synthetic strategies to provide naphthalene-methacrylates proceed upon reaction of naphthylmethanol with acryloyl chloride or via substitution of (bromomethyl)naphthalene with methacrylic acid (Scheme V.3). It should be noted that phenol-type substrates (e.g. naphthol) are also frequently employed, but are unqualified in the current work. Indeed, such electron rich substrates swiftly undergo electrophilic aromatic substitution reactions with TADs – both under thermal and photochemical conditions – which would lead to the formation of undesired irreversible TAD-adducts.



Scheme V.3. Synthetic routes towards naphthalene-containing methacrylate monomers.

Before the synthesis was carried out, however, the effect of incorporating a substituent on the naphthalene core with respect to its TAD reactivity needed to be investigated. Moreover, two different positions are susceptible to serve as a functional handle for the monomer synthesis, which might influence both the forward cycloaddition as well as the cycloreversion process. Thus, both 1- and 2-substituted commercially available naphthalene building blocks – that can be applied in the monomer synthesis (*cf.* Scheme V.3) – were transformed into their acetylated derivatives **6** and **7**, so to mimic the eventual monomer structure once included into a polymer (see Figure V.8). For a better understanding, the model compounds **6** and **7** will also be denoted as **1-NaphtMeOAc** and **2-NaphtMeOAc**, respectively.

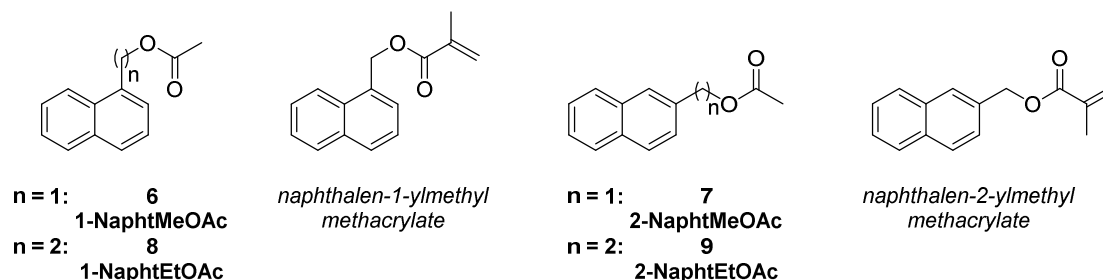


Figure V.8. Model compounds **6** and **7** as mimics for the targeted naphthalene-containing methacrylate monomers, used to investigate the substitution effect on the visible light-induced TAD-based cycloaddition reaction.

The acylated model compounds were next evaluated in terms of their photoinduced [4+2] cycloadduct formation with BuTAD. Irradiation of **1** (15 mM, Me₂CO-*d*₆, 1.0 eq.) in the presence of **6** or **7** (1.2 eq.) with green LEDs gave a clear colourless solution within 45 minutes. In contrast to the plain naphthalene derivative, the cycloaddition onto the substituted naphthalene compound can either occur on the substituted or non-substituted benzene ring, thereby potentially leading to a mixture of different regioisomers (see Figure V.9a). This was indeed observed for **2-NaphtMeOAc** (**7**) with a slight regioisomeric excess in favour of addition onto the more electron rich substituted ring, i.e. [1+7]-C_A: [1+7]-C_B = 58:42, where C_A denotes adduct formation on the substituted and C_B onto the non-substituted ring (Figure V.9a). The ratio of the different regioisomers was quantified via integration of the respective bridge head and methylene proton signals in the ¹H-NMR spectrum (refer to Appendix D), which were assigned based on two-dimensional NMR homonuclear correlation spectroscopy (COSY). Interestingly, the 1-substituted naphthalene substrate **6** was found to exclusively give

cycloaddition onto the non-substituted ring, i.e. $[1+6]-C_B$ (refer to Appendix D for structure elucidation). Breton and Newton observed a similar selectivity during the cycloaddition of MeTAD to the least electron rich ring system of 1-methylnaphthalene.³¹⁸ This result is rather counter-intuitive, but was attributed to the transient nature of $[1+6]-C_A$, the cycloadduct formed on the substituted ring, which is provoked by a steric destabilising interaction between the C1-naphthalene methyl group and the TAD dienophile. In other words, both regioisomers would be initially formed, but suffer from a difference in cycloadduct stability which is translated into their respective cycloreversion rates. Hence, once formed, the less stable adduct $[1+6]-C_A$ rapidly diminishes whilst the more stable cycloadduct $[1+6]-C_B$ accumulates throughout the course of the TAD-naphthalene photoreaction.

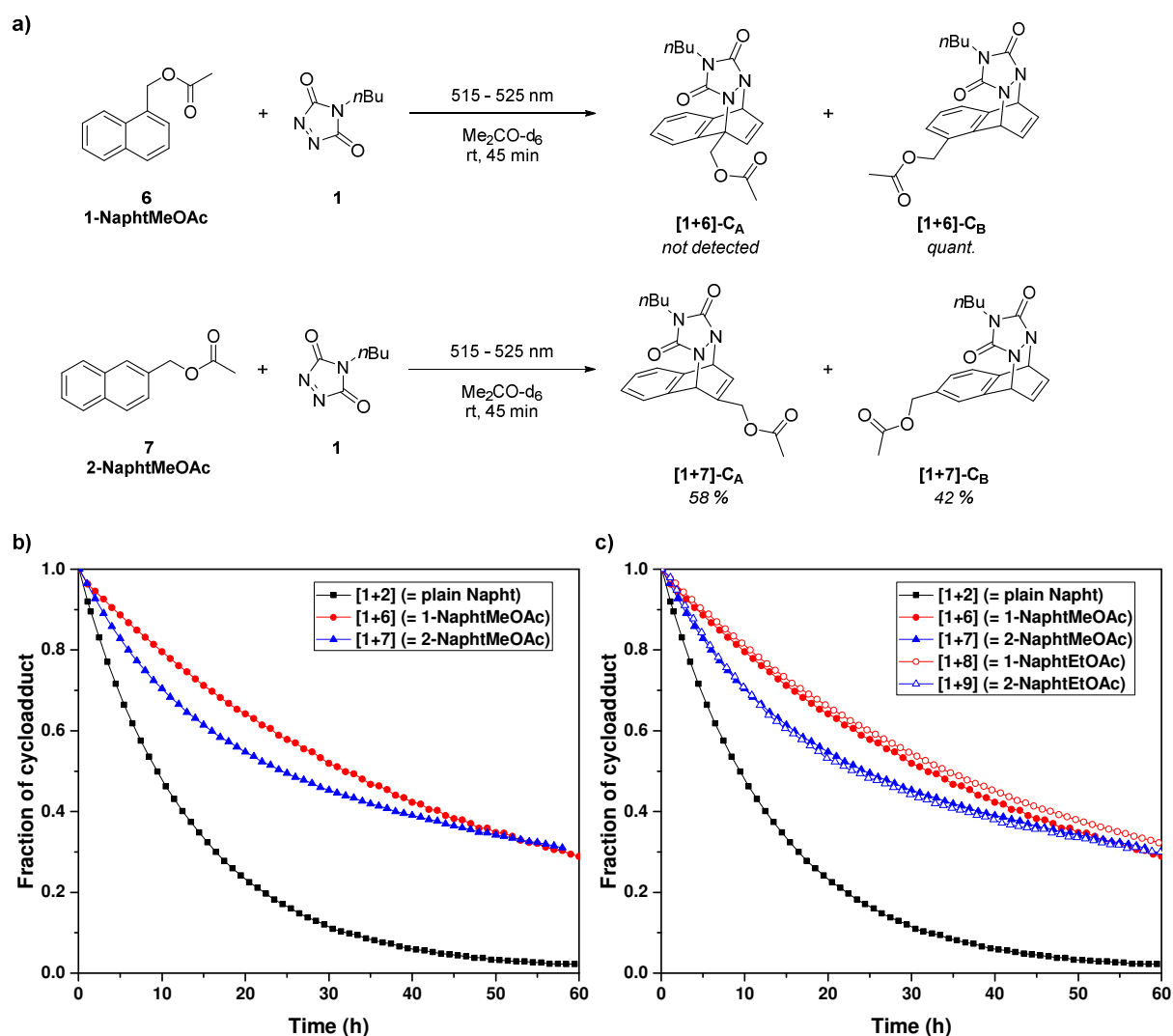


Figure V.9. a) Light-driven cycloaddition reaction of BuTAD ($\lambda = 515 - 525$ nm, 3 x 3 W LEDs, 45 min) to the model naphthalene compounds **6** and **7** gives a mixture of regioisomers on both the substituted C_A and/or non-substituted ring C_B . b) Thermal cycloreversion profiles (25 °C, $\text{Me}_2\text{CO}-d_6$) of the BuTAD-adducts with **6** and **7** indicate a much less pronounced debonding compared to plain naphthalene **2**. c) Similar cycloreversion profiles (25 °C, $\text{Me}_2\text{CO}-d_6$) are obtained for **8** and **9**, in which an ethyl instead of a methyl spacer is introduced between the naphthalene scaffold and the acetate group.

Having identified the different regioisomers that are formed during the photo-cycloaddition reaction of **6** and **7** with BuTAD, kinetic $^1\text{H-NMR}$ measurements were subsequently carried out to examine the substituent effect on the cycloreversion kinetics. From the obtained cycloreversion plots depicted in Figure V.9b, a much less pronounced dynamic behaviour compared to the plain unsubstituted naphthalene **2** was observed when a methyl acetate group was introduced onto the 1- or 2-naphthalene position (i.e. **6** and **7**, respectively). In fact, even after standing in the dark for 60 hours at 25 °C, more than 30 % of the total amount of cycloadducts was still detected (vs. 2 % for cycloadduct **[1+2]**, Figure V.9b). Introduction of an extra carbon atom in between the naphthalene and the acetate group, i.e. **1-NaphtEtOAc** (**8**) and **2-NaphtEtOAc** (**9**), gave similar results as judged by the almost superimposable cycloreversion profiles (open symbols in Figure V.9c).

The high fraction of covalent bonds that are kept intact over several days upon standing in the dark (> 30 %) when using the substituted naphthalene model compounds was detrimental for the design of the envisioned naphthalene monomer. Indeed, generating a light-triggered crosslinked material upon reaction with a bivalent TAD reagent is expected to refrain from the necessary macroscopic reversibility that is needed to ensure a complete debonding of the material when kept in the dark. Nonetheless, valuable information could be extracted from the cycloreversion plots when the different regioisomers were evaluated.

Evidently, the overall cycloreversion rate of the BuTAD-cycloadduct with **1-NaphtMeOAc** (**6**) was exclusively determined by **[1+6]-C_B**, the only cycloadduct formed (Figure V.10a). For the two regioisomers that are obtained with the 2-substituted counterpart **2-NaphtMeOAc** (**7**), however, a significantly different effect on the backward cycloaddition process became apparent. The TAD-addition product formed onto the non-substituted naphthalene ring, i.e. **[1+7]-C_B**, was shown to have a 7-fold rate accelerating effect on the cycloreversion process compared to its substituted counterpart **[1+7]-C_A** (i.e. $k_{\text{obs}} = 0.31 \cdot 10^{-5} \text{ s}^{-1}$ vs. $2.23 \cdot 10^{-5} \text{ s}^{-1}$, see Table V.1). In fact, within 30 hours of standing in the dark, the fraction of **[1+7]-C_B** almost completely diminished whereas the amount of **[1+7]-C_A** only decreased to half of its original value (Figure V.10b).

Intrigued by the observed difference on the cycloreversion rate of the regioisomers, efforts were devoted to direct cycloadduct formation onto the non-substituted naphthalene ring as this would lead to faster cycloreversion rates (*cf.* Figure V.10). Electron withdrawing groups were expected to introduce such directionality since they would deactivate the substituted ring to participate in the cycloaddition reaction with TAD. Thus, the above conducted model studies were repeated with the methyl ester-substituted naphthalene compounds **1-NaphtCOOMe** (**10**) and **2-NaphtCOOMe** (**11**).

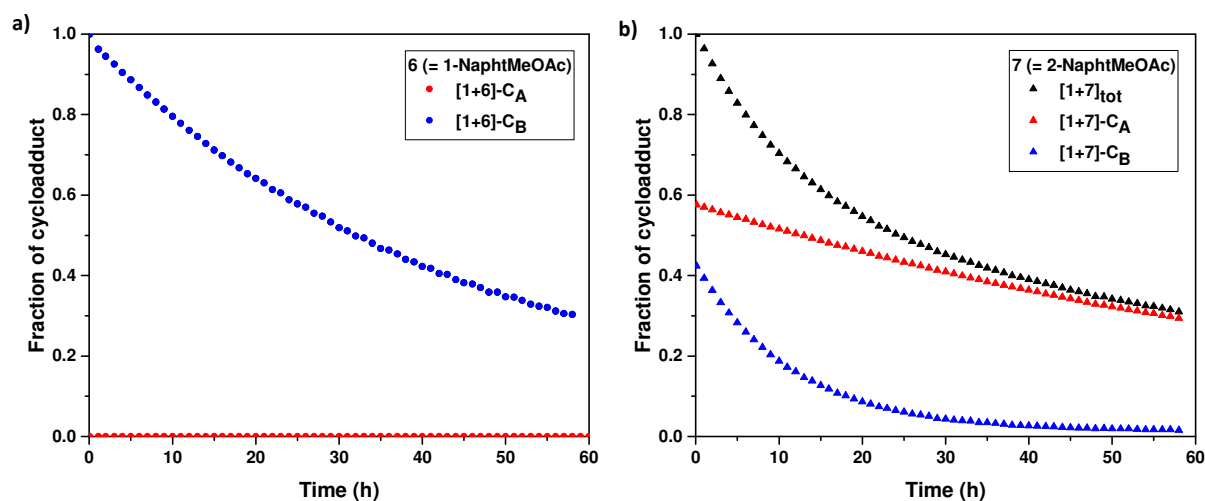


Figure V.10. Cycloreversion profiles in the dark at 25 °C ($\text{Me}_2\text{CO}-d_6$) for the individually formed regioisomers, obtained after 45 minute irradiation with green LEDs ($\lambda = 515 - 525 \text{ nm}$, $3 \times 3 \text{ W}$). a) The dissociation rate for $[1+6]$ (blue) is exclusively determined by the regioisomer formed at the non-substituted ring of 1-NaphtMeOAc **6**, the only photoproduct formed. b) The two regioisomers formed upon TAD-addition to its 2-substituted methyl acetate derivative **7** show a remarkable difference in cycloreversion rate, with the non-substituted adduct $[1+7]-\text{C}_\text{B}$ being considerably more labile.

Table V.1. Naphthalene compounds studied in the visible light-induced BuTAD-cycloaddition reaction (15 mM, $\text{Me}_2\text{CO}-d_6$, room temperature, $\lambda = 515 - 525 \text{ nm}$) with their corresponding regioisomer composition reached after 45 minutes of irradiation and the subsequent cycloreversion rates upon standing in the dark at 25 °C.

	R	Cycloaddition		Cycloreversion	
		C_A (%)	C_B (%)	$k_{\text{obs}} (\text{C}_\text{A}) (10^{-5} \text{ s}^{-1})$	$k_{\text{obs}} (\text{C}_\text{B}) (10^{-5} \text{ s}^{-1})$
2	H	100 %, with $\text{C}_\text{A} = \text{C}_\text{B}$		2.03 ^a	2.03 ^a
6	1-MeOAc	0	100	-	0.63
7	2-MeOAc	58	42	0.31	2.23
8	1-EtOAc	0	100	-	0.58
9	2-EtOAc	53	47	0.33	1.94
10	1-COOMe	0	100	-	0.41
11	2-COOMe	42	58	1.07	1.53

^aAddition of **1** to plain naphthalene **2** does not give a mixture of regioisomers due to its symmetry.

As anticipated, green light irradiation of **10** in the presence of **1** ($\lambda = 515 - 525$ nm, 45 min) exclusively gave cycloadduct formation on the non-substituted ring, as was previously observed for the 1-alkyl-substituted naphthalenes **6** and **8** (Table V.1). Moreover, no desired acceleration in the dissociation rate of **[1+10]** was established from the thermal cycloreversion profile (Figure V.11a). In fact, the thermal dissociation reaction was found to be significantly slower (i.e. $k_{\text{obs}} = 0.41 \cdot 10^{-5} \text{ s}^{-1}$ vs. $0.63 \cdot 10^{-5} \text{ s}^{-1}$ for **[1+6]-C_B**, see Table V.1). In contrast to the retained regioselectivity of **10**, its 2-substituted naphthalene ester derivative **11** was found to alter the preferred reaction site of the cycloaddition process compared to its 2-alkyl analogues **7** and **9**. Indeed, addition of **1** to **11** was now observed to slightly favour the non-substituted ring, containing a more electron rich character, thereby reversing the regioisomer composition to **[1+11]-C_A**:**[1+11]-C_B** = 42:58 (Appendix D). Interestingly, significantly faster cycloreversion kinetics were detected, which resemble the plain TAD-naphthalene system **[1+2]** much more closely (Figure V.11a). From the individual regioisomer formation over time, the non-substituted adduct **[1+11]-C_B** was identified to be the more thermally labile one (Figure V.11b), thereby confirming the proposed strategy to accelerate the cycloreversion process by directing the cycloaddition to the non-substituted ring.

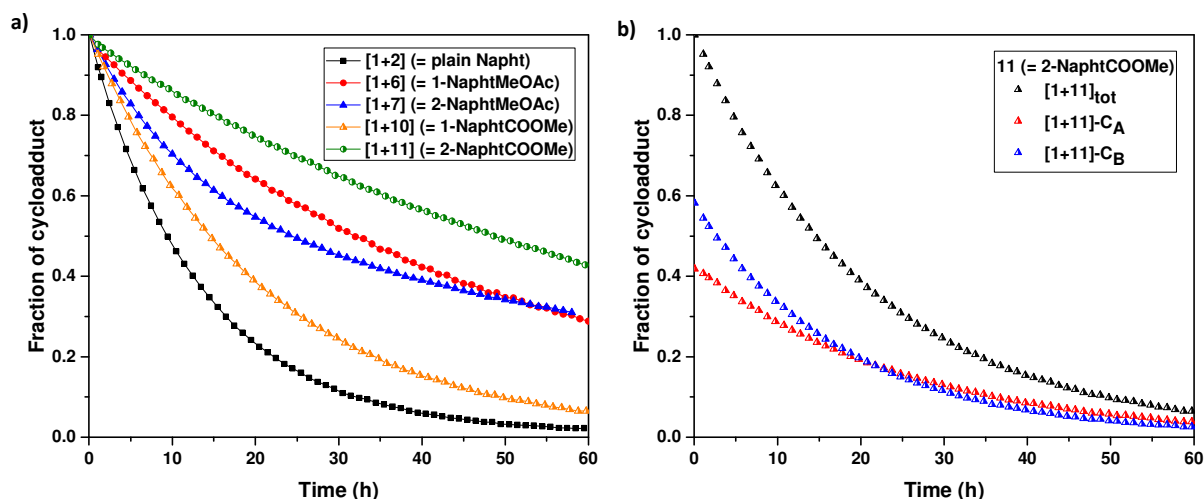
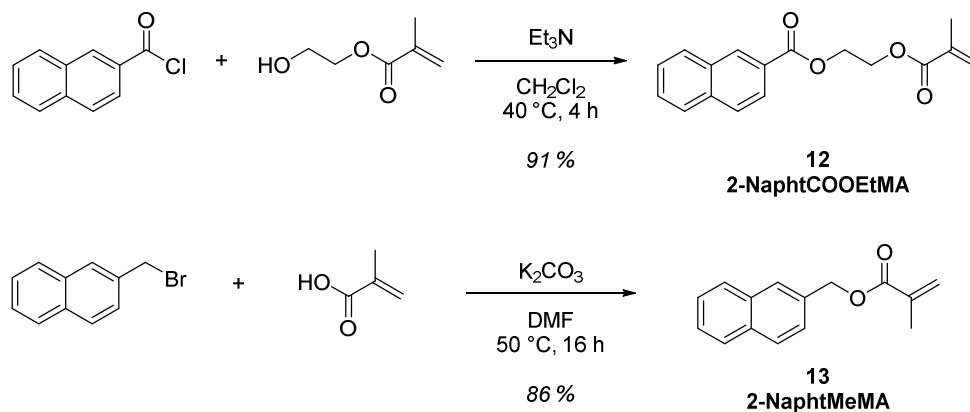


Figure V.11. a) Overview of the thermal cycloreversion kinetics of the investigated TAD-naphthalene adduct (25 °C, $\text{Me}_2\text{CO}-d_6$), indicating the ester-functionalised 2-NaphtCOOMe (**11**) to most closely mimic plain naphthalene **2**. b) Cycloreversion profiles of the individual **[1+11]** regioisomers demonstrate the non-substituted adduct **C_B** to have the most dynamic behaviour.

Given the results obtained with an electron withdrawing ester group in the naphthalene 2-position to most closely mimic the cycloreversion kinetics of plain naphthalene **2**, a new naphthalene-containing monomer was next targeted. The synthesis route comprised the straightforward modification of 2-naphthoyl chloride with 2-hydroxyethyl methacrylate, giving excellent multi-gram yields of the corresponding naphthalene-containing methacrylate monomer **12** (Scheme V.4). In addition, the initially projected naphthalen-2-ylmethyl methacrylate monomer **13** (2-NaphtMeMA) was also prepared. Although the resulting TAD-cycloadducts were shown to be considerably less labile at room temperature when the naphthalene substrate is

substituted with a methyl group instead of an ester (*cf.* [1+7] vs. [1+11] in Figure V.11a), monomer **13** was included in the following polymer studies in order to examine whether slight modulations on the molecular level can offer an additional tunable control over the debonding process in the final material.

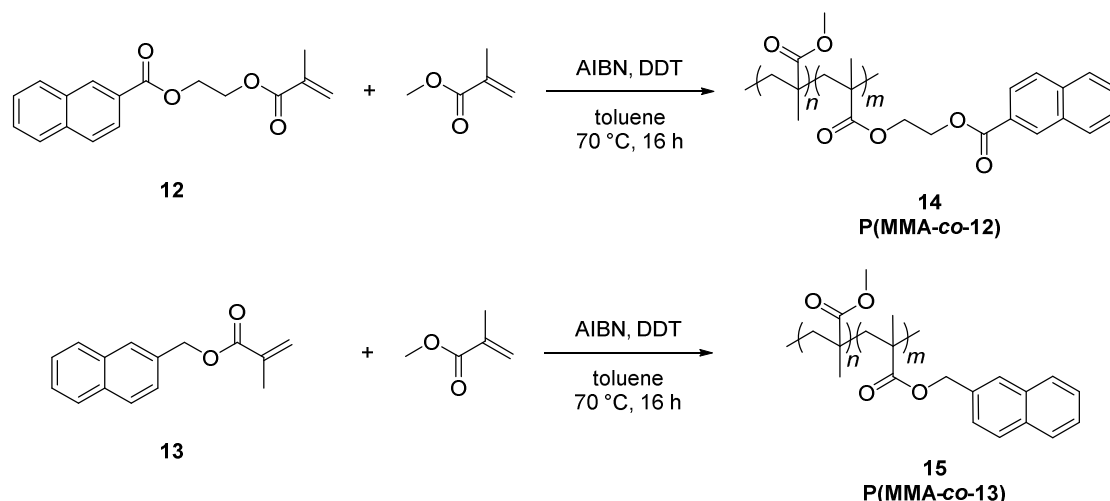


Scheme V.4. Synthesis route towards naphthalene-containing methacrylate monomers **12** and **13**, introduced on the naphthalene C2-position.

V.3.2 Polymer design and crosslinking test

Having identified a naphthalene methacrylate monomer characterised by a favourable cycloreversion rate, the monomer units were next incorporated into a linear polymer. As the intended application was to embed the dynamic TAD/naphthalene system into a crosslinked network, a precise control over molecular weight and dispersity of the resulting naphthalene-containing polymer was considered less important. Thus, a straightforward free radical process was here preferred over controlled radical polymerisation techniques.

The naphthalene monomers **12** and **13** (15 mol %) were copolymerised with methyl methacrylate (MMA) to give the linear polymethacrylates **14** and **15**, respectively (refer to Scheme V.5 and Table V.2). The free radical polymerisation was initiated by 2,2'-azobisisobutyronitrile (AIBN) and carried out in the presence of 1-dodecanethiol (DDT) as a chain transfer agent in order to suppress the molecular weight of the resulting polymer ([**12**]:[MMA]:[AIBN]:[DDT] = 15:85:1:2). ¹H-NMR analysis of the obtained copolymers indicated the effective incorporation of 14 mol % of the naphthalene units, which corresponded well to the theoretical 15 mol % of monomer feed. Although the exact molecular weight of the polymers could not be derived from the ¹H-NMR spectrum, the weight percentage of naphthalene that is embedded into the polymer was readily calculated from the molar monomer ratio (Table V.2), from which the desired amount of TAD crosslinking agent could later be determined.



Scheme V.5. Free radical polymerisation of monomers **12** and **13** to give the corresponding naphthalene-containing polymethacrylates **14** and **15**, respectively.

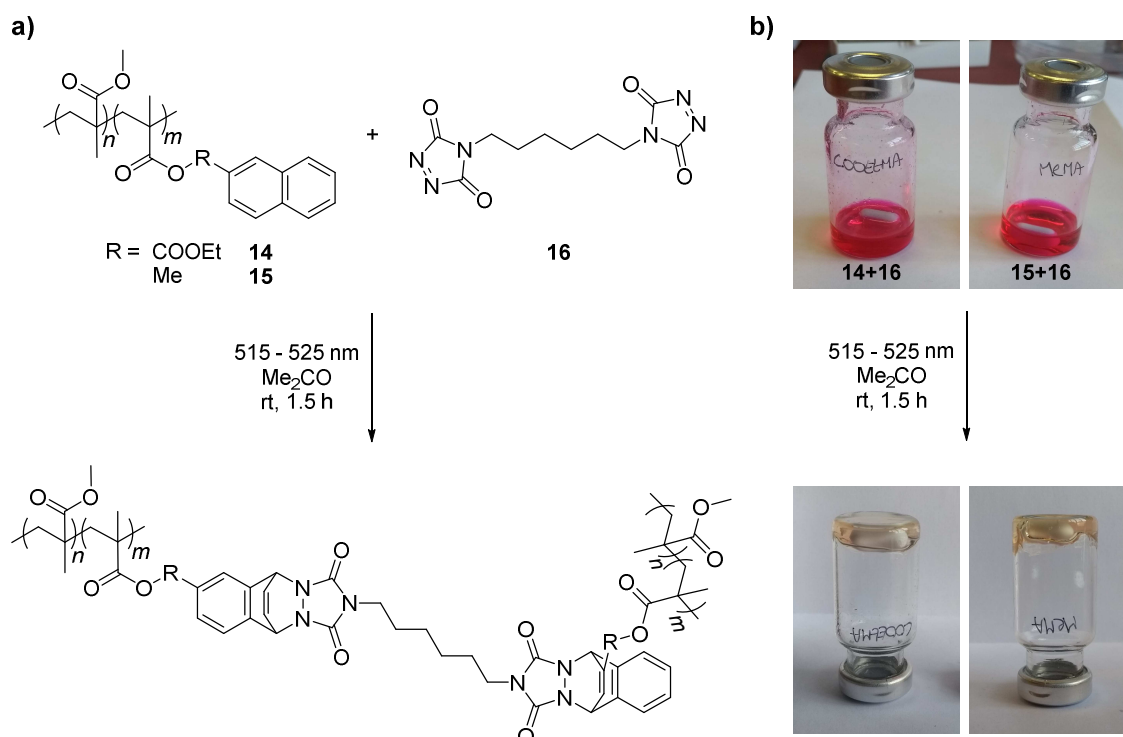
Table V.2. Molecular weight data on the naphthalene-containing polymethacrylates **14** and **15** obtained from size-exclusion chromatography (SEC, CHCl₃, calibrated on PMMA), together with the incorporated fraction of naphthalene units determined from ¹H-NMR analysis.

Polymer	M_n (kDa)	M_w (kDa)	M_p (kDa)	D	Fraction naphthalene		
					Monomer	mol %	wt %
14	5.0	9.5	8.6	1.90	12	14.1	31.8
15	4.7	9.5	8.7	2.01	13	14.2	27.2

Once the naphthalene-containing polymers were available, their TAD reactivity was next screened in crosslinking experiments with a bisfunctional TAD reagent (Scheme V.6a). Thus, the naphthalene copolymers **14** and **15** were dissolved in anhydrous acetone (200 mg mL⁻¹) together with 0.5 equivalents of bisTAD **16** (i.e. relative to the amount of naphthalene) and the resulting purple solutions were subjected to green LED light ($\lambda = 515 - 525$ nm, Scheme V.6). As expected, photobleaching of the TAD/naphthalene formulations was observed after 1.5 hours of irradiation and crosslinking of both polymers was demonstrated by means of a vial inversion test (Scheme V.6b). In a control experiment, blank reference solutions of the naphthalene-containing polymers were subjected to the same conditions of irradiation, but no gelation was observed. Moreover, no changes before and after irradiation were detected in the ¹H-NMR spectrum and SEC chromatogram, which indicated the photostability of the PMMA copolymers under visible light impact.

Following photocuring of the naphthalene polymers in the presence of bisTAD **16**, the initial purple colour readily reappeared in both gels and a weakening of the formed networks was observed over time. Eventually, both gels collapsed to give a purple solution at the bottom of the vial only a few hours after the green light was switched off. Interestingly, the networks based on copolymer **14**, wherein the naphthalene side chains are attached to the polymer backbone via

an ester functionality directly onto the aromatic scaffold (*cf.* Scheme V.6), were shown to collapse after 3 hours whereas its analogue with **15** required a slightly longer dark time to achieve a loss of its network integrity (i.e. 4 hours).



Scheme V.6. a) Visible light-induced crosslinking of naphthalene polymers **14** and **15** with bisfunctional TAD **16**.
b) Gelation was confirmed by a vial inversion test of the resulting photobleached polymer mixture.

Although routine ¹H-NMR analysis has found very little use to characterise crosslinked polymer networks because of excessively broad and overlapping peaks,⁴⁰⁷⁻⁴⁰⁸ TAD/naphthalene gelation experiments were repeated directly in an NMR tube with deuterated acetone in an attempt to gain some more quantitative insights into the formed network. Since low crosslinked and highly swollen networks have been reported to behave as linear polymers in solution,⁴⁰⁷ the visible light-induced curing of naphthalene-containing polymer **15** with bisTAD **16** (0.5 eq. vs. naphthalene) was carried out under more dilute conditions, (i.e. 75 mg of **15** in 0.75 mL Me₂CO-*d*₆). The obtained ¹H-NMR spectrum of the crosslinked gel immediately after irradiation revealed the presence of the expected TAD-naphthalene cycloadduct signals, which slowly decreased over time upon standing in the dark (refer to Appendix D). Unfortunately, no release of the TAD crosslinker could be observed because of overlapping proton signals with the polymer backbone and methyl side chain. Therefore, an alternative naphthalene-containing polymer was synthesised making use of *n*-butyl methacrylate as the comonomer. Upon repeating the gelation experiment in deuterated acetone with the newly formed polymer, the release of bisTAD **16** – and thus decrosslinking – was now clearly appreciated from the NMR spectra recorded after standing in the dark (Figure V.12).

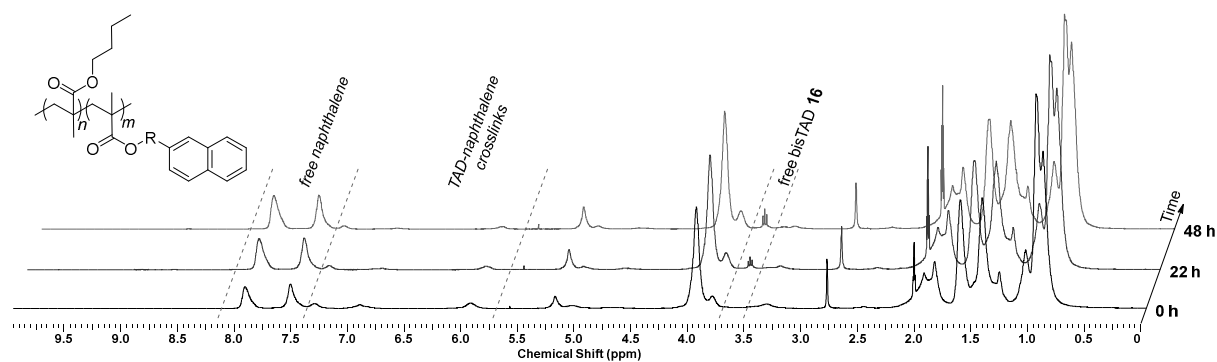


Figure V.12. Gelation experiment of bisTAD **16** with a copolymer of naphthalene-containing methacrylate **13** and *n*-butyl methacrylate upon green light irradiation. The decrosslinking reaction in the dark is evidenced by the decreasing TAD-naphthalene cycloadduct signals and increasing signals attributed to the naphthalene **13** and bisTAD **16** over time, which can be observed from the $^1\text{H-NMR}$ spectra ($\text{Me}_2\text{CO-}d_6$) recorded immediately after irradiation and after standing for 22 h and 48 h away from ambient light.

V.4 Light-stabilised dynamic materials

Having demonstrated the curing and subsequent collapse of TAD/naphthalene-based networks in preliminary experiments, the herein introduced light-stabilised dynamic materials (LSD materials) were next evaluated in more detail by assessing their rheological behaviour (V.4.1). Specifically, the ability to maintain the integrity of the crosslinked networks whilst subjected to continuous irradiation, together with the efficiency of the decrosslinking reaction when the resulting materials are kept in the dark, will be examined. Following the rheology experiments, some macroscopic demonstrations will be provided on a material level in order to illustrate the light-induced stabilisation of the covalent network linkages as well as the switchable sol-gel transitions upon alternating periods of irradiation and dark times (V.4.2).

V.4.1 Rheological behaviour

To investigate whether the TAD/naphthalene-based networks fulfil the imposed properties of LSD materials, rheological experiments under oscillatory shear mode were performed on the naphthalene-containing polymers **14** and **15** in the presence of bisTAD **16**. The viscoelastic response was monitored over prolonged periods of time at 25 °C and the storage and loss moduli G' and G'' , respectively, were determined from the torque measured throughout the experiments, which were conducted within the linear viscoelastic regime (refer to Appendix D for a strain sweep of the cured material).

A first aspect that was explored is whether the TAD/naphthalene materials that are formed upon photocuring remain stable whilst the light is continuously switched on. In a previous model study addressing light-stabilised dynamic covalent bonds (*cf.* V.2.3), the TAD-naphthalene cycloadduct was shown to remain near-quantitatively formed under prolonged times of visible light irradiation (*i.e.* > 95 % after 2 h), whilst retaining its dynamic nature. An important consideration, however, is that the model study had to be carried out in the presence of a TAD

quenching agent and therefore hardly reflects the bonding stability of the autonomous TAD/naphthalene system that would be embedded in the LSD materials.

Rheology measurements equipped with a visible light irradiation source, however, enable to detect the formation of cured TAD/naphthalene materials and allow for their stability to be monitored. Thus, solutions of the naphthalene-containing poly(methyl methacrylate)s **14** and **15** in the presence of bisTAD **16** were prepared, so to obtain an equimolar ratio of naphthalene and TAD moieties. In contrast to earlier investigations, propylene carbonate was used as the solvent instead of acetone in order to prevent evaporation during rheology measurements. Moreover, propylene carbonate is more viscous, which results in an improved detection of the storage and loss moduli of the resulting TAD/naphthalene formulations. Nonetheless, the prepared solutions remain very low viscous and therefore risk to flow from underneath the measuring system (parallel plate configuration). To prevent the solutions from flowing away and drying out during measurements, mineral oil was applied to the edges of the rheological samples.

The curing profiles of the resulting TAD/naphthalene solutions (0.5 M bisTAD **16** in a 0.84 g mL⁻¹ solution of **14**, or 0.8 g mL⁻¹ solution of **15**, in propylene carbonate), depicted in Figure V.13, indicated low initial storage moduli G' (below the limit of detection), together with low G'' values, which remained constant over the course of one hour when the sample is kept in the dark. Irradiation of the TAD/naphthalene formulations with light filtered in the visible range, i.e. $\lambda = 400 - 500$ nm, resulted in an abrupt increase in the G' and G'' . Within 30 minutes of irradiation, a sol-gel transition was observed as the intersect of the storage and loss moduli, and a plateau in G' (ca. 3 kPa) was reached after 3 hours, indicating complete photocuring was established. Importantly, no deviation in the storage modulus was detected when the samples were subjected to visible light for an additional 7 hours (i.e. 10 h of total irradiation time). Regardless of some minor fatigue that was detected for **14** (the copolymer of 2-NaphtCOOEtMA **12**, cf. Scheme V.5), both cured TAD/naphthalene materials are indeed evidenced to retain their crosslink density and can thus be regarded to be light-stabilised.

Next to evidencing the stability of the TAD/naphthalene crosslinked materials upon visible light irradiation, the subsequent decrosslinking process under the mildest trigger of all, i.e. switching the light off, can also be readily studied by means of rheology. Hence, similar formulations of **14** + **16** and **15** + **16**, were again cured in the rheometer upon visible light impact ($\lambda = 400 - 500$ nm). Since the material is expected to shrink upon photocuring, a small normal force was applied onto the material after the crosslinking was completed in order to better anticipate the volume expansion during the decrosslinking process. Indeed, by imposing a constant normal force throughout the rheological measurement, the volume changes can be compensated by allowing the gap width to adjust. Making use of such normal force controlled rheology was critical to prevent a drift in the storage modulus to erroneous values, particularly during measurements over very long periods of time.⁴⁰⁹

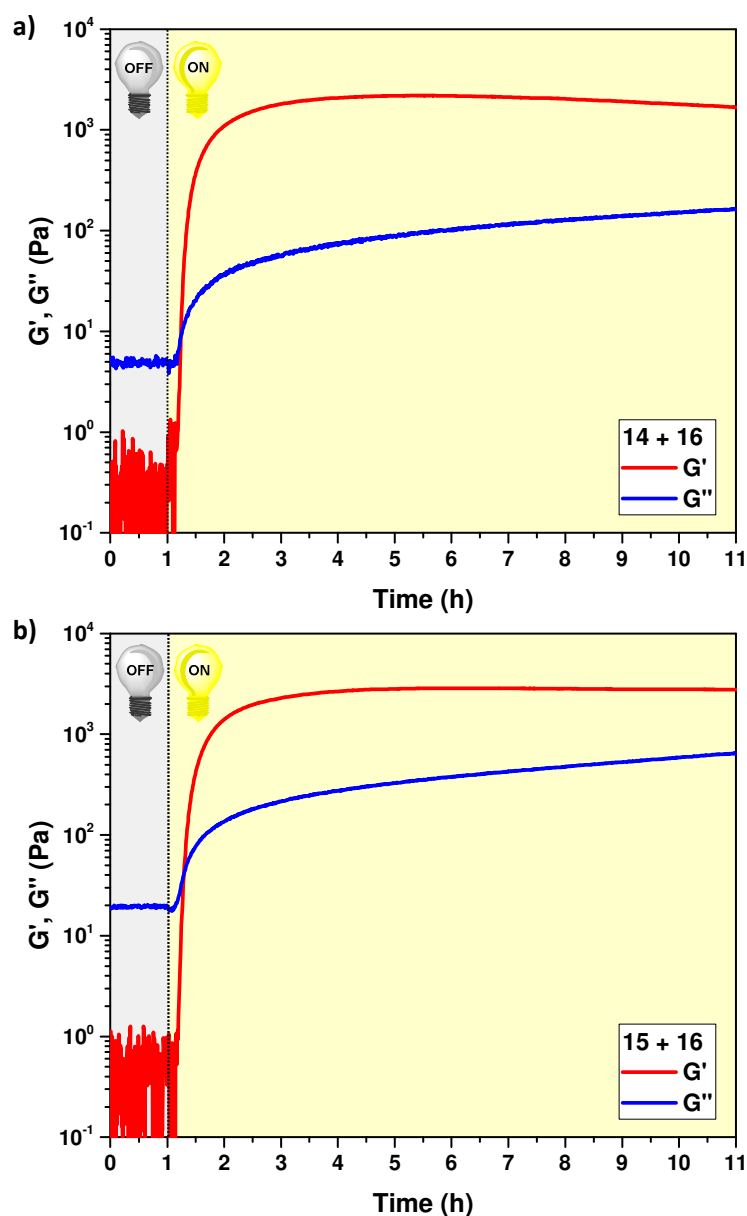


Figure V.13. Rheological behaviour of the naphthalene-containing polymers, (a) **14** and (b) **15**, and bisTAD **16** upon prolonged visible light irradiation ($\lambda = 400 - 500$ nm), indicating the light-induced stabilisation of the crosslinked TAD/naphthalene material.

Thus, when full curing was reached after 3 hours of irradiation of **14** + **16** containing an equimolar ratio of TAD vs. naphthalene, a small normal force of 0.2 N was applied to the material after which the light was subsequently switched off and the response in viscoelastic behaviour was monitored over the course of 12 hours at 25 °C (Figure V.14). Immediately after the sample is kept in the dark, a significant decrease in the storage modulus was detected, which correlates to a reduction in the crosslinking density and hence in the loss of the network integrity. After 4.5 hours of standing in the dark, a crossover of G' and G'' was again observed, evidencing the decrosslinking process as a result of the cycloreversion of the initially formed TAD-naphthalene crosslinks.

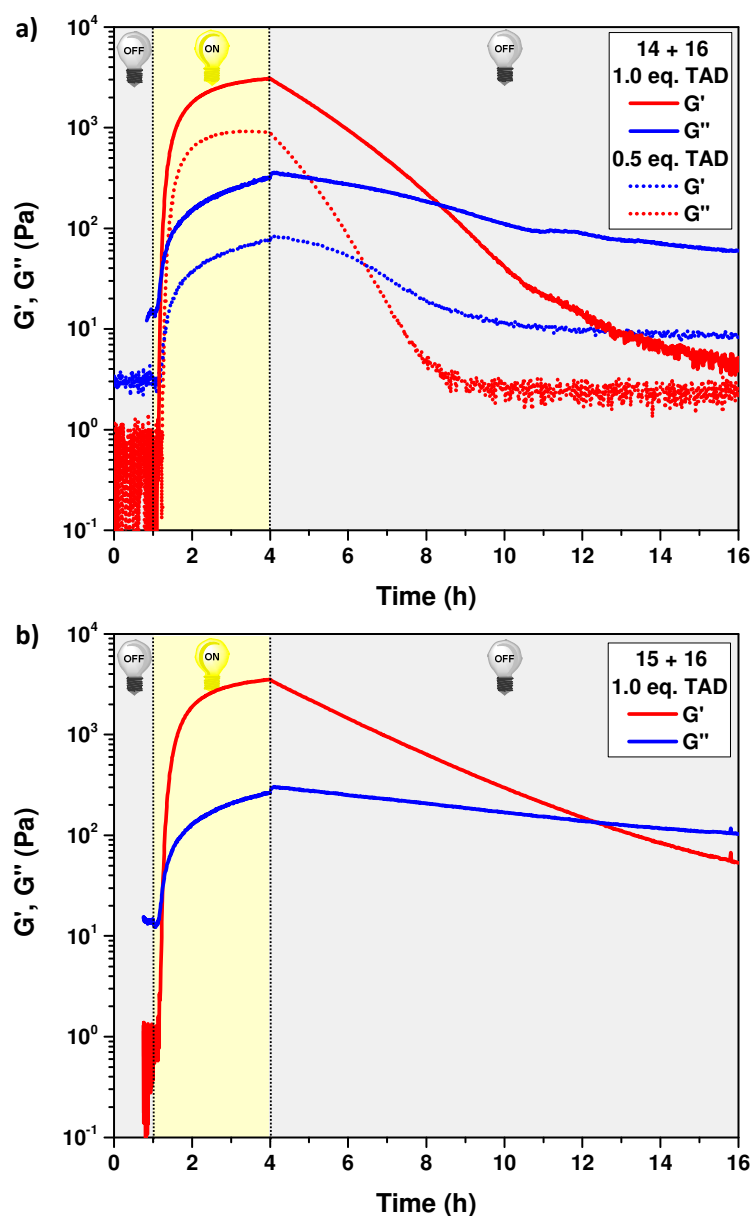


Figure V.14. Rheological behaviour of the naphthalene-containing polymers, (a) **14** and (b) **15**, in the presence of bisTAD **16** upon visible light irradiation for 3 hours ($\lambda = 400 - 500$ nm), followed by standing in the dark for 12 hours at 25 °C. The collapse of the network after photocuring is evidenced by the decrease in storage and loss modulus. The decrosslinking through thermal cycloreversion of the TAD/naphthalene systems can be tuned depending on the molecular modulations onto the naphthalene scaffold.

The correlation of the declining storage modulus to the crosslinking density was also demonstrated when only half the amount of bisTAD equivalents was used (i.e. 0.25 eq. **16**, thus $[\text{TAD}]/[\text{Naphthalene}] = 0.5$). Indeed, a lower amount of TAD reagents leads to a lower crosslinking density – and hence a less stronger material – upon photocuring, which gave a steeper decline in G' when kept in the dark (Figure V.14a). It should be noted that the equilibrium values of G' and G'' obtained after the collapse are not identical to the initial values, which can be attributed to the equilibrium fraction of TAD-naphthalene cycloadducts that is established at room temperature (refer to the model studies in V.3). An alternative explanation might be the

formation of irreversibly crosslinked products, yet is unlikely since no such degradation or side reactions were detected during the model studies on both low and high molecular weight compounds.

Although similar curing profiles were obtained for both naphthalene-containing polymers, the material obtained from **15** gave a markedly delayed sol-gel transition compared to its derivative **14** (i.e. > 8 h instead of 4.5 h dark time, Figure V.14b). This delayed collapse of the network when the naphthalene units are built into the polymer side chains through an alkyl spacer on the 2-position of the aromatic scaffold instead of an ester, is consistent with the knowledge derived from the kinetic cycloreversion studies of the respective naphthalene monomer mimics **7** and **11** (refer to Table V.1 and Figure V.11a). The thermal debonding triggered by placing the TAD/naphthalene-based LSD materials in the dark can thus be readily tuned by making slight molecular modulations on the naphthalene scaffold.

A critical aspect of the rheological investigations of the light-stabilised materials was devoted to assess whether the visible light-induced crosslinking and ambient temperature triggered decrosslinking can be repeatedly accessed. The ability to reversibly form and dissociate the TAD/naphthalene crosslinking points was evidenced from G' and G'' during consecutive cycles of visible light irradiation for 3 hours, followed by standing in the dark at 25 °C for another 15 hours. The obtained viscoelastic response for both formulations (i.e. **14** + **16** and **15** + **16**), depicted in Figure V.15, indicated several sol-gel transitions being reached after distinct time intervals. Similar to earlier observations, the storage and loss moduli did not regain their initial values obtained before light-induced crosslinking, which was devoted to the remaining equilibrium concentration of the TAD-naphthalene adducts.

Another notable effect was noticed from the lower G' values reached after the second photocuring step (Figure V.15). The apparent slightly weaker materials formed in the second cycle might be attributed to the loss of liquefied material from underneath the parallel plate measuring system to the edges of the lower plate geometry, arising during the preceding long period of decrosslinking in the dark, or to partial degradation of the reactive TAD crosslinking agents. Nonetheless, the recrosslinked sample was shown to collapse again when the light was switched off and even a third visible light/dark cycle could be successfully carried out.

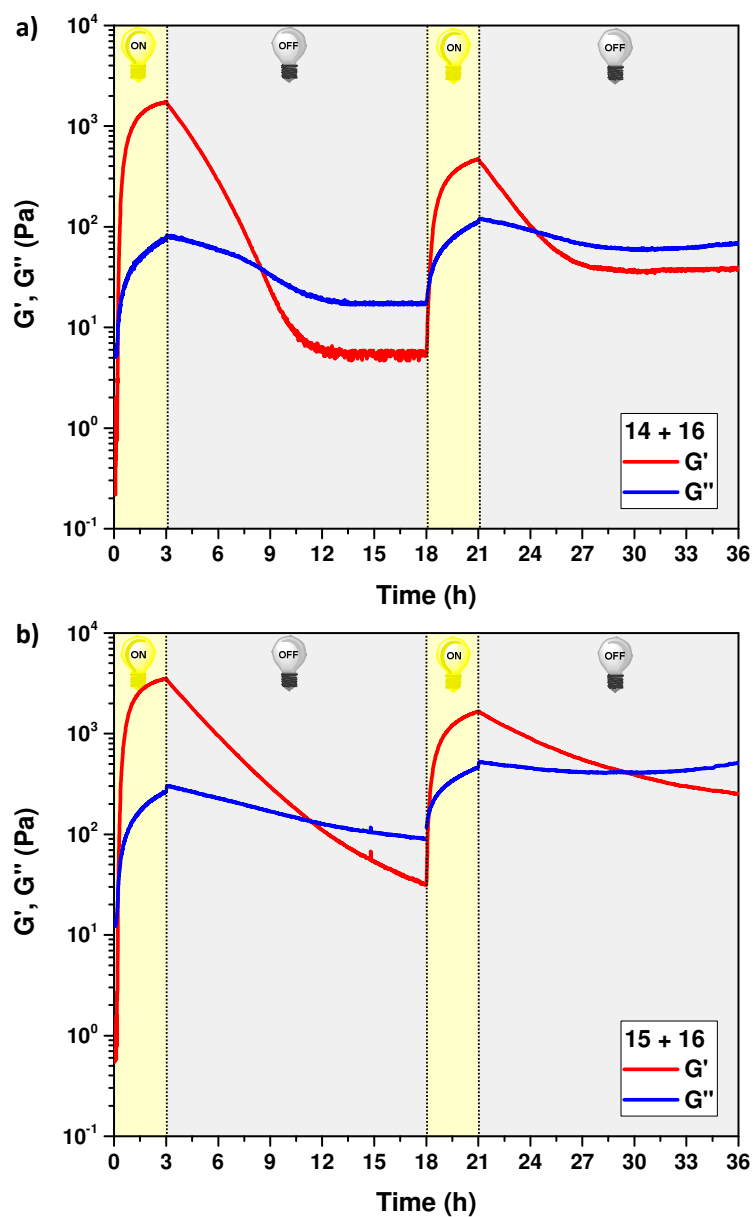


Figure V.15. Rheological behaviour of the naphthalene-containing polymers, (a) 14 and (b) 15, in the presence of bisTAD 16 during consecutive cycles of visible light irradiation for 3 hours ($\lambda = 400 - 500$ nm), followed by a 15-hour period of dark time at 25 °C, indicating a series of reversibly switchable transitions from a network to a liquid, and vice versa.

V.4.2 Macroscopic demonstrations

The rheological behaviour of the light-stabilised dynamic TAD/naphthalene materials was next demonstrated on a macroscopic scale by means of two proof-of-concept macroscopic experiments.

In a first visual demonstration, the retention of crosslinking under continuous irradiation and subsequent decrosslinking triggered by switching the light off was illustrated. For this, a formulation of the most labile TAD-reactive naphthalene-containing polymer **14** in propylene carbonate (0.84 g mL^{-1}) was prepared and mixed with bisTAD **16** to provide an equimolar ratio of TAD and naphthalene moieties. The dark red TAD/naphthalene solution **14** + **16** was placed in a rectangular silicon mould and cured under green light irradiation ($\lambda = 515 - 525 \text{ nm}$) to give a relatively firm colourless material after 5 hours. Rapidly after the light is switched off, a faint pink colour was rapidly reinstated throughout the material upon removal from the mould (Figure V.16a). The cured sample was next placed onto a metal grid (Figure V.16b) and subjected to green light for an additional 5 hours (Figure V.16c). The material was shown to have an identical appearance as the pristine sample (Figure V.16d), indicating the retained crosslinked integrity and thus illustrating the light-stabilised nature of the TAD/naphthalene material.

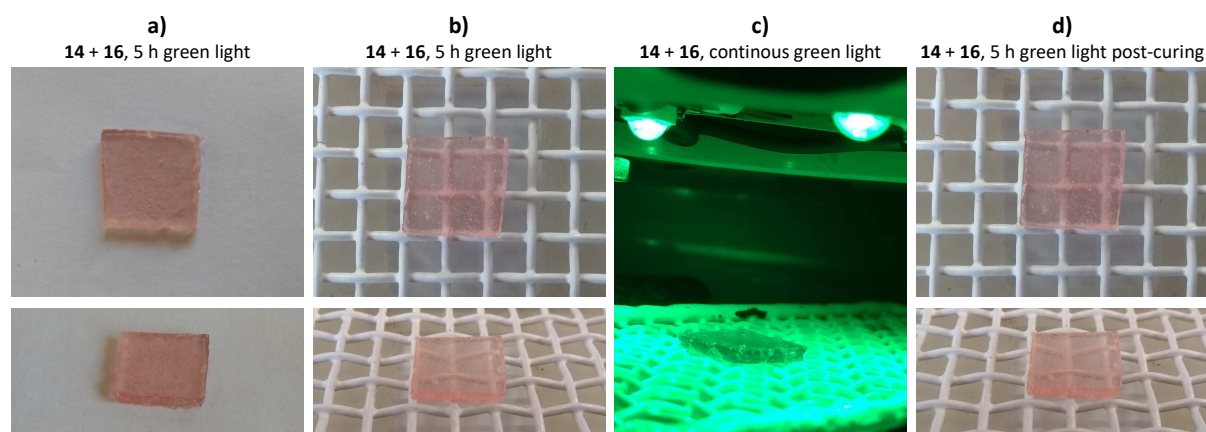


Figure V.16. Macroscopic demonstration of TAD/naphthalene-based light-stabilised materials. a) Curing of a solution of naphthalene-containing polymer **14** and bisTAD **16** in propylene carbonate with green light ($\lambda = 515 - 525 \text{ nm}$, 5 h) gives a clear colourless material, which rapidly regains a pink colour. b-d) The resulting material was placed on top of a metal grid and irradiated for an additional 5 hours, without affecting the crosslinked integrity.

When the LSD material was subsequently kept in the dark (Figure V.17a), a deep red colour, arising from the released bisTAD crosslinker, was observed after 2 hours (Figure V.17b). After an additional 3 hours of standing in the dark at ambient temperature, the decrosslinking process was evidenced more clearly by the dripping formulation and material migration through the metal grid (Figure V.17c). The collapse of the network continued over time (Figure V.17d and e) until a red solution was eventually collected on the glass plate underneath the grid, 40 hours after the green light was switched off (Figure V.17f).

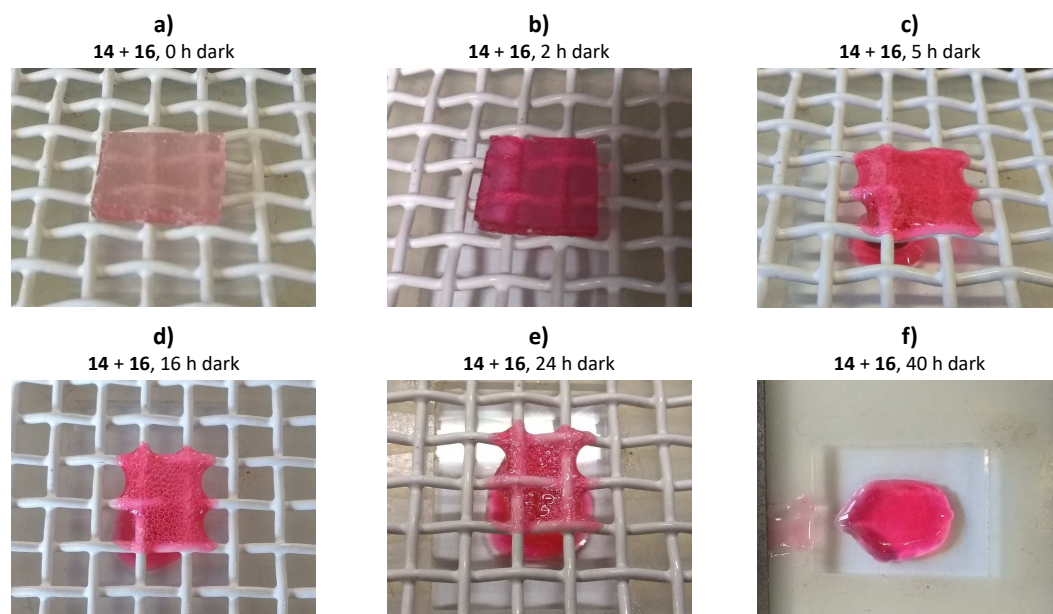


Figure V.17. Macroscopic demonstration of the decrosslinking process in the dark. Quickly after curing of **14 + 16** (propylene carbonate) with green light ($\lambda = 515 - 525$ nm, 5 h) the material placed on the metal grid regains a deep red colour upon when the light is switched off. Eventually, the decrosslinking process leads to a liquefied material that drops and migrates through the grid to finally give a purple solution.

Next to evidencing the light-stabilisation and dark collapse of TAD/naphthalene materials, a second and last macroscopic experiment aimed to demonstrate the switchable sol-gel transition, observed from the rheological measurements. To illustrate the repeatably accessible transition of a network into a solution, and vice versa, a series of shape transformations was conducted with the above employed formulation of **14 + 16** (0.42 g mL^{-1} **14** in propylene carbonate, equimolar ration of TAD and naphthalene moieties). Thus, the red TAD/naphthalene resist was first placed into a triangle shaped mould (Figure V.18, left) and crosslinked after 3 hours of green light impact ($\lambda = 515 - 525$ nm). The clear and colourless triangle was subsequently placed into a rectangular shaped mould, left overnight in the dark to give a red solution which spread across the template and eventually cured a second time with green light to yield a transparent rectangular gel (Figure V.18, middle). A third cycle was finally conducted with a circular shaped mould (Figure V.18, right). Thus, the TAD/naphthalene-based LSD material can be readily transformed into different shapes by exploiting their switchable sol-gel transition.

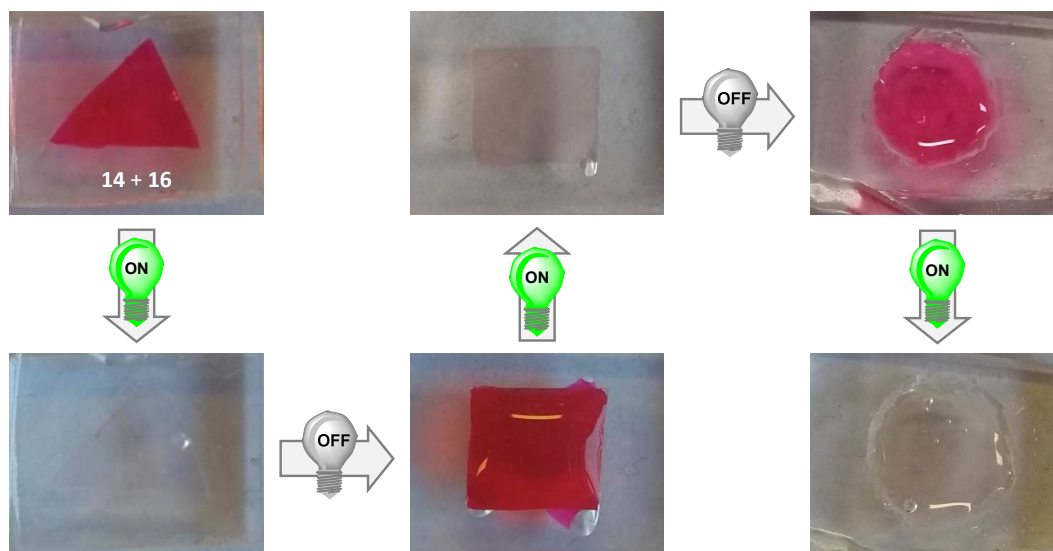


Figure V.18. Macroscopic demonstration of the switchable sol-gel transition, illustrated by the transformation of a propylene carbonate solution of **14** and **16** from a triangle network into a rectangular mould and eventually a circular shape. Crosslinking was affected by green light ($\lambda = 515 - 525$ nm, 3 h), whereas decrosslinking and flow across the newly shaped mould took place overnight upon standing in the dark at ambient temperature.

V.5 Conclusions and perspectives of light-stabilised materials

An unprecedented conceptual approach was postulated in the present chapter, which introduced an advanced polymer system that can be reversibly switched between two states of matter, i.e. from a covalently crosslinked material to a liquid and back, using only one colour of light. More specifically, a single photochemical trigger was sought for, which can induce crosslinking when the light is switched on, keep the resulting network stable whilst being irradiated, and finally allow for covalent bond cleavage that is affected when the light is switched off. The visible light-driven cycloaddition reaction of TADs to naphthalene compounds was identified as highly promising dynamic covalent chemistry to devise the here so-called light-stabilised dynamic materials (LSD materials).

The TAD/naphthalene system was subjected to detailed model studies, which demonstrated the desired features of green light-induced cycloadduct formation in combination with thermal dissociation through cycloreversion of the resulting adduct upon standing in the dark at ambient temperature. Importantly, the light-stabilised aspect of the thus formed dynamic covalent bond was established under continuous green light irradiation. It was shown that over the course of several hours, the TAD/naphthalene photostationary state remains predominantly, and in fact, near-quantitatively populated.

The identified promising characteristics were next translated to the material level via the synthesis of naphthalene methacrylate monomers that are readily incorporated into polymer materials. A crucial aspect herein was the assessed substitution effect on the naphthalene scaffold

on both the regioselectivity during cycloadduct formation as well as their characteristic cycloreversion kinetics. Alteration to the chemical environment of the naphthalene moieties to direct adduct formation onto the non-substituted aromatic ring was shown to significantly accelerate the cycloreversion kinetics.

Following photocuring of the resulting naphthalene-containing polymers with a bisTAD crosslinker, LSD materials were thus successfully obtained. An interesting observation is the ability to tune the thermal cycloreversion kinetics of the formed TAD-naphthalene adducts also on a material level by incorporating different functionalities onto the naphthalene scaffold. The light-stabilised dynamic behaviour of the TAD/naphthalene materials was finally identified by means of rheological measurements. Besides the visible light triggered crosslinking reaction and subsequent collapse when placed in the dark, the ability to keep the formed materials stabilised under the action of continuous irradiation was also visually demonstrated. Indeed, when subjected to green light the polymer network was observed to retain its crosslinked integrity, while in the dark a deformation into the liquid state was evidenced as the material dripped through a metal grid. In addition, the observed transformation from a crosslinked structure into a liquefied state can be repeatably accessed, which was illustrated by consecutive bonding-and-debonding cycles to enable reshaping of the TAD/naphthalene materials.

Given the sound proof-of-concept of TAD/naphthalene-based LSD materials that was delivered, future endeavours should focus on the optimisation of TAD/naphthalene-based networks in order to fully exploit this unprecedented class of materials, for instance in the design of photoresists. A highly interesting challenge would be to fabricate LSD materials that can respond to the external photonic field without the need for solvents. Thus far, a high boiling point solvent is required to guarantee mobility on the molecular level, so that the dissociation of the TAD/naphthalene network points can take place. Incorporating TAD/naphthalene systems into different polymer matrices with a much lower glass transition temperature (e.g. acrylates) would therefore be a highly interesting approach to incorporate light-stabilised dynamic behaviour also in bulk materials. In addition, the reversible nature of the TAD-naphthalene adducts can be tuned into an irreversible connection by taking away the driving force for the thermal cycloreversion. This has already been demonstrated via the reduction of the isolated endocyclic double bond (*cf.* V.2.2) and offers future perspectives to permanently freeze the covalent dynamic crosslinks by an additional chemical trigger.

A particular concern of the TAD/naphthalene materials, however, is the observed fatigue leading to a decrease in material properties when multiple sol-gel transitions are desired. Indeed, prolonged reshaping of the materials was shown to eventually deplete the reactivity of the TAD-crosslinking agent over the course of several days. Nonetheless, the careful modulation of the naphthalene scaffold was already demonstrated to have a significant effect on the cycloreversion rates. Further molecular manipulations are therefore expected to accelerate the collapse of the materials and thereby shorten the lifetime of free TAD moieties, thus extending the lifetime of

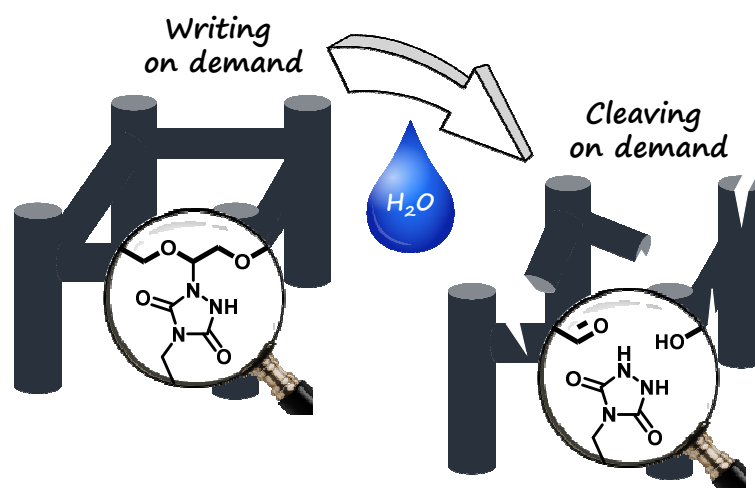
the corresponding LSD materials. One approach, for instance, could be the use of naphthalene anhydrides, which are commercially available and can be readily incorporated into a polymer backbone by means of polycondensation reactions. Given the introduction of two ester functionalities, TAD-addition is expected to be directed even more to the non-substituted ring, thereby resulting in a more rapidly debonding.

Next to a further acceleration of the debonding process to decrease the exposure time of free TADs, which leads to a reduction in their reactivity, an alternative approach is to identify other types of light-stabilised dynamic chemistries. The TAD/naphthalene-based networks developed in the present chapter would ideally serve as a pioneering example to trigger such future endeavours and open a vast array of opportunities for LSD materials in spatio-resolved applications that require an on demand debonding under the mildest trigger of all; switching the lights off.

Chapter VI.

Photoaddition of triazolinediones to polyethers

Brief motivation and content



Backbone functionalised poly(ethylene glycol)s (PEGs) are a promising class of macromolecular drug carriers as a result of improved drug loading capacities, yet their synthesis relies on the challenging ring-opening copolymerisation of tailored monomers. Based on the rarely reported side reaction of triazolinediones (TADs) to ethers under irradiation, this chapter introduces an alternative one-step approach for the backbone functionalisation of readily available polyethers. Whereas the visible light-induced TAD-addition to PEG is demonstrated to be an accessible strategy towards low-degrees of modification, the formed backbone conjugates are shown to be sensitive to hydrolysis. However, the TAD-PEG system is identified as a highly promising platform for the design of crosslinked PEG-based materials under benign visible light irradiation ($\lambda > 515$ nm), whereby the resulting material can be cleaved in water, even at neutral pH. Importantly, the developed TAD-PEG photoresists can be triggered by means of multiphoton absorption, without the need for any additives. Thus, three-dimensional laser writing becomes applicable for the fabrication of erasable PEG-based microscopic structures. The pioneered cleavable PEG-based photoresists are believed to constitute a platform technology for subtractive lithography, whereby support structures can be selectively removed, as well as tissue engineering applications, whereby the cell scaffolds can be degraded in the applied cell media *in situ* without the need for an additional trigger.

Parts of this chapter have been submitted as a manuscript

VI.1 Introduction

Poly(ethylene glycol) (PEG) is an omnipresent polymer in multifaceted daily life applications including cosmetics, food additives and lithium-ion batteries.⁴¹⁰⁻⁴¹² Moreover, PEG is regarded as the bench-mark of biocompatible polymers and is a renowned macromolecular drug carrier used in polymer therapeutics.⁴¹³⁻⁴¹⁴ The extremely diverse end-use of linear PEGs is driven by the straightforward introduction of functional end groups, either during or after the conventional ethylene oxide ring-opening polymerisation (ROP).⁴¹⁴⁻⁴¹⁵ In particular the post-polymerisation modification of PEG-hydroxyl groups forms a well-established method to incorporate a vast amount of functionalities that are amendable to further (bio)conjugation reactions in a process often referred to as PEGylation.⁴¹⁶⁻⁴¹⁸ In addition, PEG-based macromolecules bearing (photo)polymerisable end groups, such as (meth)acrylates, are also readily accessible via this manner, which have been of particular value in the synthesis of complex PEG-based macromolecular architectures and networks, including dendrimers and hydrogels.⁴¹⁹ In particular, PEG-based hydrogels have been extensively explored as three-dimensional scaffolds for tissue engineering.⁴²⁰

The degree of functionalisation that can be achieved via end group modification of linear PEGs, however, is limited and in fact inadequate for specialty applications, thereby urging the need to install functionalities directly onto the PEG polymer backbone.⁴²¹ Indeed, in pharmaceuticals and polymer supported catalysis, for example, backbone functionalities severely improve drug or catalyst loading capacities,⁴²² whilst in lithium-ion batteries such backbone modification allows for a tunable crystalline behaviour, making them useful electrolytes at room temperature.⁴²³ However, as a result of the chemical inertness that polyethers possess, backbone-functionalised PEGs – coined multifunctional PEGs (*mf*-PEGs) by Frey and coworkers⁴²² – can only be obtained by means of a ROP of ethylene oxide with tailored epoxide comonomers.^{421, 424} Critically, the functionalities that are incorporated onto the epoxide comonomer need to be compatible with the stringent ROP conditions, which rather limits the scope of backbone modification. Nonetheless, a variety of *mf*-PEGs with pendant vinyl⁴²⁵ or allyl ether-,^{421, 424} methylthioether-,⁴²⁶ hydroxyl-,⁴²⁷⁻⁴²⁸ catechol-,⁴²⁹ alkyne-⁴³⁰ and amino-groups⁴³¹ have been successfully introduced, albeit through protecting group chemistries and/or highly efficient click-like post-modification reactions. The degree of functionalisation, however, can be readily tuned by the monomer feed which enables the systematic adjustment of the resulting PEG properties, such as crystallinity and thermo-responsiveness.⁴³²

The knowledge concerning the photochemical reactivity of triazolinediones (TAD) that is gathered throughout the current doctoral work lead to identify an alternative approach to introduce functionalities throughout the PEG polymer backbone. TADs namely exhibit good hydrogen abstraction reactivity with ether substrates upon UV-light irradiation (see Figure VI.1). This photochemical TAD-addition was first reported in the 1970s and considered to be an

undesired side reaction that occurs when TAD reagents are used in ether-containing solvents, e.g. 1,4-dioxane and tetrahydrofuran (*cf.* II.2.3.2).²⁵¹ Instead of refraining from the use of TADs in the presence of ethers, Risi and coworkers exploited this observed side reaction for the functionalisation of crown ethers under UV- and green light irradiation.³⁰⁶ Apart from this sole synthetic study, however, no useful transformations of the photochemically triggered TAD addition to ethers have been reported to our knowledge.

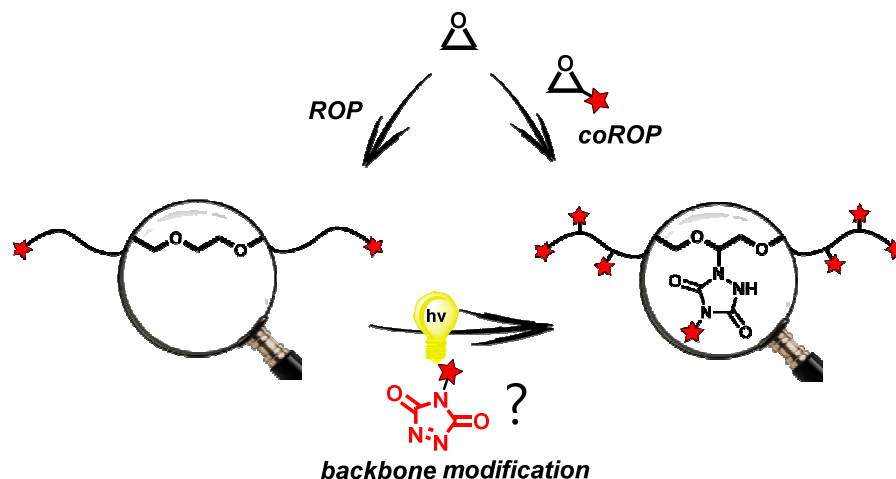


Figure VI.1. Common modification strategies to obtain end group (left) and backbone functional polyethers (right) and the alternative approach through the light-induced addition reaction of triazolinediones to commercial polyethers (bottom), investigated herein.

The final chapter of the current doctoral work aims to exploit the originally observed side reaction of TADs in the presence of ethers in a polymer context to serve as a potentially elegant strategy to enable the light-induced backbone modification of commercially available polyethers (Figure VI.1). Ideally, this alternative functionalisation method would offer a more straightforward approach than the conventional ring-opening copolymerisation to introduce tailored substituents or tune the resulting polymer properties. Therefore, the light-triggered addition reaction of TADs will first be investigated on low molecular weight as well as polymeric model compounds after which the stability of the resulting adducts will briefly be evaluated (VI.2). The insights gained from the model study allowed to identify another emerging application for which crosslinked materials are generated in a spatio-resolved manner on both the macro- and microscale (VI.3).

VI.2 Model studies of the photoaddition reaction

VI.2.1 Investigations on low molecular weight compounds

Before TAD-based polyether modification can be examined, the photoaddition reaction of TADs to low molecular weight ether compounds was first reinvestigated in order to assess the selectivity of the ether product formation with respect to the previously established photochemical TAD reactivity (*cf.* Chapter IV and V). Initially, purple solutions of BuTAD **1**

(5 mg mL⁻¹) in ether solvents were subjected to UV-light ($\lambda_{\max} = 365$ nm, 3 x 36 W Arimed B6) until complete photobleaching was observed. Tetrahydrofuran (THF) was selected as a readily available cyclic ether solvent, whereas dibutyl ether (*n*Bu₂O) was identified as a good acyclic representative to mimic the perspective poly(ethylene glycol) substrate. Moreover, both employed substrates are symmetrical ethers, which simplifies the model study as the formation of different regioisomers is avoided.

Thus, the respective BuTAD-ether mixtures were irradiated to give the expected α -TAD-addition products **3** and **4** within 1 hour (Figure VI.2a). ¹H-NMR spectra of the resulting reaction mixtures, depicted in Figure VI.2b-c (in DMSO-*d*₆) indeed indicated the formation of the α -urazolyl ether adducts, with the characteristic proton resonance above 5 ppm assigned to the substituted α -CH (i.e. signal *f*). Next to the desired adducts **3** and **4**, substantial traces of *n*-butylurazole **2** were also detected. Since the BuTAD reagent was sublimed before use, thereby removing any residual urazole precursor arising from the TAD synthesis, the generation of **2** indicated the photoaddition reaction to proceed via a reductive pathway, presumably through urazolyl radicals.³⁰⁶ Interestingly, the amount of urazole byproduct observed for the photoreaction in THF (ca. 30 %) is considerably more pronounced than for its acyclic dibutyl ether counterpart (i.e. < 12 %). This is somewhat surprising since the cyclic ether substrates tend to react faster with TAD and even form the corresponding adduct upon heating, whereas TAD-addition to acyclic analogues only proceeds under photochemical conditions.²⁵¹ Regardless, the photoaddition of BuTAD to the investigated ether compounds proceeded swiftly in moderate to high yields (i.e. 70 to 88 %), yet more importantly without the formation of products arising from photodegradation or photopolymerisation.

Although TADs swiftly undergo photoaddition in ethers as a solvent, the targeted polyether backbone modification would preferentially be conducted in solution and in an equimolar manner. A critical aspect is to find an appropriate solvent for the photoaddition reaction to take place. Indeed, solvents that either compete with the radical addition process (e.g. ethers) or induce unwanted TAD reactivity such as light-induced cycloaddition (i.e. aromatics) or photopolymerisation (e.g. halogenated solvents) should be avoided. A judicious solvent was found in acetonitrile, which was previously identified as an inert solvent for **1** and was even used to assess its photostability (*cf.* Chapter IV). Thus, similar irradiation experiments as before were carried out with equimolar amounts of **1** (5 mg mL⁻¹) and THF or *n*Bu₂O in anhydrous acetonitrile. Although identical photoproducts were observed (refer to Appendix E for ¹H- and ¹³C-NMR spectra), prolonged irradiation times were required to achieve full TAD conversion (i.e. 2 hours), along with considerably lower yields of the desired TAD-ether adducts **3** and **4** (i.e. 66 % and 73 %, respectively).

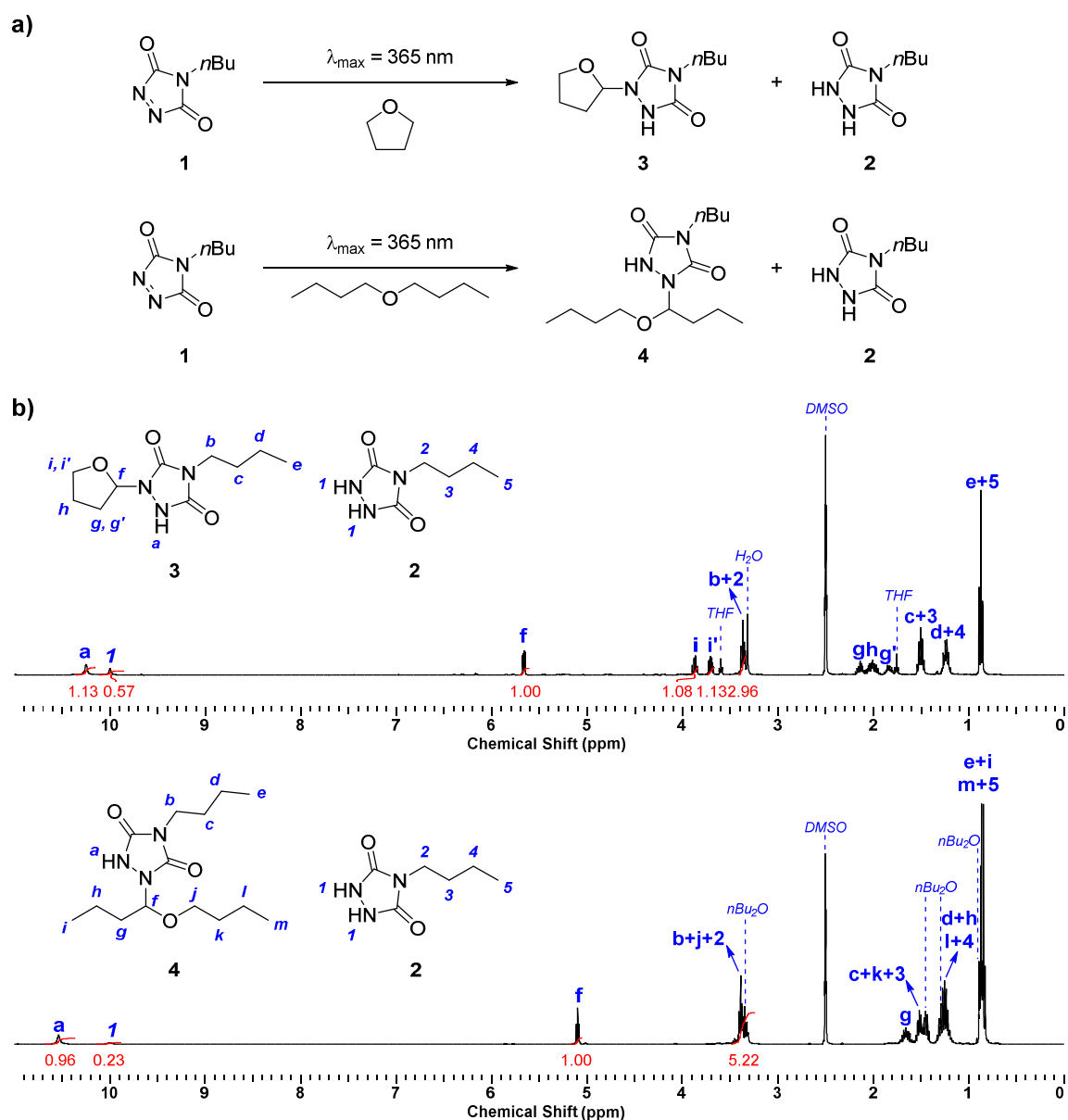


Figure VI.2. Low molecular weight study of the photoinduced TAD-ether addition reaction. a) UV-light irradiation of BuTAD **1** (5 mg mL⁻¹) in tetrahydrofuran and dibutyl ether readily gives the corresponding TAD- α -addition products **3** and **4**, together with traces of **2**. b) The expected TAD-ether adducts were readily observed in the ¹H-NMR spectra (DMSO-*d*₆) via the characteristic proton resonance of the newly substituted α -CH above 5 ppm (signal *f*) and allowed to determine the yield of the photoaddition.

In an attempt to reduce the urazole byproduct formation, thereby improving the TAD-ether photoaddition efficiency, the model reactions were repeated at different wavelengths (i.e. $\lambda = 320$ up to 600 nm). Remarkably, photobleaching was observed at every wavelength investigated, yet the yield of the TAD-ether adducts remained constant throughout the UV- and visible light regime of the spectrum. Nonetheless, the ability to conduct the phototriggered addition of TAD to ethers under visible light impact is an important observation as it indicates that the formation of the addition products is truly devoted to the light-induced activation of the TAD moieties rather than the ether substrates, which do not absorb in the visible light range.

VI.2.2 Backbone modification of poly(ethylene glycol)

Following the investigations of the UV- and visible light-induced addition of BuTAD to small molecule ethers, the backbone functionalisation of polymeric ethers was next examined. For this, poly(ethylene glycol) (PEG) with an average number molecular weight of 2000 Da was selected as cheap and readily available bench-mark aliphatic polyether. Before investigating the photoreactivity of PEG with TAD, the hydroxyl end groups of the commercial polymer were modified in order to exclude competitive TAD reactivity that might arise from the nucleophilic polymer ends (*cf.* II.2.3.3).²⁶⁰ Thus, PEG 2000 was reacted with *tert*-butyl isocyanate to transform the polymer end groups into the corresponding urethane. ¹H-NMR, SEC and ESI-MS analysis confirmed the quantitative conversion of PEG 2000 into the resulting *t*BuPEG 2000 (refer to Appendix E). An additional advantage of incorporating the *tert*-butyl groups at both ends of the polyether is their well-resolved singlet in the ¹H-NMR spectrum (i.e. signal *a* in Figure VI.3, bottom), which elegantly serves as an internal standard to later determine the degree of TAD-functionalisation onto the polymer backbone.

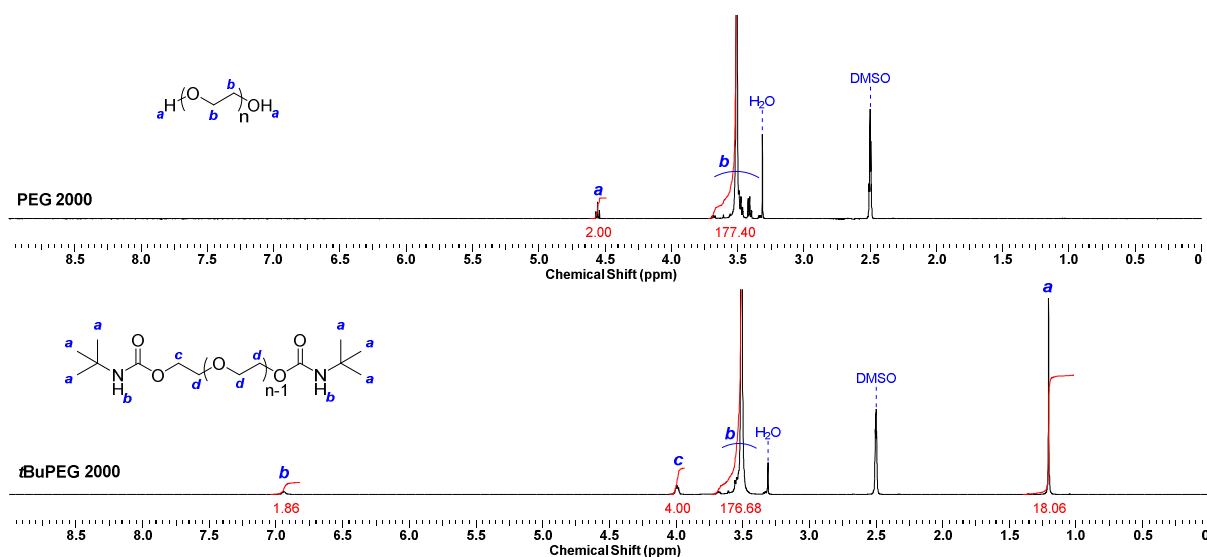
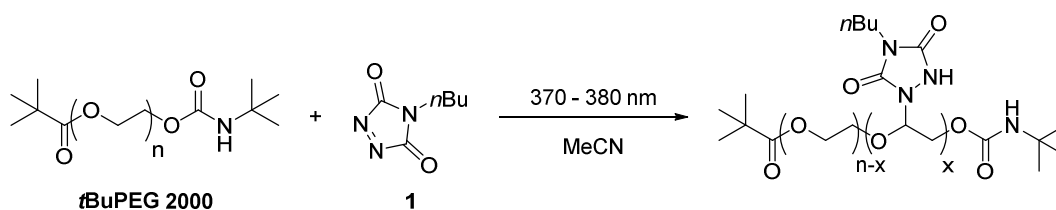


Figure VI.3. ¹H-NMR spectra (DMSO-*d*₆) before and after end capping of PEG 2000 with *tert*-butyl isocyanate. The well-resolved proton singlet arising from the *tert*-butyl group (signal *a*, bottom) can serve as an internal standard to determine the degree of backbone functionalisation.

Having assessed the photostability of the end capped *t*BuPEG 2000 upon UV-A impact (refer to Appendix E), the polyether was next irradiated in the presence of different BuTAD ratios ranging from 1 to 35 equivalents, relative to a single polymer chain (Scheme VI.1). No adduct formation was observed when **1** was added to a solution of *t*BuPEG 2000 in anhydrous acetonitrile (25 mg mL⁻¹) and kept in the dark. Photobleaching was only observed when the reaction mixtures were exposed to light ($\lambda = 370 - 380$ nm, 3 x 3 W LEDs, 24 h).



Scheme VI.1. Photoinduced modification of *tert*-butyl end capped poly(ethylene glycol) 2000 (*t*BuPEG 2000) with BuTAD 1.

The average amount of covalently attached BuTAD to the polyether backbone was derived from the $^1\text{H-NMR}$ spectra of the crude reaction mixtures, from which the yield of the photoaddition process could be determined (refer to Table VI.1 and Figure VI.4a). In addition, the backbone functionalisation could also be derived and was here defined as the ratio of the average number of TAD molecules incorporated onto the polymer backbone to the degree of polymerisation of the *t*BuPEG 2000 substrate (i.e. $\text{DP} = 46$, $^1\text{H-NMR}$). It should be noted that the obtained degree of functionalisation is based on the assumption that only one TAD-reaction site is provided per ethylene glycol monomer unit, whereas two $\alpha\text{-C}$ atoms are present. It should therefore be interpreted as an indicative measure that allows to evaluate the efficiency of the TAD-polyether addition reaction.

From the results, presented in Table VI.1, PEG modification with up to 10 equivalents of BuTAD was observed to proceed with a similar efficiency as for low molecular weight ether substrates (i.e. yields above 79 %), with up to 17 % of PEG monomer units being functionalised in 80 % yield. Higher degrees of functionalisation were also successfully achieved but suffered from a significant loss in yield as a result of an increased formation of urazole byproduct. In addition, irradiation times exceeding 24 hours were required to affect complete discolouration of the reaction mixtures when 20 or more TAD equivalents were used.

Table VI.1. Average number of BuTADs per polymer chain, yield and degree of functionalisation determined by $^1\text{H-NMR}$ analysis of the crude reaction mixtures obtained after UV-A irradiation ($\lambda = 370 - 380$ nm, 3×3 W LEDs, 24 h) of *t*BuPEG 2000 (25 mg mL^{-1} , MeCN) in the presence of BuTAD.

Targeted eq. 1	Experimental eq. 1 (from $^1\text{H-NMR}$)	Average TADs per polymer chain	Yield (%)	Degree of functionalisation (%)
1	1.04	0.86	85.5	1.86
2	2.03	1.68	82.9	3.65
5	4.75	3.77	79.2	8.19
10	9.77	7.86	80.4	17.1
20	17.65	10.70	60.6	23.3
35	28.44	13.41	47.2	29.1

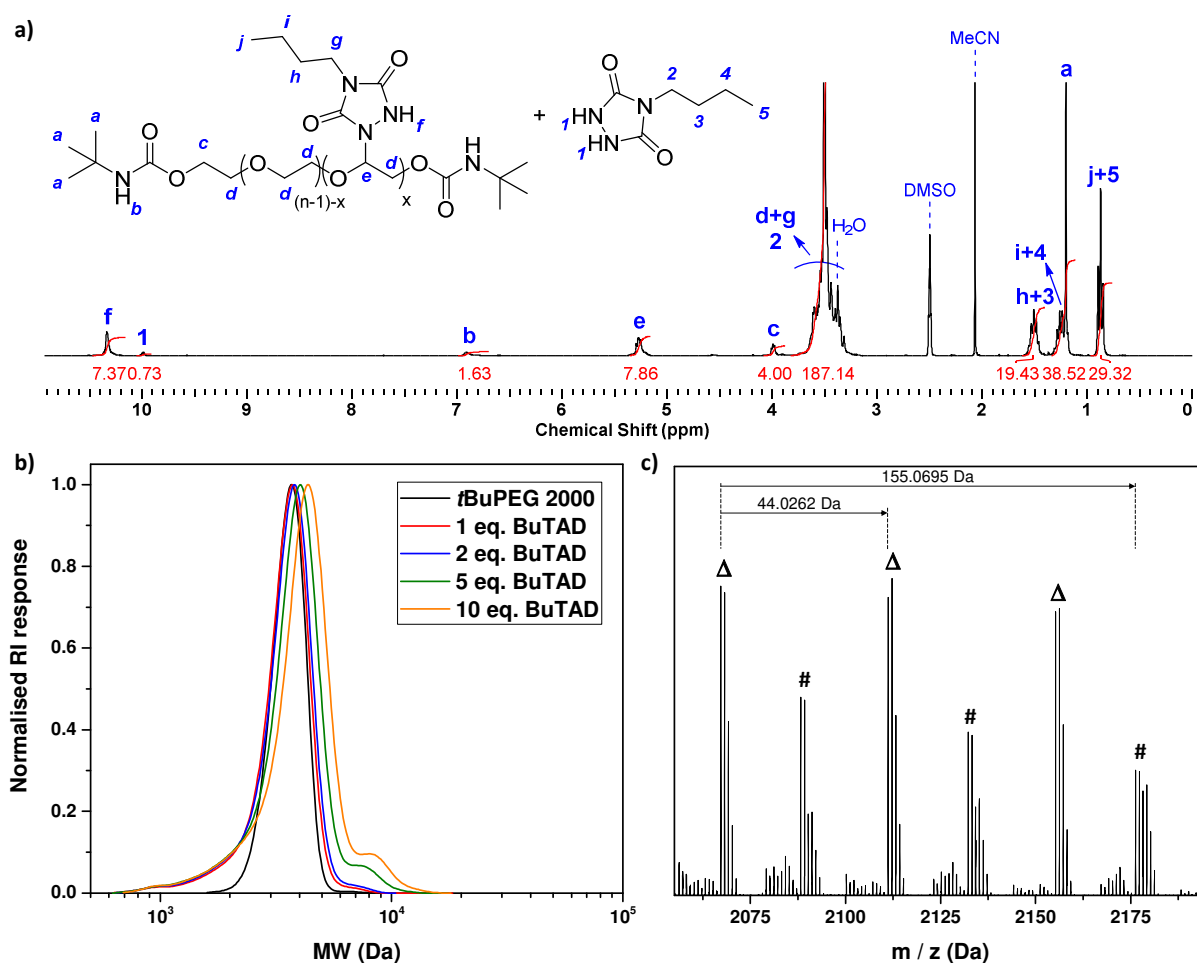


Figure VI.4. Analysis of the photoaddition of BuTAD to *t*BuPEG 2000 (25 mg⁻¹ mL, MeCN) upon UV-A irradiation ($\lambda = 370 - 380$ nm, 3 x 3 W LEDs). a) ¹H-NMR spectrum (DMSO-*d*₆) of the crude reaction mixture, illustrated for 10 equivalents BuTAD relative to *t*BuPEG 2000, indicated the covalent attachment onto the polyether backbone and allows for the determination of the yield and degree of functionalisation. b) SEC traces (THF, calibrated on polystyrene) of the crude reaction mixtures evidenced a shift to higher molecular weight values upon TAD-addition. c) The TAD-PEG conjugate was also identified in the ESI-MS spectrum, illustrated for the photoaddition of one equivalent BuTAD.

The successful polyether backbone modification upon irradiation was further evidenced by a shift in the SEC chromatograms to higher molecular weight distributions (Figure VI.4b and Table VI.2). Evidently, higher equivalents of BuTAD resulted in a more pronounced shift, although a high molecular weight shoulder also became apparent. Changing the irradiation source to LEDs that emit at higher wavelengths (i.e. $\lambda = 440 - 450$ nm and $\lambda = 515 - 525$ nm) did not improve nor deteriorate the reaction outcome, although decreasing the distance between the recipient and LEDs significantly reduced the times needed to affect photobleaching (e.g. less than 1 h instead of 18 h for 5 eq. BuTAD at $\lambda = 515 - 525$ nm). Attempts to elucidate the high molecular weight moieties that are present after irradiation via a hyphenated mass spectrometric technique (SEC-ESI-MS) unfortunately failed. However, the obtained mass spectrum did confirm the attachment of the TAD reagent onto the polymer backbone, as illustrated for the crude

reaction mixture obtained after irradiation of *t*BuPEG 2000 in the presence of one equivalent BuTAD (see Figure VI.4c and Table VI.3).

Table VI.2. SEC data (THF, polystyrene calibration) of the crude BuTAD-*t*BuPEG 2000 mixtures (25 mg⁻¹ mL *t*BuPEG in MeCN), obtained after irradiation with UV-A light ($\lambda = 370 - 380$ nm, 3 x 3 W LEDs).

Eq. BuTAD (1)	Irradiation time (h)	M_n (kDa)	M_w (kDa)	M_p (kDa)	\bar{D}
0	0	3.1	3.3	3.4	1.03
0	24	3.3	3.5	3.6	1.05
1	5	3.2	3.5	3.7	1.10
2	7	3.2	3.6	3.8	1.11
5	18	3.4	3.9	4.0	1.14
10	22	3.7	4.3	4.3	1.17

Table VI.3. Theoretical and experimental m/z values observed in the ESI-MS spectrum of the crude reaction mixture after UV-A irradiation of *t*BuPEG (25 mg⁻¹ mL, MeCN) in the presence of 1 equivalent BuTAD (relative to the amount of polyether).

$\Delta = [t\text{BuPEG-BuTAD} + \text{Na}]^+$				$\# = [t\text{BuPEG} + \text{Na}]^+$			
n	m/z_{theor} (Da)	m/z_{exp} (Da)	Δ (Da)	n	m/z_{theor} (Da)	m/z_{exp} (Da)	Δ (Da)
36	2067.2003	2067.2021	0.0018	40	2088.2408	2088.2374	0.0034
37	2111.2247	2111.2283	0.0036	41	2132.2655	2132.2637	0.0018
38	2155.2584	2155.2545	0.0039	42	2176.2883	2176.2899	0.0016

The formation of urazole byproducts during the TAD photoaddition proved inevitable both with low molecular weight as well as with macromolecular substrates. Whereas in the former case the removal of urazole **2** is readily achieved by means of chromatographic purification, applying such a technique to polymers is considerably less practical. It was thus desired to remove the small urazole byproducts from the polymer-TAD conjugate obtained after irradiation via more conventional and large scale purification methodologies. Although attempts to precipitate the modified *t*BuPEG upon addition of the crude reaction mixture into cold diethyl ether failed, dialysis in tetrahydrofuran was found to successfully remove the urazole byproducts (Figure VI.5).

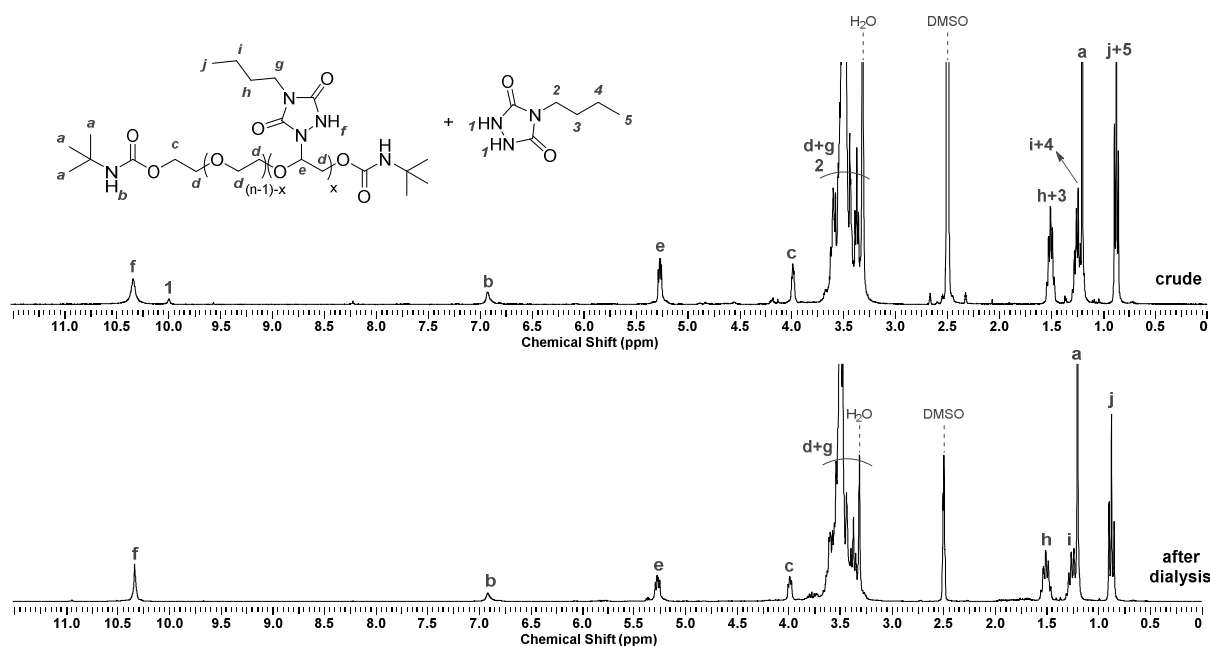
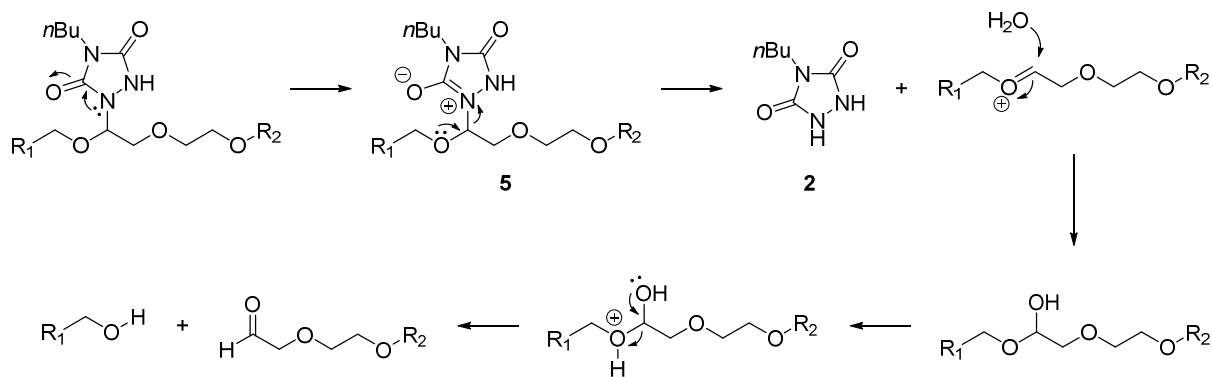


Figure VI.5. $^1\text{H-NMR}$ spectra ($\text{DMSO-}d_6$) before and after dialysis of the BuTAD-*t*BuPEG 2000 conjugate, obtained after green light irradiation ($\lambda = 515 - 525$ nm, 3 x 3 W LEDs, 1.5 h).

VI.2.3 Hydrolytic stability

A particular concern of the TAD-ether photoproducts is their stability towards hydrolysis, since the resulting adducts contain a hemiaminal-type linkage. In fact, the hydrolytic sensitivity of similar hemiaminal ether compounds has been reported by Cookson in 1965 during his studies on the photochemical reactivity of diethyl azodicarboxylate (DEAD) with ethers.³⁰⁵ Since DEAD can be regarded as an acyclic TAD mimic, the synthesised TAD-ether adducts could be expected to undergo a similar hydrolysis into alcohol, aldehyde and urazole derivatives. Indeed, when the TAD-PEG conjugates are exposed to water at 60 °C for 24 hours, several hydrolysis products became apparent in the $^1\text{H-NMR}$ spectrum, amongst aldehydes, alcohols and the initial butylurazole **2** (refer to Appendix E for NMR spectra before and after hydrolysis). In contrast, when the formed backbone functionalised TAD-polyether was kept in anhydrous acetonitrile for several days, no such degradation products were observed.

A plausible mechanism for the hydrolysis of TAD-polyether adducts likely proceeds through a zwitterionic urazole intermediate (**5**, Scheme VI.2) via electron delocalisation within the ring structure of the adduct. The neutral urazole moiety **2** can hence be kicked out of the polymer backbone. The thus formed oxonium ether can subsequently be hydrolysed to give the corresponding aldehyde and alcohol products, via the intermediate formation of a hemiacetal. Given the acidic nature of the urazole, the latter stage of the hydrolysis is presumably self-catalysed.



Scheme VI.2. Simplified, plausible mechanism for the hydrolysis of TAD-polyether adducts, thereby cleaving the backbone into its corresponding alcohol and aldehyde with the formation of the neutral urazole **2**.

VI.2.4 Concluding remarks on the model studies

In summary, it is feasible to statistically modify poly(ethylene glycol) in one step through the photochemical addition of TADs under both UV- and visible light impact. In principle, any substituent that is present on an aliphatic TAD reagent, such as a carboxylic acid or amine, can hence be introduced along the polyether backbone. This light-triggered TAD modification therefore offers promising potential and can, for instance, serve as an alternative approach for the synthesis of PEGs bearing multiple functionalities or modulate their physical properties.

Nonetheless, the degree of functionalisation that can be achieved in high yields (i.e. > 80 %), yet without affecting the polydisperse properties, is rather limited and the formed adducts were shown to be quite labile in the presence of water, as can be expected from hemiaminal ether linkages. The proposed strategy should therefore be carefully evaluated in view of the intended application, but appears to be well-suited if low degrees of functionalisation (i.e. < 10 %) are desired. In addition, the resulting modified PEGs are best employed in a non-aqueous environment to prevent hydrolysis of the polymer backbone. Given PEGs are praised for their water-borne utility, the photoaddition of TADs might therefore be a more valuable approach for different types of polyether substrates, e.g. polytetrahydrofuran,⁴³³ that lean themselves more to non-aqueous applications.

VI.3 Writing and cleaving of poly(ethylene glycol)-based materials

As alluded to above, the backbone TAD-modification of PEG is best carried out at low degrees, but severely suffered from hydrolysis even in the absence of acids and bases. This hydrolytic instability of the TAD-polyether conjugates initially hampered the enthusiasm of the established light-induced modification strategy as it is detrimental to their use in an aqueous environment. Yet, the ability to cleave the polyether backbone under extremely mild conditions, i.e. neutral pH, can also provide a highly interesting tool in chemically triggered debonding applications. The photoaddition of TADs to polyethers that are embedded into a crosslinked material, for instance, can provide a highly unique platform to degrade the linear polymer backbone, so to reduce the crosslinking density, potentially enabling recyclability of the resulting thermoplastic.

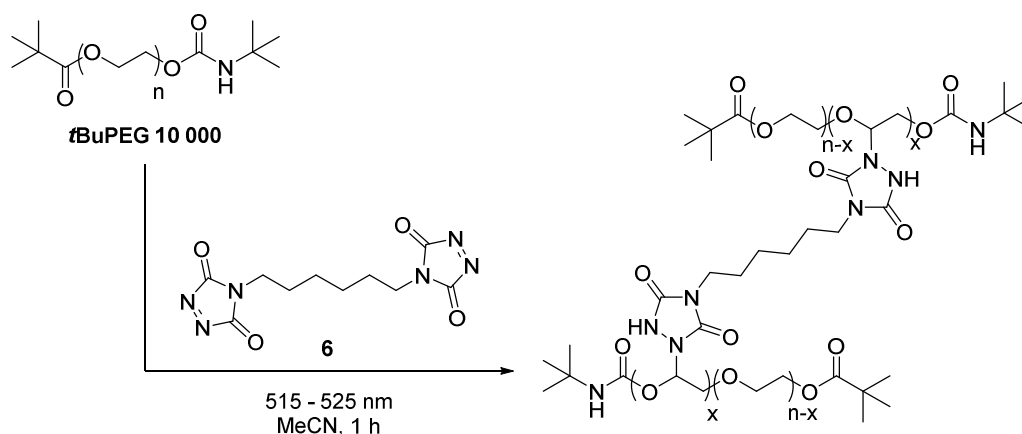
Another challenging application of the triggered bonding and debonding of TAD-polyether systems was identified during an extensive research stay at the Queensland University of Technology in Brisbane, Australia. Herein, the spatially resolved three-dimensional fabrication of microstructures was targeted since PEG-based crosslinked materials are widely applied scaffolds for biomedical purposes, including cell studies and soft tissue engineering.^{166, 387, 434} A strongly emerging topic in the construction of cell scaffolds is the implementation of biodegradable motifs, which allow for the scaffold to be removed once they become redundant.⁴³⁵ However, removing the cell scaffolds often requires harsh conditions that are incompatible towards cells and the quest for triggered scaffold degradation under mild stimuli is still ongoing.

Inspired by the above challenge, the remainder of the current chapter aimed at the development of a TAD-polyether based photoresist that enables 3D direct laser writing (3D-DLW, *cf.* II.1.3.4) of highly resolved microstructure scaffolds, which can be debonded under extremely mild conditions through hydrolytic cleavage. The possibility to affect visible light-induced TAD-based crosslinking of polyethers will first be investigated through macroscopic gelation experiments and their hydrolytic stability will be assessed (VI.3.1). Subsequently, direct laser writing experiments will be carried out to evaluate the TAD-PEG system on a microscopic level to potentially serve as a cleavable 3D cell scaffold (VI.3.2). It is noteworthy that such on demand cleavable DLW photoresists are highly desired in the fabrication of complex architectures that require selectively removable support frames (e.g. to construct hanging objects), yet their development is still very much in its infancy.^{169, 436-437}

VI.3.1 Macroscopic investigation

The synthesis and subsequent cleavage of PEG-based materials was first examined through the synthesis of macroscopic gels. Given the many research efforts that are devoted to generate materials under visible light irradiation,^{134, 438} green LEDs ($\lambda = 515 - 525$ nm, 3 x 3 W) were employed as the preferential emission source to affect the TAD-ether crosslinking reaction under

benign conditions, rather than UV-light. A high molecular weight PEG ($M_n = 10$ kDa) was selected as the polyether substrate to provide a multitude of possible TAD-reaction sites along the polymer backbone. Similar as to the model studies conducted in VI.2.2, the polyether was first end capped with *tert*-butyl isocyanate in order to suppress any undesired side reactions that might arise from the polymer end groups. The resulting *t*BuPEG 10 000 was next dissolved in anhydrous acetonitrile (100 mg mL^{-1}) in the presence of the aliphatic TAD crosslinker **6** (10 wt % with regard to *t*BuPEG) and subjected to green light (Scheme VI.3).



Scheme VI.3. Crosslinking of *tert*-butyl end capped PEG 10 000 with a bisfunctional TAD **6** under green light irradiation ($\lambda = 515 - 525 \text{ nm}$, 3 x 3 W LEDs, 1 h).

Within 1 hour of irradiation, the purple formulation was transformed into a colourless gel, which was evidenced upon vial inversion (Figure VI.6a). No regeneration of the purple TAD colour was observed and the gel was shown to remain stable for several days. Subsequent addition of water, however, caused the network to collapse upon standing overnight at ambient temperature and a clear colourless solution was eventually obtained (Figure VI.6b-d). Addition of buffered acid or base solutions (at pH = 5 and 9, respectively) instead of neutral water resulted in an accelerated collapse of the TAD-PEG networks, although several hours were still required for the aqueous media to diffuse into the gel to affect cleavage (i.e. 12 – 14 h).

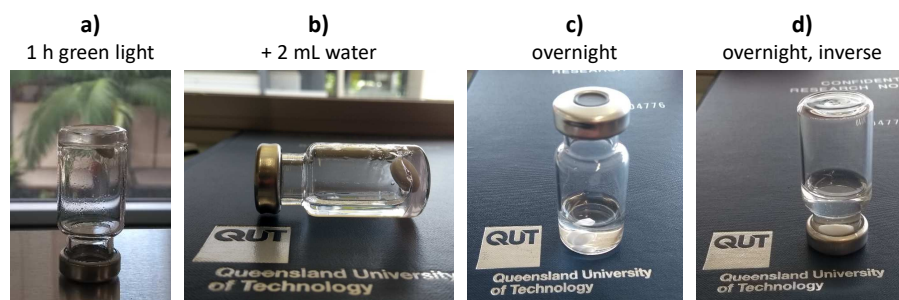


Figure VI.6. Macroscopic crosslinking and cleavage test of poly(ethylene glycol) with TAD. a) Green light irradiation ($\lambda = 515 - 525 \text{ nm}$, 3 x 3 W LEDs) of *t*BuPEG 10 000 (100 mg) and bisTAD **6** (10 mg) in anhydrous acetonitrile (1 mL) gives a colourless and stable TAD-polyether network. b) Cleavage of the PEG-based material is initiated upon addition of water (2 mL). c-d) After standing overnight, the polymer network is hydrolysed and a clear colourless solution is obtained.

VI.3.2 Direct laser written microstructures

Having successfully synthesised PEG-based materials through the green light-induced reaction with TAD crosslinkers, the fabrication of more complex 3D structures via direct laser writing (DLW, *cf.* II.1.3.4) was next targeted. Again, a collaboration was initiated with the physics group of Martin Wegener at the Karlsruhe Institute of Technology (KIT) to conduct the DLW experiments. Thus, a photoresist containing *t*BuPEG 10 000 (50 mg) and bisTAD **6** (10 mg) in anhydrous acetonitrile (250 μ L) was prepared and subjected to DLW with both a custom-built setup (Institute of Nanotechnology, KIT) as well as a commercial 3D laser lithography system (Nanoscribe GmbH).

Before 3D microstructures can be written, some basic parameters were first screened in order to establish good writing conditions for the tailored photoresist. For this, the custom-built setup was employed as it allows to tune the wavelength of the emission source. To evaluate the writing process at different wavelengths, a so-called dose test was performed to determine the writing efficiency as a function of the laser power and the position of the sample relative to the voxel of the laser beam (Figure VI.7). More specifically, a distinct line pattern is written into the photoresist at increasing laser powers (bottom to top in Figure VI.7, right). Only when a certain threshold energy is overcome to induce the TAD-based polyether addition reaction, a crosslinked material will be effectively formed. Besides the writing power, also the *z*-direction of the laser beam is screened (left to right in Figure VI.7, right) in order to identify the interface of the photoresist and the substrate. Evidently, no lines are written when the voxel is directed below the interface, whereas for higher *z*-values the cured PEG-material is not attached to the substrate and therefore diffuses throughout the non-crosslinked photoresist.

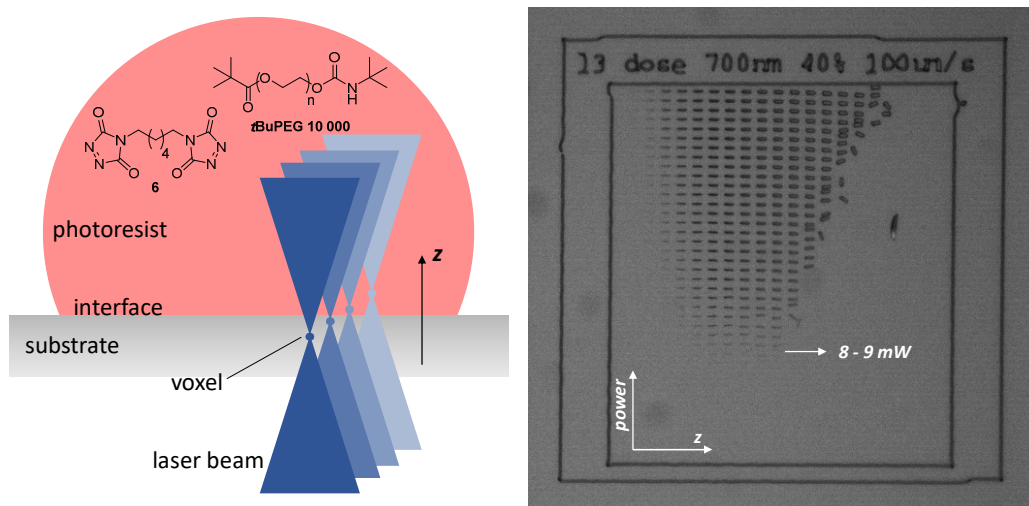


Figure VI.7. Visual representation of the direct laser writing process to conduct a dose test, whereby the position of the laser voxel is moved into the photoresist along the *z*-direction. Only at the interface of the substrate and the TAD-PEG resist, the line patterns that are generated as a result of photo-induced crosslinking adhere to the substrate. In addition to the position of the laser in the *z*-direction, the laser power is also screened. This ultimately leads to a distinct pattern that can be visualised under a microscope and allows to evaluate the optimal writing parameters (i.e. 8 – 9 mW, right).

The best results for the TAD-PEG photoresist were obtained at 700 nm laser light and a threshold energy of 8 – 9 mW at writing speeds of $100 \mu\text{m s}^{-1}$ was derived from the dose tests. In fact, the threshold energy and the writing speeds achieved for the tailored resist are in good agreement with commercially available acrylate-based photoresists. Further evaluation of the writing threshold for different laser powers revealed the non-linearity of the photoinduced crosslinking reaction and thus the underlying multi-photon absorption process, which is a prerequisite to fabricate high resolution 3D microstructures. Furthermore, no writing was detected when blank solutions of the TAD crosslinker or *t*BuPEG were used as the photoresist, thereby indicating that network formation relies on the photoaddition of TAD to the polyether backbone. Interestingly, DLW was also observed to proceed at 780 nm laser light, potentially enabling lithographic experiments with the TAD-PEG photoresist to be conducted with the commercial Nanoscribe setup. Furthermore, no additives such as multiphoton absorbing photoinitiators are required to induce the photocuring reaction, in contrast to many commercially available and tailored photoresist that have been developed.⁴³⁹

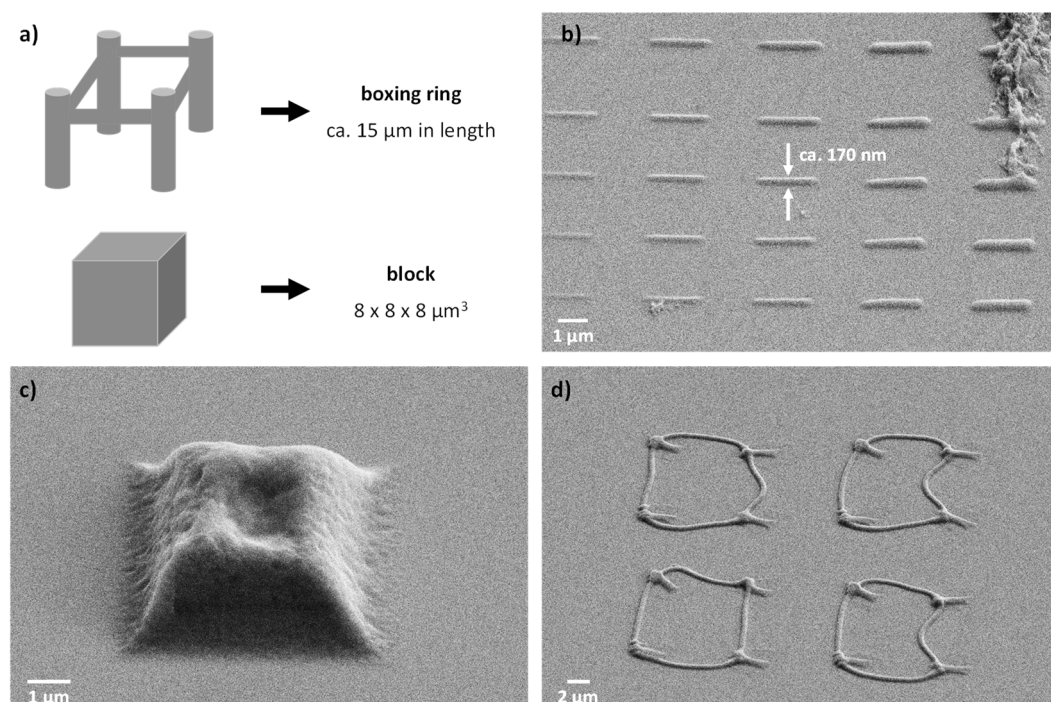


Figure VI.8. Direct laser writing of 3D objects with the TAD-PEG photoresist and visualisation by means of scanning electron microscopy (SEM). a) Representation of the three-dimensional boxing ring and cubic block pattern. b) SEM image of the dose test, from which a linewidth of ca. 170 nm can be derived. c-d) SEM images of the block and boxing rings, indicating the collapse of the written structures.

Having identified the basic parameters to enable spatially resolved laser lithography of TAD-PEG photoresists, the design of more complex 3D structures was next examined. Hence, in addition to a dose test, micrometre sized cubic blocks and boxing rings, displayed in Figure VI.8a, were written on a glass substrate containing a droplet of the TAD-PEG photoresist solution ($\lambda = 700 \text{ nm}$, at a power of 8 – 10 mW). After a development step, the three-dimensionality of

the written structures was demonstrated by scanning electron microscope (SEM) images. The line patterns written during the dose test were clearly observed in the SEM image and a linewidth of approximately 170 nm could be deduced (Figure VI.8b). The 3D block and boxing ring patterns, however, were only vaguely identified as the structures were shown to have collapsed prior to SEM imaging, presumably upon drying during the development step (Figure VI.8c-d). An alternative imaging technique was found in laser scanning microscopy (LSM), which is an indispensable tool for biological imaging. Although the TAD-polyether materials are only weakly fluorescent, sufficiently high laser powers allowed for the 3D reconstruction of the written samples while being immersed in water (Figure VI.9). Thus, DLW of the TAD-based photoresist proceeds quite efficiently and, more importantly, enables the fabrication of complex 3D microstructures, including boxing rings that can serve as cell scaffolds.

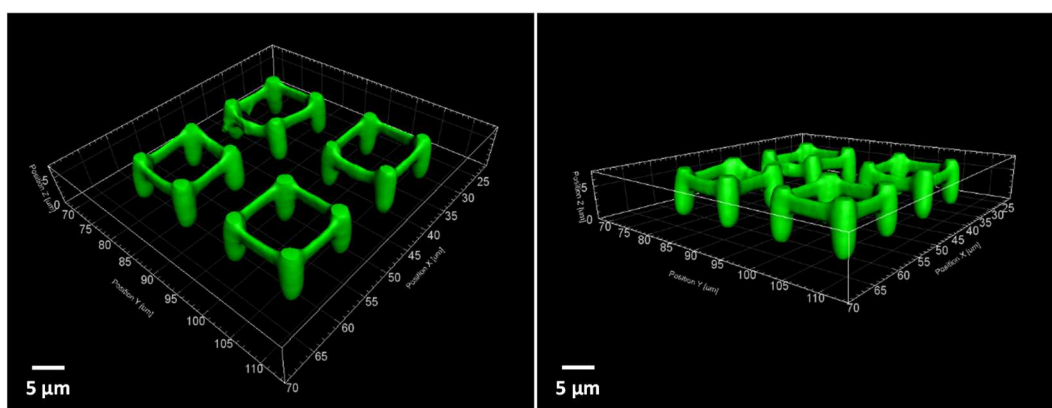


Figure VI.9. Light scanning microscopic imaging in water, allowing for a 3D reconstruction of the written TAD-PEG boxing ring materials.

The ultimate goal in the evaluation of the 3D objects fabricated from TAD-PEG photoresists was to investigate the possibility to cleave the written structures through hydrolysis. To examine the hydrolytic degradability, a series of cubic blocks and boxing rings were written on a glass substrate and subsequently immersed in water, after any residual photoresist was removed. Different powers were utilised to fabricate the microstructure to study the effect of the crosslinking density, since higher writing powers are expected to result in more crosslinking points. The hydrolysis of the materials was imaged via time-lapse optical microscopy, for which a customised sample holder was used to provide a continuous aqueous environment while preventing water evaporation (refer to Appendix E). Moreover, inspired by the potential application in cell scaffold design, the hydrolysis was monitored at 37 °C, a biologically relevant temperature regime.

Time-lapse microscopy of a first cleavage experiment readily indicated the microstructures to swell and detach from the glass substrate upon immersion in water at 37 °C, with the objects written at lower powers detaching first (refer to Appendix E). However, the obtained images remained inconclusive as to whether the structures solely detach or if they actually degrade. Nonetheless, a reference sample kept in acetonitrile over several days remained intact.

In a second experiment, the attachment of the written objects to the glass substrate upon immersion in water was improved by incorporating a support structure underneath the pillars of the boxing rings (refer to Figure VI.10). To investigate the effect of crosslinking density, both the support structure as well as ropes of the boxing rings were written with varying powers (Figure VI.10, bottom). The pillars of the boxing rings, however, were fabricated at a constant power of 32 %. The blocks (Figure VI.10, top) are also written at different laser powers, increasing from left to right (100 % power = 33 mW). Within this series of blocks, the threshold power that is required to fabricate well defined structures is clearly demonstrated, with no writing occurring below 25 %. This 25 % power corresponds to an energy of approximately 8.3 mW, which is in perfect agreement with the threshold energy derived from the dose test (*vide supra*).

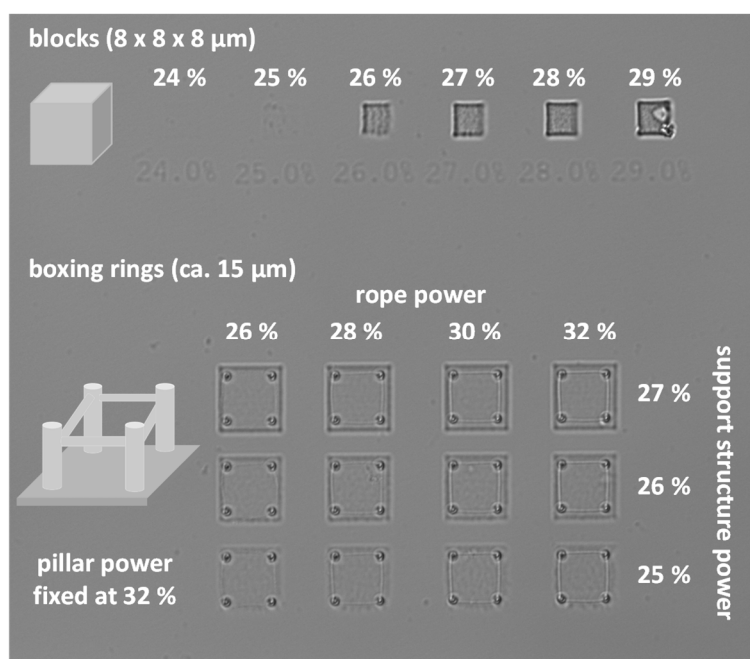


Figure VI.10. Blocks (top) and boxing rings (bottom) obtained after direct laser writing with the TAD-PEG photoresist (100 % corresponds to 33 mW). The writing power for the different objects is varied to assess the effect of crosslinking density on the cleavage behaviour.

Time-lapse microscope images, displayed in Figure VI.11, allowed for the visualisation of the newly written structures when kept in water at 37 °C. Shortly after the writing process, the cured TAD-PEG objects were shown to swell and the structures started to disintegrate after several hours. The boxing rings remained attached to the glass substrate whilst the ropes faded away over time and completely disappeared within 24 h. Eventually, also the pillars that were written at higher powers and the dense cubic blocks disintegrated as a result of hydrolysis. An interesting observation is that the structures written with the lowest power, and hence the least densely crosslinked, were shown to degrade significantly faster compared to those fabricated at higher power. Furthermore, the cubic blocks showed an increased resistance towards hydrolysis compared to the boxing ring structures, which can be devoted to the slower diffusion into such dense objects. Changing the laser power during the lithographic writing process thus allows for the modulation of the degradation kinetics of the microstructures. In other words, the collapse

of the structures can be regulated without altering the photoresist, but simply by changing the DLW parameters.

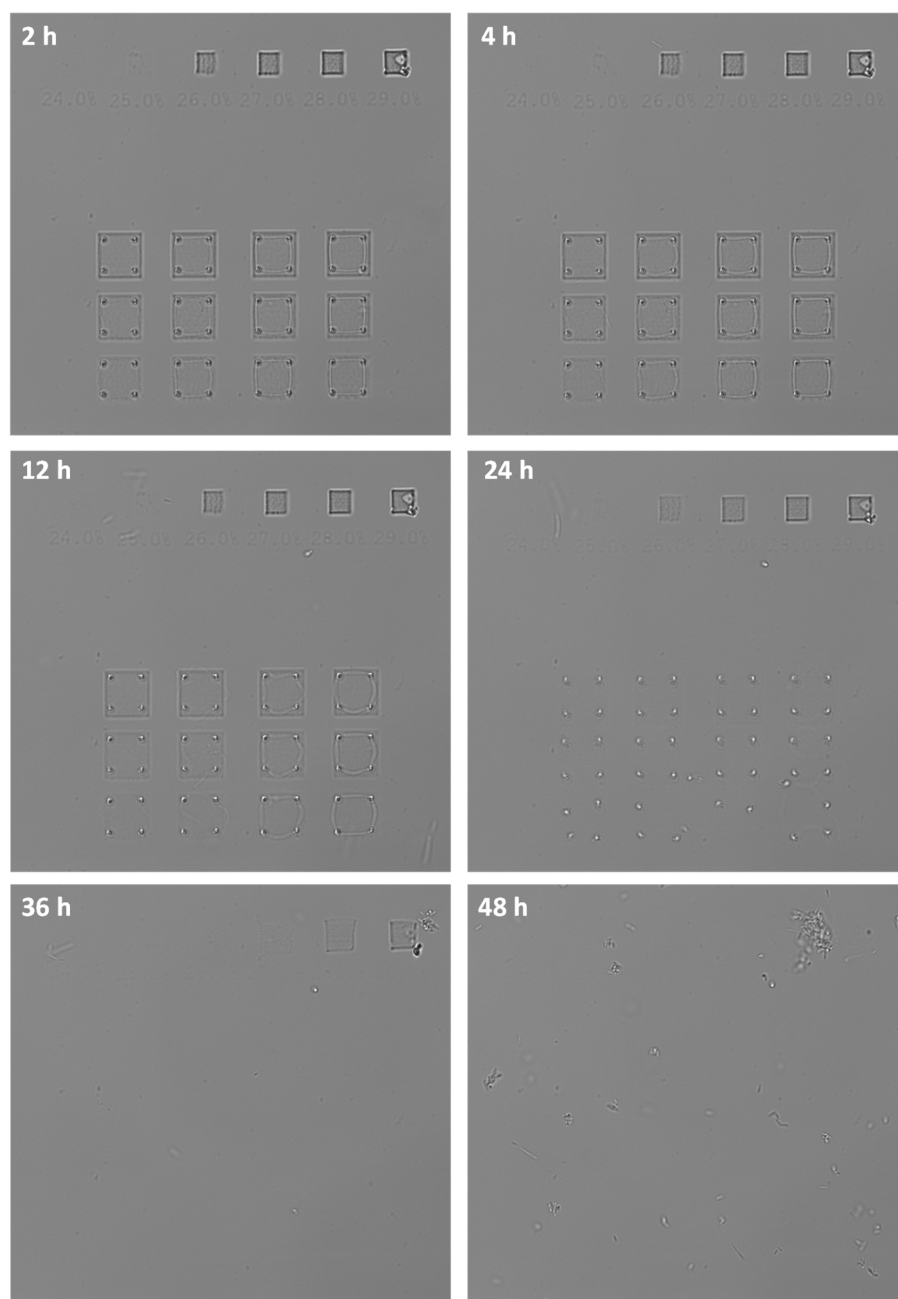


Figure VI.11. Time-lapse microscopic images of direct laser written blocks and boxing rings, indicating the cleavage of the three-dimensional TAD-PEG structures over time when immersed in water at 37 °C. Particles observed after 48 h are attributed to contamination as a result of bacterial growth.

VI.4 Conclusions and perspectives

In the present chapter, the rarely reported UV-triggered side reaction of TADs to low molecular weight aliphatic ethers was reinvestigated to exploit this photoaddition as an alternative and convenient strategy to modify polyether substrates. It was demonstrated that it is perfectly feasible to statistically introduce TAD compounds along the backbone of poly(ethylene glycol) in a single step with both UV- as well as visible light. While the TAD-based functionalisation can be carried out in high yields at low modification degrees (i.e. < 10 %), and the formed urazole byproducts can be successfully removed, the formation of TAD-PEG conjugates negatively impacts their polydisperse nature. Moreover, the formed TAD-ether adducts are sensitive to hydrolysis, which can be a considerable drawback for many waterborne applications.

Yet, the TAD-based photoaddition reaction can readily be utilised to introduce tailored functionalities or properties – by tuning the TAD-substituent – onto other types of polyethers that find applications under non-aqueous conditions.⁴⁴⁰ Indeed, the visible light modification of PEG with TADs could, for example, severely disrupt the crystallinity of the polyether, thereby making ambient temperature electrolytes for lithium ion batteries accessible.⁴²³ Thus, the TAD-ether addition might potentially evolve into a powerful platform to enable a more accessible approach for polyether functionalisation, parallel to the conventional ring-opening polymerisation protocols.

Having examined the TAD-addition reaction to PEG and recognised the obstacle of hydrolysis, the application of the introduced approach was revisited. Instead of targeting non-aqueous applications, the advantage of water to act as a chemical trigger to induce on demand debonding of a polymer along the backbone was identified and cleavable yet crosslinked PEG-based materials were hence developed, including microfeatured objects. A real breakthrough of the TAD-PEG crosslinking system was established through their applicability as photoresist in direct laser writing lithography, which is a commonly applied technique to create, for example, cell scaffolds for tissue engineering. Critically, by using different laser powers in the DLW process, the hydrolysis and thus degradation of the scaffold can be tuned, without changing the composition of the resist itself. Additionally, no (toxic) additives such as photocatalysts are required to affect the fabrication of 3D microstructures, which provides a considerable advantage over many state-of-the-art PEG-based photoresists.⁴⁴¹

Given the highly promising results of the TAD-PEG photoresist in 3D lithography, future research efforts will be devoted to fabricate real-life applicable cell scaffolds that can be removed under very mild conditions, for instance physiological saline, once they become redundant. Hence, a collaboration was started with the cell- and neurobiology group of prof. Martin Bastmeyer (Karlsruhe Institute of Technology) to firstly assess the biocompatibility of both the TAD-PEG crosslinked scaffolds as well as the degradation products formed upon hydrolytic cleavage.

Following the thus far promising preliminary results with regard to the biocompatibility and -toxicity, the hydrolysis rate can next be carefully tuned based on changing the laser power to write the initial cell scaffolds or alter the pH to add additional responsiveness, which might introduce site-selective drug release properties. Next to biological applications, the cleavable TAD-based photoresist also paves the way to fabricate 3D nano- and microstructures with additional complexity by means of removable support structures that are inaccessible through conventional manufacturing techniques, including flying or hanging objects.^{169, 437}

VI.5 Notes on the collaboration

A collaboration with the research group of Prof. Martin Wegener at the Karlsruhe Institute of Technology, Germany was initiated to investigate the applicability of the TAD-based photoaddition to polyethers in direct laser writing laser lithography. Patrick Müller and Dr. Eva Blasco (Karlsruhe Institute of Technology) designed, performed and analysed the DLW experiments described in section VI.3.2. Hannes Houck synthesised the TAD crosslinker and *tert*-butyl end capped poly(ethylene glycol) compounds that make up the photoresist. All collaboration partners involved discussed and commented on the obtained results at all stages.

Chapter VII.

General conclusions and perspectives

VII.1 Conclusions

The presented doctoral work aimed to develop external triggers to control the reactivity of triazolinediones (TADs) – powerful coupling agents^{9, 15} – to introduce TAD-based conjugation reactions into the realm of temporally and spatially resolved polymer applications. Whereas TAD chemistry is a highly enabling platform for polymer modification and crosslinking because of its ultrafast, additive-free and ambient temperature click-type characteristics, some fundamental issues of TAD reagents negatively impact these highly enabling synthetic tools. Hence, the widespread use of TADs is still hampered both in an academic and industrial context as a result of their extremely high reactivity, which often translates to a limited stability, tedious tailored synthesis and complicated handling. Therefore, the implementation of defined stimuli, such as temperature and light, to selectively switch TAD reactivity on-and-off was explored in this collaborative PhD project between Ghent University, Belgium and the Karlsruhe Institute of Technology, Germany in order to address the remaining shortcomings associated with TAD reagents.

Despite the fact that the ultrafast reactivity of TADs (e.g. instantaneous with cyclopentadiene at -78 °C)¹⁸⁵ is generally considered as a key advantage over other modular ligation chemistries, numerous applications in polymer science require a defined and on demand control over covalent bonding and/or debonding reactions.^{22, 442} Hence, **Chapter II** provides a concise overview of thermally and photochemically triggered covalent chemistries that have (recently) been embedded in polymer systems to regulate smart and adaptive material behaviour, including self-repair, recycling and controlled degradation. Following illustrative examples of how externally triggered (dynamic) covalent chemistries can be exploited in temporally and spatially resolved applications, the fascinating chemistry of triazolinediones was highlighted in the second part of Chapter II. In addition to the synthesis of TAD reagents, their extraordinary reputation and use in polymer modification and crosslinking, insights into the many different modes of TAD reactivity were provided, with an emphasis on thermally and photochemically induced transformations that possess a dynamic nature.

One of the most critical limitations associated with TAD compounds is their inherent reactivity which, for instance, results in ultrafast crosslinking kinetics of polydienes already at room temperature. **Chapter III** was therefore devoted to develop blocked TAD reagents that can be activated on demand upon heating, thereby resulting in a controlled and *in situ* release of active TAD moieties. A series of easy-to-synthesise substituted indole substrates were

identified as highly attractive blocking agents for TADs to provide the desired temporal control over their reactivity.⁴⁴³ Upon providing a full investigation concerning both the forward and backward TAD-indole reaction, including thermal kinetic reversibility studies and mechanistic rationalisations, a tunable dynamic behaviour was established which can be modulated by simple alterations on both the indole scaffold as well as the nature of the TAD-substituent. As a result, an exceptionally broad temperature regime to promote the deblocking reaction was established, making it possible to activate TADs *in situ* from above 100 °C down to 35 °C. The applicability of the indole-blocked TAD reagents was demonstrated in the time-resolved polymer modification with a bench-stable TAD-dye while the tunability of the introduced blocking concept was illustrated for bivalent TAD compounds to enable on demand curing of a one-pot diene-containing polyurethane formulation, at temperatures as low as 50 °C. In addition, the orthogonal reactivity between two different TAD-indole systems unfolded during the course of Chapter III, which allowed for the introduction of an unprecedented indole-to-indole exchange reaction of TAD-moieties without sacrificing their dynamic properties.²⁵

In addition to the ability to switch on TAD reactivity in a thermally controlled manner, light can serve as an efficient trigger to selectively render chemical reactivity on-and-off, and in fact is more defined since it also offers spatial resolution next to temporal control. In search of light-triggered TAD-based transformations, **Chapter IV** hence examined the photopolymerisation of TADs upon visible light irradiation as an elegant approach to photochemically deactivate TAD moieties and thus switch off their unique reactivity.⁴⁴⁴ Importantly, the polymerisation is reversible and rapidly regenerates TAD reagents *in situ* as soon as the light is switched off. The obtained on-and-off switch over TADs was successfully combined with the well-established UV-induced generation of photoenols, which act as a suitable TAD-reaction partner. Given the wavelength-independent nature of both processes, a one-pot reaction manifold was generated, where the outcome is orthogonally triggered between photochemical and thermal ligation products, depending on the employed colour of light. The resulting pioneering light-switchable reactivity was eventually explored in the highly emerging field of sub-diffraction STED-inspired lithography, thereby introducing for the first time TAD chemistry into the realm of spatially resolved applications.

In contrast to several reports that describe the photoinduced degradation of triazolinediones, a crucial finding in Chapter IV was the remarkable photostability of TADs, which was identified in both the UV- and visible range of the spectrum. This served as motivation for the continued development of the thus far little explored light-induced TAD conjugation reactions and their implementation in spatio-temporal controlled polymer network formation.

A first photochemical mode of reactivity that was explored, is the visible light-induced cycloaddition reaction of TAD with naphthalene. Whereas only minor traces of the TAD-naphthalene cycloadduct are formed under thermal conditions, green light irradiation shifts the equilibrium of the cycloaddition quantitatively towards the covalently bound products. In

Chapter V, this fascinating light-driven dynamic conjugation reaction was identified to enable an unprecedented polymer system that can be reversibly switched between two states of matter, namely a covalently crosslinked network when the system is irradiated and a liquefied polymer formulation when kept in the dark.⁴⁴⁵ The TAD-naphthalene system was therefore subjected to detailed model studies, after which the naphthalene scaffold was modified into a suitable benchmark methacrylate monomer. Importantly, the influence of the introduced naphthalene substituents was shown to greatly influence the regioselectivity of the TAD-cycloadducts formed under green light impact. Moreover, the corresponding cycloreversion rates when the adducts were kept in the dark can be readily tuned by making small alterations to the aromatic reaction partner. The insights gained from the model studies were in perfect agreement with the observed rheological behaviour of the polymer networks, obtained upon photocuring of the naphthalene-containing polymers with a bifunctional TAD crosslinking agent. A crucial aspect of the thus formed materials was the ability to maintain the crosslinking integrity under continuous green light irradiation, which we coined light-stabilised dynamic (LSD) materials. This LSD behaviour was also demonstrated on a macroscopic scale whereby the light-stabilisation of the TAD/naphthalene material was evidenced when the light was kept on, whereas in the dark the material started to flow as a liquid.

A final photochemical mode of reactivity that was exploited in a polymer context is provided in **Chapter VI**, where the light-induced addition of TADs to ethers was investigated. Although initially reported as a side reaction, the TAD-ether conjugation was reinvestigated to serve as a potentially elegant one-step approach for the backbone functionalisation of polyethers. Although successful modification of poly(ethylene glycol) was feasible under both UV- and visible light irradiation, only low degrees of functionalisation were efficiently achieved and the formed TAD-polymer conjugates were found to be hydrolytically unstable. Nonetheless, the established light-induced backbone modification reaction was found to be highly promising towards crosslinking applications and the designed TAD-polyether photoresist was proven compatible with multiphoton laser lithography, thereby enabling the construction of 3D scaffolds without the need of any additives (e.g. photoinitiator). Furthermore, the written microstructures were readily degraded under extremely mild conditions, including in a neutral aqueous environment.

VII.2 Future perspectives

Since a detailed topic-specific outlook was already provided in the conclusions sections at the end of each experimental chapter, only some general future perspectives will here be summarised.

As mentioned earlier, the developed blocked TAD concept undoubtedly opens a whole array of TAD chemistry applications that require an on demand reactivity, particularly in an industrial context. Indeed, latent TAD reagents have an increased shelf-life, are much safer to handle and offer the potential to be used in a one-pot complex formulation. Mirrored to the well-established blocked isocyanate strategy, blocked TADs might even enable waterborne curing applications

whereby hydrolytic degradation of TADs could be suppressed via their controlled *in situ* release in the presence of a suitable co-reactant. In this context, the designed water soluble PEGylated indole blocking agent with a characteristic temperature of deblocking at 40 °C might serve as a valuable approach to deliver TAD click-type reagents for bioconjugation purposes. With an additional experimental effort, such a bioconjugation reaction can readily be investigated via TAD-dye demonstrators.

A crucial bottleneck of TAD chemistry is the availability of tailored TAD reagents, which typically falls back to the chemoselectivity issues that are persistently observed during the post-modification of their functionalised urazole precursors. Indeed, the inherent acidity and nucleophilicity of the urazole moieties prevents access to conventional ligation methods, including esterification and amide formation. Besides the time-controlled activation of TAD reactivity, an additional future perspective of the established indole blocking agents is therefore found in their use as urazole protecting groups whereby the chemoselectivity problems are eliminated by the introduced steric bulk of the indole scaffold. This challenge is being tackled in an ongoing PhD project at Ghent University and a general synthetic platform towards tailored TAD reagents is currently being developed, which is based on the indole blocking agents that were introduced in the presented doctoral work.

Apart from the general advancements in the widespread use of TAD chemistry that arise from the time-controlled reactivity provided by thermally reversible blocking agents, the established light-triggered TAD reactivity also allows to identify future research avenues, mainly in the context of material sciences. For example, the possibility of fabricating 3D structures via direct laser writing (DLW) lithographic techniques was evidenced for the TAD-polyether systems. An interesting application that is targeted with the developed resist is the construction of scaffolds for tissue engineering that can degrade in the same environment wherein the cells are grown, once the scaffold becomes redundant. A biological screening is currently ongoing in order to assess the cytotoxicity of the degradation products that are formed upon hydrolytic cleavage of TAD-PEG networks. If the results are supportive for the required cell viability, future endeavours will focus on real-life cell applications and evaluate the tailored photoresist with regard to state-of-the-art PEG-based scaffolds. An interesting research question that is raised in this context is the difference of the mechanical properties of the fabricated cell scaffolds. Since conventional PEG-scaffolds are typically crosslinked via the end groups of linear PEG precursors, it is envisioned that the alternative crosslinking approach directly and at multiple positions along the polyether backbone may significantly alter the properties of the scaffold and hence influence the behaviour of the cells. Furthermore, the crosslinking density can readily be modulated by changing the amount of TAD crosslinker, or even simply upon altering the laser power during manufacturing.

A crucial advantage of the developed PEG-based photoresist is the apparent multiphoton absorption of the TAD crosslinking agents, which eliminates the need for additives such as potentially toxic photoinitiators. Given the promising results that were obtained during the final

months of the current doctoral work, alternative TAD-based photoresist might also be developed, for instance based on the evaluated TAD-naphthalene system. In combination with a conventional photoresist, it should hence be possible to develop a subtractive photoresist platform whereby the TAD-naphthalene-based light-stabilised dynamic microstructures can serve as support objects that can be removed without the need for an additional development step or chemical additives. Simply upon switching the light off, the TAD-naphthalene support structures would thus degrade.

In summary, the current doctoral work advanced the development of temperature and light triggered TAD-based reactions to enable temporally and spatially resolved applications. Yet, a chemistry platform never reveals all its secrets in the course of just one PhD project and many challenges remain ahead in order to truly emerge TAD reagents into the standard chemistry toolbox. Nonetheless, whereas TADs might set limits to knowledge today, they should not set limits to its future unprecedented applications.

Chapter VIII.

Abstract

Triazolinediones (TADs) are a unique class of reagents that have found a vast array of applications across multiple research disciplines; most notably in organic synthesis, bioconjugation and polymer science. Their remarkable reactivity towards a range of simple electron rich olefin substrates, giving them the reputation of most reactive dienophiles and enophiles to be isolated, highlighted these TAD reagents as attractive tools in modular ligation methods. Typically, TAD-based reactions swiftly proceed at ambient temperatures, and even far below (e.g. -78 °C), without the need of a catalyst in only a few seconds or less, even with macromolecular substrates. As a result, the click-like reactivity of TAD coupling agents has been extensively investigated, in particular for low-temperature polymer modification and crosslinking, which is discussed within the current thesis.

However, the extraordinary reactivity of triazolinediones currently limits their widespread use, especially in an industrial context, as a result of its limited stability, cumbersome tailored synthesis and reaction kinetics that are often too fast to be controlled. In the current doctoral work, conducted at Ghent University in Belgium and the Karlsruhe Institute of Technology in Germany, externally triggered TAD-based reactions have therefore been developed in order to resolve the remaining shortcomings of TAD reagents by enabling a well-defined on-and-off switch over their unique reactivity. Specifically, temperature and light were identified as highly interesting stimuli to provide a selective start and stop switch, thereby enabling temporally and/or spatially resolved applications, whereby the developed triggered TAD reactions were demonstrated in the controlled design of advanced polymer materials. Ultimately, this has resulted in conceptual, unprecedented TAD-based materials that can adapt in a controllable and even repeatable manner via temperature or light-induced covalent bonding and/or debonding reactions.

In a first conceptual approach towards on demand triazolinedione-based reactivity, *blocked TAD reagents* were developed that allow for the controlled *in situ* release of active TAD moieties upon heating. This was achieved by readily available indole blocking agents, whereby the temperature of deblocking can be precisely modulated by making minor alterations to the indole structure. The indole blocking platform was demonstrated to enable the synthesis of a tailored TAD-dye, time-delayed polymer modifications as well as the on demand crosslinking of a one-pot polyurethane formulation.

In addition to thermal control, phototriggered TAD transformations were also shown to have promising potential as a switch to render TAD reactivity on-and-off. For example, visible light

was identified as an elegant approach to photochemically deactivate TADs via their reversible transformation into a photopolymer, which resulted in a pioneering *light-switchable one-pot reaction system*, thereby introducing site-selective TAD-based reactivity into the realm of spatially resolved surface lithography. Furthermore, unprecedented *light-stabilised dynamic materials* have been established based on the photodriven TAD-naphthalene cycloaddition reaction, whereby a polymer material can be reversibly tuned from a covalently crosslinked state to a liquefied formulation upon switching only one colour of light on or off. Importantly, the resulting polymer network retained its crosslinked integrity under continuous irradiation. Finally, a *unique poly(ethylene glycol)-based photoresist* that facilitates three-dimensional direct laser writing was developed through the photochemically triggered addition of TAD to the polyether backbone. This readily enabled the fabrication of microstructures that could be cleaved under extremely mild aqueous conditions.

The TAD-based approaches introduced in this joint PhD thesis are considered to serve as a basis in externally controlled TAD reactivity, not only for their tailored synthesis or small molecule ligations, but importantly in on demand modification and crosslinking of advanced and adaptive polymer systems. Although the ability to control unique TAD reagents has not been light play, the pioneered temporal and spatially resolved applications of TAD chemistry, including surface patterning and 3D laser lithography, have only just been triggered.

Chapter IX.

Samenvatting

Triazolinedionen (TAD-verbindingen) omvatten een specifieke groep van reagentia die talrijke toepassingen gevonden hebben in verschillende onderzoeksrichtingen, onder meer in organische synthese, bioconjugatie en polymeerchemie. De unieke reactiviteit ten aanzien van een breed spectrum aan onverzadigde verbindingen, brandmerkte TAD-verbindingen reeds snel tot meest reactieve, nog steeds isoleerbare diëno- en enofielen, hetgeen deze componenten zeer aantrekkelijk maakt in modulaire koppelingsmethoden. Typerend voor TAD-gebaseerde koppelingen is het zeer gezwinde reactieverloop dat reeds plaatsgrijpt bij kamertemperatuur, maar ook ver daaronder (bv. $-78\text{ }^{\circ}\text{C}$), zonder behoefte aan een katalysator. Zelfs met macromoleculaire verbindingen zijn TAD-reacties typisch afgelopen in slechts luttele seconden. Als gevolg van de ‘klik’-reactiviteit zijn TAD-koppelingscomponenten reeds intensief onderzocht, voornamelijk in het modificeren en vernetten van polymeren bij lage temperaturen, hetgeen in deze scriptie later wordt aangehaald.

Desalniettemin is de buitengewone reactiviteit van TAD-verbindingen ook zorgwekkend inzake hun beperkte stabiliteit, omslachtige synthese en vaak te snelle en oncontroleerbare reactietijden, wat het algemene gebruik ervan sterk verhindert, voornamelijk in een industriële context. In het voorgelegde doctoraatsproefstuk, dat werd uitgevoerd aan zowel de Universiteit Gent (UGent) in België als aan de Karlsruhe Institute of Technology (KIT) in Duitsland, werden bijgevolg TAD-gebaseerde reacties ontwikkeld die door een externe stimulus gecontroleerd kunnen worden. Zodoende zou het mogelijk moeten zijn om de unieke reactiviteit van TAD-verbindingen op een gedefinieerde manier aan of uit te zetten, waardoor de huidige nadelen omtrent het gebruik van triazolinedionen omzeild kunnen worden. In het bijzonder werden licht en temperatuur als interessante stimuli vooropgesteld om een selectief start- of stopsignaal over de reactiviteit te geven. Hierdoor worden specifieke toepassingen die een zekere controle in zowel tijd en/of ruimte vereisen, toegankelijk waarbij de ontwikkelde gecontroleerde TAD-activiteit voor het ontwerpen van functionele polymeer-materialen wordt vooropgesteld. Dit gaf aanleiding tot het introduceren van conceptuele en innovatieve TAD-gebaseerde materialen die zich op een gecontroleerde en repetitieve manier kunnen aanpassen naargelang de aangewende stimulus. Om dit te bereiken werden dergelijke materialen opgebouwd uit covalente bindingen die gevormd en/of gebroken kunnen worden onder invloed van licht of temperatuur.

In een eerste conceptuele aanpak om de triazolinedion-gebaseerde reactiviteit op aanvraag te introduceren, werden geblokkeerde TAD-componenten ontwikkeld die bij verwarmen op een gecontroleerde manier de actieve TAD-verbindingen ter plaatse kunnen vrijstellen. Dit werd gerealiseerd door zeer toegankelijke indoolbevattende blokkeringsreagentia, waarbij de temperatuur van TAD-vrijstelling systematisch kan worden aangepast door de indool-kern

minimaal te wijzigen. De bekomen indool-geblokkeerde TAD-activiteit maakte het mogelijk om specifieke TAD-bevattende kleurstoffen te synthetiseren, polymeren uitgesteld te modificeren, alsook polyurethanen tijdsgecontroleerd te vernetten in een éénpotsreactie.

TAD-reacties die worden gecontroleerd door bestraling zijn – naast thermische controle – een andere veelbelovende methode om de activiteit van triazolinedionen te initiëren of te stoppen. Zo werd bijvoorbeeld aangetoond dat zichtbaar licht een elegante methode vormt om TAD-verbindingen fotochemisch te deactiveren. Hiervoor werd TAD op omkeerbare wijze omgezet in een fotopolymeer waardoor een revolutionair *licht-aangestuurde éénpotsreactie* werd geïntroduceerd, waarbij de verkregen ruimtelijke controle over TAD-activiteit het gebruik ervan toepasbaar maakte in oppervlaktelithografie. Voorts werden ook ongekende *lichtgestabiliseerde dynamische materialen* ontwikkeld, steunend op door licht aangedreven TAD-naftaleen cycloaddities, waarbij een polymeermateriaal herhaaldelijk kan worden omgezet van een covalent vernette toestand naar een viskeus vloeibare fase door slechts één welbepaalde lichtkleur in of uit te schakelen. Van belang hierbij is dat het gevormde polymeernetwerk een vernette toestand kan blijven behouden zolang dit bestraald wordt. Finaal werd ook een *unieke polyethyleenglycol-gebaseerde fotoresist* ontwikkeld die het driedimensionale “direct laserschrijven” vergemakkelijkt aan de hand van de fotochemische additiereactie van TAD-verbindingen aan de polyether-hoofdketen. Hierdoor werd de constructie van complexe microscopisch kleine structuren mogelijk, die onder zeer milde omstandigheden gedegradeerd kunnen worden in water.

De TAD-gebaseerde concepten die zijn samengevat in dit doctoraatsproefschrift en waarvan de meeste enkel ontwikkeld konden worden door de samenwerking tussen de twee universiteiten, dienen als basis voor een extern gecontroleerde TAD-activiteit, die niet alleen toepasbaar is voor de gespecialiseerde synthese van laag moleculaire componenten, maar voornamelijk ook voor de modificatie en vernetting van functionele en responsieve polymeersystemen. Hoewel de activiteitscontrole van de unieke TAD-reagentia een uitdaging blijft, betekent de hierin ontwikkelde tijdelijke en ruimtelijke controle over TAD-chemie, die ze openstelt tot veeleisende toepassingen zoals het modificeren van oppervlakken en 3D laserschrijven structuren, een zeer grote stap voorwaarts.

Chapter X.

Zusammenfassung

1,2,4-Triazol-3,5-dione (TAD-Verbindungen) gehören zu einer einzigartigen Gruppe an Reagenzien, die umfangreiche Anwendungen in zahlreichen Forschungsrichtungen – besonders in der organischen Synthese, in der Biokonjugation und in der Polymerwissenschaft – gefunden haben. Ihre bemerkenswerte Reaktivität gegenüber einem breiten Spektrum einfacher elektronenreicher Olefinsubstrate unterstreicht die Tatsache, dass TAD-Verbindungen zu Recht den Ruf der reaktivsten, noch isolierbarer Dienophile und Enophile darstellen, und sich daher exzellent für modulare Ligation eignen. Charakteristisch für TAD-basierte Reaktionen ist die zügige Umsetzung bei Umgebungstemperatur oder weit darunter (z.B. $-78\text{ }^{\circ}\text{C}$), ohne dass ein Katalysator zugesetzt werden muss. Selbst mit makromolekularen Substraten findet diese innerhalb weniger Sekunden oder sogar schneller statt. Aufgrund ihrer „Click“-ähnlichen Reaktivität wurden TAD-Kopplungsreagenzien intensiv untersucht speziell hinsichtlich Polymermodifikation und Vernetzung, die mit niedrigen Temperaturen ablaufen können. Solche Resultate werden in der vorliegenden Arbeit diskutiert.

Nichtsdestotrotz beschränkt die außergewöhnliche Reaktivität der Triazolindione deren derzeitige breite Anwendung – besonders in industrieller Hinsicht – aufgrund der langfristigen Stabilität, der umständlichen Synthese für spezielle Substrate und der Reaktionsgeschwindigkeit, die eine Reaktionskontrolle erschwert. In der vorliegenden Doktorarbeit, die sowohl an der Universität Gent in Belgien als auch am Karlsruher Institut für Technologie in Deutschland durchgeführt wurde, wurden TAD-Verbindungen entwickelt, deren Reaktion erst nach einem externen Stimulus ausgelöst wird. Durch den so angebrachten, klar differenzierten An- und Ausschalter, der die einzigartige Reaktivität regelt, sollen aktuelle Nachteile der TAD-Reagenzien umgangen werden. Besonders wurden hierbei Licht und Temperatur als hochinteressante Stimuli identifiziert, um so einen gezielten Wechsel von Reaktionsstart und -ende zur Verfügung zu stellen. Hierdurch werden zeitlich und/oder örtlich aufgelöste Anwendungen ermöglicht, wobei die Entwicklung von TAD-Reaktionen zur kontrollierten Darstellung funktionaler Polymermaterialien im Vordergrund steht. Letztendlich hat dies zu konzeptionellen und noch nie dagewesenen TAD-basierten Materialien geführt, die auf kontrollierte und wiederholbare Art und Weise an die jeweilige Anwendung angepasst werden können. Um dies zu bewirken, werden im Material kovalente Bindungen geknüpft und/oder gebrochen.

In einem ersten konzeptionellen Vorgehen, um die triazolindion-basierte Reaktivität auf Abruf zu erzeugen, wurden *blockierte TAD-Reagenzien* entwickelt, die nach Erhitzen kontrolliert an Ort und Stelle die aktivierte TAD-Gruppe freigibt. Dies wurde durch leicht zugängliche Blockierungsreagenzien auf Indol-Basis erzielt, wobei die präzise Substratfreigabe durch geringe

Modifizierungen am Indol Grundgerüst ermöglicht werden kann. Auf Grundlage der Indol-Blockade wurde die Synthese von TAD-Farbstoffen, zeitverzögerter Polymermodifikationen und die Vernetzung auf Abruf von Polyurethanen in einer Eintopfreaktion ermöglicht.

TAD-Umsetzungen, die nach Bestrahlung ausgelöst werden, sind – neben der thermischen Kontrolle – ein weiterer vielversprechender Schalter, um die TAD-Reaktivität einzuleiten beziehungsweise zu stoppen. Zum Beispiel wurde gezeigt, dass sichtbares Licht einen eleganten Ansatz darstellt, um TAD-Verbindungen photochemisch zu deaktivieren. Hierbei wird TAD in ein Photopolymer überführt, das sich als wegweisende *lichtschaltbare Eintopfreaktion* erwiesen hat, wobei die seitenselektive TAD-basierte Reaktivität den Einsatz im Forschungsgebiet der räumlich aufgelösten Oberflächenlithographie ermöglicht. Darüber hinaus wurden noch nie dagewesene *lichtstabilisierte dynamische Materialien* etabliert, die auf Grundlage der lichtgesteuerten TAD-Naphthalen-Cycloaddition funktionieren. Dabei wird ein Polymermaterial reversibel von einem kovalent vernetzten Zustand in einen verflüssigten Zustand überführt, wobei nur je eine Beleuchtungsfarbe die Reaktion auslöst oder stoppt. Von besonderer Bedeutung sind dabei die *einzigartigen auf polyethylenglycol basierenden Fotolacke*, die das dreidimensionale „direkte Laserschreiben“ vereinfachen und dabei die photochemische Additionsreaktion von TAD-Verbindungen an das Polyether-Rückgrat ermöglicht. Hierdurch wird die Herstellung von Mikrostrukturen ermöglicht, die unter besonders milden, wässrigen Bedingungen wieder gespalten werden können.

Die TAD-basierten Ansätze, die in der gemeinsamen Zusammenarbeit zweier Universitäten in der vorliegenden Doktorarbeit zusammengefasst wurden, dienen als Grundlage zu externen Kontrolle der TAD Reaktivität – nicht nur für die hochgenaue Synthese oder der Ligation kleiner Moleküle, sondern auch zur Modifikation und Vernetzung von funktionalen und anpassungsfähigen Polymersystemen. Obwohl die Kontrolle einzigartiger TAD-Reagenzien eine Herausforderung ist, stellt die hier demonstrierte zeitliche und räumliche Auflösung der TAD-Chemie im Hinblick auf Oberflächenstrukturierung und 3D direktes Laserschreiben den ersten Schritt auf dem Weg einer vielversprechenden Reise dar.

Appendix A.

Materials and instrumentation

A.1 Materials

Acetic acid (> 99.5 %, Sigma-Aldrich); acetyl chloride (> 99 %, Acros); aluminium chloride (> 99.9 %, Alfa Aesar); aluminium oxide, activated basic, Brockmann I (Sigma); 4-aminoazobenzene (98 %, TCI Europe); anhydrous anisole (99 %, ACROS Organics); anhydrous benzene (99.8 %, Sigma Aldrich); azodicarboxamide (97 %, Sigma); benzhydrol (diphenylmethanol, 99 %, Sigma); 2,2-bis(hydroxymethyl)propionic acid (98 %, Sigma-Aldrich); 1,2-bis(4-methoxyphenyl)ethanone (deoxyanisoin; 98 %, Alfa Aesar); α -bromoisobutyryl bromide (98 %, Acros); 2-(bromomethyl)naphthalene (96 %, Alfa); celite (Sigma-Aldrich); chloroform-*d* (CDCl₃, 99.8 %, Euriso-top); citronellol (95 %, Sigma-Aldrich); 4'-chloropropiophenone (98 %, Alfa Aesar); concentrated aqueous hydrochloric acid (36 %, Chem-Lab); concentrated sulfuric acid (99 %, Sigma-Aldric); deuterated acetone-*d*₆ (Me₂CO-*d*₆, 99.9 %, Euriso-top); deuterated dimethyl sulfoxide-*d*₆ (DMSO-*d*₆, 99.8 %, Euriso-top); dibutyltin dilaurate (DBTL, \geq 98 %, TCI Europe); di-*n*-butyl ether (99 %, Sigma); *N,N*-dicyclohexyldicarbodiimide (DCC; 99 %, ACROS Organics); 4-(dimethylamino)pyridine (DMAP; 99 %, ACROS Organics); 2,2-dimethoxypropane (98 %, Sigma-Aldrich); 1,1-diphenylethanol (98 %, Sigma-Aldrich); 1-dodecanethiol (DDT, > 98 %, Sigma); ethyl carbazate (97 %; Acros Chemicals); 4'-fluoropropiophenone (> 97 %, Alfa Aesar); 4'-(trifluoromethyl)propiophenone (99 %, Fluorochem); hexamethylene diisocyanate (\geq 98 %, TCI Europe); 4-hydrazino benzoic acid (97 %, Sigma-Aldrich); hydrochloric acid (36 %, Chem-Lab); hydrochloric acid in dioxane (4 N, ACROS Organics); hydrochloric acid in isopropanol (5-6 N, ACROS Organics); 2-hydroxyethyl methacrylate (98 %, Sigma); magnesium sulfate monohydrate (\geq 99 %, Roth); methacrylic acid (99 %, Sigma); 4-methoxyphenylacetic acid (99 %, Sigma-Aldrich); 4'-methoxypropiophenone (99 %, Alfa Aesar); 3-methylbutyraldehyde (98 %, Sigma-Aldrich); methyl methacrylate (99 %, Sigma); naphthalene (99 %, Acros); 1-naphthalenemethanol (98 %, Alfa); 2-(naphthalen-1-yl)ethan-1-ol (> 95 %, TCI); 2-(naphthalen-2-yl)ethan-1-ol (2-naphthaleneethanol, > 95 %, TCI); 1-naphthoic acid (98 %, Alfa); 2-naphthoic acid (98 %, Sigma); 2-naphthoyl chloride (98 %, TCI); 4-nitrophenylacetic acid (99 %, Sigma-Aldrich); *n*-butyl methacrylate (99 %, Sigma); *n*-butyllithium (2.5 M in hexane, Sigma-Aldrich); *o*-toluidine (98 %, Sigma-Aldrich); palladium on activated charcoal (5 % Pd basis, Sigma-Aldrich); PEG monomethyl ether 2000 (*m*PEG 2000, Sigma-Aldrich); 2-phenyl-1*H*-indole (> 98 %, TCI Europe); 2-phenyl-2-propanol (97 %, Sigma-Aldrich); 2-phenylacetophenone (97 %, Sigma Aldrich); phenylacetyl chloride (98 %, Sigma Aldrich); phenylhydrazine (97 %, Sigma-Aldrich); poly(ethylene glycol) 10 000 (PEG 10 000, Sigma); poly(ethylene glycol) 2000 (PEG 2000, Sigma); poly(propylene oxide) 2000 (PPO 2000, Sigma Aldrich); polyisoprene, *cis*

35 000 (*cis*, Sigma Aldrich); potassium carbonate ($\geq 99\%$, Roth); potassium hydroxide (99 %, Roth); propiophenone (99 %, Sigma-Aldrich); *p*-toluenesulfonic acid monohydrate (97.5 %, Acros); SEC Bio-Beads S-X1 Support (Bio-Rad); silica (60 Å, $\geq 99.5\%$, ROCC); sodium bicarbonate (99 %, Roth); sodium hydrogen bicarbonate ($\geq 99\%$, Roth); sodium hydroxide ($\geq 99\%$, Roth); sodium sulfate (99 %, Roth); sulfuric acid (99 %, Sigma-Aldrich); *tert*-butyl isocyanate (97 %, Sigma); thionyl chloride (97 %, Sigma Aldrich); *trans,trans*-2,4-hexadien-1-ol (HDEO; $> 97\%$, Sigma Aldrich); triethylamine (99 %, Sigma-Aldrich); trifluoroacetic acid (99 %, Sigma-Aldrich); trimethylacetyl chloride (99 %, Sigma-Aldrich); triphenylmethanol (97 %, Acros); triphosgene (98 %, TCI Europe): were used as received from the supplier.

All solvents (Sigma-Aldrich) and products were used without any pre-treatment or purification.

Desmodur XP 2489 polyisocyanate (21% isocyanate content) was kindly provided by Bayer MaterialScience and used as received.

Cyclopentadiene (Cp) was obtained as a colorless liquid by thermal cracking of dicyclopentadiene (95 %, Acros) at 180 °C, which was stored at -18 °C and used within 3 days.

2,2'-azobisisobutyronitrile (AIBN, 98 %, Sigma) was recrystallised twice from methanol.

DABCO-Br,⁴⁴⁶ BuTAD,⁷ PhTAD,⁴⁴⁷ 2,2,2-trimethyl-1,3-dioxane-5-carboxylic acid⁴⁴⁸ and 4-(6-aminohexyl) urazole hydrochloride¹² were synthesized according to literature procedures.

A.2 Instrumentation

Custom-built photoreactor. Irradiation experiments with UV-emitting Arimed B6 (3 x 36W) compact fluorescent lamps ($\lambda_{\max} = 320$ nm) were carried out in a custom-built photoreactor, equipped with a circular sample holder, which is rotated with an angular velocity of 0.5 rad s⁻¹ and ventilator to maintain ambient temperature.

Differential scanning calorimetry (DSC). Differential Scanning Calorimetry (DSC) measurements were carried out with a Mettler Toledo 1/700 calorimeter, equipped with Full Range Sensor (FRS5) containing 56 thermocouples, a liquid nitrogen cooling system that enables a temperature range of -150 °C to 700 °C and an automatic sample robot. All measurements were carried out under a nitrogen atmosphere in standard 40 µL aluminium crucibles containing 5 to 15 mg of the polymeric material, which are hermetically sealed. A consecutive heating-cooling-heating run was performed in a broad temperature range of -150 °C to 150 °C at a rate of 10 °C min⁻¹. The resulting thermograms were analysed with the STARe Excellence Software and the glass transition temperature (T_g) that is reported was taken as the midpoint from the second heating run, which is defined as the intercept of the DSC curve and the bisector of the angle formed by extrapolation of the baselines before and after the transition.

Direct laser writing (DLW). Direct laser writing experiments were carried out using two different setups. A first setup is the commercially available Photonic Professional GT DLW system supplied by Nanoscribe GmbH, equipped with a frequency doubled Erbium fiber laser centered around $\lambda = 780$ nm with pulse duration of approximately 90 fs and a Zeiss Plan-Apochromat 63x/1.4 Oil DIC objective. 3D patterns were constructed by laser scanning via galvo-mirrors and mechanical stages, conducted in immersion oil mode. A second setup is a custom-built 3D DLW system, based on a Ti:Sapphire oscillator (Coherent Chameleon Ultra II) centered around 700 nm with 140 fs pulses and a repetition rate of 80 MHz. The pulse energy is modulated by an acousto-optic AOM, AA Optic-Electronic MTS40-A3-750.850. The laser beam of the setup was focused through an oil-immersion lens with a numerical aperture of 1.4 (Leica HCX PL APO 100x/1.4-0.7 OIL CS). Pulse energies were measured at the back focal plane of the objective lens with aperture of 5.6 mm in diameter. An additional dedicated diode laser at 675 nm was used during writing to find the interface of the glass substrate and photoresist in the z -direction with high accuracy by means of confocal detection. Exposures were carried out at a scan velocity of $100 \mu\text{m s}^{-1}$ and average laser powers of 8 to 10 mW, unless specified otherwise.

Electrospray ionisation mass spectrometry (ESI-MS). Mass spectra were recorded on a LTQ Orbitrap XL Q Exactive mass spectrometer (ThermoFischer Scientific), equipped with a HESI II probe and calibrated by means of premixed calibration standards containing caffeine, Met-Arg-Phe-Ala acetate and a mixture of fluorinated phosphazenes in the mass range $m/z = 74 - 1822$. Samples were dissolved in THF:MeOH (3:2) (HPLC grade) that is doped with 100 μmol sodium trifluoroacetate, and manually injected with a flow rate of $5 \mu\text{L min}^{-1}$ at a constant spray voltage of 4.6 kV, capillary temperature of 320 °C and S-lens RF level set to 62.0.

Hyphenated liquid chromatography-mass spectrometry (LC-MS). LC-MS measurements were carried out on an 1100 series LC/MSD system (Agilent Technologies) containing a diode array detector and single quad MS. Analytical reversed phase HPLC was performed on a Phenomenex Luna C18 (2) column (dimensions $5 \mu\text{m} \times 250 \text{ mm} \times 4.6 \text{ mm}$) in a solvent mixture of acetonitrile and water (gradient of 0 to 100 % in 15 minutes) and the eluted compounds were detected by UV-absorbance at 214 nm. High resolution mass spectrometry (HRMS) was carried out with an Agilent 6220 accurate-mass time-of-flight (TOF) analyser containing a multimode ionisation (MMI) source. The ACD/Labs Spectrus software package was used to analyse the elugram and mass spectra.

Laser scanning microscopy (LSM). Fluorescence micrographics of the obtained microstructures via DLW were recorded with a Zeiss LSM 510 Meta laser scanning microscope by making use of a laser diode with emission wavelength at 405 nm as the excitation source and an oil immersion objective lens with a 63x magnification and 1.4 numerical aperture.

Matrix-assisted laser desorption-ionisation time-of-flight spectrometry (MALDI-TOF). MALDI-TOF analysis was carried out on an Applied Biosystems Voyager spectrometer,

equipped with linear (2 m) and reflector flight tubes (3 m) and a nitrogen laser operating at 337 nm, pulsed ion extraction source, and a reflectron. Mass spectra were obtained at an accelerating potential of 20 kV in positive ion mode and reflector mode, calibrated on poly(ethylene glycol) standards ($M_n = 2000 \text{ g mol}^{-1}$) and analysed using the Data Explorer 4.0.0.0 (Applied Biosystems) software.

Melting point determination. Melting points of synthesised crystalline compounds were measured using the IA 9000 Digital Melting Point Apparatus (Electrothermal) at a heating rate of $1 \text{ }^\circ\text{C min}^{-1}$. The melting points obtained were compared to those reported in literature.

Nuclear magnetic resonance (NMR) spectroscopy. NMR spectra were recorded on a Bruker Avance 300 (300 MHz), Bruker Ascend 400 (400 MHz) or Bruker Avance II (500 MHz) FT-NMR spectrometer at $25 \text{ }^\circ\text{C}$ in the solvent as indicated. Chemical shifts (δ) are expressed in parts per million (ppm) whereby the residual solvent peaks serve as an internal standard. The resonance multiplicities are abbreviated as follows: s (singlet), d (doublet), t (triplet), q (quadruplet), quint (quintuplet), sext (sextuplet) or m (multiplet). Standard parameters in terms of number of scans, pulse delay, acquisition time, tilt angle and pulse time:

^1H spectra (300 MHz: ns = 16, D1 = 1.0 s, AQ = 2.65 s, 30° , P1 = 7.25 μs ; 400 MHz: ns = 16, D1 = 1.0 s, AQ = 4.10 s, 30° , P1 = 7.75 μs ; 500 MHz: ns = 16, D1 = 1.0 s, AQ = 3.28 s, 30° , P1 = 13.83 μs);

^{13}C spectra (300 MHz: ns = 3072, D1 = 2.0 s, AQ = 1.82 s, 30° , P1 = 7.50 μs ; 400 MHz: ns = 3072, D1 = 2.0 s, AQ = 1.36 s, 30° , P1 = 7.50 μs ; 500 MHz: ns = 3072, D1 = 2.0 s, AQ = 1.10 s, 30° , P1 = 7.50 μs).

Rheology. Rheology experiments were conducted with a Modular Compact Rheometer (MCR) 302 (Anton Paar) containing an air-bearing-supported synchronous Electrically Commutated (EC) motor, integrated normal force sensor, TruRateTM sample-adaptive controller, TruStrainTM real-time position control and a Convection Temperature Device 180 (CTD 180) heating unit. Measurements were designed and analysed using of the RheoCompassTM software.

Measurements were conducted with a 50 mm diameter parallel-plate geometry (PP50), or glass parallel plate (33 mm diameter) for photocuring, with a viscoelastic moving profile in oscillatory mode with a pre-set shear gap (typically between 0.3 mm and 0.1 mm), 0.1 % shear strain and 1 Hz angular frequency, whilst keeping the normal force constant (e.g. set at 0 N, or 0.2 N). The lower detection limit, defined by the generated torque in the specific deformation applied, is specified at 0.5 nN m. For delayed crosslinking experiments, the temperature was either increased linearly from $25 \text{ }^\circ\text{C}$ up to $150 \text{ }^\circ\text{C}$ at $2.25 \text{ }^\circ\text{C min}^{-1}$, or kept constant (e.g. at $50 \text{ }^\circ\text{C}$) for isothermal curing. Experiments requiring constant heating were followed by a 5-minute isotherm period at $150 \text{ }^\circ\text{C}$ to assess complete curing of the sample. For photocuring experiments, irradiation was performed with a UV-lamp equipped with a visible light filter in the

range of 400 – 500 nm. Amplitude sweeps with a logarithmic increase in shear strain (oscillating) from 0.01 % to 10 % at a constant frequency of 1 Hz were carried out on each crosslinked sample in order to ensure the experiments were conducted within the linear viscoelastic region.

Size-exclusion chromatography (SEC). Size-exclusion chromatography (SEC) was performed on the following instruments, in the solvent as indicated;

For DMF (containing 5 g L⁻¹ lithium bromide) at 35 °C on a closed system Waters instrument equipped with Polymer Standards Services GPC serial columns (GRAM Analytical, 10 μm, 30 Å or 1000 Å) and a 2414 Waters Refractive Index detector. A solvent flow rate of 1 mL min⁻¹ was applied and the system was calibrated on poly(methyl methacrylate) standards. Analysis was carried out with the Empower software.

For THF at 40 °C on a Varian PL-GPC 50 Plus instrument equipped with a refractive index detector and two PL-gel 5 μm MIXED-D columns. Polystyrene standards were used as calibration and samples were injected with a PL AS RT autosampler and measured at a flow rate of 1 mL min⁻¹.

For CHCl₃ at 35 °C on a Waters instrument equipped with Styragel HR3-5 serial columns 5 μm (Waters) and 2410 Waters Refractive Index detector. A solvent flow rate of 1 mL min⁻¹ was applied and the system was calibrated on polystyrene and poly(methyl methacrylate) standards. Analysis was performed with the Breeze Millennium software

Thermal gravimetric analysis (TGA). Thermal gravimetric measurements were performed on a Mettler Toledo TGA/SDTA851e equipped with Julabo FP50 circulator and HP control unit which is calibrated using three indium pills and ca. 6 mg aluminium. Samples were placed in 70 μL alumina crucibles with a lid and subjected to heating from 25 °C up to 800 °C at 10 °C min⁻¹ under a nitrogen atmosphere. The thermograms were analysed with the STARe Excellence Software and the temperature of degradation was reported at 5 % weight loss (T_{d, 5%}).

Tunable laser system. Wavelength-tunable UV- and visible laser light was generated by a Splitlight 600 OPO Nd:YAG Tunable Laser System, supplied by Innolas, making use of an Optical Parametric Oscillator (OPO) to produce a tunable laser output between 410 and 670 nm or, with a second modular unit, between 270 and 410 nm. The OPO is operated by a diode pumped Nd:YAG laser at a 100 Hz repetition rate and the output energy was regulated by a variable attenuator (polariser) coupled to a Coherent Energy Max PC power meter to measure the energy of the incident laser pulses. The generated laser light was guided through a prism and directed to the bottom of the sample, placed in a home-made sample holder. The temperature in the laser room was regulated at 18 °C.

UV/vis emission spectrometer. Emission spectra of irradiation sources were recorded with a UV/vis SR600 spectrometer containing a polychromator and a silicon photodiode array. The device is calibrated to enable accurate spectral radiometric measurements, which are processed

with the SR600 spectral software. A dark measurement was carried out prior to each calibrated measurement and the integration time was changed appropriately to obtain a recording level of approximately 90%.

UV/vis spectrometry. UV/vis spectra were recorded on a Varian Cary 300 Bio spectrometer at 25 °C and on a Shimadzu UV-2700 spectrophotometer coupled to a CPS-100 cell positioner for thermoelectrically temperature controlled measurements.

Appendix B.

Experimental section Chapter III

B.1 Additional figures

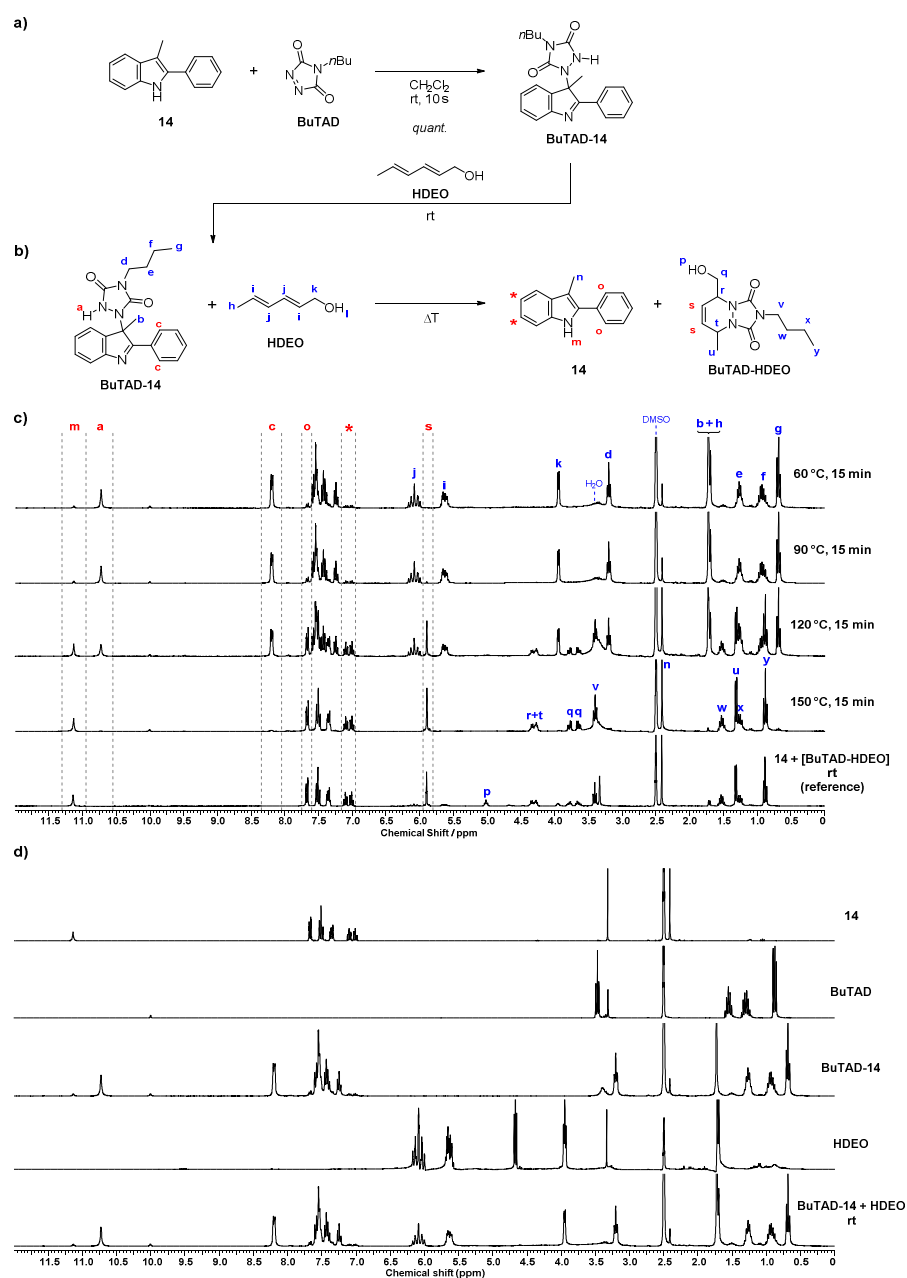


Figure B.1. a) Reaction of 3-methyl-2-phenyl-1H-indole **14** with BuTAD to give the corresponding TAD-indole adduct. b) A slight excess of HDEO was next added to enable the quantitative analysis of the TAD-indole retro-reaction by trapping the liberated TAD into the HDEO Diels-Alder adduct upon heating. c) Integration of well-resolved signals in the offline $^1\text{H-NMR}$ spectrum after 15 minutes of heating allows to determine the equilibrium the BuTAD-**14** and **14** concentrations, from which a kinetic thermal reversibility profile can be deduced. d) Reference spectra of the individual compounds used in the model study of **14**.

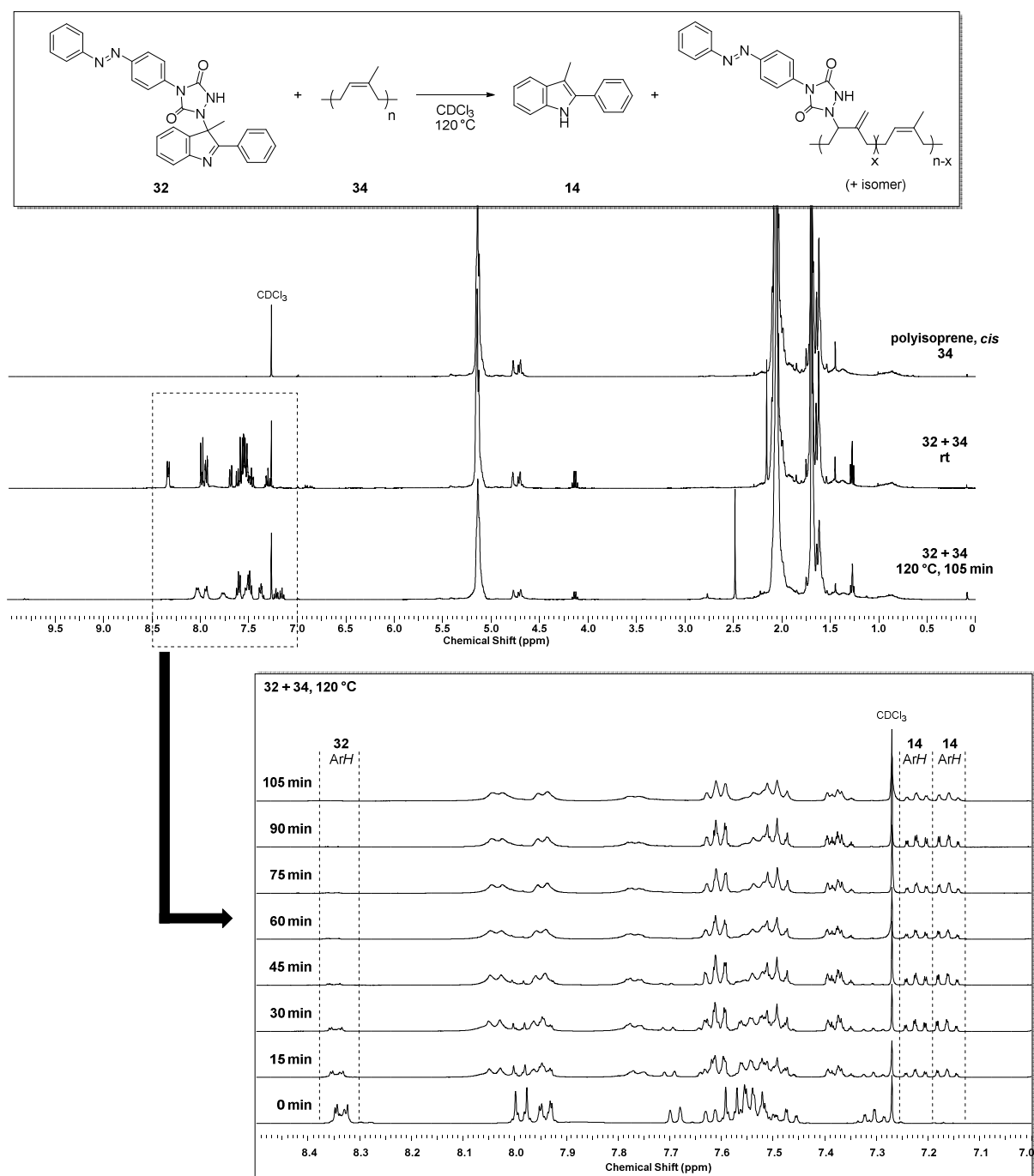


Figure B.2. Kinetic $^1\text{H-NMR}$ measurements of the TAD-dye transfer from the indole blocking agent (adduct **32**) to the polyisoprene backbone **34**, indicating complete transfer within 105 minutes at $120\text{ }^\circ\text{C}$.

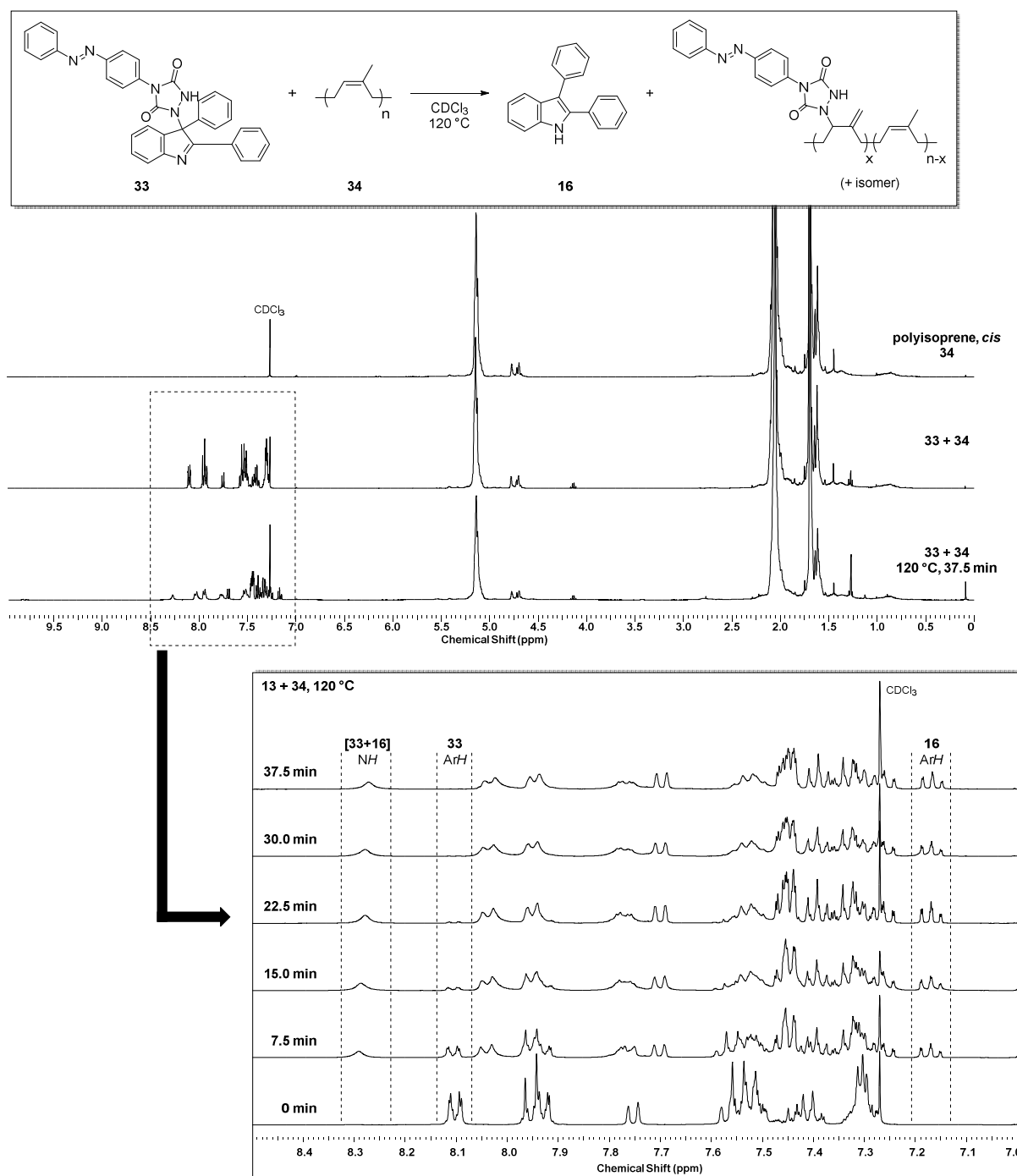


Figure B.3. Kinetic $^1\text{H-NMR}$ measurements of the TAD-dye transfer from the indole blocking agent (adduct **33**) to the polyisoprene backbone **34**, indicating complete transfer within 40 minutes at $120\text{ }^\circ\text{C}$.

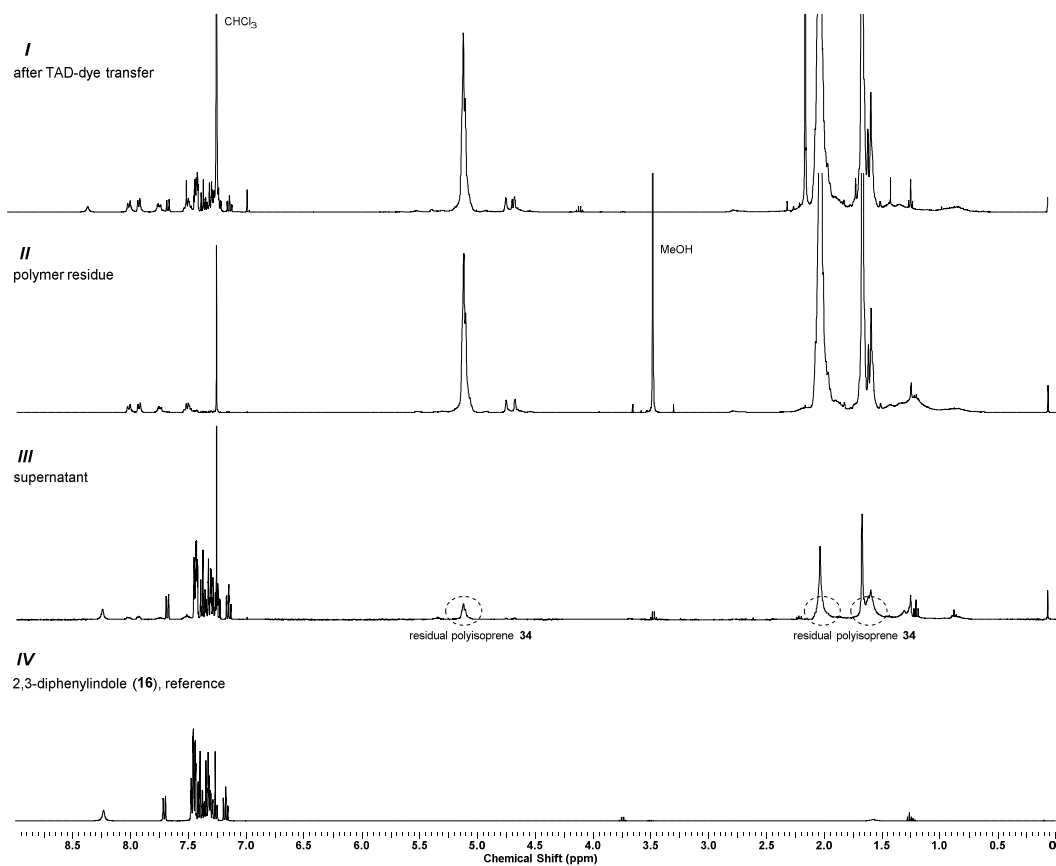


Figure B.4. $^1\text{H-NMR}$ spectra of the covalent TAD-dye polymer modification. Following the complete transfer of TAD-dye from indole-conjugate **33** to polyisoprene **34** (spectrum *I*), the resulting reaction mixture was precipitated in cold methanol to give the TAD-dye-functionalised polyisoprene as an orange residue (evidenced by the aromatic signals in spectrum *II*). The supernatant after solvent evaporation only contained the initial 2,3-diphenyl-1*H*-indole blocking agent **16**, which is cleaved off during the reaction (spectrum *III* vs. *IV*).

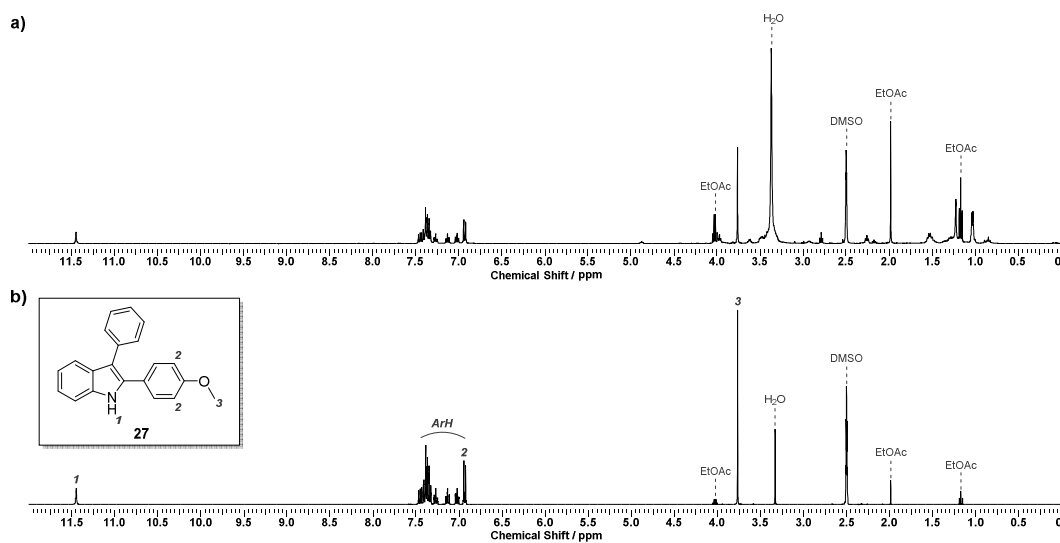


Figure B.5. a) ¹H-NMR spectra (in DMSO-*d*₆) of the soluble fraction obtained after conducting a Soxhlet extraction (from ethyl acetate) on the isothermally cured HDEO-PU with blocked bisTAD **43**. b) overlay with the NMR spectrum of initial indole **27**, indicates the successful removal of the blocking agent from the network.

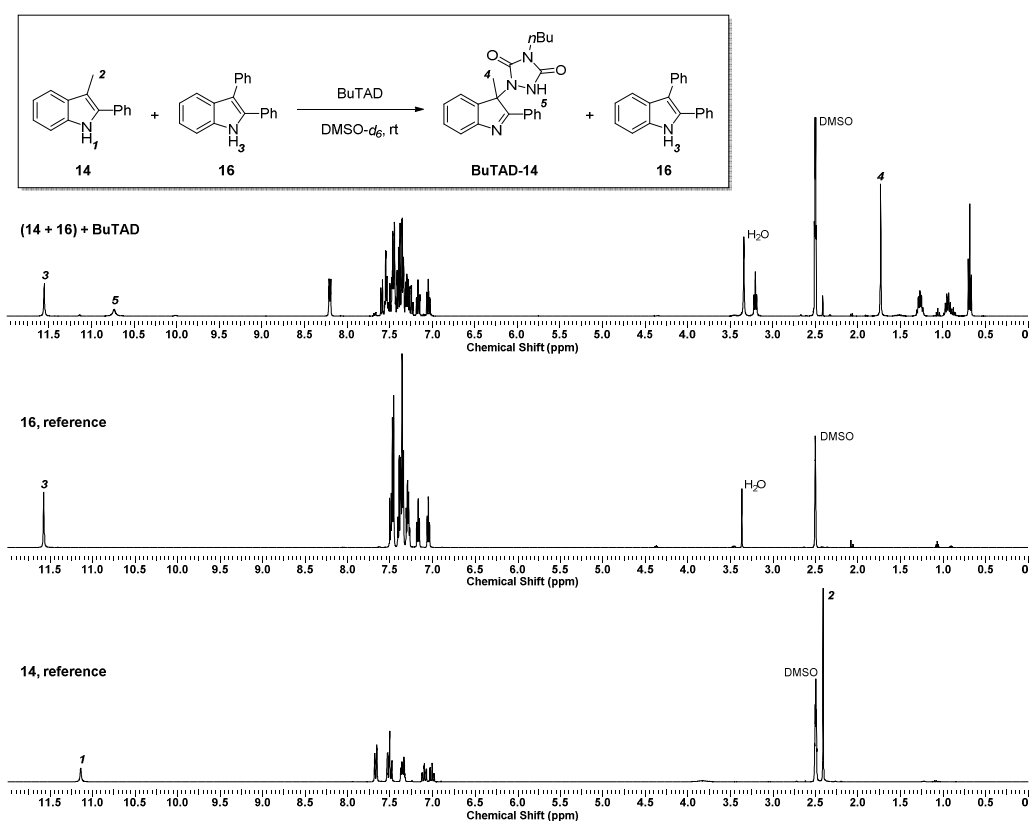


Figure B.6. Competition experiment at room temperature, whereby an equimolar amount of BuTAD is added to a pre-mixed solution of 3-methyl-2-phenyl-1*H*-indole (**14**) and 2,3-diphenyl-1*H*-indole (**16**) in DMSO-*d*₆. The resulting ¹H-NMR spectrum (top) indicates the kinetic preference of TAD-addition to the least sterically hindered indole **14**, resulting in the disappearance of the initial indole *NH* signal **1** (bottom) into signal **3** corresponding to BuTAD-14 whilst indole **16** remained unaltered (middle).

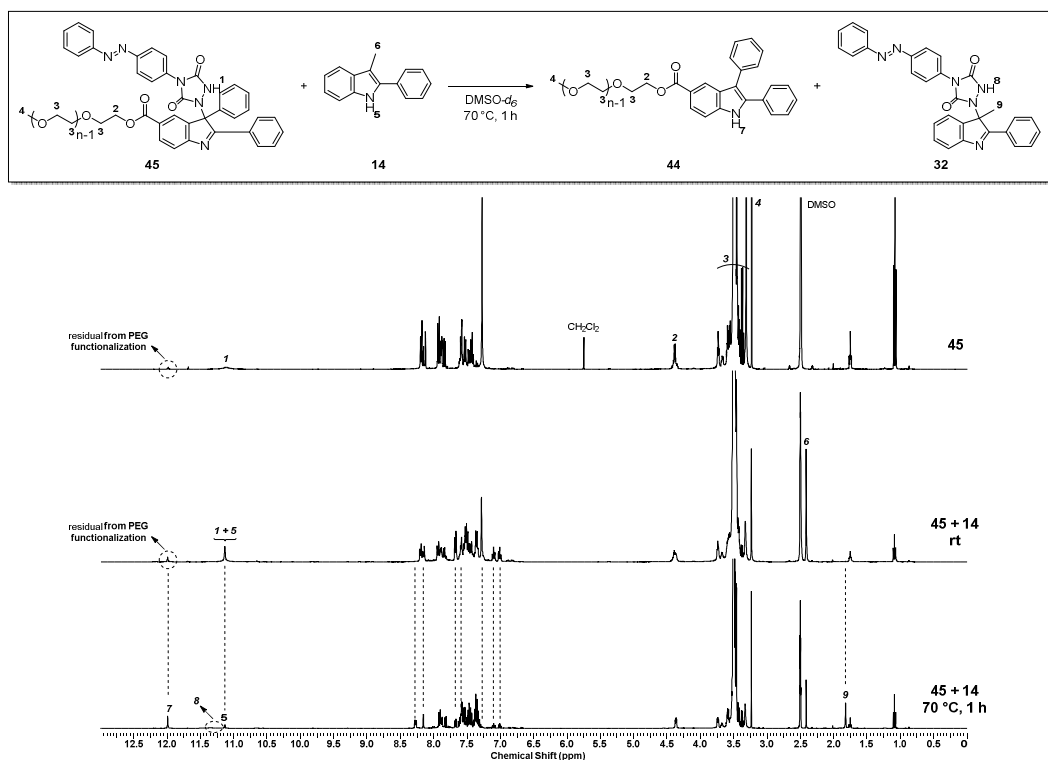


Figure B.7. $^1\text{H-NMR}$ spectra of the TAD-dye transfer from PEGylated donor indole blocking agent **44** to the non-functional indole acceptor **14** upon standing at $70\text{ }^\circ\text{C}$ for 1 hour.

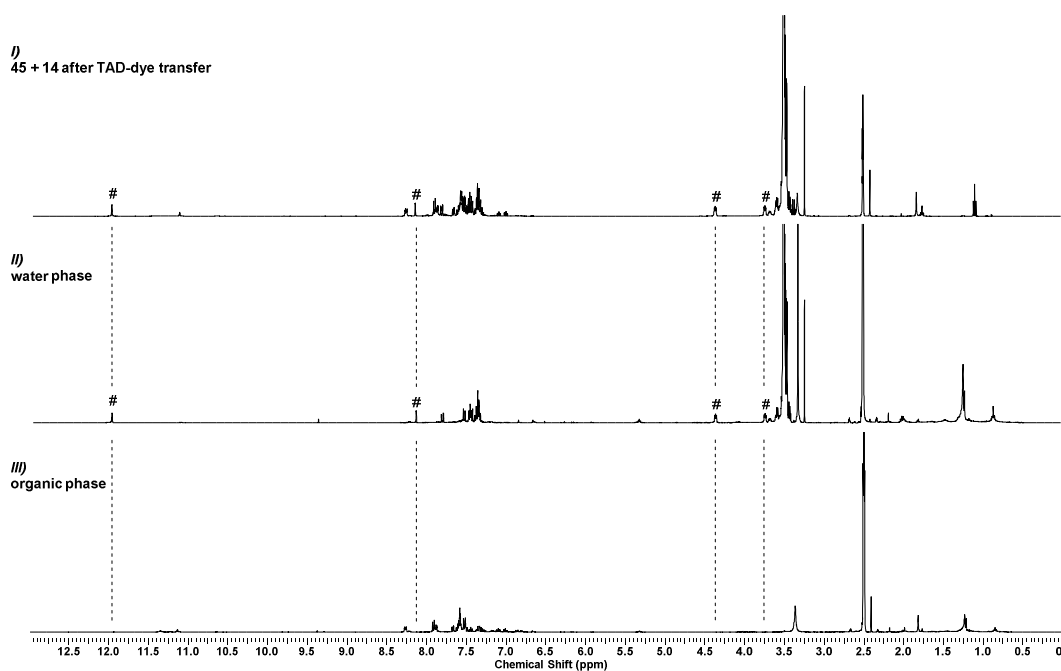
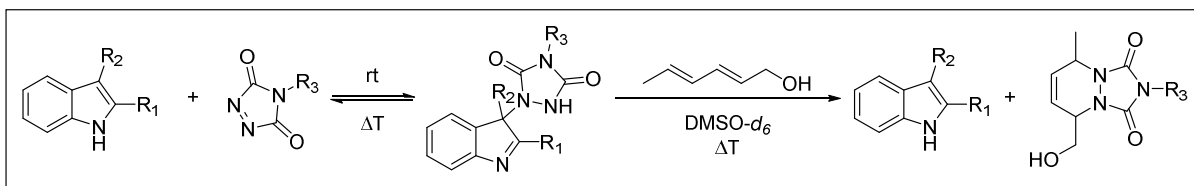


Figure B.8. $^1\text{H-NMR}$ analysis after phase separation following the TAD-dye transfer from PEGylated donor indole blocking agent **44** to non-functional indole acceptor **14** ($70\text{ }^\circ\text{C}$, 1 h, spectrum *I*), indicates the released indole-PEG to preferentially residue in the water phases (signals denoted with # in spectrum *II*), whereas the newly formed TAD-indole adduct BuTAD-14 is to be found in the organic phase (*III*).

B.2 Experimental procedures

B.2.1 Kinetic thermal reversibility studies of TAD-indole systems



General procedure for the TAD-indole kinetic thermal reversibility studies of indoles **12-14**, **16**, **18** and **21-29** with BuTAD (i.e. $R_3 = -n\text{Bu}$), indoles **14**, **16** and **27** with PhTAD (i.e. $R_3 = -\text{Ph}$) and indole **16** with azobenzene TAD-dye **31** (i.e. adduct **33**, $R_3 = -\text{Ph-N=N-Ph}$), in the following illustrated for **BuTAD-14**. The synthesis of the TAD-indole adducts is described in B.4.3.

The deblocking behaviour of **BuTAD-14** at elevated temperatures was determined by monitoring the fraction of the *in situ* liberated **BuTAD** and indole **14** that are released from the initial TAD-indole adduct within a 15-minute heating period at a distinct temperature. In order to enable a straightforward analysis of the backward TAD-indole reaction by means of offline $^1\text{H-NMR}$ analysis, it is crucial to suppress the recombination reaction between the released **BuTAD** and indole **14** to reform the initial adduct. As this would occur when the heated sample is cooled down to room temperature prior to NMR analysis, the kinetic thermal reversibility study was conducted in the presence of *trans,trans*-2,4-hexadien-1-ol (HDEO), which serves as a suitable trapping agent that quantitatively transforms the released **BuTAD** into the corresponding irreversible Diels-Alder adduct. Since the reaction kinetics of the TAD-diene reaction supersede the forward TAD-indole reaction by several orders of magnitude (i.e. $k_{\text{TAD-HDEO}} > 10^3 k_{\text{TAD-indole}}$), the recombination reaction of the released TAD and indole at elevated temperatures can thus be neglected.

More specifically, a stock solution of **BuTAD-14** (87.0 mg, 0.24 mmol, 1.0 eq.) in 6 mL DMSO- d_6 (0.04 M) in the presence of *trans,trans*-2,4-hexadien-1-ol (HDEO, 25.9 mg, 0.26 mmol, 1.1 eq.) was divided over numerous NMR tubes. The corresponding samples were placed in a preheated oil bath for 15 minutes at a defined temperature, i.e. from 40 °C to 160 °C in 10 °C intervals. After the heating period, the NMR tubes were immediately cooled down under running tap water and submitted for $^1\text{H-NMR}$ analysis.

From the obtained $^1\text{H-NMR}$ spectra (*cf.* Figure III.2), the concentration of released indole blocking agent as a function of temperature was determined from the integrated NMR signals as the ratio of released blocking agent **14** over the initial TAD-indole adduct **BuTAD-14**. Several well-resolved proton signals could be followed during the course of the deblocking reaction. For example, the urazole NH signal *a* (refer to Figure III.2) of the TAD-indole adduct decreased at the dispense of the NH signal *m* arising from the released indole (with a characteristic down-field

resonance shift), whilst the increase in signal s clearly indicated the formation of the new Diels-Alder BuTAD-HDEO adduct (which can be directly correlated to the amount of released BuTAD). Despite the distinct shift of the NH proton resonance signals of **BuTAD-14**, the urazole proton is rather acidic ($pK_a \approx 5$) and is therefore prone to exchange reactions which result in peak broadened and hence results in erroneous integration values. Therefore, the resolved aromatic proton signals c and o (integrating for 2 protons) of the TAD-indole and released indole blocking agent, respectively, were preferred to set the integration values of both compounds. In those cases that signal o overlaps with other aromatic signals, the resolved peaks denoted with * in Figure III.2 ($2 \times 1H$) were used as an alternative to determine the fraction of released indole **14**. The obtained integration ratio of **14** over **BuTAD-14** (= signal o/c) was determined for each 15-minute heating period at a distinct temperature and represented the degree of deblocking.

B.2.2 Calculation of the observed activation energies

The kinetic thermal reversibility profiles of the TAD-indole systems (*cf.* Figure III.3) express the fraction of deblocking when the system is heated for 15 minutes at a well-defined temperature. The presence of HDEO as a kinetic trap for the *in situ* liberated TAD compounds at elevated temperatures, and the therewith associated ultrafast reaction kinetics compared to the forward TAD-indole reaction (i.e. $k_{TAD-HDEO} > 10^3 k_{TAD-indole}$), allows for a simplified expression of the observed first-order deblocking rate coefficient k_{obs} (Equation B.1). Given the deblocking ratio determined from the 1H -NMR spectra, k_{obs} was hence calculated at each investigated temperature.

$$\begin{aligned} -\frac{d[TAD - indole]}{dt} &= k_{obs} [TAD - indole] \\ \Rightarrow \ln[TAD - indole] - \ln[TAD - indole]_0 &= -k_{obs}t \\ \Rightarrow \ln \frac{[TAD - indole]_t}{[TAD - indole]_0} &= -k_{obs}t \\ \Rightarrow k_{obs} &= \frac{-1}{t} \ln \frac{[TAD - indole]_t}{[TAD - indole]_0} \end{aligned}$$

Equation B.1. Simplified mathematical expression for the observed first-order deblocking rate coefficient k_{obs} . The reaction time t of the kinetic thermal reversibility studies is fixed at 15 minutes, whilst the fraction of deblocking (i.e. $\ln([TAD-indole]_t/[TAD-indole]_0)$) can be determined via integration of the resulting 1H -NMR spectrum.

Having determined k_{obs} as a function of temperature from the above first-order reaction kinetics, the observed activation energy $E_{a, obs}$ of the respective TAD-indole systems was subsequently determined via the Arrhenius equation (Equation B.2).

$$\ln k_{obs} = \frac{-E_{a,obs}}{RT} + \ln A$$

Equation B.2. Arrhenius equation.

By plotting $\ln k_{\text{obs}}$ as a function of T^{-1} , an Arrhenius plot was obtained by taking the best-fit linear interpolation of four data points corresponding to the highest coefficient of determination R^2 , from which the observed activation energy $E_{a, \text{obs}}$ for each TAD-indole system could be calculated from the slope by means of Equation B.3. The results are presented in Table B.1.

$$y = ax + b$$

$$\Rightarrow a = \frac{-E_{a, \text{obs}}}{R}$$

$$\Rightarrow E_{a, \text{obs}} = -aR$$

Equation B.3. Expression for the observed activation energy of the deblocking reaction $E_{a, \text{obs}}$ (J mol^{-1}) which was determined from the slope of the Arrhenius plot, with the gas constant $R = 8.314 \text{ J K}^{-1} \text{ mol}^{-1}$ and a the slope expressed in K.

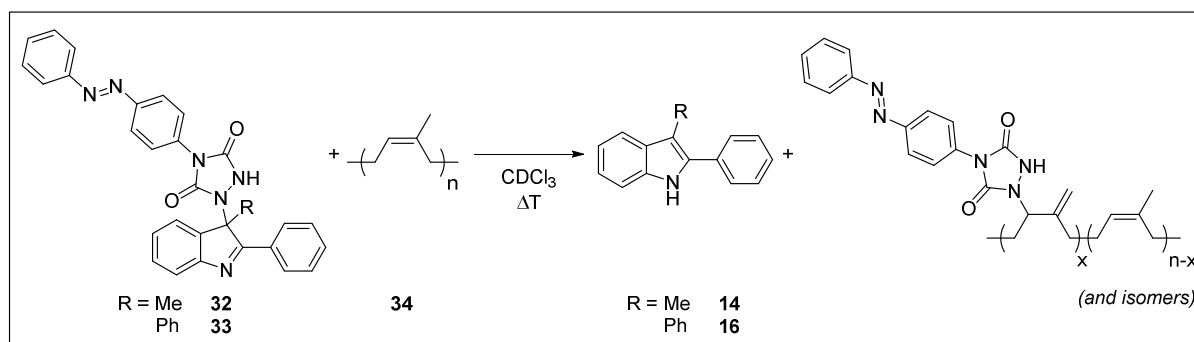
Table B.1. Overview of the observed activation energies $E_{a, \text{obs}}$ for the deblocking reaction and the standard deviation thereof, determined from the Arrhenius plot equations with coefficient of determination R^2 that were obtained from the kinetic thermal reversibility studies of the investigated TAD-indole systems.

Indole	R_1	R_2	R_3	R_4
12	<i>t</i> Bu	isopentyl	H	<i>n</i> Bu
13	Ph	isopentyl	H	<i>n</i> Bu
14	Ph	Me	H	<i>n</i> Bu
16	Ph	Ph	H	<i>n</i> Bu
18	Ph	Ph	COOMe	<i>n</i> Bu
21	4-MeOPh	Me	H	<i>n</i> Bu
22	4-FPh	Me	H	<i>n</i> Bu
23	4-ClPh	Me	H	<i>n</i> Bu
24	4-CF ₃ Ph	Me	H	<i>n</i> Bu
25	Ph	4-NO ₂ OPh	H	<i>n</i> Bu
26	Ph	4-MeOPh	H	<i>n</i> Bu
27	4-MeOPh	Ph	H	<i>n</i> Bu
28	4-MeOPh	4-NO ₂ OPh	H	<i>n</i> Bu
29	4-MeOPh	4-MeOPh	H	<i>n</i> Bu
14	Ph	Me	H	Ph
16	Ph	Ph	H	Ph
27	4-MeOPh	Ph	H	Ph
16	Ph	Ph	H	-Ph-N=N-Ph

Table B.1 (continued)

Indole	Linear regression equation	R ₂	E _{a, obs} (kJ mol ⁻¹)	Standard deviation on E _{a, obs} (kJ mol ⁻¹)
12	y = -14016 x + 28.14	0.992	116.5	6.0
13	y = -13802 x + 27.94	0.992	114.8	7.1
14	y = -13773 x + 30.71	0.997	114.5	4.7
16	y = -12484 x + 26.41	0.999	103.8	1.4
18	y = -12801 x + 28.06	0.997	106.4	4.0
21	y = -13235 x + 28.69	0.997	110.0	4.2
22	y = -13984 x + 29.62	0.997	116.3	4.4
23	y = -14252 x + 31.58	0.997	118.5	4.3
24	y = -14676 x + 29.08	0.997	122.0	5.1
25	y = -12300 x + 25.98	0.999	102.3	1.5
26	y = -12300 x + 26.58	0.999	102.3	2.0
27	y = -11565 x + 24.92	0.997	96.2	3.4
28	y = -10930 x + 22.77	1.000	90.9	0.3
29	y = -11434 x + 23.31	0.999	95.1	1.3
<hr/>				
14	y = -13097 x + 28.70	0.996	108.9	4.0
16	y = -11870 x + 26.66	0.999	98.7	0.7
27	y = -10121 x + 22.60	0.999	84.2	1.9
<hr/>				
16	y = -10496 x + 23.13	0.999	87.3	1.3

B.2.3 Time-controlled modification of polyisoprene with indole-blocked TAD-dyes



Polyisoprene, *cis* (**34**, 40 mg, $1.1 \cdot 10^{-6}$ mol) and 25 wt% of indole-blocked TAD-dye **32** (10 mg, $2.1 \cdot 10^{-5}$ mol) or **33** (10 mg, $1.8 \cdot 10^{-5}$ mol) were dissolved in 0.75 mL deuterated chloroform-*d* and transferred into a pressure tube (). The resulting orange solution was placed in a preheated oil bath at 120 °C (or 70 °C). After distinct time intervals, the pressure tube was taken out of the oil bath, cooled under running tap water and subjected to ¹H-NMR analysis (refer to B.1). The NMR sample was recovered and again placed in the oil bath. The procedure was repeated until the TAD-dye was completely transferred from the indole blocking agent onto the

polyisoprene backbone (confirmed by $^1\text{H-NMR}$). The obtained solution was added to a 10-fold excess of cold methanol and an orange precipitate was recovered, which was separated via decantation from the light yellow supernatant. The resulting orange residue was dried overnight in a vacuum oven at 40 °C and analysed by $^1\text{H-NMR}$, which indicated the covalent attachment of the TAD-dye to the polymer (refer to B.1). The light yellow supernatant was evaporated *in vacuo*, dried in a vacuum oven overnight at 40 °C and subjected to $^1\text{H-NMR}$ analysis, from which the released indole blocking agents **14** and **16** were identified.

B.2.4 Temperature triggered transfer of indole-blocked TAD-dyes from solution onto an insoluble resin

A solution of indole blocked TAD-dye **32** (5.2 mg, 0.011 mmol) or **33** (6.2 mg, 0.011 mmol) in 10 mL butyl acetate was added to 70 mg of the TAD-reactive network (*cf.* B.4.6 for the synthesis of the network) and the resulting orange heterogeneous mixture was heated in an oil bath at 120 °C for 24 h. The orange polymeric resin was taken out of the mixture and subjected to a Soxhlet extraction in ethyl acetate for 4 h to yield a dark orange network, thereby demonstrating the covalent attachment of the TAD-dye onto the polymer resin. The remaining light orange mixture was treated several times (3-5) with extra network (approx. 70 mg) to finally give a clear light yellow solution.

B.2.5 On demand polymer crosslinking of a diene-containing polyurethane

Preparation of a HDEO-PU stock solution.

A stock solution of 6.0 g of HDEO_{15wt%}-PU **35** in 15 mL DMF was prepared and used to carry out all crosslinking experiments. The synthesis of the diene-containing polyurethane **35** is described in B.4.7.

Direct crosslinking at room temperature.

A solution of the bisTAD crosslinking agent **36** (29.4 mg, 0.105 mmol, 0.5 eq.) or **37** (38.0 mg, 0.105 mmol, 0.5 eq.) in 0.25 mL DMF was added to 0.75 mL of the HDEO-PU stock solution (**35**, 300 mg, 0.210 mmol diene, 1.0 eq.) at room temperature whilst stirring. Immediately following addition, gelation was observed within one second and complete disappearance of the red coloured crosslinker was observed after 5 minutes. The resulting polymer networks were dried in a vacuum oven at 40 °C for 5 days and subjected to DSC and TGA analysis.

[**35+36**]: T_g (DSC) = -57 °C, $T_{d, 5\%}$ (TGA) = 253 °C; [**35+37**]: T_g (DSC) = -57 °C, $T_{d, 5\%}$ (TGA) = 278 °C.

Delayed crosslinking upon heating.

0.75 mL of the HDEO-PU stock solution (**35**, 300 mg, 0.210 mmol diene, 1.0 eq.) was added to the indole-blocked TAD crosslinking agents **38-43** (73.0 mg of **38**, 81.6 mg of **41**, 86.0 mg of **39**, 94.6 mg of **42**, 92.3 mg of **40**, 100.9 mg of **43**, 0.105 mmol, 0.5 eq.) and thoroughly mixed

at room temperature using a vortex mixer. The resulting polymer solution were carefully deposited on the lower parallel plate (PP50) of the rheometer (*cf.* instrumentation section), thereby avoiding the formation of air bubbles. The upper part of the moving profile of the geometry was lowered (0.3 mm gap) and the excess amount of formulation was trimmed at the edges of the measuring system. The sample was subjected to a temperature ramp from 25 °C up to 150 °C at a heating rate of 2.25 °C min⁻¹ whilst applying a constant oscillating shear strain of 0.1 %. Following complete curing (*cf.* Scheme III.11a), the resulting material was cooled to room temperature and recovered as a brown residue. The recovered network was dried in a vacuum oven at 40 °C for 5 days to remove the residual solvent and subjected to DSC and TGA analysis.

Network [35+38]: T_g (DSC) = -52 °C, $T_{d, 5\%}$ (TGA) = 225 °C; [35+41]: T_g (DSC) = -53 °C, $T_{d, 5\%}$ (TGA) = 232 °C;

Network [35+39]: T_g (DSC) = -36 °C, $T_{d, 5\%}$ (TGA) = 253 °C; [35+42]: T_g (DSC) = -37 °C, $T_{d, 5\%}$ (TGA) = 242 °C;

Network [35+40]: T_g (DSC) = -34 °C, $T_{d, 5\%}$ (TGA) = 260 °C; [35+43]: T_g (DSC) = -39 °C, $T_{d, 5\%}$ (TGA) = 253 °C.

Delayed crosslinking under isothermal conditions.

0.75 mL of the HDEO-PU stock solution (35, 300 mg, 0.210 mmol diene, 1.0 eq.) was added to the indole-blocked TAD crosslinking agents 43 (100.9 mg, 0.105 mmol, 0.5 eq.) and thoroughly mixed at room temperature using a vortex mixer. The resulting polymer solution were carefully deposited on the lower parallel plate (PP50) of the rheometer (*cf.* instrumentation section), thereby avoiding the formation of air bubbles. The upper part of the moving profile of the geometry was lowered (0.3 mm gap) and the excess amount of formulation was trimmed at the edges of the measuring system. The sample was heated in a prewarmed oven at 50 °C whilst applying a constant oscillating shear strain of 0.1 %. From the curing profile (*cf.* Scheme III.11b), a gelation time of 110 minutes could be observed. After cooling to room temperature, the formed brown network was recovered, dried in a vacuum oven at 40 °C for 5 days to remove any residual solvent and subjected to DSC and TGA analysis. A part of the network was transferred into a Soxhlet thimble and extracted several times with ethyl acetate to remove the residual indole blocking agent (27) that is released upon curing.

Network [35+43] after curing: T_g (DSC) = -35 °C, $T_{d, 5\%}$ (TGA) = 262 °C;

Network [35+43] after Soxhlet extraction T_g (DSC) = -56 °C, $T_{d, 5\%}$ (TGA) = 281 °C.

B.2.6 Orthogonal indole-to-indole TAD-exchange reaction

A solution of BuTAD (85.0 mg, 0.5 mmol, 1.0 eq.) in 6 mL dichloromethane was added to 2,3-diphenyl-1*H*-indole 16 (135 mg, 0.5 mmol, 1.0 eq.) in 6 mL dichloromethane. After stirring at room temperature for 30 minutes, the reaction was observed to have reached full conversion, which was determined by the visual disappearance of the red TAD colour. To ensure the

equimolarity of both reagents, a few additional drops of a BuTAD solution in dichloromethane were added to the reaction mixture until a slight pink colour persisted. Solvent removal *in vacuo* followed by drying in a vacuum oven overnight at 40 °C gave pure adduct **BuTAD-16** (210 mg – 99%).

BuTAD-16: ¹H-NMR (500 MHz, DMSO-*d*₆): δ (ppm) = 0.67 (t, 3H, CH₂-CH₃), 0.85 (m, 2H, CH₂-CH₃), 1.25 (m, 2H, N-CH₂-CH₂), 3.25 (t, 2H, N-CH₂), 7.13-7.19 (m, 2H, ArH), 7.19-7.25 (m, 3H, ArH), 7.28 (t, 1H, ArH), 7.34-7.45 (m, 4H, ArH), 7.50 (t, 1H, ArH), 7.67 (d, 1H, ArH), 8.07 (m, 2H, ArH), 10.37 (s, 1H, NH). ¹³C-NMR (125 MHz, DMSO-*d*₆): δ (ppm) = 13.29 (CH₃), 18.63 (CH₂), 28.89 (CH₂), 38.13 (CH₂), 81.35 (C), 120.97 (CH), 123.38 (CH), 126.79 (CH), 128.07 (CH), 128.26 (CH), 128.64 (CH), 128.73 (CH), 130.23 (CH), 130.73 (CH), 132.28 (C), 135.03 (C), 139.03 (C), 154.59 (C), 154.86 (C), 156.53 (C), 176.19 (C). LC-MS (m/z): 425.2 [M+H]⁺. HRMS (m/z): *calc.*: 425.1972, *found*: 425.1970 [M+H]⁺.

Next, aliquots of the resulting adduct **BuTAD-16** (100 mg, 0.24 mmol, 1.0 eq.) and 3-methyl-2-phenyl-1*H*-indole **14** (49 mg, 0.24 mmol, 1.0 eq.) were dissolved in 6 mL of deuterated DMSO-*d*₆ (see Figure B.9a). The resulting stock solution was divided over numerous NMR samples and placed in a preheated oil bath for 15 minutes at a defined temperature in the range of 90 – 140 °C, in 10 °C intervals. Comparison of the ¹H-NMR spectra before and after heating allowed for the characterisation of the indole-to-indole exchange reaction of BuTAD (Figure B.9c). From the resulting ¹H-NMR spectra, a quantitative exchange of the BuTAD moiety from the most dynamic indole **16** to the least dynamic indole **14** was observed upon a 15-minute heating period at 120 °C.

In a final experiment, a solution of HDEO (26 mg, 0.26 mmol, 1.1 eq.) in 1.5 mL DMSO-*d*₆ was added and the resulting mixture was heated for 15 minutes at 150 °C (Figure B.9b). Again, offline ¹H-NMR analysis allowed to determine the composition of the reaction mixture, indicating the quantitative formation of the BuTAD-HDEO Diels-Alder adduct, together with the complete release of both initial indole substrates **14** and **15** (Figure B.9c).

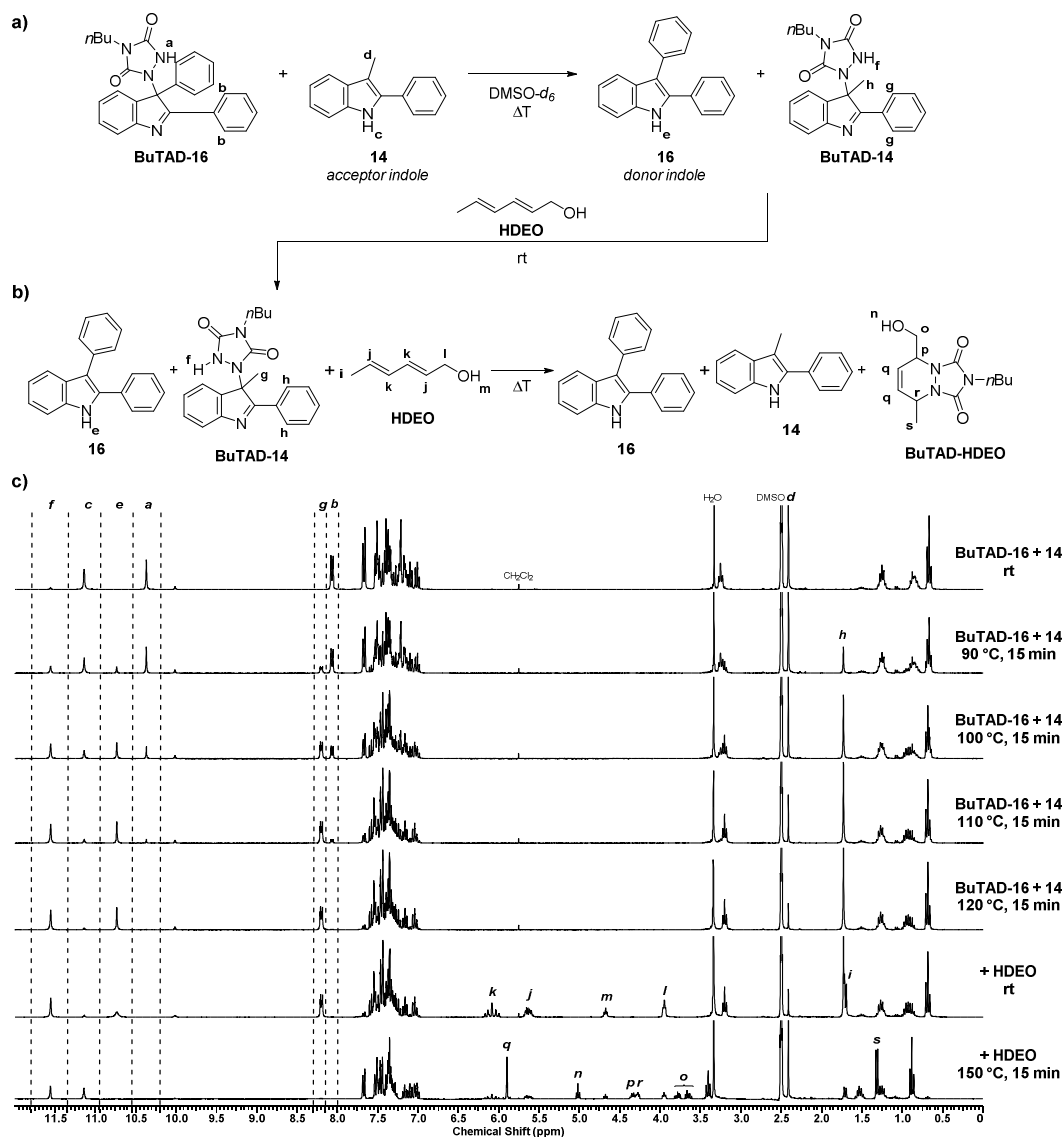
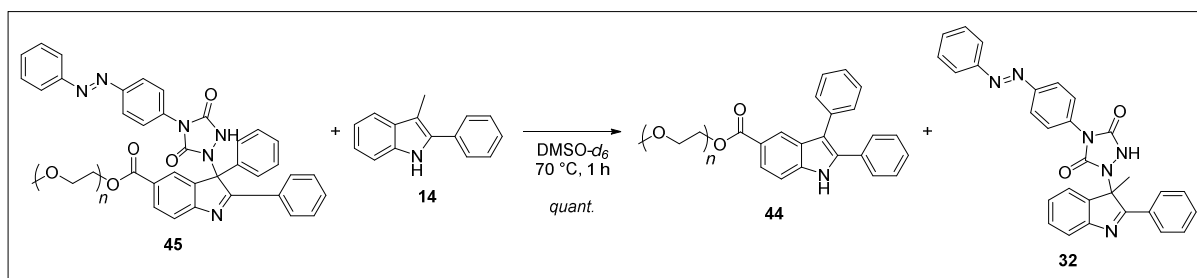


Figure B.9. a) Selective transfer of BuTAD from the donor indole **16** to acceptor indole **14** upon heating. b) Addition of HDEO to the reaction mixture and subsequent heating at 150 °C for 15 minutes eventually traps all BuTAD into the irreversible Diels-Alder adduct with the release of both original indole substrates. c) $^1\text{H-NMR}$ spectra of the indole-to-indole exchange reaction before and after heating for 15 minutes and the consecutive irreversible TAD-transfer to the conjugated diene HDEO upon a second 15-minute heating period at 150 °C.

B.2.6.1 Visual TAD-dye indole-to-indole phase transfer



TAD-dye conjugate **45** (50 mg, 0.019 mmol, 1.0 eq.) – obtained upon reaction of PEGylated 2,3-diphenyl-1*H*-indole **16** with azobenzene TAD-dye **31** – and 3-methyl-2-phenyl-1*H*-indole **14** (4.4 mg, 0.021 mmol, 1.1 eq.) were dissolved in 0.75 mL deuterated DMSO-*d*₆. The resulting solution was heated at 70 °C for 1 h after which complete transfer of the TAD-dye to the acceptor indole **14** was evidenced from the ¹H-NMR spectrum. The resulting mixture was allowed to cool to room temperature and 2 mL water was added to give an orange-yellow mixture after vigorous shaking, followed by the addition of 2.5 mL of ethyl acetate. The resulting mixture was phase separated with a centrifuge (4500 rpm, 5 minutes, 20 °C) to give a clear orange coloured organic phase and a light yellow aqueous phase. The aqueous phase was taken up with a syringe in order to separate both layers and the remaining organic phase was washed with 1 mL water, dried over magnesium sulfate and evaporated to dryness *in vacuo*. The resulting dark orange oil was submitted for ¹H-NMR analysis, which indicated the presence of the newly formed TAD-dye conjugate **32** (refer to B.1). In addition, the yellow water phase was also dried *in vacuo*, leading to a yellow residue which contained the initial PEGylated indole blocking agent **44**, again evidenced from the corresponding ¹H-NMR-spectrum (refer to B.1).

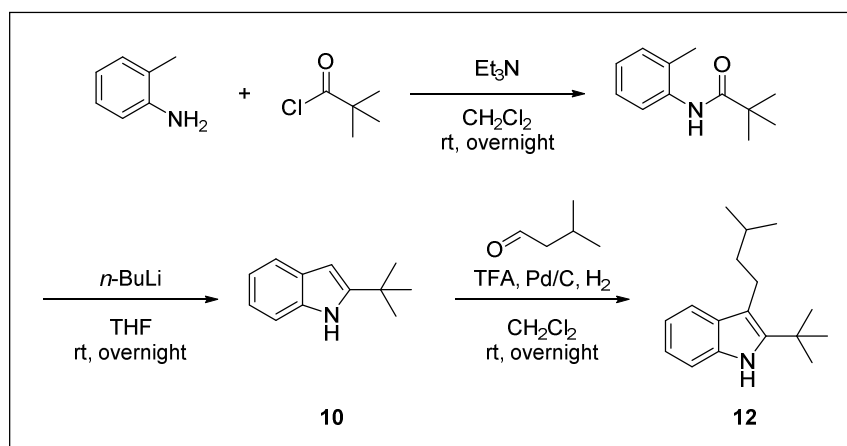
B.3 Computational methods and theoretical data

An overview of the computational methods used as well as the therefrom resulting theoretical data can be found in the electronic supporting information of the original manuscript (10.1039/C7SC00119C), on: www.rsc.org/suppdata/c7/sc/c7sc00119c/c7sc00119c1.pdf.

B.4 Synthetic procedures

B.4.1 Synthesis of indole model compounds

B.4.1.1 Synthesis of 2-*tert*-butyl-3-isopentyl-1*H*-indole (12)



Triethylamine (31.2 g, 0.308 mol, 1.1 eq.) was added to a solution of *o*-toluidine (30.0 g, 0.280 mol, 1.0 eq.) in 240 mL dichloromethane. The mixture was cooled in a water bath and trimethylacetyl chloride (37.9 mL, 0.308 mol, 1.1 eq.) was added dropwise. The resulting mixture was placed under inert atmosphere and stirred overnight. The resulting mixture was washed with 5 vol% aqueous hydrochloric acid solution (1 x 360 mL), saturated aqueous sodium bicarbonate solution (1 x 360 mL) and brine (1 x 360 mL). The organic phase was dried over magnesium sulfate and the solvent was removed *in vacuo* to give *N*-*o*-tolylpivalamide as an ivory white powder (52.4 – 98%).

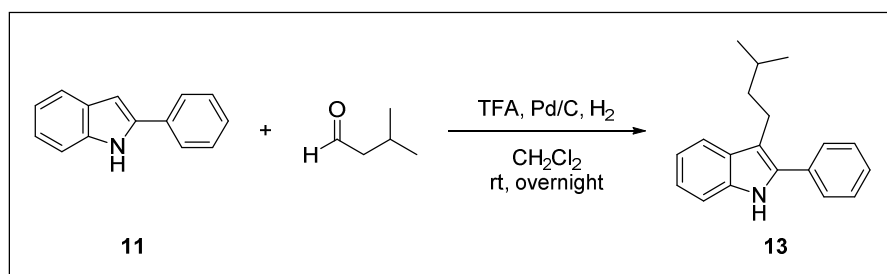
Next, a solution of *N*-*o*-tolylpivalamide (35.0 g, 0.183 mol, 1.0 eq.) in 120 mL anhydrous tetrahydrofuran was placed under inert atmosphere. After cooling in a water bath, a 2.5 M solution of *n*-butyllithium in hexane (220 mL, 0.55 mol, 3.0 eq.) was added dropwise and the resulting mixture was stirred at room temperature overnight. After cooling the mixture in an ice water bath, 340 mL of a saturated aqueous ammonium chloride solution was added slowly. The water phase was extracted with 340 mL ethyl acetate and the combined organic phases were dried over magnesium sulfate and concentrated *in vacuo* to give 2-*tert*-butyl-1*H*-indole as a brown solid (30.0 g – 95 %).

In a final step, a mixture of trifluoroacetic acid (2.30 mL, 30.0 mmol, 1.5 eq.) and palladium (5 % on activated carbon, 0.30 g) in 40 mL dichloromethane was placed under a hydrogen atmosphere and cooled in an ice water bath at 0 °C. To this, a solution of 2-*tert*-butyl-1*H*-indole (3.46 g, 20.0 mmol, 1 eq.) and 3-methylbutyraldehyde (1.90 g, 22.0 mmol, 1.1 eq.) in 60 mL dichloromethane was added dropwise and the resulting mixture was stirred overnight in a water bath. The setup was regularly flushed with hydrogen gas throughout the course of the reaction, which was monitored via thin layer chromatography (hexane:ethyl acetate 9:1). After complete

consumption of the indole substrate, the mixture was filtered over celite and washed with 100 mL of a saturated aqueous sodium bicarbonate solution. The organic phase was dried over magnesium sulfate and concentrated *in vacuo* to give 2-*tert*-butyl-3-isopentyl-1*H*-indole **12** as a brown oil (4.83 g – 99 %).

¹H-NMR (500 MHz, CDCl₃): δ (ppm) = 0.93 (d, 6H, CH-(CH₃)₂), 1.37 (s, 9H, C(CH₃)₃), 1.47 (m, 2H, *i*Pr-CH₂), 1.65 (m, 1H, CH-(CH₃)₂), 2.76 (m, 2H, C=C-CH₂), 7.00 (m, 2H, ArH), 7.18 (d, 1H, ArH), 7.42 (d, 1H, ArH), 7.70 (s, 1H, NH). **¹³C-NMR (125 MHz, CDCl₃):** δ (ppm) = 22.69 (CH₃), 23.43 (CH₂), 28.87 (CH), 30.59 (CH₃), 32.95 (C), 40.81 (CH₂), 110.33 (CH), 111.36 (C), 118.16 (CH), 118.94 (CH), 120.97 (CH), 129.83 (C), 134.07 (C), 141.6 (C). **HRMS (m/z):** *calc.*: 244.2060, *found*: 244.2067 [M+H]⁺.

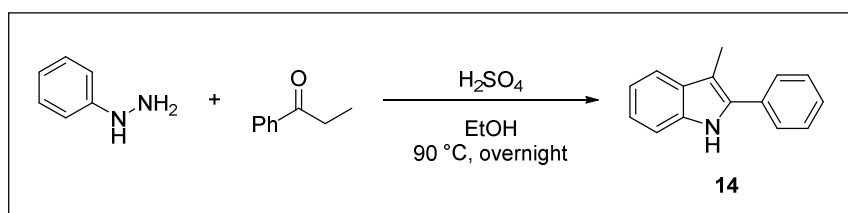
B.4.1.2 Synthesis of 3-isopentyl-2-phenyl-1*H*-indole (**13**)



A mixture of trifluoroacetic acid (0.60 mL, 7.76 mmol, 1.5 eq.) and palladium (5 % on activated carbon, 0.08 g) in 12 mL dichloromethane was placed under hydrogen atmosphere and stirred in an ice water bath at 0 °C. To this, a solution of 2-phenyl-1*H*-indole (1.00 g, 5.17 mmol, 1.0 eq.) and 3-methylbutyraldehyde (0.61 mL, 5.69 mmol, 1.1 eq.) in 18 mL dichloromethane was added dropwise. The resulting mixture was stirred vigorously in a water bath overnight, thereby regularly flushing the setup with hydrogen gas. The reaction was monitored by means of thin layer chromatography (heptane:ethyl acetate 9:1, R_F = 0.20) until completion. The reaction mixture was filtered over celite, washed with 30 mL saturated aqueous sodium bicarbonate solution and the organic phase was dried over magnesium sulfate. Solvent removal *in vacuo* gave 3-isopentyl-2-phenyl-1*H*-indole **13** as a brown oil (1.34 g – 96 %).

¹H-NMR (300 MHz, DMSO-*d*₆): δ (ppm) = 0.92 (d, 6H, CH₃), 1.55 (m, 2H, *i*Pr-CH₂), 1.62 (m, 1H, CH-(CH₃)₂), 2.84 (t, 2H, CH₂-CH₂-*i*Pr), 7.00 (t, 1H, ArH), 7.10 (t, 1H, ArH), 7.36 (m, 2H, ArH), 7.50 (m, 3H, ArH), 7.62 (m, 2H, CH₂-C=C-C=CH), 11.11 (s, 1H, NH). **LC-MS (m/z):** 264.2 [M+H]⁺. **HRMS (m/z):** *calc.*: 264.1747, *found*: 264.1735 [M+H]⁺.

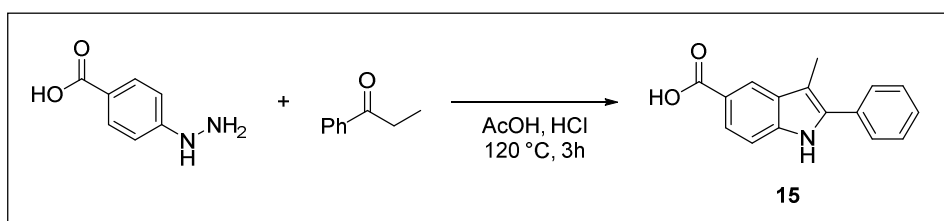
B.4.1.3 Synthesis of 3-methyl-2-phenyl-1*H*-indole (14)



A mixture of phenylhydrazine (14.1 mL, 0.143 mol, 1.1 eq.), propiophenone (17.3 mL, 0.130 mol, 1.0 eq.) and concentrated sulfuric acid (13.9 mL, 0.260 mol, 2.0 eq.) in 120 mL ethanol was placed under inert atmosphere and heated to reflux at 90 °C overnight. The reaction was monitored by means of thin layer chromatography (ethyl acetate:heptane 1:9, $R_F = 0.23$) until complete consumption of the starting ketone. The resulting mixture was cooled to room temperature and precipitated in a 10-fold excess of ice water. The formed precipitate was filtered off, dried in a vacuum oven to give a beige powder and recrystallized from water:ethanol 1:2 to yield 3-methyl-2-phenyl-1*H*-indole **14** as greenish needles (25.1 g – 93 %).

Melting point (°C): exp.: 92 - 93 °C, lit.⁴⁴⁹: 92 - 93 °C. **¹H-NMR (500 MHz, DMSO-*d*₆):** δ (ppm) = 2.41 (s, 3H, CH₃), 7.01 (t, 1H, NH-C-CH=CH-CH, $J = 6.8$ Hz), 7.11 (t, 1H, NH-C-CH=CH, $J = 7.5$ Hz), 7.35 (m, 2H, ArH), 7.51 (t, 3H, ArH, $J = 7.4$ Hz), 7.67 (dd, 2H, ArH, $J = 8.5$ Hz), 11.15 (s, 1H, NH). **¹³C-NMR (125 MHz, DMSO-*d*₆):** δ (ppm) = 9.82 (CH₃), 106.74 (C), 110.99 (CH), 118.39 (CH), 118.54 (CH), 121.52 (CH), 126.94 (CH), 127.46 (CH), 128.68 (CH), 129.36 (C), 133.06 (C), 133.71 (C), 135.90 (C). **LC-MS (m/z):** 208.1 [M+H]⁺. **HRMS (m/z):** calc.: 208.1121, found: 208.1113 [M+H]⁺.

B.4.1.4 Synthesis of 3-methyl-2-phenyl-1*H*-indole-5-carboxylic acid (15)

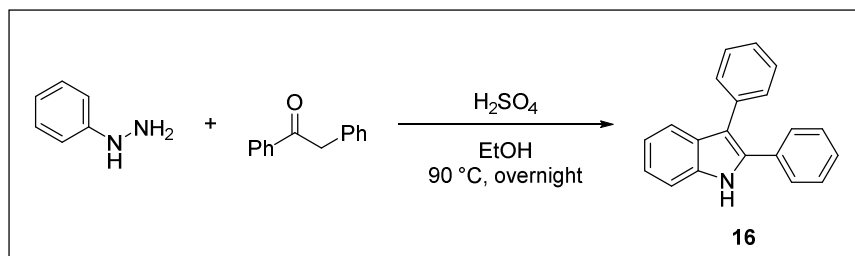


A mixture of 4-hydrazinobenzoic acid (1.00 g, 6.57 mmol, 1.0 eq.) and propiophenone (0.87 mL, 6.57 mmol, 1.0 eq.) in 50 mL concentrated acetic acid and 15 mL concentrated hydrochloric acid was refluxed at 120 °C for 3 hours until completion (monitored by thin layer chromatography, heptane:ethyl acetate 9:1, $R_F = 0.21$). The resulting mixture was cooled to room temperature and 60 mL of water was slowly added. The formed precipitate was filtered, thoroughly washed with water and dried in a vacuum oven overnight at 40 °C to give 3-methyl-2-phenyl-1*H*-indole-5-carboxylic acid **15** as a green powder (0.92 g – 56 %).

¹H-NMR (500 MHz, DMSO-*d*₆): δ (ppm) = 2.44 (s, 3H, CH₃), 7.35-7.43 (m, 2H, ArH), 7.53 (t, 2H, ArH), 7.65-7.71 (m, 2H, ArH), 7.74 (d, 1H, ArH), 8.21 (s, 1H, HOOC-C-CH-C),

11.54 (s, 1H, NH), 12.40 (s, 1H, COOH). $^{13}\text{C-NMR}$ (125 MHz, DMSO- d_6): δ (ppm) = 9.62 (CH₃), 108.06 (C), 110.70 (CH), 121.07 (CH), 121.13 (C), 122.85 (CH), 127.40 (CH), 127.62 (CH), 128.76 (CH), 128.88 (C), 132.45 (C), 135.27 (C), 138.38 (C), 168.37 (C). LC-MS (m/z): 252.1 [M+H]⁺.

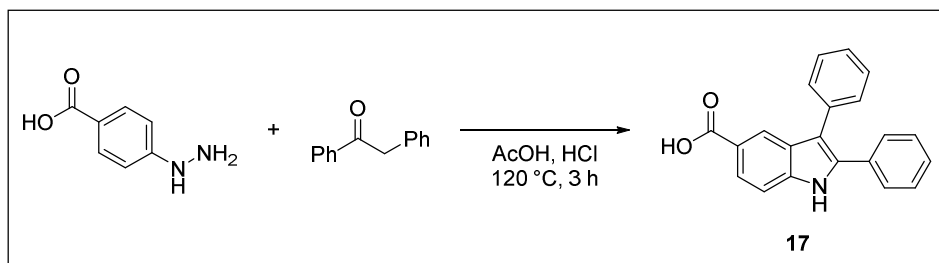
B.4.1.5 Synthesis of 2,3-diphenyl-1*H*-indole (16)



A mixture of phenylhydrazine (10.8 mL, 0.11 mol, 1.1 eq.), 2-phenylacetophenone (20.3 g, 0.10 mol, 1.0 eq.) and concentrated sulfuric acid (10.7 mL, 0.20 mol, 2.0 eq.) in 100 mL ethanol was placed under inert atmosphere and heated to reflux at 90 °C overnight. The reaction was monitored by means of thin layer chromatography (ethyl acetate:heptane 1:9, R_F = 0.30) until complete consumption of the starting ketone. The resulting mixture was cooled to room temperature and precipitated in a 10-fold excess of ice water (1 L). The precipitate was filtered off, dried in a vacuum oven at 40 °C and the resulting brown powder was recrystallized from water:ethanol 1:2 to give 2,3-diphenyl-1*H*-indole **16** as brown crystals (26.9 g – 99 %).

Melting point (°C): exp.: 123 - 124 °C, lit.⁴⁵⁰: 123 - 124 °C. $^1\text{H-NMR}$ (500 MHz, DMSO- d_6): δ (ppm) = 7.05 (m, 1H, NH-C-CH-CH-CH), 7.17 (m, 1H, NH-C-CH-CH), 7.25-7.32 (m, 2H, ArH), 7.32-7.43 (m, 6H, ArH), 7.44-7.52 (m, 4H, ArH), 11.57 (s, 1H, NH). $^{13}\text{C-NMR}$ (125 MHz, DMSO- d_6): δ (ppm) = 111.49 (CH), 113.28 (C), 118.56 (CH), 119.70 (CH), 121.99 (CH), 126.05 (CH), 127.50 (CH), 127.96 (C), 128.16 (CH), 128.48 (CH), 128.62 (CH), 129.75 (CH), 132.46 (C), 134.07 (C), 135.29 (C), 136.09 (C). LC-MS (m/z): 270.1 [M+H]⁺. HRMS (m/z): calc.: 270.1277, found: 270.1285 [M+H]⁺.

B.4.1.6 Synthesis of 2,3-diphenyl-1*H*-indole-5-carboxylic acid (17)

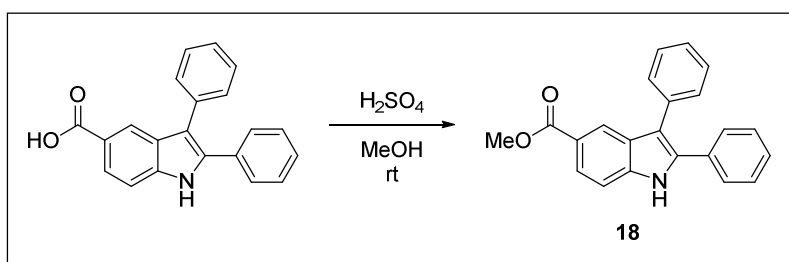


A mixture of 4-hydrazinobenzoic acid (3.00 g, 19.7 mmol, 1.0 eq.) and 2-phenylacetophenone (3.87 g, 19.7 mmol, 1.0 eq.) in 200 mL concentrated acetic acid and 60 mL concentrated hydrochloric acid was refluxed at 120 °C for 3 hours until completion (monitored by thin layer

chromatography, heptane:ethyl acetate 9:1, $R_F = 0.19$). The resulting mixture was cooled to room temperature and 250 mL of water was slowly added. The formed precipitate was filtered, thoroughly washed with water and dried in a vacuum oven overnight at 40 °C to give 2,3-diphenyl-1*H*-indole-5-carboxylic acid **17** as a brown powder (4.62 g – 75 %).

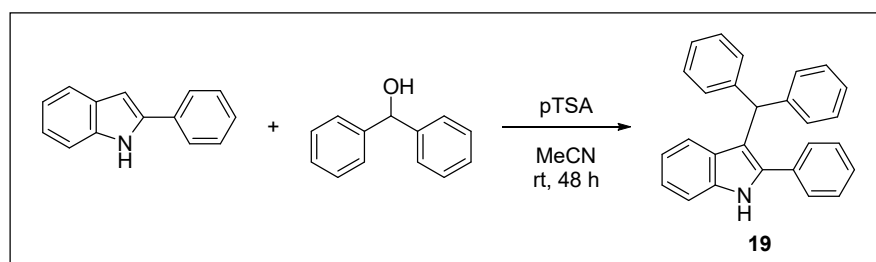
$^1\text{H-NMR}$ (500 MHz, DMSO- d_6): δ (ppm) = 7.28-7.54 (m, 11H, ArH), 7.80 (d, 1H, ArH), 8.13 (s, 1H, HOOC-C-CH-C), 11.94 (s, 1H, NH), 12.48 (s, 1H, COOH). **$^{13}\text{C-NMR}$ (125 MHz, DMSO- d_6):** δ (ppm) = 111.28 (CH), 114.41 (C), 121.28 (CH), 122.23 (C), 123.27 (CH), 126.53 (CH), 127.71 (C), 127.90 (CH), 128.18 (CH), 128.59 (CH), 128.81 (CH), 129.82 (CH), 131.88 (C), 134.61 (C), 135.54 (C), 138.54 (C), 168.23 (C). **LC-MS (m/z):** 312.0 [M-H]⁻.

B.4.1.7 Synthesis of methyl 2,3-diphenyl-1*H*-indole-5-carboxylate (**18**)



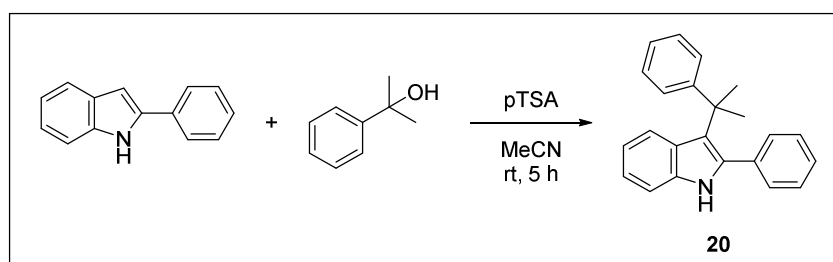
A mixture of 2,3-diphenyl-1*H*-indole-5-carboxylic acid (**17**, 0.300 g, 1.19 mmol) and 1 mL concentrated sulfuric acid in 10 mL anhydrous methanol was placed under inert atmosphere and stirred at room temperature until no starting compound was detected via thin layer chromatography (heptane:ethyl acetate 9:1, $R_F = 0.48$). The resulting mixture was extracted with 40 mL ethyl acetate and the organic phase was washed with saturated aqueous sodium bicarbonate solution (2 x 10 mL). Drying over magnesium sulfate, followed by solvent removal *in vacuo* gave methyl 2,3-diphenyl-1*H*-indole-5-carboxylate **18** (0.283 g – 90%).

$^1\text{H-NMR}$ (400 MHz, DMSO- d_6): δ (ppm) = 3.82 (s, 3H, CO-O- CH_3), 7.32-7.41 (m, 6H, ArH), 7.41-7.50 (m, 4H, ArH), 7.53 (d, 1H, ArH), 7.81 (dd, 1H, ArH), 8.13 (s, 1H, CO-C-CH-C), 11.99 (s, 1H, NH). **$^{13}\text{C-NMR}$ (100 MHz, DMSO- d_6):** δ (ppm) = 51.71 (CH_3), 111.50 (CH), 114.46 (C), 121.05 (CH), 121.12 (C), 122.97 (CH), 126.62 (CH), 127.72 (C), 127.97 (CH), 128.16 (CH), 128.59 (CH), 128.84 (CH), 129.81 (CH), 131.73 (C), 134.44 (C), 135.74 (C), 138.61 (C), 167.06 (C). **LC-MS (m/z):** 328.1 [M-H]⁻.

B.4.1.8 Synthesis of 3-benzhydryl-2-phenyl-1*H*-indole (**19**)

A solution of 2-phenyl-1*H*-indole (1.00 g, 5.17 mmol, 1.0 eq.), benzhydrol (1.43 g, 7.76 mmol, 1.5 eq.) and *p*-toluenesulfonic acid monohydrate (0.20 g, 1.04 mmol, 0.2 eq.) in 20 mL acetonitrile was placed under inert atmosphere and stirred at room temperature. After 48 hours, the reaction went to completion (monitored via TLC, heptane:ethyl acetate 9:1, $R_F = 0.23$). The resulting mixture was filtered off and washed with 10 mL acetonitrile. The filtrate was diluted with 80 mL ethyl acetate and washed with saturated aqueous sodium bicarbonate solution (2 x 10 mL). After drying over magnesium sulfate, the solvent was removed *in vacuo* to give an off-white residue, which was purified by means of crystallisation from water:ethanol 1:2 to give indole **19** as white crystals (1.51 g – 81%).

¹H-NMR (300 MHz, DMSO-*d*₆): δ (ppm) = 5.79 (s, 1H, Ar-CH-Ar), 6.77 (t, 1H, NH-C-CH=CH-CH), 6.91 (d, 1H, Ar*H*), 7.03 (t, 1H, NH-C-CH=CH), 7.08-7.33 (m, 10H, Ar*H*), 7.33-7.55 (m, 6H, Ar*H*), 11.39 (s, 1H, NH). ¹³C-NMR (75 MHz, DMSO-*d*₆): δ (ppm) = 47.30 (CH), 111.42 (CH), 113.37 (C), 118.75 (CH), 120.34 (CH), 121.10 (CH), 126.05 (CH), 127.55 (C), 127.77 (CH), 128.22 (CH), 128.37 (CH), 128.66 (CH), 128.72 (CH), 132.62 (C), 135.65 (C), 136.37 (C), 143.94 (C).

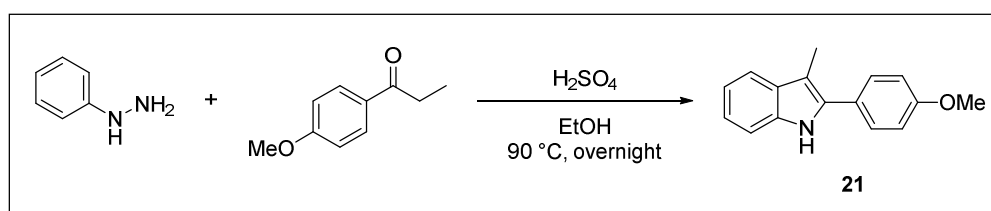
B.4.1.9 Synthesis of 2-phenyl-3-(2-phenylpropan-2-yl)-1*H*-indole (**20**)

A solution of 2-phenyl-1*H*-indole (1.00 g, 5.17 mmol, 1.0 eq.), 2-phenyl-2-propanol (1.06 g, 7.76 mmol, 1.5 eq.) and *p*-toluenesulfonic acid monohydrate (0.20 g, 1.04 mmol, 0.2 eq.) in 20 mL acetonitrile was placed under inert atmosphere and stirred at room temperature. After 5 hours, the reaction went to completion (monitored via TLC, heptane:ethyl acetate 9:1, $R_F = 0.26$). The resulting mixture was filtered off and washed with 10 mL acetonitrile. The filtrate was diluted with 80 mL ethyl acetate and washed with saturated aqueous sodium bicarbonate solution (2 x 10 mL). After drying over magnesium sulfate, the solvent was removed *in vacuo* to give a green

oil, which was purified by means of column chromatography (silica, heptane:ethyl acetate 9:1, $R_F = 0.26$) to give 2-phenyl-3-(2-phenylpropan-2-yl)-1*H*-indole **20** as a white solid (0.63 g – 39%).

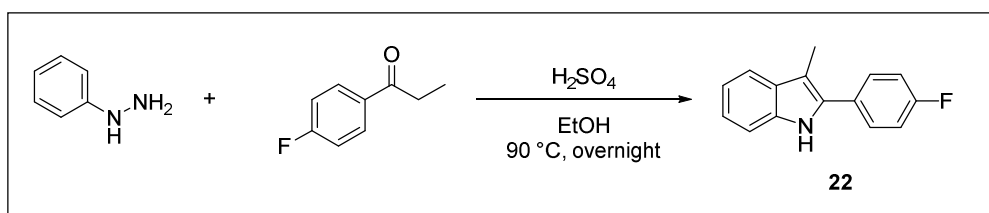
¹H-NMR (400 MHz, DMSO-*d*₆): δ (ppm) = 1.49 (s, 6H, *CH*₃), 6.69 (t, 1H, *ArH*), 6.78 (d, 1H, *ArH*), 6.95 (t, 1H, *ArH*), 7.11 (m, 1H, *ArH*), 7.23 (m, 3H, *ArH*), 7.33 (m, 2H, *ArH*), 7.41-7.48 (m, 3H, *ArH*), 7.50-7.56 (m, 2H, *ArH*), 10.96 (s, 1H, *NH*). **¹³C-NMR (100 MHz, DMSO-*d*₆):** δ (ppm) = 32.04 (*CH*₃), 40.15 (C), 110.77 (CH), 117.95 (CH), 119.20 (C), 120.52 (CH), 120.86 (CH), 125.22 (CH), 125.97 (CH), 126.81 (C), 127.51 (CH), 127.89 (CH), 128.03 (CH), 130.66 (CH), 134.83 (C), 135.67 (C), 136.08 (C), 151.41 (C). **LC-MS (m/z):** 312.1 [M+H]⁺. **HRMS (m/z):** *calc.*: 312.1747, *found*: 312.1728 [M+H]⁺.

B.4.1.10 Synthesis of 2-(4-methoxyphenyl)-3-methyl-1*H*-indole (**21**)



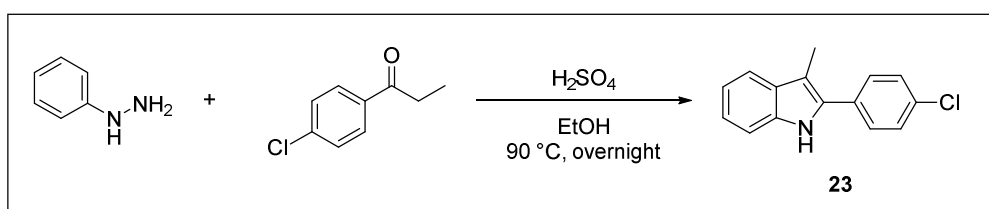
A mixture of phenylhydrazine (2.8 mL, 0.028 mol, 1.1 eq.), 4'-methoxypropiophenone (4.2 g, 0.026 mol, 1.0 eq.) and concentrated sulfuric acid (2.8 mL, 0.052 mol, 2.0 eq.) in 60 mL ethanol was placed under inert atmosphere and heated overnight to reflux at 90 °C, until complete consumption of the starting ketone was detected by thin layer chromatography (ethyl acetate:heptane 1:9, $R_F = 0.20$). The resulting mixture was cooled to room temperature and precipitated in a 10-fold excess of ice water (ca. 200 mL). The resulting precipitate was filtered off and dried in a vacuum oven overnight at 40 °C to give 2-(4-methoxyphenyl)-3-methyl-1*H*-indole **21** as a beige powder (5.27 g – 85 %).

¹H-NMR (500 MHz, DMSO-*d*₆): δ (ppm) = 2.38 (s, 3H, *CH*₃), 3.82 (s, 3H, O-*CH*₃), 6.99 (t, 1H, NH-C-CH-CH-*CH*, $J = 7.3$ Hz), 7.04-7.12 (m, 1H, NH-C-CH-CH – 2H, MeO-C-*CH*), 7.33 (d, 1H, NH-C-*CH*, $J = 8.1$ Hz), 7.49 (d, 1H, NH-C-C-*CH*, $J = 7.8$ Hz), 7.60 (d, 2H, MeO-C-CH-*CH*, $J = 8.7$ Hz), 11.04 (s, 1H, *NH*). **¹³C-NMR (125 MHz, DMSO-*d*₆):** δ (ppm) = 9.77 (*CH*₃), 55.18 (*CH*₃), 105.57 (C), 110.80 (CH), 114.17 (CH), 118.10 (CH), 118.43 (CH), 121.09 (CH), 125.56 (C), 128.75 (CH), 129.47 (C), 133.77 (C), 135.70 (C), 158.36 (C). **LC-MS (m/z):** 238.2 [M+H]⁺. **HRMS (m/z):** *calc.*: 239.1226, *found*: 238.1223 [M+H]⁺.

B.4.1.11 Synthesis of 2-(4-fluorophenyl)-3-methyl-1*H*-indole (22)

A mixture of phenylhydrazine (0.78 mL, 7.92 mmol, 1.1 eq.), 4'-fluoropropiophenone (1.00 mL, 7.20 mmol, 1.0 eq.) and concentrated sulfuric acid (0.77 mL, 14.40 mmol, 2.0 eq.) in 20 mL ethanol was placed under inert atmosphere and heated to reflux at 90 °C overnight, until complete consumption of the starting ketone was detected by thin layer chromatography (ethyl acetate:heptane 1:9, $R_F = 0.20$). The resulting orange mixture was cooled to room temperature and precipitated in a 10-fold excess of ice water. The precipitate was filtered off and dried in a vacuum oven overnight at 40 °C to give 2-(4-fluorophenyl)-3-methyl-1*H*-indole **22** as an off-white powder (1.37 g – 84 %).

¹H-NMR (500 MHz, DMSO-*d*₆): δ (ppm) = 2.39 (s, 3H, CH₃), 7.01 (m, 1H, ArH), 7.10 (m, 1H, ArH), 7.30-7.40 (m, 3H, ArH), 7.52 (d, 1H, ArH, $J = 7.9$ Hz), 7.64-7.74 (m, 2H, ArH), 11.16 (s, 1H, NH). **¹³C-NMR (125 MHz, DMSO-*d*₆):** δ (ppm) = 9.69 (CH₃), 106.68 (C), 110.97 (CH), 115.52 (CH), 115.69 (CH), 118.41 (CH), 118.60 (CH), 121.57 (CH), 129.29 (C), 129.43 (CH), 129.50 (CH), 132.81 (C), 135.85 (C), 160.25 (C), 162.19 (C). **LC-MS (m/z):** 224.1 [M-H]⁻. **HRMS (m/z):** *calc.*: 226.1027, *found*: 226.1020 [M+H]⁺.

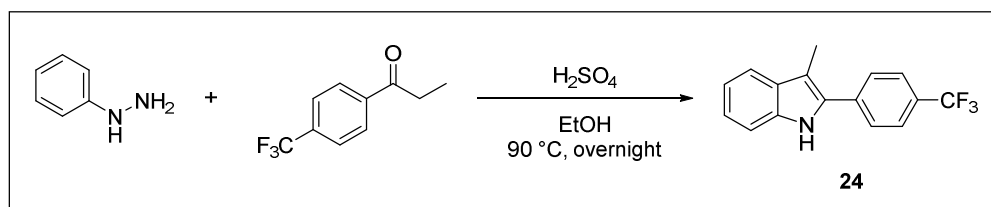
B.4.1.12 Synthesis of 2-(4-chlorophenyl)-3-methyl-1*H*-indole (23)

A mixture of phenylhydrazine (1.29 mL, 13.1 mmol, 1.1 eq.), 4'-chloropropiophenone (2.00 g, 11.9 mmol, 1.0 eq.) and concentrated sulfuric acid (1.26 mL, 23.7 mmol, 2.0 eq.) in 40 mL ethanol was placed under inert atmosphere and heated to reflux at 90 °C overnight, until complete consumption of the starting ketone was detected by thin layer chromatography (ethyl acetate:heptane 1:9, $R_F = 0.24$). The resulting mixture was cooled to room temperature and precipitated in 200 mL ice water. The resulting precipitate was filtered off and dried in a vacuum oven overnight at 40 °C to give 2-(4-chlorophenyl)-3-methyl-1*H*-indole **23** as an off-white powder (2.37 g – 83 %).

¹H-NMR (500 MHz, DMSO-*d*₆): δ (ppm) = 2.40 (s, 3H, CH₃), 7.02 (m, 1H, ArH), 7.12 (m, 1H, ArH), 7.36 (d, 1H, ArH, $J = 8.1$ Hz), 7.50-7.59 (m, 3H, ArH), 7.68 (m, 2H, ArH), 11.14 (s, 1H, NH). **¹³C-NMR (125 MHz, DMSO-*d*₆):** δ (ppm) = 9.69 (CH₃), 107.44 (C), 111.03

(CH), 118.47 (CH), 118.67 (CH), 121.81 (CH), 128.65 (CH), 129.02 (CH), 129.28 (C), 131.52 (C), 131.89 (C), 132.44 (C), 136.01 (C). **LC-MS (m/z):** 242.1 [M+H]⁺. **HRMS (m/z):** *calc.*: 242.0731, *found*: 242.0723 [M+H]⁺.

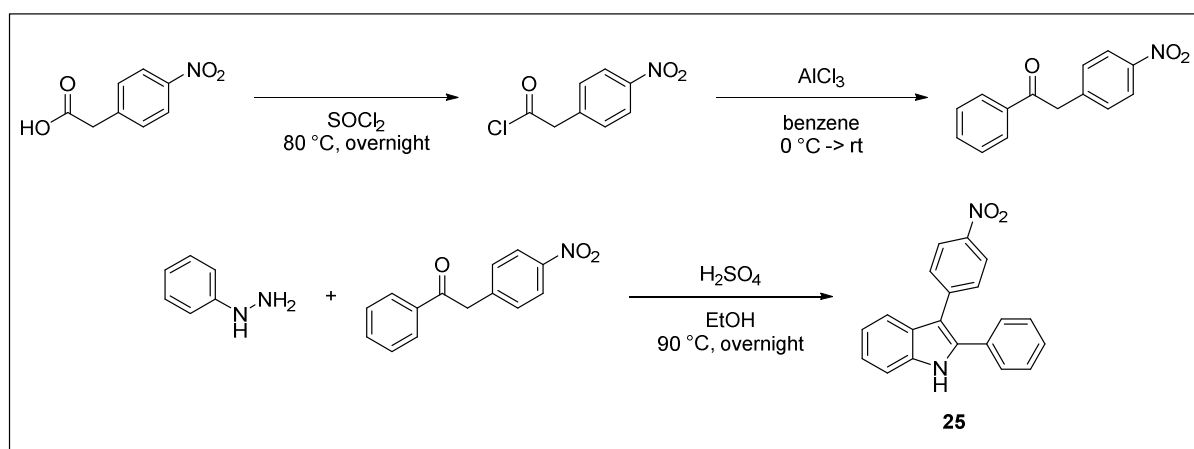
B.4.1.13 Synthesis of 3-methyl-2-(4-(trifluoromethyl)phenyl)-1*H*-indole (**24**)



A mixture of phenylhydrazine (0.40 mL, 4.08 mmol, 1.1 eq.), 4'-(trifluoromethyl)propiophenone (0.75 g, 3.71 mmol, 1.0 eq.) and concentrated sulfuric acid (0.40 mL, 7.42 mmol, 2.0 eq.) in 15 mL ethanol was placed under inert atmosphere and heated to reflux at 90 °C overnight, until complete consumption of the starting ketone was detected by thin layer chromatography (ethyl acetate:heptane 1:9, $R_F = 0.22$). The resulting orange mixture was cooled to room temperature and precipitated in a 10-fold excess of ice water (150 mL). The resulting precipitate was filtered off and dried in a vacuum oven overnight at 40 °C to give 3-methyl-2-(4-(trifluoromethyl)phenyl)-1*H*-indole **24** as an off-white powder (0.95 g – 93 %).

¹H-NMR (500 MHz, DMSO-*d*₆): δ (ppm) = 2.46 (s, 3H, CH₃), 7.04 (m, 1H, ArH), 7.15 (m, 1H, ArH), 7.39 (d, 1H, ArH, $J = 8.1$ Hz), 7.57 (d, 1H, ArH, $J = 7.9$ Hz), 7.88 (dd, 4H, ArH, $J = 18.2, 8.7$ Hz), 11.34 (s, 1H, NH). **¹³C-NMR (125 MHz, DMSO-*d*₆):** δ (ppm) = 9.91 (CH₃), 108.82 (C), 111.23 (CH), 118.83 (CH), 118.86 (CH), 122.36 (CH), 125.59 (q, CF₃), 126.89 (q, C-CF₃), 127.78 (CH), 129.23 (C), 132.00 (C), 136.25 (C), 137.00 (C). **LC-MS (m/z):** 274.0 [M-H]⁻. **HRMS (m/z):** *calc.*: 276.0995, *found*: 276.0985 [M+H]⁺.

B.4.1.14 Synthesis of 3-(4-nitrophenyl)-2-phenyl-1*H*-indole (**25**)



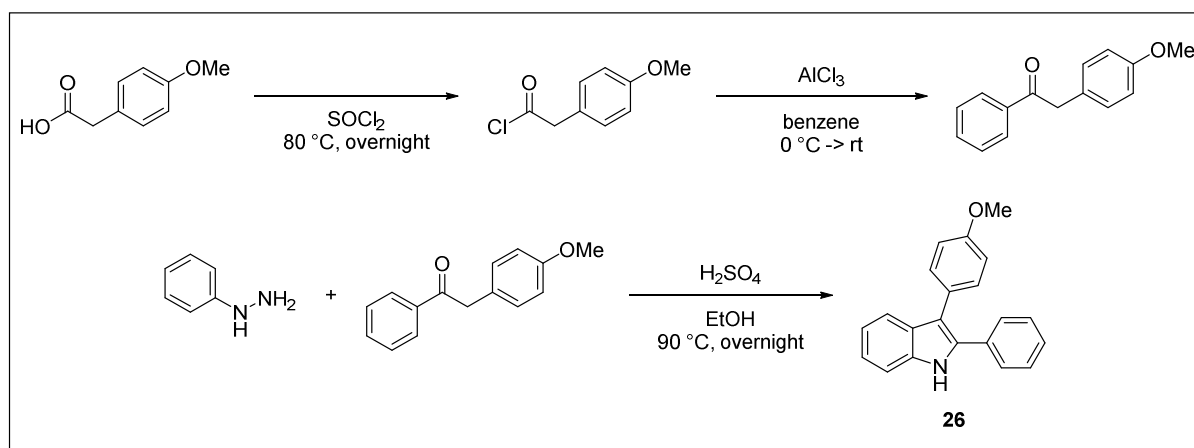
A mixture of 4-nitrophenylacetic acid (2.50 g, 13.8 mmol, 1.0 eq.) in 10 mL thionyl chloride was heated to reflux overnight (80 °C). The resulting yellow clear solution was evaporated *in vacuo* to give an orange oil. The corresponding acid chloride was dissolved in 5 mL anhydrous

benzene and added dropwise to a mixture of aluminium chloride (2.76 g, 20.7 mmol, 1.5 eq.) in 10 mL anhydrous benzene at 0 °C, which was precooled in an ice water bath and placed under inert atmosphere before the addition took place. After stirring for 30 minutes at 0 °C, followed by overnight stirring at room temperature, the mixture was poured into 100 mL ice water, which contained 3 mL of concentrated aqueous hydrochloric acid. After stirring for 1 h at room temperature, the resulting mixture was extracted with 100 mL dichloromethane. The aqueous phase was washed with dichloromethane (2 x 20 mL) and the combined organic phases were dried over magnesium sulfate. Solvent removal *in vacuo* gave the substituted acetophenone 2-(4-nitrophenyl)-1-phenylethan-1-one as an off-white powder (2.65 g – 80 %).

¹H-NMR (400 MHz, DMSO-*d*₆): δ (ppm) = 4.64 (s, 2H, CH₂), 7.53-7.60 (m, 4H, ArH), 7.68 (t, 1H, ArH, *J* = 7.3 Hz), 8.07 (d, 2H, ArH, *J* = 7.3 Hz), 8.20 (d, 2H, ArH, *J* = 9.0 Hz). **¹³C-NMR (100 MHz, DMSO-*d*₆):** δ (ppm) = 44.34 (CH₂), 123.18 (CH), 128.29 (CH), 128.80 (CH), 131.34 (CH), 133.50 (CH), 136.22 (C), 143.53 (C), 146.33 (C), 196.71 (C). **LC-MS (m/z):** 242.1 [M+H]⁺. **HRMS (m/z):** *calc.*: 240.0666, *found*: 240.0674 [M-H]⁻.

Next, a mixture of phenylhydrazine (0.30 mL, 3.0 mmol, 1.1 eq.), 2-(4-nitrophenyl)-1-phenylethan-1-one (0.65 g, 2.7 mmol, 1.0 eq.) and concentrated sulfuric acid (0.29 mL, 5.4 mmol, 2.0 eq.) in 10 mL ethanol was placed under inert atmosphere and heated to reflux at 90 °C overnight, until complete consumption of the starting ketone was detected by thin layer chromatography (ethyl acetate:heptane 1:9, R_F = 0.12). The resulting orange-red mixture was cooled to room temperature and precipitated in a 10-fold excess of ice water (100 mL). The resulting precipitate was filtered off and dried overnight in a vacuum oven to give 3-(4-nitrophenyl)-2-phenyl-1*H*-indole **25** as an orange powder (0.65 g – 76 %).

¹H-NMR (500 MHz, DMSO-*d*₆): δ (ppm) = 7.13 (m, 1H, ArH), 7.22 (m, 1H, ArH), 7.36-7.51 (m, 6H, ArH), 7.60 (d, 2H, ArH, *J* = 8.9 Hz), 7.63 (d, 1H, ArH, *J* = 7.9 Hz), 8.23 (d, 2H, ArH, *J* = 8.7 Hz), 11.88 (s, 1H, NH). **¹³C-NMR (125 MHz, DMSO-*d*₆):** δ (ppm) = 111.13 (C), 111.87 (CH), 118.31 (CH), 120.50 (CH), 122.51 (CH), 123.91 (CH), 127.04 (C), 128.29 (CH), 128.71 (CH), 128.84 (CH), 130.21 (CH), 131.76 (C), 136.27 (C), 143.02 (C), 145.04 (C). **LC-MS (m/z):** 315.2 [M+H]⁺. **HRMS (m/z):** *calc.*: 315.1128, *found*: 315.1142 [M+H]⁺.

B.4.1.15 Synthesis of 3-(4-methoxyphenyl)-2-phenyl-1*H*-indole (26)

A mixture of 4-methoxyphenylacetic acid (5.0 g, 30.1 mmol, 1.0 eq.) in 50 mL thionyl chloride was heated to reflux overnight at 80 °C. The resulting clear solution was evaporated *in vacuo* to give a brown oil. The corresponding acid chloride was dissolved in 10 mL anhydrous benzene and added dropwise to a mixture of aluminium chloride (8.0 g, 60.2 mmol, 2.0 eq.) in 20 mL anhydrous benzene at 0 °C, which was precooled in an ice water bath and placed under inert atmosphere before the addition took place. The reaction mixture turned dark red and was stirred for an additional 3 h at room temperature before poured into 400 mL ice water, which contained 10 mL of concentrated aqueous hydrochloric acid. After stirring for at room temperature 1 h, the organic phase was separated and the aqueous phase was washed with dichloromethane (3 x 50 mL). The combined organic phases were washed with saturated aqueous sodium bicarbonate solution (2 x 20 mL) and brine (1 x 20 mL) and dried over magnesium sulfate. Solvent removal *in vacuo* followed by recrystallisation from water:methanol 1:4 gave 2-(4-methoxyphenyl)-1-phenylethan-1-one as white crystals (5.72 g – 84 %).

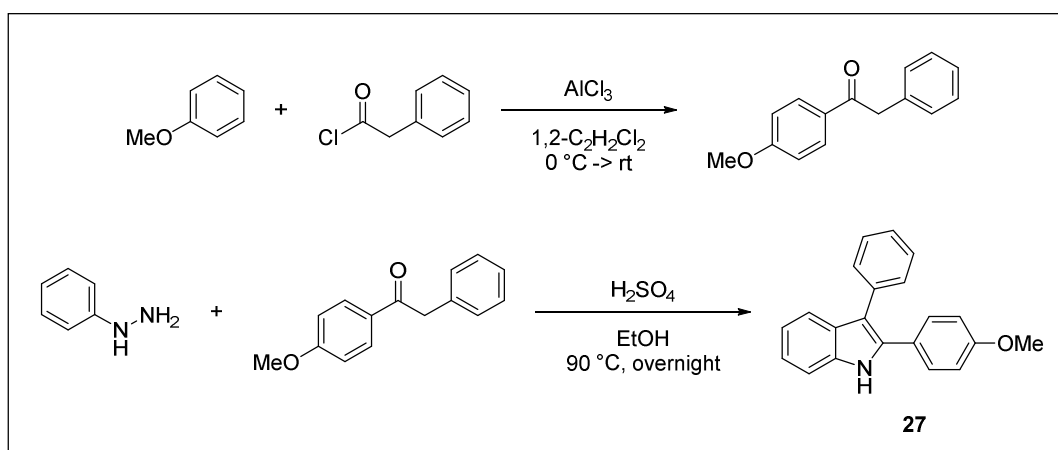
¹H-NMR (400 MHz, DMSO-*d*₆): δ (ppm) = 3.72 (s, 3H, OCH₃), 4.30 (s, 2H, CH₂), 6.87 (d, 2H, ArH, *J* = 8.6 Hz), 7.18 (d, 2H, ArH, *J* = 8.7 Hz), 7.52 (t, 2H, ArH, *J* = 7.6 Hz), 7.63 (t, 1H, ArH, *J* = 7.3 Hz), 8.04 (d, 2H, ArH, *J* = 7.7 Hz). **¹³C-NMR (100 MHz, DMSO-*d*₆):** δ (ppm) = 44.82 (CH₂), 54.97 (CH₃), 113.78 (CH), 128.38 (CH), 128.71 (CH), 128.86 (C), 130.62 (CH), 133.17 (CH), 136.31 (C), 157.93 (C), 197.92 (C). **LC-MS (m/z):** 227.1 [M+H]⁺. **HRMS (m/z):** *calc.*: 227.1067, *found*: 227.1059 [M+H]⁺.

Next, a mixture of phenylhydrazine (3.13 mL, 31.8 mmol, 1.2 eq.), 2-(4-methoxyphenyl)-1-phenylethan-1-one (6.00 g, 26.5 mmol, 1.0 eq.) and concentrated sulfuric acid (2.83 mL, 53.0 mmol, 2.0 eq.) in 90 mL ethanol was placed under inert atmosphere and heated to reflux at 90 °C, until complete consumption of the starting ketone was detected by thin layer chromatography (ethyl acetate:heptane 1:9, R_F = 0.23). After 5 days, the resulting mixture was cooled to room temperature and diluted with 110 mL ethyl acetate before being washed with aqueous saturated sodium bicarbonate solution (2 x 40 mL) and brine (2 x 40 mL). The organic

phase was dried over magnesium sulfate, evaporated *in vacuo* to give a brown oil and subsequently purified by means of column chromatography (silica, ethyl acetate:heptane 1:9, $R_F = 0.23$). Recrystallisation of the resulting residue from water:methanol gave 3-(4-methoxyphenyl)-2-phenyl-1*H*-indole **26** as bright yellow crystals (5.39 g – 68 %).

Melting point (°C): exp.: 186 – 188 °C, lit.⁴⁵¹: 185 – 188 °C. **¹H-NMR (500 MHz, DMSO-*d*₆):** δ (ppm) = 3.79 (s, 3H, O-CH₃), 6.97 (d, 2H, ArH, $J = 8.5$ Hz), 7.02 (t, 1H, ArH, $J = 7.9$ Hz), 7.15 (t, 1H, ArH, $J = 7.6$ Hz), 7.22-7.31 (m, 3H, ArH), 7.36 (t, 2H, ArH, $J = 7.6$ Hz), 7.41-7.48 (m, 4H, ArH), 11.47 (s, 1H, NH). **¹³C-NMR (125 MHz, DMSO-*d*₆):** δ (ppm) = 54.99 (CH₃), 111.38 (CH), 113.00 (C), 114.15 (CH), 118.58 (CH), 119.51 (CH), 121.87 (CH), 127.31 (C), 127.33 (CH), 127.96 (CH), 128.22 (C), 128.47 (CH), 130.81 (CH), 132.59 (C), 133.58 (C), 136.00 (C), 157.67 (C). **LC-MS (m/z):** 300.2 [M+H]⁺. **HRMS (m/z):** calc.: 300.1383, found: 300.1386 [M+H]⁺.

B.4.1.16 Synthesis of 2-(4-methoxyphenyl)-3-phenyl-1*H*-indole (**27**)



A mixture aluminium chloride (6.1 g, 45.4 mmol, 2.0 eq.) in 75 mL 1,2-dichloroethane was placed under inert atmosphere and cooled to $0\text{ }^\circ\text{C}$ in an ice water bath. To this, phenylacetyl chloride (3.0 mL, 22.7 mmol, 1.0 eq.) was added dropwise and the mixture was stirred for 30 minutes at $0\text{ }^\circ\text{C}$. Next, anhydrous anisole (2.7 mL, 25.0 mmol, 1.1 eq.) was added dropwise at $0\text{ }^\circ\text{C}$ and stirred for at $0\text{ }^\circ\text{C}$ for 30 minutes, followed by an additional 1.5 h at room temperature. The orange-brown reaction mixture was poured into 120 mL ice water, which contained 10 mL of concentrated aqueous hydrochloric acid, and stirred for 1 h at room temperature. The organic phase was separated and the aqueous phase was washed with 1,2-dichloroethane (3 x 45 mL). The combined organic phases were washed with water (1 x 60 mL) and 2 M aqueous sodium hydroxide solution (3 x 60 mL), followed by drying over magnesium sulfate. Solvent removal *in vacuo* and subsequent recrystallisation from water:methanol 1:1 gave 1-(4-methoxyphenyl)-2-phenylethan-1-one as white crystals (4.08 g – 79 %).

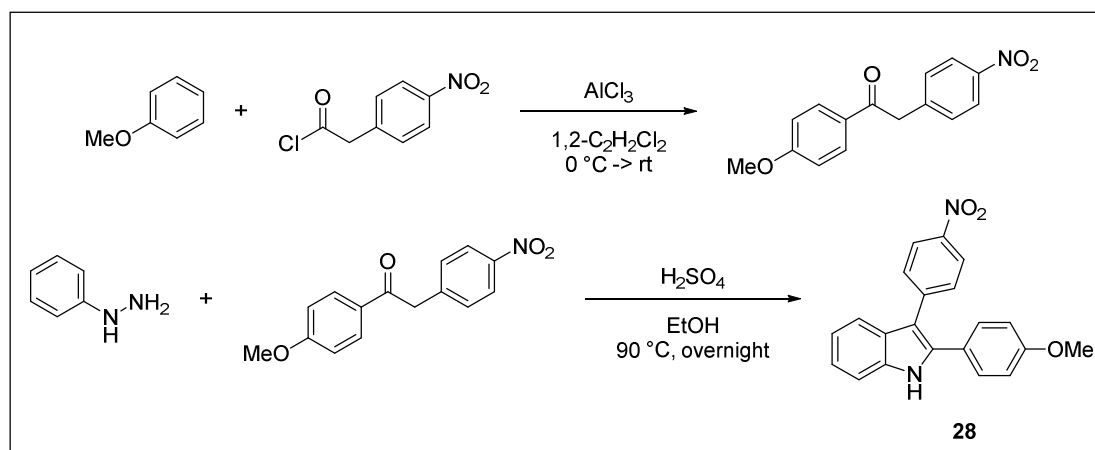
¹H-NMR (400 MHz, DMSO-*d*₆): δ (ppm) = 3.84 (s, 3H, OCH₃), 4.31 (s, 2H, CH₂), 7.04 (d, 2H, ArH, $J = 8.7$ Hz), 7.19-7.33 (m, 5H, ArH), 8.03 (d, 2H, ArH, $J = 9.6$ Hz). **¹³C-NMR**

(100 MHz, DMSO- d_6): δ (ppm) = 44.40 (CH₂), 55.52 (CH₃), 113.92 (CH), 126.38 (CH), 128.28 (CH), 129.20 (C), 129.56 (CH), 130.77 (CH), 135.47 (C), 163.16 (C), 196.04 (C). LC-MS (m/z): 227.1 [M+H]⁺. HRMS (m/z): *calc.*: 227.1067, *found*: 227.1069 [M+H]⁺.

Next, a mixture of phenylhydrazine (3.13 mL, 31.8 mmol, 1.2 eq.), 1-(4-methoxyphenyl)-2-phenylethan-1-one (6.00 g, 26.5 mmol, 1.0 eq.) and concentrated sulfuric acid (2.83 mL, 53.0 mmol, 2.0 eq.) in 90 mL ethanol was placed under inert atmosphere and heated to reflux at 90 °C, until complete consumption of the starting ketone was detected by thin layer chromatography (ethyl acetate:heptane 1:9, = R_F 0.23). After 5 days, the resulting mixture was cooled to room temperature and diluted with 110 mL ethyl acetate. The resulting mixture was washed with aqueous saturated sodium bicarbonate solution (2 x 40 mL) and brine (2 x 40 mL) and the organic phase was dried over magnesium sulfate. Solvent removal *in vacuo* gave a brown oil which was purified by means of column chromatography (silica, ethyl acetate:heptane 1:9, R_F = 0.23) to give 2-(4-methoxyphenyl)-3-phenyl-1*H*-indole **27** as a dark yellow powder (6.63 g – 84 %).

¹H-NMR (500 MHz, DMSO- d_6): δ (ppm) = 3.76 (s, 3H, O-CH₃), 6.94 (d, 2H, ArH, *J* = 8.7 Hz), 7.03 (t, 1H, ArH, *J* = 7.5 Hz), 7.14 (t, 1H, ArH, *J* = 7.6 Hz), 7.27 (t, 1H, ArH, *J* = 7.5 Hz), 7.32-7.41 (m, 6H, ArH), 7.43 (d, 1H, ArH, *J* = 8.1 Hz), 7.47 (d, 1H, ArH, *J* = 7.9 Hz), 11.46 (s, 1H, NH). ¹³C-NMR (125 MHz, DMSO- d_6): δ (ppm) = 55.11 (CH₃), 111.31 (CH), 112.30 (C), 113.99 (CH), 118.28 (CH), 119.57 (CH), 121.61 (CH), 124.78 (C), 125.89 (CH), 128.04 (C), 128.59 (CH), 129.43 (CH), 129.70 (CH), 134.14 (C), 135.50 (C), 135.93 (C), 158.74 (C). LC-MS (m/z): 300.2 [M+H]⁺. HRMS (m/z): *calc.*: 300.1383, *found*: 300.1383 [M+H]⁺.

B.4.1.17 Synthesis of 2-(4-methoxyphenyl)-3-(4-nitrophenyl)-1*H*-indole (**28**)



A mixture of 4-nitrophenylacetic acid (10.0 g, 0.055 mol, 1.0 eq.) in 90 mL thionyl chloride was heated to reflux overnight at 80 °C. The resulting yellow clear solution was evaporated *in vacuo* and an orange oil was collected. The corresponding acid chloride was dissolved in 20 mL 1,2-dichloroethane and added dropwise to a mixture of aluminium chloride (11.0 g, 0.083 mol, 1.5 eq.) in 100 mL 1,2-dichloroethane at 0 °C, which was precooled in an ice water bath and

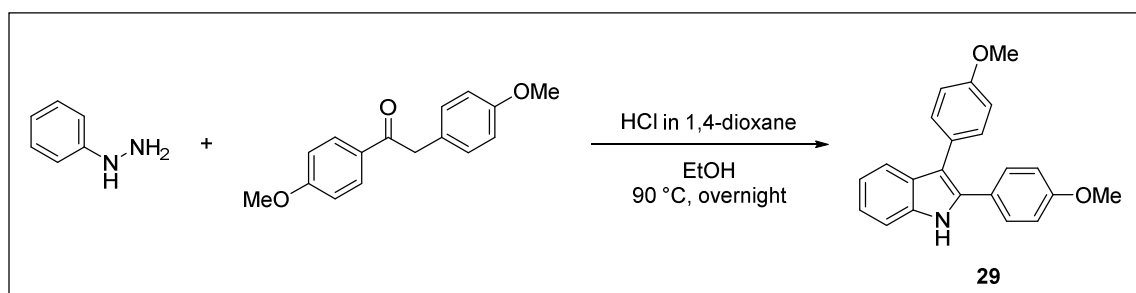
placed under inert atmosphere before the addition took place. After stirring for 30 minutes at 0 °C, anhydrous anisole (6.7 mL, 0.061 mol, 1.1 eq.) was added dropwise. The resulting dark red reaction mixture was stirred for 15 minutes at 0 °C, followed by overnight stirring at room temperature before being poured into 400 mL ice water, which contained 10 mL of concentrated aqueous hydrochloric acid. After stirring at room temperature for 1 h, the organic phase was separated and evaporated *in vacuo*. The obtained residue was dissolved in 250 mL ethyl acetate and washed with saturated aqueous sodium bicarbonate solution (2 x 25 mL) and brine (1 x 25 mL). The organic phase was dried over magnesium sulfate and evaporated *in vacuo* to give the substituted acetophenone 1-(4-methoxyphenyl)-2-(4-nitrophenyl)ethan-1-one as a yellow residue (13.7 g – 92 %).

¹H-NMR (500 MHz, DMSO-*d*₆): δ (ppm) = 3.85 (s, 3H, O-CH₃), 4.55 (s, 2H, CH₂), 7.07 (d, 2H, ArH, *J* = 9.0 Hz), 7.54 (d, 2H, ArH, *J* = 8.9 Hz), 8.04 (d, 2H, ArH, *J* = 9.3 Hz), 8.18 (d, 2H, ArH, *J* = 8.7 Hz). **¹³C-NMR (125 MHz, DMSO-*d*₆):** δ (ppm) = 44.02 (CH₃), 55.56 (CH₂), 113.97 (CH), 123.17 (CH), 129.10 (C), 130.70 (CH), 131.20 (CH), 143.85 (C), 146.27 (C), 163.38 (C), 195.02 (C). **LC-MS (m/z):** 272.1 [M+H]⁺. **HRMS (m/z):** *calc.*: 272.0917, *found*: 272.0911 [M+H]⁺.

Next, a mixture of phenylhydrazine (0.7 mL, 7.0 mmol, 1.2 eq.), 1-(4-methoxyphenyl)-2-(4-nitrophenyl)ethan-1-one (1.59 g, 5.86 mmol, 1.0 eq.) and concentrated sulfuric acid (0.6 mL, 11.7 mmol, 2.0 eq.) in 5 mL ethanol was placed under inert atmosphere and heated to reflux at 90 °C, until complete consumption of the starting ketone was detected by thin layer chromatography (ethyl acetate:heptane 1:9, R_F = 0.17). After 4 days, the resulting mixture was cooled to room temperature and diluted with 20 mL ethyl acetate before being washed with aqueous saturated sodium bicarbonate solution (2 x 2 mL) and brine (2 x 2 mL). The organic phase was dried over magnesium sulfate and evaporated *in vacuo*. Purification by means of column chromatography (silica, ethyl acetate:heptane 1:4, R_F = 0.17) gave 2-(4-methoxyphenyl)-3-(4-nitrophenyl)-1*H*-indole **28** as a dark red powder (1.26 g – 62 %).

¹H-NMR (500 MHz, DMSO-*d*₆): δ (ppm) = 3.79 (s, 3H, O-CH₃), 7.00 (d, 2H, ArH, *J* = 8.7 Hz), 7.11 (t, 1H, ArH, *J* = 8.1 Hz), 7.20 (t, 1H, ArH, *J* = 7.8 Hz), 7.39 (d, 2H, ArH, *J* = 8.7 Hz), 7.47 (d, 1H, ArH, *J* = 8.7 Hz), 7.56-7.65 (m, 3H, ArH), 8.23 (d, 2H, ArH, *J* = 8.7 Hz), 11.78 (s, 1H, NH). **¹³C-NMR (125 MHz, DMSO-*d*₆):** δ (ppm) = 55.20 (CH₃), 110.31 (C), 111.72 (CH), 114.33 (CH), 118.07 (CH), 120.39 (CH), 122.20 (CH), 123.91 (CH), 123.97 (C), 127.11 (C), 130.03 (CH), 130.08 (CH), 136.16 (C), 136.44 (C), 143.33 (C), 144.85 (C), 159.31 (C). **LC-MS (m/z):** 345.1 [M+H]⁺. **HRMS (m/z):** *calc.*: 345.1234, *found*: 345.1230 [M+H]⁺.

B.4.1.18 Synthesis of 2,3-bis(4-methoxyphenyl)-1*H*-indole (**29**)

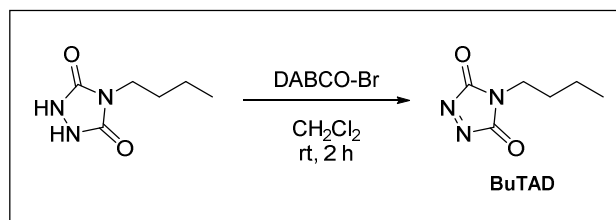


A mixture of phenylhydrazine (5.6 mL, 56.2 mmol, 1.2 eq.), 1,2-bis(4-methoxyphenyl)ethanone (12.0 g, 46.8 mmol, 1.0 eq.), 24 mL hydrochloric acid in 1,4-dioxane (4 N) and 96 mL anhydrous ethanol was placed under inert atmosphere and heated to reflux at 90 °C for 24 h, until complete consumption of the starting ketone was detected by thin layer chromatography (ethyl acetate:heptane 1:7, $R_F = 0.17$). The resulting mixture was cooled to room temperature and diluted with 80 mL ethyl acetate before being washed with aqueous saturated sodium bicarbonate solution (2 x 15 mL) and brine (2 x 15 mL). The organic phase was dried over magnesium sulfate and evaporated *in vacuo* to give a brown oil, which was purified by means of column chromatography (silica, ethyl acetate:heptane 1:7 with a gradient to 1:4, $R_F = 0.24$ (ethyl acetate:heptane 1:4)) to give 2,3-bis(4-methoxyphenyl)-1*H*-indole **29** as a yellow powder (11.3 g – 73 %).

¹H-NMR (500 MHz, DMSO-*d*₆): δ (ppm) = 3.76 (s, 3H, O-CH₃), 3.79 (s, 3H, O-CH₃), 6.92-7.03 (m, 5H, ArH), 7.12 (m, 1H, ArH), 7.25 (d, 2H, ArH, $J = 8.7$ Hz), 7.36-7.44 (m, 4H, ArH), 11.36 (s, 1H, NH). ¹³C-NMR (125 MHz, DMSO-*d*₆): δ (ppm) = 54.97 (CH₃), 55.11 (CH₃), 111.20 (CH), 112.00 (C), 113.98 (CH), 114.12 (CH), 118.30 (CH), 119.38 (CH), 121.49 (CH), 124.95 (C), 127.54 (C), 128.32 (C), 129.23 (CH), 130.77 (CH), 133.65 (C), 135.83 (C), 157.55 (C), 158.61 (C). LC-MS (m/z): 330.2 [M+H]⁺. HRMS (m/z): *calc.*: 330.1489, *found*: 330.1488 [M+H]⁺.

B.4.2 Synthesis of triazolinedione model reagents

B.4.2.1 Synthesis of 4-*n*-butyl-1,2,4-triazoline-3,5-dione (BuTAD)

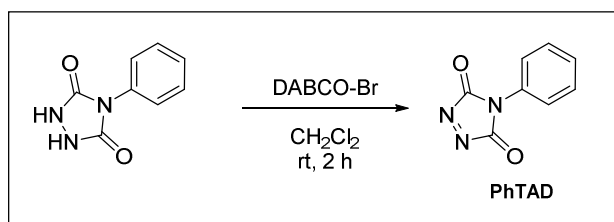


A mixture of 4-*n*-butyl-1,2,4-triazolidine-3,5-dione⁷ (2.0 g, 12.7 mmol, 1.0 eq.) and DABCO-Br⁴⁴⁶ (4.0 g, 2.54 mmol, 0.2 eq.) in 60 mL dichloromethane was placed under inert atmosphere and stirred at room temperature in the dark for 2 h. The resulting mixture was filtered, washed with 2 x 60 mL dichloromethane and evaporated *in vacuo* to dryness, thereby keeping the

temperature below 35 °C. The resulting carmine red crystals (1.41 g – 72 %) were stored in the dark at -18 °C and regularly checked for purity prior to use.

¹H-NMR (400 MHz, DMSO-*d*₆): δ (ppm) = 0.88 (t, 3H, CH₃, *J* = 7.3 Hz), 1.30 (sext, 2H, CH₂-CH₃, *J* = 7.3 Hz), 1.56 (quint, 2H, N-CH₂-CH₂, *J* = 7.3 Hz), 3.47 (t, 2H, N-CH₂, *J* = 7.0 Hz). **¹³C-NMR (100 MHz, DMSO-*d*₆):** δ (ppm) = 13.32 (CH₃), 19.11 (CH₂), 28.72 (CH₂), 40.34 (CH₂), 160.15 (C).

B.4.2.2 Synthesis of 4-phenyl-1,2,4-triazoline-3,5-dione (PhTAD)



A mixture of 4-phenyl-1,2,4-triazolidine-3,5-dione¹³ (2.00 g, 11.3 mmol, 1.0 eq.) and DABCO-Br⁴⁴⁶ (3.56 g, 2.26 mmol, 0.2 eq.) in 60 mL dichloromethane was placed under inert atmosphere and stirred in the dark at room temperature for 2 h. The resulting mixture was filtered, washed with 2 x 60 mL dichloromethane and evaporated *in vacuo* to dryness, thereby keeping the temperature below 35 °C. The resulting carmine red crystals (1.41 g – 71 %) were stored in the dark at -18 °C and regularly checked for purity prior to use.

¹H-NMR (400 MHz, DMSO-*d*₆): δ (ppm) = 7.42-7.46 (m, 2H, ArH), 7.49-7.55 (m, 1H, ArH), 7.57-7.63 (m, 2H, ArH).

B.4.3 Synthesis of model TAD-indole adducts

General procedure for the synthesis of BuTAD-indole adducts

4-*n*-butyl-1,2,4-triazoline-3,5-dione (BuTAD, 150 mg, 1.0 eq., 0.97 mmol) in 2.5 mL dichloromethane was added to a solution of the respective indole (1.0 eq., 0.97 mmol) in 2.5 mL dichloromethane at room temperature. The resulting mixture was stirred until the red purple colour disappeared (*cf.* Table III.2 and Table III.4 for indicative reaction times). Subsequently, a slight excess of BuTAD in dichloromethane was added until a faint purple colour persisted, in order to ensure complete reaction of the indole. Solvent removal *in vacuo* at room temperature gave the respective pure TAD-indole addition products in quantitative yield.

BuTAD-[2-*tert*-butyl-3-isopentyl-1H-indole] adduct (***BuTAD-12***).

As a pale brown powder. **¹H-NMR (300 MHz, DMSO-*d*₆):** δ (ppm) = 0.73 (m, 6H, CH(CH₃)₂ + CH₃-CH₂), 0.89 (m, 2H, CH₂-CH₃), 1.03 (m, 2H, N-CH₂-CH₂), 1.32 (s, 9H, C(CH₃)₃), 1.71 (dd, 3H, CH₂-CH(CH₃)₂), 2.29 (m, 2H, NH-N-C-CH₂), 3.24 (t, 2H, N-CH₂), 6.75-7.50 (m, 4H, ArH), 10.62 (s, 1H, NH).

BuTAD-[3-isopentyl-2-phenyl-1H-indole] adduct (BuTAD-13).

As a brown powder. **¹H-NMR (300 MHz, DMSO-*d*₆):** δ (ppm) = 0.65 (t, 3H, CH₃-CH₂-CH₂-CH₂), 0.78 (sext, 2H, CH₃-CH₂-CH₂-CH₂), 0.92 (d, 6H, (CH₃)₂-CH), 1.25 (quin, 2H, CH₃-CH₂-CH₂-CH₂), 1.55 (m, 2H, *i*Pr-CH₂), 1.70 (m, 1H, CH-(CH₃)₂), 1.84 (t, 2H, *i*Pr-CH₂-CH₂), 3.28 (t, 2H, N-CH₂), 7.20-7.45 (m, 7H, ArH), 8.11 (d, 2H, ArH), 10.50 (s, 1H, NH).

BuTAD-[3-methyl-2-phenyl-1H-indole] adduct (BuTAD-14).

As a white powder. **¹H-NMR (400 MHz, DMSO-*d*₆):** δ (ppm) = 0.69 (t, 3H, CH₂-CH₃, *J* = 7.3 Hz), 0.93 (m, 2H, CH₂-CH₃), 1.27 (m, 2H, N-CH₂-CH₂), 1.73 (s, 3H, C-CH₃), 3.20 (t, 2H, N-CH₂, *J* = 6.8 Hz), 7.25 (t, 1H, ArH, *J* = 7.5 Hz), 7.38-7.46 (m, 2H, ArH), 7.50-7.62 (m, 4H, ArH), 8.16-8.23 (m, 2H, ArH), 10.73 (s, 1H, NH). **¹³C-NMR (100 MHz, DMSO-*d*₆):** δ (ppm) = 13.22 (CH₃), 18.77 (CH₂), 22.81 (CH₃), 28.97 (CH₂), 37.93 (CH₂), 72.33 (C), 120.88 (CH), 121.16 (CH), 126.44 (CH), 127.94 (CH), 128.67 (CH), 129.53 (CH), 131.18 (CH), 131.58 (C), 139.44 (C), 152.77 (C), 154.66 (C), 154.93 (C), 176.04 (C). **LC-MS (m/z):** 361.2 [M-H]⁻. **HRMS (m/z):** *calc.*: 363.1816, *found*: 363.1826 [M+H]⁺.

BuTAD-[3-methyl-2-phenyl-1H-indole-5-carboxylic acid] adduct (BuTAD-15).

As a greenish white powder. **¹H-NMR (300 MHz, DMSO-*d*₆):** δ (ppm) = 0.68 (t, 3H, CH₂-CH₃), 0.90 (m, 2H, CH₂-CH₃), 1.23 (m, 2H, N-CH₂-CH₂), 1.68 (s, 3H, C-CH₃), 3.20 (t, 2H, N-CH₂), 7.11-7.62 (m, 6H, ArH), 8.20 (d, 2H, ArH), 10.60 (s, 1H, NH), 12.49 (s, 1H, COOH).

BuTAD-[2,3-diphenyl-1H-indole] adduct (BuTAD-16).

As a pale brown powder. **¹H-NMR (500 MHz, DMSO-*d*₆):** δ (ppm) = 0.67 (t, 3H, CH₂-CH₃, *J* = 7.0 Hz), 0.85 (m, 2H, CH₂-CH₃), 1.25 (m, 2H, N-CH₂-CH₂), 3.25 (m, 2H, N-CH₂), 7.13-7.19 (m, 2H, ArH), 7.19-7.25 (m, 3H, ArH), 7.28 (m, 1H, ArH), 7.34-7.45 (m, 4H, ArH), 7.50 (t, 1H, ArH, *J* = 7.6 Hz), 7.67 (m, 1H, ArH), 8.07 (m, 2H, ArH), 10.37 (s, 1H, NH). **¹³C-NMR (125 MHz, DMSO-*d*₆):** δ (ppm) = 13.29 (CH₃), 18.63 (CH₂), 28.89 (CH₂), 38.13 (CH₂), 81.35 (C), 120.97 (CH), 123.38 (CH), 126.79 (CH), 128.07 (CH), 128.26 (CH), 128.64 (CH), 128.73 (CH), 130.23 (CH), 130.73 (CH), 132.28 (C), 135.03 (C), 139.03 (C), 154.59 (C), 154.86 (C), 156.53 (C), 176.19 (C). **LC-MS (m/z):** 425.2 [M+H]⁺. **HRMS (m/z):** *calc.*: 425.1972, *found*: 425.1970 [M+H]⁺.

BuTAD-[2,3-diphenyl-1H-indole-5-carboxylic acid] adduct (BuTAD-17).

As a brown powder. **¹H-NMR (300 MHz, DMSO-*d*₆):** δ (ppm) = 0.67 (t, 3H, CH₂-CH₃), 0.78 (m, 2H, CH₂-CH₃), 1.27 (m, 2H, N-CH₂-CH₂), 3.21 (m, 2H, N-CH₂), 7.09-7.52 (m, 11H, ArH), 8.08 (m, 2H, ArH), 10.32 (s, 1H, NH), 12.19 (s, 1H, COOH).

BuTAD-[methyl 2,3-diphenyl-1H-indole-5-carboxylate] adduct (BuTAD-18).

As a brown powder. **¹H-NMR (300 MHz, DMSO-*d*₆):** δ (ppm) = 0.67 (t, 3H, CH₂-CH₃), 0.78 (m, 2H, CH₂-CH₃), 1.27 (m, 2H, N-CH₂-CH₂), 3.21 (m, 2H, N-CH₂), 3.80 (s, 3H, CH₃-OOC), 7.09-7.52 (m, 11H, ArH), 8.08 (m, 2H, ArH), 10.32 (s, 1H, NH).

BuTAD-[2-(4-methoxyphenyl)-3-methyl-1H-indole] adduct (BuTAD-21).

As a yellow powder. **¹H-NMR (400 MHz, DMSO-*d*₆):** δ (ppm) = 0.69 (t, 3H, CH₂-CH₃, $J = 7.3$ Hz), 0.95 (m, 2H, CH₂-CH₃), 1.27 (m, 2H, N-CH₂-CH₂), 1.71 (s, 3H, C-CH₃), 3.20 (t, 2H, N-CH₂, $J = 6.8$ Hz), 3.84 (s, 3H, O-CH₃), 7.08 (d, 2H, ArH, $J = 9.2$ Hz), 7.20 (m, 1H, ArH), 7.35-7.44 (m, 2H, ArH), 7.53 (d, 1H, ArH, $J = 7.6$ Hz), 8.14 (d, 2H, ArH, $J = 8.8$ Hz), 10.70 (s, 1H, NH). **¹³C-NMR (100 MHz, DMSO-*d*₆):** δ (ppm) = 13.23 (CH₃), 18.80 (CH₂), 23.10 (CH₃), 29.00 (CH₂), 37.92 (CH₂), 55.40 (CH₃), 72.17 (C), 114.12 (CH), 120.41 (CH), 121.04 (CH), 124.22 (C), 125.85 (CH), 129.43 (CH), 129.80 (CH), 139.36 (CH), 153.05 (C), 154.56 (C), 154.91 (C), 161.63 (C), 175.62 (C). **LC-MS (m/z):** 391.2 [M-H]⁻. **HRMS (m/z):** *calc.*: 393.1921, *found*: 393.1934 [M+H]⁺.

BuTAD-[2-(4-fluorophenyl)-3-methyl-1H-indole] adduct (BuTAD-22).

As an off-white powder. **¹H-NMR (500 MHz, DMSO-*d*₆):** δ (ppm) = 0.68 (t, 3H, CH₂-CH₃, $J = 7.4$ Hz), 0.94 (m, 2H, CH₂-CH₃), 1.27 (m, 2H, N-CH₂-CH₂), 1.72 (s, 3H, CH₃), 3.20 (t, 2H, N-CH₂-CH₂, 6.9 Hz), 7.25 (t, 1H, ArH, $J = 7.9$ Hz), 7.34-7.47 (m, 4H, ArH), 7.58 (d, 1H, ArH, $J = 7.6$ Hz), 8.25 (m, 2H, ArH), 10.72 (s, 1H, NH). **¹³C-NMR (125 MHz, DMSO-*d*₆):** δ (ppm) = 13.21 (CH₃), 18.76 (CH₂), 22.72 (CH₃), 28.96 (CH₂), 37.95 (CH₂), 72.35 (C), 115.72 (CH), 115.89 (CH), 120.87 (CH), 121.21 (CH), 126.47 (CH), 129.58 (CH), 130.42 (CH), 130.49 (CH), 139.24 (C), 152.71 (C), 154.81 (C), 154.92 (C), 162.81 (C), 164.80 (C), 175.01 (C). **LC-MS (m/z):** 381.2 [M+H]⁺. **HRMS (m/z):** *calc.*: 381.1721, *found*: 381.1726 [M+H]⁺.

BuTAD-[2-(4-chlorophenyl)-3-methyl-1H-indole] adduct (BuTAD-23).

As an off-white powder. **¹H-NMR (500 MHz, DMSO-*d*₆):** δ (ppm) = 0.68 (t, 3H, CH₂-CH₃, $J = 7.3$ Hz), 0.93 (m, 2H, CH₂-CH₃), 1.27 (m, 2H, N-CH₂-CH₂), 1.72 (s, 3H, CH₃), 3.20 (t, 2H, N-CH₂-CH₂, 6.7 Hz), 7.26 (t, 1H, ArH, $J = 7.6$ Hz), 7.38-7.49 (m, 2H, ArH), 7.56-7.65 (m, 3H, ArH), 8.20 (d, 2H, ArH, $J = 8.7$ Hz), 10.73 (s, 1H, NH). **¹³C-NMR (125 MHz, DMSO-*d*₆):** δ (ppm) = 13.21 (CH₃), 18.77 (CH₂), 22.60 (CH₃), 28.96 (CH₂), 37.96 (CH₂), 72.37 (C), 121.03 (CH), 121.27 (CH), 126.68 (CH), 128.85 (CH), 129.65 (CH), 130.41 (C), 135.99 (C), 139.26 (C), 152.62 (C), 154.88 (C), 175.04 (C). **LC-MS (m/z):** 397.1 [M+H]⁺. **HRMS (m/z):** *calc.*: 397.1426, *found*: 397.1438 [M+H]⁺.

BuTAD-[3-methyl-2-(4-(trifluoromethyl)phenyl)-1H-indole] adduct (BuTAD-24).

As an off-white powder. **¹H-NMR (500 MHz, DMSO-*d*₆):** δ (ppm) = 0.67 (t, 3H, CH₂-CH₃, $J = 7.6$ Hz), 0.92 (m, 2H, CH₂-CH₃), 1.26 (m, 2H, N-CH₂-CH₂), 1.75 (s, 3H, CH₃), 3.20 (t,

2H, N-CH₂-CH₂, 6.8 Hz), 7.30 (t, 1H, ArH, *J* = 7.6 Hz), 7.42-7.51 (m, 2H, ArH), 7.65 (d, 1H, ArH, *J* = 7.6 Hz), 7.91 (d, 2H, ArH, *J* = 8.4 Hz), 8.39 (d, 2H, ArH, *J* = 8.2 Hz), 10.79 (s, 1H, NH). **¹³C-NMR (125 MHz, DMSO-*d*₆):** δ (ppm) = 13.18 (CH₃), 18.74 (CH₂), 22.36 (CH₃), 28.94 (CH₂), 37.98 (CH₂), 72.49 (C), 121.40 (CH), 125.66 (CH), 127.15 (CH), 128.59 (CH), 129.75 (CH), 135.24 (C), 139.27 (C), 152.44 (C), 154.86 (C), 174.83 (C). **LC-MS (m/z):** 431.1 [M+H]⁺. **HRMS (m/z):** *calc.*: 431.1689, *found*: 431.1689 [M+H]⁺.

BuTAD-[3-(4-nitrophenyl)-2-phenyl-1H-indole] adduct (***BuTAD-25***).

As a yellow brown powder. **¹H-NMR (400 MHz, DMSO-*d*₆):** δ (ppm) = 0.68 (t, 3H, CH₂-CH₃, *J* = 7.2 Hz), 0.87 (m, 2H, CH₂-CH₃), 1.28 (m, 2H, N-CH₂-CH₂), 3.29 (m, 2H, N-CH₂), 7.32 (m, 1H, ArH), 7.36-7.50 (m, 6H, ArH), 7.55 (m, 1H, ArH), 7.73 (d, 1H, ArH, *J* = 7.1 Hz), 8.05-8.11 (m, 4H, ArH), 10.53 (s, 1H, NH). **¹³C-NMR (100 MHz, DMSO-*d*₆):** δ (ppm) = 13.28 (CH₃), 18.66 (CH₂), 28.89 (CH₂), 38.26 (CH₂), 81.08 (C), 121.35 (CH), 123.57 (CH), 123.77 (CH), 127.26 (CH), 128.30 (CH), 128.38 (CH), 128.69 (CH), 130.78 (CH), 131.12 (CH), 131.65 (C), 138.42 (C), 142.62 (C), 147.19 (C), 154.56 (C), 156.40 (C), 175.13 (C). **LC-MS (m/z):** 470.1 [M+H]⁺. **HRMS (m/z):** *calc.*: 470.1823, *found*: 470.1821 [M+H]⁺.

BuTAD-[3-(4-methoxyphenyl)-2-phenyl-1H-indole] adduct (***BuTAD-26***).

As a yellow powder. **¹H-NMR (500 MHz, DMSO-*d*₆):** δ (ppm) = 0.67 (t, 3H, CH₂-CH₃, *J* = 7.3 Hz), 0.86 (m, 2H, CH₂-CH₃), 1.26 (m, 2H, N-CH₂-CH₂), 3.25 (m, 2H, N-CH₂), 3.65 (s, 3H, O-CH₃), 6.78 (d, 2H, ArH, *J* = 8.9 Hz), 7.08 (d, 2H, ArH, *J* = 8.9 Hz), 7.28 (t, 1H, ArH, *J* = 7.4 Hz), 7.36-7.45 (m, 4H, ArH), 7.48 (t, 1H, ArH, *J* = 7.6 Hz), 7.65 (d, 1H, ArH, *J* = 7.8 Hz), 8.08 (d, 2H, ArH, *J* = 7.0 Hz), 10.33 (s, 1H, NH). **¹³C-NMR (125 MHz, DMSO-*d*₆):** δ (ppm) = 13.29 (CH₃), 18.64 (CH₂), 28.91 (CH₂), 38.10 (CH₂), 55.04 (CH₃), 80.86 (C), 114.09 (CH), 120.93 (CH), 123.31 (CH), 126.43 (C), 126.70 (CH), 128.08 (CH), 128.26 (CH), 128.66 (CH), 130.14 (CH), 130.67 (CH), 132.48 (C), 139.03 (C), 154.45 (C), 154.80 (C), 156.43 (C), 159.02 (C), 176.38 (C). **LC-MS (m/z):** 455.2 [M+H]⁺. **HRMS (m/z):** *calc.*: 455.2078, *found*: 455.2062 [M+H]⁺.

BuTAD-[2-(4-methoxyphenyl)-3-phenyl-1H-indole] adduct (***BuTAD-27***).

As a bright yellow powder. **¹H-NMR (500 MHz, DMSO-*d*₆):** δ (ppm) = 0.67 (t, 3H, CH₂-CH₃, *J* = 7.3 Hz), 0.88 (m, 2H, CH₂-CH₃), 1.25 (m, 2H, N-CH₂-CH₂), 3.25 (m, 2H, N-CH₂), 3.77 (s, 3H, O-CH₃), 6.93 (d, 2H, ArH, *J* = 8.9 Hz), 7.15-7.20 (m, 2H, ArH), 7.20-7.26 (m, 4H, ArH), 7.39 (d, 1H, ArH, *J* = 7.5 Hz), 7.46 (t, 1H, ArH, *J* = 7.6 Hz), 7.60 (d, 1H, ArH, *J* = 7.6 Hz), 8.04 (d, 2H, ArH, *J* = 8.9 Hz), 10.31 (s, 1H, NH). **¹³C-NMR (125 MHz, DMSO-*d*₆):** δ (ppm) = 13.30 (CH₃), 18.66 (CH₂), 28.91 (CH₂), 38.12 (CH₂), 55.25 (CH₃), 81.24 (C), 113.53 (CH), 120.52 (CH), 123.30 (CH), 124.77 (C), 126.26 (CH), 126.76 (CH), 128.13 (CH), 128.68 (CH), 130.12 (CH), 130.50 (CH), 135.57 (C), 139.21 (C), 154.75 (C), 154.86 (C), 156.41 (C), 161.28

(C), 175.68 (C). **LC-MS (m/z):** 455.2 [M+H]⁺. **HRMS (m/z):** *calc.*: 455.2078, *found*: 455.2078 [M+H]⁺.

BuTAD-[2-(4-methoxyphenyl)-3-(4-nitrophenyl)-1H-indole] adduct (BuTAD-28).

As a bright dark yellow powder. **¹H-NMR (500 MHz, DMSO-*d*₆):** δ (ppm) = 0.69 (t, 3H, CH₂-CH₃, *J* = 7.5 Hz), 0.88 (m, 2H, CH₂-CH₃), 1.28 (m, 2H, N-CH₂-CH₂), 3.28 (m, 2H, N-CH₂), 3.77 (s, 3H, O-CH₃), 6.94 (d, 2H, ArH, *J* = 8.9 Hz), 7.26 (t, 1H, ArH, *J* = 7.6 Hz), 7.40 (m, 1H, ArH), 7.47 (d, 2H, ArH, *J* = 8.9 Hz), 7.51 (t, 1H, ArH, *J* = 7.6 Hz), 7.66 (d, 1H, ArH, *J* = 7.8 Hz), 8.03 (d, 2H, ArH, *J* = 8.9 Hz), 8.09 (d, 2H, ArH, *J* = 9.0 Hz), 10.45 (s, 1H, NH). **¹³C-NMR (125 MHz, DMSO-*d*₆):** δ (ppm) = 13.28 (CH₃), 18.68 (CH₂), 28.89 (CH₂), 38.22 (CH₂), 55.30 (CH₃), 113.75 (CH), 120.87 (CH), 123.49 (CH), 123.71 (CH), 124.10 (C), 126.71 (CH), 128.32 (CH), 130.60 (CH), 138.55 (C), 143.14 (C), 147.07 (C), 154.73 (C), 156.35 (C), 161.55 (C), 174.62 (C). **LC-MS (m/z):** 500.2 [M+H]⁺. **HRMS (m/z):** *calc.*: 500.1929, *found*: 500.1193 [M+H]⁺.

BuTAD-[2,3-bis(4-methoxyphenyl)-1H-indole] adduct (BuTAD-29).

As a pale orange powder. **¹H-NMR (500 MHz, DMSO-*d*₆):** δ (ppm) = 0.67 (t, 3H, CH₂-CH₃, *J* = 7.1 Hz), 0.86 (m, 2H, CH₂-CH₃), 1.25 (m, 2H, N-CH₂-CH₂), 3.25 (t, 2H, N-CH₂, *J* = 6.7 Hz), 3.67 (s, 3H, O-CH₃), 3.78 (s, 3H, O-CH₃), 6.79 (d, 2H, ArH, *J* = 8.9 Hz), 6.94 (d, 2H, ArH, *J* = 8.9 Hz), 7.08 (d, 2H, ArH, *J* = 8.9 Hz), 7.22 (t, 1H, ArH, *J* = 7.0 Hz), 7.39 (d, 1H, ArH, *J* = 7.5 Hz), 7.45 (m, 1H, ArH), 7.58 (d, 1H, ArH, *J* = 7.6 Hz), 8.04 (d, 2H, ArH, *J* = 9.1 Hz), 10.28 (s, 1H, NH). **¹³C-NMR (125 MHz, DMSO-*d*₆):** δ (ppm) = 13.29 (CH₃), 18.67 (CH₂), 28.94 (CH₂), 38.09 (CH₂), 55.05 (CH₃), 55.25 (CH₃), 80.73 (C), 113.52 (CH), 114.04 (CH), 120.48 (CH), 123.20 (CH), 124.94 (C), 126.16 (CH), 127.02 (C), 128.21 (CH), 130.01 (CH), 130.50 (CH), 139.23 (C), 154.58 (C), 154.79 (C), 156.30 (C), 158.91 (C), 161.23 (C), 175.87 (C). **LC-MS (m/z):** 485.2 [M+H]⁺. **HRMS (m/z):** *calc.*: 485.2183, *found*: 485.2182 [M+H]⁺.

General procedure for the synthesis of PhTAD-indole adducts

4-phenyl-1,2,4-triazoline-3,5-dione (**PhTAD**, 150 mg, 1.0 eq., 0.86 mmol) in 2.5 mL dichloromethane was added to a solution of the respective indole **14**, **16** or **27** (1.0 eq., 0.86 mmol) in 2.5 mL dichloromethane at room temperature. The resulting mixture was stirred until the red purple colour disappeared. Solvent removal *in vacuo* at room temperature gave the pure TAD-indole addition product in quantitative yield.

PhTAD-[3-methyl-2-phenyl-1H-indole] adduct (PhTAD-14).

As a white powder. **¹H-NMR (400 MHz, DMSO-*d*₆):** δ (ppm) = 1.81 (s, 3H, CH₃), 7.16-7.23 (m, 2H, ArH), 7.27-7.47 (m, 5H, ArH), 7.52-7.64 (m, 5H, ArH), 8.19-8.30 (m, 2H, ArH), 11.17 (s, 1H, NH). **¹³C-NMR (100 MHz, DMSO-*d*₆):** δ (ppm) = 22.92 (CH₃), 72.41 (C), 120.95 (CH), 121.20 (CH), 125.72 (CH), 126.72 (CH), 127.99 (CH), 128.10 (CH), 128.77 (CH),

128.89 (CH), 129.67 (CH), 130.91 (C), 131.28 (C), 131.48 (C), 139.50 (C), 152.75 (C), 153.37 (C), 175.95 (C).

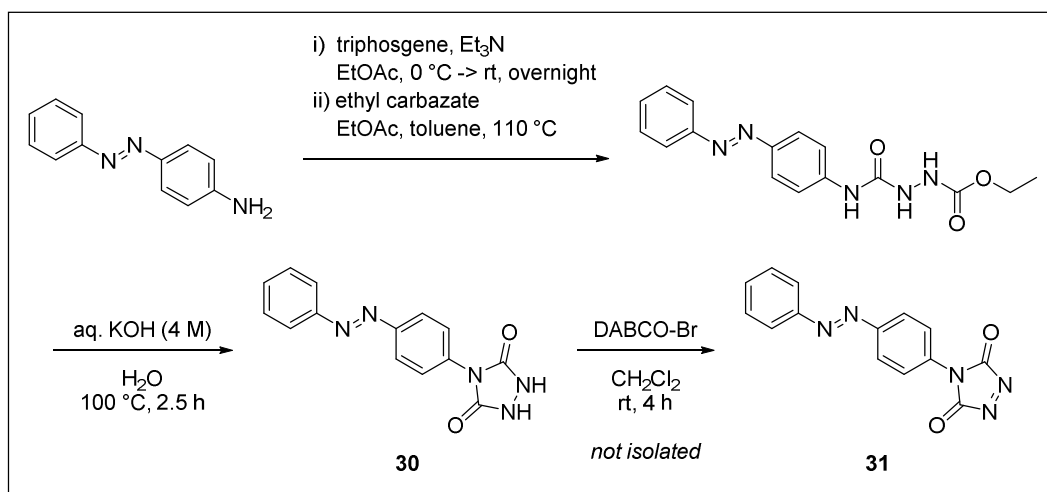
PhTAD-[2,3-diphenyl-1H-indole] adduct (PhTAD-16).

As a pale brown powder. $^1\text{H-NMR}$ (400 MHz, $\text{DMSO-}d_6$): δ (ppm) = 7.15-7.28 (m, 7H, ArH), 7.31-7.49 (m, 7H, ArH), 7.49-7.58 (m, 2H, ArH), 7.69 (d, 1H, ArH, $J = 7.5$ Hz), 8.13 (m, 2H, ArH), 10.81 (s, 1H, NH). $^{13}\text{C-NMR}$ (100 MHz, $\text{DMSO-}d_6$): δ (ppm) = 81.18 (C), 121.09 (CH), 123.42 (CH), 125.88 (CH), 126.90 (CH), 127.08 (CH), 128.11 (CH), 128.22 (CH), 128.37 (CH), 128.76 (CH), 128.80 (CH), 128.94 (CH), 130.39 (CH), 130.82 (CH), 130.91 (C), 132.20 (C), 134.87 (C), 154.52 (C), 176.16 (C).

PhTAD-[2-(4-methoxyphenyl)-3-phenyl-1H-indole] adduct (PhTAD-27).

As a bright yellow powder. $^1\text{H-NMR}$ (500 MHz, $\text{DMSO-}d_6$): δ (ppm) = 3.78 (s, 3H, O-CH_3), 6.95 (d, 2H, ArH, $J = 9.0$ Hz), 7.15-7.33 (m, 8H, ArH), 7.33-7.39 (m, 1H, ArH), 7.39-7.46 (m, 2H, ArH), 7.46-7.55 (m, 2H, ArH), 7.6 (d, 1H, ArH, $J = 7.6$ Hz), 8.11 (d, 2H, ArH, $J = 9.4$ Hz), 10.76 (s, 1H, NH). $^{13}\text{C-NMR}$ (125 MHz, $\text{DMSO-}d_6$): δ (ppm) = 55.26 (CH_3), 81.09 (C), 113.57 (CH), 120.65 (CH), 123.37 (CH), 124.73 (C), 125.87 (CH), 126.54 (CH), 126.90 (CH), 128.22 (CH), 128.71 (CH), 128.94 (CH), 130.29 (CH), 130.68 (CH), 130.95 (CH), 135.41 (C), 139.31 (C), 153.10 (C), 154.58 (C), 154.76 (C), 161.36 (C), 175.65 (C).

B.4.4 Synthesis of 4-(4-azobenzene)-1,2,4-triazoline-3,5-dione (31)



Triphosgene (5.70 g, 19.2 mmol, 0.35 eq.) was dissolved in 100 mL ethyl acetate and cooled in an ice water bath at $0\text{ }^\circ\text{C}$. To this, a mixture of 4-aminodiphenylamine (10.82 g, 55.0 mmol, 1.00 eq.) and dry triethylamine (16.8 mL, 0.121 mol, 2.20 eq.) in 40 mL ethyl acetate was slowly added at $0\text{ }^\circ\text{C}$ under inert atmosphere. The ice water bath was removed and the solution was stirred overnight before filtered directly into a mixture of ethyl carbazate (6.29 g, 60.4 mmol, 1.10 eq.) in 20 mL ethyl acetate and the residue was washed with another 100 mL ethyl acetate. A precipitate was rapidly formed in the clear filtrate and after stirring for 5 minutes, the reaction

mixture was evaporated *in vacuo*. 200 mL toluene and 100 mL ethyl acetate were added to the crude product and the resulting mixture was heated to reflux. Another 100 mL toluene was added before the mixture was cooled to room temperature. The formed precipitate was filtered and dried overnight in a vacuum oven at 40 °C to give 4-(4-azobenzene)-1-(ethoxycarbonyl) semicarbazide as an orange powder (10.2 g – 56 %).

¹H-NMR (400 MHz, DMSO-*d*₆): δ (ppm) = 1.21 (t, 3H, CH₃), 4.08 (q, 2H, CH₂), 7.48-7.61 (m, 3H, ArH), 7.64-7.78 (m, 2H, ArH), 7.81-7.89 (m, 4H, ArH), 8.21 (s, 1H, Ar-NH), 8.63 + 9.01 (s, 1H, Ar-NH-C(O)-NH), 9.20 (s, 1H, Ar-NH-C(O)-NH-NH). **¹³C-NMR (100 MHz, DMSO-*d*₆):** δ (ppm) = 14.54 (CH₃), 60.59 (CH₂), 122.22 (CH), 123.72 (CH), 129.37 (CH), 130.78 (CH), 143.21 (C), 146.66 (C), 152.08 (C). **LC-MS (m/z):** 328.20 [M+H]⁺. **HRMS (m/z):** *calc.*: 328.1404, *found*: 328.1395 [M+H]⁺.

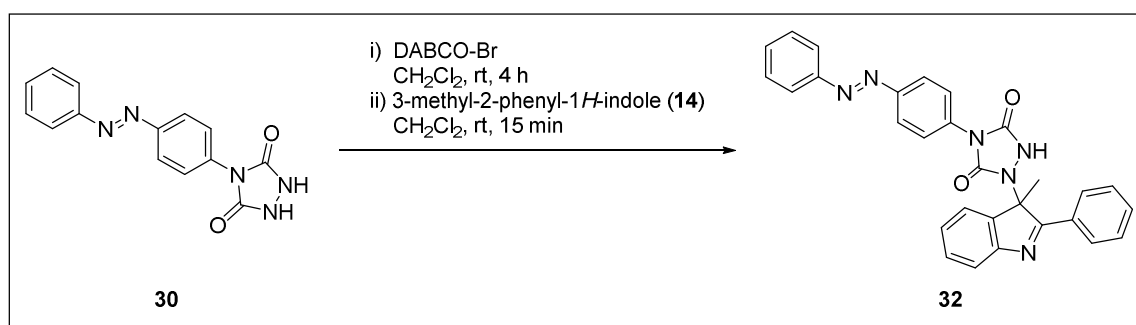
Next, 4-(4-azobenzene)-1-(ethoxycarbonyl) semicarbazide (1.00 g, 3.05 mmol, 1.0 eq.) in 2.5 mL of 4 M aqueous potassium hydroxide solution was placed under inert atmosphere. The mixture was refluxed for at 100 °C for 2.5 h and the resulting dark orange-brown solution was cooled to room temperature before being acidified to pH = 1 using 1 M aqueous hydrochloric acid solution. The obtained precipitate was filtered, washed with water (3 x 5 mL) and dried in a vacuum oven overnight at 40 °C to give 4-(4-azobenzene) urazole (**30**) as an orange powder (0.817 g – 95 %).

¹H-NMR (400 MHz, DMSO-*d*₆): δ (ppm) = 7.55-7.66 (m, 3H, ArH), 7.76 (dt, 2H, ArH), 7.92 (m, 2H, ArH), 8.00 (dt, 2H, ArH), 10.65 (s, 2H, NH). **¹³C-NMR (100 MHz, DMSO-*d*₆):** δ (ppm) = 122.64 (CH), 122.89 (CH), 126.23 (CH), 129.51 (CH), 131.73 (CH), 134.63 (C), 150.34 (C), 151.88 (C), 152.85 (C). **LC-MS (m/z):** 282.10 [M+H]⁺. **HRMS (m/z):** *calc.*: 282.0986, *found*: 282.0994 [M+H]⁺.

Finally, a mixture of 4-(4-azobenzene) urazole (**30**, 500 mg, 1.78 mmol, 1.0 eq.) and DABCO-Br (559 mg, 0.356 mmol, 0.2 eq.) in 25 mL dry dichloromethane was placed under inert atmosphere and stirred in the dark at room temperature for 4 h. The resulting red mixture was taken up with a syringe and the heterogenous oxidant was removed by means of a syringe filter to give a clear dark red solution of 4-(4-azobenzene)-1,2,4-triazoline-3,5-dione **31**. The TAD-dye was used without isolation.

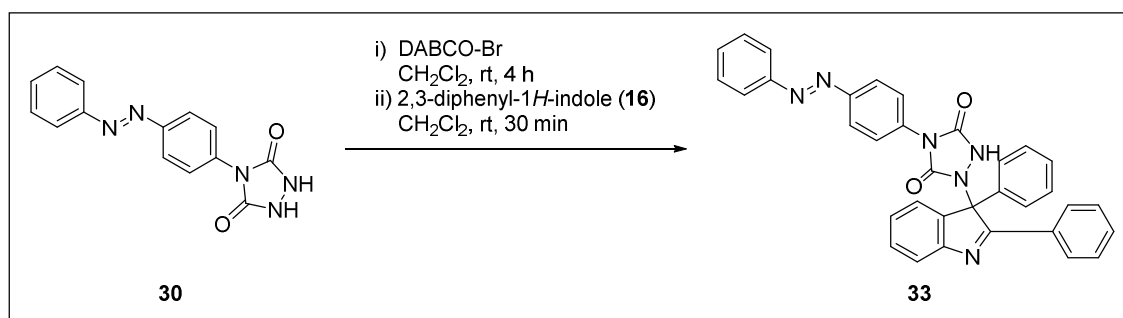
B.4.5 Synthesis of indole-blocked TAD-dye adducts **32** and **33**

B.4.5.1 Synthesis of 3-methyl-2-phenyl-1*H*-indole blocked TAD-dye (**32**)



A mixture of 4-(4-azobenzene) urazole (**30**, 250 mg, 0.90 mmol, 1.0 eq.) and DABCO-Br⁴⁴⁶ (280 mg, 0.18 mmol, 0.2 eq.) in 10 mL anhydrous dichloromethane was placed under inert atmosphere and stirred at room temperature for 4 h away from ambient light. The resulting dark red mixture was taken up with a syringe and added to a solution of 3-methyl-2-phenylindole (**14**, 184 mg, 0.90 mmol, 1.0 eq.) in 3 mL anhydrous dichloromethane through a syringe filter. The syringe and filter were washed with an additional 2 mL anhydrous dichloromethane. The resulting mixture was stirred under inert atmosphere at room temperature for 15 minutes, whereby the red colour completely disappeared. Solvent removal *in vacuo* (< 35 °C) gave a bright orange residue, which was purified by means of column chromatography (silica, hexane:ethyl acetate 1:1, $R_F = 0.29$) in order to remove traces of unreacted indole. An inseparable diastereomeric mixture ($de = 80\%$) of the 3-methyl-2-phenyl-1*H*-indole-blocked TAD-dye **32** was obtained as a bright orange powder (305 mg – 71 %).

¹H-NMR (400 MHz, DMSO-*d*₆): major diastereomer: δ (ppm) = 1.82 (s, 3H, CH₃), 7.31 (t, 1H, ArH), 7.44 (t, 1H, ArH), 7.50-7.64 (m, 10H, ArH), 7.85-7.94 (m, 4H, ArH), 8.24-8.30 (m, 2H, ArH), 11.34 (s, 1H, NH); Some resolved resonances of the minor diastereomer: δ (ppm) = 1.77 (s, 3H, CH₃), 6.81 (m, 2H, ArH), 6.87 (m, 2H, ArH), 7.14 (m, 1H, ArH), 8.19-8.24 (m, 2H, ArH). ¹³C-NMR (100 MHz, DMSO-*d*₆): δ (ppm) = 22.96 (CH₃), 72.28 (C), 119.77 (CH), 120.40 (CH), 120.97 (CH), 121.27 (CH), 122.64 (CH), 122.93 (CH), 125.84 (CH), 126.03 (CH), 126.78 (CH), 128.02 (CH), 128.79 (CH), 128.94 (CH), 129.49 (CH), 129.70 (CH), 131.31 (CH), 131.47 (C), 131.82 (CH), 133.58 (C), 139.50 (C), 150.51 (C), 151.80 (C), 152.35 (C), 152.75 (C), 152.96 (C), 175.92 (C). LC-MS (m/z): 487.20 [M+H]⁺. HRMS (m/z): *calc.*: 487.1877, *found*: 487.1862 [M+H]⁺.

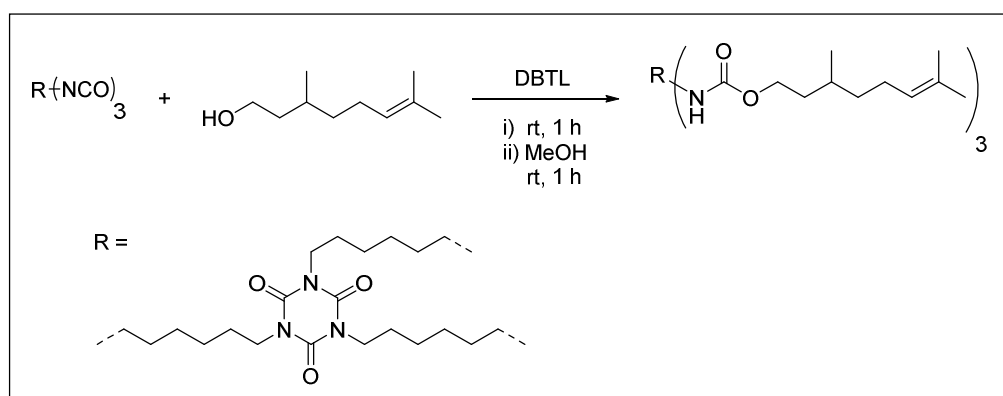
B.4.5.2 Synthesis of 2,3-diphenyl-1*H*-indole blocked TAD-dye (**33**)

A mixture of 4-(4-azobenzene) urazole (**30**, 500 mg, 1.78 mmol, 1.0 eq.) and DABCO-Br⁴⁴⁶ (559 mg, 0.356 mmol, 0.2 eq.) in 25 mL anhydrous dichloromethane was placed under inert atmosphere and stirred at room temperature for 4 h away from ambient light. The resulting dark red mixture was taken up with a syringe and added to a solution of 2,3-diphenyl-1*H*-indole (**33**, 479 mg, 1.78 mmol, 1.0 eq.) in 5 mL anhydrous dichloromethane through a syringe filter. The syringe and filter were washed with an additional 5 mL anhydrous dichloromethane. The resulting mixture was stirred under inert atmosphere at room temperature for 30 minutes, whereby the red colour completely disappeared. Solvent removal *in vacuo* (< 35 °C) gave a bright orange residue, which was purified by means of column chromatography (silica, hexane:ethyl acetate 7:3 with a gradient to 1:1, $R_F = 0.25$ (hexane: ethyl acetate 1:1)) in order to remove traces of unreacted indole. An inseparable diastereomeric mixture (*de* = 77 %) of the 2,3-diphenyl-1*H*-indole-blocked TAD-dye **33** was obtained as a bright orange powder (859 mg – 88 %).

¹H-NMR (500 MHz, DMSO-*d*₆): major diastereomer: δ (ppm) = 7.21-7.48 (m, 9H, Ar*H*), 7.49-7.64 (m, 7H, Ar*H*), 7.70 (d, 1H, Ar*H*), 7.87-7.92 (m, 2H, Ar*H*), 7.94 (d, 2H, Ar*H*), 8.16 (d, 2H, Ar*H*), 11.01 (s, 1H, NH); Some resolved resonances of the minor diastereomer: δ (ppm) = 6.83 (d, 2H, Ar*H*), 6.90 (d, 2H, Ar*H*), 7.68 (d, 1H, Ar*H*), 8.10 (d, 2H, Ar*H*). **¹³C-NMR (125 MHz, DMSO-*d*₆):** δ (ppm) = 80.91 (C), 121.11 (CH), 122.65 (CH), 122.98 (CH), 123.49 (CH), 126.25 (CH), 126.93 (CH), 127.16 (CH), 128.13 (CH), 128.41 (CH), 128.77 (CH), 128.85 (CH), 129.51 (CH), 130.43 (CH), 130.85 (CH), 131.84 (CH), 132.19 (C), 133.52 (C), 134.80 (C), 150.63 (C), 151.81 (C), 154.52 (C), 176.11 (C). **LC-MS (m/z):** 549.20 [MH]⁺. **HRMS (m/z):** *calc.*: 549.2034 [M+H]⁺ and 270.1277 [**16**+H]⁺ (fragment ion), *found*: 270.1267 [**16**+H]⁺ (fragment ion).

B.4.6 Synthesis of TAD-reactive network

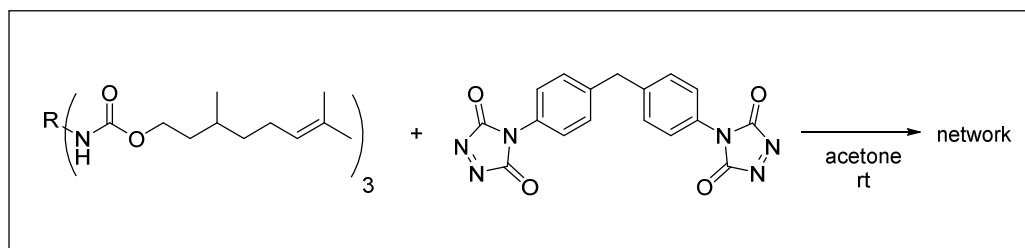
B.4.6.1 Synthesis of multifunctional citronellol derivative



Desmodur XP 2489 polyisocyanate (5.20 g, 26.0 mmol NCO, 1.0 eq.) and citronellol (4.07 g, 26.0 mmol, 1.0 eq.) in 5 mL ethyl acetate were thoroughly mixed until a homogeneous solution was formed. Dibutyltin dilaurate (DBTL, 100 μ L) was subsequently added and the resulting solution was mixed for 1 h. Next, 5 mL methanol was added and the resulting mixture was stirred for an additional hour. The solvent was removed *in vacuo* followed by overnight drying in a vacuum oven at 40 $^{\circ}$ C to give the multifunctional citronellol derivative as a clear viscous liquid, containing 2.8 mmol g^{-1} of alkenes.

1H -NMR (300 MHz, $CDCl_3$): δ (ppm) = 0.92 (d, 9H, $CH-CH_3$), 1.19 (m, 3H, CH_3-CH), 1.28–1.72 (m, 54H, $N-CH_2-(CH_2)_4-CH_2-NH + O-CH_2-CH_2 + CH_2-CH_2-CH + C-(CH_3)_2$), 1.98 (m, 6H, $CH_2-CH=C$), 3.16 (q, 6H, $NH-CH_2$), 3.86 (t, 6H, $N-CH_2$), 4.09 (m, 6H, $O-CH_2$), 4.69 (s, 3H, NH), 5.09 (t, 3H, $CH=C$).

B.4.6.2 Synthesis of TAD-reactive polymer resin by crosslinking of the multifunctional citronellol derivative



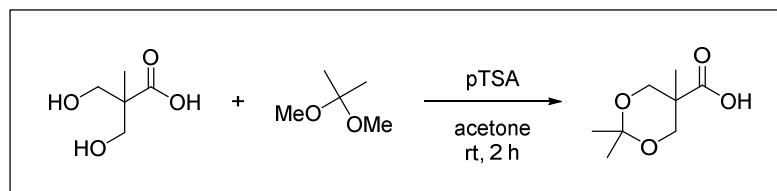
A solution of the aromatic bisTAD (**37**, 0.41 g, 1.12 mmol, 0.4 eq., *cf.* B.4.8) in 3 mL acetone was added to a solution of the multifunctional citronellol derivative (1.00 g, 2.80 mmol alkene, 1.0 eq.) in 3 mL acetone. Once addition was complete, the mixture was quickly shaken and poured into a petri dish. Gelation was observed within 5 seconds and complete curing was evidenced by the complete disappearance of the red TAD colour. One minute after mixing of the solutions, a yellowish-white precipitate was formed, which after drying to the air overnight at

room temperature became almost transparent. The resulting crosslinked material containing an excess of TAD-reactive moieties was thus obtained.

B.4.7 Synthesis of diene-containing polyurethane (HDEO-PU, 35)

B.4.7.1 Monomer synthesis

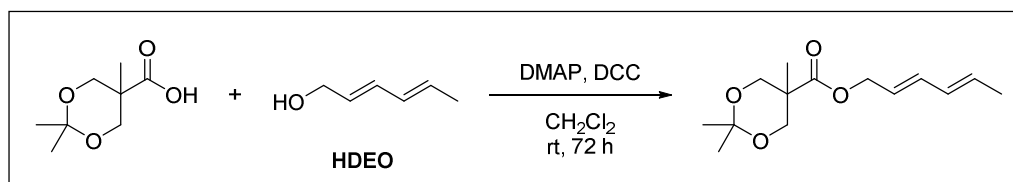
2,2,5-trimethyl-1,3-dioxane-5-carboxylic acid.



2,2,2-trimethyl-1,3-dioxane-5-carboxylic acid was synthesised according to a literature procedure,⁴⁴⁸ giving a white waxy solid (11.42 g – 82 %).

¹H-NMR (400 MHz, DMSO-*d*₆): δ (ppm) = 1.07 (s, 3H, C(O)-C-CH₃), 1.26 (s, 3H, O-C-CH₃), 1.34 (s, 3H, O-C-CH₃), 3.55 (d, 2H, CH₂, *J* = 11.9 Hz), 4.01 (d, 2H, CH₂, *J* = 11.6 Hz), 12.50 (s, 1H, COOH). **¹³C-NMR (100 MHz, DMSO-*d*₆):** δ (ppm) = 18.44 (CH₃), 22.92 (CH₃), 24.45 (CH₃), 40.71 (C), 65.24 (CH₂), 97.22 (C), 175.54 (C). **LC-MS (m/z):** 175.2 [M+H]⁺.

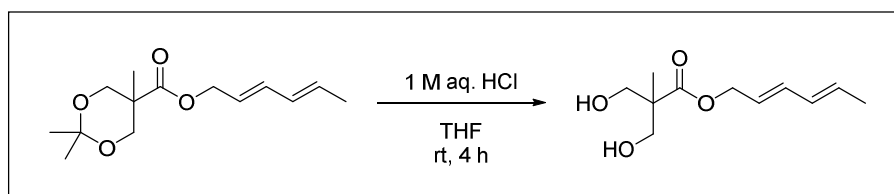
trans,trans-hexa-2,4-dien-1-yl 2,2,5-trimethyl-1,3-dioxane-5-carboxylate.



A mixture of 2,2,2-trimethyl-1,3-dioxane-5-carboxylic acid (4.90 g, 28.2 mmol, 1.0 eq.), 4-(dimethylamino)pyridine (DMAP, 1.38 g, 11.3 mmol, 0.4 eq.) and *trans,trans*-2,4-hexadien-1-ol (HDEO, 3.31 g, 33.8 mmol, 1.2 eq.) in 200 mL dichloromethane was placed under inert atmosphere and stirred in an ice water bath at 0 °C. To this, a solution of *N,N*-dicyclohexyldicarbodiimide (DCC, 6.97 g, 33.8 mmol, 1.2 eq.) in 50 mL dichloromethane was added dropwise and the mixture was stirred over the weekend (i.e. 72 h). The resulting mixture was concentrated *in vacuo* to approximately 15 mL volume before the salts were removed by filtration. The yellowish filtrate was diluted with 200 mL dichloromethane, washed with water (2 x 40 mL) and dried over magnesium sulfate. Solvent removal *in vacuo* gave a yellow-brown oil, which was purified by means of column chromatography (silica, ethyl acetate:cyclohexane 1:7, *R*_F = 0.43). The obtained residue was dried in a vacuum oven overnight at 40 °C to give *trans,trans*-hexa-2,4-dien-1-yl 2,2,5-trimethyl-1,3-dioxane-5-carboxylate as a dark yellow oil (4.33 g – 60 %).

¹H-NMR (400 MHz, DMSO-*d*₆): δ (ppm) = 1.06 (s, 3H, C(O)-C-CH₃), 1.25 (s, 3H, O-C-CH₃), 1.36 (s, 3H, O-C-CH₃), 1.72 (d, 3H, CH₃-CH=CH, *J* = 6.7 Hz), 3.62 (d, 2H, CH₃-C-CH₂, *J* = 11.7 Hz), 4.04 (d, 2H, CH₃-C-CH₂, *J* = 11.7 Hz), 4.61 (d, 2H, O-CH₂-CH, *J* = 6.0 Hz), 5.62 (m, 1H, CH₃-CH=CH), 5.73 (m, 1H, O-CH₂-CH), 6.07 (m, 1H, CH₃-CH=CH), 6.28 (m, 1H, O-CH₂-CH=CH). **¹³C-NMR (100 MHz, DMSO-*d*₆):** δ (ppm) = 17.82 (CH₃), 18.09 (CH₃), 21.85 (CH₃), 25.35 (CH₃), 41.32 (C), 64.29 (CH₂), 65.06 (CH₂), 97.34 (C), 124.21 (CH), 130.40 (CH), 130.59 (CH), 133.50 (CH), 173.41 (C). **HR-ESI-MS (m/z):** *calc.*: 277.14103, *found*: 277.14132 [M+Na]⁺.

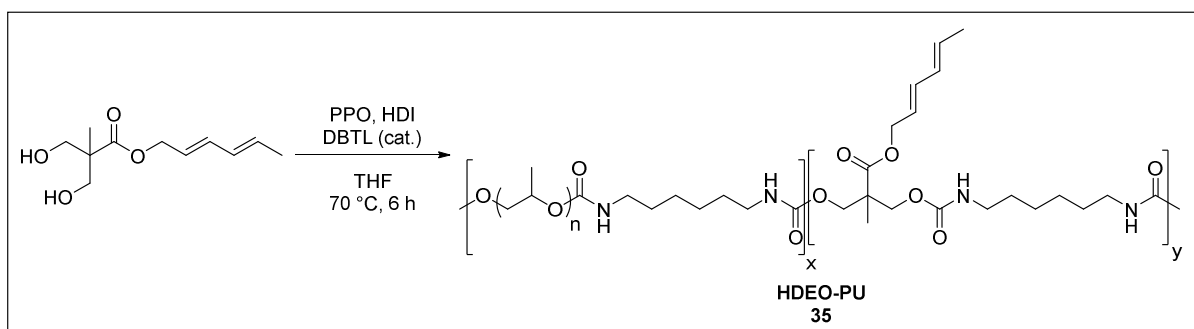
trans,trans-hexa-2,4-dien-1-yl 3-hydroxy-2-(hydroxymethyl)-2-methylpropanoate.



A suspension of *trans,trans*-hexa-2,4-dien-1-yl 2,2,5-trimethyl-1,3-dioxane-5-carboxylate (3.33 g, 13.1 mmol, 1.0 eq.) in 10 mL diluted aqueous hydrochloric acid (1 M) and 10 mL tetrahydrofuran was stirred at room temperature. After 4 h, the reaction went to completion as detected by thin layer chromatography (ethyl acetate:cyclohexane 1:7). The formed salts were removed by filtration and the clear filtrate was evaporated *in vacuo*. The residue was dissolved in 100 mL dichloromethane and washed with water (1 x 20 mL), aqueous saturated sodium bicarbonate solution (1 x 20 mL) and brine (1 x 20 mL). The organic phase was dried over magnesium sulfate followed by solvent removal and the obtained product was dried in a vacuum oven overnight at 60 °C to give the HDEO-derived monomer *trans,trans*-hexa-2,4-dien-1-yl 3-hydroxy-2-(hydroxymethyl)-2-methylpropanoate as a yellow oil (2.58 g – 92 %).

¹H-NMR (400 MHz, DMSO-*d*₆): δ (ppm) = 1.05 (s, 3H, CH₃-C), 1.72 (d, 3H, CH₃-CH=CH, *J* = 6.6 Hz), 3.46 (m, 4H, CH₂-OH), 4.52 (d, 2H, O-CH₂-CH, *J* = 6.0 Hz), 4.65 (t, 2H, OH, *J* = 5.4 Hz), 5.61 (m, 1H, CH₃-CH=CH), 5.73 (m, 1H, O-CH₂-CH), 6.07 (m, 1H, CH₃-CH=CH), 6.26 (m, 1H, O-CH₂-CH=CH). **¹³C-NMR (100 MHz, DMSO-*d*₆):** δ (ppm) = 16.89 (CH₃), 17.86 (CH₃), 50.52 (C), 63.88 (CH₂), 124.70 (CH), 130.21 (CH), 130.68 (CH), 133.20 (CH), 174.44 (C). **HR-ESI-MS (m/z):** *calc.*: 237.10973, *found*: 237.10952 [M+Na]⁺.

B.4.7.2 Polymer synthesis

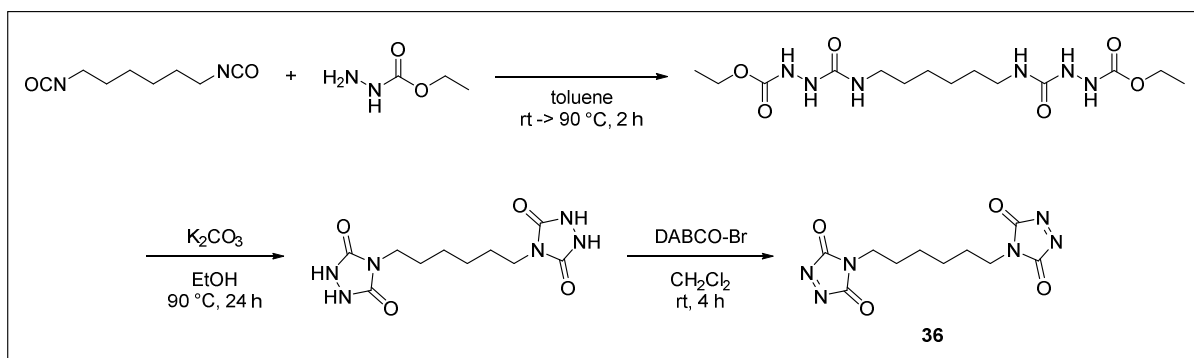


A mixture of the HDEO-derived monomer *trans,trans*-hexa-2,4-dien-1-yl 3-hydroxy-2-(hydroxymethyl)-2-methylpropanoate (1.669 g, 7.79 mmol, 0.68 eq.) and poly(propylene oxide) 2000 (PPO, 7.331 g, 3.67 mmol, 0.32 eq.) in 10 mL anhydrous tetrahydrofuran was placed under inert atmosphere. To this, hexamethylene diisocyanate (HDI, 1.927 g, 11.50 mmol, 1.00 eq.) was added, followed by 120 μ L dibutyltin dilaurate (DBTL) and the resulting mixture was refluxed for 6 h at 70 °C. Cooling to room temperature open to the air, followed by solvent removal *in vacuo* and drying in a vacuum oven at 40 °C for 48 h gave the sticky polyurethane (10.3 g – 94 %).

SEC (DMAc): $M_n = 12.5$ kDa, $D = 2.25$. DSC: $T_g = -54$ °C. TGA: $T_{d, 5\%} = 255$ °C.

B.4.8 Synthesis of triazolinedione crosslinking agents

B.4.8.1 Synthesis of 4,4'-(hexane-1,6-diyl)bis(1,2,4-triazoline-3,5-dione) (36)



A mixture of ethyl carbazate (16.2 g, 155.6 mmol, 2.0 eq.) in 100 mL toluene was placed under inert atmosphere and stirred at room temperature. To this, a solution of hexamethylene diisocyanate (12.5 mL, 77.8 mmol, 1.0 eq.) in 50 mL toluene was added dropwise. Following complete addition, the resulting mixture was heated at 90 °C for 2 h. The resulting mixture was cooled to room temperature and the waxy solid was filtered, washed with toluene (2 x 75 mL) and dried overnight in a vacuum at 40 °C to give 4,4'-(hexane-1,6-diyl)bis(1-(ethoxycarbonyl)semicarbazide) as a white powder (28.8 g – 98 %).

$^1\text{H-NMR}$ (400 MHz, DMSO- d_6): δ (ppm) = 1.17 (t, 6H, CH_3 , $J = 7.1$ Hz), 1.22 (m, 4H, $\text{N-CH}_2\text{-CH}_2\text{-CH}_2$), 1.35 (m, 4H, $\text{N-CH}_2\text{-CH}_2$), 2.97 (q, 4H, N-CH_2 , $J = 14.5, 6.6$ Hz), 4.01 (q, 4H,

$\text{CH}_3\text{-CH}_2$, $J = 14.2, 7.1$ Hz), 6.28 (s, 2H, $\text{CH}_2\text{-NH}$), 7.60 (s, 2H, C(O)-NH), 8.34 + 8.70 (s, 2H, C(O)-NH). $^{13}\text{C-NMR}$ (100 MHz, $\text{DMSO-}d_6$): δ (ppm) = 14.54 (CH_3), 26.04 (CH_2), 29.85 (CH_2), 38.99 (CH_2), 60.30 (CH_2), 156.89 (C), 158.21 (C). **LC-MS (m/z):** 377.2 $[\text{M}+\text{H}]^+$. **HR-MS (m/z):** *calc.*: 377.2143, *found*: 377.2156 $[\text{M}+\text{H}]^+$.

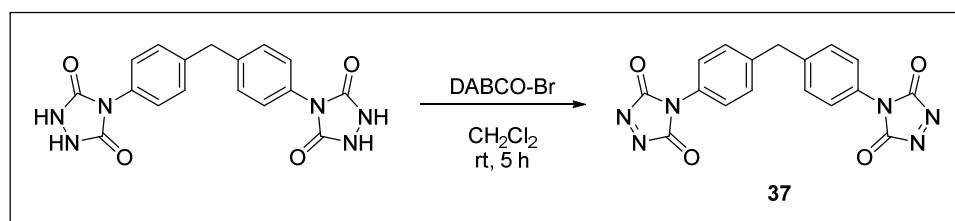
Next, a suspension of the obtained 4,4'-(hexane-1,6-diyl)bis(1-(ethoxycarbonyl)semicarbazide) (5.0 g, 13.3 mmol, 1.0 eq.) and potassium carbonate (6.2 g, 44.9 mmol, 3.4 eq.) in 150 mL ethanol was placed under inert atmosphere and heated to reflux for 24 h at 90 °C. The resulting mixture was filtered warm, and the obtained filtrate was cooled to room temperature before being acidified to pH 1 upon addition of a hydrochloric acid (5-6 N) solution in isopropanol. Filtration of the formed salts, solvent removal *in vacuo* and overnight drying in a vacuum oven at 40 °C gave 4,4'-(hexane-1,6-diyl)bis(1,2,4-triazolidine-3,5-dione) as a white powder (3.42 g – 90 %).

$^1\text{H-NMR}$ (300 MHz, $\text{DMSO-}d_6$): δ (ppm) = 1.24 (m, 4H, $\text{N-CH}_2\text{-CH}_2\text{-CH}_2$), 1.50 (t, 4H, $\text{N-CH}_2\text{-CH}_2$, $J = 6.8$ Hz), 3.33 (t, 4H, N-CH_2 , $J = 7.1$ Hz), 10.0 (s, 4H, NH). $^{13}\text{C-NMR}$ (75 MHz, $\text{DMSO-}d_6$): δ (ppm) = 25.53 (CH_2), 27.36 (CH_2), 37.73 (CH_2), 155.05 (C). **LC-MS (m/z):** 285.1 $[\text{M}+\text{H}]^+$. **HR-MS (m/z):** *calc.*: 285.1306, *found*: 285.1301 $[\text{M}+\text{H}]^+$.

Finally, a mixture of 4,4'-(hexane-1,6-diyl)bis(1,2,4-triazolidine-3,5-dione) (1.50 g, 5.28 mmol, 1.0 eq.) and DABCO- Br^{446} (3.32 g, 2.12 mmol, 0.4 eq.) in 40 mL dichloromethane was placed under inert atmosphere and stirred at room temperature, away from ambient light. After 4 h, the heterogenous mixture was filtered and washed with dichloromethane (4 x 40 mL). Solvent removal *in vacuo*, keeping the temperature below 35 °C, gave 4,4'-(hexane-1,6-diyl)bis(1,2,4-triazoline-3,5-dione) **36** as a red crystalline residue (1.07 g – 72 %), which was stored in a dark recipient at -18 °C.

$^1\text{H-NMR}$ (300 MHz, $\text{DMSO-}d_6$): δ (ppm) = 1.29 (m, 4H, $\text{N-CH}_2\text{-CH}_2\text{-CH}_2$), 1.55 (m, 4H, $\text{N-CH}_2\text{-CH}_2\text{-CH}_2$), 3.45 (t, 4H, $\text{N-CH}_2\text{-CH}_2\text{-CH}_2$, $J = 7.2$ Hz). $^{13}\text{C-NMR}$ (75 MHz, $\text{DMSO-}d_6$): δ (ppm) = 25.24 (CH_2), 26.46 (CH_2), 40.51 (CH_2), 160.13 (C).

B.4.8.2 Synthesis of 4,4'-(methylenebis(4,1-phenylene))bis(1,2,4-triazoline-3,5-dione) (**37**)



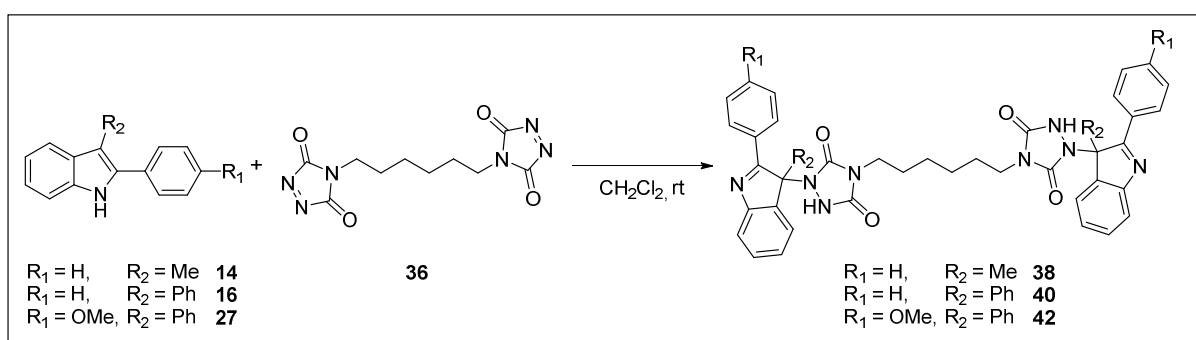
A mixture of 4,4'-(methylenebis(4,1-phenylene))bis(1,2,4-triazolidine-3,5-dione) ⁷ (2.0 g, 5.46 mmol, 1.00 eq.) and DABCO- Br^{446} (5.0 g, 3.17 mmol, 0.58 eq.) in 55 mL dichloromethane was placed under inert atmosphere and stirred at room temperature for 5 h. The resulting mixture

was filtered, washed with dichloromethane (2 x 55 mL) and evaporated to dryness *in vacuo*, keeping the temperature below 35 °C. 4,4'-(methylenebis(4,1-phenylene))bis(1,2,4-triazoline-3,5-dione) **37** was obtained as a pink powder (1.63 g – 83 %), which was stored in a dark recipient at -18 °C.

¹H-NMR (400 MHz, DMSO-*d*₆): δ (ppm) = 4.10 (s, 2H, CH₂), 7.37 (d, 4H, ArH, *J* = 8.4 Hz), 7.47 (d, 4H, ArH, *J* = 8.8 Hz). ¹³C-NMR (100 MHz, DMSO-*d*₆): δ (ppm) = 125.43 (CH), 128.26 (C), 129.84 (CH), 141.86 (C), 158.66 (C).

B.4.9 Synthesis of indole-blocked triazolinedione crosslinking agents 38-43

B.4.9.1 Synthesis of blocked aliphatic crosslinkers



36-[3-methyl-2-phenyl-1*H*-indole (**14**)]₂ adduct (**38**).

A solution of 4,4'-(hexane-1,6-diyl)bis(1,2,4-triazoline-3,5-dione) (**36**, 250 mg, 0.89 mmol, 1.0 eq.) in 5 mL dichloromethane was added to a solution of 3-methyl-2-phenyl-1*H*-indole (**14**, 370 mg, 1. mmol, 2.0 eq.) in 5 mL dichloromethane. The resulting mixture was stirred for 5 minutes at room temperature, until the red colour completely faded. Solvent removal *in vacuo* (< 35 °C) gave the corresponding indole-blocked aliphatic TAD crosslinker **38** as a white powder (606 mg – 98 %).

¹H-NMR (400 MHz, DMSO-*d*₆): δ (ppm) = 0.67 (m, 4H, N-CH₂-CH₂-CH₂), 1.09 (m, 4H, N-CH₂-CH₂-CH₂), 1.73 (s, 6H, CH₃), 3.10 (m, 4H, N-CH₂-CH₂-CH₂), 7.13-7.22 (m, 2H, ArH), 7.30-7.37 (m, 2H, ArH), 7.39-7.46 (m, 2H, ArH), 7.47-7.58 (m, 8H, ArH), 8.19 (m, 4H, ArH), 10.73 (s, 2H, NH). ¹³C-NMR (100 MHz, DMSO-*d*₆): δ (ppm) = 22.81 (CH₃), 25.00 (CH₂), 26.84 (CH₂), 38.09 (CH₂), 72.28 (C), 120.87 (CH), 121.12 (CH), 126.44 (CH), 127.94 (CH), 128.66 (CH), 129.54 (CH), 131.18 (CH), 131.58 (C), 139.35 (C), 152.77 (C), 154.90 (C), 176.02 (C). LC-MS (*m/z*): 695.30 [M+H]⁺. HRMS (*m/z*): *calc.*: 695.3089, *found*: 695.3102 [M+H]⁺.

36-[2,3-diphenyl-1*H*-indole (**16**)]₂ adduct (**40**).

A solution of 4,4'-(hexane-1,6-diyl)bis(1,2,4-triazoline-3,5-dione) (**36**, 250 mg, 0.89 mmol, 1.0 eq.) in 7.5 mL dichloromethane was added to a solution of 2,3-diphenyl-1*H*-indole (**16**, 481 mg, 1.78 mmol, 2.0 eq.) in 7.5 mL dichloromethane. The mixture was stirred for 30 minutes at room temperature, until the red colour completely faded. Solvent removal *in vacuo* (< 35 °C)

gave the corresponding indole-blocked aliphatic TAD crosslinker **40** as a beige powder (685 mg – 94 %).

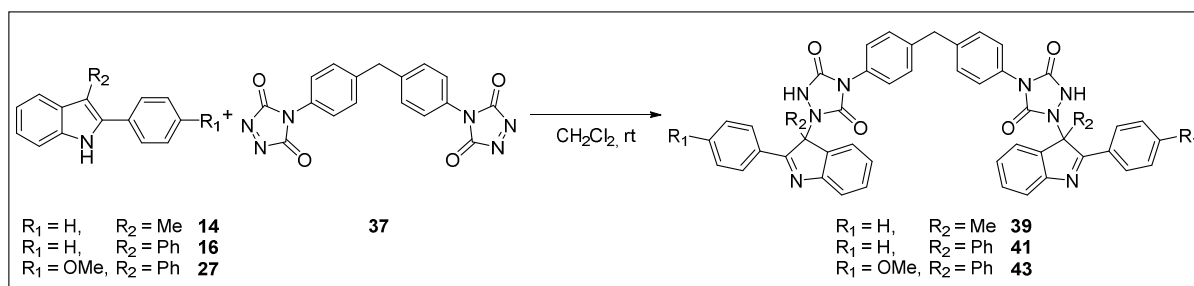
¹H-NMR (400 MHz, DMSO-*d*₆): δ (ppm) = 0.61 (m, 4H, N-CH₂-CH₂-CH₂), 1.10 (m, 4H, N-CH₂-CH₂-CH₂), 3.18 (m, 4H, N-CH₂-CH₂-CH₂), 7.12-7.18 (m, 4H, ArH), 7.18-7.28 (m, 8H, ArH), 7.33-7.49 (m, 10H, ArH), 7.63 (m, 2H, ArH), 8.07 (m, 4H, ArH), 10.38 (s, 2H, NH). **¹³C-NMR (100 MHz, DMSO-*d*₆):** δ (ppm) = 24.94 (CH₂), 26.71 (CH₂), 38.37 (CH₂), 81.29 (C), 120.95 (CH), 123.35 (CH), 126.79 (CH), 128.07 (CH), 128.27 (CH), 128.64 (CH), 128.75 (CH), 130.28 (CH), 130.72 (C), 132.31 (C), 135.03 (C), 138.97 (C), 154.61 (C), 154.84 (C), 156.43 (C), 156.48 (C), 176.22 (C). **LC-MS (m/z):** 819.30 [M+H]⁺. **HRMS (m/z):** *calc.*: 819.3402, *found*: 819.3423 [M+H]⁺.

36-[2-(4-methoxyphenyl)-3-phenyl-1H-indole (**27**)]₂ adduct (**42**).

A solution of 4,4'-(hexane-1,6-diyl)bis(1,2,4-triazoline-3,5-dione) (**36**, 250 mg, 0.89 mmol, 1.0 eq.) in 5 mL dichloromethane was added to a solution of 2-(4-methoxyphenyl)-3-phenyl-1H-indole (**27**, 534 mg, 1.78 mmol, 2.0 eq.) in 5 mL dichloromethane. The mixture was stirred for 10 minutes at room temperature, until the red colour completely faded. Solvent removal *in vacuo* (< 30 °C) gave the corresponding indole-blocked TAD crosslinker **42** as a dark yellow powder (759 mg – 97 %).

¹H-NMR (400 MHz, DMSO-*d*₆): δ (ppm) = 0.62 (m, 4H, N-CH₂-CH₂-CH₂), 1.11 (m, 4H, N-CH₂-CH₂-CH₂), 3.18 (m, 4H, N-CH₂-CH₂-CH₂), 3.75 (s, 6H, CH₃), 6.89-6.96 (m, 4H, ArH), 7.11-7.28 (m, 12H, ArH), 7.35-7.44 (m, 4H, ArH), 7.57 (d, 2H, ArH, *J* = 7.6 Hz), 8.05 (m, 4H, ArH), 10.32 (s, 2H, NH). **¹³C-NMR (100 MHz, DMSO-*d*₆):** δ (ppm) = 24.98 (CH₂), 26.72 (CH₂), 38.36 (CH₂), 55.24 (CH₃), 81.21 (C), 113.52 (CH), 120.49 (CH), 123.26 (CH), 124.82 (C), 126.27 (CH), 126.76 (CH), 128.13 (CH), 128.70 (CH), 130.18 (CH), 130.48 (CH), 135.55 (C), 139.11 (C), 154.82 (C), 156.40 (C), 161.25 (C), 175.68 (C). **LC-MS (m/z):** 879.30 [M+H]⁺. **HRMS (m/z):** *calc.*: 879.3613, *found*: 879.3614 [M+H]⁺.

B.4.9.2 Synthesis of blocked aromatic crosslinkers



37-[3-methyl-2-phenyl-1H-indole (**14**)]₂ adduct (**39**).

A suspension of 4,4'-(methylenebis(4,1-phenylene))bis(1,2,4-triazoline-3,5-dione) (**37**, 0.20 g, 0.55 mmol, 1.0 eq.) in 5 mL dichloromethane was added to a solution of 3-methyl-2-phenyl-1H-

indole (**14**, 0.23 g, 1.10 mmol, 2.0 eq.) in 5 mL dichloromethane. The mixture was stirred for 15 minutes at room temperature, until the red colour faded completely. Solvent removal *in vacuo* (< 30 °C) gave the corresponding indole-blocked aromatic TAD crosslinker **39** as a white powder (0.40 g – 93 %).

¹H-NMR (500 MHz, DMSO-*d*₆): δ (ppm) = 1.78 (s, 6H, CH₃), 3.90 (s, 2H, CH₂), 7.09 (d, 4H, ArH, *J* = 8.5 Hz), 7.18 (d, 4H, ArH, *J* = 8.7 Hz), 7.28 (m, 2H, ArH), 7.42 (m, 2H, ArH), 7.52-7.63 (m, 10H, ArH), 8.23 (m, 4H, ArH), 11.09 (s, 2H, NH). **¹³C-NMR (125 MHz, DMSO-*d*₆):** δ (ppm) = 22.92 (CH₃), 72.41 (C), 120.95 (CH), 121.19 (CH), 125.70 (CH), 126.72 (CH), 127.99 (CH), 128.77 (CH), 128.95 (C), 129.12 (CH), 129.65 (CH), 131.28 (CH), 131.47 (C), 139.52 (C), 140.85 (C), 152.73 (C), 152.99 (C), 153.37 (C), 175.95 (C). **LC-MS (m/z):** 777.20 [M+H]⁺. **HRMS (m/z):** *calc.*: 777.2932, *found*: 777.2927 [M+H]⁺.

37-[2,3-diphenyl-1H-indole (16**)]₂ adduct (**41**).**

A suspension of 4,4'-(methylenebis(4,1-phenylene))bis(1,2,4-triazoline-3,5-dione) (**37**, 2.43 g, 6.70 mmol, 1.0 eq.) in 30 mL dichloromethane was added to a solution of 2,3-diphenyl-1H-indole (**16**, 3.61 g, 13.4 mmol, 2.0 eq.) in 30 mL dichloromethane. The mixture was stirred for 1 h at room temperature, until the red colour faded completely. Solvent removal *in vacuo* (< 30 °C) gave the corresponding indole-blocked aromatic TAD crosslinker **41** as a yellow-brown powder (5.75 g – 95 %).

¹H-NMR (400 MHz, DMSO-*d*₆): δ (ppm) = 3.93 (s, 2H, CH₂), 7.09 (d, 4H, ArH, *J* = 8.5 Hz), 7.19-7.44 (m, 22H, ArH), 7.48-7.56 (m, 4H, ArH), 7.68 (d, 2H, ArH, *J* = 7.4 Hz), 8.11 (m, 4H, ArH), 10.76 (s, 2H, NH). **¹³C-NMR (100 MHz, DMSO-*d*₆):** δ (ppm) = 81.18 (C), 121.08 (CH), 123.40 (CH), 125.86 (CH), 126.90 (CH), 127.08 (CH), 128.12 (CH), 128.35 (CH), 128.74 (CH), 128.80 (CH), 128.94 (C), 129.18 (CH), 130.37 (CH), 130.82 (CH), 132.17 (C), 134.89 (C), 140.97 (C), 154.49 (C), 176.14 (C). **LC-MS (m/z):** 901.20 [M+H]⁺. **HRMS (m/z):** *calc.*: 901.3245, *found*: 901.3223 [M+H]⁺.

37-[2-(4-methoxyphenyl)-3-phenyl-1H-indole (27**)]₂ adduct (**43**).**

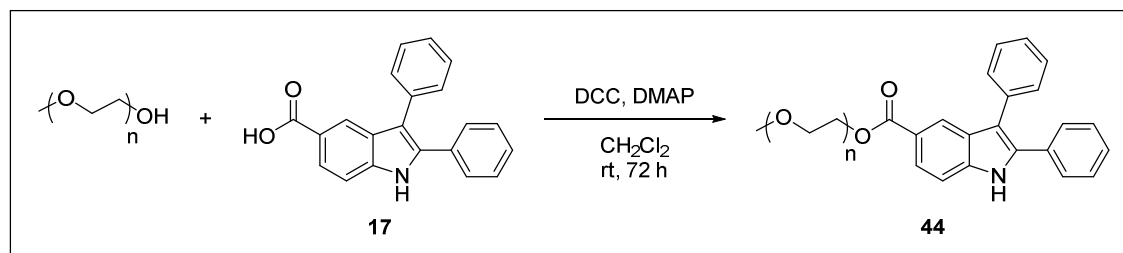
A suspension of 4,4'-(methylenebis(4,1-phenylene))bis(1,2,4-triazoline-3,5-dione) (**37**, 0.20 g, 0.55 mmol, 1.0 eq.) in 7.5 mL dichloromethane was added to a solution of 2-(4-methoxyphenyl)-3-phenyl-1H-indole (**27**, 0.33 g, 1.10 mmol, 2.0 eq.) in 7.5 mL dichloromethane. The mixture was stirred for 30 minutes at room temperature, until the red colour faded completely. Solvent removal *in vacuo* (< 25 °C) gave the corresponding indole-blocked aromatic TAD crosslinker **43** as an orange-brown powder (0.49 g – 94 %).

¹H-NMR (400 MHz, DMSO-*d*₆): δ (ppm) = 3.77 (s, 6H, CH₃), 3.94 (s, 2H, CH₂), 6.94 (d, 4H, ArH, *J* = 9.0 Hz), 7.10 (d, 4H, ArH, *J* = 8.3 Hz), 7.18-7.32 (m, 16H, ArH), 7.49 (d, 4H, ArH, *J* = 7.7 Hz), 7.62 (d, 2H, ArH, *J* = 7.4 Hz), 8.09 (d, 4H, ArH, *J* = 9.0 Hz), 10.71 (s, 2H, NH). **¹³C-NMR (100 MHz, DMSO-*d*₆):** δ (ppm) = 55.27 (CH₃), 81.08 (C), 113.57 (CH),

120.62 (CH), 123.33 (CH), 124.67 (C), 125.86 (CH), 126.53 (CH), 126.87 (CH), 128.20 (CH), 128.67 (CH), 128.97 (C), 129.18 (CH), 130.26 (CH), 130.65 (CH), 135.40 (C), 139.26 (C), 140.96 (C), 153.09 (C), 154.70 (C), 161.33 (C), 175.60 (C). **LC-MS (m/z):** 961.20 [M+H]⁺. **HRMS (m/z):** *calc.*: 961.3457, *found*: 961.3433 [M+H]⁺.

B.4.10 Synthesis of poly(ethylene glycol)-supported blocked TAD-dye 45

B.4.10.1 Synthesis of PEG-supported 2,3-diphenyl-1*H*-indole blocking agent 44



A mixture of 2,3-diphenyl-1*H*-indole-5-carboxylic acid (**17**, 0.940 g, 3.00 mmol, 6.0 eq.), poly(ethylene glycol) monomethyl ether 2000 (mPEG, 1.00 g, 0.50 mmol, 1.0 eq.) and 4-(dimethylamino)pyridine (DMAP, 0.061 g, 0.50 mmol, 1.0 eq.) in 5 mL anhydrous dichloromethane was placed under inert atmosphere and cooled in an ice water bath at 0 °C. To this, a solution of *N,N*-dicyclohexylcarbodiimide (DCC, 0.516 g, 2.50 mmol, 5.0 eq.) in 5 mL anhydrous dichloromethane was added dropwise and the mixture was stirred for 72 h at room temperature. The resulting mixture was filtered directly into a 10-fold excess of cold diethyl ether, to give a yellowish-brown precipitate. The residue was collected via filtration, washed with cold diethyl ether and dissolved in a minimal amount of dichloromethane. A second precipitation in a 10-fold excess of cold diethyl ether, followed by filtered and overnight drying in a vacuum oven at 30 °C gave the PEG-supported 2,3-diphenyl-1*H*-indole **44** as a brown powder (0.896 g – 78 %).

¹H-NMR (400 MHz, DMSO-*d*₆): δ (ppm) = 3.24 (s, 3H, CH₃), 3.40-3.69 (m, 176 H, O-CH₂), 3.74 (t, 2H, C(O)-O-CH₂-CH₂), 4.37 (t, 2H, C(O)-O-CH₂), 7.28-7.40 (m, 5H, ArH), 7.40-7.51 (m, 5H, ArH), 7.54 (d, 1H, ArH), 7.82 (dd, 1H, ArH), 8.16 (s, 1H, O-C(O)-CH), 11.99 (s, 1H, NH). **MALDI-TOF-MS:** refer to Figure B.10 and Table B.2.

Table B.2. Theoretical and experimentally found masses in the obtained MALDI-TOF spectrum of PEG-supported 2,3-diphenyl-1*H*-indole **44** (Δ).

Δ = [44+Na] ⁺		
n	Theoretical m/z (Da)	Experimental m/z (Da)
44	2287.2685	2287.4503
45	2331.2947	2331.4248
46	2375.3209	2375.3720

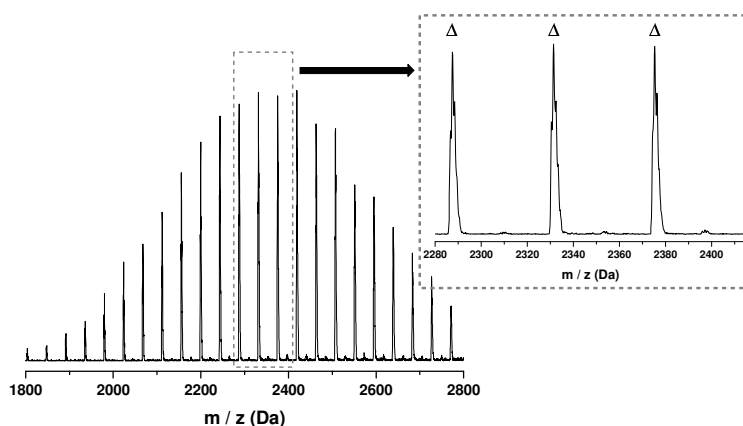
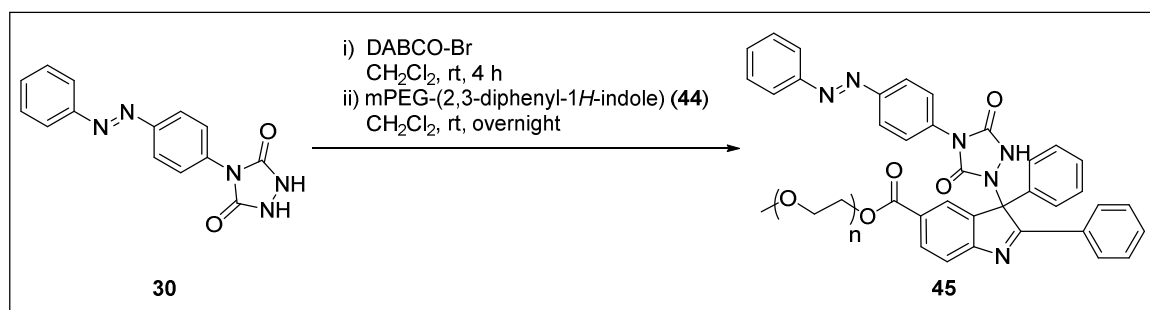


Figure B.10. MALDI-TOF analysis of PEG-supported 2,3-diphenyl-1*H*-indole **44** (Δ).

B.4.10.2 Synthesis of PEG-supported blocked TAD-dye **45**



A mixture of 4-(4-azobenzene) urazole (**30**, 214 mg, 0.76 mmol, 3.0 eq.) and DABCO-Br⁴⁴⁶ (239 mg, 0.15 mmol, 0.2 eq.) in 10 mL anhydrous dichloromethane was placed under inert atmosphere and stirred at room temperature for 4 h. The resulting red mixture was taken up with a syringe and added to a solution of mPEG-(2,3-diphenyl-1*H*-indole) **44** (574 mg, 0.25 mmol, 1.0 eq.) in 3 mL anhydrous dichloromethane through a syringe filter. The syringe and filter were washed with an additional 2 mL anhydrous dichloromethane and the resulting mixture was stirred overnight at room temperature under inert atmosphere. The orange-red mixture was precipitated into 150 mL of cold diethyl ether and filtered off. The orange residue was dissolved in a minimal amount of tetrahydrofuran and purified by means of column chromatography (SEC Bio-Beads S-X1 Support, tetrahydrofuran, R_F (silica, heptane:ethyl acetate 1:1) = 0.00). The fractions containing polymeric material were evaporated to dryness *in vacuo* (< 30 °C), followed by precipitation in cold diethyl ether (10-fold excess). Filtration followed by overnight drying to the air at room temperature gave the PEG-supported blocked TAD-dye **45** as a dark orange residue (445 mg – 68%).

¹H-NMR (400 MHz, DMSO-*d*₆): δ (ppm) = 3.24 (s, 3H, CH₃), 3.41-3.70 (m, 176 H, O-CH₂), 3.74 (t, 2H, C(O)-O-CH₂-CH₂), 4.39 (t, 2H, C(O)-O-CH₂), 7.28 (m, 5H, ArH), 7.40-7.49 (m, 3H, ArH), 7.53 (d, 2H, ArH), 7.57-7.64 (m, 3H, ArH), 7.84 (dd, 1H, ArH), 7.89 (m, 2H, ArH), 7.94 (dt, 2H, ArH), 8.11-8.23 (m, 4H, ArH), 11.11 (s, 1H, NH). MALDI-TOF-MS: refer to Figure B.11 and Table B.3.

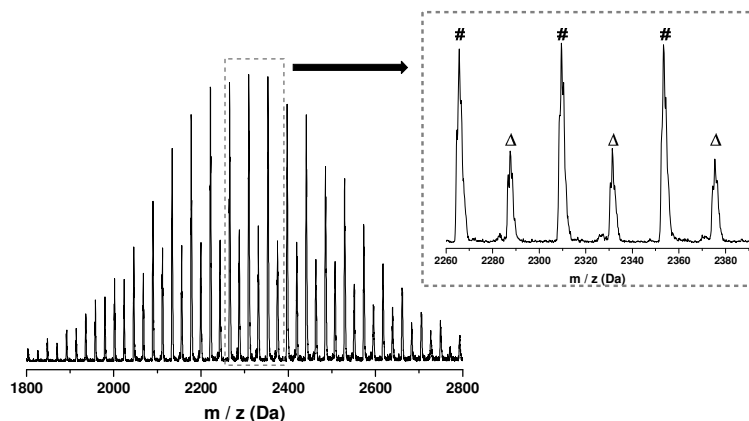


Figure B.11. MALDI-TOF analysis of PEG-supported blocked TAD-dye **45** gives a bimodal distribution, which can be attributed to the PEG-indole-TAD-dye conjugate after fragmentation (#) and the initial – unreacted or also fragmented – PEGylated 2,3-diphenyl-1*H*-indole blocking agent **44** (Δ).

Table B.3. Theoretical and experimentally found masses in the obtained MALDI-TOF spectrum of PEG-supported 2,3-diphenyl-1*H*-indole-blocked TAD-dye **45** (Δ).

$\# = [44+H]^+$			$\Delta = [44+Na]^+$		
n	Theoretical m/z (Da)	Experimental m/z (Da)	n	Theoretical m/z (Da)	Experimental m/z (Da)
44	2265.2860	2265.6200	44	2287.2685	2287.5962
45	2309.3122	2309.5318	45	2331.2947	2331.4248
46	2353.3348	2353.4211	46	2375.3209	2375.3720

Appendix C.

Experimental section Chapter IV

C.1 Additional figures and table

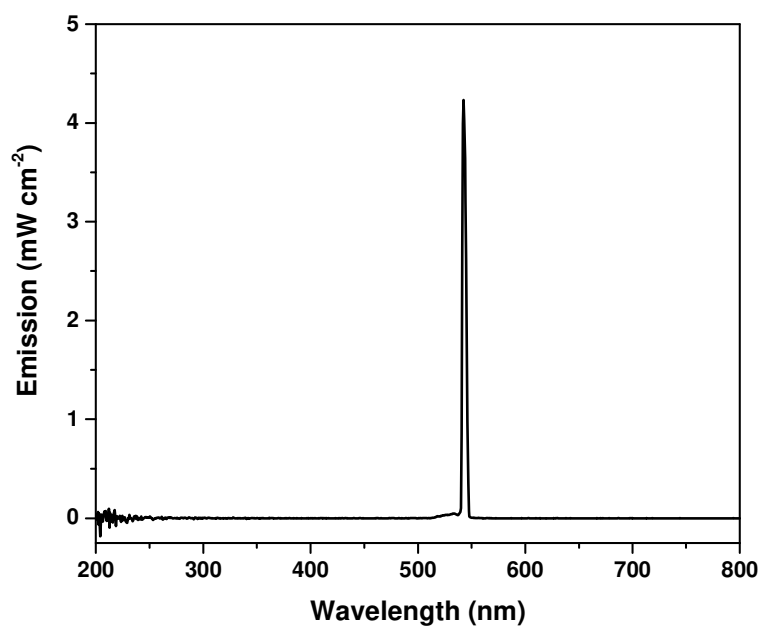


Figure C.1. Emission spectrum of the laser set at 544 nm, employed in the visible light irradiation experiments.

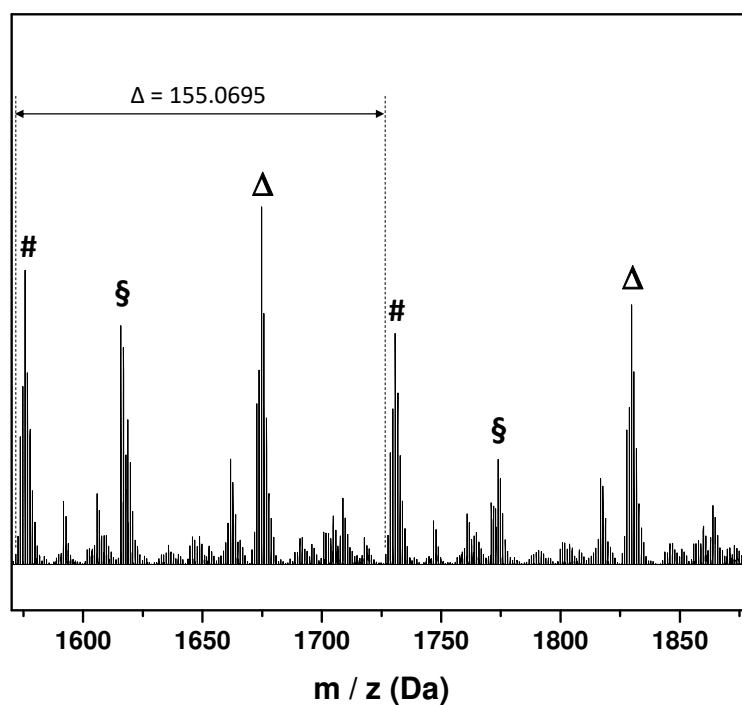


Figure C.2. Zoom of the ESI-MS spectrum of photopolymer **2**, recorded immediately after visible light irradiation (544 nm, 4 mW cm⁻², 10 min) of **1** in CCl₄ (0.3 M).

Table C.1. Theoretical (theor.) and experimentally (exp.) found masses (m/z in Da) in the obtained ESI-MS spectrum of photopolymer **2**, recorded immediately after visible light irradiation (544 nm, 4 mW cm⁻², 10 min) of **1** in CCl₄ (0.3 M). The plausible structures corresponding to the listed m/z values are depicted in **Figure C.3**.

n	# = [2+Na] ⁺		Δ = [2*+Na] ⁺		§ = [2**+Na] ⁺	
	Theor. m/z	Exp. m/z	Theor. m/z	Exp. m/z	Theor. m/z	Exp. m/z
9	1418.6145	1418.6179	1517.6830	1517.6864	1616.7514	1616.7559
10	1573.6840	1573.6871	1672.7524	1672.7685	1771.8209	1771.8393
11	1728.7535	1728.7697	1827.8219	1827.8395	1926.8904	1926.9092

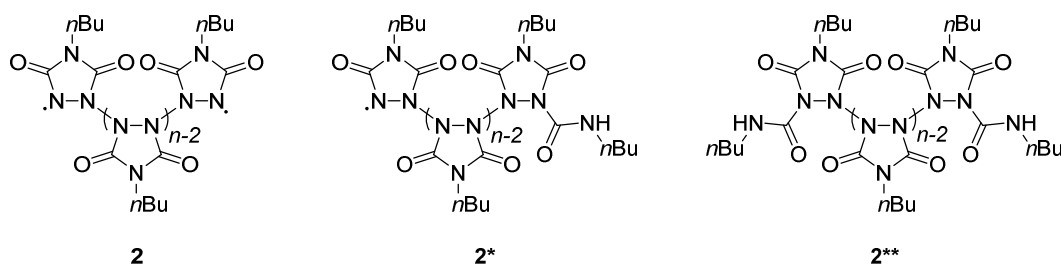


Figure C.3. Plausible structures that correspond to the experimentally found m/z values in the ESI-MS spectrum of photopolymer **2**, recorded immediately after visible light irradiation (544 nm, 4 mW cm⁻², 10 min) of **1** in CCl₄ (0.3 M).

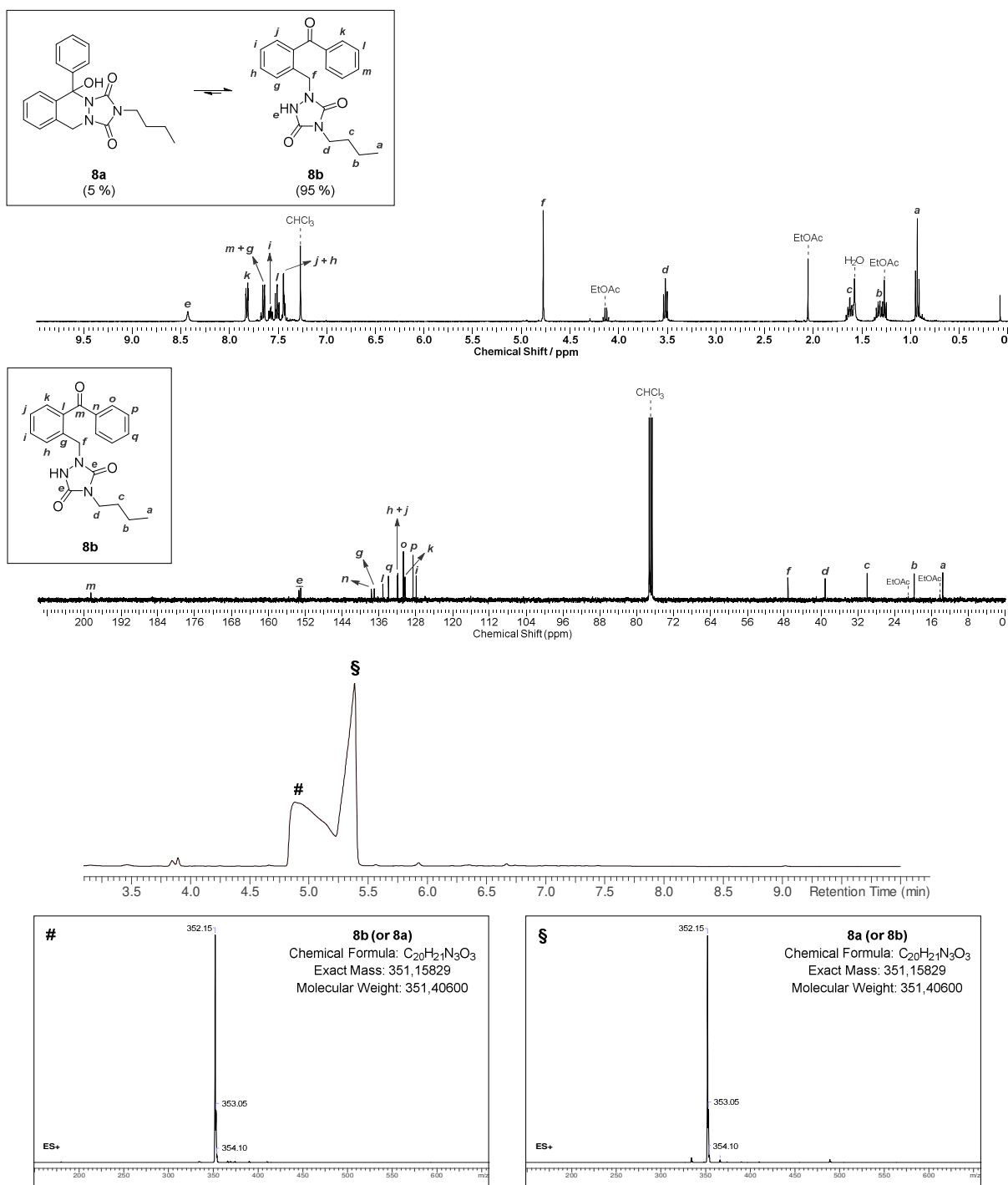


Figure C.4. ^1H - and ^{13}C -NMR spectra, recorded in CDCl_3 , and LC-MS trace with the corresponding mass spectra, used for the structure elucidation of the TAD-photoenol product mixture **8a+8b**. All peaks in the depicted NMR spectra were assigned in agreement with the corresponding 2D spectra (i.e. COSY, HSQC and HMBC).

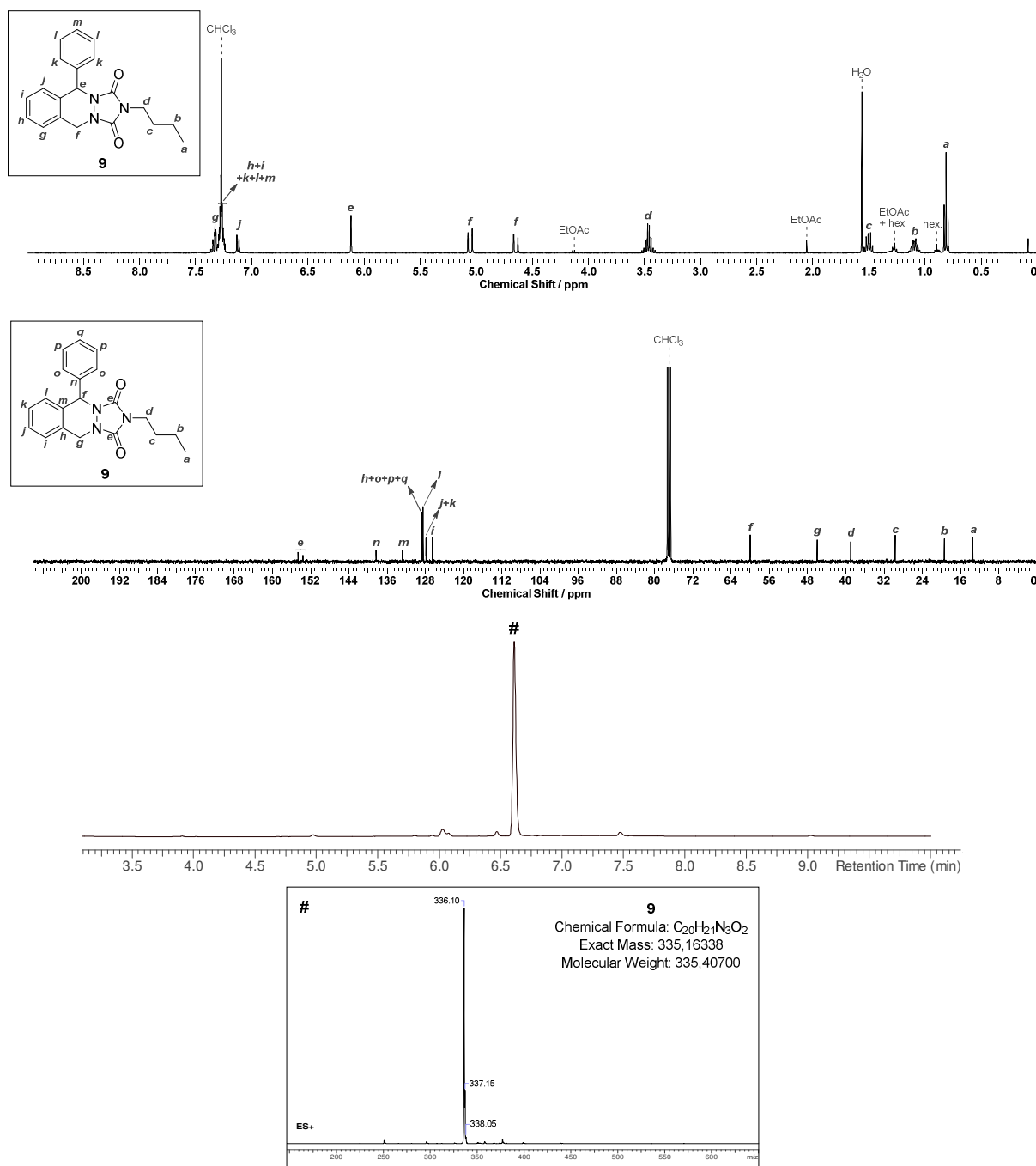


Figure C.5. ^1H - and ^{13}C -NMR spectra, recorded in CDCl_3 , and LC-MS trace with the corresponding mass spectrum, used for the structure elucidation of the cyclic reduction product **9**. All peaks in the depicted NMR spectra were assigned in agreement with the corresponding 2D spectra (i.e. COSY, HSQC and HMBC).

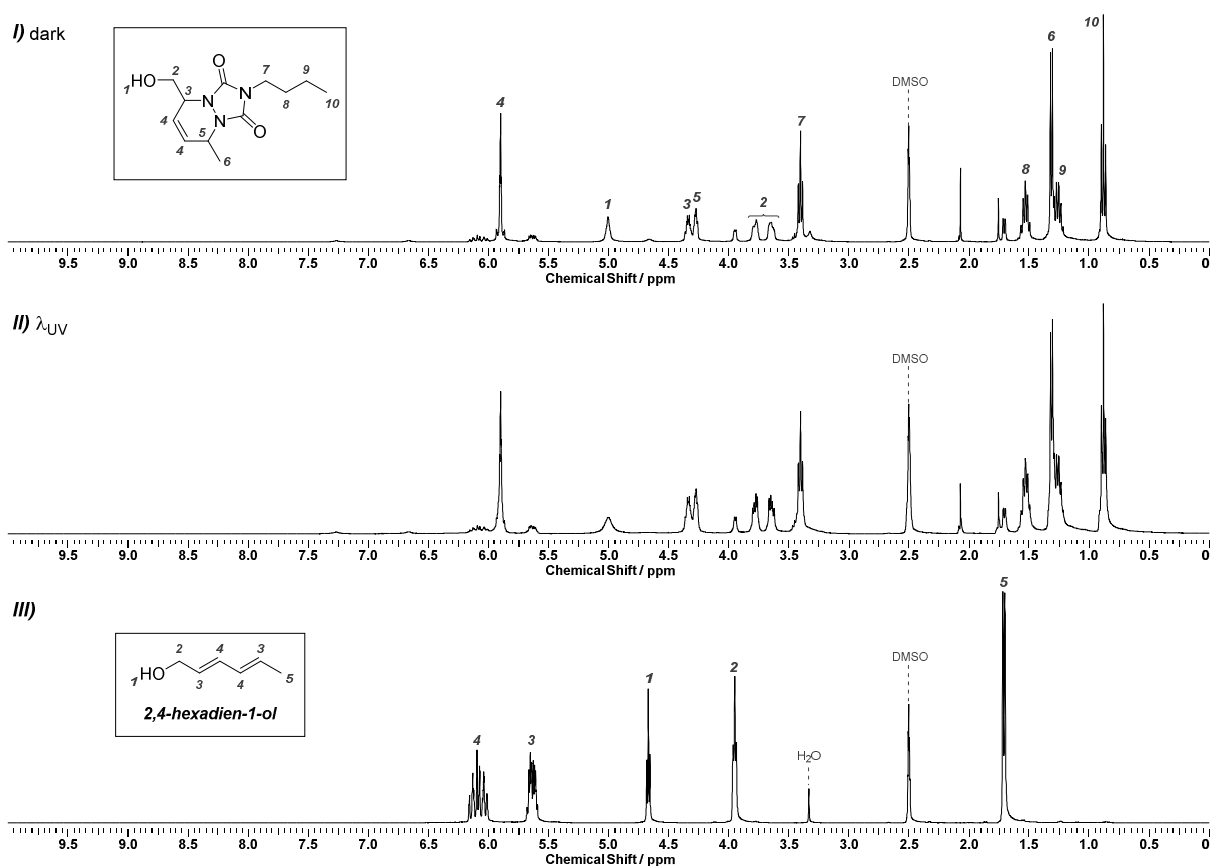


Figure C.6. $^1\text{H-NMR}$ spectra of BuTAD 1 after addition of *trans,trans*-2,4-hexadien-1-ol (1.1 eq.) before (spectrum I) and after irradiation with UV-light at $\lambda_{\text{max}} = 320 \text{ nm}$ (4 h, Arimed B6, 3 x 36 W, spectrum II) indicating the absence of photodegradation. The residual signals in spectrum II are attributed to the slight excess of the diene TAD-trap, evidenced by comparison with reference spectrum III. Spectra were recorded in $\text{DMSO-}d_6$ in order to provide better solubility of the potential photodegradation products.

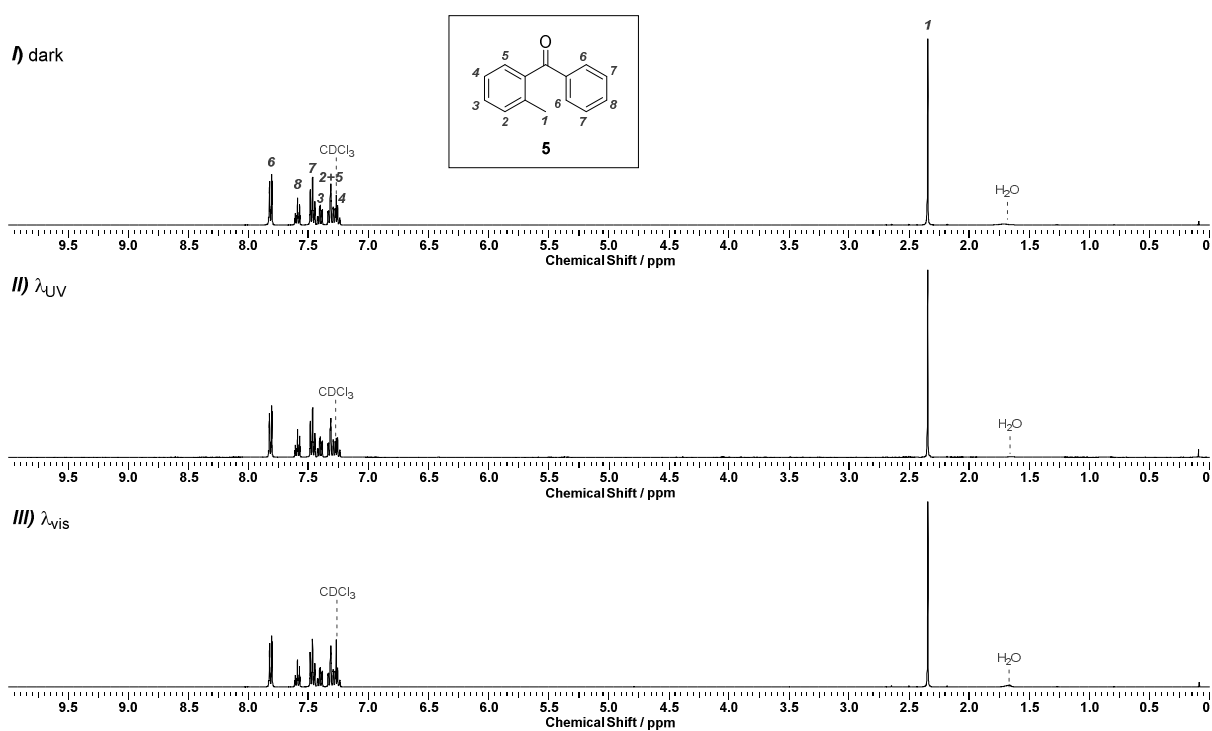


Figure C.7. $^1\text{H-NMR}$ spectra of *o*-methylbenzophenone (5, 0.15 M in CDCl_3) before (spectrum I) and after irradiation with UV-light at $\lambda_{\text{max}} = 320$ nm (4 h, Arimed B6, 3 x 36 W, spectrum II) or visible light at $\lambda = 544$ nm (1 h, 4 mW cm^{-2} , 100 Hz, Innolas tunable laser, spectrum III), indicating the absence of photodegradation.

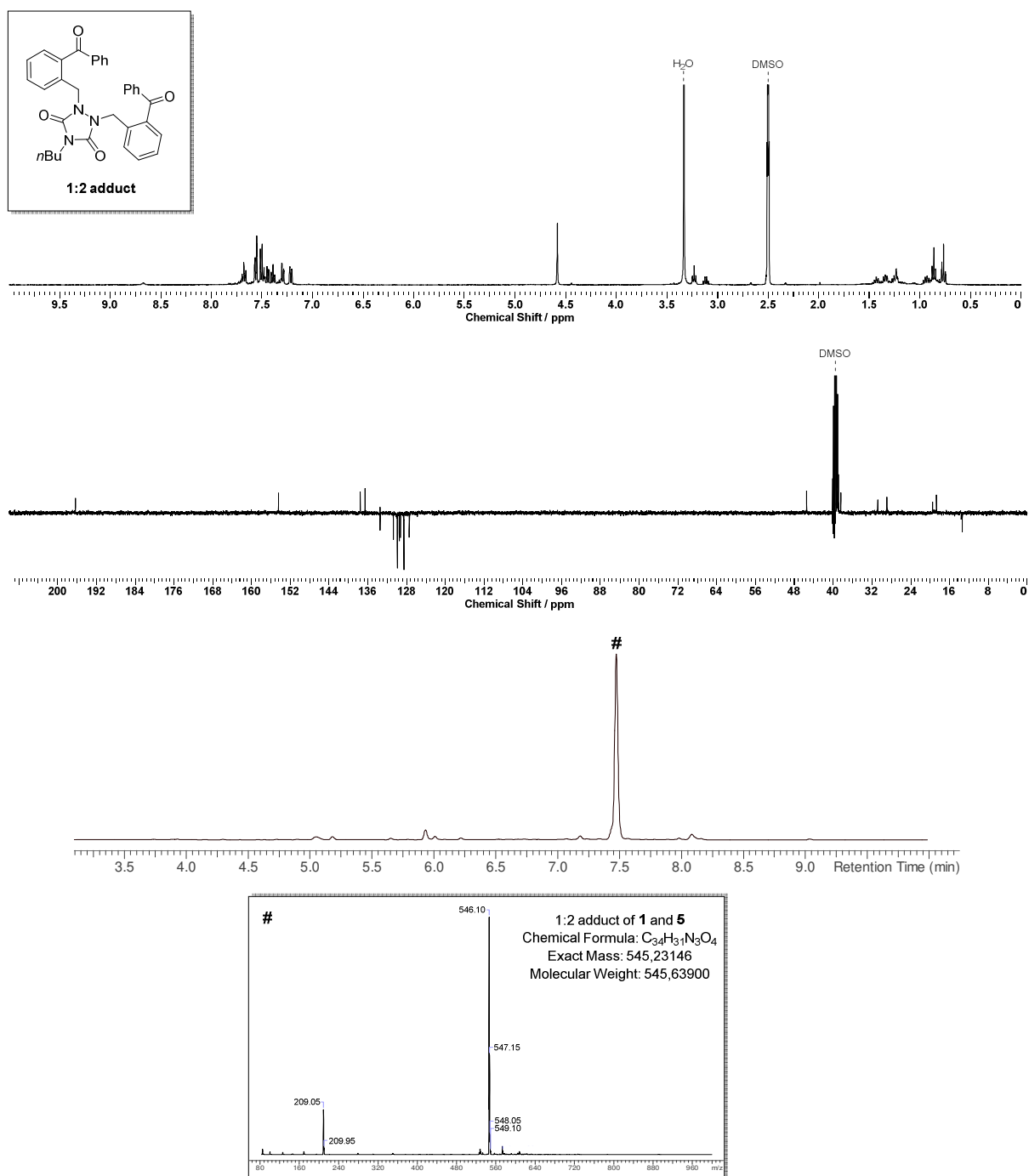


Figure C.8. ^1H - and ^{13}C -NMR spectra (APT), recorded in CDCl_3 , and LC-MS trace with the corresponding mass spectrum, indicating the presence of a 1:2 addition product, formed upon reaction of **1** and **5**. A double benzylic addition product was suggested, based on 2D NMR spectra (i.e. COSY, HSQC and HMBC).

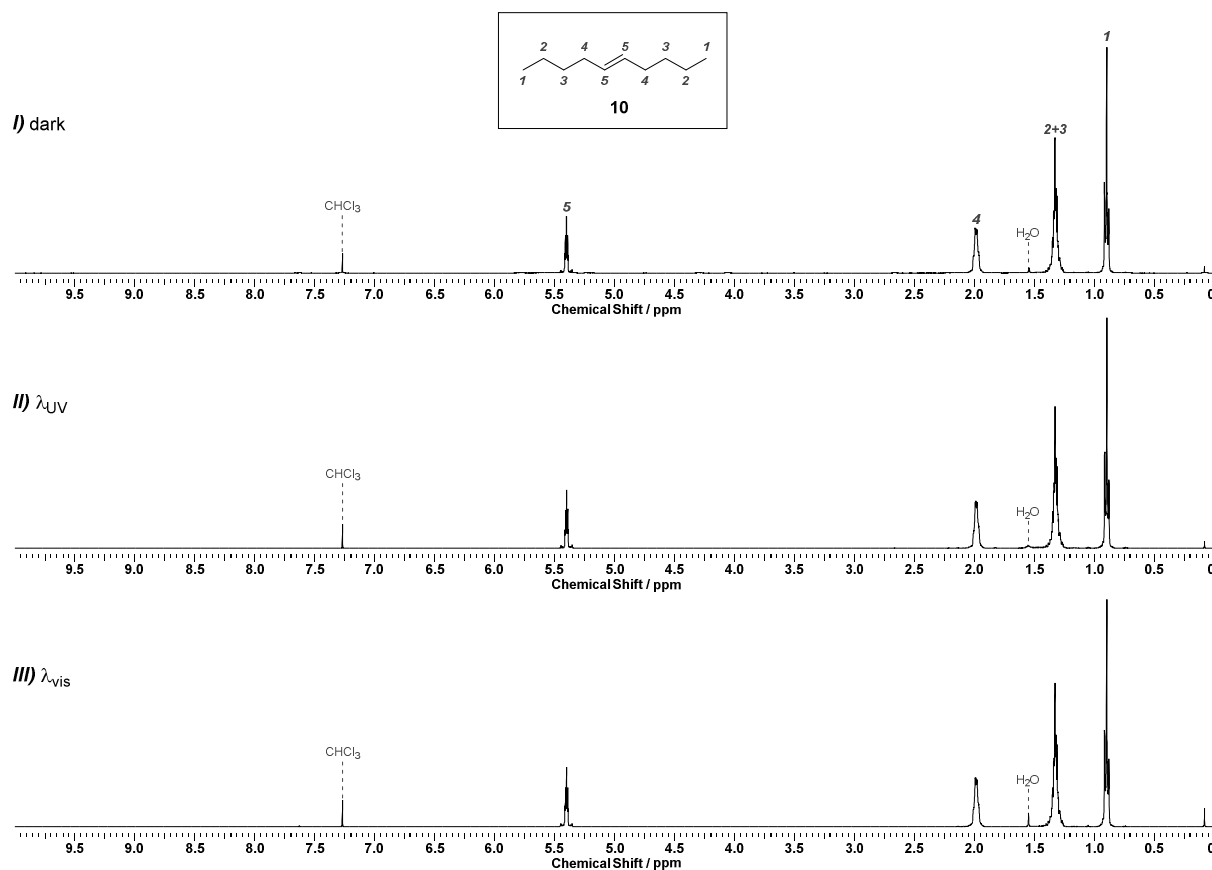


Figure C.9. $^1\text{H-NMR}$ spectra of *trans*-5-decene (**10**, 0.15 M in CDCl_3) before (spectrum I) and after irradiation with UV-light at $\lambda_{\text{max}} = 320$ nm (4 h, Arimed B6, 3 x 36 W, spectrum II) or visible light at $\lambda = 544$ nm (1 h, 4 mW cm^{-2} , 100 Hz, Innolas tunable laser, spectrum III), indicating no photodegradation to occur.

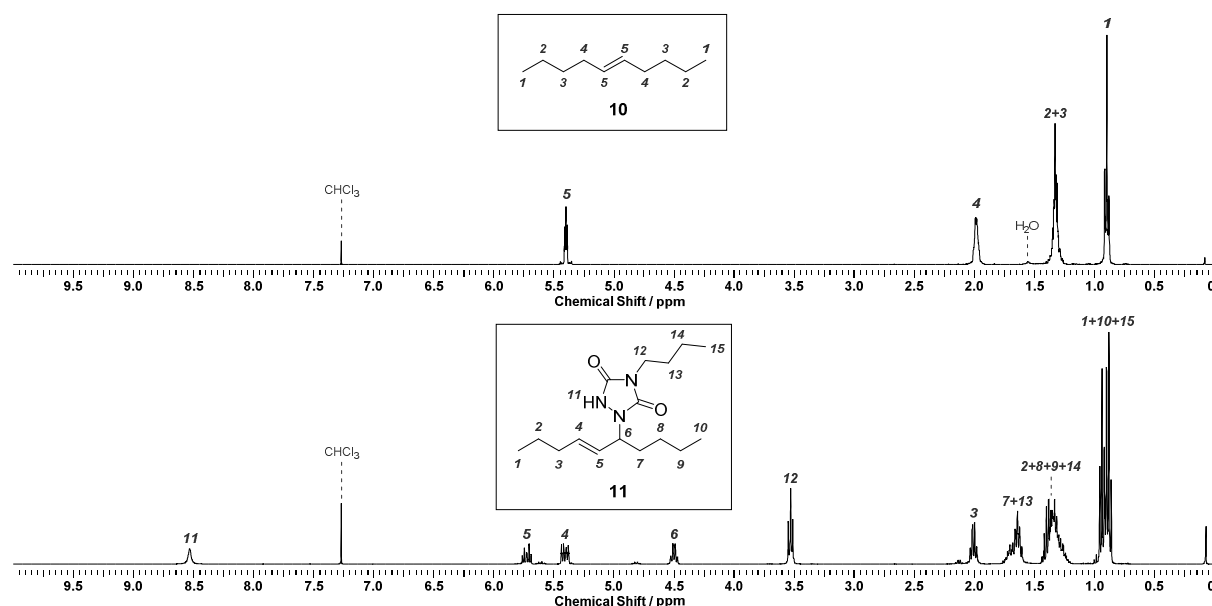


Figure C.10. $^1\text{H-NMR}$ spectra of *trans*-5-decene (**10**, 0.15 M in CDCl_3) before (spectrum I) and after addition of an equimolar amount of BuTAD (**1**, 0.15 M in CDCl_3), indicating the exclusive formation of a 1:1 Alder-ene addition product.

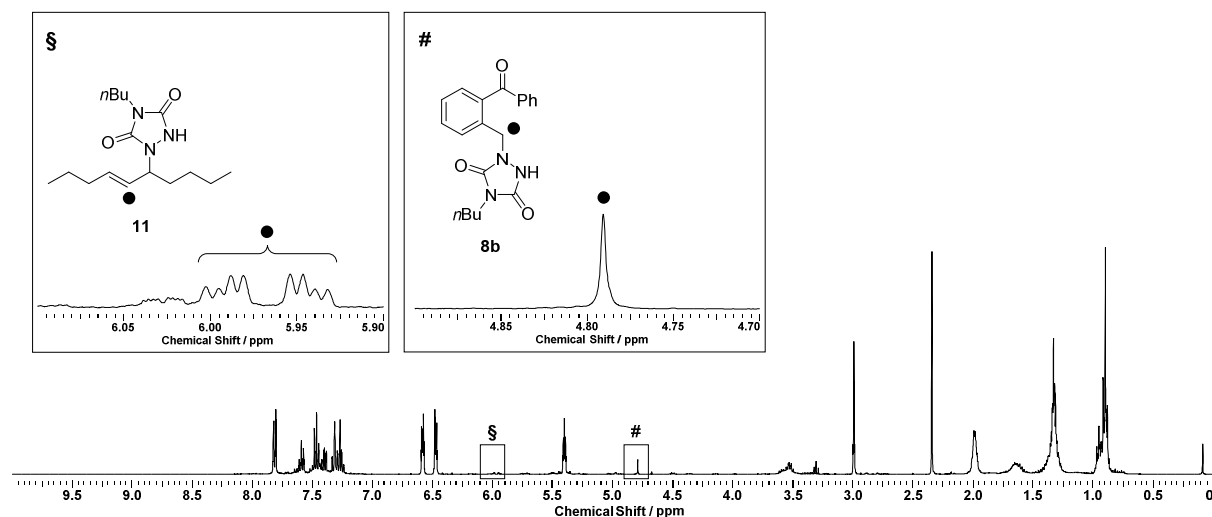
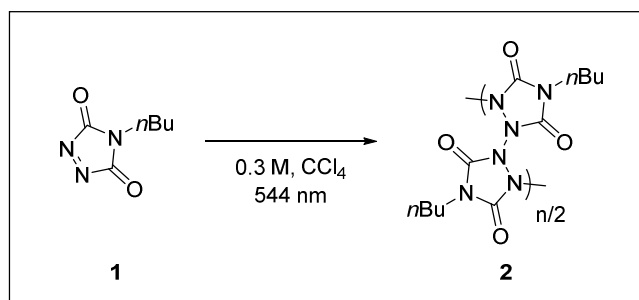


Figure C.11. Representative $^1\text{H-NMR}$ spectrum, obtained from the reaction mixture of the light-switchable one-pot manifold (containing an equimolar mixture of the TAD-photopolymer **2**, photocaged diene **5** and thermal alkene substrate **10**, 0.15 M in CDCl_3) after 2 h UV-light, followed by 8 h standing in the dark, 1 h of visible light impact, 4 h of UV-irradiation and finally 8 h of dark time. The conversion of the photoaddition products **8a+8b** as well as thermal TAD-conjugation product **11** was determined via integration of the well-resolved proton signals # and §, respectively (see inset).

C.2 Experimental procedures

C.2.1 Photopolymerisation of BuTAD (1) upon visible light irradiation



A stock solution of **1** (0.3 M, 69.8 mg, 0.60 mmol) in 1.5 mL carbon tetrachloride was sealed with a septum and deoxygenated by flushing with N_2 -gas for 15 minutes. The resulting solution was divided into 0.2 mL portions in crimp neck vials (0.7 mL volume) which were quickly flushed with N_2 -gas and crimped airtight. The bright purple solution was placed in the sample holder of the wavelength-tunable laser and irradiated at 544 nm (4.0 mW cm^{-2} , 100 Hz) until a clear colorless solution of photopolymer **2** was obtained (i.e. within 10 minutes).

Upon standing in the dark, the reaction mixture quickly regained a faint purple color which was evidenced by UV/vis kinetic measurements at $\lambda_{\text{max}} = 544 \text{ nm}$ upon diluting the sample with carbon tetrachloride (1 mM) (refer to Figure IV.2).

The photopolymerisation was also successfully carried out at lower wavelengths (i.e. down to 440 nm) – keeping the number of incident photons constants (*vide infra*) – although longer irradiation times were required (i.e. up to 30 min).

Similar results were obtained when the solvent was changed to deuterated chloroform, thereby readily enabling $^1\text{H-NMR}$ analysis (*cf.* Figure IV.3).

$^1\text{H-NMR}$ (400 MHz, CDCl_3): δ (ppm) = 0.95 (broad m, 3H, CH_3), 1.40 (broad m, 3H, $\text{CH}_3\text{-CH}_2$), 1.68 (broad m, 3H, $\text{N-CH}_2\text{-CH}_2$), 3.31 + 3.60 (t + broad m, 2H, N-CH_2); recorded 8 minutes after irradiation.

Solutions of **1** in acetonitrile did not give a clear colorless solution upon irradiation, even after prolonged times of 1 h (refer to Figure IV.5). Furthermore, no increase in absorbance was observed over time.

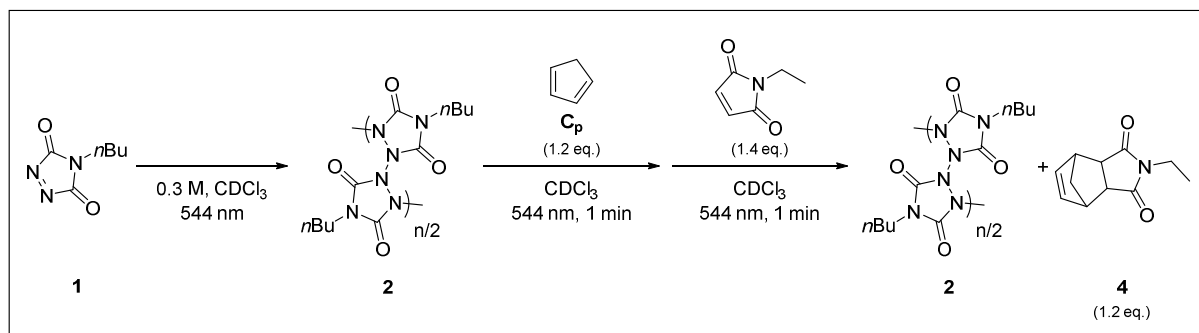
C.2.2 Photostability assessment of BuTAD (**1**) as a function of the applied wavelength

An airtight crimped headspace vial containing **1** (36 mg, 0.23 mmol) was placed under $\text{N}_2(\text{g})$ atmosphere. To this, 7.2 mL of beforehand deoxygenated (flushed with N_2 -gas for 20 min) anhydrous acetonitrile was added. The resulting purple stock solution was divided into over crimp neck vials (0.7 mL) in 0.25 mL portions which were quickly flushed with N_2 -gas and crimped airtight. Each sample was placed in the sample holder of the wavelength-tunable laser and irradiated at a distinct wavelength in the range of 320 to 560 nm with 10 nm intervals. The targeted pulse energy of the laser was set carefully to maintain a constant number of incident photons that were introduced into the sample, independent of the applied wavelength (see Table IV. 1). The targeted energy was calculated according to a calibration curve that was reported elsewhere,^{131, 392} yet for the same laser system applied in the current study, in which the absorption of the incident laser light by the glass of the sample recipient is corrected for. The total number of incident photons was readily altered by changing the number of pulses that are emitted by the laser, which is directly proportional to the irradiation time. After irradiation, 0.1 mL of the resulting solution was diluted with acetonitrile (3.4 mL) and subjected to UV/vis analysis. The photostability was determined by the ratio of the absorbance (at $\lambda_{\text{max}} = 527$ nm) of the respective sample before and after irradiation. The results are depicted in Figure IV.5b.

Table IV. 1. Parameters used to assess the photostability of **1** in acetonitrile (5 mg mL⁻¹) at distinct wavelengths (i.e. from 320 to 560 nm in 10 nm intervals) for three different numbers of incident photons. The targeted pulse energy was calculated, thereby taking into account the absorbance of the glass recipients (determined by means of a calibration curve reported elsewhere^{131, 392}), in order to maintain a constant number of incident photons that were deposited into the sample at the distinct wavelengths under investigation. N_p = number of incident photons.

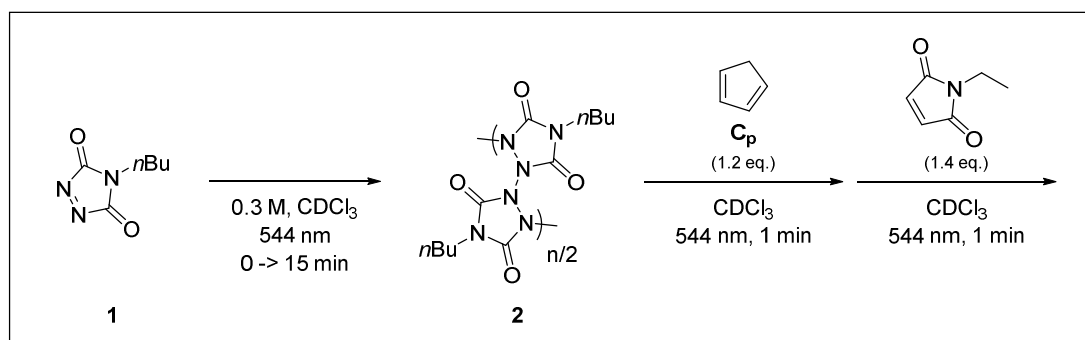
λ (nm)	Targeted pulse energy (μJ)	Measured pulse energy output (μJ)		
		$N_p = 3.42 \cdot 10^{18}$	$N_p = 8.54 \cdot 10^{18}$	$N_p = 1.71 \cdot 10^{19}$
320	627.2	628	628	628
330	562.1	567	563	562
340	537.3	537	535	536
350	500.0	502	499	502
360	471.2	470	472	470
370	470.3	469	470	470
380	454.7	456	454	454
390	428.9	429	430	429
400	422.5	421	427	423
410	384.4	385	385	385
420	366.2	365	366	366
430	349.3	349	348	349
440	338.6	338	340	337
450	327.9	329	328	327
460	318.6	323	314	315
470	310.3	309	308	310
480	300.5	298	299	301
490	291.8	293	290	293
500	284.0	286	284	285
510	276.3	278	277	278
520	268.9	270	271	268
530	261.8	262	262	261
540	255.1	254	253	254
550	248.5	250	248	250
560	242.3	242	243	241

C.2.3 Trapping experiment to demonstrate the photodeactivation of BuTAD (1)



An airtight crimped headspace vial containing **1** (93.1 mg, 0.60 mmol) was placed under N₂-gas atmosphere, followed by the addition of 2.0 mL of deuterated chloroform (beforehand deoxygenated by flushing with N₂-gas for 20 min). The resulting 0.3 M stock solution of **1** (9.31 mg, 0.060 mmol, 1 eq.) was next divided into 0.2 mL portions in a crimp neck vial (0.7 mL) and briefly flushed with N₂-gas before being crimped airtight. The sample was placed in the sample holder of a wavelength-tunable laser and irradiated at 544 nm (4.0 mW cm⁻², 100 Hz) for 10 min to give a clear colorless solution of **2**. Subsequently, under continuous irradiation with green laser light, 0.2 mL of a 0.3 M stock solution of cyclopentadiene (C_p, 4.76 mg, 0.072 mmol, 1.2 eq.) was added through the septum of the crimp neck vial. Whilst the visible light was kept switched on, the mixture was allowed to stand for 1 additional minute to ensure for any active TAD to be trapped by C_p. Next, *N*-ethylmaleimide (10.5 mg, 0.084 mmol, 1.4 eq.) in 0.2 mL deuterated chloroform was added and allowed to react for 1 minute thereby quenching any non-reacted C_p in the Diels-Alder adduct **4** before the visible light was eventually switched off. The resulting mixture quickly reinstated a faint purple colour indicating the regeneration of **1**. Offline ¹H-NMR analysis (*cf.* Figure IV.6) indicated the complete absence of the C_p-**1** Diels-Alder adduct. Thus, no active TAD species were present upon visible light irradiation, thereby demonstrating that quantitative photodeactivation of **1** took place.

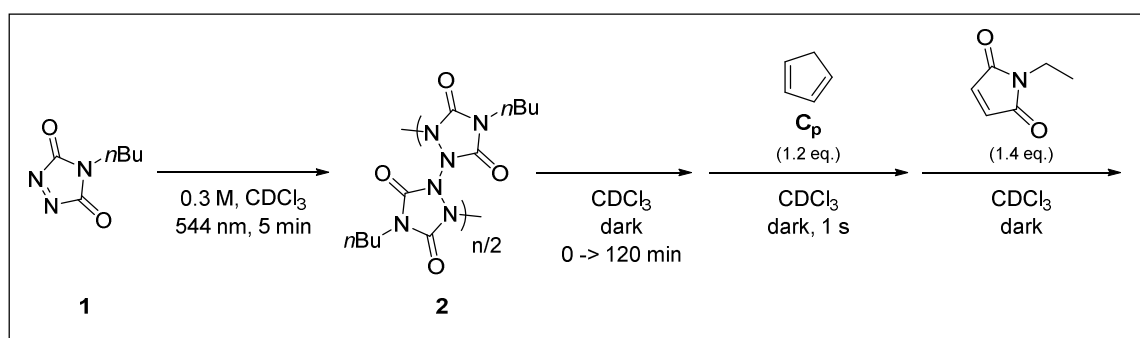
C.2.4 Kinetic study of the photopolymerisation of BuTAD (1)



An airtight crimped headspace vial containing **1** (93.1 mg, 0.60 mmol) was placed under N₂-gas atmosphere, followed by the addition of 2.0 mL of deuterated chloroform (beforehand

deoxygenated by flushing with N_2 -gas for 20 min). The resulting 0.3 M stock solution of **1** (9.31 mg, 0.060 mmol, 1 eq.) was next divided into 0.2 mL portions in a crimp neck vial (0.7 mL) and briefly flushed with N_2 -gas before being crimped airtight. The resulting solutions of **1** (9.31 mg, 0.060 mmol, 1 eq.) were subsequently placed in the sample holder of a wavelength-tunable laser and irradiated at 544 nm (4.0 mW cm^{-2} , 100 Hz). Each sample was subjected to a distinct period of visible light (i.e. 0, 0.5, 1.0, 1.5, 2.5, 5.0, 7.5, 10.0, 12.5 and 15.0 minutes). The fraction of any remaining monomer **1** was locked-in upon addition of 0.2 mL of a 0.3 M stock solution of cyclopentadiene (C_p , 4.76 mg, 0.072 mmol, 1.2 eq.). The mixture was allowed to stand for 1 additional minute to ensure complete trapping of all remaining TAD into the C_p -**1** Diels-Alder adduct **3**, whilst the visible light was kept switched on. Subsequently, *N*-ethylmaleimide (10.5 mg, 0.084 mmol, 1.4 eq.) in 0.2 mL deuterated chloroform was added and allowed to stand for 1 additional minute under irradiation to quench the excess of C_p in a second Diels-Alder adduct **4** before the visible light was eventually switched off. The obtained reaction mixtures were subjected to offline $^1\text{H-NMR}$ analysis from which the monomer conversion over time was determined (refer to Figure IV.7a).

C.2.5 Regeneration kinetics of BuTAD (**1**) after photopolymerisation



An airtight crimped headspace vial containing **1** (93.1 mg, 0.60 mmol) was placed under N_2 -gas atmosphere, followed by the addition of 2.0 mL of deuterated chloroform (beforehand deoxygenated by flushing with N_2 -gas for 20 min). The resulting 0.3 M stock solution of **1** (9.31 mg, 0.060 mmol, 1 eq.) was next divided into 0.2 mL portions in a crimp neck vial (0.7 mL) and briefly flushed with N_2 -gas before being crimped airtight. The resulting solutions of **1** (9.31 mg, 0.060 mmol, 1 eq.) were subsequently placed in the sample holder of a wavelength-tunable laser and irradiated at 544 nm (4.0 mW cm^{-2} , 100 Hz) for 5 minutes to give a clear colourless solution of **2**. Each sample was allowed to stand in the dark (at $18 \text{ }^\circ\text{C}$) for a well-defined period of time (i.e. 0, 5, 10, 15, 30, 45, 60, 90 and 120 minutes) to regenerate the initial purple coloured monomer. The fraction of regenerated **1** after a certain dark time was locked-in by the addition of 0.2 mL of a 0.3 M solution of cyclopentadiene (C_p , 4.76 mg, 0.072 mmol, 1.2 eq.) in deuterated chloroform to form the C_p -**1** Diels-Alder adduct **3**. After 1 second, *N*-ethylmaleimide (10.5 mg, 0.084 mmol, 1.4 eq.) in 0.2 mL deuterated chloroform was added in order to quench the excess, non-reacted C_p in a second Diels-Alder adduct (**4**). The obtained reaction mixtures quickly regained a faint

purple colour as a result of the continued release of **1** over time in the non-reactive mixture. The fraction of regenerated **1** was determined over time via offline $^1\text{H-NMR}$ analysis (refer to Figure IV.7c).

The same experiment was repeated, yet with addition of C_p immediately after the visible light-induced photopolymerisation as to determine the regeneration of **1** in the presence of C_p as an *in situ* trap (refer to Figure IV.7c). In this case, the fraction of regenerated **1** was effectively locked-in upon addition of *N*-ethylmaleimide after standing in the dark (18 °C) for a well-defined period in time (i.e. 0, 5, 10, 15, 30, 45, 60, 90 and 120 minutes). Alternatively, the exact same regeneration experiment, i.e. with the addition of C_p immediately after the visible light-induced photopolymerisation, was repeated upon UV-irradiation at $\lambda_{\text{max}} = 320$ nm with 3 x 36 W Arimed B6 lamps in a custom-built photoreactor (at 25 °C) (refer to Figure IV.7c).

The regeneration kinetics were also monitored over time at different temperatures (i.e. 18 °C, 25 °C and 35 °C) for 5 h via the absorbance of **1** at $\lambda_{\text{max}} = 540$ nm in a UV/vis spectrophotometer coupled to a temperature control unit. For this, the solution of **2** obtained after visible light irradiation was diluted with chloroform to a concentration of 7.5 mM before being transferred into a cuvette (refer to Figure IV.7d).

C.2.6 Photostability assessment of *o*-methylbenzophenone (**5**) and *trans*-5-decene (**10**)

Upon UV-light irradiation

An airtight crimped headspace vial with septum containing *o*-methylbenzophenone **5** (29.4 mg, 0.15 mmol) and/or *trans*-5-decene **10** (21.0 mg, 0.15 mmol) was placed under N_2 -gas atmosphere followed by the addition of 1.0 mL deuterated chloroform (beforehand deoxygenated by flushing with N_2 -gas for 20 min). The resulting 0.15 M solution was transferred into a custom-built photoreactor and irradiated for 4 h at $\lambda_{\text{max}} = 320$ nm with 3 x 36 W Arimed B6 compact fluorescent lamps. The photostability was assessed by comparison of the $^1\text{H-NMR}$ spectra before and after irradiation (refer to C.1).

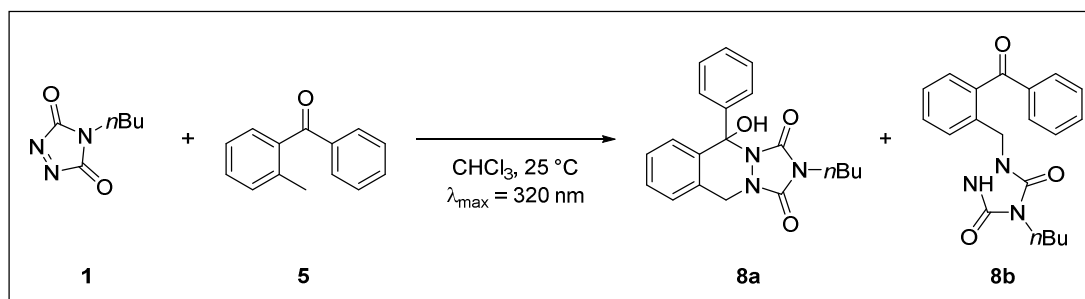
Upon visible light irradiation

An airtight crimped headspace vial with septum containing *o*-methylbenzophenone **5** (29.4 mg, 0.15 mmol) and/or *trans*-5-decene **10** (21.0 mg, 0.15 mmol) was placed under N_2 -gas atmosphere followed by the addition of 1.0 mL deuterated chloroform (beforehand deoxygenated by flushing with N_2 -gas for 20 min). 0.4 mL of the resulting 0.15 M stock solution was transferred into a crimp neck vial (0.7 mL) and quickly flushed with N_2 -gas before being crimped airtight. The sample was placed in the sample holder of the wavelength-tunable laser and irradiated for 1 hour at 544 nm (4.0 mW cm^{-2} , 100 Hz). The photostability was assessed by comparison of the $^1\text{H-NMR}$ spectra before and after irradiation (refer to C.1).

C.2.7 Photostability assessment of BuTAD (1) under UV-light

An airtight crimped headspace vial with septum containing BuTAD **1** (9.31 mg, 0.06 mmol, 1.0 eq.) was placed under N₂-gas atmosphere. To this, 0.2 mL of deuterated chloroform (beforehand deoxygenated by flushing with N₂-gas for 20 min) was added. The resulting 0.3 M stock solution was transferred into a custom-built photoreactor and irradiated with 3 x 36 W Arimed B6 compact fluorescent lamps ($\lambda_{\max} = 320$ nm) for 4 h. Immediately after irradiation, a slight excess of *trans,trans*-2,4-hexadien-1-ol (HDEO, 6.5 mg, 0.07 mmol, 1.1 eq.) in 0.3 mL deuterated chloroform was added. The photostability was eventually determined by comparing the ¹H-NMR spectra obtained after irradiation with a dark non-irradiated reference sample (refer to C.1).

C.2.8 Light-induced photoenol reaction of 1 with 5

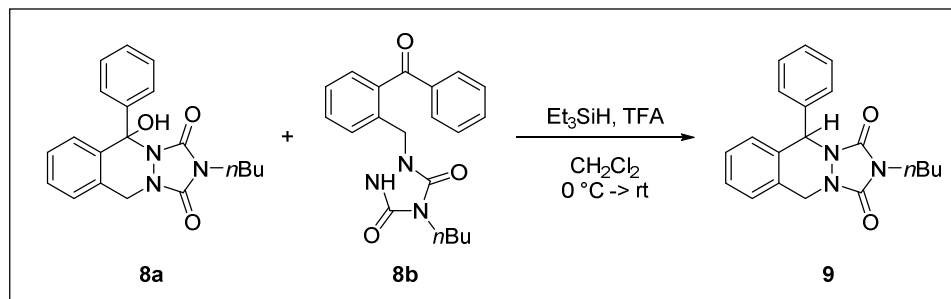


A mixture of BuTAD (**1**, 93.1 mg, 0.6 mmol, 1.0 eq.) and *o*-methylbenzophenone **5** (118 mg, 0.6 mmol, 1.0 eq.) in 20 mL chloroform, deoxygenated by flushing with N₂-gas for 10 min, was added to an airtight crimped headspace vial which was placed under nitrogen atmosphere. The mixture was transferred into a custom-built photoreactor and irradiated with 3 x 36 W Arimed B6 compact fluorescent lamps ($\lambda_{\max} = 320$ nm) for 2.5 hours to give a clear faint yellow solution. Solvent removal *in vacuo* resulted in a yellow oil that contained an equilibrium mixture of **8a** and **8b**. Purification by means of column chromatography (silica, eluent: various mixtures of ethyl acetate and hexanes) failed to separate the product mixture (156 mg – 74 %). Found product ratio **8a**:**8b** = 1:14 in CDCl₃ and **8a**:**8b** = 1:3 in DMSO-*d*₆.

¹H-NMR (500 MHz, CDCl₃): **8b**, δ (ppm) = 0.93 (t, 3H, CH₃), 1.32 (m, 2H, CH₃-CH₂), 1.62 (m, 2H, N-CH₂-CH₂), 3.52 (t, 3H, N-CH₂), 4.77 (s, 2H, Ar-CH₂), 7.40-7.47 (m, 2H, ArH), 7.48-7.54 (t, 2H, ArH), 7.55-7.60 (m, 1H, ArH), 7.62-7.69 (m, 2H, ArH), 7.82 (m, 2H, ArH), 8.43 (s, 1H, NH); **8a**, some resolved resonances: 4.80 (d, 1H, CH₂), 4.96 (d, 1H, CH₂). ¹³C-NMR (500 MHz, CDCl₃): δ (ppm) = 13.58 (CH₃), 19.81 (CH₂), 30.02 (CH₂), 39.12 (CH₂), 47.19 (CH₂), 127.91 (CH), 128.61 (CH), 130.30 (CH), 130.74 (CH), 131.86 (CH), 132.02 (CH), 133.92 (CH), 135.15 (C), 137.04 (C), 137.62 (C), 152.99 (C), 153.38 (C), 198.55 (C). ¹H-NMR (500 MHz, DMSO-*d*₆): **8b**, δ (ppm) = 0.82 (t, 3H, CH₃), 1.12 (m, 2H, CH₃-CH₂), 1.39 (m, 2H, N-CH₂-CH₂), 3.25 (t, 3H, N-CH₂), 4.70 (s, 2H, Ar-CH₂), 7.32-7.39 (m, 1H, ArH), 7.41-7.48 (m, 2H, ArH), 7.50-7.61 (m, 3H, ArH), 7.63-7.75 (m, 3H, ArH), 10.28 (s, 1H, NH); **8a**, some

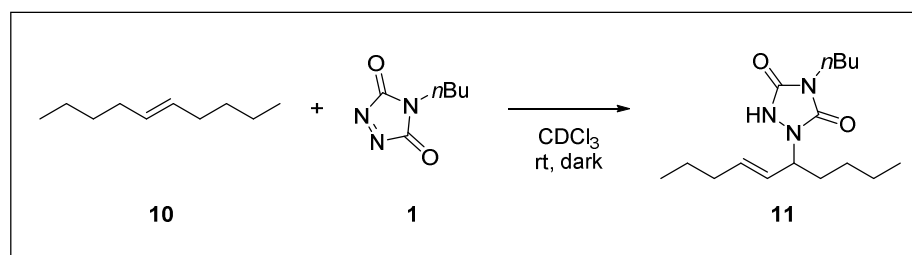
resolved resonances: 4.74 (d, 1H, Ar-CH₂), 4.96 (d, 1H, Ar-CH₂), 6.89 (d, 1H, OH), 7.19 (t, 1H, ArH). LC-MS (m/z): 352.15 [MH]⁺. HRMS (m/z): *calc.*: 352.1656, *found*: 352.1701 [MH]⁺.

C.2.9 Reduction of the photoenol product mixture 8a+8b into cyclic 9



A mixture of BuTAD (**1**, 93.1 mg, 0.6 mmol, 1.0 eq.) and *o*-methylbenzophenone **5** (118 mg, 0.6 mmol, 1.0 eq.) in 20 mL of chloroform (deoxygenated by flushing with N₂-gas for 10 min) was added to an airtight crimped headspace vial placed under nitrogen atmosphere. The mixture was placed in a custom-built photoreactor and irradiated for 2.5 hours with 3 x 36 W Arimed B6 compact fluorescent lamps ($\lambda_{\text{max}} = 320$ nm) to give a clear faint yellow solution. Solvent removal *in vacuo* afforded a yellow oil that contained an equilibrium mixture of **8a** and **8b**, together with traces of unreacted **5**. The obtained crude reaction mixture was subsequently dissolved in 5 mL of anhydrous dichloromethane and added dropwise at 0 °C to a cooled solution of triethylsilane (1.15 mL, 7.2 mmol, 6.0 eq.) and trifluoroacetic acid in 5 mL of anhydrous dichloromethane. The mixture was allowed to react for 30 minutes at 0 °C, followed by overnight stirring at room temperature before being quenched with 1 M aqueous sodium hydroxide to pH = 7 (approximately 20 mL). The yellow suspension was phase-separated and the aqueous phase was washed with dichloromethane (15 mL). The combined organic phases were washed with brine (30 mL), dried over magnesium sulfate and concentrated *in vacuo*. The resulting yellow oil was purified by means of column chromatography (silica, ethyl acetate:hexanes 1:9 with a gradient to 1:4) to yield unreacted **5** (14 mg – 12 %, R_F (ethyl acetate:hexanes 1:4) = 0.52) together with the cyclic reduction product **9** (169 mg – 84 %, R_F (ethyl acetate:hexanes 1:4) = 0.15) that was obtained as a white waxy solid.

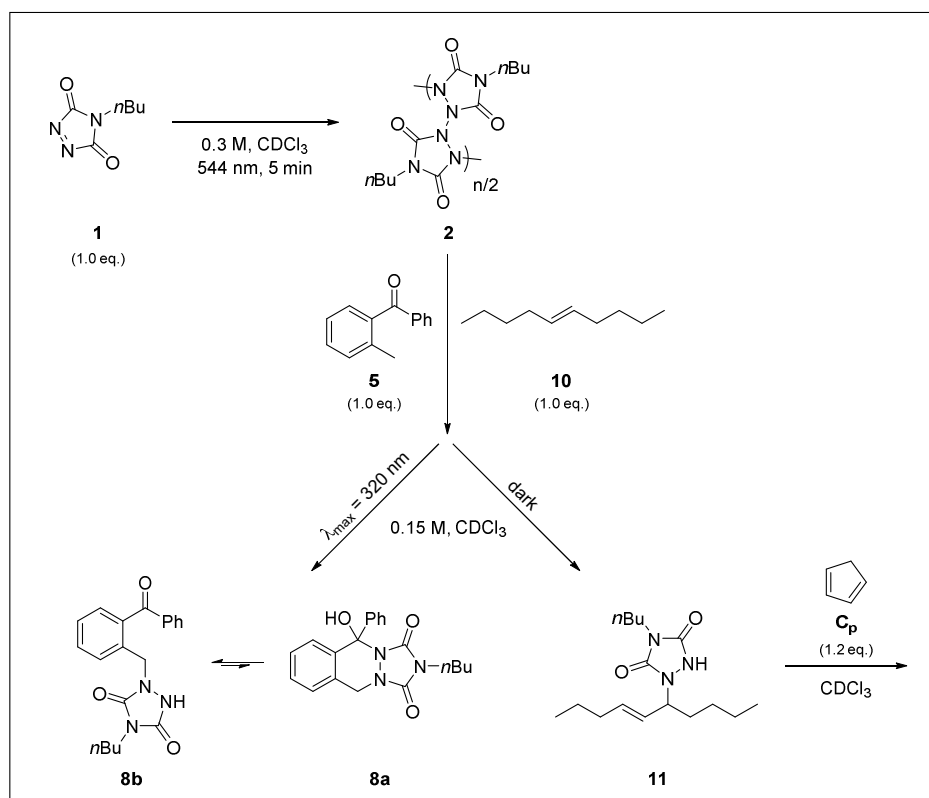
¹H-NMR (500 MHz, CDCl₃): δ (ppm) = 0.81 (t, 3H, CH₃), 1.09 (m, 2H, CH₂-CH₃), 1.50 (m, 2H, N-CH₂-CH₂), 3.46 (m, 2H, N-CH₂-CH₂), 4.65 (d, 1H, Ar-CH₂), 5.06 (d, 1H, Ar-CH₂), 6.12 (s, 1H, Ar-CH), 7.12 (d, 1H, ArH), 7.22-7.38 (m, 8H, ArH). ¹³C-NMR (500 MHz, CDCl₃): δ (ppm) = 13.46 (CH₃), 19.41 (CH₂), 29.69 (CH₂), 38.98 (CH₂), 45.98 (CH₂), 60.03 (CH), 126.56 (CH), 127.81 (CH), 217.85 (CH), 128.45 (CH), 128.54 (CH), 128.57 (CH), 128.65 (C), 128.75 (CH), 132.75 (C), 138.32 (C), 153.62 (C), 154.62 (C). LC-MS (m/z): 336.10 [MH]⁺. HRMS (m/z): *calc.*: 336.1707, *found*: 336.1708 [MH]⁺.

C.2.10 Alder-ene addition of **1** to **10** in the dark

A solution of BuTAD (**1**, 9.31 mg, 0.06 mmol, 1.0 eq.) in 0.2 mL deuterated chloroform was added to a solution of *trans*-5-decene (**7**, 8.42 mg, 0.06 mmol) in 0.2 mL deuterated chloroform and stirred in the absence of light at room temperature. Complete discoloration was observed after 20 minutes to give a colorless solution of the addition product **11** in quantitative yield.

¹H-NMR (400 MHz, CDCl₃): δ (ppm) = 0.84-0.97 (m, 9H, 3 x CH₃), 1.20-1.46 (m, 8H, 3 x CH₃-CH₂ + N-CH-CH₂-CH₂), 1.58-1.77 (m, 4H, N-CH-CH₂ + N-CH₂-CH₂), 2.01 (q, 2H, CH=CH-CH₂), 3.53 (t, 2H, N-CH₂), 4.50 (q, 1H, N-CH), 5.41 (m, 1H, CH=CH-CH), 5.73 (m, 1H, CH=CH-CH), 8.53 (s, 1H, NH).

C.2.11 Light-switchable reaction manifold

Preparation of a 0.30 M stock solution of **1**

An airtight crimped headspace vial with septum containing **1** (186.2 mg, 1.20 mmol, 1.0 eq.) was placed under N₂-gas atmosphere followed by the addition of 4.0 mL deuterated chloroform (beforehand deoxygenated by flushing with N₂-gas for 20 min).

Preparation of a 0.30 M stock solution of 5 and 10

An airtight crimped headspace vial with septum containing a mixture of *o*-methylbenzophenone **5** (235.5 mg, 1.20 mmol, 1.0 eq.) and *trans*-5-decene **10** (168.3 mg, 1.20 mmol, 1.0 eq.) was placed under N₂-gas atmosphere followed by the addition of 4.0 mL deuterated chloroform (beforehand deoxygenated by flushing with N₂-gas for 20 min).

Preparation of a 0.36 M stock solution of C_p

An airtight crimped headspace vial with septum containing cyclopentadiene C_p (95.2 mg, 1.44 mmol, 1.2 eq.) was placed under N₂-gas atmosphere followed by the addition of 4.0 mL deuterated chloroform (beforehand deoxygenated by flushing with N₂-gas for 20 min).

Procedure

The 0.30 M stock solution of **1** in deuterated chloroform was divided into portions of 0.2 mL over several crimp neck vials (0.7 mL), quickly flushed with N₂-gas and crimped airtight. The solutions of **1** were next placed in the sample holder of a wavelength-tunable laser and irradiated at 544 nm (4.0 mW cm⁻², 100 Hz) for 5 minutes to give a clear colourless solution of **2**. Whilst the visible laser light was continuously kept switched on, 0.2 mL of the **5** + **10** stock solution was added through the septum of the crimp neck vial. The resulting mixture was then immediately transferred into a custom-built photoreactor (25 °C) and irradiated at λ_{max} = 320 nm for 2 h with 3 x 36 W Arimed B6 compact fluorescence lamps in order to initiate the formation of the photoproducts **8a**+**8b** (**A**, Figure C.12.). After being subjected to UV-light irradiation, the mixture was kept in the dark (18 °C) for 8 h, thereby enabling the thermal TAD-reaction to proceed to result in the formation of TAD-adduct **11** (**B**). Next, the sample was again placed into the sample holder of a wavelength-tunable laser and irradiated 1 hour at 544 nm (4.0 mW cm⁻², 100 Hz) to give a non-reactive mixture without the formation of any products being detected (**C**). To demonstrate the possibility to initiate the on/off switchability of the reaction manifold a second time, the sample was again transferred into the photoreactor and subjected to 4 hours of UV-light (**D**), followed by standing in the dark for an additional 8 h (**E**).

At each point (i.e. **A**, ... , **E**), 0.2 mL of the 0.36 M C_p stock solution in deuterated chloroform was injected into the samples in order to lock-in the TAD-concentrations upon standing in the dark. In other words, all *in situ* regenerated TAD was now kinetically trapped into the cyclopentadiene Diels-Alder adduct **3** without affecting the concentrations of the formed reaction products during offline ¹H-NMR measurements. The reaction outcome at each point during the experiment was eventually determined via integration of well resolved signals in the obtained ¹H-NMR spectra (*cf.* C.1). Moreover, each experiment (i.e. **A**, ... , **E**) was reproduced in threefold and the average obtained conversions were plotted at the distinct times (refer to Figure C.12.).

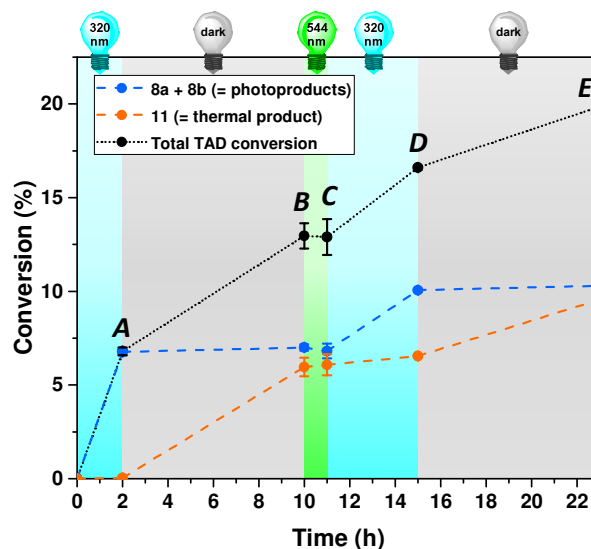


Figure C.12. Outcome of the light-switchable reaction manifold (**2** + **5** + **11**) upon UV-light irradiation (2 hours, point A) followed by standing in the dark (8 hours, point B). During a one-hour period of visible light irradiation, no product conversion was observed (point C), whilst a second on/off cycle demonstrated the possibility for the reaction channels to be accessed again (point D and E). Yields of the photoenol products **8a** + **8b** and thermal addition product **11** were determined via $^1\text{H-NMR}$ and reproduced in threefold. Minor traces ($< 2\%$) of a 2:1 adduct of **1** and **5** were also detected, but did not increase over time.

C.2.12 STED-inspired sub-diffraction lithography experiments

Preparation of the photoresist

The photoresist was prepared by making a 10 mM stock solution of the bromine containing TAD compound **13** in chloroform.

Surface functionalisation

The used glass substrates were functionalised with the silane-containing photoenol precursor **12** according to a literature procedure.¹¹⁸

General procedure

The glass substrate, functionalised with the photoenol precursor **12**, was mounted onto a sample holder comprising an airtight chamber to avoid solvent evaporation during surface lithography. The chamber was filled with the photoresist, sealed and inserted into the lithographic setup, described elsewhere.⁴⁵² A 150 fs pulsed tunable Ti:sapphire oscillator (Coherent Chameleon Ultra II) at a wavelength centred around 700 nm was used as the source of excitation, whereas the depletion was affected by a picosecond pulsed diode laser (Picoquant LDH-P-FA-530XL). The beam intensities were controlled by an Acousto-optic modulators (AA Optic-Electronic) and the beams were focussed through an oil immersion objective lens with a 1.4 numerical aperture (Leica HCX PL APO 100x/1.4-0.7 OIL CS). The sample was held by a three-dimensional piezo stage (Physik Instrumente), allowing for a relative translational motion with respect to the laser beam focus. Samples were exposed to a scan speed of $100\ \mu\text{m s}^{-1}$. After

the writing process of the desired patterns, the samples were immersed into chloroform and additionally rinsed with isopropanol to remove any non-covalently attached TAD compounds from the surface.

Surface-initiated atom-transfer radical polymerisation (SI-ATRP)

Surface-initiated atom-transfer radical polymerisation (SI-ATRP) was carried out conform a literature procedure.^{118, 394}

C.3 Synthetic procedures

C.3.1 Synthesis of 4-*n*-butyl-triazoline-3,5-dione (BuTAD, 1)

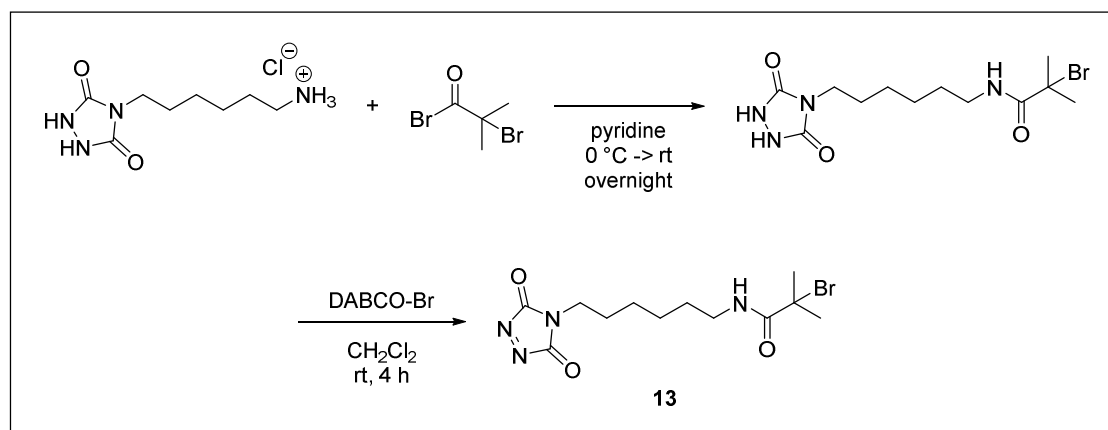
4-*n*-butyl-1,2,4-triazoline-3,5-dione (BuTAD, **1**) was synthesized as described in B.4.3, followed by sublimation under reduced pressure (0.1 mbar) at 40 °C, to give BuTAD (**1**) as a carmine red crystalline product. The reactive compound was stored in the dark at -18 °C and typically used within several weeks. Purity was regularly checked via ¹H-NMR prior to use.

¹H-NMR (400 MHz, DMSO-*d*₆): δ (ppm) = 0.88 (t, 3H, CH₃, *J* = 7.3 Hz), 1.30 (sext, 2H, CH₂-CH₃, *J* = 7.3 Hz), 1.56 (quint, 2H, N-CH₂-CH₂, *J* = 7.3 Hz), 3.47 (t, 2H, N-CH₂, *J* = 7.0 Hz). ¹³C-NMR (100 MHz, DMSO-*d*₆): δ (ppm) = 13.32 (CH₃), 19.11 (CH₂), 28.72 (CH₂), 40.34 (CH₂), 160.15 (C).

C.3.2 Synthesis of triethoxysilane-containing photoenol precursor 12

The triethoxysilane-containing photoenol precursor **12** was prepared following a procedure described elsewhere.¹²¹ Courtesy of Markus Ziegler (Karlsruhe Institute of Technology).

C.3.3 Synthesis of bromine-containing triazolinedione 13



A mixture of 4-(6-aminohexyl) urazole hydrochloride (1.12 g, 4.71 mmol, 1.0 eq.) in 10 mL anhydrous pyridine was placed under inert atmosphere and cooled in an ice water bath. To this, α -bromoisobutyryl bromide (0.58 mL, 4.71 mmol, 1.0 eq.) was added dropwise at 0 °C. The

resulting mixture was allowed to warm to room temperature and stirred overnight. The yellow solution was evaporated *in vacuo* to dryness and dissolved in a minimal amount of methanol before being purified by means of column chromatography (silica, (ethyl acetate:methanol:acetic acid 95:5:1):(petroleum ether) 2:1, $R_F = 0.35$). After isolation, the product was subjected to co-evaporation with petroleum ether (3 x) to remove traces of residual pyridine and acetic acid. The bromine-containing urazole was obtained as a brown-yellow oil (0.74 g – 45 %).

$^1\text{H-NMR}$ (400 MHz, DMSO- d_6): δ (ppm) = 1.25 (m, 4H, NH-CH₂-CH₂-(CH₂)₂), 1.41 (m, 2H, NH-CH₂-CH₂), 1.51 (m, 2H, C(O)-N-CH₂-CH₂), 3.06 (q, 2H, NH-CH₂, $J = 6.8$ Hz), 3.33 (t, 2H, C(O)-N-CH₂, $J = 7.1$ Hz), 8.01 (t, 1H, NH-CH₂, $J = 5.6$ Hz), 10.01 (s, 2H, NH-NH).

Next, a mixture of the bromine-containing urazole (100 mg, 0.29 mmol, 1.0 eq.) and DABCO-Br (94 mg, 0.06 mmol, 0.2 eq.) in 5 mL dichloromethane was placed under inert atmosphere and stirred at room temperature for 4 hours. The resulting heterogeneous mixture was filter, washed with dichloromethane (2 x 5 mL) and evaporated *in vacuo* to dryness, keeping the temperature below 35 °C. The resulting bromine-containing triazolinedione **13** was obtained as a red oil, which was stored at -18 °C kept away from ambient light (74 mg – 73 %).

$^1\text{H-NMR}$ (400 MHz, DMSO- d_6): δ (ppm) = 1.36 (m, 4H, NH-CH₂-CH₂-(CH₂)₂), 1.55 (m, 2H, NH-CH₂-CH₂), 1.70 (m, 2H, C(O)-N-CH₂-CH₂), 3.26 (m, 2H, NH-CH₂), 3.66 (t, 2H, C(O)-N-CH₂, $J = 7.2$ Hz), 6.73 (s, 1H, NH-CH₂).

Appendix D.

Experimental section Chapter V

D.1 Additional figures

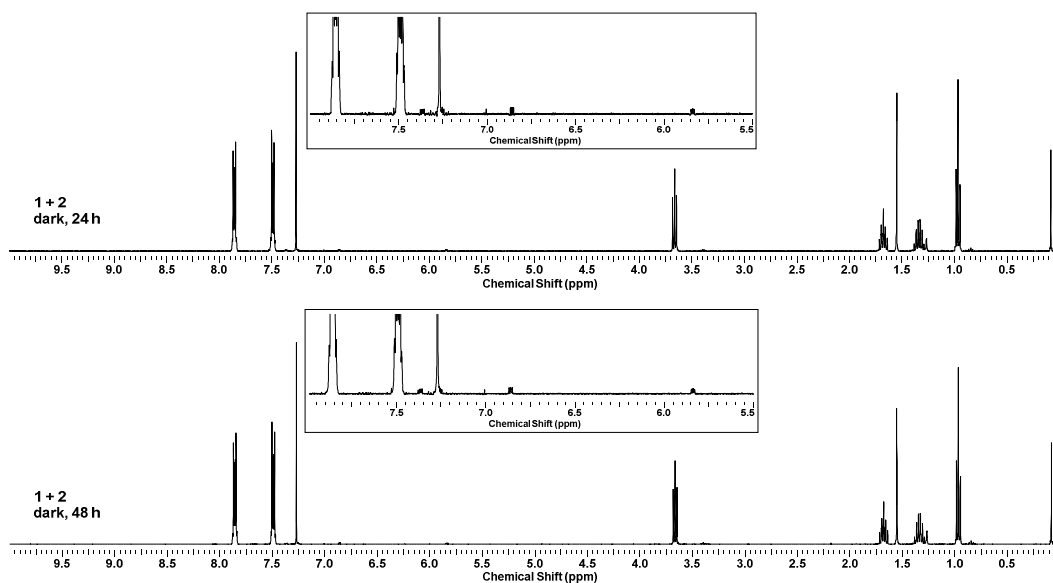


Figure D.1. $^1\text{H-NMR}$ spectra obtained upon mixing BuTAD (**1**) with equimolar amounts of plain naphthalene (**2**) in deuterated chloroform (CDCl_3 , 15 mM), kept in the dark. An equilibrium concentration is reached after 24 hours, whereby ca. 2 % of the corresponding cycloadduct **3** is formed (top). No change in concentration of **3** was observed over the course of 48 hours (bottom).

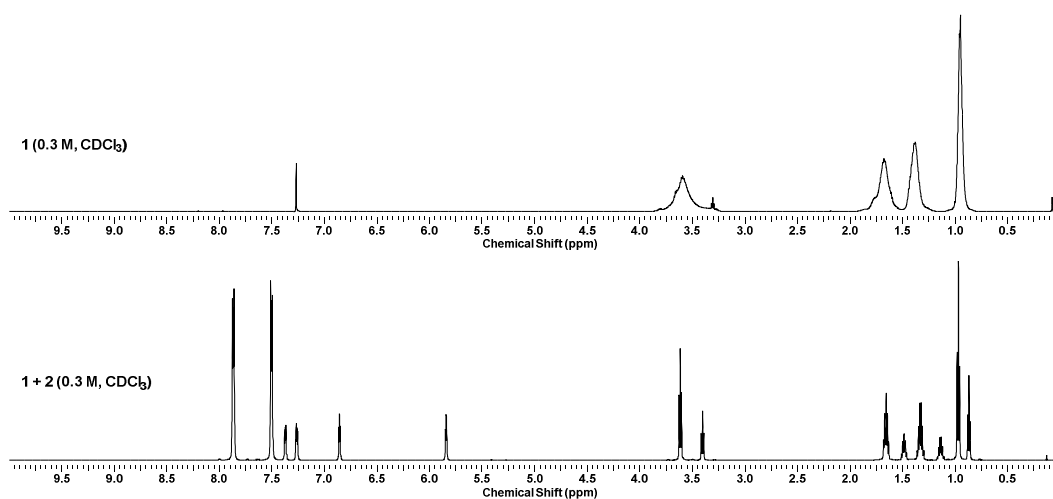


Figure D.2. $^1\text{H-NMR}$ spectrum of a 0.3 M solution of BuTAD (**1**) in CDCl_3 obtained after green light irradiation ($\lambda = 515 - 525$ nm, 3 x 3 W LEDs, 20 min), indicating the formation of a TAD-photopolymer (top). In the presence of an equimolar amount of naphthalene **2**, however, no polymerisation is observed. Instead, the cycloaddition reaction of **1** + **2** is exclusively observed.

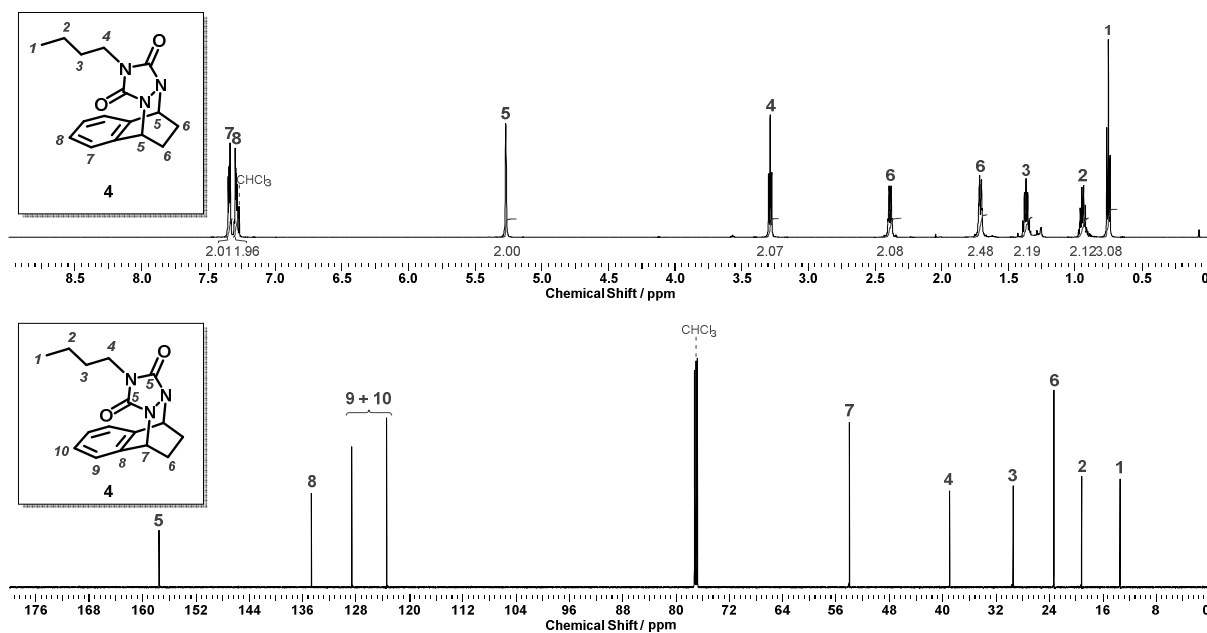


Figure D.3. ^1H - and ^{13}C -NMR spectra (CDCl₃) of the reduced cycloadduct **4**.

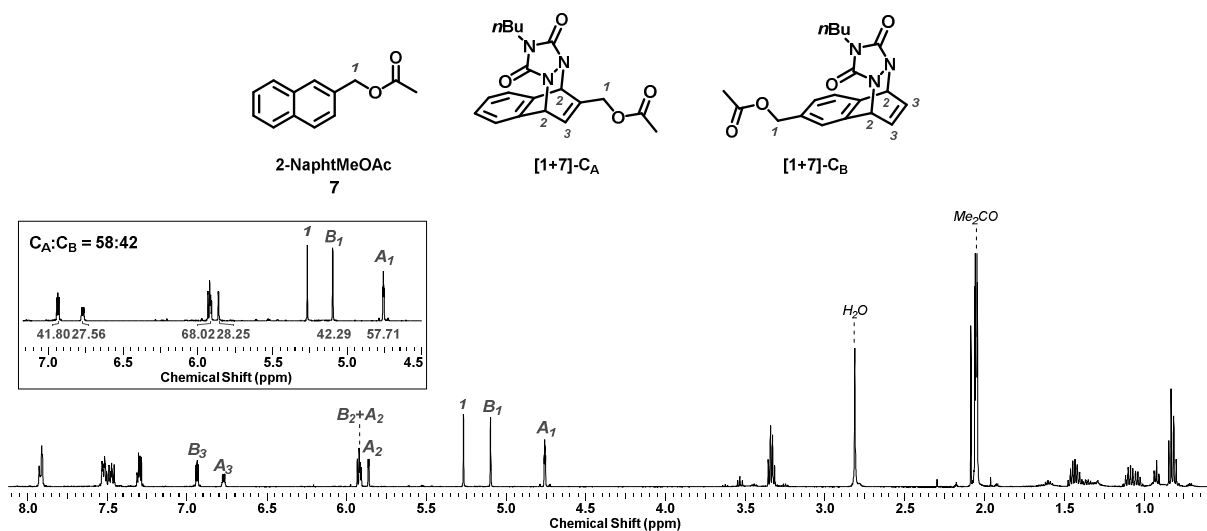


Figure D.4. ^1H -NMR spectrum obtained after green light irradiation ($\lambda = 515 - 525$ nm, 3 x 3 W LEDs, 45 min) of naphthalene **7** and BuTAD (Me₂CO-*d*₆), indicating the formation of two regioisomers. The regioisomeric excess was determined based on the proton integration values of well resolved signals (inset). Peaks were assigned in accordance with 2D COSY-NMR.

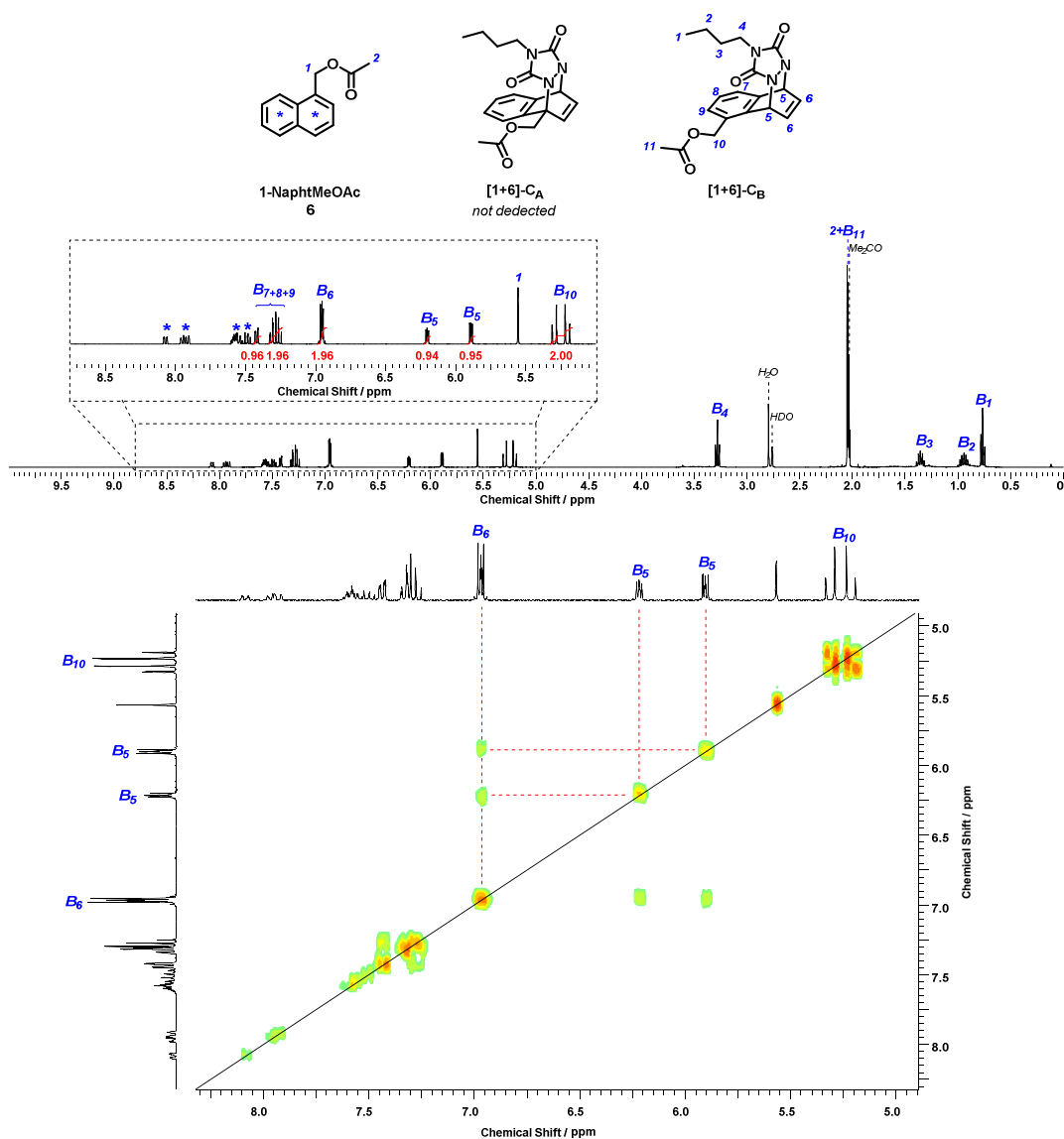


Figure D.5. $^1\text{H-NMR}$ spectrum obtained after green light irradiation ($\lambda = 515 - 525$ nm, 3 x 3 W LEDs, 45 min) of naphthalene **6** and BuTAD ($\text{Me}_2\text{CO-}d_6$), indicating the formation of only one regioisomers, i.e. on the non-substituted ring C_B. Peaks were assigned in accordance with 2D COSY-NMR from which the exclusive regioselectivity was confirmed (bottom).

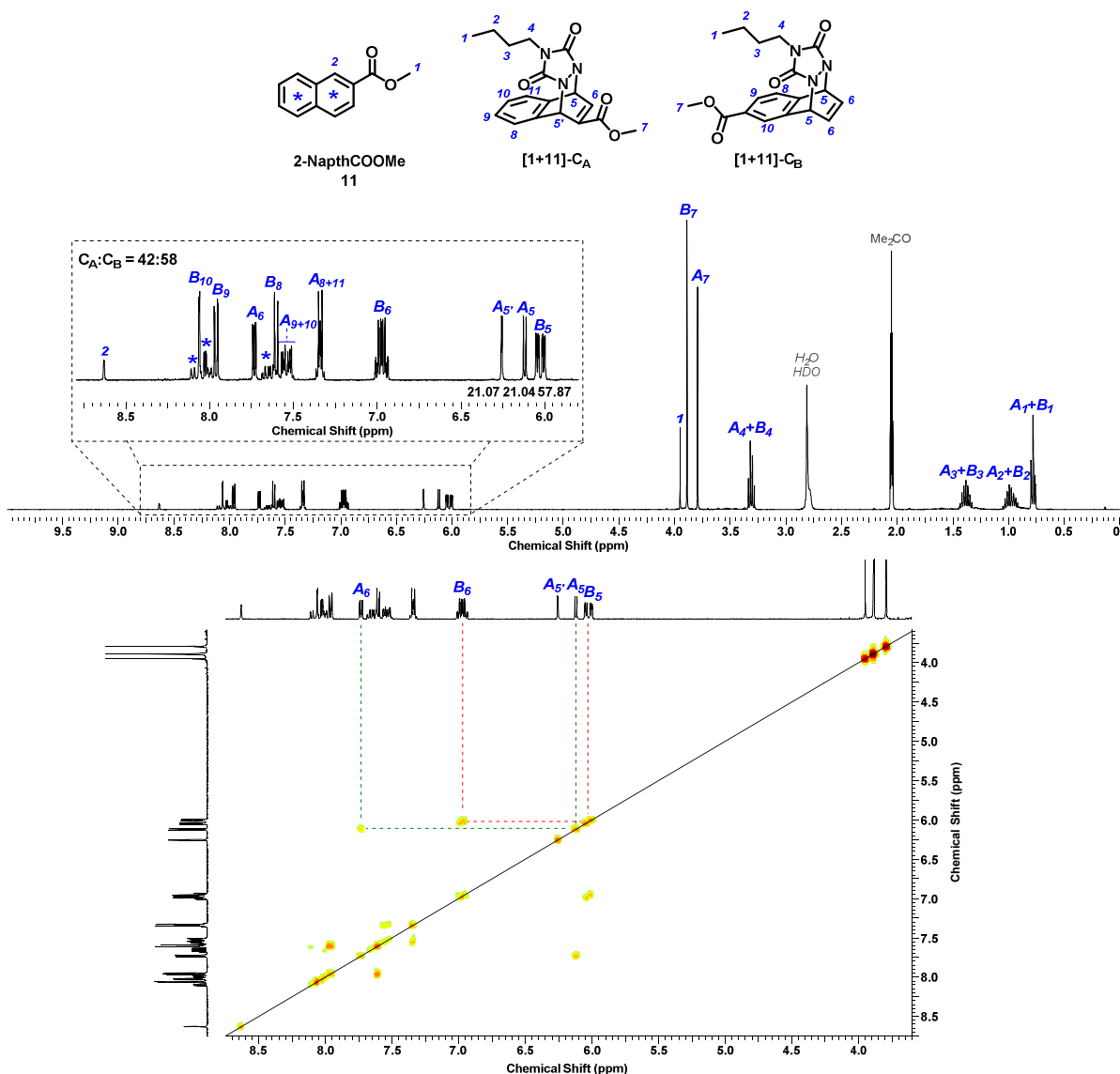


Figure D.6. $^1\text{H-NMR}$ spectrum obtained after green light irradiation ($\lambda = 515 - 525$ nm, 3 x 3 W LEDs, 45 min) of naphthalene **11** and BuTAD ($\text{Me}_2\text{CO}-d_6$), indicating the formation of two regioisomers. The regioisomeric excess was determined based on the proton integration values of well resolved signals (inset). Peaks were assigned in accordance with 2D COSY-NMR (bottom).

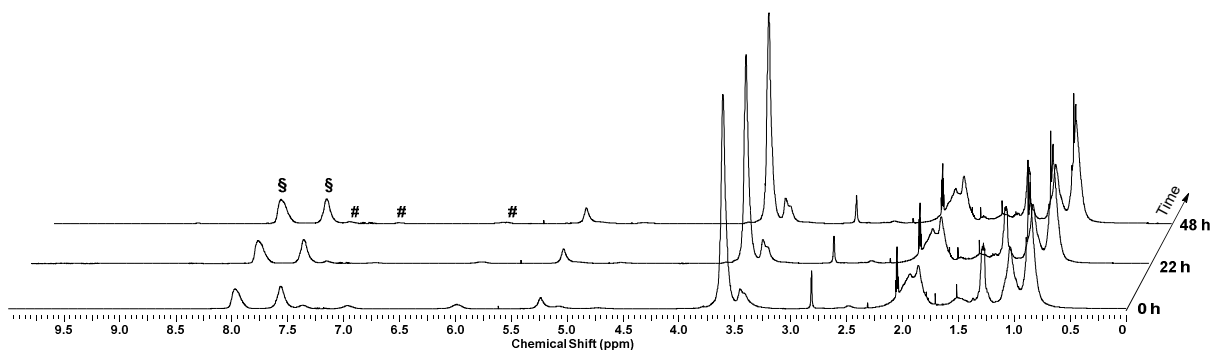


Figure D.7. Gelation experiment of bisTAD **16** with a naphthalene-containing polymer **15** upon green light irradiation. The decrosslinking reaction in the dark is evidenced by the decreasing TAD-naphthalene cycloadduct signals (**#**) and increasing signals attributed to the release of naphthalene over time (**S**), observed in the $^1\text{H-NMR}$ spectra ($\text{Me}_2\text{CO}-d_6$) recorded immediately after irradiation and after standing for 22 h and 48 h away from ambient light.

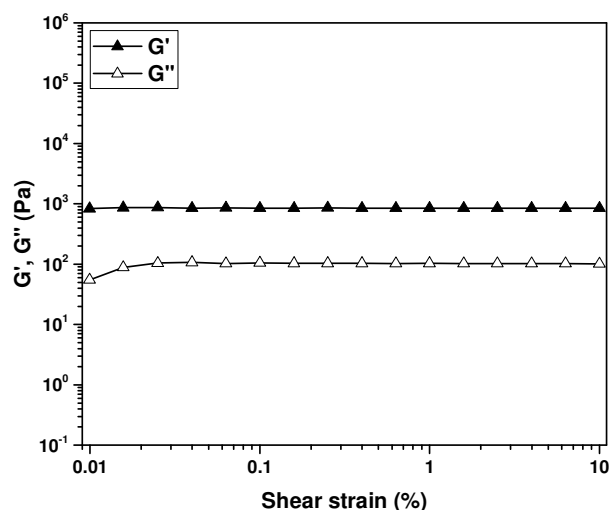
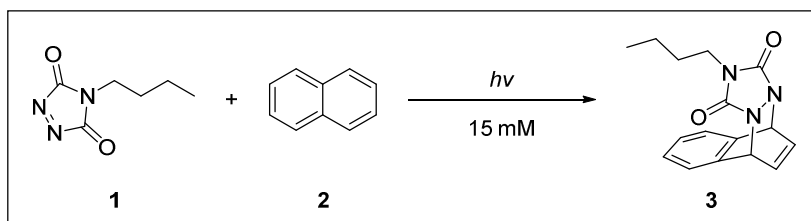


Figure D.8. Strain sweep at 25 °C of the material obtained after visible light-induced crosslinking of naphthalene-containing polymer **14** in the presence of bisTAD **16** ($\lambda = 400 - 500$ nm, 3 x 3 W LEDs, 3 h), indicating that the rheology measurements conducted at 1 % shear strain are carried out in the viscoelastic regime.

D.2 Experimental procedures

D.2.1 Visible light-induced formation of cycloadduct **3**



A solution of 4-*n*-butyl-1,2,4-triazoline-3,5-dione (BuTAD, **1**, 4.65 mg, $3.0 \cdot 10^{-5}$ mol, 1.0 eq.) and naphthalene (**2**, 3.94 mg, $3.0 \cdot 10^{-5}$ mol, 1.0 eq.) in 2 mL carbon tetrachloride was transferred into a crimped neck glass vial and placed in the sample holder of the Innolas tunable laser. Irradiation with green laser light $\lambda = 544$ (4 mW cm^{-2} , 100 Hz) gave a clear colourless solution within 5 minutes. After photobleaching was observed, 0.05 mL of the reaction mixture was diluted to 0.033 mM upon addition of carbon tetrachloride and subjected to UV/vis analysis (refer to Figure V.2). Comparison with a reference sample kept in the dark indicated the complete consumption of **1** immediately after irradiation. Upon standing in the dark in the UV/vis spectrophotometer, **1** was rapidly regenerated.

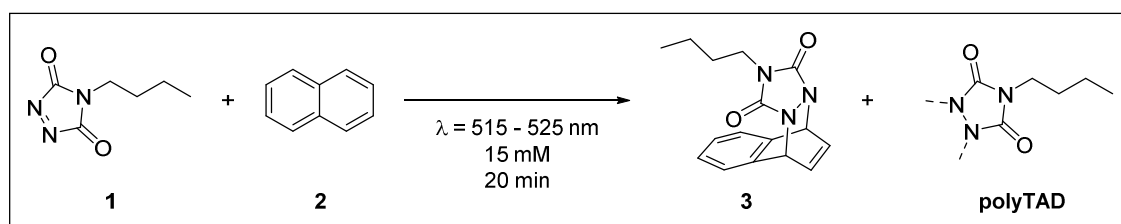
In a similar experiment, the photoreaction was carried out with LED irradiation sources (3 x 3 W). Both with UV-A ($\lambda = 370 - 380$ nm) and green light ($\lambda = 515 - 525$ nm), photobleaching was observed within 30 and 20 minutes, respectively. Changing the solvent to acetonitrile also resulted in photobleaching upon green light irradiation ($\lambda = 515 - 525$ nm, 3 x 3 W LEDs), albeit within 1 hour instead of 20 minutes.

More quantitative insights into the photobleaching process were obtained by affecting the photoreaction in deuterated solvent, enabling $^1\text{H-NMR}$ -analysis. Thus, solutions of 4-*n*-butyl-

1,2,4-triazoline-3,5-dione (BuTAD, **1**, 4.65 mg, $3.0 \cdot 10^{-5}$ mol, 1.0 eq.) and naphthalene (**2**, 3.94 mg, $3.0 \cdot 10^{-5}$ mol, 1.0 eq.) in 2 mL deuterated chloroform or deuterated acetone- d_6 (15 mM) were subjected to green LED light ($\lambda = 515 - 525$ nm, 3 x 3 W) until photobleaching was observed after 20 or 45 minutes, respectively. The resulting mixture was transferred into an NMR-tube and immediately subjected to $^1\text{H-NMR}$ analysis. NMR spectra are depicted in Figure V.3b-c (CDCl_3) and Figure V.4a-b ($\text{Me}_2\text{CO-}d_6$).

$^1\text{H-NMR}$ (400 MHz, CDCl_3): δ (ppm) = 0.84 (t, 3H, CH_3 , $J = 7.3$ Hz), 1.12 (m, 2H, $\text{CH}_3\text{-CH}_2$), 1.47 (m, 2H, $\text{N-CH}_2\text{-CH}_2$), 3.40 (t, 2H, N-CH_2 , $J = 7.0$ Hz), 5.84 (t, 2H, Ar-CH-N $J = 3.7$ Hz), 6.86 (t, 2H, Ar-CH-CH=CH , $J = 4.0$ Hz), 7.25 (m, 2H, ArH), 7.36 (m, 2H, ArH). **$^1\text{H-NMR}$ (400 MHz, $\text{Me}_2\text{CO-}d_6$):** δ (ppm) = 0.81 (t, 3H, CH_3 , $J = 7.2$ Hz), 1.05 (m, 2H, $\text{CH}_3\text{-CH}_2$), 1.41 (m, 2H, $\text{N-CH}_2\text{-CH}_2$), 3.32 (t, 2H, N-CH_2 , $J = 7.0$ Hz), 5.89 (dd, 2H, Ar-CH-N $J = 4.0, 3.2$ Hz), 6.93 (dd, 2H, Ar-CH-CH=CH , $J = 4.2, 3.1$ Hz), 7.27 (m, 2H, ArH), 7.45 (m, 2H, ArH).

D.2.2 Visible light-induced cycloaddition or polymerisation



In order to address the competition that might occur between the visible light-induced cycloaddition reaction of **1** with **2** and the exclusive homopolymerisation of **1** as established in Chapter IV, irradiation experiments were carried out in deuterated chloroform to enable $^1\text{H-NMR}$ analysis of the reaction outcome.

As a reference experiment, a plain solution of 4-*n*-butyl-1,2,4-triazoline-3,5-dione (BuTAD, **1**, 4.65 mg, $3.0 \cdot 10^{-5}$ mol, 1.0 eq.) in 2 mL deuterated chloroform (15 mM) was subjected to green light at $\lambda = 515 - 525$ nm (3 x 3 W LEDs). After 20 minutes, a clear colourless solution was obtained, which was immediately submitted for $^1\text{H-NMR}$ analysis. As expected, the resulting mixture exclusively contained the TAD-photopolymer (refer to Figure V.3a).

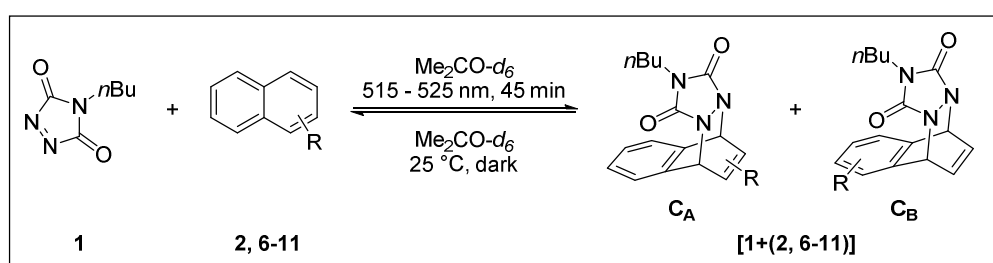
$^1\text{H-NMR}$ (400 MHz, CDCl_3): δ (ppm) = 0.95 (broad m, 3H, CH_3), 1.40 (broad m, 3H, $\text{CH}_3\text{-CH}_2$), 1.68 (broad m, 3H, $\text{N-CH}_2\text{-CH}_2$), 3.31 + 3.60 (t + broad m, 2H, N-CH_2).

Next, a solution of 4-*n*-butyl-1,2,4-triazoline-3,5-dione (BuTAD, **1**, 4.65 mg, $3.0 \cdot 10^{-5}$ mol, 1.0 eq.) in the presence of naphthalene (**2**, 3.94 mg, $3.0 \cdot 10^{-5}$ mol) in 2 mL deuterated chloroform (15 mM) was irradiated with green light at ($\lambda = 515 - 525$ nm, 3 x 3 W LEDs). Again, photobleaching was observed within 20 minutes and the colourless mixture was analysed via $^1\text{H-NMR}$. The TAD-naphthalene cycloadduct **3** was shown to be predominantly formed, with only minor traces (i.e. $< 2\%$) of the photopolymer detected (refer to Figure V.3b). In contrast to a reference sample that was kept in the dark for 20 minutes, less than 1 % of cycloadduct **3**

was detected, indicating the true light-induced nature of the TAD-naphthalene cycloaddition reaction (refer to Figure V.3c).

Finally a more concentrated solution of 4-*n*-butyl-1,2,4-triazoline-3,5-dione (BuTAD, **1**, 9.4 mg, $6.0 \cdot 10^{-5}$ mol, 1.0 eq.) and naphthalene (**2**, 7.7 mg, $6.0 \cdot 10^{-5}$ mol) in 4 mL deuterated chloroform (15 mM) was irradiated with green light at ($\lambda = 515 - 525$ nm, 3 x 3 W LEDs). In contrast to the more diluted experiment (i.e. 15 mM), not even a single trace of the TAD-polymer was detected in the resulting $^1\text{H-NMR}$ spectrum (refer to C.1). Thus, the cycloaddition reaction was found to be the exclusive pathway when irradiation a 0.3 M solution of **1** and **3** (which is the same TAD-concentration as employed for the photopolymerisation experiments discussed in Chapter IV).

D.2.3 Kinetic measurements of the cycloreversion process



General procedure to determine the cycloreversion kinetics of TAD-naphthalene adducts, in the following illustrated for plain naphthalene **2**.

A solution of 4-*n*-butyl-1,2,4-triazoline-3,5-dione (BuTAD, **1**, 3.53 mg, $2.25 \cdot 10^{-5}$ mol, 1.0 eq.) and plain naphthalene **2** (3.18 mg, $2.48 \cdot 10^{-5}$ mol, 1.1 eq.) in 1.5 mL deuterated acetone- d_6 (15 mM) was transferred into two NMR-tubes.

A first NMR tube was irradiated with green LED light ($\lambda = 515 - 525$ nm, 3 x 3 W) for 45 minutes. Complete photobleaching was observed and the resulting mixture was immediately submitted for $^1\text{H-NMR}$ analysis. From then onwards, the NMR sample remained in the autosampler of the NMR spectrometer at 25 °C, shielded from ambient light and $^1\text{H-NMR}$ spectra were recorded over the course of 60 hours in 1 hour intervals. Integration of well-resolved signals in the NMR spectra allowed to determine the concentration of the TAD-naphthalene cycloadduct at distinct times when kept in the dark at 25 °C, from which cycloreversion profiles were determined. Clean first order kinetics were observed over several half-life times and the respective cycloreversion rate coefficients could be calculated from the logarithmic relationship of the decrease in cycloadduct concentration over time (refer to Table V.1). Peaks in the $^1\text{H-NMR}$ spectra were assigned based on correlations observed in the respective 2D COSY spectrum.

The second NMR tube was kept in the dark and served as a reference to determine the thermal equilibrium concentration of the cycloadduct after a prolonged period of time, without being irradiated.

Cycloadduct [1+2] (= 3).

Only one product is formed (i.e. $[1+2]-C_A = [1+2]-C_B$). $^1\text{H-NMR}$ (400 MHz, $\text{Me}_2\text{CO}-d_6$): δ (ppm) = 0.81 (t, 3H, CH_3 , $J = 7.2$ Hz), 1.05 (m, 2H, $\text{CH}_3\text{-CH}_2$), 1.41 (m, 2H, $\text{N-CH}_2\text{-CH}_2$), 3.32 (t, 2H, N-CH_2 , $J = 7.0$ Hz), 5.89 (dd, 2H, Ar-CH-N , $J = 4.0, 3.2$ Hz), 6.93 (dd, 2H, Ar-CH-CH=CH , $J = 4.2, 3.1$ Hz), 7.27 (m, 2H, ArH), 7.45 (m, 2H, ArH).

Cycloadduct [1+6].

$[1+6]-C_A:[1+6]-C_B = 0:100$. $^1\text{H-NMR}$ (400 MHz, $\text{Me}_2\text{CO}-d_6$): $[1+6]-C_B$: δ (ppm) = 0.77 (t, 3H, CH_3 , $J = 7.3$ Hz), 0.95 (m, 2H, $\text{CH}_3\text{-CH}_2$), 1.36 (m, 2H, $\text{N-CH}_2\text{-CH}_2$), 2.06 (s, 3H, C(O)CH_3), 3.29 (t, 2H, N-CH_2 , $J = 6.8$ Hz), 5.26 (dd, 2H, C(O)-O-CH_2 , $J = 37.2, 12.5$ Hz), 5.90 (m, 1H, Ar-CH-N), 6.21 (m, 1H, Ar-CH-N), 6.96 (m, 2H, Ar-CH-CH=CH), 7.24-7.35 (m, 2H, ArH), 7.43 (dd, 1H, ArH , $J = 7.1, 1.2$ Hz).

Cycloadduct [1+7].

$[1+7]-C_A:[1+7]-C_B = 58:42$. $^1\text{H-NMR}$ (400 MHz, $\text{Me}_2\text{CO}-d_6$): $[1+7]-C_A$: δ (ppm) = 0.83 (t, 3H, CH_3 , $J = 7.3$ Hz), 1.08 (m, 2H, $\text{CH}_3\text{-CH}_2$), 1.43 (m, 2H, $\text{N-CH}_2\text{-CH}_2$), 2.05 (s, 3H, C(O)CH_3), 3.34 (t, 2H, N-CH_2 , $J = 6.9$ Hz), 4.75 (m, 2H, Ar-CH_2), 5.86 (d, 1H, Ar-CH-N ; $J = 1.8$ Hz), 5.92 (m, 1H, Ar-CH-N), 7.43-7.56 (m, 4H, ArH). $[1+7]-C_B$: some resolved resonances, δ (ppm) = 5.09 (s, 2H, Ar-CH_2), 5.92 (m, 2H, Ar-CH-N), 6.93 (m, 2H, Ar-CH-CH=CH).

Cycloadduct [1+8].

$[1+8]-C_A:[1+8]-C_B = 0:100$. $^1\text{H-NMR}$ (400 MHz, $\text{Me}_2\text{CO}-d_6$): $[1+8]-C_B$: δ (ppm) = 0.78 (t, 3H, CH_3 , $J = 7.2$ Hz), 0.96 (m, 2H, $\text{CH}_3\text{-CH}_2$), 1.38 (m, 2H, $\text{N-CH}_2\text{-CH}_2$), 1.99 (s, 3H, C(O)CH_3), 3.13 (m, 2H, Ar-CH_2), 3.30 (t, 2H, N-CH_2 , $J = 6.8$ Hz), 4.24 (m, 2H, C(O)-O-CH_2), 5.86 (dd, 1H, Ar-CH-N , $J = 5.0, 2.4$ Hz), 6.20 (dd, 1H, Ar-CH-N , $J = 4.9, 2.2$ Hz), 6.96 (m, 2H, Ar-CH-CH=CH), 7.18-7.25 (m, 2H, ArH), 7.30-7.35 (m, 1H, ArH).

Cycloadduct [1+9].

$[1+9]-C_A:[1+9]-C_B = 53:47$. $^1\text{H-NMR}$ (400 MHz, $\text{Me}_2\text{CO}-d_6$): δ (ppm) = 0.82 (t, 3H, CH_3 , $J = 7.1$ Hz), 1.06 (m, 2H, $\text{CH}_3\text{-CH}_2$), 1.42 (m, 2H, $\text{N-CH}_2\text{-CH}_2$), 1.92 (s, 3H, C(O)CH_3), 2.64 (m, 1H, Ar-CH_2), 3.33 (t, 2H, N-CH_2 , $J = 6.9$ Hz), 4.09 + 4.23 (m, 2H, O-CH_2), 5.81 (d, 2H, Ar-CH-N , $J = 1.9$ Hz), 5.85 (d, 2H, Ar-CH-N , $J = 6.1$ Hz), 6.58 (m, 1H, Ar-CH-CH=CH), 7.36-7.53 (m, 4H, ArH). $[1+9]-C_B$: some resolved resonances, δ (ppm) = 2.94 (t, 1H, Ar-CH_2 , $J = 7$ Hz), 4.23 (s, 2H, O-CH_2), 5.86 (m, 2H, Ar-CH-N), 6.92 (m, 2H, Ar-CH-CH=CH).

Cycloadduct [1+10].

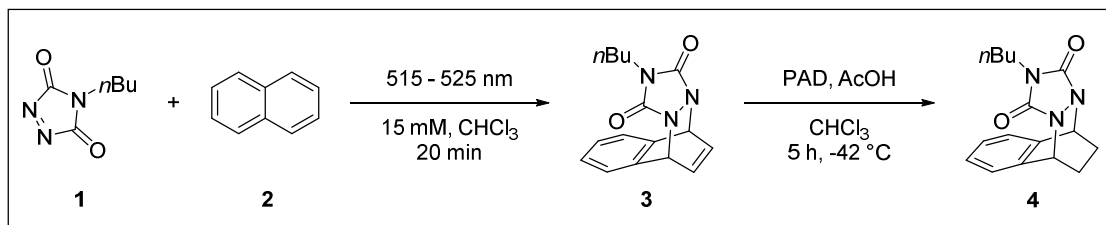
$[1+10]-C_A:[1+10]-C_B = 0:100$. $^1\text{H-NMR}$ (400 MHz, $\text{Me}_2\text{CO}-d_6$): $[1+10]-C_B$: δ (ppm) = 0.82 (t, 3H, CH_3 , $J = 7.4$ Hz), 1.09 (m, 2H, $\text{CH}_3\text{-CH}_2$), 1.43 (m, 2H, $\text{N-CH}_2\text{-CH}_2$), 3.34 (t, 2H, N-CH_2 , $J = 7.0$ Hz), 3.95 (s, 3H, OCH_3), 5.98 (dd, 1H, Ar-CH-N , $J = 5.1, 2.3$ Hz), 6.92-7.03 (m,

2H, Ar-CH-CH=CH), 7.41 (dd, 1H, ArH, $J = 8.0, 7.4$ Hz), 7.72 (dd, 1H, ArH, $J = 7.3, 0.8$ Hz), 7.87 (dd, 1H, ArH, $J = 8.0, 1.2$ Hz).

Cycloadduct [1+11].

[1+11]-C_A: [1+11]-C_B = 42:58. ¹H-NMR (400 MHz, Me₂CO-*d*₆): [1+11]-C_A: δ (ppm) = 0.78 (t, 3H, CH₃, $J = 7.2$ Hz), 0.98 (m, 2H, CH₃-CH₂), 1.39 (m, 2H, N-CH₂-CH₂), 3.32 (t, 2H, N-CH₂, $J = 6.8$ Hz), 3.79 (s, 3H, OCH₃), 6.12 (d, 1H, Ar-CH-N, $J = 6.4$ Hz), 6.26 (d, 1H, Ar-CH-N, $J = 1.5$ Hz), 7.34 (m, 2H, ArH), 7.49-7.59 (m, 2H, ArH), 7.73 (dd, 1H, Ar-CH-CH=C, $J = 6.1, 1.8$ Hz). [1+11]-C_B: some resolved resonances, δ (ppm) = 3.89 (s, 3H, OCH₃), 6.01 (dd, 1H, Ar-CH-N, $J = 5.2, 1.6$ Hz), 6.04 (dd, 1H, Ar-CH-N, $J = 5.3, 1.9$ Hz), 6.97 (m, 2H, Ar-CH-CH=CH), 7.62 (m, 1H, ArH), 7.96 (m, 1H, ArH), 8.06 (m, 1H, ArH).

D.2.4 Reduction of cycloadduct 3 into 4

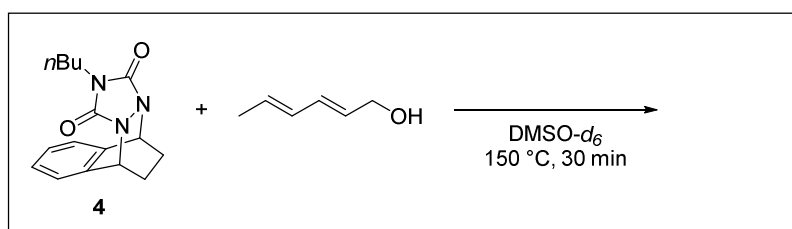


A solution of 4-*n*-butyl-1,2,4-triazoline-3,5-dione (BuTAD, **1**, 46.5 mg, 0.3 mmol, 1.0 eq.) and naphthalene (**2**, 39.4 mg, 0.3 mmol, 1.0 eq.) in 20 mL anhydrous chloroform (beforehand deoxygenated by flushing with nitrogen gas for 20 min) was placed in a photoreactor and irradiated at $\lambda = 515 - 525$ nm for 20 minutes (3 x 3 W green LEDs). After photobleaching was observed, the reaction mixture was transferred into a flask and cooled at -42 °C in a liquid nitrogen-acetonitrile bath. To this, potassium azodicarboxylate (PAD, 0.58 g, 3.0 mmol, 10 eq.) was added at -42 °C. Next, acetic acid (0.86 mL, 15.0 mmol, 50 eq.) was added to the cloudy yellow suspension and the mixture was stirred at -42 °C. The suspension slowly turned into a solution and after 2 hours, the mixture was slowly warmed in an ice water bath to 0 °C. After 5 hours, the obtained faint yellow cloudy suspension was allowed to warm to room temperature and 10 mL water was added. The mixture was washed with 20 mL aqueous saturated sodium bicarbonate solution and phase separated. The aqueous phase was washed with 20 mL chloroform and the combined organic phases were washed with 20 mL brine. Drying over magnesium sulfate, followed by solvent removal *in vacuo* gave a dark yellow oil, which was purified by means of preparative thin layer chromatography (silica, ethyl acetate:hexane 1:1, $R_F = 0.91$). The resulting yellow oil was subjected a second time to preparative thin layer chromatography (silica, ethyl acetate:hexane 1:4, $R_F = 0.75$) to remove traces of unreacted naphthalene, leaving a pure fraction of reduced cycloadduct **4** as a yellow oil (25 mg – 29 %).

¹H-NMR (400 MHz, CDCl₃): δ (ppm) = 0.75 (t, 3H, CH₃, $J = 7.3$ Hz), 0.94 (m, 2H, CH₂-CH₃), 1.37 (m, 2H, N-CH₂-CH₂), 1.71 (m, 2H, Ar-CH-CH₂), 2.39 (m, 2H, Ar-CH-CH₂), 3.29 (t, 2H, N-CH₂, $J = 7.0$ Hz), 5.27 (s, 2H, N-CH-Ar), 7.29 (m, 2H, ArH), 7.34 (m, 2H, ArH). ¹³C-

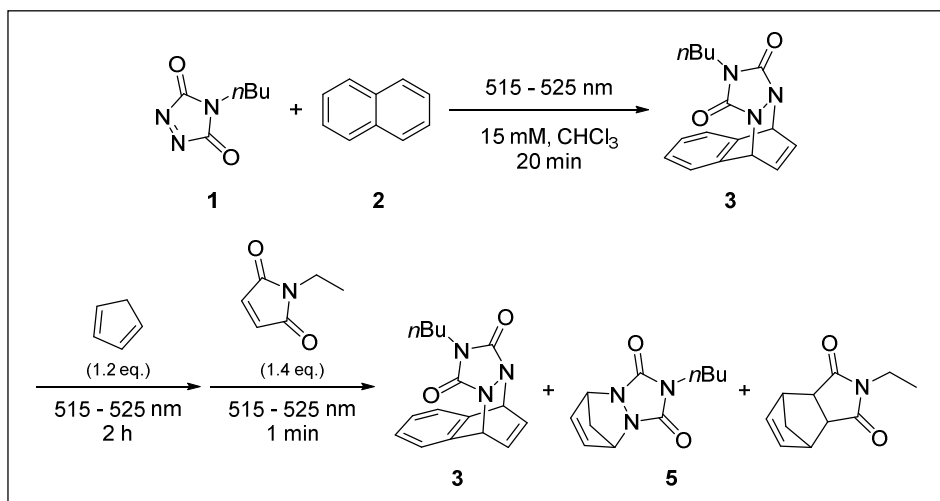
NMR (100 MHz, CDCl₃): δ (ppm) = 13.41 (CH₃), 19.17 (CH₂), 23.30 (CH₂), 29.44 (CH₂), 38.97 (CH₂), 54.01 (CH), 123.42 (CH), 128.65 (CH), 134.70 (C), 157.54 (C). **¹H-NMR (400 MHz, DMSO-*d*₆):** δ (ppm) = 0.65 (t, 3H, CH₃, *J* = 7.0 Hz), 0.74 (m, 2H, CH₂-CH₃), 1.22 (m, 2H, N-CH₂-CH₂), 1.62 (m, 2H, Ar-CH-CH₂), 2.26 (m, 2H, Ar-CH-CH₂), 3.17 (t, 2H, N-CH₂, *J* = 6.6 Hz), 5.30 (s, 2H, N-CH-Ar), 7.35 (s, 4H, ArH) (refer to Figure V.6a)

D.2.5 Thermal cycloreversion test of reduced cycloadduct 4



A solution of reduced cycloadduct **4** (25 mg, 0.09 mmol, 1.0 eq.) and *trans,trans*-2,4-hexadien-1-ol (HDEO, 12 mg, 0.12 mmol, 1.4 eq.) in 0.7 mL deuterated DMSO-*d*₆ was transferred into an NMR tube and placed in a preheated oil bath at 150 °C for 30 minutes. After cooling to room temperature, the resulting mixture was submitted for ¹H-NMR analysis, indicating the lack of thermal reversibility of **4** since no trace of cycloreversion could be observed. ¹H-NMR spectra before and after heating are depicted in Figure V.6.

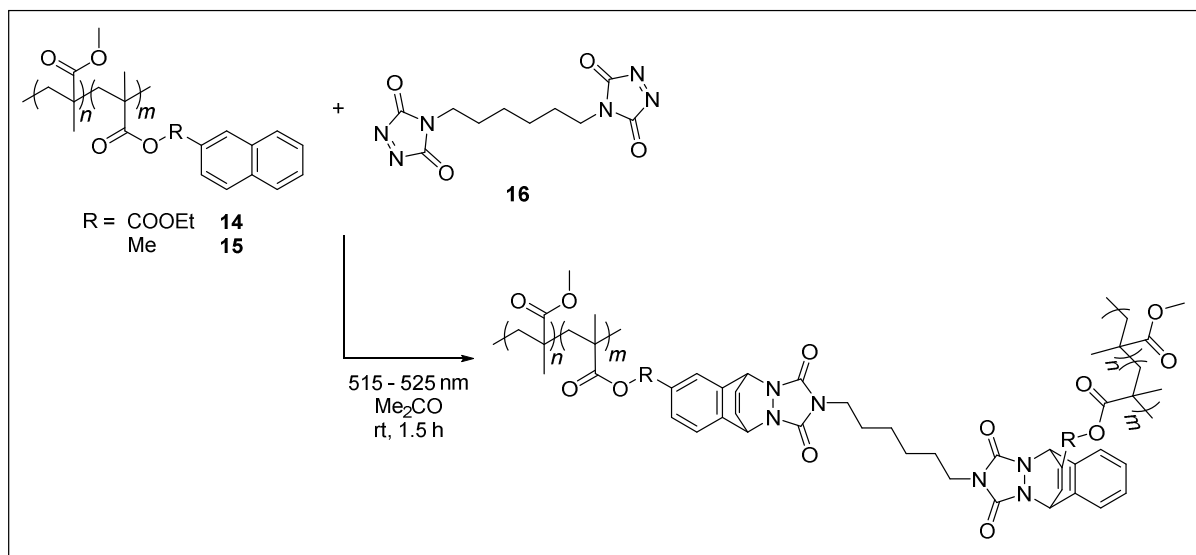
D.2.6 Light-stabilised formation of cycloadduct 3



A solution of 4-*n*-butyl-1,2,4-triazoline-3,5-dione (BuTAD, **1**, 9.31 mg, 0.060 mmol, 1.0 eq.) and naphthalene (**2**, 8.46 mg, 0.066 mmol, 1.1 eq.) in 4 mL deuterated chloroform (beforehand deoxygenated by flushing with nitrogen gas for 20 min) was placed in a photoreactor and irradiated at $\lambda = 515 - 525$ nm for 20 minutes (3 x 3 W green LEDs). After complete photobleaching, cyclopentadiene (4.76 mg, 0.072 mmol, 1.2 eq.) in 0.1 mL deuterated chloroform was added, whilst the green light was kept switched on. Irradiation was continued for 2 hour, followed by addition of *N*-ethyl maleimide (10.5 mg, 0.084 mmol, 1.4 eq.) in 0.1 mL deuterated chloroform. The resulting reaction mixture was submitted for ¹H-NMR analysis to determine the

light-stabilisation of the formed TAD-naphthalene cycloadduct (refer to Figure V.7). Simultaneous, a similar experiment was performed in the dark to serve as a reference.

D.2.7 Photo-induced crosslinking of triazolinedione-naphthalene networks



Crosslinking in solution

A solution of naphthalene-containing polymer **14** (210 mg, 0.24 mmol naphthalene, 1.0 eq.) or **15** (200 mg, 0.24 mmol, 1.0 eq.) and bisfunctional TAD **16** (34 mg, 0.12 mmol, 0.5 eq.) in 1 mL anhydrous acetone was irradiated with 3 x 3 W green LEDs at $\lambda = 515 - 525$ nm. Within 1.5 hours, photobleaching was observed and a crosslinked gel was formed (*cf.* Scheme V.6).

Crosslinking in solution for $^1\text{H-NMR}$ analysis

A solution of naphthalene-containing polymer **15** (75 mg, 0.09 mmol naphthalene, 1.0 eq.) and bisfunctional TAD **16** (13 mg, 0.05 mmol, 0.5 eq.) in 0.75 mL deuterated acetone- d_6 was transferred into an NMR tube and irradiated with 3 x 3 W green LEDs at $\lambda = 515 - 525$ nm. Within 1 hour, photobleaching was observed and a crosslinked gel was formed, verified by inversion of the NMR tube. Immediately after the light was switched off, the gel was submitted for $^1\text{H-NMR}$ analysis (refer to Figure V.12). The experiment was repeated with a butyl methacrylate derivative of naphthalene-containing polymer **15** (75 mg, 0.12 mmol naphthalene, 1.0 eq.) in the presence of **16** (17 mg, 0.06 mmol, 0.5 eq.) as the N-CH_2 signal of the TAD crosslinker does not overlap with those of the polymer backbone.

Crosslinking in solution for rheology

A polymer formulation of naphthalene-containing polymer **14** (210 mg, 0.24 mmol naphthalene, 1.0 eq.) or **15** (200 mg, 0.24 mmol, 1.0 eq.) and bisfunctional TAD **16** (34 mg, 0.12 mmol, 0.5 eq.) in 0.25 mL anhydrous acetone was prepared to assess the rheological behaviour of the TAD-naphthalene system. 8 drops of the formulation were deposited on the lower parallel glass plate (33 mm diameter) of the rheometer (refer to instrumentation section), thereby avoiding the formation of air bubbles. The upper part of the moving profile (PP25) was

lowered (0.10 to 0.20 mm gap) and the excess amount of the formulation was trimmed at the edges of the moving profile. The samples were measured in oscillatory mode in an oven at 25 °C. After a certain time in the dark, photocuring was affected by switching on a broad emitting UV-lamp equipped with a filter in the visible range, i.e. $\lambda = 400 - 500$ nm. After curing, a normal force of 0.2 N was applied whilst the sample was kept irradiated. Afterwards, the light was switched off and the collapse of the material was monitored in the dark. At the end of the dark time, the normal force was reinstated to 0 N and a second photocuring was carried out, if desired. The rheology profiles, showing G' and G'' as a function of time are depicted in Figure V.13-15.

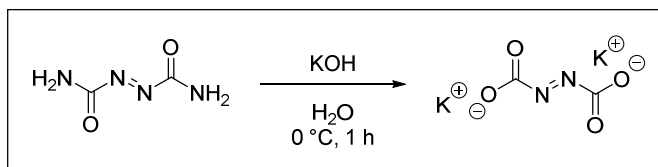
D.3 Synthetic procedures

D.3.1 Synthesis of 4-*n*-butyl-triazoline-3,5-dione (BuTAD, 1)

4-*n*-butyl-1,2,4-triazoline-3,5-dione (BuTAD, **1**) was synthesized as described in B.4.3, followed by sublimation under reduced pressure (0.1 mbar) at 40 °C, to give BuTAD (**1**) as a carmine red crystalline product. The reactive compound was stored in the dark at -18 °C and typically used within several weeks. Purity was regularly checked via ¹H-NMR prior to use.

¹H-NMR (400 MHz, DMSO-*d*₆): δ (ppm) = 0.88 (t, 3H, CH₃, $J = 7.3$ Hz), 1.30 (sext, 2H, CH₂-CH₃, $J = 7.3$ Hz), 1.56 (quint, 2H, N-CH₂-CH₂, $J = 7.3$ Hz), 3.47 (t, 2H, N-CH₂, $J = 7.0$ Hz). ¹³C-NMR (100 MHz, DMSO-*d*₆): δ (ppm) = 13.32 (CH₃), 19.11 (CH₂), 28.72 (CH₂), 40.34 (CH₂), 160.15 (C).

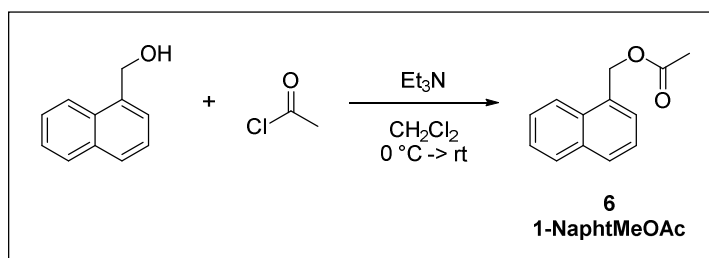
D.3.2 Synthesis of potassium azodicarboxylate



A solution of potassium hydroxide (6.2 g, 0.110 mol, 40 wt %) in 15.5 mL water was cooled in an ice water bath at 0 °C. To this, azodicarboxamide (2.5 g, 0.021 mol, 1.0 eq.) was added in small portions, maintaining the temperature below 5 °C. The yellow suspension was stirred at 0 – 5 °C for 1 hour, filtered and dried to air overnight at room temperature to give potassium azodicarboxylate (PAD) as a yellow powder (2.52 g – 62 %).

D.3.3 Synthesis of naphthalene model compounds

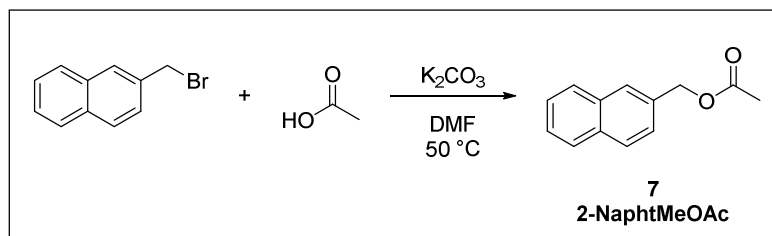
D.3.3.1 Synthesis of naphthalen-1-ylmethyl acetate (1-NaphtMeOAc, 6)



A solution of 1-naphthalenemethanol (1.00 g, 6.32 mmol, 1.0 eq.) in 20 mL dichloromethane was placed under inert atmosphere and cooled at 0 °C. Triethylamine (1.06 mL, 7.59 mmol, 1.2 eq.) was added at 0 °C, followed by the dropwise addition of acetyl chloride (0.54 mL, 7.59 mmol, 1.2 eq.). The resulting mixture was stirred overnight at room temperature, diluted with 20 mL dichloromethane and quenched with 40 mL 1 M aqueous hydrochloric acid. The organic phase was separated and the aqueous phase was washed with dichloromethane (2 x 40 mL). The combined organic phases were washed with brine (2 x 20 mL) and dried over magnesium sulfate. Solvent removal *in vacuo*, followed by overnight drying in a vacuum oven at 40 °C, gave naphthalen-1-ylmethyl acetate **6** as a dark yellow oil (1.20 g – 95 %).

¹H-NMR (400 MHz, CDCl₃): δ (ppm) = 2.13 (s, 3H, CH₃), 5.59 (s, 2H, CH₂), 7.45-7.50 (m, 1H, ArH), 7.51-7.62 (m, 3H, ArH), 7.84-7.94 (m, 2H, ArH), 8.04 (d, 1H, ArH, $J = 8.4$ Hz). **¹³C-NMR (100 MHz, CDCl₃):** δ (ppm) = 21.00 (CH₃), 64.55 (CH₂), 123.51 (CH), 125.25 (CH), 125.93 (CH), 126.55 (CH), 127.48 (CH), 128.70 (CH), 129.29 (CH), 131.41 (C), 131.60 (C), 133.71 (C), 170.95 (C). **¹H-NMR (400 MHz, Me₂CO-*d*₆):** δ (ppm) = 2.06 (s, 3H, CH₃), 5.57 (s, 2H, CH₂), 7.49 (dd, 1H, ArH, $J = 8.2, 7.0$ Hz), 7.62-7.62 (m, 3H, ArH), 7.89-7.99 (m, 2H, ArH), 8.08 (m, 1H, ArH). **¹³C-NMR (100 MHz, Me₂CO-*d*₆):** δ (ppm) = 20.88 (CH₃), 64.82 (CH₂), 124.59 (CH), 126.25 (CH), 126.88 (CH), 127.43 (CH), 128.16 (CH), 129.56 (CH), 129.96 (CH), 132.61 (C), 133.03 (C), 134.81 (C), 170.96 (C). **LC-MS (m/z):** 218.2 [M+NH₄]⁺. **HRMS (m/z):** *calc.*: 218.1176, *found*: 218.1180 [M+NH₄]⁺.

D.3.3.2 Synthesis of naphthalen-2-ylmethyl acetate (2-NaphtMeOAc, 7)

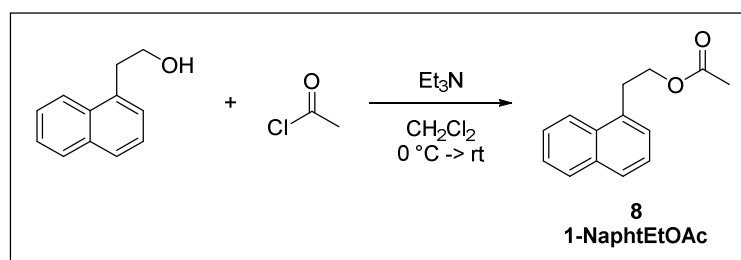


A mixture of 2-(bromomethyl)naphthalene (1.00 g, 4.74 mmol, 1.0 eq.) and potassium carbonate (0.98 g, 7.11 mmol, 1.5 eq.) in 20 mL anhydrous DMF was placed under inert atmosphere. Acetic acid (0.40 mL, 7.11 mmol, 1.5 eq.) was added and the resulting mixture was

heated at 50 °C for 16 hours. After cooling to room temperature, 40 mL ethyl acetate was added and the mixture was washed with water (1 x 40 mL) and brine (2 x 40 mL). The organic phase was dried over magnesium sulfate, followed by solvent removal *in vacuo* and the residue was dried overnight in a vacuum oven at 40 °C. Naphthalen-2-ylmethyl acetate **7** was obtained as an off-white powder (0.85 g – 90 %).

¹H-NMR (400 MHz, CDCl₃): δ (ppm) = 2.15 (s, 3H, CH₃), 5.29 (s, 2H, CH₂), 7.45-7.55 (m, 3H, ArH), 7.82-7.89 (m, 4H, ArH). **¹³C-NMR (100 MHz, CDCl₃):** δ (ppm) = 21.02 (CH₃), 66.42 (CH₂), 125.87 (CH), 126.25 (CH), 126.28 (CH), 127.35 (CH), 127.67 (CH), 127.94 (CH), 128.35 (CH), 133.08 (C), 133.16 (C), 133.32 (C), 170.90 (C). **¹H-NMR (400 MHz, Me₂CO-*d*₆):** δ (ppm) = 2.08 (s, 3H, CH₃), 5.26 (s, 2H, CH₂), 7.49-7.55 (m, 3H, ArH), 7.89-7.93 (m, 4H, ArH). **¹³C-NMR (100 MHz, Me₂CO-*d*₆):** δ (ppm) = 20.92 (CH₃), 66.62 (CH₂), 126.86 (CH), 127.13 (CH), 127.24 (CH), 127.89 (CH), 128.61 (CH), 128.84 (CH), 129.12 (CH), 134.12 (C), 134.31 (C), 135.18 (C), 170.98 (C). **LC-MS (m/z):** 218.2 [M+NH₄]⁺. **HRMS (m/z):** *calc.*: 218.1176, *found*: 218.1175 [M+NH₄]⁺.

D.3.3.3 Synthesis of 2-(naphthalen-1-yl)ethyl acetate (1-NaphtEtOAc, **8**)

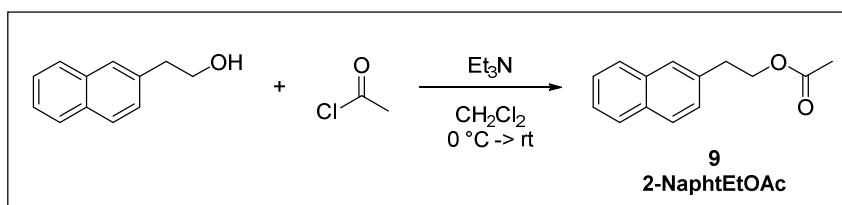


A solution of 2-(naphthalen-1-yl)ethan-1-ol (1.00 g, 5.81 mmol, 1.0 eq.) in 20 mL dichloromethane was placed under inert atmosphere and cooled at 0 °C. Triethylamine (0.97 mL, 6.97 mmol, 1.2 eq.) was added at 0 °C, followed by the dropwise addition of acetyl chloride (0.50 mL, 6.97 mmol, 1.2 eq.). The resulting mixture was stirred overnight at room temperature, diluted with 20 mL dichloromethane and quenched with 40 mL 1 M aqueous hydrochloric acid. The organic phase was separated and the aqueous phase was washed with dichloromethane (2 x 40 mL). The combined organic phases were washed with brine (2 x 20 mL) and dried over magnesium sulfate. Solvent removal *in vacuo* followed by overnight drying in a vacuum oven at 40 °C gave 2-(naphthalen-1-yl)ethyl acetate **8** as a dark yellow oil (1.18 g – 95 %).

¹H-NMR (400 MHz, CDCl₃): δ (ppm) = 2.08 (s, 3H, CH₃), 3.45 (t, 2H, Ar-CH₂, *J* = 7.4 Hz), 4.45 (t, 2H, O-CH₂, *J* = 7.4 Hz), 7.38-7.48 (m, 2H, ArH), 7.49-7.61 (m, 2H, ArH), 7.79 (d, 1H, ArH, *J* = 8.1 Hz), 7.89 (d, 1H, ArH, *J* = 8.8 Hz), 8.13 (d, 1H, ArH, *J* = 8.5 Hz). **¹³C-NMR (100 MHz, CDCl₃):** δ (ppm) = 20.93 (CH₃), 32.13 (CH₂), 64.39 (CH₂), 123.50 (CH), 125.41 (CH), 125.59 (CH), 126.10 (CH), 126.88 (CH), 127.38 (CH), 128.75 (CH), 131.99 (C), 133.63 (C), 133.79 (C), 171.00 (C). **¹H-NMR (400 MHz, Me₂CO-*d*₆):** δ (ppm) = 1.98 (s, 3H, CH₃), 3.42 (t, 2H, Ar-CH₂, *J* = 7.3 Hz), 4.37 (t, 2H, O-CH₂, *J* = 7.2 Hz), 7.41-7.48 (m,

2H, ArH), 7.49-7.60 (m, 2H, ArH), 7.78-7.83 (m, 1H, ArH), 7.92 (dt, 1H, ArH, $J = 8.1, 0.7$ Hz), 8.18 (m, 1H, ArH). $^{13}\text{C-NMR}$ (100 MHz, $\text{Me}_2\text{CO-}d_6$): δ (ppm) 20.91 (CH_3), 32.85 (CH_2), 64.94 (CH_2), 124.62 (CH), 126.50 (CH), 126.57 (CH), 127.03 (CH), 128.02 (CH), 128.23 (CH), 129.67 (CH), 133.11 (C), 135.02 (C), 135.08 (C), 171.09 (C). **LC-MS (m/z):** 232.2 $[\text{M}+\text{NH}_4]^+$. **HRMS (m/z):** *calc.*: 232.1332, *found*: 232.1337 $[\text{M}+\text{NH}_4]^+$.

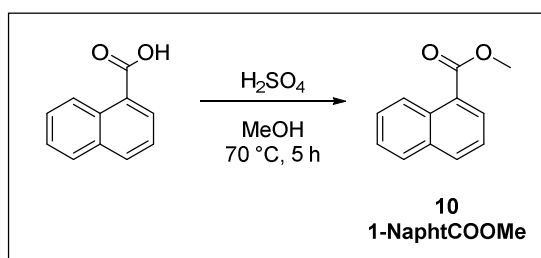
D.3.3.4 Synthesis of 2-(naphthalen-2-yl)ethyl acetate (2-NaphtEtOAc, 9)



A solution of 2-(naphthalen-2-yl)ethan-1-ol (1.00 g, 5.81 mmol, 1.0 eq.) in 20 mL dichloromethane was placed under inert atmosphere and cooled at $0\text{ }^\circ\text{C}$. Triethylamine (0.97 mL, 6.97 mmol, 1.2 eq.) was added at $0\text{ }^\circ\text{C}$, followed by the dropwise addition of acetyl chloride (0.50 mL, 6.97 mmol, 1.2 eq.). The resulting mixture was stirred overnight at room temperature, diluted with 20 mL dichloromethane and quenched with 40 mL 1 M aqueous hydrochloric acid. The organic phase was separated and the aqueous phase was washed with dichloromethane (2 x 40 mL). The combined organic phases were washed with brine (2 x 20 mL) and dried over magnesium sulfate. Solvent removal *in vacuo* followed by overnight drying in a vacuum oven at $40\text{ }^\circ\text{C}$ gave 2-(naphthalen-2-yl)ethyl acetate **9** as a yellow oil (1.15 g – 93 %).

$^1\text{H-NMR}$ (400 MHz, CDCl_3): δ (ppm) = 2.07 (s, 3H, CH_3), 3.13 (t, 2H, Ar- CH_2 , $J = 7.0$ Hz), 4.41 (t, 2H, O- CH_2 , $J = 7.1$ Hz), 7.39 (dd, 1H, ArH, $J = 8.4, 1.6$ Hz), 7.44-7.54 (m, 2H, ArH), 7.70 (s, 1H, ArH), 7.78-7.88 (m, 3H, ArH). $^{13}\text{C-NMR}$ (100 MHz, CDCl_3): δ (ppm) = 20.90 (CH_3), 35.15 (CH_2), 64.76 (CH_2), 125.45 (CH), 126.00 (CH), 127.21 (CH), 127.22 (CH), 127.44 (CH), 127.58 (CH), 128.04 (CH), 132.22 (C), 133.48 (C), 135.24 (C), 170.97 (C). $^1\text{H-NMR}$ (400 MHz, $\text{Me}_2\text{CO-}d_6$): δ (ppm) = 1.97 (s, 3H, CH_3), 3.10 (t, 2H, Ar- CH_2 , $J = 7.0$ Hz), 4.34 (t, 2H, O- CH_2 , $J = 7.0$ Hz), 7.41-7.51 (m, 3H, ArH), 7.76 (s, 1H, ArH), 7.82-7.90 (m, 3H, ArH). $^{13}\text{C-NMR}$ (100 MHz, $\text{Me}_2\text{CO-}d_6$): δ (ppm) = 20.87 (CH_3), 35.89 (CH_2), 65.33 (CH_2), 126.38 (CH), 126.95 (CH), 128.18 (CH), 128.39 (CH), 128.43 (CH), 128.51 (CH), 128.91 (CH), 133.38 (C), 134.70 (C), 136.88 (C), 171.00 (C). **LC-MS (m/z):** 232.2 $[\text{M}+\text{NH}_4]^+$. **HRMS (m/z):** *calc.*: 232.1332, *found*: 232.1342 $[\text{M}+\text{NH}_4]^+$.

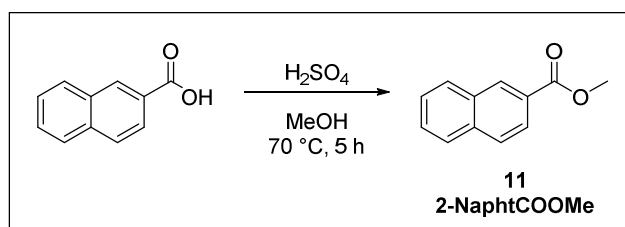
D.3.3.5 Synthesis of methyl 1-naphthoate (1-NaphtCOOMe, 10)



A mixture of 1-naphthoic acid (1.00 g, 5.81 mmol, 1.0 eq.) and concentrated sulfuric acid (0.31 g, 5.81 mmol, 1.0 eq.) in 5 mL anhydrous methanol was placed under inert atmosphere and refluxed at 70 °C. After 5 hours, the clear solution was cooled to ambient temperature and evaporated *in vacuo* to dryness. The residue was dissolved in 20 mL dichloromethane and washed with 20 mL water. The aqueous phase was extracted with dichloromethane (2 x 20 mL) and the combined organic phases washed with water (1 x 20 mL), saturated aqueous sodium bicarbonate solution (2 x 20 mL) and brine (1 x 20 mL). The clear organic phase was dried over magnesium sulfate followed by solvent removal *in vacuo* and overnight drying in a vacuum oven at 40 °C. Methyl 1-naphthoate **10** was obtained as a faint yellow oil (0.92 g – 85 %).

¹H-NMR (400 MHz, CDCl₃): δ (ppm) = 4.02 (s, 3H, CH₃), 7.47-7.58 (m, 2H, ArH), 7.64 (ddd, 1H, ArH, J = 8.6, 6.9, 1.3 Hz), 7.90 (dt, 1H, ArH, J = 8.1, 0.6 Hz), 8.03 (d, 1H, ArH, J = 8.2 Hz), 8.21 (dd, 1H, ArH, J = 7.3, 1.3 Hz), 8.95 (dd, 1H, ArH, J = 8.7, 0.9 Hz). **¹³C-NMR (100 MHz, CDCl₃):** δ (ppm) = 52.07 (CH₃), 124.42 (CH), 125.76 (CH), 126.14 (CH), 127.01 (C), 127.69 (CH), 128.48 (CH), 130.16 (CH), 131.28 (C), 133.30 (CH), 133.78 (C), 169.96 (C). **¹H-NMR (400 MHz, Me₂CO-*d*₆):** δ (ppm) = 3.98 (s, 3H, CH₃), 7.55-7.62 (m, 2H, ArH), 7.65 (m, 1H, ArH), 8.00 (dt, 1H, ArH, J = 8.1, 0.8 Hz), 8.15 (d, 1H, ArH, J = 8.2 Hz), 8.19 (dd, 1H, ArH, J = 7.3, 1.3 Hz), 8.90 (m, 1H, ArH). **¹³C-NMR (100 MHz, Me₂CO-*d*₆):** δ (ppm) = 52.44 (CH₃), 125.59 (CH), 126.51 (CH), 127.16 (CH), 128.11 (C), 128.54 (CH), 129.54 (CH), 130.91 (CH), 132.11 (C), 134.17 (CH), 134.90 (C), 168.28 (C). **LC-MS (m/z):** 187.1 [M+H]⁺.

D.3.3.6 Synthesis of methyl 2-naphthoate (2-NaphtCOOMe, 11)



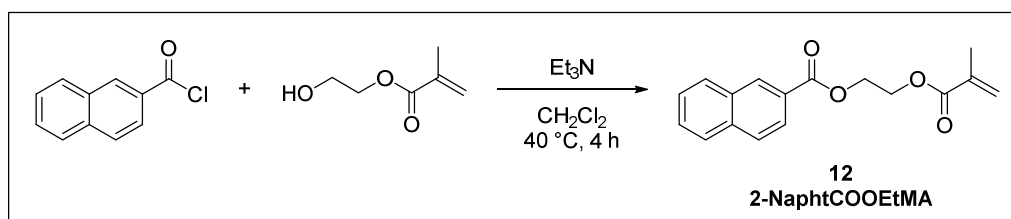
A mixture of 2-naphthoic acid (1.00 g, 5.81 mmol, 1.0 eq.) and concentrated sulfuric acid (0.31 g, 5.81 mmol, 1.0 eq.) in 5 mL anhydrous methanol was placed under inert atmosphere and refluxed at 70 °C. After 5 hours, the clear solution was cooled to ambient temperature and evaporated *in vacuo* to dryness. The residue was dissolved in 20 mL dichloromethane and washed

with 20 mL water. The aqueous phase was extracted with dichloromethane (2 x 20 mL) and the combined organic phases washed with water (1 x 20 mL), saturated aqueous sodium bicarbonate solution (2 x 20 mL) and brine (1 x 20 mL). The clear organic phase was dried over magnesium sulfate, followed by solvent removal *in vacuo* and overnight drying in a vacuum oven at 40 °C, to give methyl 2-naphthoate **11** as a white powder (0.94 g – 87 %).

¹H-NMR (400 MHz, CDCl₃): δ (ppm) = 4.00 (s, 3H, CH₃), 7.54-7.64 (m, 2H, ArH), 7.90 (d, 2H, ArH, J = 8.7 Hz), 7.97 (dd, 1H, ArH, J = 7.9, 0.6 Hz), 8.08 (dd, 1H, ArH, J = 8.5, 1.7 Hz), 8.63 (s, 1H, ArH). **¹³C-NMR (100 MHz, CDCl₃):** δ (ppm) = 52.22 (CH₃), 125.22 (CH), 126.62 (CH), 127.40 (C), 127.75 (CH), 128.14 (CH), 128.22 (CH), 129.34 (CH), 131.06 (CH), 132.49 (C), 135.51 (C), 167.27 (C). **¹H-NMR (400 MHz, Me₂CO-*d*₆):** δ (ppm) = 3.95 (s, 3H, CH₃), 7.58-7.70 (m, 2H, ArH), 7.96-8.07 (d, 2H, ArH), 8.09 (d, 1H, ArH, J = 8.1 Hz), 8.63 (s, 1H, ArH). **¹³C-NMR (100 MHz, Me₂CO-*d*₆):** δ (ppm) = 52.53 (CH₃), 125.94 (CH), 127.83 (CH), 128.56 (C), 128.73 (CH), 129.24 (CH), 129.37 (CH), 130.28 (CH), 131.61 (CH), 133.59 (C), 136.54 (C), 167.41 (C). **LC-MS (m/z):** 187.1 [M+H]⁺.

D.3.4 Synthesis of naphthalene-containing methacrylate monomers

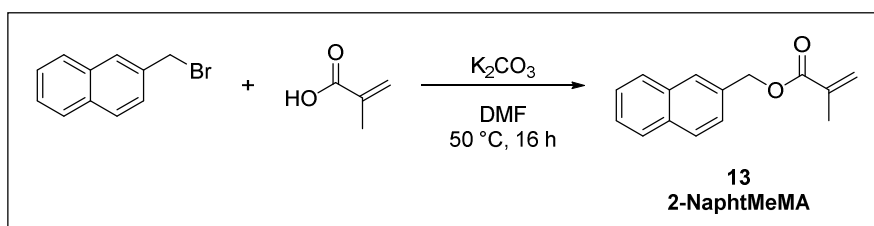
D.3.4.1 Synthesis of 2-(methacryloyloxy)ethyl 2-naphthanoate (2-NaphtCOOEtMA, **12**)



A solution of 2-naphthoyl chloride (5.00 g, 26.2 mmol, 1.0 eq.) was placed under inert atmosphere and cooled at 0 °C. Triethylamine (4.02 mL, 28.9 mmol, 1.1 eq.) was added at 0 °C, followed by the dropwise addition of 2-hydroxyethyl methacrylate (3.50 mL, 28.9 mmol, 1.1 eq.). The resulting mixture was heated to mild reflux at 40 °C for 4 hours. The resulting cloudy mixture was cooled to room temperature and diluted with 20 mL dichloromethane and quenched with 20 mL aqueous saturated ammonium chloride solution. The clear suspension was phase separated and the aqueous phase was washed with dichloromethane (1 x 20 mL). The combined organic phases were washed with brine (1 x 20 mL), dried over magnesium sulfate and the solvent was removed *in vacuo*. The crude colorless oil was dissolved in a minimal amount of ethyl acetate and purified by means of column chromatography (silica, ethyl acetate:hexanes 1:9, R_F = 0.25). 4-Methoxyphenol was added as an inhibitor prior to solvent evaporation *in vacuo* to eventually give 2-(methacryloyloxy)ethyl 2-naphthanoate **12** as a clear and colorless oil that solidified to a white powder upon standing at room temperature (6.81 g – 91 %).

¹H-NMR (400 MHz, CDCl₃): δ (ppm) = 1.98 (dd, 3H, CH₃, J = 0.5 (x2) Hz), 4.55 (m, 2H, Ar-CO-O-CH₂), 4.65 (m, 2H, Ar-CO-O-CH₂-CH₂), 5.61 (quin, 1H, C=CH, J = 1.6 Hz), 6.20 (dq, 1H, C=CH, J = 1.7, 0.9 Hz), 7.52-7.65 (m, 2H, ArH), 7.90 (m, 1H, ArH), 7.97 (m, 1H, ArH), 8.07 (dd, 1H, ArH, J = 8.5, 1.7 Hz), 8.63 (s, 1H, ArH). **¹³C-NMR (100 MHz, CDCl₃):** δ (ppm) = 18.28 (CH₃), 62.44 (CH₂), 62.74 (CH₂), 125.17 (CH), 126.11 (CH₂), 126.68 (CH), 127.05 (C), 127.75 (CH), 128.20 (CH), 128.34 (CH), 129.37 (CH), 131.25 (CH), 132.44 (C), 135.59 (C), 135.94 (C), 166.47 (C), 167.18 (C). **LC-MS (m/z):** 302.2 [M+NH₄]⁺. **HRMS (m/z):** *calc.*: 302.1387, *found*: 302.1396 [M+H]⁺.

D.3.4.2 Synthesis of naphthalen-2-ylmethyl methacrylate (2-NaphtMeMA, **13**)

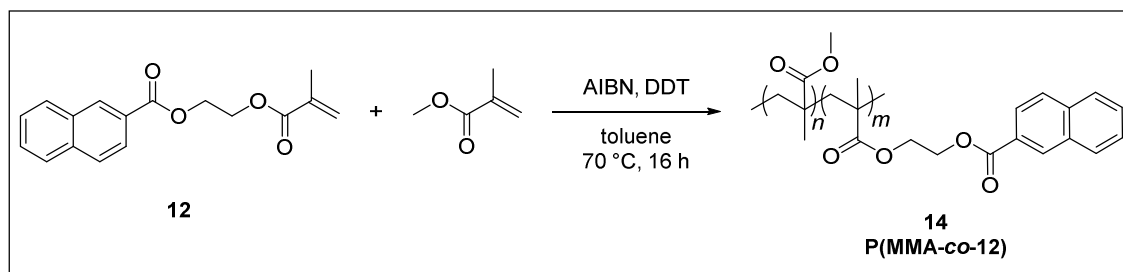


A mixture of methacrylic acid (3.37 mL, 39.6 mmol, 1.0 eq.) and potassium carbonate (6.1 g, 43.6 mmol, 1.1 eq.) in 200 mL anhydrous DMF was placed under inert atmosphere. 2-(Bromomethyl)naphthalene (9.2 g, 43.6 mmol, 1.1 eq.) was added dropwise and the resulting mixture was heated at 50 °C for 16 hours. After cooling to room temperature, 400 mL ethyl acetate was added and the organic phase was washed with brine (3 x 400 mL) and dried over magnesium sulfate. Solvent evaporation *in vacuo* gave a clear yellow oil that solidified upon standing at room temperature. The crude residue was dissolved in a minimal amount of ethyl acetate and purified by means of column chromatography (silica, ethyl acetate:hexanes 1:5, R_F = 0.45). 4-Methoxyphenol was added as an inhibitor prior to solvent evaporation *in vacuo* to give naphthalen-2-ylmethyl methacrylate **13** as an off-white residue (7.70 g – 86 %).

¹H-NMR (300 MHz, CDCl₃): δ (ppm) = 2.00 (dd, 3H, CH₃, J = 1.32 (x2) Hz), 5.37 (s, 2H, CH₂), 5.61 (m, 1H, C=CH), 6.20 (m, 1H, C=CH), 7.45-7.56 (m, 3H, ArH), 7.81-7.91 (m, 4H, ArH). **¹³C-NMR (75 MHz, CDCl₃):** δ (ppm) = 18.36 (CH₃), 66.56 (CH₂), 125.80 (CH), 125.87 (CH₂), 126.22 (CH), 126.27 (CH), 127.18 (CH), 127.70 (CH), 127.97 (CH), 128.35 (CH), 133.08 (C), 133.18 (C), 133.52 (C), 136.24 (C), 167.28 (C). **LC-MS (m/z):** 244.2 [M+NH₄]⁺. **HRMS (m/z):** *calc.*: 244.1332, *found*: 244.1340 [M+NH₄]⁺.

D.3.5 Synthesis of naphthalene-containing polymers

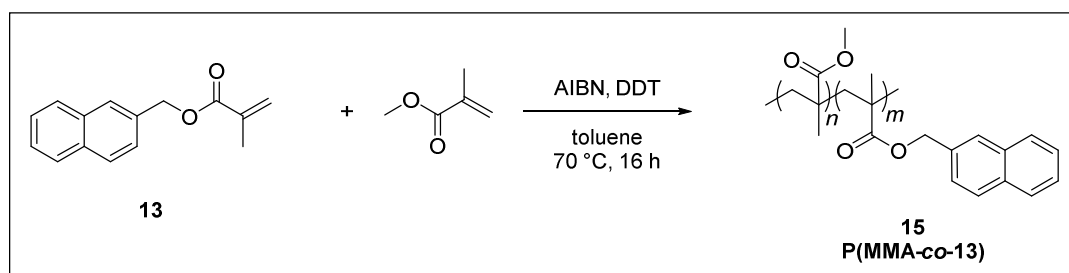
D.3.5.1 Synthesis of 2-(methacryloyloxy)ethyl 2-naphthanoate (**12**) into polymer **14**



2-(Methacryloyloxy)ethyl 2-naphthanoate (**12**, 2.56 g, 9.0 mmol, 15 eq.) was dissolved in 4 mL of toluene and passed over a column of basic aluminium oxide to remove the inhibitor. The column was flushed with another 2 mL of toluene. Methyl methacrylate (MMA, 5.46 mL, 51.0 mmol, 85 eq.) was next added to the toluene solution, after the inhibitor was removed by passing over a column of basic aluminium oxide. The combined monomer solution was added to an airtight crimped headspace vial containing 2,2'-azobisisobutyronitrile (AIBN, 98.5 mg, 0.60 mmol, 1.0 eq.) and a stirring bar, which was placed under inert atmosphere prior to monomer addition. Another 6 mL of toluene was added and the resulting mixture was flushed for 20 minutes by bubbling with nitrogen gas. Subsequently, 1-dodecanethiol (DDT, 0.29 mL, 1.20 mmol, 2.0 eq.), which was deoxygenated by bubbling with nitrogen gas for 20 minutes, was added and the mixture was placed in a preheated oil bath at 70 °C. After 16 hours, the polymer mixture was opened to the air and cooled in liquid nitrogen after which 6 mL of tetrahydrofuran was added. The polymer solution was precipitated in 300 mL of ice cold methanol and the white precipitate was collected through filtration. The residue was dissolved in a minimal amount of tetrahydrofuran and precipitated a second time in a 10-fold excess of ice cold *n*-hexane. Drying of the obtained residue in a vacuum oven at 40 °C overnight gave the naphthalene-containing polymer **14** as a white powder (5.87 g – ca. 81 %). Fraction of naphthalene, determined via ¹H-NMR: 14.1 mol % or 31.8 wt %.

¹H-NMR (400 MHz, CDCl₃): δ (ppm) = 0.66-2.13 (CH₃ + CH₂ polymer backbone), 3.30-3.69 (O-CH₃), 4.06-4.71 (4H, C(O)O-CH₂), 7.40-7.68 (2H, ArH), 7.77-8.17 (4H, ArH), 8.48-8.74 (1H, ArH). SEC (CHCl₃, PMMA standards): M_n = 5.0 kDa, M_w = 9.5 kDa, M_p = 8.6 kDa, Đ = 1.90. DSC: T_g = 82 °C. TGA: T_{d, 5%} = 267 °C.

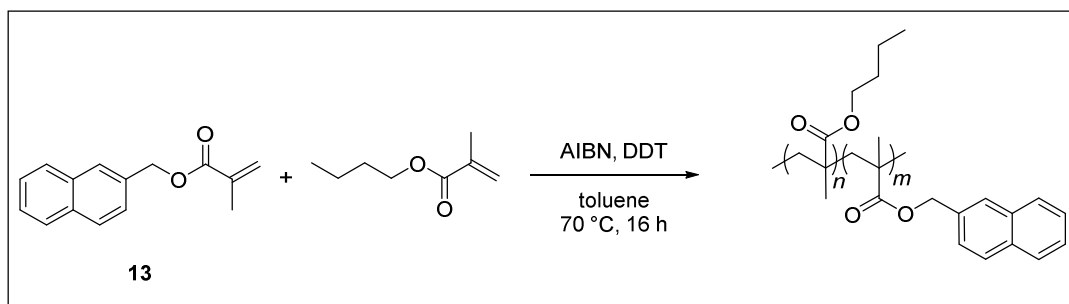
D.3.5.2 Synthesis of naphthalen-2-ylmethyl methacrylate (**13**) into polymer **15**



Naphthalen-2-ylmethyl methacrylate (**13**, 2.04 g, 9.0 mmol, 15 eq.) was dissolved in 4 mL of toluene and passed over a column of basic aluminium oxide to remove the inhibitor. The column was flushed with another 2 mL of toluene. Methyl methacrylate (MMA, 5.46 mL, 51.0 mmol, 85 eq.) was next added to the toluene solution, after the inhibitor was removed by passing over a column of basic aluminium oxide. The combined monomer solution was added to an airtight crimped headspace vial containing (AIBN, 98.5 mg, 0.60 mmol, 1.0 eq.) and a stirring bar, which was placed under inert atmosphere prior to monomer addition. Another 6 mL of toluene was added and the resulting mixture was flushed for 20 minutes by bubbling with nitrogen gas. Subsequently, 1-dodecanethiol (DDT, 0.29 mL, 1.20 mmol, 2.0 eq.), which was deoxygenated by bubbling with nitrogen gas for 20 minutes, was added and the mixture was placed in a preheated oil bath at 70 °C. After 16 hours, the polymer mixture was opened to the air and cooled in liquid nitrogen after which 6 mL of tetrahydrofuran was added. The polymer solution was precipitated in 300 mL of ice cold methanol and the white precipitate was collected through filtration. The residue was dissolved in a minimal amount of tetrahydrofuran and precipitated a second time in a 10-fold excess of ice cold *n*-hexane. Drying of the obtained residue in a vacuum oven at 40 °C overnight gave the naphthalene-containing polymer **15** as a white powder (6.09 g – ca. 85 %). Fraction of naphthalene, determined via ¹H-NMR: 14.2 mol % or 27.2 wt %.

¹H-NMR (400 MHz, CDCl₃): δ (ppm) = 0.44-2.25 ($CH_3 + CH_2$ polymer backbone), 3.24-3.70 (O- CH_3), 4.84-5.33 (2H, Ar CH_2), 7.33-7.62 (3H, Ar H), 7.66-8.01 (4H, Ar H). **SEC (CHCl₃, PMMA standards):** $M_n = 4.7$ kDa, $M_w = 9.5$ kDa, $M_p = 8.7$ kDa, $D = 2.01$. **DSC:** $T_g = 87$ °C. **TGA:** $T_{d, 5\%} = 263$ °C.

D.3.5.3 Copolymerisation of naphthalen-2-ylmethyl methacrylate (**13**) with butyl methacrylate



Naphthalen-2-ylmethyl methacrylate (**13**, 649 mg, 3.0 mmol, 15 eq.) was dissolved in 2 mL of toluene and passed over a column of basic aluminium oxide to remove the inhibitor. The column was flushed with another 1 mL of toluene. *n*-Butyl methacrylate (BuMA, 2.70 mL, 17.0 mmol, 85 eq.) was next added to the toluene solution, after the inhibitor was removed by passing over a column of basic aluminium oxide. The combined monomer solution was added to an airtight crimped headspace vial containing (AIBN, 32.8 mg, 0.20 mmol, 1.0 eq.) and a stirring bar, which was placed under inert atmosphere prior to monomer addition. Another 1 mL of toluene was added and the resulting mixture was flushed for 20 minutes by bubbling with nitrogen gas. Subsequently, 1-dodecanethiol (DDT, 0.05 mL, 0.20 mmol, 1.0 eq.), which was deoxygenated by bubbling with nitrogen gas for 20 minutes, was added and the mixture was placed in a preheated oil bath at 70 °C. After 16 hours, the polymer mixture was opened to the air and cooled in liquid nitrogen after which 6 mL of tetrahydrofuran was added. The polymer solution was precipitated in 300 mL of ice cold methanol and the white precipitate was collected through filtration. The residue was dissolved in a minimal amount of tetrahydrofuran and precipitated a second time in a 10-fold excess of ice cold *n*-hexane. Drying of the obtained residue in a vacuum oven at 40 °C overnight gave the naphthalene-containing butyl methacrylate polymer as a brittle white powder (2.35 g – ca. 63 %). Fraction of naphthalene, determined via ¹H-NMR: 15.4 mol % or 22.5 wt %.

¹H-NMR (400 MHz, CDCl₃): δ (ppm) = 0.57-2.15 (CH₃-(CH₂)₃ + CH₂ polymer backbone), 3.54-4.16 (O-CH₂), 4.79-5.38 (2H, ArCH₂), 7.63-7.63 (3H, ArH), 7.66-7.99 (4H, ArH). SEC (CHCl₃, PMMA standards): M_n = 8.6 kDa, M_w = 14.6 kDa, M_p = 14.0 kDa, Đ = 1.70. DSC: T_g = 31 °C.

D.3.6 Synthesis of bisfunctional triazolinedione crosslinker **16**

BisTAD crosslinker **16** was synthesized as described in B.4.8.

Appendix E.

Experimental section Chapter VI

E.1 Additional figures

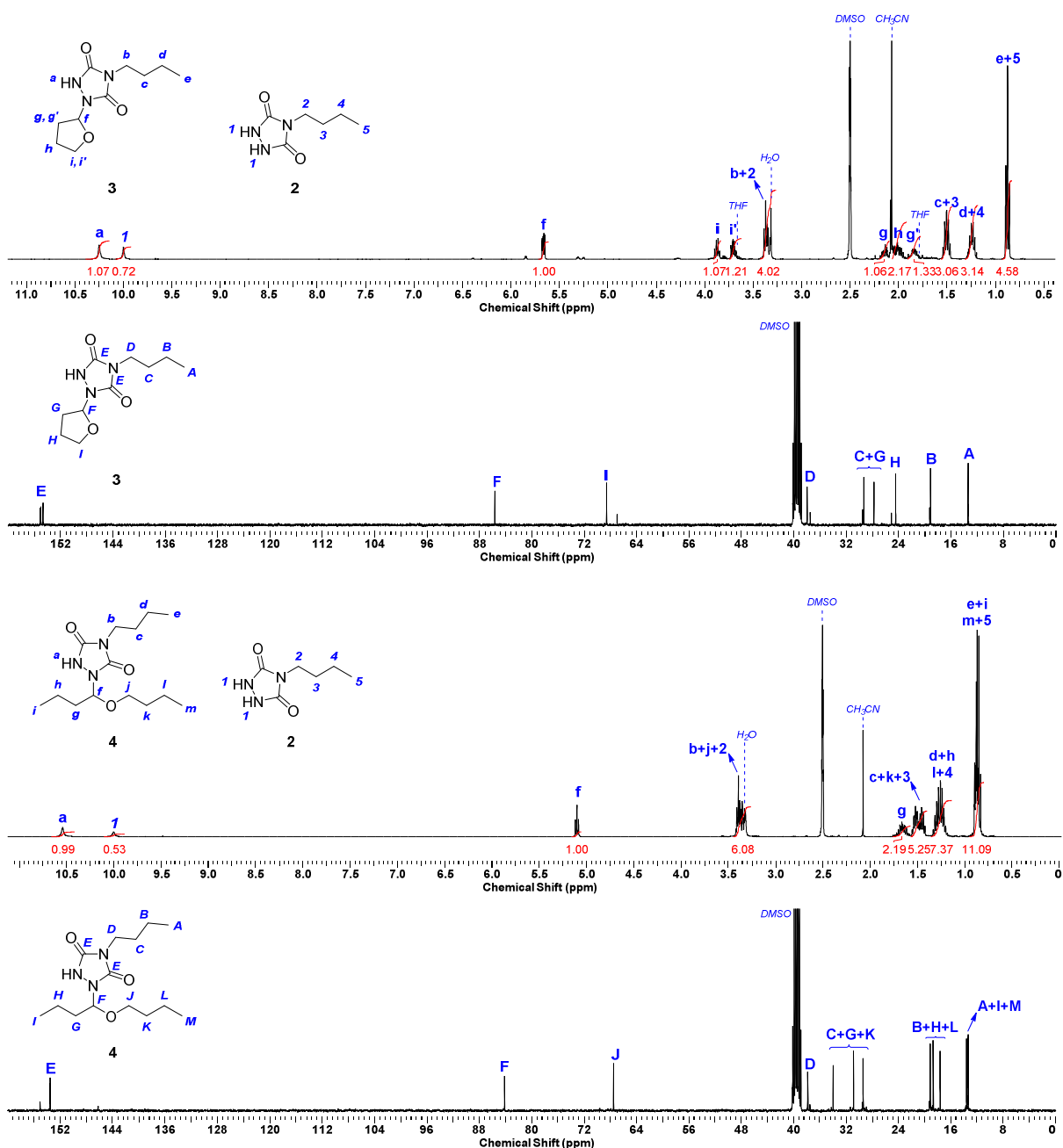


Figure E.1. ^1H -NMR and ^{13}C -NMR spectra (DMSO- d_6) obtained after UV-irradiation of BuTAD 1 in the presence of an equimolar amount of tetrahydrofuran or di-*n*-butyl ether in anhydrous acetonitrile (5 mg mL^{-1}) to give the corresponding TAD- α -addition products 3 and 4, respectively. Traces of the urazole 2 are also observed.

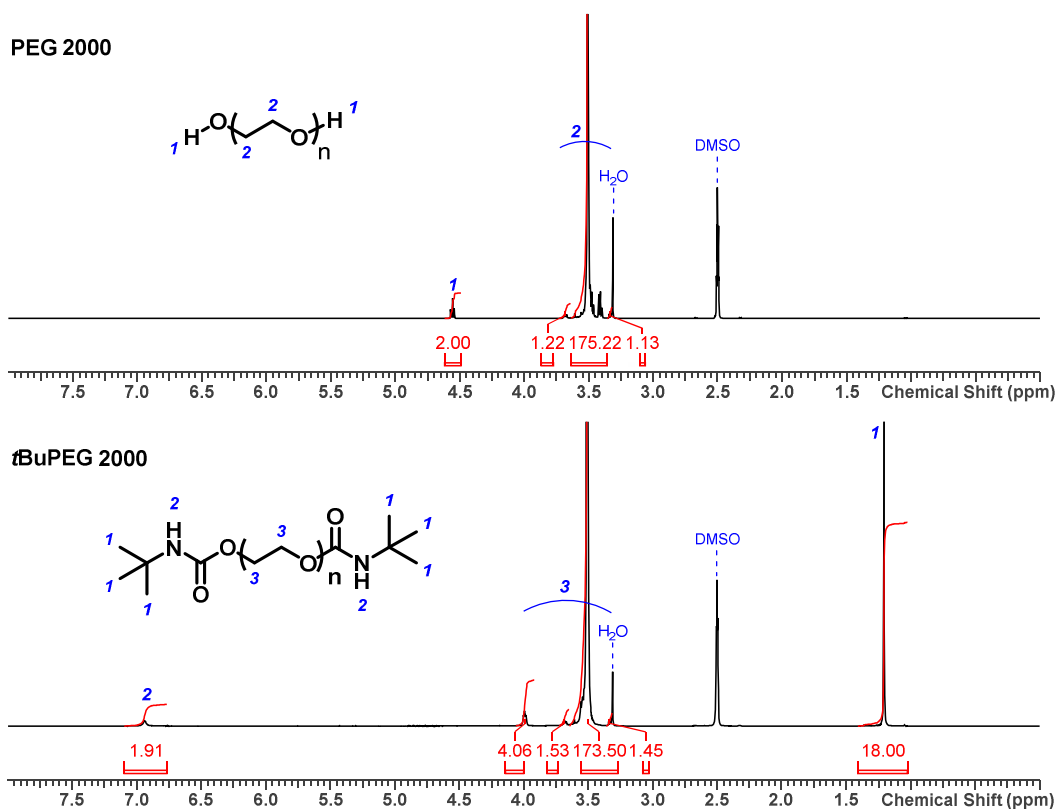


Figure E.2. ^1H -NMR spectra, indicating the quantitative end group conversion of PEG 2000 (top) into its *tert*-butyl end capped derivative *t*BuPEG 2000 (bottom).

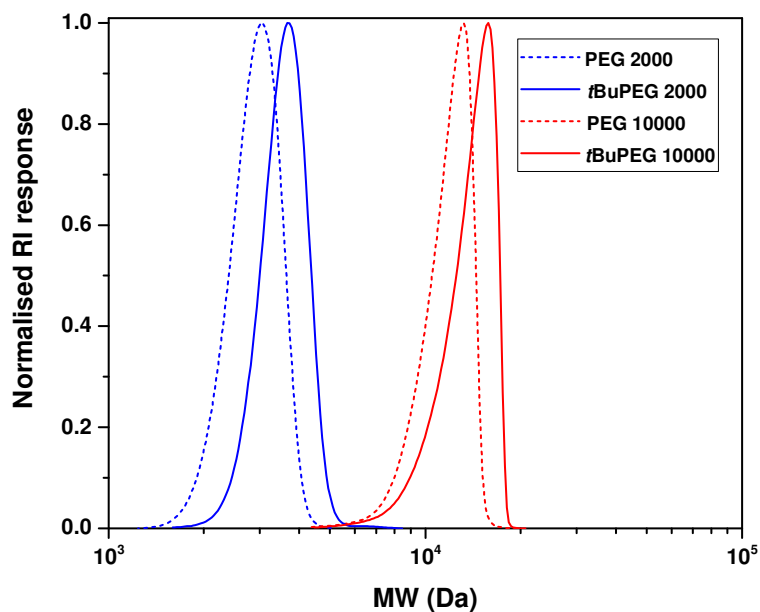


Figure E.3. SEC traces (THF, polystyrene standards), indicating the quantitative end group modification of PEG 2000 (dashed blue line) and 10 000 (dashed red line) into its *tert*-butyl end capped derivative *t*BuPEG 2000 (full blue line) and 10 000 (full red line).

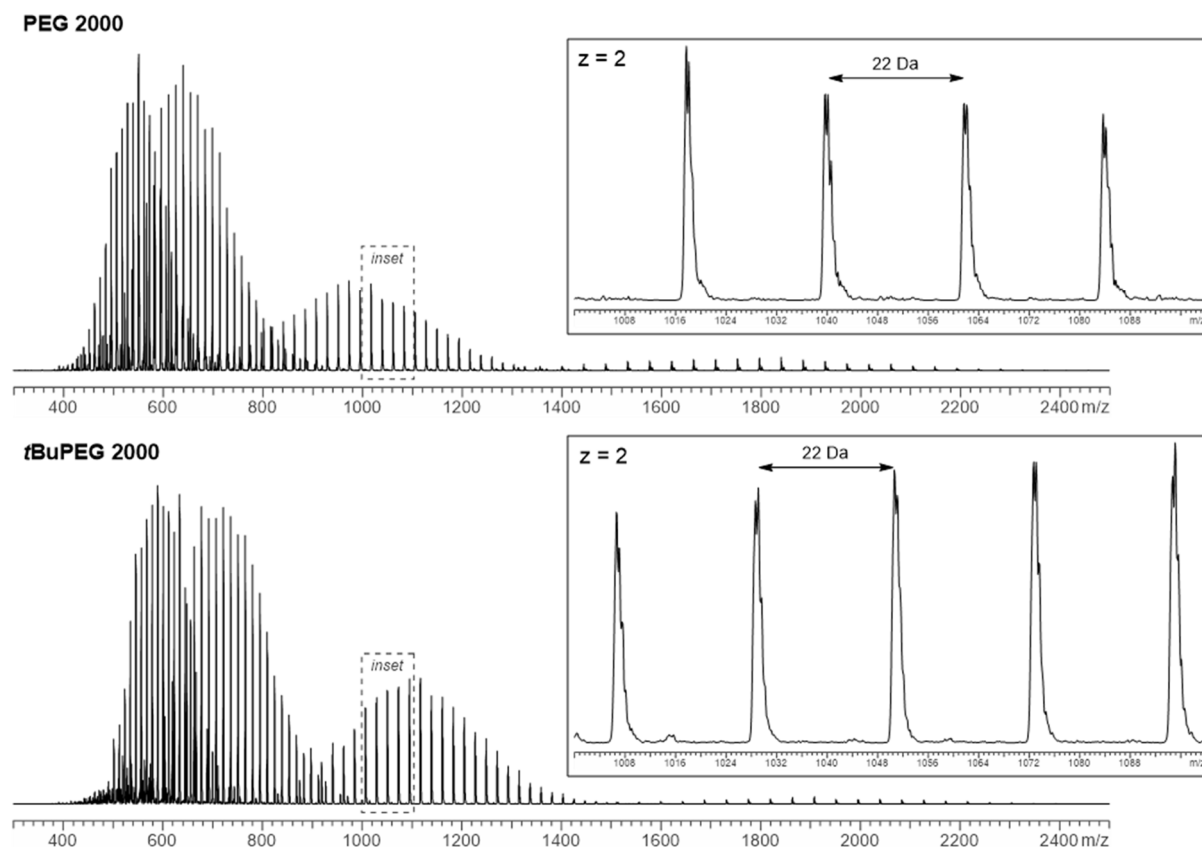


Figure E.4. ESI-MS spectra obtained before (top) and after (bottom) end capping of PEG 2000 into its tBuPEG derivative, indicating quantitative conversion of the hydroxyl end groups.

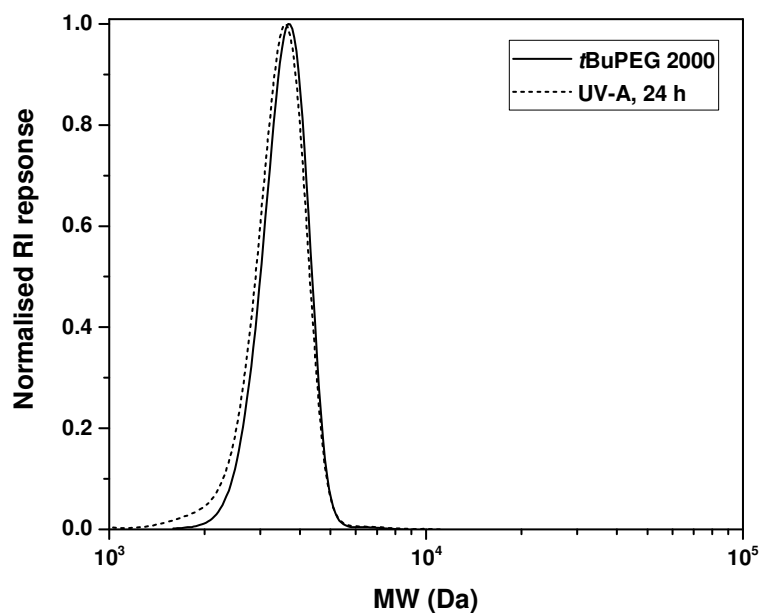


Figure E.5. SEC traces (THF, polystyrene standards) of tBuPEG 2000 before (full line) and after (dashed line) irradiation with UV-A light for 24 hours ($\lambda = 370 - 380$ nm, 3×3 W LEDs), demonstrating the required photostability.

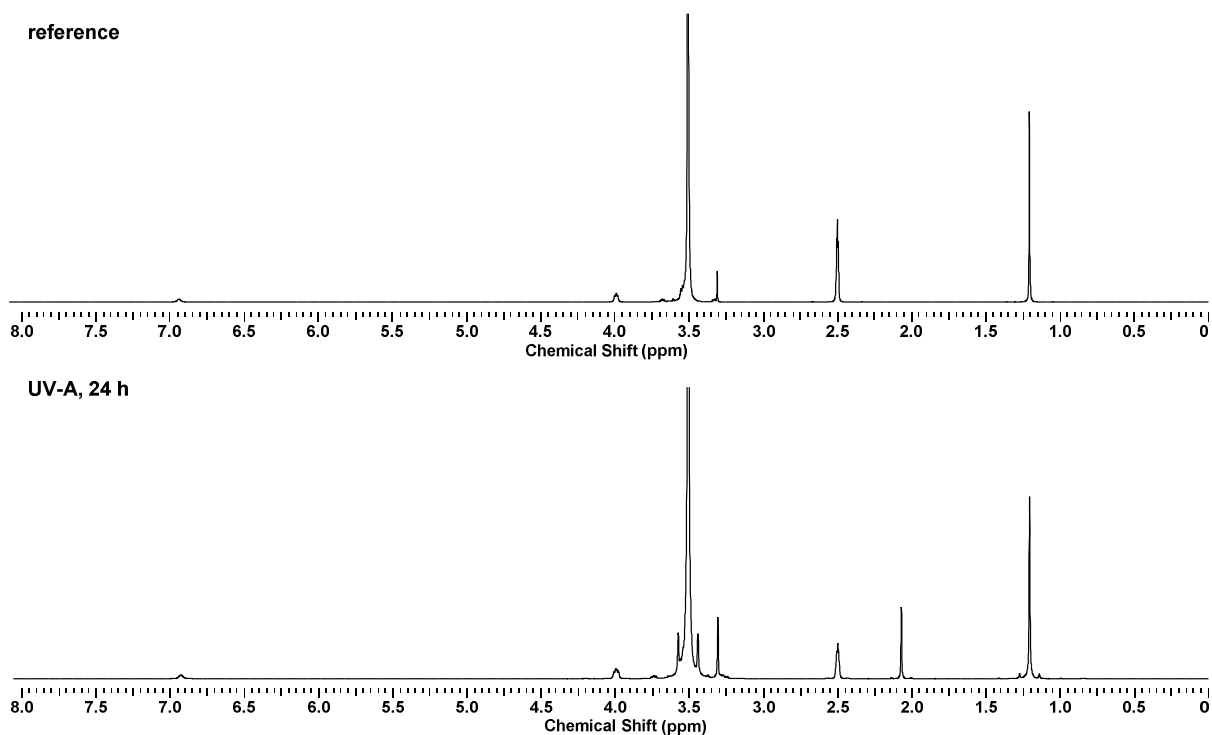


Figure E.6. ¹H-NMR spectra of tBuPEG 2000 before (top) and after (bottom) irradiation with UV-A light for 24 hours ($\lambda = 370 - 380$ nm, 3 x 3 W LEDs), demonstrating the required photostability.

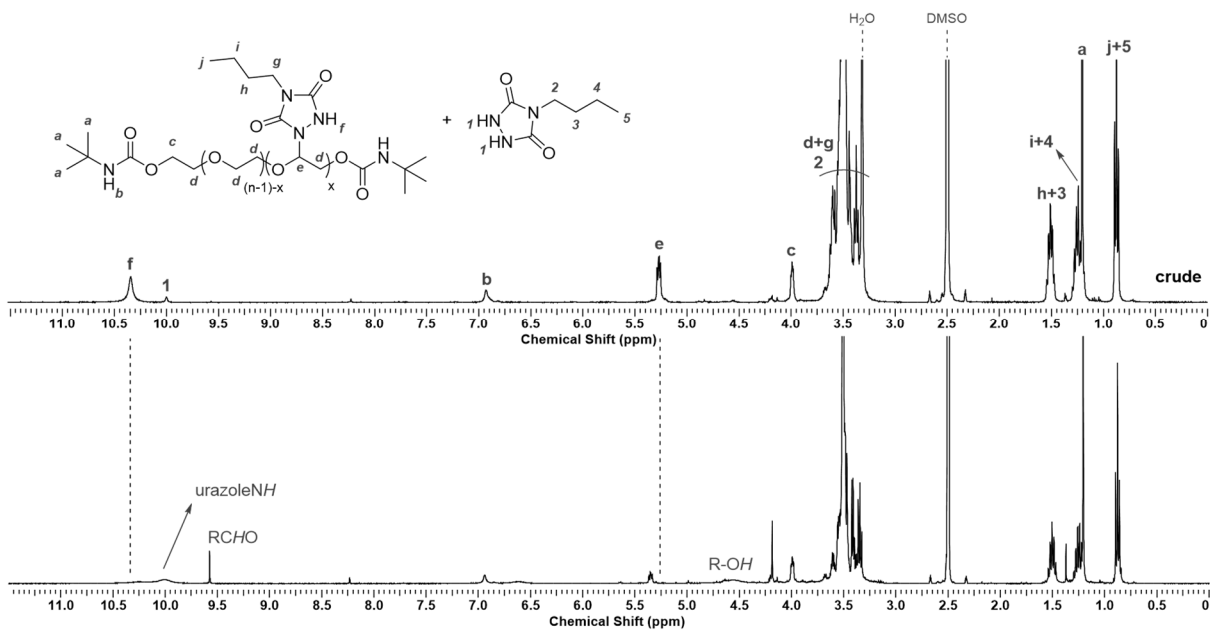


Figure E.7. ¹H-NMR spectra of tBuPEG 2000 irradiated in the presence of 10 equivalents BuTAD, kept in anhydrous acetonitrile (top) or water at 60 °C (bottom) for 24 hours after irradiation, indicating the disappearance of the TAD-PEG conjugate and the formation of several hydrolysis products

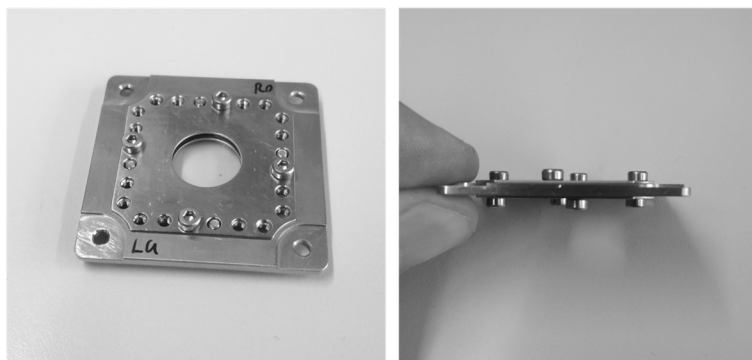


Figure E.8. Customised sample holder, used in the time-lapse optical microscopic imaging of the hydrolytic cleavage of the direct laser written TAD-PEG microstructures.

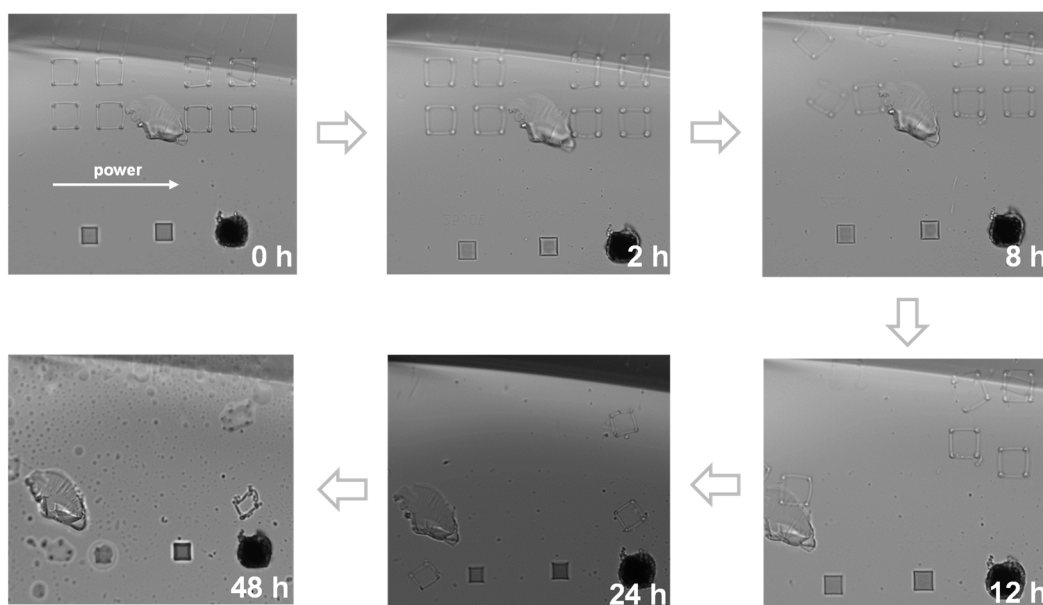
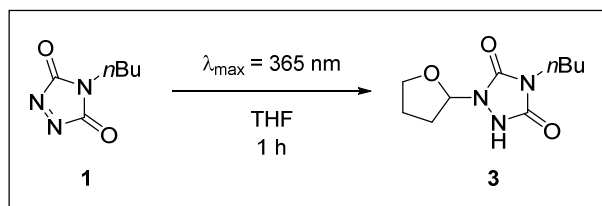


Figure E.9. Time-lapse microscopy of direct laser written TAD-PEG structures, immersed in water at 40 °C. Swelling and of the boxing rings and blocks is observed, yet remains inconclusive whether the structures are degraded or solely detached from the glass substrate.

E.2 Experimental procedures

E.2.1 Photoaddition to low molecular weight compounds

E.2.1.1 Photoaddition of BuTAD in tetrahydrofuran

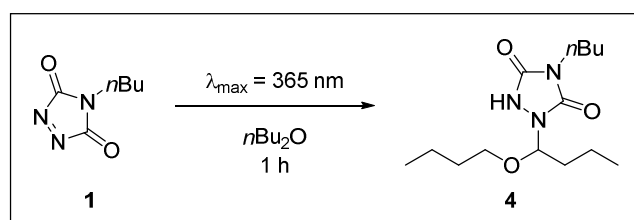


An airtight crimped headspace vial containing a solution of sublimed BuTAD (**1**, 10 mg, $6.44 \cdot 10^{-5}$ mol, 1.0 eq.) in 2 mL anhydrous tetrahydrofuran was placed under inert atmosphere

and transferred into a custom-built photoreactor. Irradiation of the purple solution with 3 x 36 W Arimed B6 compact fluorescence lamps ($\lambda_{\max} = 365$ nm) gave a clear colourless solution within 1 h. Solvent removal *in vacuo* gave photoadduct **3** as a clear colourless oil (10.3 mg – 70 %). Traces of *n*-butylurazole (**2**) were also detected. No product formation was observed when a reference sample was kept in the dark.

¹H-NMR (400 MHz, DMSO-*d*₆): δ (ppm) = 0.87 (t, 3H, CH₃, *J* = 7.4 Hz), 1.25 (m, 2H, CH₃-CH₂), 1.51 (m, 2H, CH₃-CH₂-CH₂), 1.83 (m, 1H, N-CH-CH₂), 2.01 (m, 2H, O-CH₂-CH₂), 2.14 (m, 1H, N-CH-CH₂), 3.37 (m, 2H, N-CH₂), 3.70 (m, 1H, O-CH₂-CH₂), 3.87 (m, 1H, O-CH₂-CH₂), 5.66 (dd, 1H, O-CH-N, *J* = 7.5, 3.9 Hz), 10.25 (s, 1H, NH). **¹³C-NMR (100 MHz, DMSO-*d*₆):** δ (ppm) = 13.39 (CH₃), 19.15 (CH₂), 24.47 (CH₂), 27.79 (CH₂), 29.35 (CH₂), 37.99 (CH₂), 68.59 (CH₂), 85.68 (CH), 154.99 (C), 155.07 (C).

E.2.1.2 Photoaddition of BuTAD in di-*n*-butyl ether



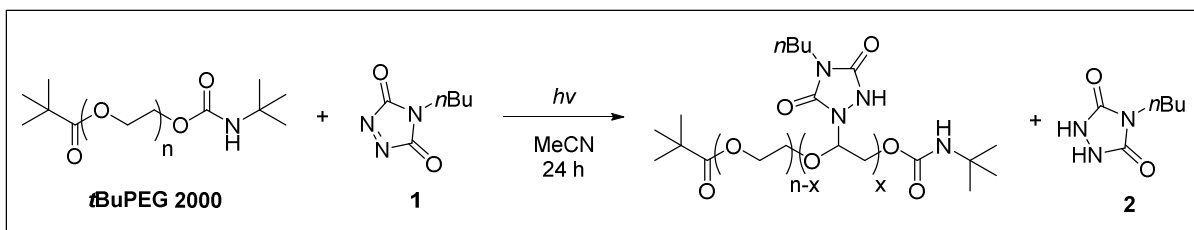
An airtight crimped headspace vial containing a solution of sublimed BuTAD (**1**, 10 mg, $6.44 \cdot 10^{-5}$ mol, 1.0 eq.) in 2 mL di-*n*-butyl ether was placed under inert atmosphere and transferred into a custom-built photoreactor. Irradiation of the purple solution with 3 x 36 W Arimed B6 compact fluorescence lamps ($\lambda_{\max} = 365$ nm) gave a clear colourless solution within 1 h. Solvent removal *in vacuo* gave photoadduct **4** as a clear colourless oil (16.2 mg – 88 %). Traces of *n*-butylurazole (**2**) were also detected. No product formation was observed when a reference sample was kept in the dark.

¹H-NMR (400 MHz, DMSO-*d*₆): δ (ppm) = 0.80-0.93 (m, 9H, CH₃), 1.16-1.38 (m, 6H, CH₃-CH₂), 1.38-1.57 (m, 5H, N-CH₂-CH₂ + O-CH₂-CH₂), 1.66 (m, 1H, N-CH-CH₂), 3.39 (m, 2H, N-CH₂), 5.10 (t, 1H, O-CH-N, *J* = 6.8 Hz), 10.54 (s, 1H, NH). **¹³C-NMR (100 MHz, DMSO-*d*₆):** δ (ppm) = 13.34 (CH₃), 13.38 (CH₃), 13.57 (CH₃), 17.63 (CH₂), 18.67 (CH₂), 19.16 (CH₂), 29.39 (CH₂), 30.83 (CH₂), 33.96 (CH₂), 37.84 (CH₂), 67.51 (CH₂), 84.14 (CH), 153.51 (C), 153.56 (C).

E.2.1.3 Photoaddition of BuTAD and equimolar amount of ethers in acetonitrile

Similar experiments were carried out with sublimed BuTAD (**1**, 10 mg, $6.44 \cdot 10^{-5}$ mol, 1.0 eq.) and equimolar amounts of anhydrous tetrahydrofuran (5.22 μ L, $6.44 \cdot 10^{-5}$ mol, 1.0 eq.) or di-*n*-butyl ether (11.0 μ L, $6.44 \cdot 10^{-5}$ mol, 1.0 eq.) in 2 mL anhydrous acetonitrile. UV-irradiation was carried out for 2 h with 3 x 36 W Arimed B6 compact fluorescence lamps ($\lambda_{\max} = 365$ nm).

E.2.2 Photoaddition to *tert*-butyl endcapped poly(ethylene glycol)



A stock solution of *tert*-butyl end capped poly(ethylene glycol) 2000 (*t*BuPEG 2000, 400 mg, $1.86 \cdot 10^{-4}$ mol, 1.0 eq.) in 16 mL anhydrous acetonitrile was prepared in an airtight crimped headspace vial and deoxygenated for 20 minutes by bubbling with a stream of nitrogen gas. 2 mL of the resulting stock solution was next added to an airtight crimped headspace vial containing a distinct amount of BuTAD (**1**), ranging from 1.0 to 35 eq. (i.e. 1.0; 2.0; 5.0; 10.0; 20.0; 35.0 eq., respectively), which was briefly flushed with nitrogen gas. The obtained purple solutions were transferred into a custom-built photoreactor and irradiated with 3 x 3 W UV-A LEDs ($\lambda = 370 - 380$ nm) for 24 hours. Complete photobleaching was observed for all samples, except when more than 20 equivalent of BuTAD were used. Solvent removal *in vacuo* gave clear colourless residues, which were subjected to $^1\text{H-NMR}$ analysis to determine the yield of the reactions via integration of well-resolved proton signals. The thus found yields are depicted in Table VI.1. Traces of *n*-butylurazole (**2**) were also detected. No product formation was observed when a reference sample was kept in the dark.

$^1\text{H-NMR}$ (400 MHz, DMSO-*d*₆): illustrated for the reaction with 10 eq. BuTAD: δ (ppm) = 0.87 (t, 30H, CH_3 + **2**), 1.14-1.35 (m, 38H, $\text{C}(\text{CH}_3)_3$ + $\text{N-CH}_2\text{-CH}_2\text{-CH}_2$ + **2**), 1.51 (m, 20H, $\text{N-CH}_2\text{-CH}_2$ + **2**), 3.20-3.78 (broad, ca. 191H, $\text{CH}_2\text{-O}$ polyether backbone + water), 3.99 (t, 4H, $\text{C}(\text{O})\text{-O-CH}_2$, $J = 4.5$ Hz), 5.28 (m, 8.43H, O-CH-N), 6.92 (s, 2H, $\text{C}(\text{O})\text{-NH}$), 9.99 (s, 0.96H, **2**), 10.33 (s, 8.15H, NH) (refer to Figure VI.4a). **SEC (THF, PS standards):** illustrated for the reaction with 10 eq. BuTAD: $M_n = 3.7$ kDa, $M_w = 4.3$ kDa, $D = 1.17$ (refer to Figure VI.4b and Table VI.2). **ESI-MS:** refer to Figure VI.4c and Table VI.3.

The modification reaction of *t*BuPEG 2000 with BuTAD was repeated with different LED sources, i.e. $\lambda = 440 - 450$ nm and $\lambda = 515 - 525$ nm, but did not improve nor deteriorate the reaction outcome. Decreasing the distance between the samples and the LEDs during irradiation, however, were found to significantly reduce the times needed to affect the photobleaching (e.g. < 1 hour for 5 eq. of **1** with *t*BuPEG 2000, when making use of green LEDs at $\lambda = 515 - 525$ nm vs. 18 h found earlier).

E.2.3 Removal of urazole byproducts via dialysis

An airtight crimped headspace vial containing a solution of sublimed BuTAD (**1**, 70.2 mg, $4.52 \cdot 10^{-4}$ mol, 10.0 eq.) and *tert*-butyl end capped poly(ethylene glycol) (*t*BuPEG 2000, 100 mg, $4.53 \cdot 10^{-5}$ mol, 1.0 eq.) in 4 mL anhydrous acetonitrile was placed under inert atmosphere and

irradiated with 3 x 3 W green LEDs ($\lambda = 515 - 525$ nm). After 3 hours, complete photobleaching was observed and a clear colourless solution was obtained. The resulting mixture was transferred into a dialysis tube (MWCO 1 kDa, regenerated cellulose), which was mildly stirred in 800 mL acetonitrile overnight. Magnesium sulfate was added to the solvent in order to preserve a water-free environment, thereby preventing hydrolysis of the TAD-PEG conjugates. After 16 h, the solvent was replaced for tetrahydrofuran and dialysis was continued for another day. Following dialysis, the reaction mixture was evaporated to dryness *in vacuo* to give a colourless oil. The obtained residue was submitted for $^1\text{H-NMR}$ analysis, indicating the successful removal of the low molecular weight urazole (**2**) byproducts (refer to Figure VI.5).

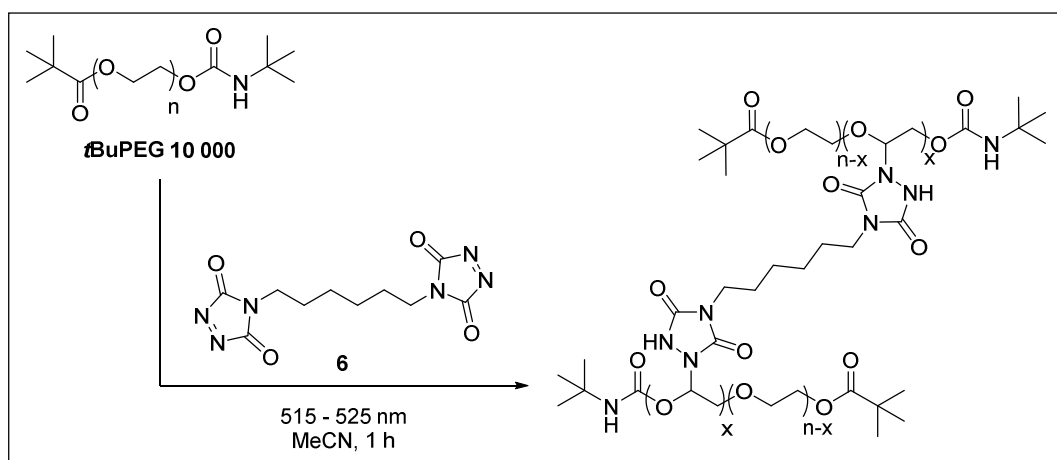
$^1\text{H-NMR}$ (400 MHz, DMSO-*d*₆): δ (ppm) = 0.88 (t, 18H, CH_3 , $J = 7.3$ Hz), 1.12-1.36 (m, 30H, $\text{C}(\text{CH}_3)_3 + \text{N-CH}_2\text{-CH}_2\text{-CH}_2$), 1.51 (m, 12, $\text{N-CH}_2\text{-CH}_2$), 3.34-3.72 (broad, ca. 206H, $\text{CH}_2\text{-O}$ polyether backbone + water), 3.99 (t, 4H, $\text{C}(\text{O})\text{-O-CH}_2$, $J = 4.5$ Hz), 5.27 (m, 6H, O-CH-N), 6.92 (s, 2H, $\text{C}(\text{O})\text{-NH}$), 10.34 (s, 6H, NH). SEC (THF, PS standards): $M_n = 3.6$ kDa, $M_w = 3.9$ kDa, $D = 1.10$.

E.2.4 Hydrolysis of BuTAD-poly(ethylene glycol) conjugates

Following photoaddition of BuTAD (**1**, 72.1 mg, $4.65 \cdot 10^{-4}$ mol, 10 eq.) to *t*BuPEG 2000 (100 mg, $4.65 \cdot 10^{-5}$ mol, 1.0 eq.) in 4 mL anhydrous acetonitrile under green light irradiation ($\lambda = 515 - 525$ nm, 3 x 3 W LEDs), as described in VI.6.3.2, the photobleached reaction mixture was divided into 2 portion. One of the samples was kept at room temperature in anhydrous acetonitrile (serving as the reference) while the other sample was diluted with 8 mL water and placed in an oil bath at 60 °C for 24 h. Following solvent removal *in vacuo*, both samples were submitted to $^1\text{H-NMR}$ analysis (refer to E.1).

E.2.5 Light-induced macroscopic network formation and cleavage

E.2.5.1 Crosslinking under green light irradiation



An airtight crimped headspace vial containing a solution of TAD crosslinker **6** (10 mg, $3.57 \cdot 10^{-5}$ mol, 10 wt %) and *tert*-butyl end capped poly(ethylene glycol) 10 000 (*t*BuPEG 10 000,

100 mg) in 1 mL anhydrous acetonitrile was irradiated with 3 x 3 W green LEDs ($\lambda = 515 - 525$ nm). After 1 hour, complete photobleaching was observed and a clear colourless gel was obtained, which was demonstrated upon vial inversion (*cf.* Figure VI.6). No visual change was detected over the course of several days.

E.2.5.2 Hydrolytic cleavage

Following photocuring of the TAD-*t*BuPEG 10 000 solution, 2 mL of anhydrous acetonitrile was added to the resulting gel. After standing overnight, no visual change was observed. Upon addition of 2 mL water, however, the gel was shown to disintegrate over time. Eventually, a clear colourless solution was obtained after 24 h.

In a similar experiment, 2 mL of an aqueous acid buffer (pH = 5) or aqueous base buffer (pH = 9) was added to the crosslinked gel. In contrast to neutral water, an accelerated collapse of the TAD-PEG networks was observed upon diffusion of the aqueous media into the gel structure.

E.2.6 Direct laser writing and cleavage of microscopic structures

A tailored resist containing *t*BuPEG 10 000 (50 mg) and bisTAD **6** (10 mg) in 250 μ L anhydrous acetonitrile was subjected to DLW to create microsized TAD-PEG blocks and boxing rings. Experiments were carried by Eva Blasco and Patrick Müller with a custom-built DLW setup (Institute of Nanotechnology (KIT), refer to A.2 for instrument specifications) at the powers indicated in VI.3.2). After writing, the substrate containing the structures was placed in a custom-built sample holder and immersed in water at 37 °C. Degradation was monitored over time via time-lapse microscopic imaging.

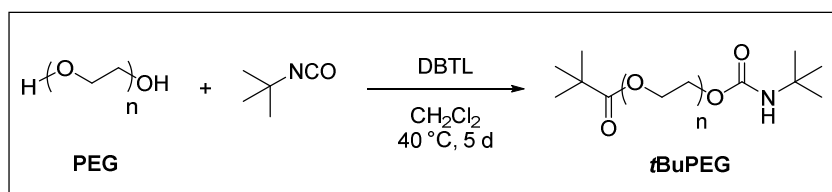
E.3 Synthetic procedures

E.3.1 Synthesis of 4-*n*-butyl-triazoline-3,5-dione (BuTAD, **1**)

4-*n*-butyl-1,2,4-triazoline-3,5-dione (BuTAD, **1**) was synthesized as described in B.4.3, followed by sublimation under reduced pressure (0.1 mbar) at 40 °C, to give BuTAD (**1**) as a carmine red crystalline product. The reactive compound was stored in the dark at -18 °C and typically used within several weeks. Purity was regularly checked via ¹H-NMR prior to use.

¹H-NMR (400 MHz, DMSO-*d*₆): δ (ppm) = 0.88 (t, 3H, CH₃, $J = 7.3$ Hz), 1.30 (sext, 2H, CH₂-CH₃, $J = 7.3$ Hz), 1.56 (quint, 2H, N-CH₂-CH₂, $J = 7.3$ Hz), 3.47 (t, 2H, N-CH₂, $J = 7.0$ Hz). ¹³C-NMR (100 MHz, DMSO-*d*₆): δ (ppm) = 13.32 (CH₃), 19.11 (CH₂), 28.72 (CH₂), 40.34 (CH₂), 160.15 (C).

E.3.2 Synthesis of *tert*-butyl end capped poly(ethylene glycol)s (*t*BuPEG)



E.3.2.1 Synthesis of *t*BuPEG 2000

A solution of poly(ethylene glycol) 2000 (PEG 2000, 10.0 g, 5.0 mmol, 1.0 eq.) in 75 mL anhydrous dichloromethane was placed under inert atmosphere. To this, *tert*-butyl isocyanate (2.3 mL, 20.0 mmol, 4.0 eq.) was added, followed by dibutyltin dilaurate (DBTL, 10 drops) and resulting mixture was refluxed at 40 °C. After 5 days, the mixture was cooled to room temperature and precipitated in a 10-fold excess of cooled diethyl ether. The precipitate was filtered and dissolved in a minimal amount of dichloromethane. Precipitation in a 10-fold excess of diethyl ether gave a white waxy solid, which was dried in a vacuum oven overnight at 40 °C to give the *tert*-butyl end capped poly(ethylene glycol) (*t*BuPEG 2000) as a white waxy solid (5.81 g – 53 %).

¹H-NMR (400 MHz, DMSO-*d*₆): δ (ppm) = 1.21 (s, 18H, 6 x CH₃), 3.38-3.64 (broad, ca. 176H, CH₂-O polyether backbone), 3.99 (t, 4H, C(O)-O-CH₂, *J* = 4.4 Hz), 6.94 (s, 2H, C(O)-NH). SEC (THF, PS standards): *M*_n = 3.5 kDa, *M*_w = 3.7 kDa, *D* = 1.03.

E.3.2.2 Synthesis of *t*BuPEG 10 000

A solution of poly(ethylene glycol) 10 000 (PEG 10 000, 10.0 g, 1.0 mmol, 1.0 eq.) in 75 mL anhydrous dichloromethane was placed under inert atmosphere. To this, *tert*-butyl isocyanate (0.46 mL, 4.0 mmol, 4.0 eq.) was added, followed by dibutyltin dilaurate (DBTL, 10 drops) and resulting mixture was refluxed at 40 °C. After 5 days, the mixture was cooled to room temperature and precipitated in a 10-fold excess of cooled diethyl ether. The precipitate was filtered and dissolved in a minimal amount of dichloromethane. Precipitation in a 10-fold excess of diethyl ether followed by overnight drying in a vacuum oven at 40 °C gave the *tert*-butyl end capped poly(ethylene glycol) (*t*BuPEG 10 000) as a white powder (9.61 g – 94 %).

¹H-NMR (400 MHz, DMSO-*d*₆): δ (ppm) = 1.21 (s, 18H, 6 x CH₃), 3.38-3.64 (broad, ca. 922H, CH₂-O polyether backbone), 3.99 (t, 4H, C(O)-O-CH₂, *J* = 4.5 Hz), 6.94 (s, 2H, C(O)-NH). SEC (THF, PS standards): *M*_n = 13.2 kDa, *M*_w = 13.8 kDa, *D* = 1.04.

E.3.3 Synthesis of bisfunctional triazolinedione crosslinker **6**

BisTAD crosslinker **6** was synthesized as described in B.4.8.

Appendix F.

List of abbreviations

1PA	one-photon absorption
2PA	two-photon absorption
3D	three dimensional
ABS	acrylonitrile butadiene styrene terpolymer
ADMET	acyclic diene metathesis polymerisation
AFM	atomic-force microscopy
AI	aziridinium imide intermediate
AIBN	2,2'-azobisisobutyronitile
CAN	covalent adaptable network
COSY	correlation spectroscopy
C _p	cyclopentadiene
DABCO-Br	tetrameric complex of 1,4-diazabicyclo[2.2.2]octane with bromine
DDT	1-dodecanethiol
DEAD	diethyl azodicarboxylate
DFT	density functional theory
DLW	Direct Laser Writing
DSC	Differential Scanning Calorimetry
ESI-MS	Electrospray Ionisation Mass Spectrometry
HDEO	<i>trans,trans</i> -2,4-hexadien-1-ol
HDI	1,6-hexamethylene
HMBC	heteronuclear multiple bond coherence
HOMO	highest occupied molecular orbital
HSQC	heteronuclear multiple quantum coherence

ISC	intersystem crossing
KIT	Karlsruhe Institute of Technology
LC-MS	hyphenated liquid Chromatography-mass spectrometry
LED	light-emitting diode
LSD materials	light-stabilised dynamic materials
LSM	laser scanning microscopy
LUMO	lower occupied molecular orbital
MALDI-TOF	matrix-assisted laser desorption-ionisation time-of-flight spectrometry
MDI	4,4'-methylene diphenyl
Napht	naphthalene
NBS	<i>N</i> -bromosuccinimide
NMR	nuclear magnetic resonance spectroscopy
PEG	poly(ethylene glycol)
<i>m</i> f-PEG	multifunctional poly(ethylene glycol)
<i>m</i> PEG	poly(ethylene glycol) monomethyl ether
<i>t</i> BuPEG	<i>tert</i> -butyl end capped poly(ethylene glycol)
PhD	doctor of philosophy
PMMA	poly(methyl methacrylate)
PU	polyurethane
ROMP	ring opening metathesis polymerisation
ROP	ring opening polymerisation
S _E Ar	electrophilic aromatic substitution
SEC	size-exclusion chromatography
SEM	scanning electron microscopy
SI-ATRP	surface-initiated atom-transfer radical polymerisation
SOMO	single occupied molecular orbital
STED	stimulated-emission depletion

TAD	1,2,4-triazoline-3,5-dione or triazolinedione
bisTAD	bisfunctional triazolinedione
BuTAD	4- <i>n</i> -butyl-1,2,4-triazoline-3,5-dione
MeTAD	4-methyl-1,2,4-triazoline-3,5-dione
PhTAD	4-phenyl-1,2,4-triazoline-3,5-dione
TCICA	trichloroisocyanuric acid
T _g	glass transition temperature
TGA	Thermal gravimetric analysis
TS	transition state
UGent	Ghent University
UV	ultraviolet
UV/vis	ultraviolet and visible light

Appendix G.

List of publications arising from this dissertation

- [01] **Triazolinediones as Highly Enabling Synthetic Tools**
De Bruycker, K.; Billiet, S.; Houck, H. A.; Chattopadhyay, S.; Winne, J. M.;
Du Prez, F. E., *Chem. Rev.* **2016**, *116*, 3919-3974.
- [02] **Design of a Thermally Controlled Sequence of Triazolinedione-Based Click and Transclick Reactions**
Houck, H. A.; De Bruycker, K.; Billiet, S.; Dhanis, B.; Goossens, H.; Catak, S.;
Van Speybroeck, V.; Winne, J. M.; Du Prez, F. E. *Chem. Sci.* **2017**, *8*, 3098-3108.
- [03] **Controlling Thermal Reactivity with Different Colors of Light**
Houck, H. A.; Du Prez, F. E.; Barner-Kowollik, C. *Nat. Commun.* **2017**, *8*, 1869.
- [04] **Tunable Blocking Agents for Temperature-Controlled Triazolinedione-Based Cross-Linking Reactions**
Houck, H. A.; De Bruycker, K.; Barner-Kowollik, C.; Winne, J. M.; Du Prez, F. E.
Macromolecules **2018**, *51*, 3156-3164.
- [05] **Light-Stabilized Dynamic Materials**
Houck, H. A.; Blasco, E.; Du Prez, F. E.; Barner-Kowollik, C. *J. Am. Chem. Soc.* **2019**,
141, 31, 12329-12337.
- [06] **Visible Light-Induced Backbone Modification and Crosslinking of Poly(ethylene glycol) through Triazolinediones for Cleavable Direct Laser Written Materials.**
Houck, H. A.; *et al.*,
Manuscript submitted.

Appendix H.

Bibliography

1. H. C. Kolb, M. G. Finn, K. B. Sharpless, *Angew. Chem., Int. Ed.* **2001**, *40*, 2004-2021.
2. C. J. Hawker, V. V. Fokin, M. G. Finn, K. B. Sharpless, *Aust. J. Chem.* **2007**, *60*, 381-383.
3. C. Barner-Kowollik, F. E. Du Prez, P. Espeel, C. J. Hawker, T. Junkers, H. Schlaad, W. Van Camp, *Angew. Chem., Int. Ed.* **2011**, *50*, 60-62.
4. P. Espeel, F. E. Du Prez, *Macromolecules* **2015**, *48*, 2-14.
5. Z. Weike, D. Jianté, L. Yingwu, Z. Qian, X. Tao, *Adv. Mater.* **2017**, *29*, 1606100.
6. Z. P. Zhang, M. Z. Rong, M. Q. Zhang, *Prog. Polym. Sci.* **2018**, *80*, 39-93.
7. S. Billiet, K. De Bruycker, F. Driessen, H. Goossens, V. Van Speybroeck, J. M. Winne, F. E. Du Prez, *Nat. Chem.* **2014**, *6*, 815-821.
8. B. T. Gillis, J. D. Hagarty, *J. Org. Chem.* **1967**, *32*, 330-&.
9. S. Rádl, in *Adv. Heterocycl. Chem., Vol. Volume 67* (Ed.: R. K. Alan), Academic Press, **1996**, pp. 119-205.
10. J. Sauer, B. Schroder, *Chem. Ber.* **1967**, *100*, 678-684.
11. G. B. Butler, *Ind. Eng. Chem. Prod. Res. Dev.* **1980**, *19*, 512-528.
12. S. Vandewalle, S. Billiet, F. Driessen, F. E. Du Prez, *ACS Macro Lett.* **2016**, *5*, 766-771.
13. O. Türünc, S. Billiet, K. De Bruycker, S. Ouadad, J. Winne, F. E. Du Prez, *Eur. Polym. J.* **2015**, *65*, 286-297.
14. N. Van Herck, F. E. Du Prez, *Macromolecules* **2018**, *51*, 3405-3414.
15. K. De Bruycker, S. Billiet, H. A. Houck, S. Chattopadhyay, J. M. Winne, F. E. Du Prez, *Chem. Rev.* **2016**, *116*, 3919-3974.
16. H. C. Kolb, K. B. Sharpless, *Drug Discovery Today* **2003**, *8*, 1128-1137.
17. J. E. Moses, A. D. Moorhouse, *Chem. Soc. Rev.* **2007**, *36*, 1249-1262.
18. W. Xi, T. F. Scott, C. J. Kloxin, C. N. Bowman, *Adv. Funct. Mater.* **2014**, *24*, 2572-2590.
19. E. Blasco, M. B. Sims, A. S. Goldmann, B. S. Sumerlin, C. Barner-Kowollik, *Macromolecules* **2017**, *50*, 5215-5252.
20. A. J. Inglis, S. Sinnwell, M. H. Stenzel, C. Barner-Kowollik, *Angew. Chem., Int. Ed.* **2009**, *48*, 2411-2414.
21. P. L. Golas, K. Matyjaszewski, *Chem. Soc. Rev.* **2010**, *39*, 1338-1354.
22. M. A. Tasdelen, B. Kiskan, Y. Yagci, *Prog. Polym. Sci.* **2016**, *52*, 19-78.
23. S. Mukherjee, J. J. Cash, B. S. Sumerlin, in *Dynamic Covalent Chemistry* (Eds.: W. Zang, Y. Jin), **2017**.
24. E. S. Gil, S. M. Hudson, *Prog. Polym. Sci.* **2004**, *29*, 1173-1222.
25. H. A. Houck, K. De Bruycker, S. Billiet, B. Dhanis, H. Goossens, S. Catak, V. Van Speybroeck, J. M. Winne, F. E. Du Prez, *Chem. Sci.* **2017**, *8*, 3098-3108.
26. W. Song, Y. Wang, J. Qu, M. M. Madden, Q. Lin, *Angew. Chem., Int. Ed.* **2008**, *47*, 2832-2835.

27. W. Song, Y. Wang, J. Qu, Q. Lin, *J. Am. Chem. Soc.* **2008**, *130*, 9654-9655.
28. S. J. Rowan, S. J. Cantrill, G. R. L. Cousins, J. K. M. Sanders, J. F. Stoddart, *Angew. Chem., Int. Ed.* **2002**, *41*, 898-952.
29. H. Sun, C. P. Kabb, M. B. Sims, B. S. Sumerlin, *Prog. Polym. Sci.* **2018**, 10.1016/j.progpolymsci.2018.1009.1006.
30. H. Sun, C. P. Kabb, Y. Dai, M. R. Hill, I. Ghiviriga, A. P. Bapat, B. S. Sumerlin, *Nat. Chem.* **2017**, *9*, 817.
31. C. J. Kloxin, T. F. Scott, B. J. Adzima, C. N. Bowman, *Macromolecules* **2010**, *43*, 2643-2653.
32. R. J. Wojtecki, M. A. Meador, S. J. Rowan, *Nat. Mater.* **2010**, *10*, 14.
33. L. P. Engle, K. B. Wagener, *J. Macromol. Sci., Part C* **1993**, *33*, 239-257.
34. F. García, M. M. J. Smulders, *J. Polym. Sci., Part A: Polym. Chem.* **2016**, *54*, 3551-3577.
35. X. Chen, M. A. Dam, K. Ono, A. Mal, H. Shen, S. R. Nutt, K. Sheran, F. Wudl, *Science* **2002**, *295*, 1698-1702.
36. N. Teramoto, Y. Arai, M. Shibata, *Carbohydr. Polym.* **2006**, *64*, 78-84.
37. S. Billiet, X. K. D. Hillewaere, R. F. A. Teixeira, F. E. Du Prez, *Macromol. Rapid Commun.* **2013**, *34*, 290-309.
38. P. Reutenauer, E. Buhler, P. J. Boul, S. J. Candau, J.-M. Lehn, *Chem. - Eur. J.* **2009**, *15*, 1893-1900.
39. D. M. Vyas, G. W. Hay, *J. Chem. Soc. D* **1971**, 1411-1412.
40. J. Zhou, N. K. Guimard, A. J. Inglis, M. Namazian, C. Y. Lin, M. L. Coote, E. Spyrou, S. Hilf, F. G. Schmidt, C. Barner-Kowollik, *Polym. Chem.* **2012**, *3*, 628-639.
41. A. J. Inglis, L. Nebhani, O. Altintas, F. G. Schmidt, C. Barner-Kowollik, *Macromolecules* **2010**, *43*, 5515-5520.
42. N. K. Guimard, J. Ho, J. Brandt, C. Y. Lin, M. Namazian, J. O. Mueller, K. K. Oehlenschlaeger, S. Hilf, A. Lederer, F. G. Schmidt, M. L. Coote, C. Barner-Kowollik, *Chem. Sci.* **2013**, *4*, 2752-2759.
43. K. K. Oehlenschlaeger, N. K. Guimard, J. Brandt, J. O. Mueller, C. Y. Lin, S. Hilf, A. Lederer, M. L. Coote, F. G. Schmidt, C. Barner-Kowollik, *Polym. Chem.* **2013**, *4*, 4348-4355.
44. K. K. Oehlenschlaeger, J. O. Mueller, J. Brandt, S. Hilf, A. Lederer, M. Wilhelm, R. Graf, M. L. Coote, F. G. Schmidt, C. Barner-Kowollik, *Adv. Mater.* **2014**, *26*, 3561-3566.
45. A. M. Schenzel, C. Klein, K. Rist, N. Moszner, C. Barner-Kowollik, *Adv. Sci.* **2016**, *3*, 1500361.
46. P. T. Corbett, J. Leclaire, L. Vial, K. R. West, J. L. Wietor, J. K. Sanders, S. Otto, *Chem. Rev.* **2006**, *106*, 3652-3711.
47. H. R. Kricheldorf, *Macromolecules* **2003**, *36*, 2302-2308.
48. M. Capelot, D. Montarnal, F. Tournilhac, L. Leibler, *J. Am. Chem. Soc.* **2012**, *134*, 7664-7667.
49. B. T. Worrell, S. Mavila, C. Wang, T. M. Kontour, C.-H. Lim, M. K. McBride, C. B. Musgrave, R. Shoemaker, C. N. Bowman, *Polym. Chem.* **2018**, *9*, 4523-4534.
50. R. Larsson, Z. Pei, O. Ramström, *Angew. Chem., Int. Ed.* **2004**, *43*, 3716-3718.
51. P. Dawson, T. Muir, I. Clark-Lewis, S. Kent, *Science* **1994**, *266*, 776-779.

52. J. Simon, F. Barla, A. Kelemen-Haller, F. Farkas, M. Kraxner, *Chromatographia* **1988**, *25*, 99-106.
53. J. O. Akindoyo, M. D. H. Beg, S. Ghazali, M. R. Islam, N. Jeyaratnam, A. R. Yuvaraj, *RSC Adv.* **2016**, *6*, 114453-114482.
54. J. Y. Chang, S. K. Do, M. J. Han, *Polymer* **2001**, *42*, 7589-7594.
55. J. Nicolas, Y. Guillaneuf, C. Lefay, D. Bertin, D. Gigmes, B. Charleux, *Prog. Polym. Sci.* **2013**, *38*, 63-235.
56. F. Wang, M. Z. Rong, M. Q. Zhang, *J. Mater. Chem.* **2012**, *22*, 13076-13084.
57. R. K. Roy, A. Meszynska, C. Laure, L. Charles, C. Verchin, J.-F. Lutz, *Nat. Commun.* **2015**, *6*, 7237.
58. E. Delebecq, J.-P. Pascault, B. Boutevin, F. Ganachaud, *Chem. Rev.* **2013**, *113*, 80-118.
59. Z. W. Wicks, *Prog. Org. Coat.* **1975**, *3*, 73-99.
60. E. Quérat, L. Tighzert, J.-P. Pascault, *Angew. Makromol. Chem.* **1994**, *219*, 185-203.
61. Y. Camberlin, P. Michaud, C. Pesando, J. P. Pascault, *Macromol. Symp.* **1989**, *25*, 91-99.
62. T. Shen, D. Zhou, L. Liang, J. Zheng, Y. Lan, M. Lu, *J. Appl. Polym. Sci.* **2011**, *122*, 748-757.
63. A. Mühlebach, *J. Polym. Sci., Part A: Polym. Chem.* **1994**, *32*, 753-765.
64. D. A. Wicks, Z. W. Wicks, *Prog. Org. Coat.* **1999**, *36*, 148-172.
65. M. S. Rolph, A. L. J. Markowska, C. N. Warriner, R. K. O'Reilly, *Polym. Chem.* **2016**, *7*, 7351-7364.
66. G. Sankar, A. Sultan Nasar, *Eur. Polym. J.* **2009**, *45*, 911-922.
67. C. J. Kloxin, C. N. Bowman, *Chem. Soc. Rev.* **2013**, *42*, 7161-7173.
68. C. N. Bowman, C. J. Kloxin, *Angew. Chem., Int. Ed.* **2012**, *51*, 4272-4274.
69. H. Ying, Y. Zhang, J. Cheng, *Nat. Commun.* **2014**, *5*, 3218.
70. H. Y. Park, C. J. Kloxin, A. S. Abuelyaman, J. D. Oxman, C. N. Bowman, *Macromolecules* **2012**, *45*, 5640-5646.
71. D. Leung, C. N. Bowman, *Macromol. Chem. Phys.* **2012**, *213*, 198-204.
72. W. Thongsomboon, M. Sherwood, N. Arellano, A. Nelson, *ACS Macro Lett.* **2013**, *2*, 19-22.
73. W. Denissen, J. M. Winne, F. E. Du Prez, *Chem. Sci.* **2016**, *7*, 30-38.
74. D. Montarnal, M. Capelot, F. Tournilhac, L. Leibler, *Science* **2011**, *334*, 965-968.
75. W. Denissen, G. Rivero, R. Nicolaÿ, L. Leibler, J. M. Winne, F. E. Du Prez, *Adv. Funct. Mater.* **2015**, *25*, 2451-2457.
76. W. Denissen, M. Droesbeke, R. Nicolaÿ, L. Leibler, J. M. Winne, F. E. Du Prez, *Nat. Commun.* **2017**, *8*, 14857.
77. B. Hendriks, J. Waelkens, J. M. Winne, F. E. Du Prez, *ACS Macro Lett.* **2017**, *6*, 930-934.
78. W. Denissen, I. De Baere, W. Van Paeppegem, L. Leibler, J. Winne, F. E. Du Prez, *Macromolecules* **2018**, *51*, 2054-2064.
79. M. Guerre, C. Taplan, R. Nicolay, J. M. Winne, F. E. Du Prez, *J. Am. Chem. Soc.* **2018**.
80. S. Chatani, C. J. Kloxin, C. N. Bowman, *Polym. Chem.* **2014**, *5*, 2187-2201.

81. R. Ruckamp, E. Benckiser, M. W. Haverkort, H. Roth, T. Lorenz, A. Freimuth, L. Jongen, A. Moller, G. Meyer, P. Reutler, B. Buchner, A. Revcolevschi, S. W. Cheong, C. Sekar, G. Krabbes, M. Gruninger, *New Journal of Physics* **2005**, *7*.
82. H. H. Jaffe, A. L. Miller, *J. Chem. Educ.* **1966**, *43*, 469.
83. C. Brieke, F. Rohrbach, A. Gottschalk, G. Mayer, A. Heckel, *Angew. Chem., Int. Ed.* **2012**, *51*, 8446-8476.
84. P. Klán, T. Šolomek, C. G. Bochet, A. Blanc, R. Givens, M. Rubina, V. Popik, A. Kostikov, J. Wirz, *Chem. Rev.* **2013**, *113*, 119-191.
85. C. G. Bochet, *Angew. Chem., Int. Ed.* **2001**, *40*, 2071-2073.
86. V. San Miguel, C. G. Bochet, A. del Campo, *J. Am. Chem. Soc.* **2011**, *133*, 5380-5388.
87. M. A. Azagarsamy, K. S. Anseth, *Angew. Chem., Int. Ed.* **2013**, *52*, 13803-13807.
88. A. M. Kloxin, A. M. Kasko, C. N. Salinas, K. S. Anseth, *Science* **2009**, *324*, 59-63.
89. C. A. DeForest, K. S. Anseth, *Nat. Chem.* **2011**, *3*, 925-931.
90. S. Petersen, J. M. Alonso, A. Specht, P. Duodu, M. Goeldner, A. del Campo, *Angew. Chem., Int. Ed.* **2008**, *47*, 3192-3195.
91. J. H. Kaplan, B. Forbush, J. F. Hoffman, *Biochemistry* **1978**, *17*, 1929-1935.
92. B. Yan, J.-C. Boyer, D. Habault, N. R. Branda, Y. Zhao, *J. Am. Chem. Soc.* **2012**, *134*, 16558-16561.
93. M. J. Hansen, W. A. Velema, M. M. Lerch, W. Szymanski, B. L. Feringa, *Chem. Soc. Rev.* **2015**, *44*, 3358-3377.
94. J. A. Barltrop, P. J. Plant, P. Schofield, *Chem. Commun. (London)* **1966**, 822-823.
95. A. Patchornik, B. Amit, R. B. Woodward, *J. Am. Chem. Soc.* **1970**, *92*, 6333-6335.
96. F. M. Houlihan, O. Nalamasu, J. M. Kometani, E. Reichmanis, *J. Imaging Sci. Technol.* **1997**, *41*, 35-40.
97. J. F. Cameron, J. M. J. Frechet, *J. Am. Chem. Soc.* **1991**, *113*, 4303-4313.
98. H. Zhao, E. S. Sterner, E. B. Coughlin, P. Theato, *Macromolecules* **2012**, *45*, 1723-1736.
99. B. T. Worrell, M. K. McBride, G. B. Lyon, L. M. Cox, C. Wang, S. Mavila, C.-H. Lim, H. M. Coley, C. B. Musgrave, Y. Ding, C. N. Bowman, *Nat. Commun.* **2018**, *9*, 2804.
100. J. Jennane, T. Boutros, R. Giasson, *Can. J. Chem.* **1996**, *74*, 2509-2517.
101. J. A. Johnson, M. G. Finn, J. T. Koberstein, N. J. Turro, *Macromolecules* **2007**, *40*, 3589-3598.
102. D. Saran, D. H. Burke, *Bioconjugate Chem.* **2007**, *18*, 275-279.
103. R. Rodebaugh, B. Fraser-Reid, H. Mario Geysen, *Tetrahedron Lett.* **1997**, *38*, 7653-7656.
104. C. G. Bochet, *Tetrahedron Lett.* **2000**, *41*, 6341-6346.
105. A. P. Pelliccioli, J. Wirz, *Photochem. Photobiol. Sci.* **2002**, *1*, 441-458.
106. A. M. Piloto, S. P. G. Costa, M. S. T. Gonçalves, *Tetrahedron* **2014**, *70*, 650-657.
107. A. del Campo, D. Boos, H. W. Spiess, U. Jonas, *Angew. Chem., Int. Ed.* **2005**, *44*, 4707-4712.
108. J. P. Olson, M. R. Banghart, B. L. Sabatini, G. C. R. Ellis-Davies, *J. Am. Chem. Soc.* **2013**, *135*, 15948-15954.
109. A. Chaudhuri, Y. Venkatesh, K. K. Behara, N. D. P. Singh, *Org. Lett.* **2017**, *19*, 1598-1601.

110. J. A. Peterson, C. Wijesooriya, E. J. Gehrman, K. M. Mahoney, P. P. Goswami, T. R. Albright, A. Syed, A. S. Dutton, E. A. Smith, A. H. Winter, *J. Am. Chem. Soc.* **2018**, *140*, 7343-7346.
111. A. Deiters, *ChemBioChem* **2010**, *11*, 47-53.
112. A. M. Rosales, K. S. Anseth, *Nat. Rev. Mater.* **2016**, *1*, 15012.
113. E. Blasco, M. Wegener, C. Barner-Kowollik, *Adv. Mater.* **2017**, *29*, 1604005.
114. N. C. Yang, C. Rivas, *J. Am. Chem. Soc.* **1961**, *83*, 2213-2213.
115. F. Nerdel, W. Brodowski, *Chem. Ber.* **1968**, *101*, 1398-1406.
116. G. Porter, M. F. Tchir, *J. Chem. Soc. D* **1970**, 1372-1373.
117. G. Porter, M. F. Tchir, *J. Chem. Soc. A* **1971**, 3772-3777.
118. P. Mueller, M. M. Zieger, B. Richter, A. S. Quick, J. Fischer, J. B. Mueller, L. Zhou, G. U. Nienhaus, M. Bastmeyer, C. Barner-Kowollik, M. Wegener, *ACS Nano* **2017**, *11*, 6396-6403.
119. A. Herner, Q. Lin, *Top. Curr. Chem.* **2015**, *374*, 1.
120. T. Gruending, K. K. Oehlenschlaeger, E. Frick, M. Glassner, C. Schmid, C. Barner-Kowollik, *Macromol. Rapid Commun.* **2011**, *32*, 807-812.
121. T. Pauloehrl, G. Delaittre, V. Winkler, A. Welle, M. Bruns, H. G. Börner, A. M. Greiner, M. Bastmeyer, C. Barner-Kowollik, *Angew. Chem., Int. Ed.* **2012**, *51*, 1071-1074.
122. M. Glassner, K. K. Oehlenschlaeger, T. Gruending, C. Barner-Kowollik, *Macromolecules* **2011**, *44*, 4681-4689.
123. G. Delaittre, A. S. Goldmann, J. O. Mueller, C. Barner-Kowollik, *Angew. Chem., Int. Ed.* **2015**, *54*, 11388-11403.
124. A. Vigovskaya, D. Abt, I. Ahmed, C. M. Niemeyer, C. Barner-Kowollik, L. Fruk, *J. Mater. Chem. B* **2016**, *4*, 442-449.
125. F. Feist, J. P. Menzel, T. Weil, J. P. Blinco, C. Barner-Kowollik, *J. Am. Chem. Soc.* **2018**, *140*, 11848-11854.
126. P. G. Sammes, *Tetrahedron* **1976**, *32*, 405-422.
127. T. Krappitz, F. Feist, I. Lamparth, N. Moszner, H. John, J. P. Blinco, T. R. Dargaville, C. Barner-Kowollik, *Mater. Horiz.* **2018**, 10.1039/C1038MH00951A.
128. T. P. Yoon, M. A. Ischay, J. Du, *Nat. Chem.* **2010**, *2*, 527.
129. J. O. Mueller, F. G. Schmidt, J. P. Blinco, C. Barner-Kowollik, *Angew. Chem., Int. Ed.* **2015**, *54*, 10284-10288.
130. P. Lederhose, K. N. R. Wust, C. Barner-Kowollik, J. P. Blinco, *Chem. Commun.* **2016**, *52*, 5928-5931.
131. B. T. Tuten, J. P. Menzel, K. Pahnke, J. P. Blinco, C. Barner-Kowollik, *Chem. Commun.* **2017**, *53*, 4501-4504.
132. E. Blasco, Y. Sugawara, P. Lederhose, J. P. Blinco, A.-M. Kelterer, C. Barner-Kowollik, *ChemPhotoChem* **2017**, *1*, 159-163.
133. J. Merz, J. Fink, A. Friedrich, I. Krummenacher, H. H. Al Mamari, S. Lorenzen, M. Haehnel, A. Eichhorn, M. Moos, M. Holzappel, H. Braunschweig, C. Lambert, A. Steffen, L. Ji, T. B. Marder, *Chem. - Eur. J.* **2017**, *23*, 13164-13180.
134. J. T. Offenloch, M. Gernhard, J. P. Blinco, H. Frisch, H. Mutlu, C. Barner-Kowollik, *Chem. - Eur. J.*, 10.1002/chem.201803755.

135. K. Hildebrandt, T. Pauloehrl, J. P. Blinco, K. Linkert, H. G. Börner, C. Barner-Kowollik, *Angew. Chem., Int. Ed.* **2015**, *54*, 2838-2843.
136. M. M. Russew, S. Hecht, *Adv. Mater.* **2010**, *22*, 3348-3360.
137. T. Junkers, *Eur. Polym. J.* **2015**, *62*, 273-280.
138. S. Poplata, A. Tröster, Y.-Q. Zou, T. Bach, *Chem. Rev.* **2016**, *116*, 9748-9815.
139. G. Delaittre, N. K. Guimard, C. Barner-Kowollik, *Acc. Chem. Res.* **2015**, *48*, 1296-1307.
140. G. Kaur, P. Johnston, K. Saito, *Polym. Chem.* **2014**, *5*, 2171-2186.
141. J. Van Damme, F. Du Prez, *Prog. Polym. Sci.* **2018**, *82*, 92-119.
142. T. K. Claus, S. Telitel, A. Welle, M. Bastmeyer, A. P. Vogt, G. Delaittre, C. Barner-Kowollik, *Chem. Commun.* **2017**, *53*, 1599-1602.
143. H. Lin, X. Wan, Z. Li, X. Jiang, Q. Wang, J. Yin, *ACS Appl. Mater. Interfaces* **2010**, *2*, 2076-2082.
144. L. Hu, X. Cheng, A. Zhang, *J. Mater. Sci.* **2015**, *50*, 2239-2246.
145. J. Van Damme, O. van den Berg, L. Vlaminck, J. Brancart, G. Van Assche, F. Du Prez, *Eur. Polym. J.* **2018**, *105*, 412-420.
146. D. E. Marschner, H. Frisch, J. T. Offenloch, B. T. Tuten, C. R. Becer, A. Walther, A. S. Goldmann, P. Tzvetkova, C. Barner-Kowollik, *Macromolecules* **2018**, *51*, 3802-3807.
147. H. Frisch, D. E. Marschner, A. S. Goldmann, C. Barner-Kowollik, *Angew. Chem., Int. Ed.* **2018**, *57*, 2036-2045.
148. M. M. Lerch, W. Szymański, B. L. Feringa, *Chem. Soc. Rev.* **2018**, *47*, 1910-1937.
149. D. Bléger, S. Hecht, *Angew. Chem., Int. Ed.* **2015**, *54*, 11338-11349.
150. M. Kathan, S. Hecht, *Chem. Soc. Rev.* **2017**, *46*, 5536-5550.
151. J.-P. Sauvage, F. Stoddart, B. L. Feringa, <https://www.nobelprize.org/prizes/chemistry/2016/press-release/>, **2016**.
152. H. D. Samachetty, V. Lemieux, N. R. Branda, *Tetrahedron* **2008**, *64*, 8292-8300.
153. M. Kathan, P. Kovaříček, C. Jurissek, A. Senf, A. Dallmann, A. F. Thünemann, S. Hecht, *Angew. Chem., Int. Ed.* **2016**, *55*, 13882-13886.
154. M. Kathan, F. Eisenreich, C. Jurissek, A. Dallmann, J. Gurke, S. Hecht, *Nat. Chem.* **2018**, *10*, 1031-1036.
155. K. Hildebrandt, K. Elies, D. R. D'hooge, J. P. Blinco, C. Barner-Kowollik, *J. Am. Chem. Soc.* **2016**, *138*, 7048-7054.
156. A. Fuhrmann, R. Göstl, R. Wendt, J. Kötteritzsch, M. D. Hager, U. S. Schubert, K. Brademann-Jock, A. F. Thünemann, U. Nöchel, M. Behl, S. Hecht, *Nat. Commun.* **2016**, *7*, 13623.
157. A. Fuhrmann, K. Broi, S. Hecht, *Macromol. Rapid Commun.* **2018**, *39*, 1700376.
158. A. Selimis, V. Mironov, M. Farsari, *Microelectron. Eng.* **2015**, *132*, 83-89.
159. M. T. Raimondi, S. M. Eaton, M. M. Nava, M. Laganà, G. Cerullo, R. Osellame, *J. Appl. Biomater. Funct. Mater.* **2012**, *10*, 56-66.
160. J. Torgersen, X.-H. Qin, Z. Li, A. Ovsianikov, R. Liska, J. Stampfl, *Adv. Funct. Mater.* **2013**, *23*, 4542-4554.
161. J. Fischer, M. Wegener, *Laser Photonics Rev.* **2013**, *7*, 22-44.
162. S. Maruo, J. T. Fourkas, *Laser Photonics Rev.* **2008**, *2*, 100-111.
163. K. Svoboda, R. Yasuda, *Neuron* **2006**, *50*, 823-839.
164. A. S. Quick, PhD Thesis thesis, Karlsruhe Institute of Technology **2015**.

165. B.-B. Xu, Y.-L. Zhang, H. Xia, W.-F. Dong, H. Ding, H.-B. Sun, *Lab Chip* **2013**, *13*, 1677-1690.
166. B. Richter, V. Hahn, S. Bertels, T. K. Claus, M. Wegener, G. Delaittre, C. Barner-Kowollik, M. Bastmeyer, *Adv. Mater.* **2017**, *29*, 1604342.
167. A. S. Quick, J. Fischer, B. Richter, T. Pauloehrl, V. Trouillet, M. Wegener, C. Barner-Kowollik, *Macromol. Rapid Commun.* **2013**, *34*, 335-340.
168. A. S. Quick, H. Rothfuss, A. Welle, B. Richter, J. Fischer, M. Wegener, C. Barner-Kowollik, *Adv. Funct. Mater.* **2014**, *24*, 3571-3580.
169. D. Gräfe, A. Wickberg, M. M. Zieger, M. Wegener, E. Blasco, C. Barner-Kowollik, *Nat. Commun.* **2018**, *9*, 2788.
170. C. Barner-Kowollik, M. Bastmeyer, E. Blasco, G. Delaittre, P. Müller, B. Richter, M. Wegener, *Angew. Chem., Int. Ed.* **2017**, *56*, 15828-15845.
171. R. R. Batchelor, E. Blasco, K. N. R. Wuest, H. Lu, M. Wegener, C. Barner-Kowollik, M. H. Stenzel, *Chem. Commun.* **2018**, *54*, 2436-2439.
172. T. K. Claus, B. Richter, V. Hahn, A. Welle, S. Kayser, M. Wegener, M. Bastmeyer, G. Delaittre, C. Barner-Kowollik, *Angew. Chem., Int. Ed.* **2016**, *55*, 3817-3822.
173. S. W. Hell, J. Wichmann, *Opt. Lett.* **1994**, *19*, 780-782.
174. E. Rittweger, K. Y. Han, S. E. Irvine, C. Eggeling, S. W. Hell, *Nat. Photonics* **2009**, *3*, 144.
175. T. F. Scott, B. A. Kowalski, A. C. Sullivan, C. N. Bowman, R. R. McLeod, *Science* **2009**, *324*, 913-917.
176. J. Fischer, G. von Freymann, M. Wegener, *Adv. Mater.* **2010**, *22*, 3578-3582.
177. O. Diels, J. H. Blom, W. Koll, *Justus Liebigs Ann. Chem.* **1925**, *443*, 242-262.
178. O. Diels, K. Alder, *Justus Liebigs Ann. Chem.* **1928**, *460*, 98-122.
179. B. T. Gillis, P. E. Beck, *J. Org. Chem.* **1962**, *27*, 1947-1951.
180. B. M. Jacobson, A. C. Feldstein, J. I. Smallwood, *J. Org. Chem.* **1977**, *42*, 2849-2853.
181. B. Franzus, J. H. Surridge, *J. Org. Chem.* **1962**, *27*, 1951-1957.
182. B. Franzus, *J. Org. Chem.* **1963**, *28*, 2954-2960.
183. G. O. Schenck, H. R. Kopp, B. Kim, E. K. von Gustorf, *Z. Naturforsch., B: Chem. Sci.* **1965**, *20*, 637-639.
184. E. Fahr, H. Lind, *Angew. Chem., Int. Ed.* **1966**, *5*, 372-384.
185. R. C. Cookson, S. S. H. Gilani, I. D. R. Stevens, *Tetrahedron Lett.* **1962**, *3*, 615-618.
186. R. C. Cookson, S. S. H. Gilani, I. D. R. Stevens, *J. Chem. Soc. C* **1967**, 1905-1909.
187. V. D. Kiselev, D. A. Kornilov, I. I. Lekomtseva, A. I. Konovalov, *Int. J. Chem. Kinet.* **2015**, *47*, 289-301.
188. G. Schön, H. Hopf, *Liebigs Ann. Chem.* **1981**, *1981*, 165-180.
189. T. J. Katz, N. Acton, *J. Am. Chem. Soc.* **1973**, *95*, 2738-2739.
190. I. K. Korobitsyna, A. V. Khalikova, L. L. Rodina, N. P. Shusherina, *Chemistry of Heterocyclic Compounds* **1983**, *19*, 117-136.
191. C. J. Moody, in *Adv. Heterocycl. Chem., Vol. 30* (Ed.: A. R. Katritzky), Academic Press, **1982**, pp. 1-45.
192. G. B. Butler, *Polymer Science U.S.S.R.* **1981**, *23*, 2587-2622.
193. H. Ban, J. Gavriluk, C. F. Barbas, *J. Am. Chem. Soc.* **2010**, *132*, 1523-1525.
194. I. C. F. Barbas, H. Ban, J. Gavriluk. WO2011079315, **2011**.

195. J. Thiele, O. Stange, *Justus Liebigs Ann. Chem.* **1894**, *283*, 1-46.
196. A. Pinner, *Ber. Dtsch. Chem. Ges.* **1887**, *20*, 2358-2360.
197. R. Stollé, *Ber. Dtsch. Chem. Ges.* **1912**, *45*, 273-289.
198. J. E. Herweh, R. M. Fantazier, *Tetrahedron Lett.* **1973**, 2101-2104.
199. F. Arndt, R. Schwarz, C. Martius, E. Aron, *Istanbul Üniversitesi Fen Fakültesi Mecmuası, Seri A: Matematik - Fizik - Kimya* **1948**, *13A*, 127-146.
200. H. Giesecke, R. Merten, L. Rottmaier. US4386213, **1983**.
201. H. Giesecke, R. Merten, L. Rottmaier. US4429135, **1984**.
202. T. Tsuji, *Pharmaceutical Bulletin* **1954**, *2*, 403-411.
203. R. L. Sowerby. CA1313179, **1987**.
204. G. Zinner, W. Deucker, *Arch. Pharm.* **1961**, *294*, 370-372.
205. R. C. Cookson, S. S. Gupte, I. D. R. Stevens, C. T. Watts, *Org. Synth.* **1971**, *51*, 121.
206. G. W. Breton, M. Turlington, *Tetrahedron Lett.* **2014**, *55*, 4661-4663.
207. K. Shimada, T. Oe, T. Mizuguchi, *Analyst* **1991**, *116*, 1393-1397.
208. S. Ogawa, S. Ooki, M. Morohashi, K. Yamagata, T. Higashi, *Rapid Commun. Mass Spectrom.* **2013**, *27*, 2453-2460.
209. J. C. Stickler, W. H. Pirkle, *J. Org. Chem.* **1966**, *31*, 3444-3445.
210. G. B. Butler, A. G. Williams, *J Polym Sci Pol Chem* **1979**, *17*, 1117-1128.
211. V. P. Arya, S. J. Shenoy, *Indian J Chem B* **1976**, *14*, 883-886.
212. A. Kiriazis, T. Rüffer, S. Jäntti, H. Lang, J. Yli-Kauhaluoma, *J. Comb. Chem.* **2007**, *9*, 263-266.
213. B. Saville, *J. Chem. Soc. D* **1971**, 635-636.
214. K. B. Wagener, S. R. Turner, G. B. Butler, *J. Polym. Sci., Part C: Polym. Lett.* **1972**, *10*, 805-816.
215. S. E. Mallakpour, M. A. Zolfigol, *Indian J Chem B* **1995**, *34*, 183-189.
216. T. Little, J. Meara, F. Ruan, M. Nguyen, M. Qabar, *Synth. Commun.* **2002**, *32*, 1741-1749.
217. T. Curtius, *Ber. Dtsch. Chem. Ges.* **1890**, *23*, 3023-3033.
218. T. Curtius, *J. Prakt. Chem.* **1894**, *50*, 275-294.
219. T. Curtius, K. Heidenreich, *Ber. Dtsch. Chem. Ges.* **1894**, *27*, 773-774.
220. K. Shimada, T. Oe, *Anal. Sci.* **1990**, *6*, 461-463.
221. S. Yamada, M. Shimizu. JP04005287, **1992**.
222. M. Shimizu, T. Takahashi, S. Uratsuka, S. Yamada, *J Chem Soc Chem Comm* **1990**, 1416-1417.
223. M. Shimizu, S. Kamachi, Y. Nishii, S. Yamada, *Anal. Biochem.* **1991**, *194*, 77-81.
224. J. M. Gardlik, L. A. Paquette, *Tetrahedron Lett.* **1979**, *20*, 3597-3600.
225. L. A. Paquette, R. F. Doehner, *J. Org. Chem.* **1980**, *45*, 5105-5113.
226. S. Mallakpour, Z. Rafiee, *Synth. Commun.* **2007**, *37*, 1927-1934.
227. L. Vlaminc, B. Van de Voorde, F. E. Du Prez, *Green Chem.* **2017**, *19*, 5659-5664.
228. S. Mallakpour, Z. Rafiee, *Synlett* **2007**, 1255-1256.
229. H. Ban, M. Nagano, J. Gavriljuk, W. Hakamata, T. Inokuma, C. F. Barbas, *Bioconjugate Chem.* **2013**, *24*, 520-532.
230. R. Adamo, M. Allan, F. Berti, E. Danieli, Q. Y. Hu. WO2013009564, **2013**.

231. A. Nilo, M. Allan, B. Brogioni, D. Proietti, V. Cattaneo, S. Crotti, S. Sokup, H. Zhai, I. Margarit, F. Berti, Q.-Y. Hu, R. Adamo, *Bioconjugate Chem.* **2014**, *25*, 2105-2111.
232. T. J. Gilbertson, T. Ryan, *Synthesis* **1982**, 159-160.
233. S. Ohashi, K.-W. Leong, K. Matyjaszewski, G. B. Butler, *J. Org. Chem.* **1980**, *45*, 3467-3471.
234. M. J. Bausch, B. David, P. Dobrowolski, C. Guadalupe-Fasano, R. Gostowski, D. Selmarten, V. Prasad, A. Vaughn, L. H. Wang, *J. Org. Chem.* **1991**, *56*, 5643-5651.
235. S. Alakurtti, T. Heiska, A. Kiriazis, N. Sacerdoti-Sierra, C. L. Jaffe, J. Yli-Kauhaluoma, *Bioorg. Med. Chem.* **2010**, *18*, 1573-1582.
236. U. Seidel, J. Hellman, D. Schollmeyer, C. Hilger, R. Stadler, *Supramol. Sci.* **1995**, *2*, 45-50.
237. G. Read, N. R. Richardson, *J. Chem. Soc., Perkin Trans. 1* **1996**, 167-174.
238. O. Roling, K. De Bruycker, B. Vonhoren, L. Stricker, M. Korsgen, H. F. Arlinghaus, B. J. Ravoo, F. E. Du Prez, *Angew. Chem., Int. Ed.* **2015**, *53*, 13126-13129.
239. L. Xiao, Y. Chen, K. Zhang, *Macromolecules* **2016**, *49*, 4452-4461.
240. M. Furdik, Mikulase.S, M. Livar, Prihrad.S, *Chemické Zvesti* **1967**, *21*, 427-&.
241. M. Thiemann, E. Scheibler, K. W. Wiegand, in *Ullmann's Encyclopedia of Industrial Chemistry*, Wiley-VCH Verlag GmbH & Co. KGaA, **2000**.
242. S. Mallakpour, G. Butler, in *Advances in Polymer Synthesis, Vol. 31* (Eds.: B. Culbertson, J. McGrath), Springer US, **1985**, pp. 1-25.
243. C. Hilger, R. Stadler, *Makromol. Chem.* **1990**, *191*, 1347-1361.
244. J. Burgert, R. Stadler, *Chem. Ber. Recl.* **1987**, *120*, 691-694.
245. S. E. Mallakpour, *J. Chem. Educ.* **1992**, *69*, 238-241.
246. M. A. Zolfigol, M. H. Zebarjadian, G. Chehardoli, S. E. Mallakpour, M. Shamsipur, *Tetrahedron* **2001**, *57*, 1627-1629.
247. G. Chehardoli, M. A. Zolfigol, E. Ghaemi, E. Madrakian, K. Niknam, S. Mallakpour, *J. Heterocycl. Chem.* **2012**, *49*, 596-599.
248. M. A. Zolfigol, E. Ghaemi, E. Madrakian, K. Niknam, *J. Chin. Chem. Soc.* **2008**, *55*, 704-711.
249. H. Wamhoff, K. Wald, *Org. Prep. Proced. Int.* **1975**, *7*, 251-253.
250. H. Bock, G. Rudolph, E. Baltin, *Chem. Ber.* **1965**, *98*, 2054-2055.
251. H. Wamhoff, K. Wald, *Chem. Ber.* **1977**, *110*, 1699-1715.
252. M. A. Zolfigol, E. Madrakian, E. Ghaemi, S. Mallakpour, *Synlett* **2002**, 1633-1636.
253. M. A. Zolfigol, G. Chehardoli, E. Ghaemi, E. Madrakian, R. Zare, T. Azadbakht, K. Niknam, S. Mallakpour, *Monatsh. Chem.* **2008**, *139*, 261-265.
254. U. Tilstam, H. Weinmann, *Org. Process Res. Dev.* **2002**, *6*, 384-393.
255. E. Dolci, V. Froidevaux, C. Joly-Duhamel, R. Auvergne, B. Boutevin, S. Caillol, *Polym. Rev. (Philadelphia, PA, U. S.)* **2016**, *56*, 512-556.
256. P. M. P. Gois, J. Ravasco, H. Faustino, A. Trindade, *Chem. - Eur. J.* **2018**, 10.1002/chem.201803174.
257. V. D. Kiselev, D. A. Kornilov, A. I. Konovalov, *Int. J. Chem. Kinet.* **2017**, *49*, 562-575.
258. A. G. Williams, G. B. Butler, *J. Org. Chem.* **1980**, *45*, 1232-1239.
259. N. Roy, J. M. Lehn, *Chem-Asian J* **2011**, *6*, 2419-2425.
260. L. H. Dao, D. Mackay, *Can. J. Chem.* **1979**, *57*, 2727-2733.

261. D. A. Singleton, C. Hang, *J. Am. Chem. Soc.* **1999**, *121*, 11885-11893.
262. W. Adam, O. De Lucchi, *Tetrahedron Lett.* **1981**, *22*, 929-932.
263. A. G. Leach, K. N. Houk, *Chem. Commun.* **2002**, 1243-1255.
264. D. K. Mandal, *Pericyclic Chemistry: Orbital Mechanisms and Stereochemistry*, Elsevier Science, **2018**.
265. H. H. Wasserman, R. W. DeSimone, K. R. X. Chia, M. G. Banwell, in *Encyclopedia of Reagents for Organic Synthesis*, **2013**.
266. M. J. S. Dewar, S. Olivella, J. J. P. Stewart, *J. Am. Chem. Soc.* **1986**, *108*, 5771-5779.
267. F. A. Carey, Sundberg, R. J., *Advanced Organic Chemistry - Part B: Reactions and Synthesis*, 5th Edition ed., **2007**.
268. B. Rickborn, in *Organic Reactions*, John Wiley & Sons, Inc., **2004**.
269. H. Kwart, K. King, *Chem. Rev.* **1968**, *68*, 415-447.
270. M. A. Fernandez-Herrera, J. Sandoval-Ramirez, S. Montiel-Smith, S. Meza-Reyes, *Heterocycles* **2013**, *87*, 571-582.
271. M. L. Poutsma, P. A. Ibarbia, *J. Am. Chem. Soc.* **1971**, *93*, 440-450.
272. A. P. Henderson, E. Mutlu, A. Leclercq, C. Bleasdale, W. Clegg, R. A. Henderson, B. T. Golding, *Chem. Commun.* **2002**, 1956-1957.
273. A. Sanyal, *Macromol. Chem. Phys.* **2010**, *211*, 1417-1425.
274. K. Alder, F. Pascher, A. Schmitz, *Ber. Dtsch. Chem. Ges.* **1943**, *76*, 27-53.
275. H. M. R. Hoffmann, *Angew. Chem. Int. Ed. Engl.* **1969**, *8*, 556-577.
276. M. L. Clarke, M. B. France, *Tetrahedron* **2008**, *64*, 9003-9031.
277. K. Mikami, M. Shimizu, *Chem. Rev.* **1992**, *92*, 1021-1050.
278. W. Oppolzer, V. Snieckus, *Angew. Chem. Int. Ed. Engl.* **1978**, *17*, 476-486.
279. W. H. Pirkle, J. C. Stickler, *Chem. Commun.* **1967**, 760-761.
280. C. C. Cheng, C. A. Seymour, M. A. Petti, F. D. Greene, J. F. Blount, *J. Org. Chem.* **1984**, *49*, 2910-2916.
281. P. S. Baran, C. A. Guerrero, E. J. Corey, *Org. Lett.* **2003**, *5*, 1999-2001.
282. A. Fernando Rodrigues de Sa, J. B. Eliezer, F. Carlos Alberto Manssour, *Mini-Rev. Med. Chem.* **2009**, *9*, 782-793.
283. C. M. Rasik, M. K. Brown, *J. Am. Chem. Soc.* **2013**, *135*, 1673-1676.
284. B. B. Snider, *Chem. Rev.* **1988**, *88*, 793-811.
285. J. H. Hall, G. Krishnan, *J. Org. Chem.* **1984**, *49*, 2498-2500.
286. E. Koerner von Gustorf, D. V. White, B. Kim, D. Hess, J. Leitich, *J. Org. Chem.* **1970**, *35*, 1155-1165.
287. G. W. Breton, J. H. Shugart, C. A. Hughey, S. M. Perala, A. D. Hicks, *Org. Lett.* **2001**, *3*, 3185-3187.
288. C. A. Seymour, F. D. Greene, *J. Am. Chem. Soc.* **1980**, *102*, 6384-6385.
289. S. F. Nelsen, D. L. Kapp, *J. Am. Chem. Soc.* **1985**, *107*, 5548-5549.
290. S. F. Nelsen, S. J. Klein, *J. Phys. Org. Chem.* **1997**, *10*, 456-460.
291. J. H. Hall, *J. Org. Chem.* **1983**, *48*, 1708-1712.
292. G. W. Breton, K. R. Hoke, *J. Org. Chem.* **2013**, *78*, 4697-4707.
293. G. W. Breton, *Tetrahedron Lett.* **2011**, *52*, 733-735.
294. G. W. Breton, *Adv. Chem. Lett.* **2013**, *1*, 68-73.

295. J. Marton, Z. Szabó, I. Csorvássy, C. Simon, S. Hosztafi, S. Makleit, *Tetrahedron* **1996**, *52*, 2449-2464.
296. S. B. Hanay, D. F. Brougham, A. A. Dias, A. Heise, *Polym. Chem.* **2017**, *8*, 6594-6597.
297. D. Kaiser, J. M. Winne, M. E. Ortiz-Soto, J. Seibel, T. A. Le, B. Engels, *J. Org. Chem.* **2018**.
298. A. V. Pocius, J. T. Yardley, *J. Am. Chem. Soc.* **1973**, *95*, 721-725.
299. A. V. Pocius, J. T. Yardley, *J. Chem. Phys.* **1974**, *61*, 2779-2792.
300. D. P. Kjell, R. S. Sheridan, *J. Photochem.* **1985**, *28*, 205-214.
301. F. Risi, L. Pizzala, M. Carles, P. Verlaque, J. P. Aycard, *J. Org. Chem.* **1996**, *61*, 666-670.
302. W. H. Pirkle, J. C. Stickler, *J. Am. Chem. Soc.* **1970**, *92*, 7497-7499.
303. H. Wang, M. I. Eremets, I. Troyan, H. Liu, Y. Ma, L. Vereecken, *Scientific reports* **2015**, *5*, 13239.
304. J. C. Stickler, Ph.D. Thesis thesis, University of Illinois **1971**.
305. R. C. Cookson, I. D. R. Stevens, C. T. Watts, *Chem. Commun. (London)* **1965**, 259-260.
306. F. Risi, A.-M. Alstanei, E. Volanschi, M. Carles, L. Pizzala, J.-P. Aycard, *Eur. J. Org. Chem.* **2000**, *2000*, 617-626.
307. G. O. Schenck, H. Formanek, *Angew. Chem.* **1958**, *70*, 505-505.
308. W. Ando, K. Ito, T. Takata, *Tetrahedron Lett.* **1982**, *23*, 3909-3912.
309. W. Adam, O. De Lucchi, K. Hill, E.-M. Peters, K. Peters, H. G. von Schnering, *Chem. Ber.* **1985**, *118*, 3070-3088.
310. F. Yoneda, K. Suzuki, Y. Nitta, *J. Am. Chem. Soc.* **1966**, *88*, 2328-&.
311. G. Ahlgren, *Tetrahedron Lett.* **1974**, *15*, 2779-2782.
312. G. E. Wilson, J. H. E. Martin, *J. Org. Chem.* **1972**, *37*, 2510-2512.
313. J. Firl, S. Sommer, *Tetrahedron Lett.* **1972**, *13*, 4713-4716.
314. R. B. Woodward, R. Hoffmann, *Angew. Chem., Int. Ed.* **1969**, *8*, 781-853.
315. N. D. Epiotis, R. L. Yates, *J. Org. Chem.* **1974**, *39*, 3150-3153.
316. S. Inagaki, Y. Hirabayashi, *Chem. Lett.* **1978**, *7*, 135-138.
317. D. P. Kjell, R. S. Sheridan, *J. Am. Chem. Soc.* **1984**, *106*, 5368-5370.
318. G. W. Breton, K. A. Newton, *J. Org. Chem.* **2000**, *65*, 2863-2869.
319. S. J. Hamrock, R. S. Sheridan, *Tetrahedron Lett.* **1988**, *29*, 5509-5512.
320. S. J. Hamrock, R. S. Sheridan, *J. Am. Chem. Soc.* **1989**, *111*, 9247-9249.
321. M. Okumura, D. Sarlah, *Synlett* **2018**, *29*, 845-855.
322. E. H. Southgate, J. Pospech, J. Fu, D. R. Holycross, D. Sarlah, *Nat. Chem.* **2016**, *8*, 922-928.
323. L. Ulmer, C. Siedschlag, J. Mattay, *Eur. J. Org. Chem.* **2003**, *2003*, 3811-3817.
324. E. H. Southgate, D. R. Holycross, D. Sarlah, *Angew. Chem., Int. Ed.* **2017**, *56*, 15049-15052.
325. M. Okumura, S. M. Nakamata Huynh, J. Pospech, D. Sarlah, *Angew. Chem., Int. Ed.* **2016**, *55*, 15910-15914.
326. M. Okumura, A. S. Shved, D. Sarlah, *J. Am. Chem. Soc.* **2017**, *139*, 17787-17790.
327. M. E. Burrage, R. C. Cookson, S. S. Gupte, I. D. R. Stevens, *J. Chem. Soc. Perk. Trans. 2* **1975**, 1325-1334.

328. W. L. F. Armarego, C. Chai, *Purification of Laboratory Chemicals*, Elsevier Science, **2009**.
329. L. H. Dao, D. Mackay, *J. Chem. Soc., Chem. Commun.* **1976**, 326-327.
330. D. W. Borhani, F. D. Greene, *J. Org. Chem.* **1986**, *51*, 1563-1570.
331. R.-J. Tang, T. Milcent, B. Crousse, *Eur. J. Org. Chem.* **2017**, *2017*, 4753-4757.
332. A. Christoforou, G. Nicolaou, Y. Elemes, *Tetrahedron Lett.* **2006**, *47*, 9211-9213.
333. R. C. Cookson, I. D. R. Stevens, C. T. Watts, *Chem. Commun.* **1966**, 744-744a.
334. E. Baumgartner. EP0390028A2, 26/03/1990, **1990**.
335. B. Ostermayer. EP0412414A2, **1990**.
336. J. Blackborow. EP0728766A2, **1996**.
337. K. Muehlbach, M. A. De Araujo, R. Stadler. EP0338425A1, **1989**.
338. B. Ostermayer, K. Muehlbach, E. Baumgartner, H. Brandt, H. Feldmann. EP0370330A2, **1989**.
339. K.-W. Leong, G. B. Butler, *J. Macromol. Sci., Chem.* **1980**, *14*, 287-319.
340. T. C. S. Chen, G. B. Butler, *J. Macromol. Sci., Part A: Pure Appl. Chem.* **1981**, *A16*, 757-768.
341. R. Stadler, M. M. Jacobi, W. Gronski, *Makromol. Chem., Rapid Commun.* **1983**, *4*, 129-135.
342. W. Gronski, R. Stadler, M. Maldaner Jacobi, *Macromolecules* **1984**, *17*, 741-748.
343. R. Stadler, L. de Lucca Freitas, *Colloid Polym. Sci.* **1986**, *264*, 773-778.
344. R. Stadler, L. de Lucca Freitas, *Polym. Bull.* **1986**, *15*, 173-179.
345. L. L. de Lucca Freitas, R. Stadler, *Macromolecules* **1987**, *20*, 2478-2485.
346. L. de Lucca Freitas, R. Stadler, *Colloid Polym. Sci.* **1988**, *266*, 1095-1101.
347. L. D. Freitas, J. Burgert, R. Stadler, *Polym. Bull.* **1987**, *17*, 431-438.
348. C. Hilger, R. Stadler, *Macromolecules* **1990**, *23*, 2095-2097.
349. R. Wragg, J. Yardley. GB1456855, **1973**.
350. R. Wragg, J. Yardley. US3899378, **1975**.
351. S. P. Rout, G. B. Butler, *Polym. Bull.* **1980**, *2*, 513-520.
352. L. L. de Lucca Freitas, M. M. Jacobi, R. Stadler, *Polym. Bull.* **1984**, *11*, 407-414.
353. R. Stadler, F. Bühler, W. Gronski, *Makromol. Chem.* **1986**, *187*, 1301-1312.
354. R. Stadler, L. L. D. L. Freitas, M. M. Jacobi, *Makromol. Chem.* **1986**, *187*, 723-729.
355. R. Stadler, M. Weber, *Polymer* **1986**, *27*, 1254-1260.
356. M. Weber, R. Stadler, *Polymer* **1988**, *29*, 1064-1070.
357. M. Weber, R. Stadler, *Polymer* **1988**, *29*, 1071-1078.
358. E. Cutts, G. T. Knight. US3966530, **1974**.
359. S. van der Heijden, K. De Bruycker, R. Simal, F. Du Prez, K. De Clerck, *Macromolecules* **2015**, *48*, 6474-6481.
360. S. van der Heijden, L. Daelemans, K. De Bruycker, R. Simal, I. De Baere, W. Van Paeppegem, H. Rahier, K. De Clerck, *Compos. Struct.* **2017**, *159*, 12-20.
361. K. De Bruycker, M. Delahaye, P. Cools, J. Winne, F. E. D. Prez, *Macromol. Rapid Commun.* **2017**, *38*, 1700122.
362. Y. Zhao, J. Chen, W. Zhu, K. Zhang, *Polymer* **2015**, *74*, 16-20.
363. L. Vlamincck, K. De Bruycker, O. Turunc, F. E. Du Prez, *Polym. Chem.* **2016**, *7*, 5655-5663.

364. G. Becker, L. Vlaminck, M. M. Velencoso, F. E. Du Prez, F. R. Wurm, *Polym. Chem.* **2017**, *8*, 4074-4078.
365. L. Vlaminck, S. Lingier, A. Hufendiek, F. E. Du Prez, *Eur. Polym. J.* **2017**, *95*, 503-513.
366. S. Chattopadhyay, F. Du Prez, *Eur. Polym. J.* **2016**, *81*, 77-85.
367. Z. Wang, L. Yuan, N. M. Trenor, L. Vlaminck, S. Billiet, A. Sarkar, F. E. Du Prez, M. Stefik, C. Tang, *Green Chem.* **2015**, *17*, 3806-3818.
368. K. Hoogewijs, D. Buyst, J. M. Winne, J. C. Martins, A. Madder, *Chem. Commun.* **2013**, *49*, 2927-2929.
369. P. Wilke, T. Kunde, S. Chattopadhyay, N. ten Brummelhuis, F. E. Du Prez, H. G. Börner, *Chem. Commun.* **2017**, *53*, 593-596.
370. S. Vandewalle, R. De Coen, B. G. De Geest, F. E. Du Prez, *ACS Macro Lett.* **2017**, *6*, 1368-1372.
371. S. B. Hanay, B. Ritzen, D. Brougham, A. A. Dias, A. Heise, *Macromol. Biosci.* **2017**, *17*, 1700016.
372. S. B. Hanay, J. O'Dwyer, S. D. Kimmins, F. C. S. de Oliveira, M. G. Haugh, F. J. O'Brien, S.-A. Cryan, A. Heise, *ACS Macro Lett.* **2018**, *7*, 944-949.
373. N. Roy, J.-M. Lehn, *Chem. - Asian J.* **2011**, *6*, 2419-2425.
374. J. Sauer, B. Schroder, R. Wiemer, *Chem. Ber. Recl.* **1967**, *100*, 306-314.
375. M. M. Jacobi, R. Stadler, *Makromol. Chem., Rapid Commun.* **1988**, *9*, 709-715.
376. M. Inman, C. J. Moody, *Chem. Sci.* **2013**, *4*, 29-41.
377. N. K. Kaushik, N. Kaushik, P. Attri, N. Kumar, C. H. Kim, A. K. Verma, E. H. Choi, *Molecules* **2013**, *18*, 6620-6662.
378. T. C. Barden, in *Heterocyclic Scaffolds II: Reactions and Applications of Indoles* (Ed.: G. W. Gribble), Springer Berlin Heidelberg, Berlin, Heidelberg, **2010**, pp. 31-46.
379. T. V. Hoang, A. Michel, A. Guyot, *Eur. Polym. J.* **1976**, *12*, 357-364.
380. W. J. Houlihan, V. A. Parrino, Y. Uike, *J. Org. Chem.* **1981**, *46*, 4511-4515.
381. L.-L. Cao, D.-S. Wang, G.-F. Jiang, Y.-G. Zhou, *Tetrahedron Lett.* **2011**, *52*, 2837-2839.
382. M. Bandini, A. Eichholzer, *Angew. Chem., Int. Ed.* **2009**, *48*, 9608-9644.
383. K. De Bruycker, Ph.D. Thesis thesis, Ghent University **2017**.
384. H. Ueda, S. Aikawa, Y. Kashima, J. Kikuchi, Y. Ida, T. Tanino, K. Kadota, Y. Tozuka, *J. Pharm. Sci.* **2014**, *103*, 2829-2838.
385. L. Tajber, O. I. Corrigan, A. M. Healy, *Eur. J. Pharm. Sci.* **2005**, *24*, 553-563.
386. A. Kerbs, P. Mueller, M. Kaupp, I. Ahmed, A. S. Quick, D. Abt, M. Wegener, C. M. Niemeyer, C. Barner-Kowollik, L. Fruk, *Chem. - Eur. J.* **2017**, *23*, 4990-4994.
387. B. Richter, T. Pauloehrl, J. Kaschke, D. Fichtner, J. Fischer, A. M. Greiner, D. Wedlich, M. Wegener, G. Delaittre, C. Barner-Kowollik, M. Bastmeyer, *Adv. Mater.* **2013**, *25*, 6117-6122.
388. W. Song, Y. Wang, Z. Yu, C. I. R. Vera, J. Qu, Q. Lin, *ACS Chem. Biol.* **2010**, *5*, 875-885.
389. V. Kottisch, Q. Michaudel, B. P. Fors, *J. Am. Chem. Soc.* **2017**, *139*, 10665-10668.
390. D. R. Griffin, J. L. Schlosser, S. F. Lam, T. H. Nguyen, H. D. Maynard, A. M. Kasko, *Biomacromolecules* **2013**, *14*, 1199-1207.
391. K. Hiltebrandt, M. Kaupp, E. Molle, J. P. Menzel, J. P. Blinco, C. Barner-Kowollik, *Chem. Commun.* **2016**, *52*, 9426-9429.

392. D. E. Fast, A. Lauer, J. P. Menzel, A.-M. Kelterer, G. Gescheidt, C. Barner-Kowollik, *Macromolecules* **2017**, *50*, 1815-1823.
393. F. Hendrik, M. D. E., G. A. S., B.-K. Christopher, *Angew. Chem., Int. Ed.* **2018**, *57*, 2036-2045.
394. C. Rodriguez-Emmenegger, C. M. Preuss, B. Yameen, O. Pop-Georgievski, M. Bachmann, J. O. Mueller, M. Bruns, A. S. Goldmann, M. Bastmeyer, C. Barner-Kowollik, *Adv. Mater.* **2013**, *25*, 6123-6127.
395. D. M. Jones, A. A. Brown, W. T. S. Huck, *Langmuir* **2002**, *18*, 1265-1269.
396. O. Prucker, C. A. Naumann, J. R uhe, W. Knoll, C. W. Frank, *J. Am. Chem. Soc.* **1999**, *121*, 8766-8770.
397. W. Szymański, J. M. Beierle, H. A. V. Kistemaker, W. A. Velema, B. L. Feringa, *Chem. Rev.* **2013**, *113*, 6114-6178.
398. J. Zhang, J. Wang, H. Tian, *Mater. Horiz.* **2014**, *1*, 169-184.
399. D. G. Flint, J. R. Kumita, O. S. Smart, G. A. Woolley, *Chem. Biol.* **2002**, *9*, 391-397.
400. J. A. Ihalainen, J. Bredenbeck, R. Pfister, J. Helbing, L. Chi, I. H. M. van Stokkum, G. A. Woolley, P. Hamm, *Proc. Natl. Acad. Sci.* **2007**, *104*, 5383-5388.
401. B. L. Feringa, *Angew. Chem., Int. Ed.* **2017**, *56*, 11060-11078.
402. E. U. Kulawardana, T. Kuruwita-Mudiyanselage, D. C. Neckers, *J. Polym. Sci., Part A: Polym. Chem.* **2009**, *47*, 3318-3325.
403. S. Helmy, F. A. Leibfarth, S. Oh, J. E. Poelma, C. J. Hawker, J. Read de Alaniz, *J. Am. Chem. Soc.* **2014**, *136*, 8169-8172.
404. K. Matsubara, M. Watanabe, Y. Takeoka, *Angew. Chem., Int. Ed.* **2007**, *46*, 1688-1692.
405. Y. Gu, E. A. Alt, H. Wang, X. Li, A. P. Willard, J. A. Johnson, *Nature* **2018**, *560*, 65-69.
406. M. Herder, J.-M. Lehn, *J. Am. Chem. Soc.* **2018**, *140*, 7647-7657.
407. A. M. Mathur, A. B. Scranton, *Biomaterials* **1996**, *17*, 547-557.
408. H. N. Cheng, A. D. English, *NMR Spectroscopy of Polymers in Solution and in the Solid State, Vol. 834*, American Chemical Society, **2002**.
409. B. Mao, T. Divoux, P. Snabre, *J. Rheol.* **2016**, *60*, 473-489.
410. C. Dingels, M. Sch omer, H. Frey, *Chem. Unserer Zeit* **2011**, *45*, 338-349.
411. R. Klein, F. R. Wurm, *Macromol. Rapid Commun.* **2015**, *36*, 1147-1165.
412. Z. Xue, D. He, X. Xie, *J. Mater. Chem. A* **2015**, *3*, 19218-19253.
413. A. A. D'souza, R. Shegokar, *Expert Opinion on Drug Delivery* **2016**, *13*, 1257-1275.
414. J. Herzberger, K. Niederer, H. Pohlit, J. Seiwert, M. Worm, F. R. Wurm, H. Frey, *Chem. Rev.* **2016**, *116*, 2170-2243.
415. A.-L. Brocas, C. Mantzaridis, D. Tunc, S. Carlotti, *Prog. Polym. Sci.* **2013**, *38*, 845-873.
416. R. d'Arcy, N. Tirelli, *Macromol. Rapid Commun.* **2015**, *36*, 1829-1835.
417. S. Zalipsky, *Bioconjugate Chem.* **1995**, *6*, 150-165.
418. F. M. Veronese, *Biomaterials* **2001**, *22*, 405-417.
419. J.-F. Lutz, *J. Polym. Sci., Part A: Polym. Chem.* **2008**, *46*, 3459-3470.
420. X. Zhang, B. Xu, D. S. Puperi, A. L. Yonezawa, Y. Wu, H. Tseng, M. L. Cuchiara, J. L. West, K. J. Grande-Allen, *Acta Biomaterialia* **2015**, *14*, 11-21.
421. Y. Koyama, M. Umehara, A. Mizuno, M. Itaba, T. Yasukouchi, K. Natsume, A. Suginaka, K. Watanabe, *Bioconjugate Chem.* **1996**, *7*, 298-301.

422. B. Obermeier, F. Wurm, C. Mangold, H. Frey, *Angew. Chem., Int. Ed.* **2011**, *50*, 7988-7997.
423. K. P. Barteau, M. Wolffs, N. A. Lynd, G. H. Fredrickson, E. J. Kramer, C. J. Hawker, *Macromolecules* **2013**, *46*, 8988-8994.
424. B. Obermeier, H. Frey, *Bioconjugate Chem.* **2011**, *22*, 436-444.
425. C. Mangold, C. Dingels, B. Obermeier, H. Frey, F. Wurm, *Macromolecules* **2011**, *44*, 6326-6334.
426. J. Herzberger, K. Fischer, D. Leibig, M. Bros, R. Thiermann, H. Frey, *J. Am. Chem. Soc.* **2016**, *138*, 9212-9223.
427. C. Mangold, F. Wurm, B. Obermeier, H. Frey, *Macromolecules* **2010**, *43*, 8511-8518.
428. A. Thomas, S. S. Müller, H. Frey, *Biomacromolecules* **2014**, *15*, 1935-1954.
429. K. Niederer, C. Schüll, D. Leibig, T. Johann, H. Frey, *Macromolecules* **2016**, *49*, 1655-1665.
430. J. Herzberger, D. Leibig, J. Langhanki, C. Moers, T. Opatz, H. Frey, *Polym. Chem.* **2017**, *8*, 1882-1887.
431. B. Obermeier, F. Wurm, H. Frey, *Macromolecules* **2010**, *43*, 2244-2251.
432. C. Mangold, B. Obermeier, F. Wurm, H. Frey, *Macromol. Rapid Commun.* **2011**, *32*, 1930-1934.
433. G. Pruckmayr, P. Dreyfuss, M. P. Dreyfuss, in *Kirk-Othmer Encyclopedia of Chemical Technology*, **2000**.
434. F. Claeysens, E. A. Hasan, A. Gaidukeviciute, D. S. Achilleos, A. Ranella, C. Reinhardt, A. Ovsianikov, X. Shizhou, C. Fotakis, M. Vamvakaki, B. N. Chichkov, M. Farsari, *Langmuir* **2009**, *25*, 3219-3223.
435. F. J. O'Brien, *Mater. Today* **2011**, *14*, 88-95.
436. M. M. Zieger, P. Mueller, A. S. Quick, M. Wegener, C. Barner-Kowollik, *Angew. Chem., Int. Ed.* **2017**, *56*, 5625-5629.
437. M. M. Zieger, P. Müller, E. Blasco, C. Petit, V. Hahn, L. Michalek, H. Mutlu, M. Wegener, C. Barner-Kowollik, *Adv. Funct. Mater.* **2018**, *28*, 1801405.
438. J. Wang, B. Durbeej, *ChemistryOpen* **2018**, *7*, 583-589.
439. A. del Campo, C. Greiner, *J. Micromech Microeng* **2007**, *17*, R81-R95.
440. P. A. Mabrouk, in *Poly(ethylene glycol)*, Vol. 680, American Chemical Society, **1997**, pp. 118-133.
441. J. B. Mueller, J. Fischer, M. Wegener, in *Three-Dimensional Microfabrication Using Two-photon Polymerization* (Ed.: T. Baldacchini), William Andrew Publishing, Oxford, **2016**, pp. 82-101.
442. P. Theato, B. S. Sumerlin, R. K. O'Reilly, I. I. I. T. H. Epps, *Chem. Soc. Rev.* **2013**, *42*, 7055-7056.
443. H. A. Houck, K. De Bruycker, C. Barner-Kowollik, J. M. Winne, F. E. Du Prez, *Macromolecules* **2018**, *51*, 3156-3164.
444. H. A. Houck, F. E. Du Prez, C. Barner-Kowollik, *Nat. Commun.* **2017**, *8*, 1869.
445. H. A. Houck, E. Blasco, F. E. Du Prez, C. Barner-Kowollik, *J. Am. Chem. Soc.* **2019**, *141*, 12329-12337.
446. M. M. Heravi, F. Derikvand, M. Ghassemzadeh, B. Neumüller, *Tetrahedron Lett.* **2005**, *46*, 6243-6245.

-
447. R. C. Cookson, S. S. Gupte, I. D. R. Stevens, C. T. Watts, *Org. Synth.* **1988**, 50-9, 936-940.
448. R. J. Williams, I. A. Barker, R. K. O'Reilly, A. P. Dove, *ACS Macro Lett.* **2012**, 1, 1285-1290.
449. D.-Q. Xu, J. Wu, S.-P. Luo, J.-X. Zhang, J.-Y. Wu, X.-H. Du, Z.-Y. Xu, *Green Chem.* **2009**, 11, 1239-1246.
450. C. F. H. Allen, J. A. VanAllan, *J. Am. Chem. Soc.* **1951**, 73, 5850-5856.
451. B. Z. Lu, W. Zhao, H.-X. Wei, M. Dufour, V. Farina, C. H. Senanayake, *Org. Lett.* **2006**, 8, 3271-3274.
452. J. Fischer, J. B. Mueller, A. S. Quick, J. Kaschke, C. Barner-Kowollik, M. Wegener, *Advanced Optical Materials* **2015**, 3, 221-232.

